Institute of Genetic Medicine

Newcastle University

Investigating the role of Rac1 in cardiovascular development

Rebecca Dodds

Submitted in accordance with the requirement for the degree of Doctor of Philosophy
September 2016

Supervisors: Dr Helen Phillips

Professor Deborah Henderson

Abstract

Rac1 is a Rho GTPase which is involved in a variety of fundamental cellular processes, such as cell proliferation, adhesion and migration. In the adult heart, Rac1 is upregulated in cardiovascular disease and is required for the development of hypertrophy through production of oxidative stress. However, its expression and function during cardiovascular development remains unclear.

Rac1 gene expression was characterised during mouse cardiac development, and using *Cre-loxP* technology it was identified that *Rac1* is essential in the cardiomycoytes within the myocardium, but not in the epicardium, for the normal development of the mouse embryonic heart. Deletion of *Rac1* specifically in the cells of the myocardium, the cardiomyocytes, using the *TnT-Cre* transgenic mouse line, resulted in severe defects of the ventricular myocardial wall as well as disrupted cardiac outflow tract alignment. $Rac1^{TnTCre}$ mutants displayed disrupted formation of ventricular trabeculae early in development. This resulted in abnormalities in the mature structures that form from the trabeculae, including the compact myocardial wall and interventricular septum. As a consequence of these myocardial defects, $Rac1^{TnTCre}$ mutant hearts become dilated and ballooned in shape leading to malalignment of the cardiac outflow tract, but with no overall loss of cardiomyocytes. This thesis shows that Rac1 and interacting partners, Mena and Vav2, are required for the organisation and movement of cardiomyocytes in the ventricular myocardial wall during early trabeculae formation.

Congenital heart defects, including those affecting the myocardium and outflow tract, are the most common form of birth abnormalities. Additionally, defects occurring *in utero* can predispose to heart disease in later life. Therefore, understanding the role of genes that regulate myocardial wall and outflow tract formation could facilitate the development of preventative measures and treatments for congenital heart defects and cardiovascular disease.

Acknowledgements

First of all I would like to express my gratitude and thanks to my supervisor Dr Helen Phillips for the continuous help, support and guidance I received throughout my PhD studies, and in writing this thesis. Additionally, I would like to thank my supervisor Professor Deborah Henderson for her support and expertise in this field of research. I would also like to express my thanks to Dr Simon Bamforth, Dr Gavin Richardson, Professor Helen Arthur and Professor Robert Anderson for their insightful comments on my PhD research. I greatly appreciate the encouragement, enthusiasm, and knowledge I received from all the formentioned people.

I would like to extend my thanks to past and present members of the cardiovascular development group for practical tips, discussion and entertainment in the lab. In particular Dr Amy-Leigh Johnson for teaching me in the initial stages of my PhD and both Dr Lorraine Eley and Kath Allison for their technical expertise and advice. In addition I would like to acknowledge the many undergraduate, postgraduate and summer students who have worked alongside me on this project over the course of my PhD studies.

I am grateful to my friends within the Institute of Genetic Medicine for their kindness and support throughout my PhD. In particular, I would like to thank Kate Bailey, Dr Vipul Sharma and Dr Alberto Briones for much needed cake Wednesdays and Friday wine time.

Thanks to all the staff at the Institute of Genetic Medicine for their help during my PhD studies and whom made my time at the institute very enjoyable.

Finally, thanks to my wonderful family and friends for their support and understanding during my PhD studies. In particular, I would like to thank Mark Ashby for the financial and emotional support during the past 4 years, and for reading this thesis many times.

Table of Contents

Abbreviations

3D	Three dimensional
ABP	Apical-basal polarity
AF	Atrial fibrillation
Afp	Alphafetoprotein
AJ	Adherens junctions
ANF	Atrial natriuretic factor
APC	Adenonatous polyposis coli
AV	Atrioventricular
AVC	Atrioventricular canal
ARSA	Anomalous right subclavian artery
AS	Atrial septum
ASD	Atrial septal defects
AVS	Atrioventricular septum
AVSD	Atrioventricular septal defects
BHF	British Heart Foundation
BMP	Bone morphogenetic protein
BrdU	Bromodeoxyuridine
Ccn1	Cysteine rich protein 61
CE	Convergent extension
Cdk	Cyclin dependent kinases
cDNA	Complementary DNA
CHD	Congenital heart defects
CreERT2	Cre-modified oestrogen receptor ligand-binding domain
CS	Chondroitin sulfate
CVD	Cardiovascular disease
Cx	Connexins
DAB	Diaminobenzine
DEPC	Diethylpyrocarbonate
dH_20	Distilled water
DMP	Dorsal mesenchyme protrusion
DORV	Double outlet right ventricle
DPW	Dorsal pericardial wall
Dvl	Dishevelled
E	Embryonic day
EC	Endothelial cells

ECM	Extracellular matrix
EDTA	Ethylenediamine tetra-acetic acid
EMT	Epithelial to mesenchymal transition
EPDC	Epicardial derived cells
EYFP	Enhanced yellow fluorescent protein
FAK	Focal adhesion kinase
FCS	Foetal calf serum
FGF	Fibroblast growth factor
FHF	First heart field
Fz	Frizzled
GAP	GTPase activating protein
Gapdh	Glyceraldehyde 3-phosphate dehydrogenase
GEF	Guanine nucleotide exchange factors
Git1	G protein coupled receptor kinase interacting protein 1
HA	Hyaluronan
Hh	Hedgehog
HREM	High resolution episcopic microscopy
HS	Heparan sulfate
ICD	Intercalated disc
KS	Keratin sulfate
IF	Immunofluorescence
IHC	Immunohistochemistry
Isl1	LIM-homeodomain protein
Irx	Iroquois homeobox
IVS	Interventricular septum
KCl	Potassium chloride
LB	Luria Bertani
LEF	Lymphoid enhancer binding factor
LVNC	Left ventricular non-compaction
MBP-C	Myosin binding protein C
MC	Mesenchymal cap
MHC	Myosin heavy chains
MI	Myocardial infarction
MLC	Myosin light chains
MRI	Magnetic Resonance Imaging
MTOC	Microtubule organising centre
N1ICD	Notch intracellular domain

NCC	Neural crest cells
Nfatc	Nuclear factor of activated T cells
Nrg	Neuregulin
Nrp	Neuropilin
OA	Overriding aorta
OFT	Outflow tract
P	Postnatal day
PAA	Pharyngeal arch artery
PAS	Primary atrial septum
PBS	Phosphate buffered saline
PCP	Planar cell polarity
PCR	Polymerase chain reaction
Pdgf	Platelet derived growth factor
PE	Pro-epicardium
phHH3	Phospho-histone H3
Pix	Pak interacting exchange factor
Pk	Prickle
PKC	Protein kinase C
PTA	Persistent truncus arteriosus
QPCR	Quantitative Real Time PCR
Rac1	Ras-related C3 botulinum toxin substrate 1
RBD	Rho binding domain
RBP-Jk	Recombining binding protein suppressor of hairless
ROS	Reactive oxygen species
RT-PCR	Reverse transcriptase PCR
RV	Right ventricle
SAS	Secondary atrial septum
SEM	Standard error of the mean
Sfrp1	Secreted frizzled related protein 1
SHF	Second heart field
SM22α	Smooth muscle 22 alpha
SMC	Smooth muscle cell
SV	Sinus venosus
TBS	Tris buffered saline
Tbx	T box transcription factor
TCF	T cell factor
TEM	Transmission electron microscopy

TF	Tetralogy of Fallot
TGA	Transposition of the great arteries
TGF	Transforming growth factor
TJ	Tight junction
TnT	Troponin
TSA	Tyramide Signal Amplification
Tx	Triton-X
VE	Vascular endothelial
VEGF	Vascular endothelial growth factor
VEGFR	Vascular endothelial growth factor receptor
vSMC	Vascular smooth muscle cell
VSD	Ventricular septal defect
WGA	Wheat germ agglutinin
WT	Wilm’s tumour
ZO	Zona occludens

List of Figures

List of Tables

Chapter 1. Introduction

1.1 Mammalian adult heart and cardiovascular disease

The mammalian adult heart is a four-chambered muscular organ that pumps blood through the blood vessels of the circulatory system to supply the body with oxygen and nutrients and to remove metabolic waste (Figure 1; adult heart schematic in A and dissected mouse heart in B). The muscular wall of the heart, or ventricular myocardium, is enveloped in a thin endocardial layer on the inside, and an epicardial layer on the outside (Figure 1A). The muscular wall contains contractile cardiomyocytes supplemented with connective tissue, and is innervated and vascularised. Cardiomyocytes account for around 30% of the total cells in the adult heart however they occupy around 75% of the total volume (Vliegen *et al*., 1991). The remaining cells and space is comprised of cardiac fibroblasts, endothelial cells and vascular smooth muscle cells which form the blood vessels and contribute to the interstitium surrounding cardiomyocytes (Camelliti *et al*., 2005) (Figure 1C).

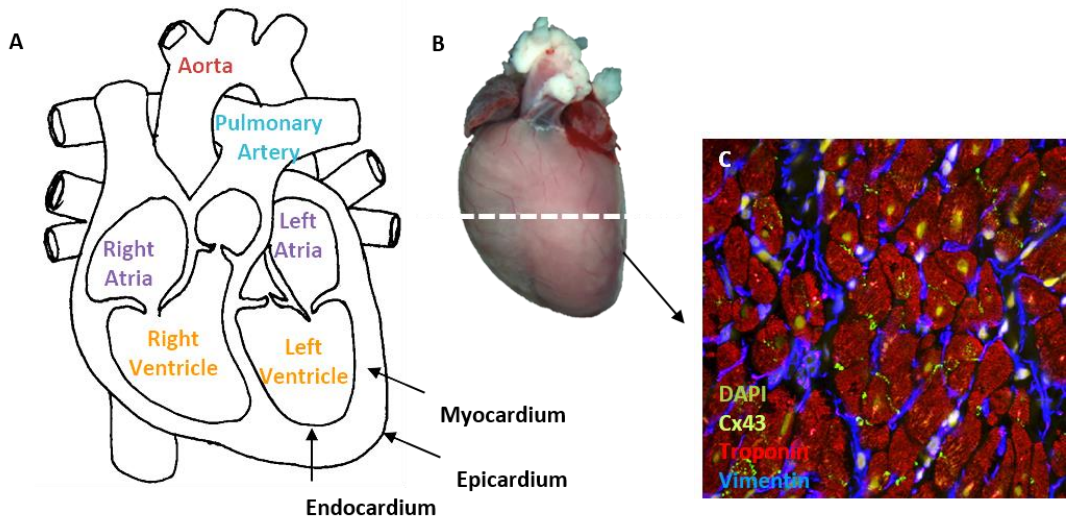

Figure 1: Adult heart structure.
The mammalian adult heart is a four-chambered pump (schematic in **A**). The muscular wall of the heart is enveloped in a thin endocardial layer on the inside and an epicardial layer on the outside (**A**). The mouse heart is similar to the human heart (dissected mouse heart in **B**) and the muscular wall, or ventricular myocardium, is comprised of contractile cardiomyocytes supplemented with connective tissue and is innervated and vascularised (**C**). Cardiomyocytes (anti-troponin red) are joined by intercalated discs (anti-connexin43, bright green) and are interspersed with fibroblasts (anti-vimentin, blue) (**C**). DAPI to label nuclei (yellow–green) (**C**) (Camelliti *et al*., 2005).

Cardiovascular disease (CVD) is the main cause of death in the United Kingdom (UK), accounting for over a quarter of all deaths and includes all diseases of the heart and circulation, including coronary heart disease, cardiomyopathy, atrial fibrillation (AF) and heart failure (British Heart Foundation (BHF)). Risk factors for CVD include genetic and environmental factors such as diabetes, smoking and poor diet. Furthermore, there is increasing evidence suggesting that abnormalities occurring *in utero* can predispose to CVD in adult life, therefore understanding the role genes play during development can help elucidate their role in disease development.

1.2 Congenital heart disease

Congenital heart defects (CHD) are the most common form of birth abnormalities, diagnosed in 1 out of 180 babies in the UK (BHF Statistics). There are many types of CHD and they can be grouped into three main categories; cyanotic heart disease, left sided obstructive defects and septation defects. The individual CHDs are listed in Table 1.

Cyanotic Heart	Left Sided Obstructive Defects	Septal Defects
Transposition of the great arteriesTetralogy of fallot Tricuspid atresia Pulmonary atresia Ebstein's anomaly of tricuspid valve Double outlet right ventricle Common arterial trunk Total anomalous pulmonary venous connection	Hypoplastic left heart syndrome Mitral stenosis Aortic stenosis Aortic coarctation Interrupted aortic arch	Atrial septal defect Ventricular septal defect Atrioventricular septal defect

Table 1: Types of congenital heart defects.
Table adapted from Bruneau *et al.* (Bruneau, 2008).

Several genetic and environmental risk factors for CHD have been identified but the majority of cases have no obvious cause. Genetic disorders such as Down's syndrome can include CHD (Mortensen *et al.*, 2012; Roberts *et al.*, 2013; Stoll *et al.*, 2015). Alternatively, maternal factors can increase the risk of CHD including diabetes, infections such as Rubella, and folate deficiency (Lee and Lupo, 2013; Cai *et al.*, 2014; Shi *et al.*, 2014; Simeone *et al.*, 2015).

Treatment for CHD is defect dependent. Mild defects, such as muscular ventricular septal defect (VSD), often heal independently and may not cause any further problems. However, surgery or interventional procedures are normally required for more severe defects. For example, in double outlet right ventricle (DORV) prostaglandin infusions are required to keep the ductus arteriosus open to allow oxygenated blood to enter the systemic circulation, followed by surgical repair (Lagopoulos *et al.*, 2010). Current surgical techniques can often restore cardiac function, with 80% survival into adulthood (BHF statistics). However, patients with treated congenital heart disease often develop problems with heart rhythm or valves in adulthood, thus, requiring lifelong treatment and review. Therefore, it is important to understand the underlying causes of CHD to develop better treatments and preventions of CHD and adult cardiovascular disease.

1.3 Embryonic heart development

1.3.1 Overview of mammalian embryonic heart development

Across vertebrates, cardiac development follows the same basic pattern; formation of a linear heart tube which undergoes lengthening and looping to form a four-chambered pump. Zebrafish, chick and mouse models have been extensively studied to dissect the pathways that initiate and regulate embryonic heart development. In mice, heart development is initiated at embryonic day (E) 6.5, when the earliest cardiac precursors are positioned in bilaterally paired cardiogenic fields around the midline in the splanchnic mesoderm of the epiblast (Tam *et al.*, 1997) (Figure 2A). These two fields, containing endocardial and myocardial precursor cells, converge on the midline to form the cardiac crescent (Figure 2B). The cardiac crescent then fuses at the midline to form the linear heart tube (DeRuiter *et al.*, 1992; Buckingham *et al.*, 2005), which consists of an inner endocardial tube, surrounded by a single layer of myocardial cells separated by cardiac jelly (Figure 2C). The linear heart tube undergoes a complex process of looping, and lengthens by the addition of both myocardial and endocardial cells to the outflow tract (OFT) pole. As the myocardial layer thickens and matures, myocardial cells begin to contract, the cardiac jelly between the endocardium and myocardium allows the contraction to pass to the endocardial tube, and the heart begins to beat at around E8.5.

During the process of looping, the heart loops to the right towards the midline forming the primordial atria, primordial ventricles and truncus arteriosus (Figure 2D). The atria are positioned above the ventricles and ventricular bulging occurs, forming the right and left sides of the ventricle (Moorman and Christoffels, 2003) (Figure 2E). Cardiac jelly dissipates from the chambers and accumulates at the atrioventricular (AV) canal and in the OFT to form endocardial cushions (Figure 2F). The endocardial cushions are infiltrated by mesenchymal cells from the endocardium that have undergone epithelial to mesenchymal transition (EMT). The endocardial cushions at the AV junction are required for the formation of the AV septum and AV valves (tricuspid and mitral valves) (Anderson *et al.*, 2003a). Similarly, the OFT endocardial cushions are necessary for OFT septation (septation of the truncus arteriosus into the pulmonary and aortic trunk) and formation of aortic and pulmonary valves (Anderson *et al.*, 2003b). During development of the thickening myocardial wall, two main processes occur; trabeculation and compaction of the myocardium. Ridges of myocardium covered in endocardium extend into the atrial or ventricular lumen; initiating at around E9.5 (Kruithof *et al.*, 2013) (Figure 2G). Trabeculation aids to increase myocardial oxygen and nutient exchange in the absence of coronary circulation, and also to enhance myocardial force generation (Sedmera *et al.*, 2000). The trabeculae coalesce to form the interventricular septum (IVS) and are thought to compact later in development, resulting in further thickening of the compact myocardium, during which ventricular septation occurs, followed by atrial septation (Anderson *et al.*, 2003a). By E13.5 the four-chambered heart is formed (Figure 2I).

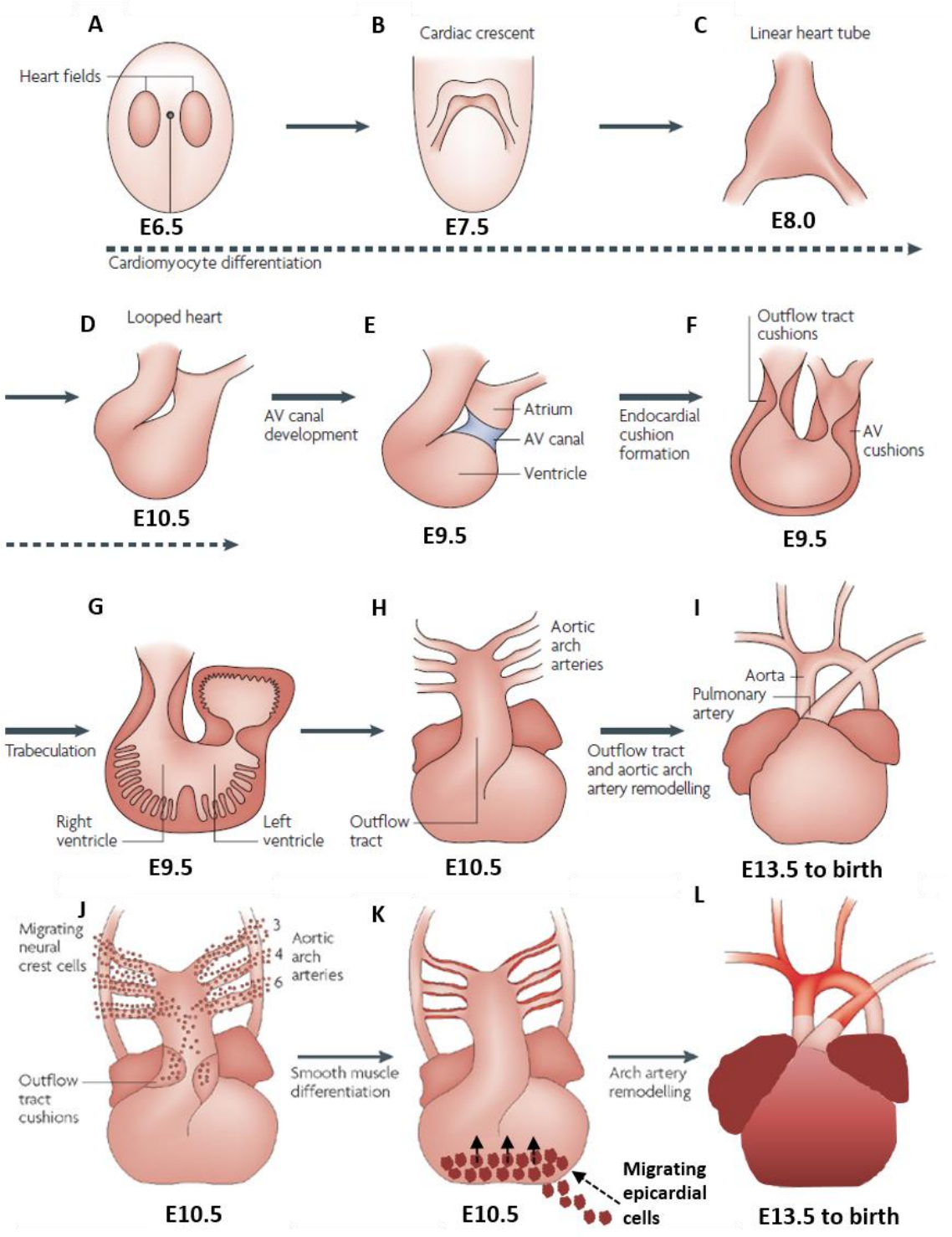

Figure 2: Schematic of mouse embryonic heart development.
Heart development is initiated at E7.0 when bilateral cardiogenic fields are positioned either side of the midline (**A**). These cardiogenic fields converge to form the cardiac crescent which then fuses to form the linear heart tube (**B**,**C**). At around E8.5 the linear heart tube loops rightwards towards the midline forming the primordial atria, primordial ventricles and truncus arteriosus (**D**,**E**). At E9.5 cardiac jelly accumulates at the atrioventricular (AV) canal and in the OFT to form endocardial cushions which are involved in AV and OFT septation (**F**). Trabeculation of the myocardium begins at around E9.5 where ridges of

myocardium covered in endocardium extend into the atrial or ventricular lumen (**G**). NCC migrate into the aortic arch arteries and OFT contributing to the septation and remodelling of the OFT (**J**). Pro-epicardial cells spread over the surface of the heart in a monolayer and form the epicardium by E10.5 (**K**) and by E13.5 the four-chambered heart is formed (**L**). E; embryonic day. Figure adapted from (High and Epstein, 2008).

1.3.2 Extracardiac cell populations

The primary, or first heart field (FHF) is responsible for the formation of the initial linear heart tube. In addition to the FHF, several extra-cardiac cell populations contribute to the development of the heart after the formation of the linear heart tube, including cells originating in the second heart field (SHF), neural tube and pro-epicardium (PE). The FHF contributes to cells in the left ventricle (LV) and atria, whereas the SHF contributes to the right ventricle (RV), OFT and atria. The cells from the PE form the epicardium.

1.3.2.1 Second heart field

Both the FHF and SHF populations originate in the cardiogenic fields, however these two populations do not differentiate into myocardium and endocardium simultaneously. The FHF is defined by the first cells to express cardiac markers, *Mesp1*, T-box transcription factor (*Tbx)5* and *Nkx2.5,* and forms the initial linear heart tube. A later wave in *Mesp1* expression defines the SHF, which also expresses *LIM-homeodomain protein* (*Islet1*), *fibroblast growth factor* (*Fgf*)*8* and *Fgf10*. SHF cells contribute to the lengthening of the heart tube by their addition to the inflow and outflow region (Kelly *et al.*, 2001; Mjaatvedt *et al.*, 2001; Waldo *et al.*, 2001; Waldo *et al.*, 2005b) (Figure 3). SHF progenitors display differentiation delay and continued elevated proliferation relative to FHF progenitors (Buckingham *et al.*, 2005). The continued proliferation and differentiation of SHF cells is regulated by FGF, bone morphogenetic protein (BMP), Hedgehog (Hh), Wnt signalling and Notch signalling pathways (Goddeeris *et al.*, 2007; Prall *et al.*, 2007; Cohen *et al.*, 2008; Park *et al.*, 2008) (Figure 4). Conditional loss-of-function analysis of these signalling pathways in the SHF results in shortening of the cardiac OFT, leading to subsequent septation defects. FGF ligands implicated in SHF deployment include FGF3, FGF8 and FGF10 and are expressed in pharyngeal mesoderm and epithelia (Ilagan *et al.*, 2006; Watanabe *et al.*, 2010; Urness *et al.*, 2011). Wnt and Hh signalling pathways are required to maintain proliferation and regulate

deployment of SHF cells (Klaus *et al.*, 2012; Xie *et al.*, 2012). Wnt/β-catenin signalling operates downstream of Notch in the regulation of progenitor cell differentiation and OFT morphogenesis (Klaus *et al.*, 2012). SHF can give rise to three major cell lineages of the heart: cardiomyocytes, smooth muscle cells (SMC) and endothelial cells (Moretti *et al.*, 2006). Endocardial cells lining the OFT are thought to derive from SHF progenitors (Laugwitz *et al.*, 2008).

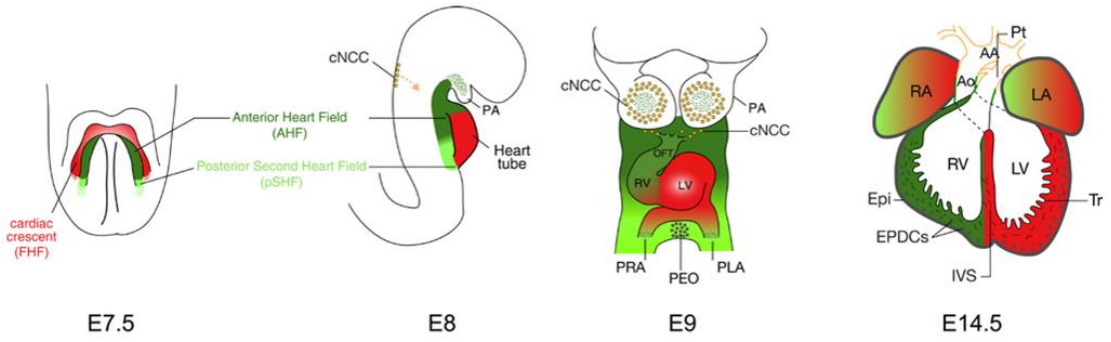

Figure 3: The contribution of the second heart field (SHF) to the developing mouse heart.
The relative position and contribution of the SHF progenitors (green) including anterior heart field (AHF) and posterior second heart field (pSHF) relative to the first heart field (FHF) cells (red) from the cardiac-crescent through to the looping stages of mouse heart development. SHF gives rise to three major cell lineages of the heart: cardiomyocytes, smooth muscle cells and also endothelial cells (Moretti *et al.*, 2006). SHF cells contribute to the lengthening of the heart tube by their addition to the heart tube through the inflow and outflow region, and ultimately form the myocardium of the OFT, right ventricle and parts of the atria (Kelly *et al.*, 2001; Mjaatvedt *et al.*, 2001; Waldo *et al.*, 2001; Waldo *et al.*, 2005b). cNCC; cardiac neural crest cells, PA; pharyngeal arches, PEO; proepicardial organ, OFT; outflow tract, LA; left atrium; LV, left ventricle; RA, right atrium; RV, right ventricle, Ao; Aorta, Pt; pulmonary trunk, AA; Aortic arch, Epi; epicardium, EPDCs; epicardial derived cells, IVS; Intraventricular septum, Tr; trabeculae, E; embryonic day (Zaffran *et al.*, 2014).

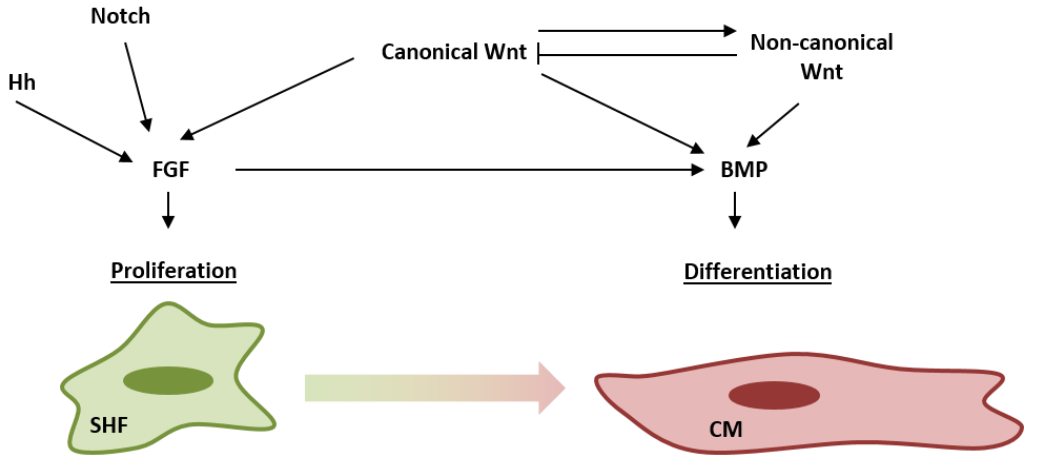

Figure 4: Signalling pathways involved in proliferation and progressive differentiation of second heart field (SHF) cardiac progenitor cells in the early embryo.
SHF cell proliferation and differentiation is regulated through various signalling pathway, including FGF, Notch, Hh, BMP and Wnt signalling (Francou *et al.*, 2013). CM; Cardiomyocyte.

1.3.2.2 Cardiac neural crest cells

Cardiac neural crest cells (NCC), originating in the dorsal neural tube, play an early role in restricting proliferation and controlling deployment of the SHF by modulating local FGF signalling (Waldo *et al.*, 2005a) (Figure 4). Additionally, NCC migrate into and stabilise the endothelial cells of the pharyngeal arch arteries, contributing to the remodelling into the great vessels of the OFT (Waldo *et al.*, 1996; Jiang *et al.*, 2000) (Figure 2J). NCC also migrate into the endocardial cushions of the distal OFT and are involved in OFT septation (Kirby *et al.*, 1983) (Figure 2J). As NCC enter the distal OFT, endothelial cells in the proximal region of the OFT undergo a process of EMT in response to myocardial-derived signals, to form, together with invading NCC, OFT cushions between the myocardial and endothelial layers (Sugishita *et al.*, 2004). Convergence of OFT cushions in a spiral structure separates laminar flow from the embryonic left and right ventricles.

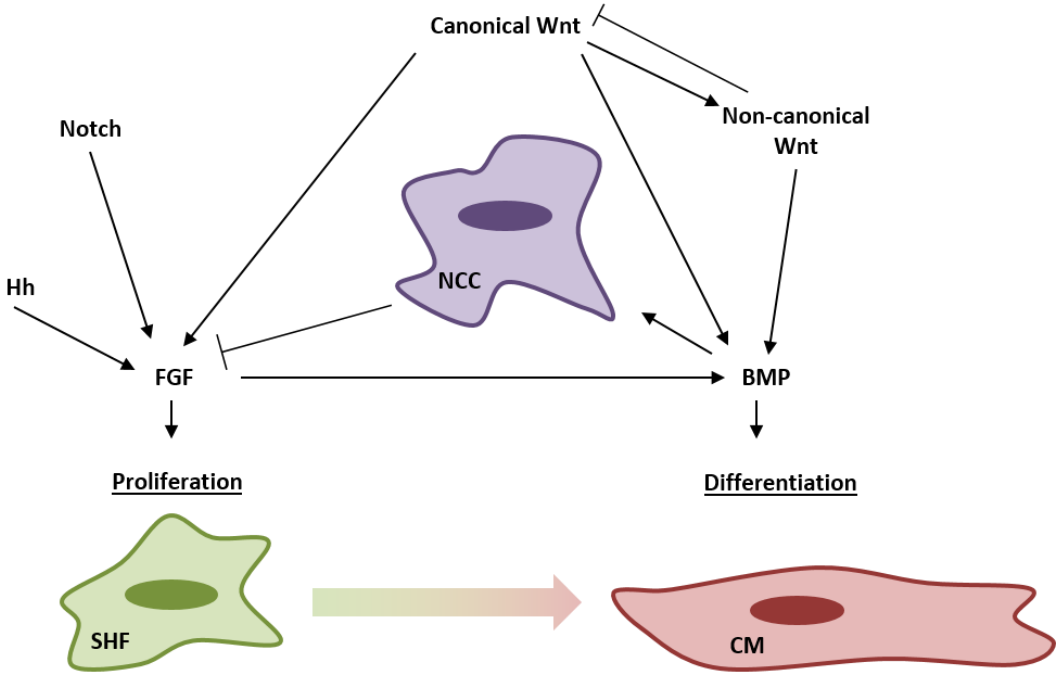

Figure 5: Neural crest cell (NCC) regulation of second heart field (SHF) proliferation and differentiation.
NCC play a regulatory role in controlling SHF cell proliferation and differentiation through FGF signalling (Francou *et al.*, 2013). CM; cardiomyocyte.

1.3.2.3 Epicardial cells

The proepicardium (PE) is a transient extra-cardiac cluster of cells, which form a cauliflower-like protrusion at the base of the developing heart (Viragh and Challice, 1981; Manner *et al.*, 2001). The PE forms villi which protrude towards the myocardium of the looping heart tube. In mice, PE cells migrate as clusters of cells and adhere to the surface of the myocardium at E9.5, forming an epicardial layer that spreads over the surface of the heart in a monolayer, covering the ventricles and atria by E10.5 (Komiyama *et al.*, 1987) (Figure 2K). Once the epicardium has completely enveloped the myocardium, a subset of epicardial cells delaminate from the epicardium and migrate into the sub-epicardial space, from E11.5 to E12.5 (Mikawa and Gourdie, 1996; Dettman *et al.*, 1998; Perez-Pomares *et al.*, 2002).These epicardial derived cells (EPDCs) then migrate into the myocardium and also populate the AV cushions where the cells undergo EMT and differentiate into SMC, endothelial cells and fibroblasts (Figure 6) and contribute to the formation of coronary vessels and heart valves (Mikawa and Gourdie, 1996; Dettman *et al.*, 1998; Perez-Pomares *et al.*, 2002). FGFs and transforming growth factor beta (TGF) promote and inhibit EMT

respectively, and play a critical role in balancing the number of cells leaving the epithelial layer as mesenchymal cells (Morabito *et al.,* 2001). Various signalling pathways regulate EPDC differentiation; Vascular endothelial growth factor (VEGF) and FGF signalling are required for endothelial cell differentiation; Tcf21, TGF-β and platelet derived growth factor (PDGF) signalling are required for cardiac fibroblast differentiation, and TGF-β and PDGF are required for smooth muscle differentiation (Figure 6). EPDCs have also been found to contribute to the cardiomyocyte lineage (Zhou *et al.*, 2008).

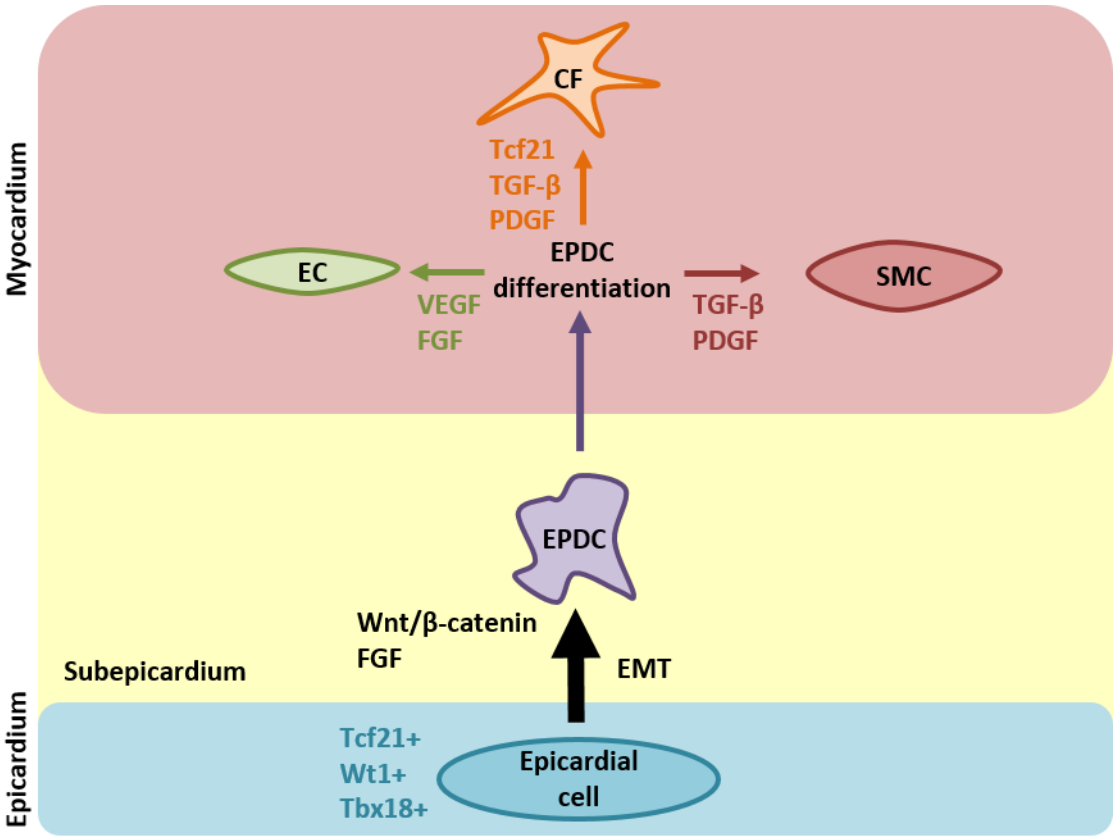

Figure 6: Epicardial epithelial to mesenchymal transition (EMT) during cardiac development.
Epicardial cells undergo EMT and enter the subepicardial space. FGFs and TGF-β promote and inhibit EMT respectively, and play a critical role in balancing the number of cells leaving the epithelial layer as mesenchymal cells. Epicardial derived cells (EPDC)s then invade the myocardium, differentiate and populate the myocardium with endocardial cells (EC)s, smooth muscle cells (SMC)s and cardiac fibroblasts (CF). Various signalling pathways regulate EPDC differentiation; VEGF and FGF signalling are required for endothelial cell differentiation, Tcf21, TGF-β and PGDF signalling are required for cardiac fibroblast differentiation and TGF-β and PDGF are required for smooth muscle differentiation.

1.4 Outflow tract development and conotruncal heart defects

Septation of the primitive cardiac chambers, the atrioventricular canal (AVC) and the OFT is necessary for the correct formation of the four-chamber heart. The morphogenic events that regulate these processes are described below.

1.4.1 Cushion and valve formation

Cardiac jelly that is secreted by the myocardium, concentrates itself into two pairs of bulges between the myocardial and endocardial layers of the primary heart tube. One pair lines the OFT, continuous through the proximal and distal regions, forming the OFT cushions (Figure 7). The second pair forms the AV cushions between the atrial and ventricle chambers. At E12.5 the cushions have fully formed and mainly consist of ECM proteins such as proteoglycans. Cushion mesenchyme is derived from the endocardium through EMT. Various signalling pathways are involved in the initiation of EMT including Wnt, BMP, TGF-β and Notch (Timmerman *et al.*, 2004; Wang *et al.*, 2013). Wnt signalling from myocardial cells to endocardial cells initiates EMT and is central to cardiac cushion formation (Hurlstone *et al.*, 2003). TGF-β, BMP and Notch signalling act to downregulate Vascular endothelial (VE)-cadherin pre EMT (Brown *et al.*, 1996; Jiao *et al.*, 2006). In response to these signals from the myocardium and ECM, a subset of endothelial cells delaminate from the surface epithelium and transdifferentiate into mesenchymal cells. These mesenchymal cells migrate into the cardiac jelly and proliferate to cellularise the cushions (Eisenberg and Markwald, 1995). EMT requires down-regulation of cadherins, leading to cell detachment from laminin and the basement membrane. The OFT cushions are subsequently remodelled into semi-lunar valves at the angular junction of the proximal and distal regions of the OFT (Anderson *et al.*, 2003b). The AV cushions are remodelled into the AV valves.

1.4.2 OFT development

The cardiac OFT forms at the arterial pole of the heart and connects the embryonic ventricles to the aortic sac. OFT morphogenesis is a complex process involving differentiation and proliferation of multiple cell types and is regulated by various signalling pathways, making it prone to abnormalities.

1.4.2.1 OFT formation

After formation of the linear heart tube by the FHF, myocardial and endocardial cells are added to the arterial pole from the SHF progenitor population in the pharyngeal mesoderm. SHF cells are continuously added, leading to elongation of the heart tube (Kelly and Buckingham, 2002; Cai *et al.*, 2003; Buckingham *et al.*, 2005) (Figure 3). Deployment of SHF cells and regulation by NCC is critical for correct vessel formation. NCC and SHF cells work in coordination and NCCs regulate proliferation of SHF cells (Waldo *et al.*, 2005a) (Figure 5).

1.4.2.2 OFT remodeling

Alongside AV septation and pharyngeal arch artery (PAA) remodeling, the OFT undergoes remodeling involving septation and rotation. OFT remodeling is a complex process with contributions from both genetics and haemodynamics, and occurs between E10.5 and E14.5 of mouse gestation (Yashiro *et al.*, 2007).

1.4.2.3 OFT Septation

The OFT is septated into the base of the ascending aorta and the base of the pulmonary trunk, while both outflow vessels remain associated with the RV. OFT septation requires the ingrowth of the aorticopulmonary septum between the 4th and 6th PAA and the formation of the OFT cushions, and is regulated by NCCs. By E10.5, NCCs have invaded the distal region of the OFT and the transient aorticopulmonary septum is visible in the dorsal wall of the aortic sac (Anderson *et al.*, 2003b). By E11.5, there is a rapid increase in the number of NCCs, due to their continuous migration into the outflow cushions and proliferation of cells already in the cushions (Sugishita *et al.*, 2004; Kirby and Hutson, 2010), filling the distal outflow cushions and the dorsal wall of the aortic sac (Figure 7B). As a consequence, the dorsal wall of the aortic sac comes in contact with the most distal regions of the expanded outflow cushions and fuses, along with the fusion of the two cushions with each other, initiating outflow septation and separating the systemic and pulmonary circulations (Anderson *et al.*, 2003b) (Figure 7C). Once septation is initiated by the fusion of the dorsal wall of the aortic sac with the distal OFT cushions, it proceeds in a distal to proximal direction (Waldo *et al.*, 1998).

1.4.2.4 Rotation of the OFT and wedging of the aorta

OFT cushion convergence is accompanied by rotation of the OFT wall in an anticlockwise direction, resulting in alignment of the aorta with the LV and pulmonary trunk with the RV (Bajolle *et al.*, 2006) (Figure 7). This process requires hypoxia-driven programmed cell death in part of the distal OFT myocardial wall (Sugishita *et al.*, 2004; Rana *et al.*, 2007). The remaining distal OFT myocardial wall is incorporated into the right ventricular subpulmonary myocardium. It has been shown that the myocardium at the base of the aorta and pulmonary trunk is prefigured in the OFT of the heart and in subdomains of the SHF (Bajolle *et al.*, 2008). 'Wedging' is the movement of the aorta behind the pulmonary trunk, between AV valves during OFT alignment and septation. The process of wedging is dependent on the retraction and rotation of the truncal myocardium and without rotation and wedging the aorta overrides the ventricular septum leading to DORV.

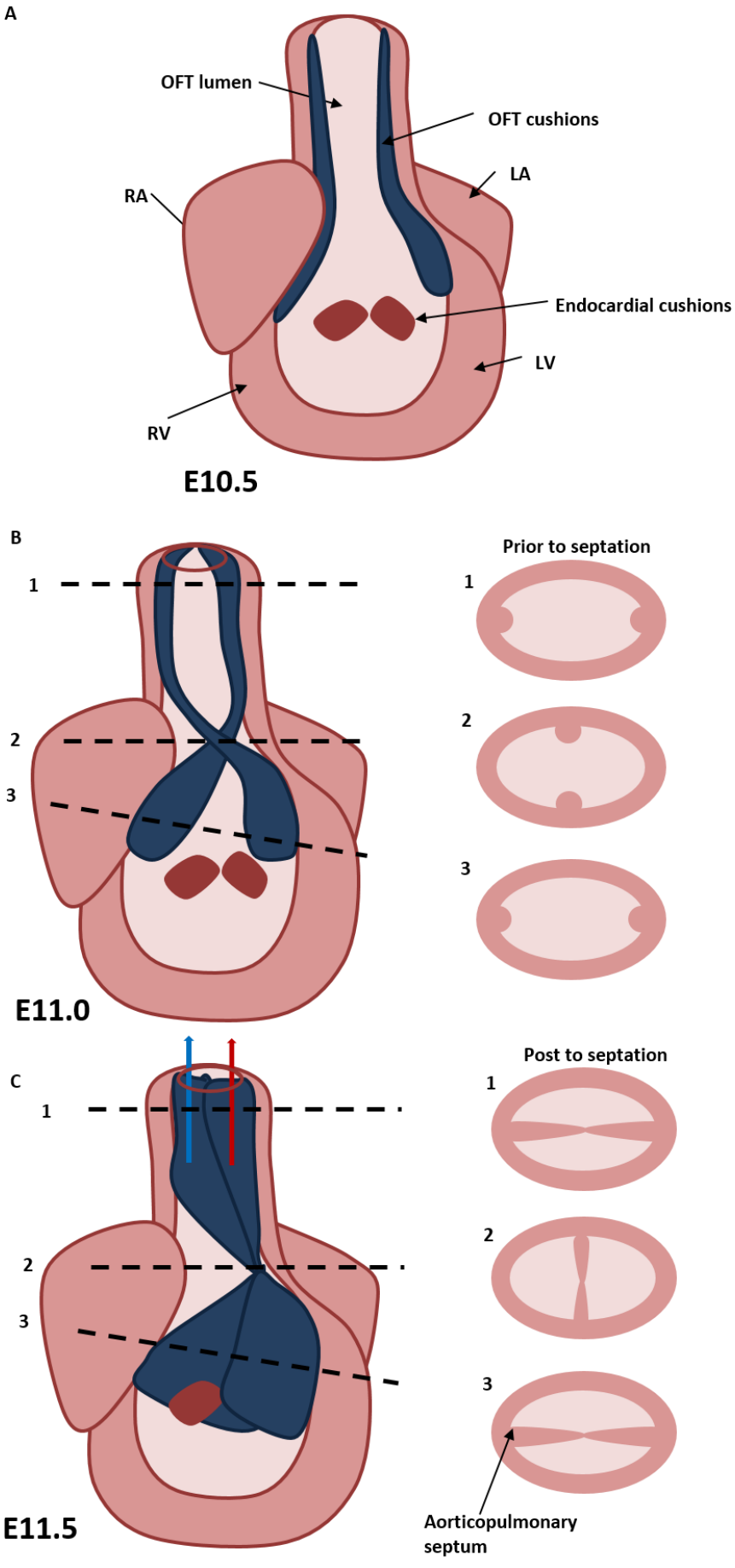
A
OFT lumen
OFT cushions
LA
RA
Endocardial cushions
LV
RV
E10.5
B
Prior to septation
1
2
3
E11.0
C
Post to septation
1
2
3
E11.5
Aorticopulmonary septum

Figure 7: Cardiac OFT Septation.
The OFT is septated into the base of the ascending aorta and the base of the pulmonary trunk. OFT cushions form through infiltration of NCC and proliferation of cells present within the cushions (**A**). The two OFT cushions spiral around each other (**B**) and then fuse with each other, initiating outflow septation and separating the systemic and pulmonary circulations (**C**). Once septation is initiated it proceeds in a distal to proximal direction.

1.4.2.5 Muscularisation of the OFT by myocardialisation

At around E12.5, as the most proximal part of the cushions fuse, cardiomyocytes migrate and invade the flanking mesenchymal OFT cushions, leading to a gradual replacement of mesenchymal tissue with myocardium (Sugishita *et al.*, 2004; Waldo *et al.*, 2005b). This process is known as myocardialisation and leads to muscularisation of the OFT cushions and produces smooth muscular walls at the base of the pulmonary trunk and ascending aorta by E17.5 (van den Hoff *et al.*, 2001; Rana *et al.*, 2007). This process depends on multiple intercellular signalling pathways, including TGF-β, FGF, BMP, VEGF, Notch and non-canonical Wnt signalling (Wagner and Siddiqui, 2007). The fusion of cushions and muscularisation continues and completes the separation between the aorta and the pulmonary trunk (van den Hoff *et al.*, 1999; Kruithof *et al.*, 2003).

1.4.3 Conotruncal congenital heart defects

Genetic or environmental factors affecting initial formation or remodeling of the OFT contribute to the spectrum of conotruncal congenital heart defects seen in humans, accounting for 30% of all congenital heart defects (Srivastava and Olson, 2000; Bruneau, 2008). The most common OFT defects are shown in Figure 8. Tetralogy of Fallot (TOF) includes pulmonary stenosis, overriding aorta (OA), VSD, and right ventricular hypertrophy (Figure 8B). DORV occurs when both of the great arteries, the pulmonary artery and aorta, arise from the RV (Figure 8C). However, DORV represents a spectrum of congenital heart defects that ranges from VSD with 50% of the blood entering the aorta coming from the RV, to complete origin of the aorta from the RV. DORV is always associated with a VSD and can be classified by the location of the VSD; DORV with a committed (underlying) VSD or DORV with a non-committed VSD. A milder form of this CHD is OA where the aorta does not wedge properly

between the AV valves and is positioned above a VSD. More severe defects of the OFT include transposition of the great arteries (TGA) where the aorta and the pulmonary trunk are swapped in position (Figure 8D) and persistent truncus arteriosus (PTA) where the truncus arteriosus fails to separate into the aorta and pulmonary trunk (Figure 8E).

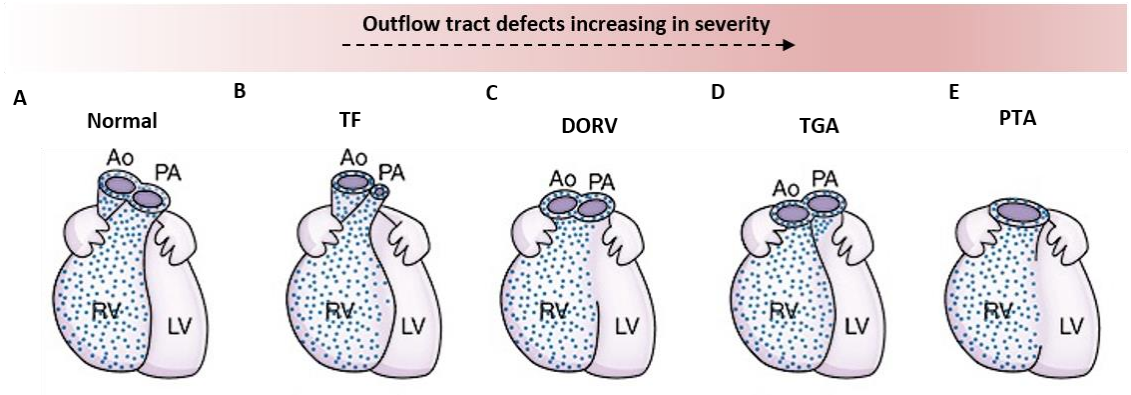

Figure 8: Schematic of conotruncal heart defects.
Tetralogy of Fallot (TOF) includes pulmonary stenosis, overriding aorta, VSD, and right ventricular hypertrophy (**B**). Double outlet right ventricle (DORV) occurs when both of the great arteries, the pulmonary artery and aorta, arise from the right ventricle (**C**). Transposition of the great arteries (TGA) is where the aorta and the pulmonary trunk are swapped in position (**D**). Persistent truncus arteriosus (PTA) is where the truncus arteriosus fails to separate into the aorta and pulmonary trunk (**E**). Adapted from (Neeb *et al.*, 2013).

As discussed above, the cardiac OFT is highly susceptible to malformations. Disruption in either SHF or NCC cell populations contributes to a spectrum of OFT defects in humans and animal developmental models. Abnormalities in SHF progenitors leads to impaired elongation of the OFT, resulting in disruption of OFT rotation and remodelling causing alignment defects, including TGA, DORV and OA (Abu-Issa and Kirby, 2007). Impaired elongation of the OFT can result from a failure of migration or addition of SHF cells to the developing OFT, or from defective arrangement, proliferation and maturation of these cells once they reach the OFT. For example, a combination of premature differentiation and defective cardiomyocyte polarity was shown to lead to defective OFT rotation, causing DORV in *Vangl2*^{SHF} mutants (Ramsbottom *et al.*, 2014). SHF deficiency is linked to OFT rotation defects, whereas abnormalities in NCCs commonly lead to a septation defect such as PTA. NCC deficiency can also

indirectly affect SHF development, resulting in a composite septation and alignment defect (Neeb *et al.*, 2013).

Alignment defects can be caused by an early disruption in either NCC and SHF contributions (Yelbuz *et al.*, 2002), however myocardial and endocardial populations have also been shown to be important during OFT alignment. Failure of rotation of the OFT myocardial wall during OFT remodeling results in alignment defects, including TGA, DORV and OA (Bamforth *et al.*, 2001; Bajolle *et al.*, 2006). For example, in *Pitx2deltac* mutant embryos, PTA and DORV are associated with a myocardial rotation defect (Bajolle *et al.*, 2006). Defects in formation of the OFT septum can also result from later failure of myocardial wall differentiation and anomalies in processes essential for remodeling, such as programmed cell death or myocardialisation. Compaction and rotation of truncal myocardium requires hypoxia driven apoptosis (Watanabe *et al.*, 2001). In *TGF-β(2)*-knockout mice, DORV and overriding tricuspid valve result from disturbances of myocardialisation, endocardial cushion differentiation, and apoptosis (Bartram *et al.*, 2001). Intrinsic defects in OFT endocardial cells have been demonstrated to lead to OFT cushion anomalies (Zhang *et al.*, 2009).

Coordinated proliferation, migration and differentiation of the cell lineages involved is required for correct OFT morphogenesis. Identification of causative genetic mutations and modifiers of conotruncal CHD will provide further insight into the signalling pathways and cellular processes that drive OFT morphogenesis.

1.5 Cardiac septation and septation defects

1.5.1 Atrial and AVC septation

Four mesenchymal tissues are required for atrial and AVC septation: the superior and inferior AV endocardial cushions, the mesenchymal cap (MC), and the dorsal mesenchymal protrusion (DMP) (Webb *et al.*, 1998; Snarr *et al.*, 2008). By E11.5 all components of the AV septal complex are formed (Figure 9). The muscular primary atrial septum (PAS) grows from the atrial roof towards the AVC, with the MC at its leading edge (Figure 9A). The PAS and secondary artial septum (SAS) then fuses to complete the septation of atrial chamber (Figure 9B) (Anderson *et al.*, 2003a).

1.5.2 Ventricular septation

Septation of the ventricle chambers occurs through three continuous processes; formation of the primitive IVS, growth of the IVS and subsequent closure of IVS. The IVS is initially formed from the coalescence of trabeculae branches which requires the absence of Hand2 in the developing IVS to inhibit regular trabeculae formation in this region (Togi *et al.*, 2006) (Figure 9A). Growth and elongation of the IVS follows (Contreras-Ramos *et al.*, 2009), leading to fusion of the IVS with AV cushions, dividing the ventricular chamber into left and right ventricle (Anderson *et al.*, 2003a; Moorman and Christoffels, 2003) (Figure 9B). The IVS also connects with the endocardial cushions to separate the ventricular outlets of the OFT. The septation process is completed by convergence of the OFT, AV and ventricular septa. The RV initially holds the whole OFT, but fusion of the cushions separates the aorta and pulmonary trunk and the septum joins the wall of RV, pushing the aorta to the LV, and leaving the pulmonary trunk exiting from the RV (Waldo *et al.*, 1998).

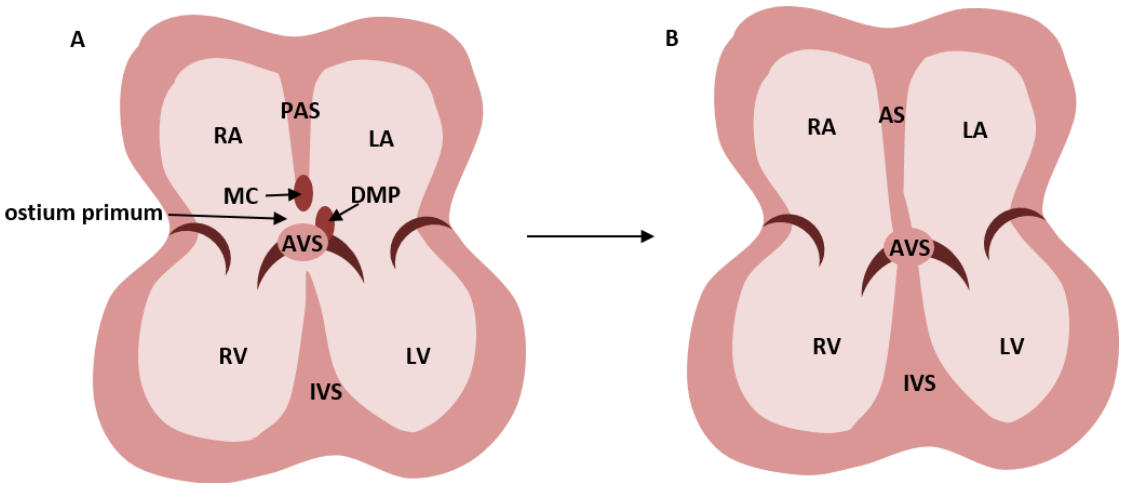

Figure 9: Atrioventricular (AV) septation during cardiac development. Formation of the major cushions between the IVS and AS is essential as all components of the AV septum fuse to them. The muscular PAS grows from the atrial roof towards the AVC, with the MC at its leading edge (**A**). This muscular outgrowth partially septates the atrial chamber and leaves an opening (the ostium primum) between the MC and the AVC (**A**). The MC then merges anteriorly with the AV cushions and posteriorly with the DMP, to seal the ostium primum (**B**). Septation of the ventricle chambers occurs through formation and growth of the IVS (**A**). Subsequent closure of IVS, as it fuses with AV cushions, divides the ventricular chamber into left and right ventricles (**B**). RA; right atria, LA; left atria, RV; right ventricle, LV; left ventricle, IVS; interventricular septum, PAS; primary atrial septum, AS; atrial septum, AVS; atrioventricular septum, MC; mesenchymal cap, DMP; dorsal mesenchymal protrusion.

1.5.3 Septal defects

Abnormal chamber septation results in CHD, including atrial septal defects (ASD), VSD and atrioventricular septal defects (AVSD). These defects cause abnormal cardiac shunting and may lead to congestive heart failure (Brickner *et al.*, 2000). ASD and VSD are a defect in the septum that separates the right and left atria and ventricle, respectively (Figure 10, B and C). The ventricular septum consists of an inferior muscular portion and superior membranous portion. Membranous VSD is more common than muscular VSD, and is the most common CHD in humans (BHF statistics). There are also many subtypes of VSD depending on the position of the septation defect, for example, subaortic or subpulmonary. AVSD occurs when there is an incomplete fusion between the atrial and ventricular septum and can either be complete or partial (Figure 10D). Complete AVSD allows blood to flow between all four chambers through the central opening and contains a single, malformed valve. In a partial AVSD there are usually two valves between the atria and ventricles, however one of the valves (usually the mitral valve) is leaky.

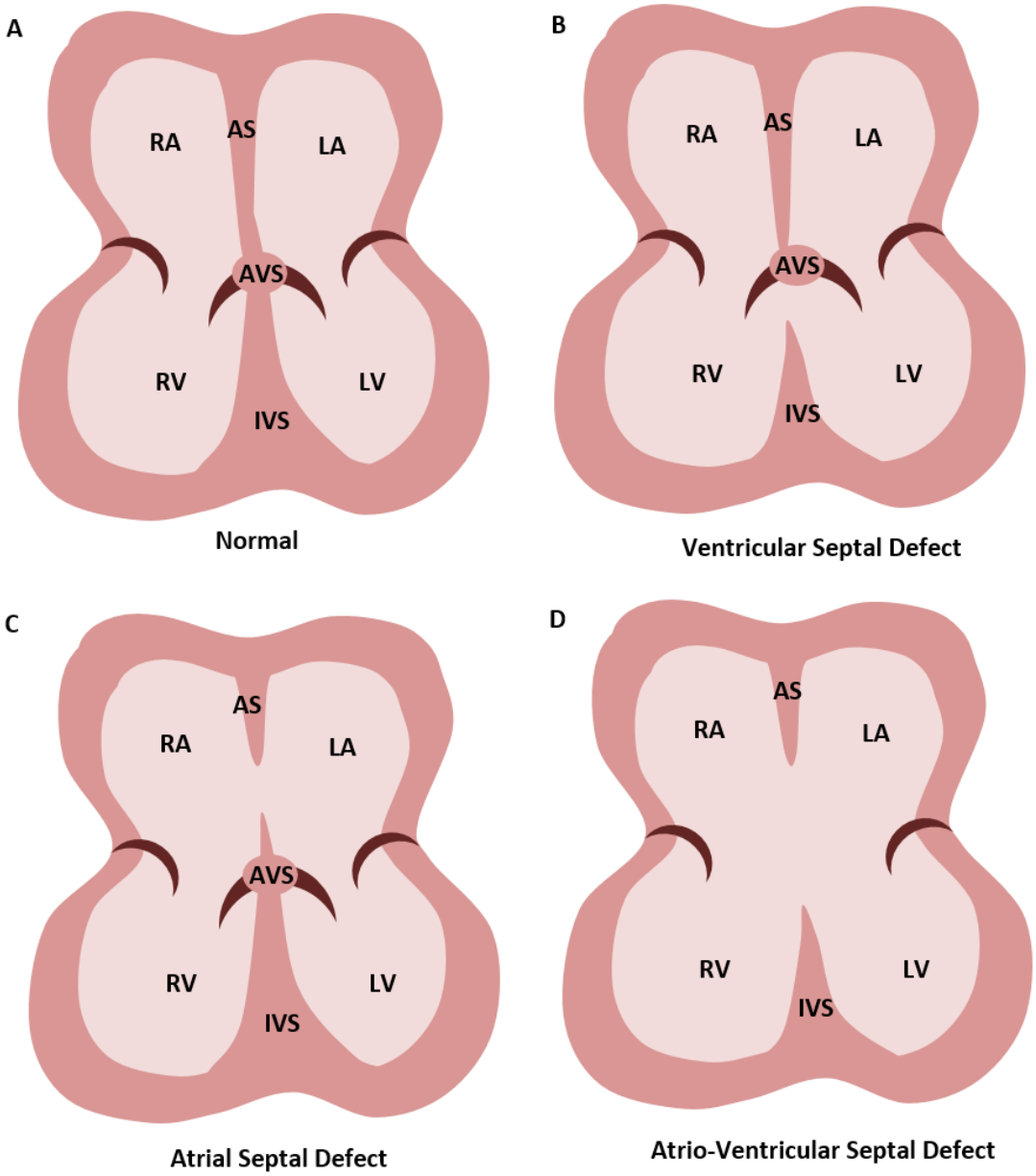

Figure 10: Septal defects.
Perturbations in the processes that lead to chamber septation can result in congenital heart diseases, including ventricular septal defects (VSD) (**B**), atrial septal defects (ASD) (**C**) and atrioventricular septal defects (AVSD) (**D**). ASD and VSD are a defect in the septum that separates the right and left atria and ventricle respectively and AVSD occurs when there is an incomplete fusion between the atrial and ventricular septum. RA; right atria, LA; left atria, RV; right ventricle, LV; left ventricle, IVS; interventricular septum, AS; atrial septum, AVS; atrioventricular septum.

1.6 Ventricular development

1.6.1 Ventricular development overview

The developing ventricle wall consists of three main layers; outer epicardium, myocardium and inner endocardium. The myocardium is separated from the endocardium and epicardium by cardiac jelly, and interstitial fibroblasts, endothelial cells and ECM surround the cardiomyocytes of the myocardium.

Following the formation of the linear heart tube, myocardial cells undergo continued maturation and differentiation to become mature ventricular cardiomyocytes (Sedmera *et al.*, 2000) (Figure 11). A subset of myocardial cells protrude into the ventricular lumen and form trabeculae, beginning at E9.5 (Kruithof *et al.*, 2013). In addition, ventricular myocardial cells proliferate rapidly, resulting in expansion of the compact myocardium (Figure 11C). Trabeculae cardiomyocytes become more differentiated than those in the compact myocardium, with reduced proliferative capacity (Harvey, 2002). Compared to compact layer cardiomyocytes, trabeculae cardiomyocytes are elongated and polarised with increased sarcomeric organization and clear myofibrils (Hirschy *et al.*, 2006; Henderson and Chaudhry, 2011). At later stages in development, it is proposed that the trabeculae cardiomyocytes undergo compaction, from around E12.5, leading to further thickening of the compact layer, although evidence of this is lacking (Captur *et al.*, 2016). Even after birth cardiomyocytes undergo structural changes; elongating into the characteristic rod-shaped structure, with fully aligned myofibrils and fully formed intercalated discs (ICD) restricted to myofibril anchorage (Hirschy *et al*., 2006; Martin-Puig *et al*., 2008) (Figure 12).

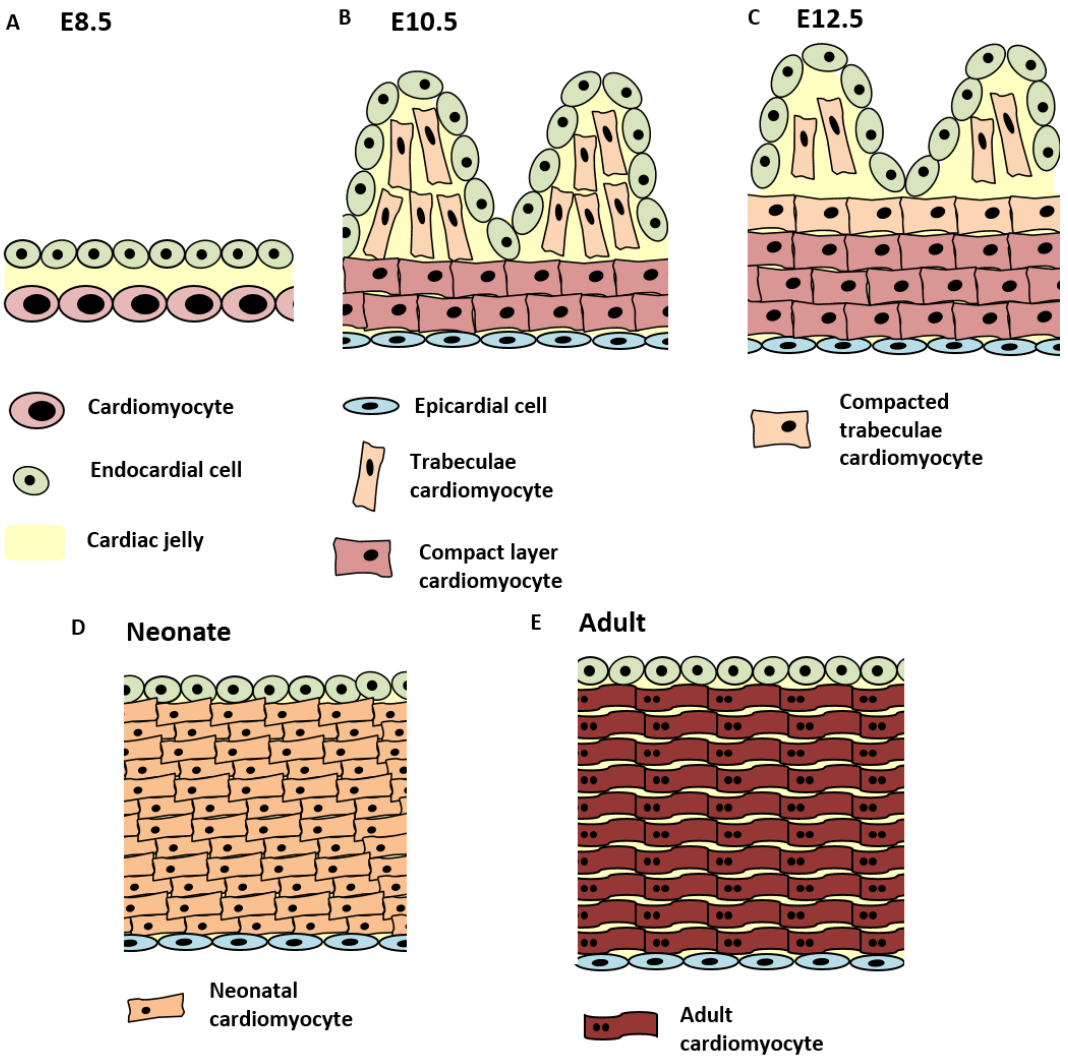

Figure 11: Ventricular cardiomyocyte formation and maturation.
Cardiac progenitors from the FHF and SHF form the linear heart tube (E7.5–8.5), which consists of an outer layer of myocardium (pink cells) and an inner layer of endocardium (green cells) separated by cardiac jelly (yellow) (**A**). The ventricular cardiomyocytes from the myocardial layer proliferate and form the compact zone (pink square-shaped cells) at around E10.5 (**B**). Furthermore epicardial cells from the proepicardium adhere to the myocardial layer and spread over the heart (blue cells) (**B**). Proliferation, differentiation, and migration of the inner layer myocardium leads to trabeculated cardiomyocytes (light orange cells) which protrude into the lumen of the ventricles at E12.5 (**B**). These trabeculated cardiomyocytes have a slower proliferative rate and show more organized sarcomeric structure. At later stages these cells undergo trabecular compaction (**C**) before becoming neonatal cardiomyocytes (**D**). Several weeks after birth the mature ventricular cardiomyocytes acquire the characteristic rod-shaped structure with intercalated discs (red cells) (**E**). Figure adapted from (Martin-Puig *et al.*, 2008).

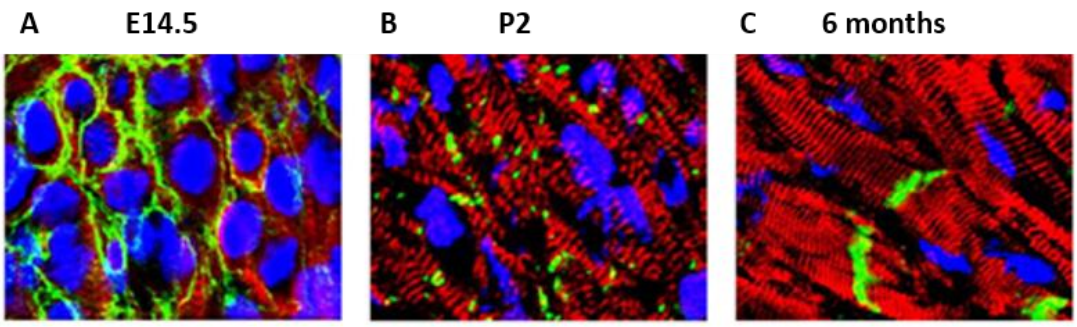

Figure 12: Changes in cardiomyocytes morphology throughout embryonic and postnatal development.
Cryosections are immunostained with anti-VE-cadherin to visualize adherens junctions (AJ) (green), sarcomeric marker titin 9D10 to show myofibrils (red) and DAPI to visualize nuclei (blue). During embryonic development (E14.5) (**A**) the AJ are distributed all around the cell, whereas during postnatal development (P2 - 6 months) (**B-C**) the AJ are restricted to the sites of myofibril anchorage, at the intercalated discs. At P2 and 6 month the cardiomyocytes are also larger and more elongated, and become polarised. Figure from (Hirschy et al., 2006).

1.6.2 Cardiomyocyte structure

Mature cardiomyocytes are characterised by binucleation, highly organised cytoskeletal structure and the appearance of mature ICD as well as high numbers of mitochondria, due to high energy demand. The actin and myosin fibres extend along the length of the cell and ICD are positioned between adjacent cardiomyocytes, to allow the transmission of contraction between cardiomyocytes.

1.6.3 Cardiomyocyte cytoskeleton and adhesion

1.6.3.1 Sarcomeric cytoskeleton

The main components of the sarcomeric cytoskeleton are thin filaments, thick filaments and the Z-discs, and are crucial for cell contractility. One sarcomeric unit consists of intermingling thin and thick filaments, flanked by two Z-discs and repeats of these sarcomeric units form a myofibril (Figure 13A). The thin actin filaments are attached to the Z-discs and extend in the opposite direction from both sides of the Z-disc. Among the actin filaments are thick myosin filaments. The thin actin filaments consist of cardiac actin, α-tropomyosin and C-, I- and T-troponins (Figure 13B). Cardiac actin fibrils are formed from two chains of G-actin monomers. Cardiac actin fibrils twist around each other, forming the double helix, sarcomeric F-actin. Each G-actin monomer has a binding area for

myosin and regulatory proteins, including tropomyosin, are also connected to the actin. There are two tropomyosin polymers per actin filament and these act to stabilise the thin filament, preventing its de-polymerisation (Mudry *et al.*, 2003). Cardiac troponin is a complex of three subunits; Troponin T (TnT), Troponin I (TnI) and Troponin C (TnC). TnT forms a complex with tropomyosin and allows protein kinase C (PKC) to regulate cardiomyocyte function (Sumandea *et al.*, 2003). TnI is a key regulatory protein involved in cardiac muscle contraction and relaxation, and suppresses the actin-myosin interaction (Layland *et al.*, 2005), and TnC binds calcium (Putkey *et al.*, 1989).

The thick filaments consist mainly of myosin and C-, H- and X-myosin binding proteins (Figure 13C). Myosin is a large complex comprised of two myosin heavy chains (MHC) and two pairs of myosin light chains (MLC1 and MLC2). Myosin heavy chains are thin molecules composed of two chains twisted around each other and contain myosin heads on one end of each chain. These myosin heads connect to the MLC and actin (Mornet *et al.*, 1979; Sutoh, 1982), and also contain ATP binding sites (Szilagyi *et al.*, 1979).

The Z-disc structure is highly complex and functions to accumulate the mechanical energy produced by the interaction between myosin and actin and then transfer it to focal adhesions at the cell membrane (Frank *et al.*, 2006). Anti-parallel actin thin filaments of opposing polarity begin from each side of the Z-disc, and are connected and stabilised in the Z-disc, through actin binding protein, α-actinin (Figure 13A) (Sjoblom *et al.*, 2008). In cardiomyocytes, α-actinin is localised in the Z line of cardiac myofibrils, as well as distributed at focal adhesions and along the cell-cell junctions (Yang and Xu, 2012).

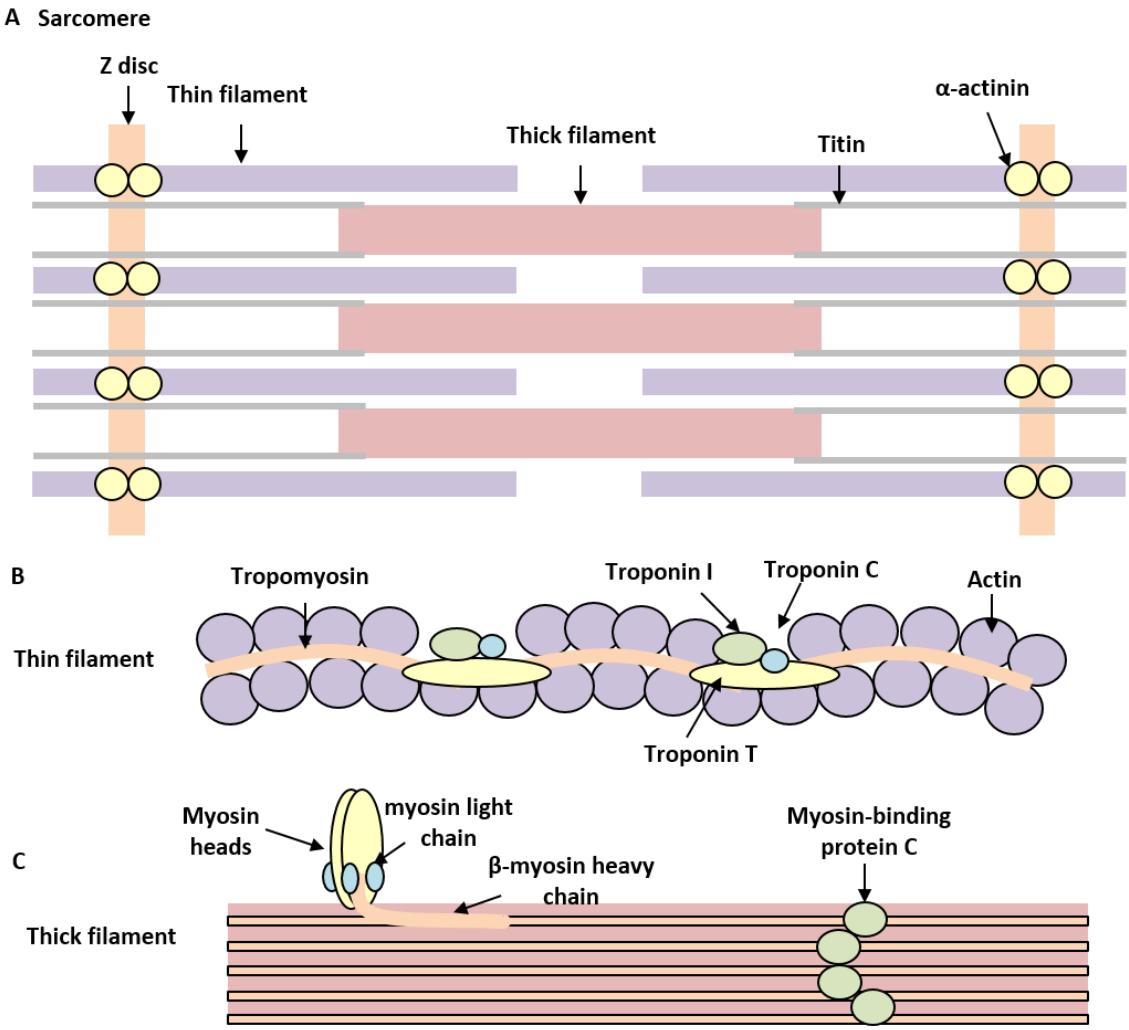

Figure 13: Sarcomere composition.
The main components of the sarcomeric cytoskeleton are thin filaments, thick filaments and the Z-discs. One sarcomeric unit consists of intermingling thin and thick filaments, flanked by two Z-discs and repeats of these sarcomeric units form a myofibril (A). Thin actin filaments are attached to the Z-discs through actin binding protein, α-actinin and extend from both sides of the Z-disc. The thin actin filaments consist of cardiac actin, α-tropomyosin and C-, I- and T-troponins (B). Among the actin filaments there are thick myosin filaments. The thick filaments consist mainly of myosin and myosin-binding protein C (C). Myosin is a large complex comprised of two myosin heavy chains and two pairs of myosin light chains (MLC). Myosin heavy chains contain myosin heads on one end of each chain that connect to the MLC and actin. Myosin binding protein C (MBP-C) plays an important structural and regulatory role between actin and myosin. Adapted from (Gautel and Djinovic-Carugo, 2016).

1.6.3.2 Generic cytoskeleton

The major and best-characterised generic cytoskeletal filaments are intermediate filaments (polymeric filaments composed of intermediate filament

proteins from a family of over 60 members), microfilaments (polymeric filaments of actin) and microtubules (polymers of tubulin dimers).

Desmin is the main protein of the intermediate filaments in cardiac muscle. Desmin intermediate filaments provide structural integrity to the cell and tissues in the form of a three-dimensional (3D) skeleton that covers the entire cytoplasm (Figure 14). Desmin intermediate filaments play an important role in the preservation and unity of the myofibrils, extending from one Z-disc to another and also to the ICD at the cell membrane. The desmin intermediate filaments are also connected to the actin filaments, the nuclear membrane and cell organelles such as microtubules (reviewed in (Lowery *et al.*, 2015)).

In addition to functioning as part of the sarcomeric cytoskeleton, actin microfilaments, consisting of polymeric filaments of actin, are also present in cardiomyocytes. Similar to the desmin, intermediate filaments, the actin microfilaments form a 3D structure connecting the Z-disc, through α-actinin, with the focal adhesions and the ICD, to provide an additional connection between the intracellular and the extracellular environment (Figure 14). Several regulatory proteins are located at the sites of actin microfilament attachment to the costameres, such as α-actinin and Rho GTPases.

Microtubules are tubular structures created by the polymerisation of α- and β-tubulin heterodimers and align along the cell's longitudinal axis (Goldstein and Entman, 1979) (Figure 14). In cardiomyocytes, only 25% of the total tubulin is polymerised in the form of microtubules, while the remaining 75% exists in the form of a non-polymerised protein in the cytoplasm (Palmer *et al.*, 1998; Yamamoto *et al.*, 1998). Microtubules are very dynamic elements with the capacity to de-polymerise and re-polymerise rapidly, therefore they can efficiently transmit chemical and mechanical stimuli within the cell and between cells leading to alterations in cytoskeleton flexibility and contraction capacity (Desai and Mitchison, 1997). Microtubule organising centre (MTOC) are polarised cell organelles and are apically expressed (Magdalena *et al.*, 2003). The two most important types of MTOCs are the basal bodies associated with cilia and the centrosome associated with spindle formation (Figure 14).

1.6.3.3 The sarcolemma

The sarcolemma is the membrane of muscle cells. During embryonic heart development, two specialised regions of the sarcolemma develop; ICD for cell-cell interaction and extracellular matrix (ECM)-integrin-cytoskeletal connections for cell-ECM contacts.

1.6.3.4 ECM-cytoskeleton interactions

Costameres (focal adhesions *in vitro* (Geiger and Bershadsky, 2001)) are lateral cell membrane attachments for many cytoskeleton networks, intercalating communication between the ECM, sarcolemma and the cytoskeleton (Hilenski *et al.*, 1992) (Figure 14) and form as dense focal adhesion plaques at the cell membrane (Terracio *et al.*, 1990). In addition to their structural role in cell attachment to the ECM, costameres transmit mechanical force between the Z-discs of the actin cytoskeleton and the ECM, regulating mechanosignal transduction during cardiomyocyte growth and differentiation (Danowski *et al.*, 1992). The interactions at costameres requires transmembrane cell surface receptors, α- and β- integrins. The extracellular part of integrins interacts with the collagens, laminin and fibronectin of the ECM. The cytoplasmic domain of integrin receptors can directly bind actin-cytoskeleton proteins including talin, vinculin, paxillin, focal adhesion kinase (FAK) and α-actinin. These proteins, in turn, interact with the actin filaments and connect the costameres with the Z-discs (Sharp *et al.*, 1997).

During the establishment of the costameres in early cardiac development, fibroblast-secreted collagens attach to cardiomyocyte cell surface and are consistent with the distribution of β1 integrin receptors at the sarcolemma and also with the formation of de novo premyofibril Z-bands internally (Markwald, 1973; Borg *et al.*, 1983; Tokuyasu, 1989; Carver *et al.*, 1994; Sharp *et al.*, 1997). Additionally, focal adhesions are important during the *de novo* formation of premyofibrils near the cell membrane at the leading edge of migrating cells (Dabiri *et al.*, 1997). Disruption of the costameres results in abnormal myofibril alignment (Shiraishi *et al.*, 1997). These findings suggest that costameres and focal adhesions play an important role in the earliest steps in myofibrillogenesis in myocyte development and in cell migration.

1.6.3.5 Cell-Cell adhesion

Cardiomyocytes are attached to each other through ICD. The ICD is exclusive to cardiomyocytes and functions to connect adjacent cells to enable the transmission of cell contraction and allow communication between cells. The ICD consists of different types of adhering cellular junctions including desmosomes, adhesions junctions (AJ) and gap junctions (Figure 14). Desmosomes and AJ allow transmission of mechanical signals, whereas gap junctions allow the passage of electrical signals. All three types of junctions are restricted to the ICD postnatally, however, desmosomes and AJ show polarised expression more rapidly than gap junctions (Angst *et al.,* 1997; Hirschy *et al*., 2006).

The desmosomes bind intermediate filaments and join cardiomyocytes together to prevent detachment of cells during normal contraction (Figure 14). The desmosomes are formed by desmoglein-2 and desmocollin-2 transmembrane proteins, which establish a transcellular connection (reviewed in (Harmon and Green, 2013; Patel and Green, 2014).

The AJ are attachment points for sarcomere actin filaments at cell-cell contacts and thus transmit contraction between neighbouring cardiomyocytes (Zuppinger *et al.*, 2000) (Figure 14). The main proteins of the AJ comprise of transmembrane proteins including E- and N-cadherin and β1D integrin and cytoplasmic proteins including α-, β-, γ- (plakoglobin) and p120-catenins, vinculin, metavinculin, and a GTPase activating protein (GAP family protein) (Tepass *et al.*, 2000). In the AJ, cadherins recruit β-catenin molecules onto their intracellular regions. β-catenin then associates with another catenin protein, α-catenin which directly binds to the actin filaments, through α-actinin. The cadherin/β-catenin/α-catenin complex is weakly associated to actin filaments, therefore is a dynamic, link to the actin cytoskeleton (Itoh *et al.*, 1997; Muller *et al.*, 2005).

The gap junctions are key structures for ion transportation between adjacent cardiomyocytes as well as non-muscle cells of the myocardium (Severs *et al.*, 2001) (Figure 14). Gap junctions are formed by six connexin molecules in the cell membrane. There are many types of connexins (Cx). In the ventricle myocardium, Cx-43 dominates and is essential for cell-cell coupling and normal cardiac function (Kolcz *et al.*, 2002; Heinzel *et al.*, 2005; Boengler *et al.*, 2006;

Boengler *et al.*, 2007), while Cx-40 and Cx-45 are associated with the cardiac conduction system (Severs *et al.*, 2001).

An additional cell junction in cardiomyocytes is the tight junction (TJ) (Hartsock and Nelson, 2008). TJ bind cells together and maintain the organisation of the plasma membrane of epithelial cells in an apical and a basolateral compartment (Figure 14). TJ are comprised of occudin and claudin membrane proteins (Furuse *et al.*, 1998). Additional proteins, zona occludens (ZO), links claudins to the actin cytoskeleton, as well as recruiting signalling components, like atypical PKC (Itoh *et al.*, 1999; Muller *et al.*, 2005).

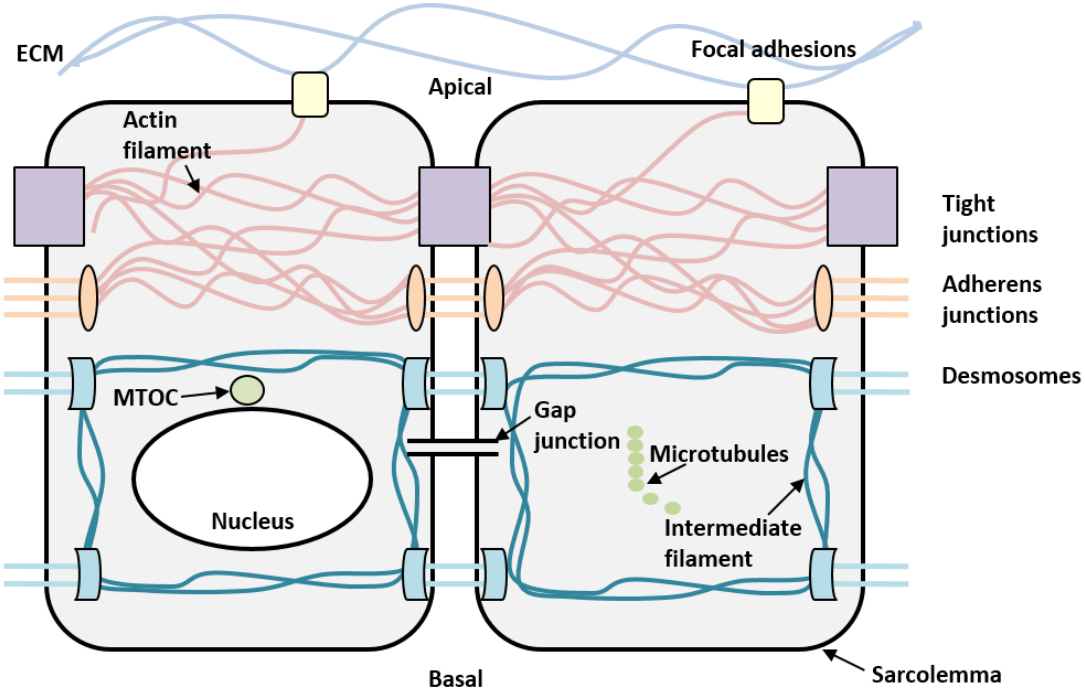

Figure 14: Cardiomyocyte cell-cell and cell-ECM junctions.
The major cytoskeletal filaments are intermediate filaments (polymeric filaments composed of intermediate filament proteins) (blue lines), microfilaments (polymeric filaments of actin) (pink lines) and microtubules (polymers of tubulin dimers) (green circles). During embryonic heart development, specialised regions of the sarcolemma develop. Intercalated discs (ICD) for cell-cell interaction, consisting of different types of adhering cellular junctions including desmosomes (blue), adhesions junctions (orange) and gap junctions (black). ECM-integrin-cytoskeletal connections (focal adhesions) (yellow) allow cell-ECM interaction. Tight junctions (purple) bind cells together and maintain the organisation of the plasma membrane in an apical and a basolateral compartment.

1.6.3.6 Alterations in cytoskeletal, ICD or FA components cause cardiac abnormalities

Studies investigating cytoskeletal and adhesion components in mice have suggested an important role of both the cytoskeleton, ICD and focal adhesion structures during cardiac development. For example, mice lacking *α-tropomyosin-1*, a regulatory protein of the actin thin filaments, are embryonic lethal at E9.5 with severe cardiac defects (McKeown *et al.*, 2014). The hearts of these mice were enlarged, misshapen and non-beating, with a thinned myocardium and fewer trabeculae. (McKeown *et al.*, 2014). *Desmin* knockout mice show evidence of haemorrhage and have fibrotic, ischemic hearts with defective mitochondria composition and function (Li *et al.*, 1996; Linden *et al.*, 2001). An alternative study found that *Desmin* null mice display cardiomyocyte cell death and abnormal cardiomyocyte ICD, sarcolemma and myofibrils (Thornell *et al.*, 1997). A more recent study showed that *Desmin* null mice develop cardiomyocyte hypertrophy and dilated cardiomyopathy with cardiomyocyte cell death, calcific fibrosis and multiple ultrastructural defects (Weisleder *et al.*, 2004). Additionally, mutations in *DESMIN* have been identified in patients with Desmin-related cardiomyopathy (Goldfarb *et al.*, 1998). *Cx-43* null mice die at birth (Zhao *et al.*, 2005) and display delayed OFT myocardialisation, as well as delayed α-smooth muscle actin (α-SMA) expression in the proximal OFT septum (Qi *et al.*, 2011).

1.6.4 Cardiomyocyte cell cycle

During embryonic development, cardiomyocytes proliferate rapidly and the rates of karyokinesis and cytokinesis are equal. Embryonic cardiomyocyte proliferation peaks at a rate of around 30% at E12.5 in the developing ventricles. The overall rate of cardiomyocyte proliferation gradually declines during later stages of embryogenesis. Following birth, cardiomyocytes lose the ability to proliferate and withdraw from the cell cycle. There is a final round of karyokinesis without the accompanied cytokinesis, resulting in binucleated cardiomyocytes. The initiation of binucleation is associated with downregulation of positive cell cycle regulators such as cyclins and cyclin dependent kinases (Cdk), as well as an increase in negative cell cycle regulators such as Cdk inhibitors p21 and p27 (Soonpaa *et al.*, 1996). Cell death in the developing

heart is rare and has been shown to be restricted to specific areas in the chick, with very low occurrence in the ventricular myocardium (van den Hoff *et al.*, 2000; Cheng *et al.*, 2002).

During early cardiac development, cardiomyocyte cell cycle activity is closely associated with cardiac differentiation and morphogenesis. The onset of cardiomyocyte differentiation during the formation of early linear heart tube is accompanied by a transient reduction in proliferation. This reduced proliferation rate recovers by E11 and contributes to the ballooning of ventricular chambers from the linear heart tube (Meilhac *et al.*, 2003).

1.6.5 Myocardial morphogenesis

The early vertebrate embryonic heart is a two layered, linear heart tube with a luminal endocardial layer and an immature myocardial layer. Maturation of the linear heart tube involves myocardial thickening, trabeculation and establishment of the coronary vasculature and cardiac conduction system, with the contribution of the epicardial layer.

The growth of the myocardium can be divided into two overlapping and parallel processes; trabeculation and expansive growth of the compact myocardial wall.

During expansive growth, the compact layer undergoes extensive proliferation and thickening. This is concurrent with the formation of the coronary vasculature and maturation of the cardiac conduction system. Compact myocardial cells remain immature and highly proliferative. Endocardial and epicardial cells invade the developing compact myocardium and differentiate into coronary endothelial cells, SMCs and fibroblasts to form the coronary vasculature. Factors regulating compact myocardial growth include FGFs, Wnts, and retinoic acid (Merki *et al.*, 2005).

Trabeculation occurs after cardiac looping and results in a network of luminal projections of myocardial cells covered by the endocardial layer. The early function of trabeculae is to allow for efficient myocardial oxygen and nutrient exchange and greater contractile function in the absence of coronary circulation (Sedmera *et al.*, 2000). Several models of trabeculation have been described, detailing trabeculae initiation, growth and remodelling.

The first stage in trabeculation is the emergence of trabeculae; after the formation of the linear heart tube, myocardial protrusions begin to appear

extending into the lumen, beginning on the outer curvature of the ventricle. The cellular and molecular mechanisms of how initial trabeculae are formed are still unclear; proposed mechanisms include buckling of myocardial wall (Figure 15, 1), invagination of cardiomyocytes into the lumen (Figure 15, 2) (Liu *et al.*, 2010; Peshkovsky *et al.*, 2011) and evagination of the endocardium (Figure 15, 3).

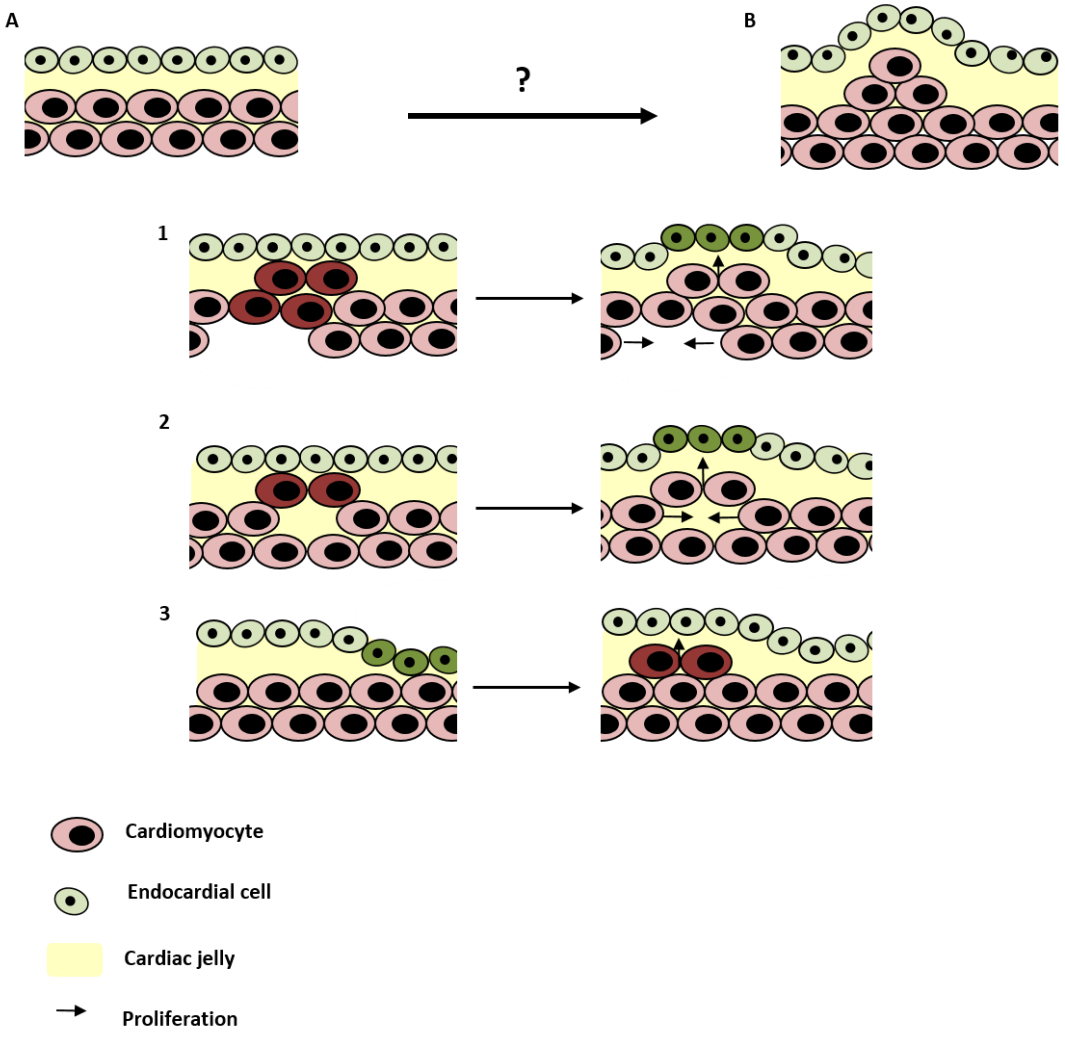

Figure 15: Three proposed mechanisms for initiation of trabeculation.
(**1**) Buckling of myocardial wall where the myocardial cells fold in towards the lumen (dark pink) which leads to movement of the endocardial cells into the lumen (dark green). (**2**) Invagination of cardiomyocytes into the lumen, where some of the cardiomyocytes move into the lumen and again leads to movement of endocardial cells into the lumen. (**3**) Evagination of the endocardium where movement of endocardial cells leads to subsequent movement of cardiomyocytes in adjacent areas.

In zebrafish, a 2-step process of trabeculation has been proposed; firstly, cardiomyocytes extend protrusions that invade luminally along neighbouring

cell-cell junctions. These protrusions can interact within the trabeculae layer to form new cell-cell contacts. Secondly, cardiomyocytes constrict their abluminal surface, moving their cell bodies into the trabeculae layer whilst extending more protrusions (Staudt *et al.*, 2014). Clonal analysis in zebrafish showed that trabeculae cardiomyocytes are clonally unrelated to adjoining compact cardiomyocytes, suggesting they delaminate from the compact myocardium and attach at a second site in the ventricle. Additionally the trabeculae are clonally mixed, meaning they do not arise solely from a single cardiomyocyte (Gupta and Poss, 2012). Trabeculation in mice has been less well defined. Trabeculation initiates after cardiac looping at E9.0 and proliferation of a single myocyte in the tubular heart is thought it give rise to early trabeculae protrusions (Staudt *et al.*, 2014).

The second step in trabeculation is the growth of trabeculae; trabecular projections propagate radially to form a network and increase in length (Sedmera *et al.*, 2000; Peshkovsky *et al.*, 2011) (Figure 11B). However, the mechanisms which control the directionality of the trabeculae growths have not been well defined. Genes that are currently thought to be involved in the trabeculation process are *Notch*, *Wnt*, *VEGF* and *Semaphorin* genes (Toyofuku *et al*., 2004b; Grego-Bessa *et al*., 2007; Nagy *et al*., 2010; Wu *et al*., 2012). Proliferation is approximately 2-fold greater in cardiomyocytes of the compact myocardium, as compared with those in the inner trabeculae (Harvey, 2002). The trabeculae cardiomyocytes increase in maturity and decrease in proliferative capacity as the distance increases from the compact myocardium, creating a gradient from base to tip (Pasumarthi and Field, 2002; Buikema *et al.*, 2013; Samsa *et al.*, 2013).

The last step in trabeculation is remodelling of the trabecular network. Trabeculae are suggested to compact or collapse at the base to become incorporated into the compact myocardial layer (Figure 11C). Some endocardial cells surrounding trabeculae are proposed to become incorporated into the compact myocardium as the trabeculae compact which then contribute to the endothelial layer of coronary capillaries and vessels (Wu *et al.*, 2012; D'Amato *et al.*, 2016). However, the efficiency and specificity of various *Cre* lines makes interpretation of this data particularly difficult and subjective leading to contradictory evidence (Zhang *et al.*, 2016).

Some trabeculae protrusions within the ventricle free wall are remodelled to become part of papillary muscle, IVS and cardiac conduction system. In mice, this late phase of trabeculation occurs post E13.5, when Notch2 expression and BMP10 expression ceases in the compact myocardium and trabeculae myocardium respectively. During this phase, coronary vasculature is established and there is a switch from dependence on trabeculae to coronary circulation for oxygenation of the myocardium (Captur *et al.*, 2015).

Defective formation and/or remodelling of the trabeculae leads to cardiac abnormalities in mice. Failure of trabeculae formation results in a hypoplastic myocardial wall and embryonic lethality due to heart failure, for example *Notch1* mutant embryos die between E9.5 and E10.5 with impaired ventricular trabeculation (Grego-Bessa *et al.*, 2007). Conversely, the excessive trabeculation or abnormal/absent remodelling typically causes a hypertrabeculated, non-compaction phenotype which can cause embryonic lethality or can lead to cardiomyopathy in adulthood (Oechslin and Jenni, 2011). Excessive trabeculation is associated with dilated cardiomyopathy, CHD and left ventricular non-compaction (LVNC) in patients.

Trabeculae form as a result of interaction between the primitive myocardium and endocardium. Various signalling pathways have been identified as being crucial for the formation and/or remodelling of ventricular trabeculae including Notch, Wnt, Semaphorin and VEGF signalling (Toyofuku *et al*., 2004b; Grego-Bessa *et al*., 2007; Nagy *et al*., 2010; Wu *et al*., 2012).

1.6.6 Signal pathways regulating myocardial proliferation and trabeculation

1.6.6.1 Notch signalling

Notch signalling is an evolutionary conserved signalling pathway which allows for communication between cells and can determine cell fate, as well as being able to initiate cell proliferation and apoptosis (Kopan and Goate, 2002) (Figure 16). The Notch pathway is one of the main signalling pathways between the endocardium and myocardium known to regulate the development of the ventricular wall (Grego-Bessa *et al.*, 2007).

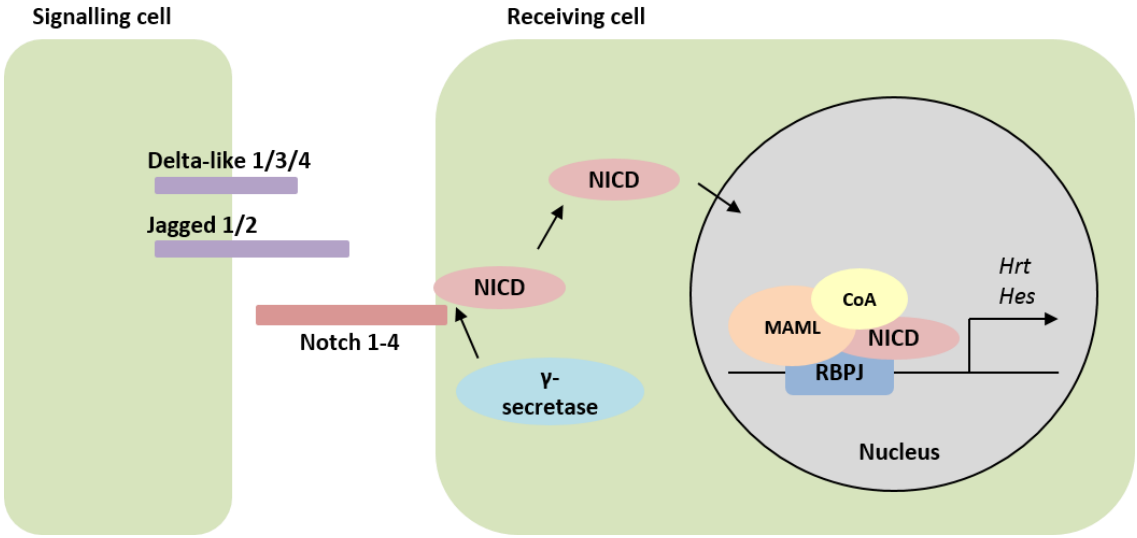

Figure 16: Notch signalling.
Notch receptors (1-4) have a large extracellular domain and an intracellular domain. The extracellular domain of the Notch receptor interacts with delta like and jagged ligands. Proteolytic cleavage of the receptor by gamma-secretase results in nuclear translocation of the Notch intracellular domain (N1ICD). N1ICD interacts with the transcriptional repressor, recombining binding protein suppressor of hairless (RBP-Jk), leading to the transcription/repression of Notch target genes such as Hes and Hey. Figure adapted from (High and Epstein, 2008).

In humans, mutations in Notch receptor and ligand genes can cause congenital heart defects and LVNC, and have also been associated with adult CVD. (Li *et al.*, 1997; Oda *et al.*, 1997; Krantz *et al.*, 1999; Eldadah *et al.*, 2001; Garg *et al.*, 2005; McDaniell *et al.*, 2006; Luxan *et al.*, 2013). Notch gene and protein expression within the developing myocardium has been extensively investigated in mouse and zebrafish models, and is summarised in (Figure 17). In mice, Notch1 and N1ICD expression is restricted to the endocardium by E8.0, with highest expression at the base of the developing trabeculae (Williams *et al.*, 1995). Notch2 protein is highly expressed in the myocardium and absent from the endocardium (McCright *et al.*, 2001). Notch ligands, Jagged and delta like, are differentially expressed. Jagged1 is expressed in the myocardium from midgestation (Loomes *et al.*, 2002), whereas delta like ligands, Dll1 and Dll4, are restricted to endocardial cells, with highest expression at the base of the trabeculae, similar to N1ICD (Del Monte *et al.*, 2007) (Figure 17).

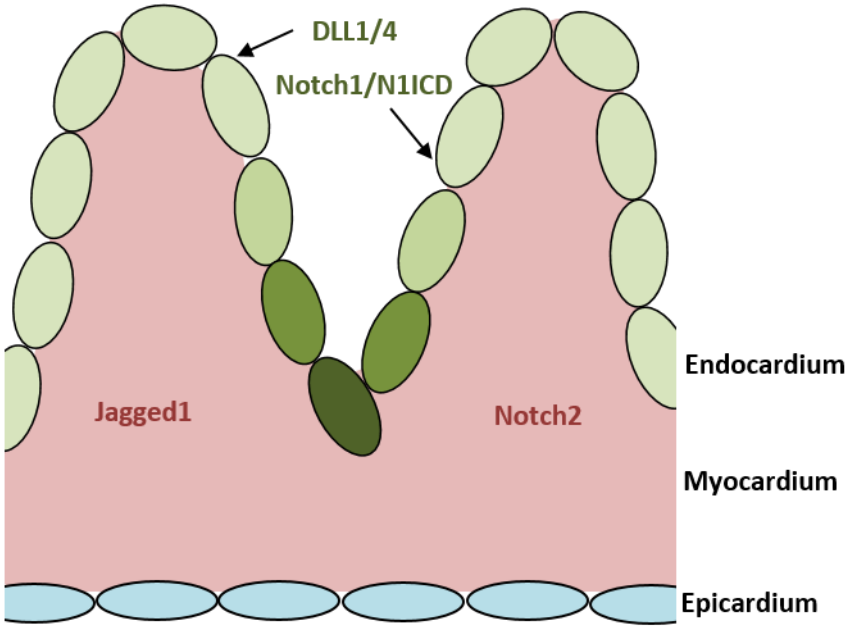

Figure 17: Notch receptor and ligand expression in the developing myocardium.
Notch1 and activated Notch1 (N1ICD) expression is restricted to the endocardium by E8.0, with highest expression at the base of the developing trabeculae. Notch2 protein is highly expressed in the myocardium and absent from the endocardium. Notch4 is expressed in the endocardium. Notch ligand, Jagged1 is expressed in the myocardium from midgestation, whereas delta like ligands, DLL1 and DLL4, are restricted to endocardial cells, with highest expression at the base of the trabeculae, similar to N1ICD.

Gene inactivation studies in mice have allowed investigation of Notch signalling during ventricular development. Notch receptors 1 and 2 are crucial for trabeculation and myocardial development (McCright *et al.*, 2001; Watanabe *et al.*, 2006; Grego-Bessa *et al.*, 2007). Global or endothelial deletion of *Notch1* results in defective trabeculation, impaired compact myocyte and trabeculae markers, and reduced cardiomyocyte proliferation (Grego-Bessa *et al.*, 2007) (Figure 18). Deletion studies of Notch ligands, *jagged* and *delta-like*, and modifier *Mib1* confirm the role of Notch signalling in myocardial development (Xue *et al.*, 1999; McCright *et al.*, 2002; Luxan *et al.*, 2013). Since a similar phenotype is observed after alteration of Notch ligands receptors in the endocardium and Notch ligands or modifiers in the myocardium, this suggests myocardial-endocardial Notch signalling is critical for normal myocardial development (Luxan *et al.*, 2013). Poor trabeculae formation in either global or endothelial *Notch1* mutants was attributable to both proliferation and differentiation defects (Grego-Bessa *et al.*, 2007) (Figure 18).

A recent paper decribes sequential Notch 1 receptor activation in the endocardium (D'Amato *et al.*, 2016). Initial signalling from endocardially expressed delta like-4 to endocardial Notch1 is involved in cardiomyocyte proliferation and differentiation, resulting in trabeculation at E9.5. Later in development, Jagged1/2 signalling from the myocardium to Notch1 in the endocardium is involved in myocardial patterning, maturation and compaction at E11.5. This sequential Notch 1 receptor activation was found to be determined by Manic fringe expression (D'Amato *et al.*, 2016).

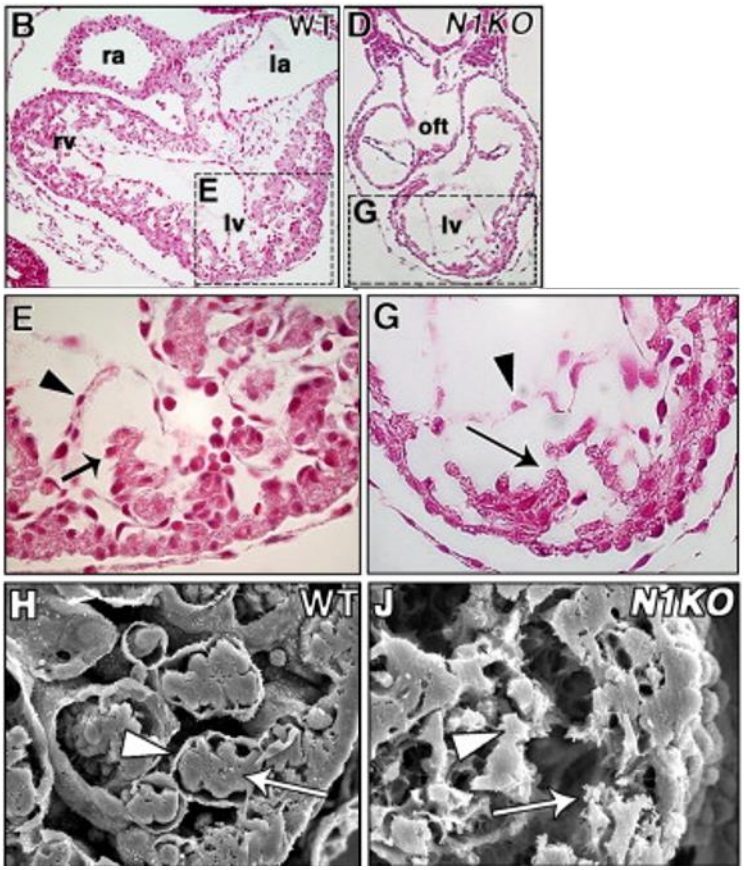

Figure 18: Defective Trabeculation in E9.5 *Notch1* Mutants.
H+E-stained transverse sections of representative wt (**B**) and *Notch1* (*N1KO*)(**D**) mutants, details of left ventricle (**E** and **G**). SEM photomicrographs of wt (**H**) and *Notch1* (J) in left ventricle. In wt, note developing trabeculae with myocardium (**E**, **H**, arrows) and endocardium (arrowheads). *Notch1* embryos show collapsed endocardium (arrowheads in **J**), disorganized myocardium (arrows in **J**) and poorly developed trabeculae. Arrowheads indicate endocardium. la, left atrium; oft, outflow tract; ra, right atrium; lv, left ventricle and rv, right ventricle. Figure taken from (Grego-Bessa *et al.*, 2007).

Hey genes, *Hey1* and *Hey2*, are downstream effectors of the Notch pathway and are known to be expressed during embryonic heart development. *Hey2* is

expressed in the ventricle compact myocardium, IVS and endocardial cells of the AV cushions at E10.5 (Leimeister *et al.*, 1999; Nakagawa *et al.*, 1999; Kokubo *et al.*, 2005a) and is crucial for normal cardiac development. Cardiac abnormalities in *Hey2* deficient embryos include perimembranous VSD, and ASD, (TOF), thin myocardium and abnormal trabeculae (Kokubo *et al.*, 2004). Increased expression of atrial markers in the LV were also observed (ANF, Tbx5, Mlc1a, Mlc2a) in *Hey2* mutants, suggesting that Hey2 acts to maintain compact ventricular phenotype and suppresses atrial phenotype (Xin *et al.*, 2007). Knockout studies have shown that *Hey1* is dispensable for heart development (Fischer *et al.*, 2004).

Two parallel Notch-dependent cardiac developmental processes have been described during trabeculation, contributing to cardiomyocyte proliferation and trabeculation, independently. The first is the differentiation of primitive myocardial cells into trabeculae and compact myocardium, which is mediated by ephrinB2-neuregulin (Nrg) signalling in the endocardium. EphrinB2/EphB4 is a ligand-receptor pair that is expressed in the ventricular endocardium. Endocardial ephrinB2/EphB4 expression and activity is impaired in *Notch* mutants (Grego-Bessa *et al.*, 2007). *EphrinB2* is a direct transcriptional target of N1ICD/RBPJk and is upstream of *Nrg-1*. Deficiency in either *EphrinB2* or *EphB4* is embryonic lethal and hearts show defective trabeculae formation (Wang *et al.*, 1998; Gerety *et al.*, 1999). Nrg-1 is expressed in endocardial cells and signals to ErbB2/4 receptors in the myocardium to initiate trabeculation of the ventricular wall (Gassmann *et al.*, 1995; Lee *et al.*, 1995; Meyer and Birchmeier, 1995; Hertig *et al.*, 1999). *Nrg-1*, *ErbB2* and *ErbB4* deficiency all result in embryonic lethality and defects in trabeculae development; mutants display a hypoplastic wall and abnormal trabeculae (Zhang *et al.*, 2013). Cardiomyocyte proliferation is unaffected in *Nrg-1* and *ErbB2/4* mutants, but cardiomyocyte differentiation is impaired. Nrg-1 and ErbB2 have been shown to have a role in directional delamination of cardiomyocytes to initiate ventricular trabeculation (Lai *et al.*, 2010; Liu *et al.*, 2010). In zebrafish, ErbB2 is involved in the formation of myocardial protrusions (Zhao *et al.*, 1998; Liu *et al.*, 2010; Staudt *et al.*, 2014; Wang and Huang, 2014; Rupert and Coulombe, 2015).

The second is maintenance of BMP-dependent proliferation of trabeculae cardiomyocytes. Impaired proliferation marker BMP10 and differentiation

marker Nrg-1 expression was observed in Notch mutants (Grego-Bessa *et al.*, 2007). *BMP10* is expressed transiently in mouse developing trabecular myocardium from E9.0-E13.5. Later in mouse embryonic development, at E16.5-E17.5, *BMP10* is only expressed in the atria. Notch signalling in the endocardium acts to conserve *BMP10* expression in trabeculae cardiomyocytes to maintain proliferation. Target genes of Notch and BMP10 in the myocardium include *Tbx20*, *Hey2* and *p57kip2* (Zhang *et al.*, 2011). BMP10 activates BMP signalling via smad phosphorylation and maintains trabeculae cardiomyocyte proliferation via p57kip2 (Pashmforoush *et al.*, 2004). BMP10 is upregulated in several mutant mice that display trabeculation abnormalities, such as *FKBP12*, *Nkx2.5* and *numb* mutants (Shou *et al.*, 1998; Pashmforoush *et al.*, 2004; Yang *et al.*, 2012). *Bmp10* deficient mice have reduced cardiomyocyte proliferation at E9-E9.5 leading to poor cardiac function and are dead by E10.5. At E9.5-E10.5 the hearts were growth retarded, had hypoplastic walls and failed to develop normal trabeculae. Endocardial cushions were acellular cushions suggesting defective myocardialisation (Chen *et al.*, 2004; Grego-Bessa *et al.*, 2007). Induced *BMP10* expression was able to rescue the proliferation defect and similarly, induced *Nrg1* rescued the differentiation defect in these Notch mutants. These results indicate that BMP10 and Nrg1 independently act downstream of Notch signalling to regulate cardiomyocyte proliferation and cardiomyocyte differentiation, respectively (Grego-Bessa *et al.*, 2007) (Figure 19).

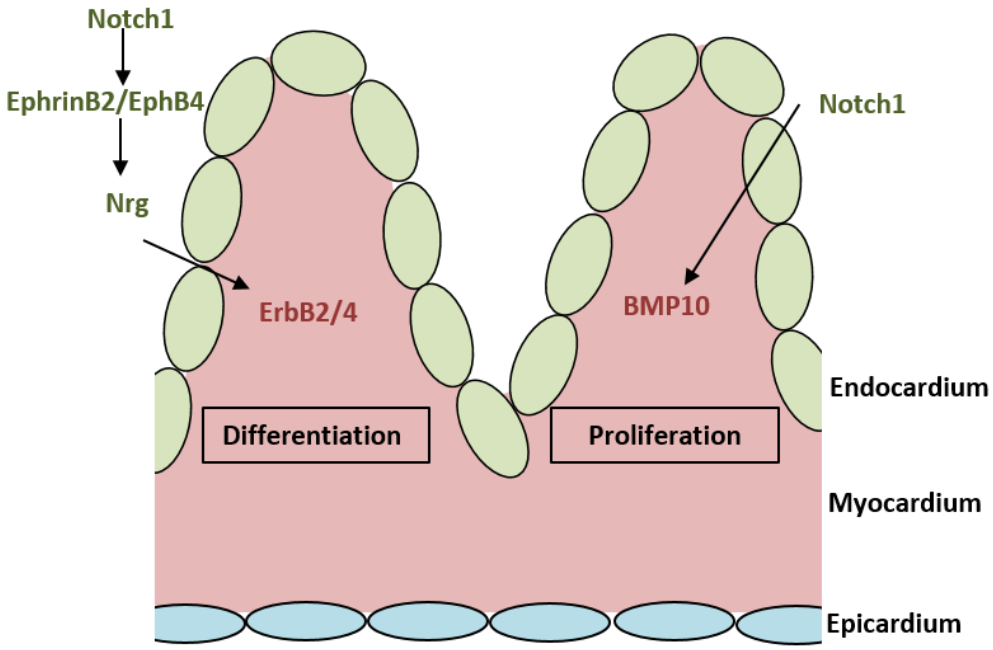

Figure 19: Endocardial-myocardial Notch signalling.
Two parallel Notch-dependent cardiac developmental processes during trabeculation. The first is the differentiation of primitive myocardial cells into trabeculae and compact myocardium, which is mediated by ephrinB2-neuregulin signalling in the endocardium. The second is maintenance of BMP-dependent proliferation of trabeculae cardiomyocytes. BMP10 and Nrg1 independently act downstream of Notch signalling to regulate cardiomyocyte proliferation and cardiomyocyte differentiation, respectively.

1.6.6.2 Non-canonical Wnt signalling (Wnt – PCP signalling)

Non-canonical Wnt signalling is important for normal myocardial development. Wnt signalling plays an important role in several cellular processes, such as cell fate specification, migration and proliferation and differentiation (Nusse, 2008). Cardiomyocytes are not an epithelial cell, however adult cardiomyocytes are highly polarised, with cell-cell junctions localised at ICD with attachment to ECM on the lateral surface, and therefore non-canonical Wnt signalling may play a role in cardiomyocyte polarisation.

Planar cell polarity (PCP) signalling is an essential mechanism by which cells establish apical-basal axis polarity. PCP is a key feature of epithelial cells. The main PCP components were defined in drosophila using genetic mutagenesis and clonal analysis. Core signalling components include Frizzled (Fz), Dishevelled (Dvl), Prickle (Pk), Vangl and Celsr1. In addition, there are a large number of PCP effectors such as Daam1, RhoA and Rac1. Activation of Wnt/PCP signalling by binding of Wnt ligands, Wnt5a and Wnt11, to Fz

receptors at the cell membrane causes Dvl to bind Daam1, which increases its affinity for downstream effectors, Rac1 and RhoA, and promotes polymerization of actin and regulates gene expression (Figure 20) (Habas *et al.*, 2001; Liu *et al.*, 2008; Young and Copeland, 2010).

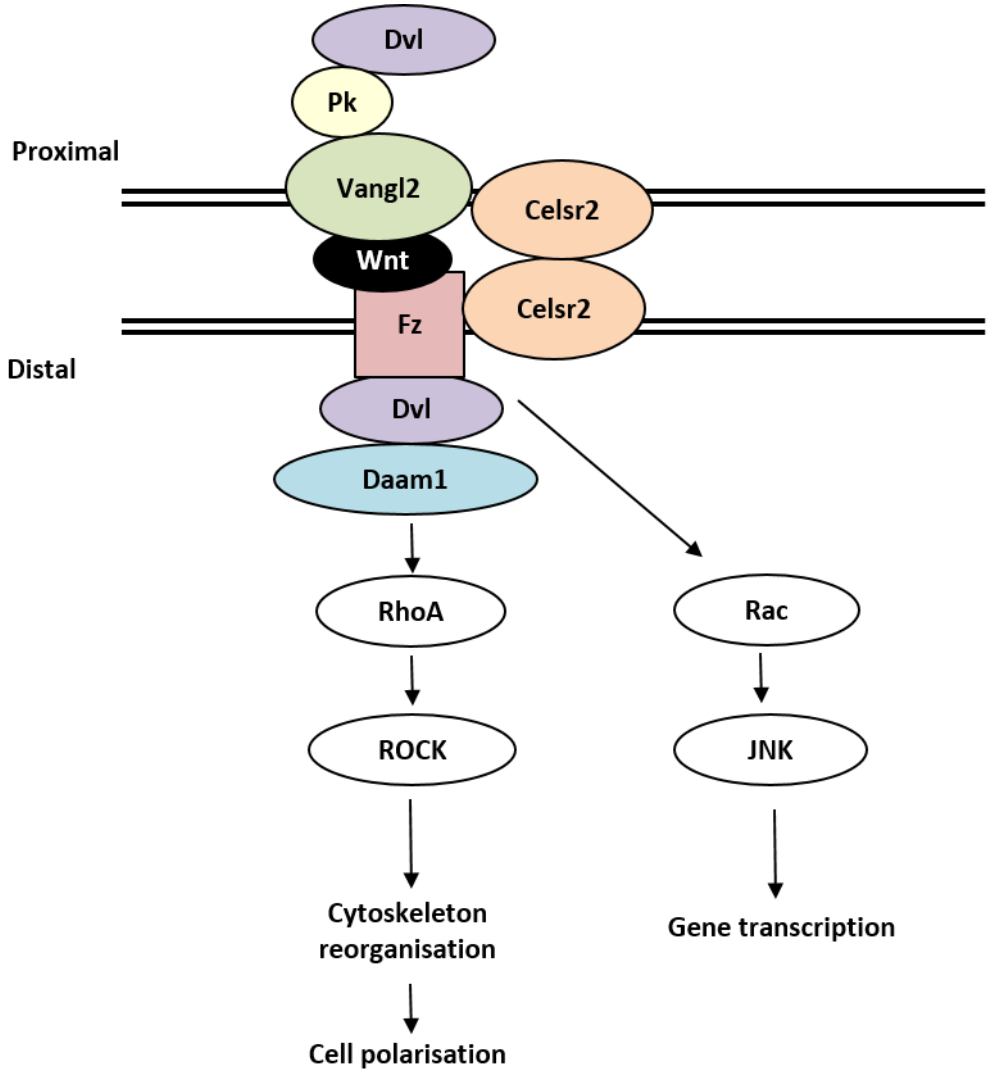

Figure 20: PCP signalling.
Core signalling components include Frizzled (Fz), Dishevelled (Dvl), Prickle (Pk), Vangl and Celsr1. In addition, there are a large number of PCP effectors such as Daam1, RhoA and Rac1. Activation of Wnt/PCP signalling by binding of Wnt ligands, Wnt5a and Wnt11, to Fz receptors at the cell membrane causes Dvl to bind Daam1, which increases its affinity for downstream effectors, Rac1 and RhoA, and regulates cytoskeletal organisation and gene expression.

Wnt ligands, Wnt11 and Wnt5a, are associated with non-canonical Wnt signalling and thought to stimulate cardiogenesis (Afouda *et al.*, 2008). Mutations in *Wnt5a* and *Wnt11* disrupt cardiac development (Schleiffarth *et al.*, 2007; Cohen *et al.*, 2012; Sinha *et al.*, 2015). Wnt11 is expressed in the

myocardium (Sinha *et al.*, 2015) and deletion of *Wnt11* results in embryonic lethality between E12.5 and E13.5. These *Wnt11* deficient hearts had dilated cardiac chambers and thin myocardial walls, with fewer, irregular trabeculae (Figure 21), disrupted AJ and cytoskeleton organisation and decreased expression of *ANF*, *Mef2c*, *Nkx2.5* and *Gata4* (Nagy *et al.*, 2010).

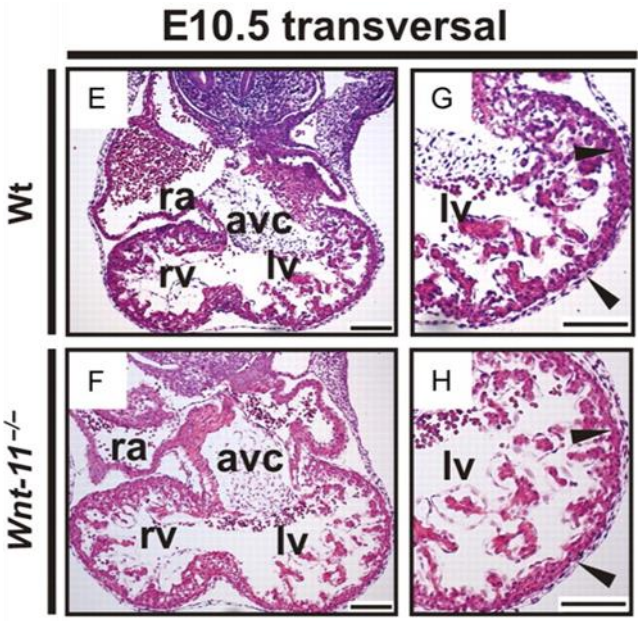

Figure 21: Defective trabeculation in *Wnt11* mutants.
H&E staining of wild type and *Wnt-11*$^{-/-}$ hearts at E10.5. The *Wnt-11*-deficient ventricles are dilated relative to controls at E10.5 (**F** compared to **E**) and the trabecular processes are hypoplastic and are located at irregular distances. The ventricular wall is also thinner (**H** compared with **G**, arrowheads). ra, right atrium; rv, right ventricle; lv, left ventricle; avc, atrioventricular cushion; Scale Bar: 100 µm (Nagy *et al.*, 2010).

Fz receptors are the principle receptors for Wnt ligands and are involved in three distinct pathways; the canonical Wnt pathway, the PCP pathway and the calcium pathway. There are 10 frizzled receptor genes and mutations in these genes cause developmental phenotypes, some including cardiac abnormalities. *Fz1* and *Fz2* are partially functionally redundant. However, double *Fz1* and *Fz2* null embryos have highly penetrant VSDs. *Fz1/2/7* receptor mutant mice have increased frequency of cardiac defects when combined with mutations in *Dvl3*, *Wnt3a*, or *Wnt11* (Yu *et al.*, 2012).

Gene deletion studies in mice have revealed functional redundancy between the three murine Dvl proteins, as well as an essential role in cardiovascular

development. *Dvl2* deficient embryos display OFT defects, including DORV, TGA and PTA (Hamblet *et al.*, 2002), *Dvl1/2* double null mutants have ventricular and OFT defects (Sinha *et al.*, 2012) and *Dvl3* null mice die perinatally with cardiac OFT abnormalities, including DORV and PTA (Etheridge *et al.*, 2008). Dishevelled associated activator of morphogenesis 1 and 2 (Daam1 and Daam2) were identified as Dvl binding proteins (Habas *et al.*, 2001). Daam1 is expressed in developing and adult hearts, and *Daam1* mutants show a ventricular non-compaction phenotype with DORV and VSD, but still have normal proliferation and BMP10 expression (Li *et al.*, 2011). This phenotype suggests that Daam1-mediated Wnt/PCP signalling may orient the cytoskeletons of trabecular cardiomyocytes and guide their integration into the compact myocardium of the adult heart. Cardiac specific deletion of *Daam1* confirmed an autonomous role of Daam1 in the polarized protrusive activity in cardiomyocytes.

Vangl2 and Scrib are both expressed in developing and adult myocardium. Natural occurring *Vangl2* mutants, *Loop-tail* mice, have thin ventricular walls and DORV (Phillips *et al.*, 2005; Henderson *et al.*, 2006; Phillips *et al.*, 2008). *Scrib* mutants have altered ventricular chamber formation and DORV (Murdoch *et al.*, 2003; Phillips *et al.*, 2007). Polarisation and organisation of cardiomyocytes in the ventricular myocardium and outflow myocardium is disrupted in both *Scrib* and *Vangl2 m*utants.

Pk1 knockout mouse embryos present with pregastrulation lethality suggesting *Pk1* plays an important role in development (Tao *et al.*, 2009). A novel mutation in *Pk1* (*Beetlejuice* (*Bj*)) resulted in OFT defects; 63% DORV, 17% OA and 20% a simple perimembranous VSD with normally positioned great arteries (Gibbs *et al.*, 2016). PCP components Scrib and Vangl2 were unchanged, however Pk1 expression was reduced in *Bj* mutants and both canonical and non-canonical Wnt signalling was perturbed in *Bj* mutants (Gibbs *et al.*, 2016).

These studies suggest that non-canonical Wnt signalling is important in cardiomyocyte polarity and organisation during cardiac development.

1.6.6.3 Semaphorin signalling

Plexin transmembrane receptors and their semaphorin ligands, as well as co-receptors, including Nrp1, Vascular endothelial growth factor receptor (VEGFR)-

2 and ErbB2, are emerging as key regulators of cardiovascular development. Semaphorins are a large, highly structurally and functionally conserved family of secreted or membrane associated glycoproteins (Huber *et al.*, 2003). There are 8 classes of semaphorins, with classes 3-7 being expressed in vertebrates. Class 3 are secreted proteins, whereas class 4-6 are membrane proteins and class 7 are anchored proteins that turn soluble after proteolytic cleavage. Semaphorins contain a sema domain for receptor binding.

Two main types of semaphorin receptors have been identified; plexins and neuropilins. There are 9 different plexin receptors, separated into 4 classes; class A (Plexin A1-A4), class B (PlexinB1-3), class C (Plexin C1) and class D (Plexin D1) (Tamagnone *et al.*, 1999). Plexins contain an extracellular sema domain which acts as an autoinhibitory element. The sema domain maintains plexins in an inactive state until a semaphorin binds. Semaphorin binding induces receptor dimerization with either another plexin receptor or one of the co-receptors. Plexins also contain an intracellular Rho-binding domain (RBD), to which Rho GTPases can bind (Tong and Buck, 2005; Tong *et al.*, 2007; Fansa *et al.*, 2013). Plexins require both extracellular and intracellular binding to become activated (Hota and Buck, 2012). Semaphorins and plexins interact on adjacent cells and within the ECM and active, phosphorylated plexins activate downstream kinases. Nrp receptors are transmembrane receptors with a small cytoplasmic domain and multiple extracellular domains which can bind class 3 semaphorins and VEGF ligands (Gu *et al.*, 2003). There are two types of Neuropilin receptors; Nrp-1 and Nrp-2 (Takashima *et al.*, 2002).

Various gene inactivation studies, in chick and mice have suggested that semaphorin signalling is involved in cardiac development including trabeculation and myocardial maturation (Figure 23) (Toyofuku *et al.*, 2004a; Toyofuku *et al.*, 2004b). Recently, semaphorin signalling has been shown to regulate ventricular chamber development in the chick (Toyofuku *et al.*, 2004a; Toyofuku *et al.*, 2004b). In particular, Sema6D, acting as both a membrane bound receptor and a soluble ligand, signals through PlexinA1 to regulate trabeculation and compact layer expansion. Sema6D is expressed in the compact layer and trabeculae myocardium, whereas PlexinA1 is expressed in the trabeculae layer and endocardial cells. Knockdown of either *Sema6D* or *PlexinA1* in the chick leads to a decrease in heart size, a thin compact myocardium and reduced

trabeculation, these changes occur in the absence of altered cardiomyocyte proliferation or apoptosis (Figure 22). It was shown that forward signalling through Sema6D-PlexinA1 is necessary for the expansion of compact layer and bending of the linear heart tube. Whereas, reverse signalling through PlexinA1-Sema6D is required for migration of cardiomyocytes into the trabeculae layer and subsequent trabeculation, through regulation of trabeculae cardiomyocyte motility and directionality (Toyofuku *et al.*, 2004b). Cardiomyocytes expressing a mutant version of mammalian enabled (*Mena*), a known Sema6d interactor, do not migrate into the trabeculae layer but remain in the compact myocardial layer (Toyofuku *et al.*, 2004b). Surprisingly, both *Sema6D* and *PlexinA1* KO mice do not have any obvious cardiac defects (Takegahara *et al.*, 2006; Takamatsu *et al.*, 2010). Several studies in mice have also suggested a role of semaphorin signalling during myocardial development. Sema3A is strongly expressed in the subendocardial regions of the trabeculae myocardium early in development, and is then restricted to the purkinje fibres later in development (Behar *et al.*, 1996; Ieda *et al.*, 2007). *Sema3A* null mice die postnatally with hypertrophy of the RV and dilation of the RA (Behar *et al.*, 1996). Knockout or overexpression of *Sema3A* in mice causes disruption of the cardiac innervation pattern and results in an increased incidence of fatal arrhythmias and sudden cardiac death (Ieda *et al.*, 2007). Additionally, a polymorphism in *Sema3a* is a risk factor for cardiac arrest with ventricular fibrillation (Nakano *et al.*, 2013).

Plexin receptors are expressed in endothelial cells during cardiovascular development, with PlexinC1 and PlexinD1 in particular shown to be expressed in the mouse endocardium (Artigiani *et al.*, 2004; Perala *et al.*, 2005). An additional study suggested that PlexinD1 along with ErbB2 are synthesised in cardiomyocytes. PlexinD1 mediates class 3 semaphorin signals and *PlexinD1* null mice display PTA and VSD, and pups die shortly after birth (Gitler *et al.*, 2004). Endothelial specific deletion of *PlexinD1* recapitulates the cardiac phenotype seen in the null *PlexinD1* mice and also reports embryonic myocardial defects with a thinned myocardial wall (Zhang *et al.*, 2009). These results suggest that PlexinD1 in the endocardium is important for signalling involved in the thickening and maturation of the ventricle wall.

Nrp-1 is expressed in multiple cell types that contribute to development of the cardiovascular system including NCC and endothelial cells (Brown *et al.*, 2001;

Feiner *et al.*, 2001). Additionally, *Nrp-1* has been found to be expressed in both neonatal rat cardiomyocytes and the adult murine heart. Nrp1 forms complexes with VEGFR-1 and VEGFR-2 in cardiomyocytes (Li *et al.*, 2008). Mice with null mutations in *Nrp-1*, or in the genes encoding Nrp-1 ligands exhibit cardiac or vascular defects (Behar *et al.*, 1996; Brown *et al.*, 2001; Feiner *et al.*, 2001; Takashima *et al.*, 2002). *Nrp-1* null mice die at around E10.5–E12.5 with cardiovascular defects (Kawasaki *et al.*, 1999). Endothelial specific disruption of either VEGF/Nrp1 or Sema3C/Nrp1 signalling revealed that VEGF/Nrp1 is critical for the cardiac septation, while Sema/Nrp1 signalling is essential for the development of the atria (Gu *et al.*, 2003). Disrupted VEGF/Nrp1 signalling resulted in PTA, VSD and coronary artery defects (Gu *et al.*, 2003).

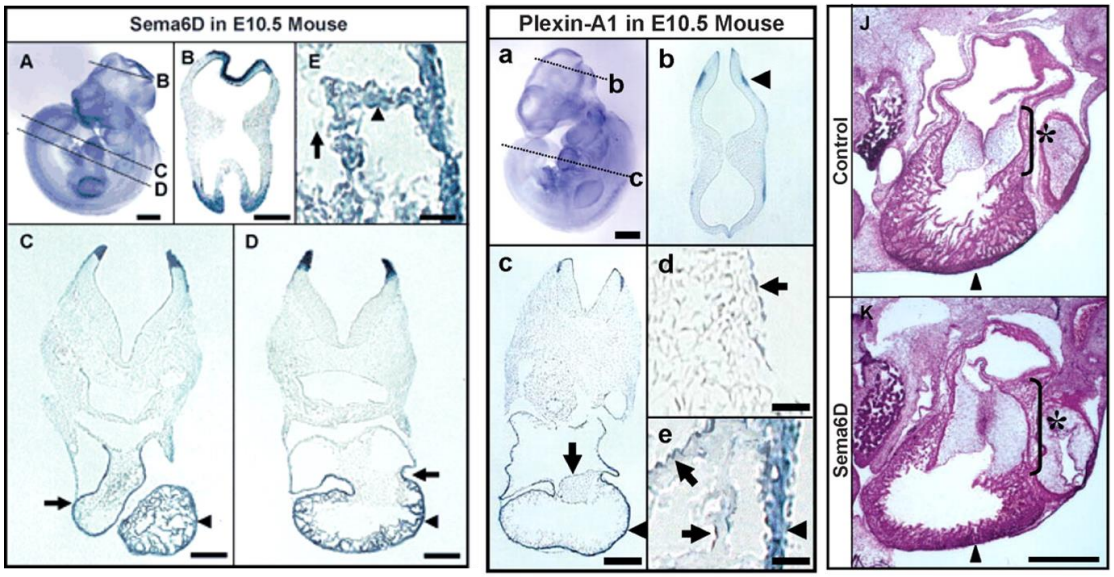

Figure 22: *Sema6D* and *PlexinA1* expression in mice and cardiac defects in knockout chick model.
E10.5 mouse embryo (**A**). Cross-sections through the E10.5 mouse embryo (**B**-**E**). *Sema6D* mRNA is expressed throughout the ventricular myocardium (**C**-**E**) including the OFT, IVS and myocardial cells in compact zone and trabeculae (arrowhead in **E**). Scale bars; A–D, 100 µm; E, 20µm (Toyofuku *et al.*, 2004a; Toyofuku *et al.*, 2004b). E10.5 mouse embryo (**a**). Cross-sections through the E10.5 mouse embryo ***(b-e)***. Plexin-A1 mRNA is expressed in the compact myocardial layer of cardiac ventricular wall (***c*** and ***e***). Scale bar C, 100 µm. Scale bar; E, 20 µm. H&E staining of cross-sections of HH stage 36 chick embryos treated with control (***J***) or Sema6D-expressing cells (***K***). In Sema6D-treated embryos, cardiac ventricle exhibits expanded cavity and poor myocardial trabeculae (***K***, arrowhead) compared with the control embryo (***J***). Figure taken from (Toyofuku *et al.*, 2004a; Toyofuku *et al.*, 2004b).

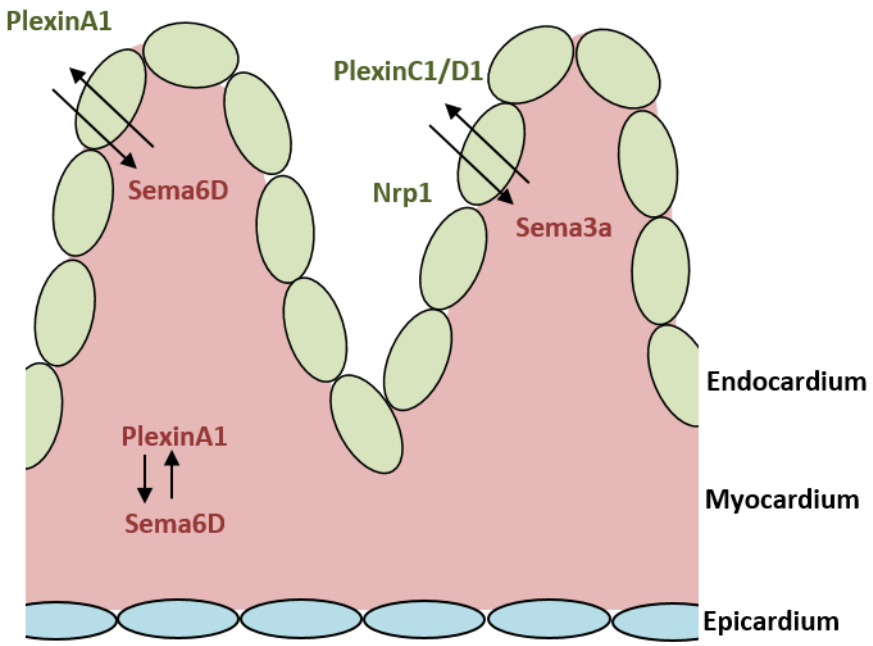

Figure 23: Semaphorin signalling during myocardial development.
Sema3A is strongly expressed in subendocardial regions of the trabeculae myocardium early in development, and is then restricted to the purkinje fibres later in development. Sema6D is expressed in the compact layer and trabeculae myocardium, whereas PlexinA1 is restricted to the compact layer myocardium and endocardial cells. Sema6D, acting as both a membrane bound receptor and a soluble ligand, signals through PlexinA1 to regulate trabeculation and compact layer expansion in chick. PlexinC1 and PlexinD1 are expressed in the mouse endocardium. *Nrp-1* is expressed in multiple cell types that contribute to development of the cardiovascular system including NCC and endothelial cells.

1.6.6.4 VEGF signalling

VEGF is a major signalling pathway between the myocardium and endocardium. Myocardial VEGF binds to VEGF receptors expressed in endocardial cells. VEGFR-2 is expressed in endocardial cells and binding of VEGF causes phosphorylation of tyrosine (Jopling *et al.*, 2011).

In mice, overexpression of endogenous *Vegf-a* causes embryonic lethality from E12.5 and severe heart detects, including a thin compact myocardium, hypertrabeculation, and defective ventricular septation and OFT remodelling (Miquerol *et al.*, 2000). *Vegfr-2* deficient mice lack some endothelial lineages and do not form trabeculae leading to embryonic lethality at E9.5 (Shalaby *et al.*, 1995; Milgrom-Hoffman *et al.*, 2011). Deletion of *Vegf-a* in the myocardium or deletion of *Vegfr-2* in the endocardium resulted in similar ventricular defects,

including the thin myocardial walls, and ruptured septa at E15.5 (Wu *et al.*, 2012). This study highlights that regulation of VEGF signalling between the myocardium and endocardium is essential for normal cardiac ventricular development (Figure 24).

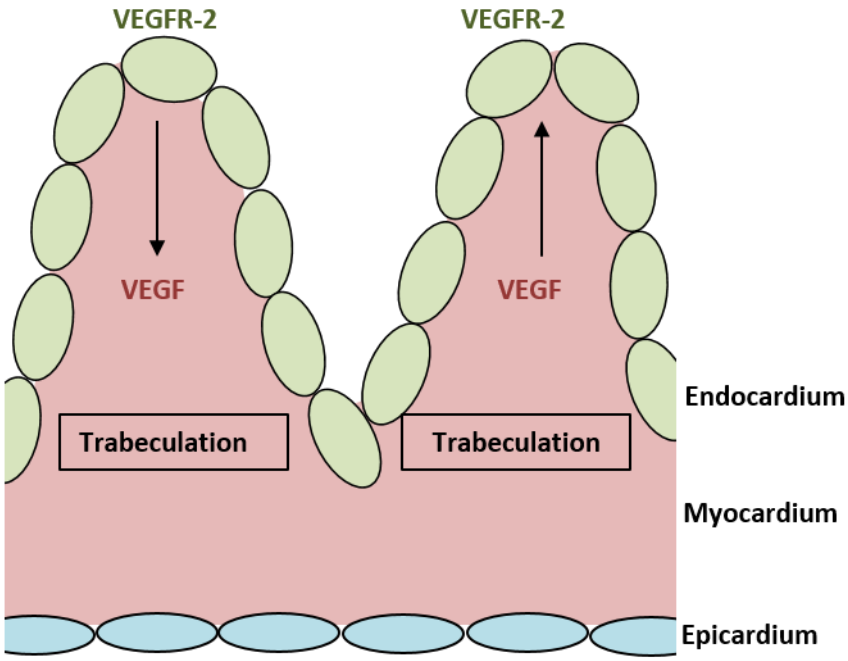

Figure 24: VEGF signalling during myocardial development.
Myocardial vascular endothelial growth factor (*VEGF*) binds to VEGF receptor 2 (VEGFR-2) expressed in endocardial cells. Deletion of *Vegf-a* in the myocardium or deletion of *Vegfr-2* in the endocardium resulted in similar ventricular defects, including the thin myocardial walls and defective trabeculation revealing that regulation of VEGF signalling between the myocardium and endocardium is essential for normal trabeculation (Wu *et al.*, 2012).

The importance of all the signalling pathways described highlights the necessity of the interaction between the endocardium and myocardium during development of the ventricular wall. Between these two layers is cardiac jelly consisting of ECM proteins. ECM is also present in the interstitial space surrounding cardiomyocytes and therefore is important component in the signalling between the endocardium and myocardium.

1.6.7 Role of ECM in trabeculation

The ECM is involved in cell signalling, differentiation and migration, and is crucial for the spatiotemporal regulation of these processes during the complex

development of the heart. Alterations in the composition of the ECM can lead to cardiac malformations (Table 2).

The ECM is secreted by the myocardium and is found in all components of the heart. In particular, there is strong expression in mesenchymal tissues of the developing heart such as the AV and OFT cushions, DMP and epicardium. The macromolecules that make up the ECM include hyaluronan, proteoglycans, collagens, elastin, fibrilin, fibronectin, and laminins. The main ECM components currently known to be important for normal heart development are shown in Figure 25, and studies perturbing these ECM proteins during development have revealed cardiac defects similar to those seen in CHD.

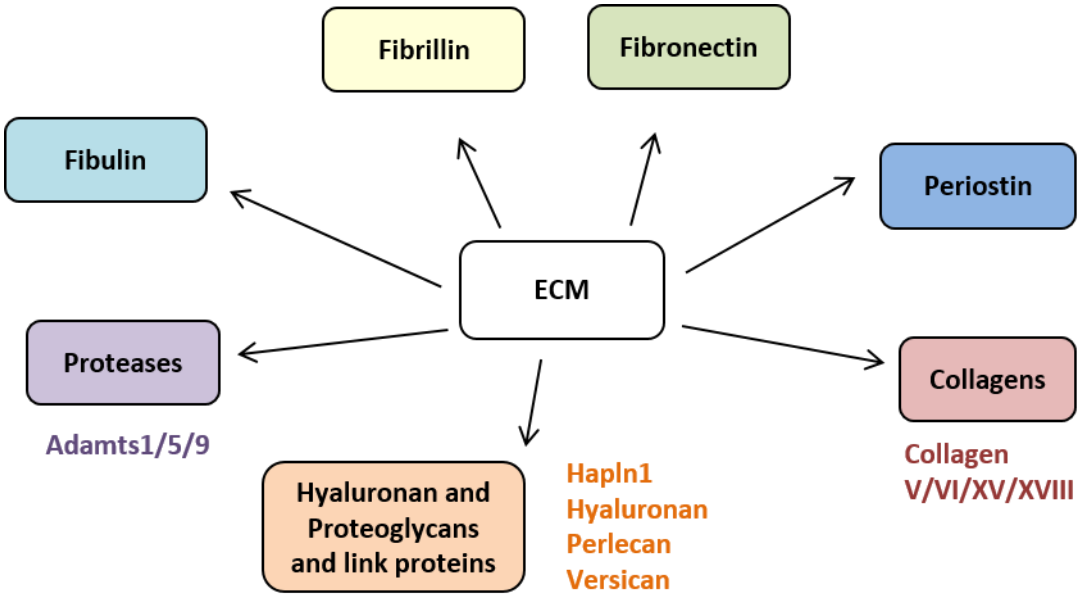

Figure 25: Main components of the ECM in heart development.

Recently, it has been highlighted that the ECM is important for normal cardiac trabeculation, for example knockout of *Has2* or *Versican* leads to defective trabeculation (Yamamura *et al.*, 1997; Camenisch *et al.*, 2000). Hyaluronan and other ECM proteins make up a pericellular matrix, which surrounds cardiomyocytes and provides a hydrated environment that facilitates cellular proliferation and motility (Toole, 2001). Since regulated cell proliferation and migration are critical during the process of trabeculation, it is unsurprising that altering the composition of the pericellular matrix can result in myocardial defects. Using mouse and chick animal models, the expression and function of

several ECM proteins during cardiac development has been investigated. These are summarised in Table 2.

Gene	Expression	Lethality	Cardiovascular Phenotype	Reference
Cartilage Link Protein (Hapln1)	AV and OFT cushions, endocardium	Perinatal	ASD, VSD, AVSD, thin myocardium	Watanabe and Yamada, 1999; Wirrig at al, 2007
Hyaluronan	Myocardium and endocardium, mesenchyme of the AV and OFT cushions, AV valves	E9.5-10	Defects in vasculogenesis, fail to form AVC	Camenish et al, 2000
Perlecan	BM, Cardiac Jelly, OFT Cushions, SMCs of Ao and PA	E10.5-12 or perinataly	Thin myocardium , defects in OFT rotation	Costell et al, 2002
Versican	Cardiac jelly, AV and OFT cushions, mesenchyme of the PAS	E10.5	Fail to form RV, OFT, AVC, and Thin myocardium;	Yamamura et al, 1997; Mjaatvedt et al, 1998; Wirrig et al, 2007
Collagen Type V	Ao, Anulous Fibrosus, Mural Leaflet	E10	Undescribed cardiovascular defects	Wenstrup et al, 2004; Roulet et al, 2006;Kruithof et al, 2007
Collagen Type VI	AV valves, myocardium, epicardium, Ao, and PA	None	None reported	Bonaldo et al, 1998; Klewer et al, 1998; Kruithof et al, 2007
Collagen Type XV	BM, Myocardial Capillaries	None	Vascular defects, cardiomyopathy	Eklund et al, 2001 Muona et al, 2002
Collagen Type XVIII	BM of myocardium and endocardium, Semilunar Valves	None	Broadened AV Valves	Carvalhaes et al, 2006; Utriainen et al, 2004
ADAMTS1	Endocardium, myocardium, AV cushion	50% Embryonic Lethality	Hypertrabeculation	Thai and Irule-Arispe, 2002; Kern et al, 2006; Stakunas et al, 2008
ADAMTS5	Endocardium, myocardium, pericardium, Ao, aortic valves	None	Normal	Majumdar et al, 2007; McCulloch et al, 2009
ADAMTS9	Myocardium, right-sided OFT cushions, SLV, Ao, mitral valve	E7.5	Haploinsufficiency results in enlarged SLV, myxomatous mitral valve, “spongy” myocardium	Jungers et al, 2005; Kern et al, 2010
Fibulin 1	AV and OFT cushions, CNDCs	Perinatal	ASD, Thin myocardium, abnormal AAA, DORV, overriding aorta, VSD, haemorrhage	Kern et al, 2006; Cooley et al, 2008
Fibronectin	Embryonic Mesoderm, AVC, endocardium, dorsal Ao	E8.5 – 10.5	Fail to form heart tube in most severely affected, vascular defects	French-Constant and Hynes, 1989; George et al, 1993; Georges-Labouesse et al, 1996

Table 2: Mouse knockout models of ECM proteins during heart development (Lockhart *et al.*, 2011).

Collagen types I, III, V, VI and XI have been shown to be expressed in the developing myocardium (Klewer *et al.*, 1998; Lincoln *et al.*, 2006). Collagen XI is thought to be involved in the regulation of collagen fibril assembly and is restricted to the trabeculated layer of the ventricular wall, with no expression in the compact layer (Lincoln *et al.*, 2006). *Collagen XI* deficient mice display

cardiac abnormalities such as an increase in the thickness of the IVS and AV valve leaflets with increased collagen I expression, as well as a pronounced change in the overall shape of the heart (Lincoln *et al.*, 2006).

Fibronectin is a multi-domain ECM protein that interacts with multiple integrins, HS proteoglycans, collagens, and fibrins to mediate cellular processes. During cardiac development, fibronectins are expressed in the endocardium and mesenchyme of the endocardial cushions, where it is required for EMT (Astrof *et al.*, 2007). Fibronectin null embryos die by E10 due to severe cardiovascular and vascular defects. The formation of the primary heart tube is affected and those that do form a heart tube display a thickened myocardium, lack of cardiac jelly, and abnormal endocardium (Astrof *et al.*, 2007). Laminin is an ECM protein present at the basal side of the cell in the basal lamina of the basement membrane and is involved in adhesion and cell migration (Timpl *et al.*, 1979).

These studies implicate the complex composition of ECM as an integral component in ventricular development.

1.7 Coronary vasculature development

As described earlier, the heart is made up of three major layers; the inner endocardium, myocardium and outer epicardium. The coronary vasculature develops within the middle myocardial layer and is absent from the embryonic heart until the myocardium becomes thickened. During the early trabeculation phase, interamural vessels are yet to be formed and only subepicardial vessels are present in the myocardium (Captur *et al.*, 2015).

The coronary vasculature is made up of coronary arteries and coronary veins, which branch into arterioles and venules and are connected by microvessels and capillaries. Coronary arteries and veins have three tissue layers; an inner layer of endothelium, a middle layer of SMCs and an outer layer of fibroblasts. Capillaries are made up of a single layer of endothelial cells to allow efficient oxygen and nutrient exchange.

Embryonic vascular development is established through two main processes; vasculogenesis and angiogenesis. During vasculogenesis, endothelial cell precursors, angioblasts, associate to form a primitive vascular network. This is followed by angiogenesis, where the primitive vascular network is remodelled with new vessels sprouting from pre-existing vessels. Hypoxia is required for

angiogenesis and hypoxic regions during development, including the atria and IVS, correlate with major coronary artery formation in the chick heart (Wikenheiser *et al.*, 2006).

1.7.1 Origin of coronary endothelial cells

The origin of the coronary vessel endothelial cells which contribute to the coronary arteries, veins and capilaries is controversial. Studies have shown that pro-epicardial cells generate SMCs of both coronary arteries and veins, however there is conflicting evidence of the origin of endothelial cells. Fate mapping studies have reported contribution from both the pro-epicardial cells and the SV, and more recently, the endocardium (Tian *et al.*, 2013; Chen *et al.*, 2014). Through nuclear factor of activated T cells cytoplasmic 1 (Nfatc1) lineage tracing, Wu *et al.* showed that the endocardium is a major source of endothelial cells in the coronary vasculature (Wu *et al.*, 2012). However, recent evidence suggests that Nfatc1 labels both SV and vascular endocardium and that the endocardium only minimally contributes to the coronary endothelium of the ventricular free walls (Zhang *et al.*, 2016). Through complex Nfatc1 lineage tracing studies, Zhang *et al.* have shown that the majority of coronary endothelium arises from the SV whereas the Nrp3 expressing endocardial cells contribute to the coronary vessels in the septum (~90%) and minimally to the coronary vessels (~3%) (Zhang *et al.*, 2016). There are numerous markers of endothelial and/or endocardial cells which have been identified and utilised to investigate coronary endothelial contributions. These are listed in Table 3.

Endothelial/endocardial marker	Expression
Apelin	Vascular endothelial cells but not endocardial cells
APJ	Endothelial cells
CD31 (pecam)	Endothelial cells of both coronary arteries and veins and endocardial cells
CD34	Endocardial cells but not epicardial cells
CD105 (endoglin)	Endothelial and endocardial cells.
Endomucin	Endothelial cells of coronary veins and endocardial cells
Nfatc1	Endocardial cells but absent from vascular endothelial cells
Nrp3	Endocardial cells
Vimentin	Endocardial and epicardial cells plus subepicardial and intramyocardial interstitial cells

Table 3: Endothelial and endocardial specific proteins.

1.7.1.1 Pro-Epicardium

The PE is a transient extra-cardiac cluster of cells which develops as a cauliflower-like protrusion from at the base of the developing heart (Viragh and Challice, 1981; Manner *et al.*, 2001). The pro-epicardium forms villi which protrude towards the myocardium of the looping heart tube, the pro-epicardial cells then migrate to the surface of the heart and envelop the myocardium, forming the epicardium. Fate mapping of pro-epicardial cells in chick and quail reveal contribution to additional lineages including perivascular fibroblasts, SMCs and endocardial cells of the coronary vessels (Manner *et al.*, 2001). Studies in mice have highlighted that PE is most likely a molecularly compartmentalized structure, with predetermined populations contributing separately to each lineage. Tbx18 and (Wilm's tumour) WT-1-expressing cells give rise to vascular SMCs, cardiomyocytes and fibroblasts with little or no contribution to endothelial cells (Cai *et al.*, 2008; Zhou *et al.*, 2008; Red-Horse *et al.*, 2010). Whereas, Scx- and Sema3D-expressing pro-epicardial cells give rise to coronary vascular endothelium including the early SV and cardiac endocardium (Katz *et al.*, 2012).

1.7.1.2 Sinus Venosus

The SV is the main vein that returns blood to the embryonic heart. The endothelial cells of SV are a heterogeneous population, composed of Apelin receptor positive and negative cells (Chen *et al.*, 2014). A recent study demonstrated that some murine coronary endothelial cells arise from both the endothelial lining of the SV and from the cardiac endocardium, with no contribution to these structures from *Tbx18* expressing pro-epicardial cells (Red-Horse *et al.*, 2010).

1.7.1.3 Endocardium

The endocardium is an epithelial layer made up of endocardial cells associated with the basement membrane of the trabeculae and OFT myocardium. Endocardial cells were initially thought to be terminally differentiated, however recent studies demonstrate a role of endocardial cells in the formation of coronary vessel endothelium. As mentioned above, a recent study discovered that some murine coronary endothelial cells arise from the cardiac endocardium

(Red-Horse *et al.*, 2010). Tian and colleagues recently proposed a mechanism in which a proportion of postnatal coronary vessels arise *de novo* in the neonatal mouse heart, through conversion of endocardial cells during ventricular compaction after birth. Genetic lineage tracing revealed that postnatal endocardial cells generate a distinct population of coronary vasculature within the inner ventricular wall. During trabeculae compaction, endocardial cells become trapped within the compacting myocardium and in response to their new hypoxic, intramyocardial environment, the endocardial cells undergo angiogenesis, migrate and form coronary vessels (Tian *et al.*, 2014). This study also revealed waves of coronary artery formation. The first wave of outer compact myocardial vessels is formed by EPDCs at E10.5. The second and third wave of vessels are formed from conversion of endocardial cells to vascular endothelial cells; the second wave at E13.5 in the IVS and the third wave postnatally in the inner compact myocardium (Tian *et al.*, 2014).

A role for endocardial cells during embryonic vessel formation has also been reported. Interestingly, Wu and colleagues described endocardial cells that were not terminally differentiated but were angiogenic and contributed to the formation of coronary endothelial networks. *Nfatc1-Cre* was used to fate map endocardial cells. It was found that Nfatc1+ endocardial derivatives make a substantial contribution to arterial endothelium, however, only a small contribution to coronary veins (Wu *et al.*, 2012). Additionally, in the human heart, it has been shown that endothelial networks in the inner myocardium are derived from endocardial cells and are guided by filopodia-projecting CD31+/CD34+/CD105+/vimentin+ endocardial tip cells, with upregulated CD105 expression in activated endocardial cells (Rusu *et al.*, 2015) (Figure 26).

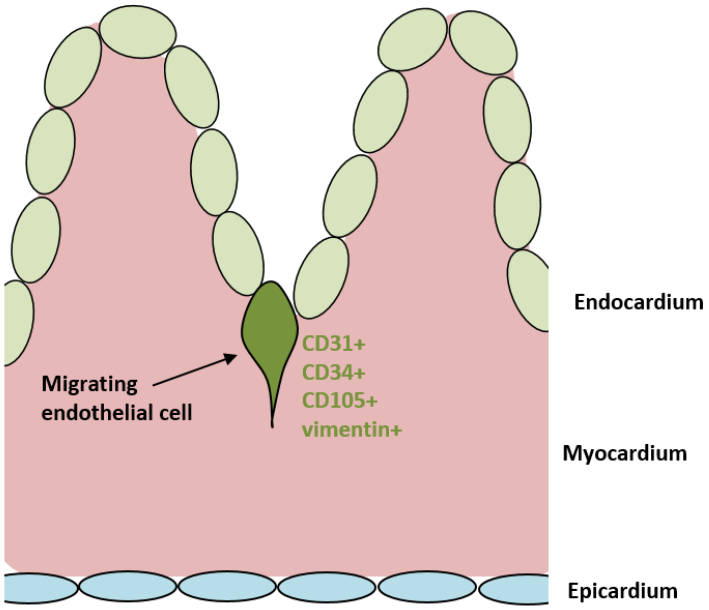

Figure 26: Endocardial contribution to the coronary endothelial networks. In the human heart endothelial networks in the inner myocardium are derived from endocardial cells and are guided by filopodia-projecting CD31+/CD34+/CD105+/vimentin+ endocardial tip cells at the base of trabeculae, with upregulated CD105 expression in activated endocardial cells (Rusu *et al.*, 2015).

1.7.2 Regulators of vascular development

Several cell surface receptors and ligands have been found to play central roles in vascular development such as tyrosine kinase receptors and associated ligands. In particular, VEGF and FGF and their receptors have been extensively investigated.

1.7.2.1 VEGF signalling

As previously discussed in Chapter 1 Section 1.6.6.4, VEGF signalling is important for trabeculation and myocardial development, but it is also critical for vasculogenesis. Genetic alterations of either *Vegf-a* or *Vegfr-2* leads to defective vasculogenesis (Carmeliet *et al.*, 1996; Ferrara *et al.*, 1996; Miquerol *et al.*, 2000). Myocardial to endocardial VEGF signalling is critical for angiogenesis and coronary vessel formation since myocardial *Vegf-a* or endocardial and SV *Vegfr-2* deletion inhibited coronary angiogenesis and arterial formation (Wu *et al.*, 2012). VEGFR-1 within the endocardium negatively regulates angiogenesis. Endocardial specific deletion of *Vegfr-1* causes increased coronary plexus formation with increased VEGF-Notch signalling.

Additionally, *Vegfr-1* null endocardial cells undergo spontaneous angiogenesis and generated extensive endothelial tubular networks in vitro (Zhang and Zhou, 2013).

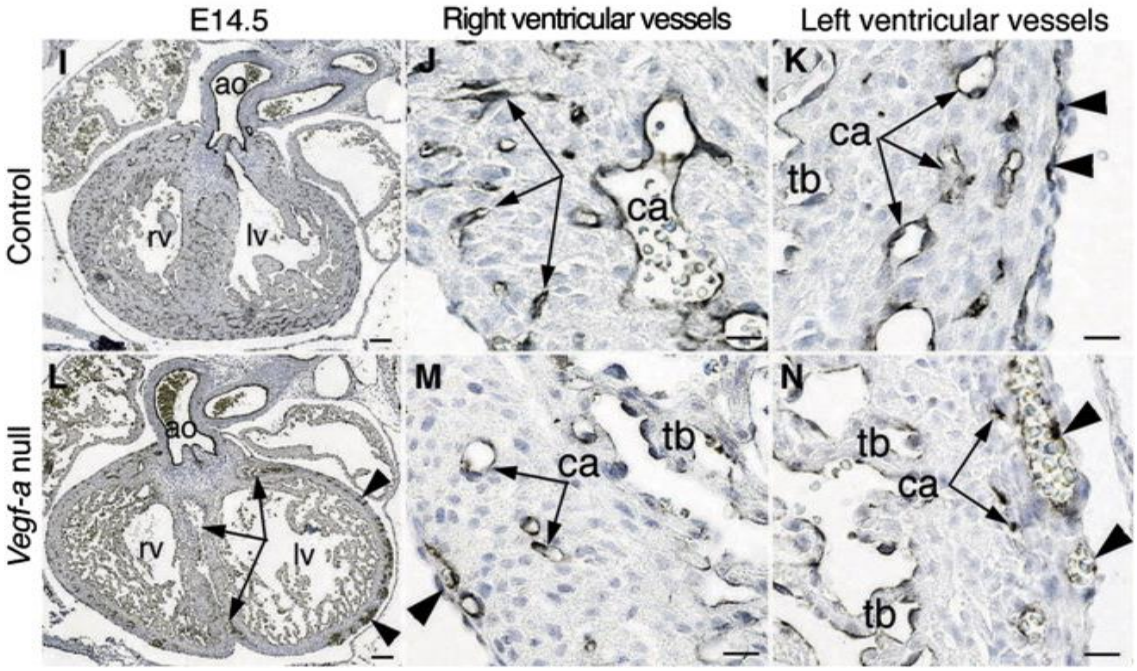

Figure 27: Disruption of *Vegf-a* in the Myocardium Reveals that Myocardial VEGFA Is Required for Coronary Angiogenesis and Artery Formation (Wu *et al.*, 2012).
Images of E14.5 control heart show the Pecam1+ coronary arteries (ca, arrows) and subepicardial vessels (**I–K**, arrowheads). Images of E14.5 *TnnT2-Cre*;*Vegfaf/f* heart show less and immaturely formed coronary arteries (**L–N**, arrows) but numerous and dilated subepicardial vessels (arrowheads). The null heart also has necrotic peritruncal and septal myocardium (**L**, arrows). Scale bars for (**I**) and (**L**), 100 μm; for all other panels, 20 μm.

1.7.2.2 Notch signalling

Notch signalling is critical for coronary vessel formation. Studies revealed substantial and specific expression of Notch signalling components in developing blood vessels as detailed in Table 4. Initial vasculogenesis is unaffected in Notch signalling mutants, including *Hey1/2*, *Jagged1* and *Notch1* knockout mice, however subsequent remodelling is disrupted. Large arteries lack expression of common arterial endothelial markers, CD44, Nrp-1 and EphrinB2, displaying defective arterial differentiation (Kokubo *et al.*, 2005b). Additionally, a recent paper shows that endothelial Dll4 to Fringe modified Notch1 receptors stimulates coronary vessel development. (D'Amato *et al.*, 2016).

Notch gene	Expression	Reference
Notch1	Arterial endothelium	(Villa *et al*., 2001)
Notch2	Not expressed	(Villa *et al*., 2001)
Notch3	Arterial smooth muscle	(Villa *et al*., 2001)
Notch4	Arterial and capillary endothelium	(Villa *et al*., 2001) (Mailhos *et al*., 2001)
Delta1/3	Not expressed	(Shutter *et al*., 2000; Mailhos *et al*., 2001)
Delta4	Arterial and capillary endothelium	(Shutter *et al*., 2000; Mailhos *et al*., 2001)
Jagged1/2	Arterial endothelium and smooth muscle	
Hey1	Vascular endothelium	(Fischer and Gessler, 2003)
Hey2	Vascular endothelium and smooth muscle	(Fischer and Gessler, 2003)
EphrinB1	Arterial and venous endothelium	(Wang *et al*., 1998)
EphrinB2	Arterial	(Villa *et al*., 2001) (Wang et al., 1998)
EphrinB3/4	Venous endothelium	(Wang *et al*., 1998)
EphB3	Venous and some arterial	(Wang *et al*., 1998)
EphB4	Venous and some arterial endothelium and endocardium	(Wang *et al*., 1998)

Table 4: Notch gene expression in the coronary vasculature.

1.7.2.3 Semaphorin-Plexin signalling during angiogenesis

Class 3 semaphorins are expressed in endothelial cells. Sema3 reduces endothelial motility and thus inhibits angiogenesis. Expectedly, *Sema3A* null mice exhibit vascular detects (Serini *et al.*, 2003), and defects in *Sema3C* and receptors *PlexinA2* and *Nrp-1* result in DiGeorge Syndrome like defects in the aortic arches and OFT septation (Zhou *et al.*, 2012). Sema4, on the other hand, promotes cell migration and angiogenesis (Conrotto *et al.*, 2005). As mentioned earlier, plexins are expressed in endothelial cells (Artigiani *et al.*, 2004). PlexinD1 is expressed in vascular cells in developing blood vessels in mice and propagates Sema3A inhibitory signals and is required with Sema3A and Nrp-1 in endothelial cells for normal cardiovascular development (Gay *et al.*, 2011; Hota and Buck, 2012).

1.7.2.4 Nfatc1

The inactive transcription factor Nfat is localised in the cytoplasm. Once dephosphorylated by Calcineurin, a heteromeric Ca(2+)-dependent serine/threonine phosphatase, Nfat undergoes translocation to the nucleus. Nfat regulates numerous biological processes, including cardiac development. Cysteine-Rich with EGF-Like Domains 1 (*Creld1*) gene, a regulator

of calcineurin/Nfactc1 signalling, is also essential for heart development. Creld1 function is required for the VEGF-dependent proliferation of endocardial cells by promoting the expression of Nfatc1 target-genes (Mass *et al.*, 2014). Wu and colleagues described a decrease in Nfatct1 expression in endocardial cells before migration into the compact layer (Wu *et al.*, 2012).

1.7.2.5 VE-cadherin

VE-cadherin plays an important role in the cessation of sprouting in angiogenesis (Abraham *et al.*, 2009). Cell-cell adhesion in endothelial cells increases actinomyosin contractility at cell junctions through VE-cadherin, suppressing VEGF stimulated Rac1-dependent migration and sprouting (Lampugnani *et al.*, 2002).

1.7.2.6 Signalling pathways common to both coronary vessel formation and myocardial development

Additional known signalling pathways active between the myocardium and endocardium that are involved in coronary vessel development include Ang-1-Tie2, BMP2-TGF-β and FGF-FGFR-1/2 (Shalaby *et al.*, 1995; Suri *et al.*, 1996; Arita *et al.*, 2014; Mima *et al.*, 1995; Lavine *et al.*, 2005; Lu *et al.*, 2008). The signalling pathways between the myocardium and endocardium important for myocardial development and coronary vessel development (described in Chapter 1 Section 1.6.6 and 1.7.2, respectively) are overlapping. Notch, VEGF, FGF and Semaphorin signalling pathways are crucial for both trabeculation and coronary vessel formation (Figure 28). Hence, disruptions in myocardium or endothelial lineages can affect myocardial development and/or coronary vessel formation. This is unsurprising since the formation of coronary vessels and the development of the myocardium is intrinsically linked. Trabeculation occurs to increase perfusion in the absence of coronary circulation. As the compact myocardium thickens, endothelial cells invade and form the coronary vasculature. Once the coronary vasculature is formed, the trabeculae are no longer required and regress into the compact myocardium, possibly through compaction at the base (Figure 11) (Tian *et al.*, 2014).

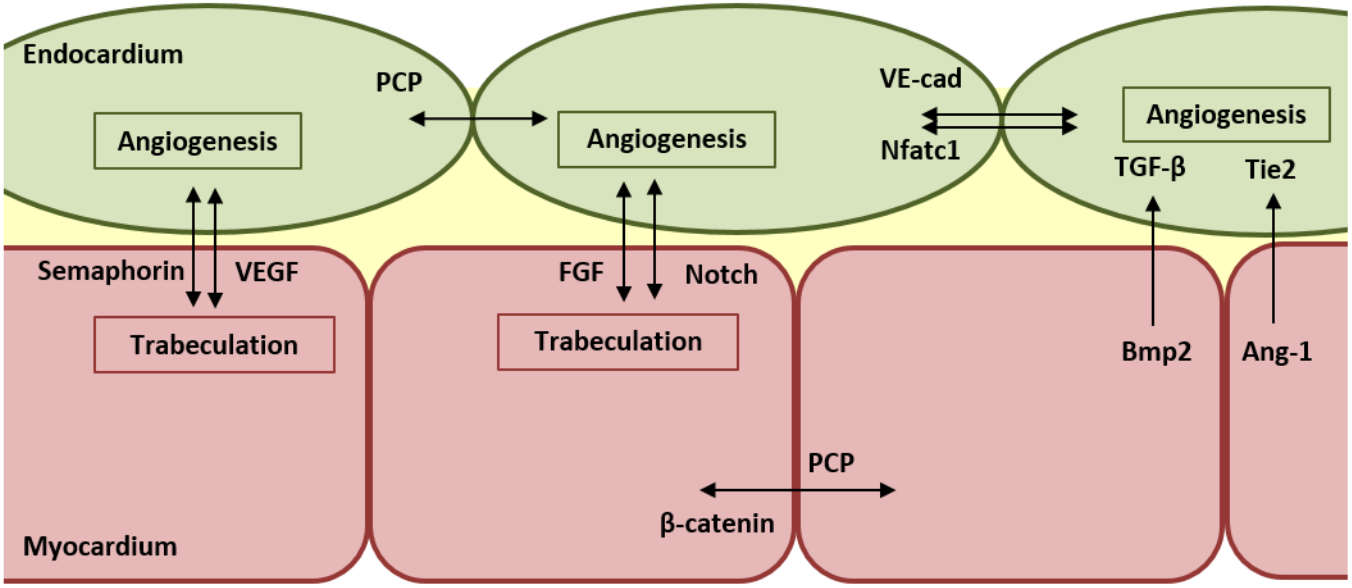

Figure 28: The signalling pathways between the myocardium and endocardium important for both myocardial development and coronary vessel development .
Notch, VEGF, FGF and Semaphorin signalling pathways are crucial for both trabeculation and coronary vessel formation. Additional known signalling pathways active involved in coronary vessel development include Ang-1-Tie2, BMP2-TGF-β and FGF-FGFR-1/2, as well as PCP, VE-cadherin and Nfatc1 signalling within the endocardial layer, and PCP and β-catenin signalling within the myocardial layer.

1.8 Rac1

1.8.1 Rho-GTPases

Rac1 (also known as Ras-related C3 botulinum toxin substrate 1) is a member of the Rho family of small GTPases, which are a subgroup within the large superfamily of Ras-related small GTPases. Rho GTPases consist of 20 members, acting as molecular switches that oscillate between an active GTP-bound state, able to activate several downstream effectors, and an inactive GDP-bound state (Jaffe and Hall, 2005). The activation of Rho-GTPases is catalysed by guanine nucleotide exchange factors (GEFs) and GAPs, resulting in GTP hydrolysis and protein activation (Tcherkezian and Lamarche-Vane, 2007) (Figure 29). GEFs have high affinity for the guanine nucleotide-free state of the GTPases and are thought to promote GDP release by stabilizing an intermediate transition state. Over 70 RhoGAPs and 80 RhoGEFs have been identified and most of them show tissue-specific expression (Jaffe and Hall, 2005; Cherfils and Zeghouf, 2013).

RhoA, Rac1, and Cdc42 are the best-characterized members of the Rho GTPase family. Previous studies have highlighted the importance of these proteins in cytoskeletal rearrangements (Tapon and Hall, 1997; Jaffe and Hall, 2005). Generally, activation of Cdc42 leads to the formation of filopodia, activation of Rac1 induces lamellipodia and membrane ruffles, while RhoA activation leads to contractile actin-myosin filaments and stress fibre formation (Ridley and Hall, 1992; Ridley *et al.*, 1992; Kozma *et al.*, 1995; Nobes and Hall, 1995). Other molecular functions regulated by these small GTPases include microtubule dynamics, signal transduction, gene expression, and enzymatic regulation, which regulate a variety of cellular processes, such as cell migration, polarity, survival, morphology, proliferation, differentiation, and regulation of the various phases of the cell cycle (Etienne-Manneville and Hall, 2002; Jaffe and Hall, 2005).

Disruption of Rho GTPase signalling, using a Rho GDP dissociation inhibitor, during mouse development, results in embryonic death at E10.5 with cardiac defects, including defective heart looping and chamber septation, hypocellular and dilated ventricles, and a lack of trabeculation and endocardial cushion formation (Wei *et al.*, 2002). Decreased proliferation in these hearts at E9.5

suggests a role of Rho GTPases in cardiac cell cycle regulation (Wei *et al.*, 2002).

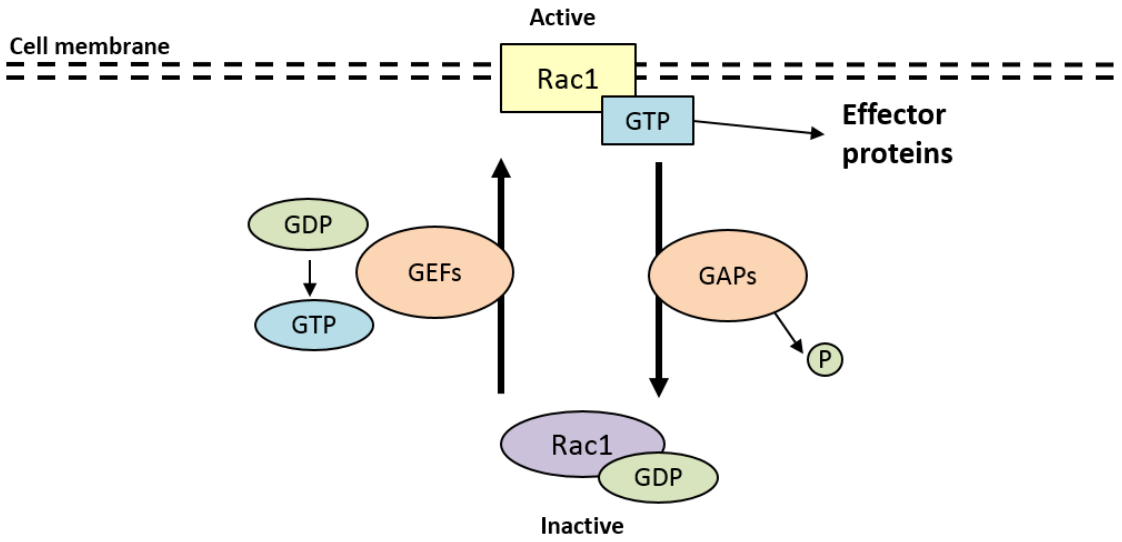

Figure 29: Activation of Rac1.
The activation of Rho-GTPases including Rac1 is catalysed by guanine nucleotide exchange factors (GEFs) and GTPase-activating proteins (GAPs), resulting in GTP hydrolysis and protein activation. Active Rac1 is associated with the cell membrane, whereas inactive Rac1 resides in the cytosol.

1.8.2 Rac proteins

The Rac subfamily is composed of three members: Rac1, Rac2 and Rac3 (Haataja *et al.*, 1997). *Rac1* is expressed ubiquitously with the strongest expression found in the heart, placenta and kidney (Matos *et al.*, 2000). *Rac2* expression is limited to hematopoietic tissues and regulates the actin cytoskeleton and superoxide generation. *Rac3* is predominantly expressed in the central nervous system and adult brain.

1.8.3 Rac1

In its active state, Rac1 is associated with the plasma membrane and binds to a variety of effector proteins to regulate cellular responses such as cytoskeleton organisation, cell adhesion, and cell migration (Ridley, 2001) (Figure 30). Rac1 regulates focal adhesion formation and organisation of actin filaments at the plasma membrane, resulting in the formation of lamellipodia and ruffles at the leading edge of migrating cells. Additional functions include regulation of gene transcription, DNA synthesis, superoxide production, cell proliferation and apoptosis (Bosco *et al.*, 2009) (Figure 30).

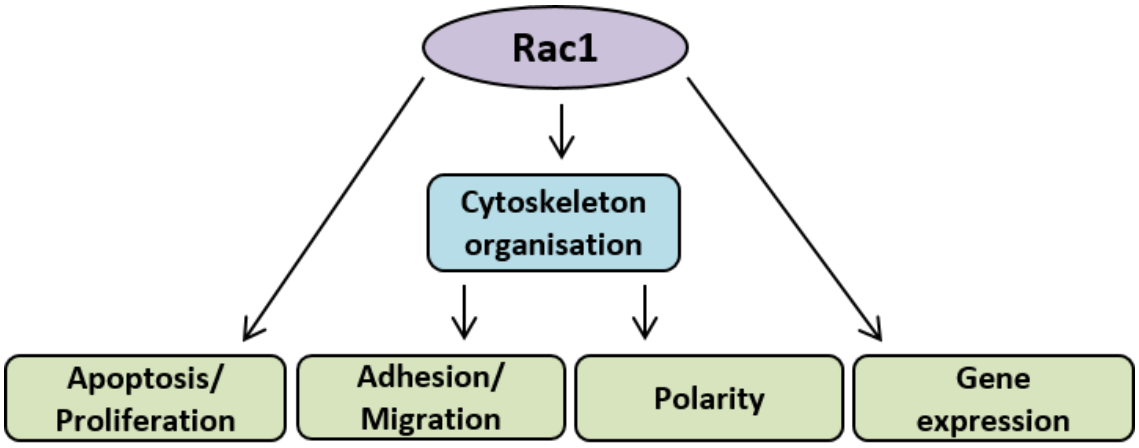

Figure 30: Downstream functions of Rac1 activation.
Rac1 binds to a variety of effector proteins to regulate cellular responses such cell adhesion, polarity and migration. Rac1 regulates actin organisation and focal adhesion formation at the plasma membrane, resulting in the formation of lamellipodia and ruffles at the leading edge of migrating cells. Additional functions include regulation of gene transcription, DNA synthesis, cell proliferation and apoptosis.

1.8.4 Rac1 gene

The human *RAC1* gene is 29kb and contains seven exons and is mapped to chromosome 7p22 (Matos *et al.*, 2000). In mice, the *Rac1* gene is located on chromosome 5p14.3. There are two protein-coding transcripts through alternative splicing of *Rac1* exon 3b (Figure 31). The first transcript contains six exons and encodes a 192 amino acid protein which is expressed ubiquitously (Figure 31A). The second transcript contains seven exons and encodes a 211 amino acid protein which is not known to be expressed (Figure 31A). The Rac1 protein is shown in Figure 31C and contains a RhoGTPase domain and is prenylated. Humans and mice share 91.6% similarity in the nucleotide sequence and 100% similarity in the amino acid sequence (GeneCards).

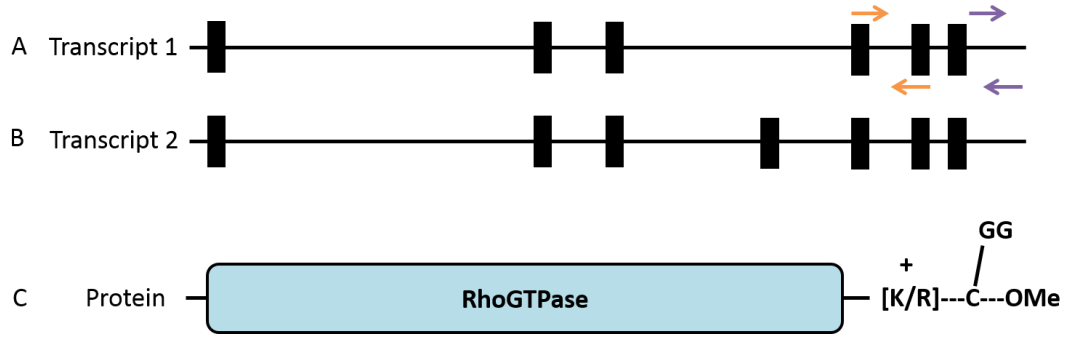

Figure 31: Rac1 Coding Transcripts and Protein.
There are two protein-coding transcripts through alternative splicing of Rac1 exon 3b. Transcript 1 contains six exons and encodes a 192 amino acid protein (**A**). Transcript is 2,325bp contains seven exons and encodes a 211 amino acid protein (**B**). Transript 1 encodes the Rac1 protein which is ubquitously expressed and contains a RhoGTPase domain and is prenylated (**C**). The arrows on A represent the primers used for in situ probes; *Rac1* (purple) and *Rac1* exons 4-5 (orange).

1.8.5 Rac1 in embryonic development

Rac1 is the only Rac gene expressed both ubiquitously and early in embryogenesis (Wang and Zheng, 2007). *Rac1* null mouse embryos die during embryogenesis (before E7.5) and display extensive cell death in the space between the endoderm and ectoderm (Sugihara *et al.*, 1998), implying that *Rac1* has a critical role during embryogenesis. Cell-specific knock-out studies in mice have shown that *Rac1* is required for endoderm and mesoderm migration (Migeotte *et al.*, 2010; Migeotte *et al.*, 2011). Epiblast-specific deletion of *Rac1* caused cardia bifida (two independent heart tubes) and *in vitro*, *Rac1* deficient epiblast cells failed to adhere to matrix, leading to cell death (Migeotte *et al.*, 2011).

1.8.6 Rac1 in cardiovascular development

The cardia bifida phenotype observed in the epiblast specific *Rac1* deletion embryos highlights the importance of *Rac1* in early heart formation. Additionally, cell-specific knock-out studies in mice have shown that *Rac1* has a continued important role in cardiac development within endothelial, NCC and cardiomyocyte lineages.

1.8.6.1 Rac1 in endothelial cells

During mouse embryonic development, studies have shown that *Rac1* is crucial in the endothelial lineage. Using an endothelial specific *Cre* line, *Tie2Cre*, *Rac1* was deleted from endothelial cells. *Rac1;Tie2Cre* embryos die at E9.5 due to developmental delay, with defective development of major vessels and complete lack of smaller branched vessels (Tan *et al.*, 2008). The presence of a complete dorsal aorta suggested that *Rac1* is primarily involved in angiogenesis rather than vasculogenesis. However, capillary like structures were absent in *Rac1;Tie2Cre* embryos suggesting *Rac1* may be required for the migration of angioblasts to promote establishment of these networks (Tan *et al.*, 2008). *Rac1+/f;Tie2Cre* heterozygous mice survive to adulthood but present with decreased eNOS, decreased endothelium-dependent vasorelaxation and mild hypertension (Sawada *et al.*, 2008). *Rac1* deficient primary endothelial cells had reduced migration and failed to form tube-like networks, as well as displaying reduced focal adhesion and lamellipodia formation, and attachment to fibronectin in response to VEGF. Endothelial cells lacking *Rac1* also had increased permeability and unorganised cell-cell interactions as labelled by β-catenin, VE-cadherin and ZO1. Additionally, it was established that Rac1 is required for cell surface signalling to downstream effectors WAVE and PAK to regulate endothelial cell migration, gene expression and cell permeability (Tan *et al.*, 2008). Since *Tie2Cre* is expressed during vasculogenesis and angiogenesis, the same group have since conditionally deleted *Rac1* in a temporally controlled and endothelial-restricted fashion using *Cdh5(PAC)-iCreERT2* transgenic mice. This confirmed that Rac1 is required for embryonic vascular integrity and angiogenesis, and is spatially involved in endothelial cell migration, invasion, and radial sprouting activities in 3D *in vitro* models (Nohata *et al.*, 2016).

Hence, *Rac1* is essential in endothelial cells for normal cardiovascular development mainly due to its role in the regulation of the actin cytoskeleton and lamellipodia protrusion formation necessary for endothelial cell migration (Tan *et al.*, 2008).

1.8.6.2 Rac1 in neural crest cells

Deletion of *Rac1* in the neural crest stem cells (NCSC) results in reduced cell proliferation in differentiated NCCs, but does not affect the migration of early NCSCs, suggesting a role of Rac1 during NCC maturation (Fuchs *et al.*, 2009). Embryos lacking in *Rac1* in NCC, using *Wnt1Cre*, have abnormal craniofacial development including a cleft palate at E12.5, as well as cardiovascular defects comprising defective remodelling of the PAA and septation of the cardiac OFT, resulting in a PTA (Thomas *et al.*, 2010). Confirming the conclusions from Fuchs *et al*, NCC migration was unaffected in *Rac1* mutants, however postmigratory NCCs showed increased cell death and attenuated proliferation, as well as a defect in smooth muscle differentiation (Thomas *et al.*, 2010). Hence, *Rac1* is not required for NCC migration but it is important for post-migratory NCC survival and differentiation in craniofacial and cardiovascular development (Thomas *et al.*, 2010).

1.8.6.3 Rac1 in valve development

Rho GTPase signalling acts to coordinate AV valve differentiation and morphogenesis (Gould *et al.*, 2016). Rac1 activity is almost absent in the early cushions but is increased substantially as the valve matures. Through gain/loss of function analysis, it was found that the Rac1 pathway is necessary to induce matrix compaction *in vitro* through increased cell adhesion, elongation, and stress fibre alignment. Additionally, cyclic mechanical signalling coordinates the RhoA to Rac1 signalling transition essential for proper embryonic mitral valve remodelling (Gould *et al.*, 2016).

1.8.6.4 Rac1 in cardiomyocytes

During the duration of this project, new publications have investigated the role of *Rac1* in cardiomyocyte populations and are discussed in detail in Chapter 3 (Abu-Issa, 2014; Leung *et al.*, 2014; Leung *et al.*, 2015). However, both Abu Issa and Leung and colleagues use conditional deletions of *Rac1* which include multiple cell types, leading to difficulties separating possible differential roles of Rac1 in specific cell types. Additionally, neither group have investigated the role of Rac1 in the formation of the trabeculae and subsequent development of the myocardium. And therefore the work presented in this thesis addresses this.

1.8.7 Rac1 in the adult heart

Rac1 was identified in a pathway-based genome-wide association analysis of coronary heart disease (de las Fuentes *et al.*, 2012). Additionally, *Rac1* mutations and elevated levels of Rac1 have been associated with types of CVD, including AF, in human patients (Adam *et al.*, 2007). In the adult mouse heart, Rac1 is known to regulate proliferation and migration of vascular SMCs, cardiomyocyte hypertrophy, and realignment of endothelial cells during cardiac pathology (Sawada *et al.*, 2010). Knockdown of *Rac1* in cultured cardiomyocytes, or cardiomyocyte specific deletion of *Rac1 in vivo,* using *MerCreMer*, reduced cardiomyocyte hypertrophy in response to angiotensin II (Hingtgen *et al.*, 2006; Satoh *et al.*, 2006). Overexpression of *Rac1* in the myocardium can cause severe cardiac hypertrophy, heart failure or AF in mice (Buscemi *et al.*, 2005; Adam *et al.*, 2007; Elnakish *et al.*, 2011; Elnakish *et al.*, 2012; Elnakish *et al.*, 2013a; Elnakish *et al.*, 2013b; Talukder *et al.*, 2013). This data suggests that *Rac1* is critical in the hypertrophic response in the adult heart.

1.8.8 Rac1 activators

The activation state of Rac1 depends on the release of GDP and the binding of GTP and this cycling is regulated by GEFs and GAPs. A number of GEFs and GAPs have been linked to Rac1 activity in the heart. GAP, G protein coupled receptor kinase interacting protein 1 (Git1), and GEF, Pak interacting exchange factor (betaPix) are both involved in Rho GTPase activation. Git1 and betaPix form a complex at the cell membrane and are thought to act as a scaffold to bring together proteins involved in cytoskeletal arrangement, cell adhesion and migration (Botrugno *et al.*, 2006). The Git1/betaPix complex is particularly located at focal adhesions where it promotes focal complex disassembly (Wilson *et al.*, 2014). Git1 is highly expressed in the mouse heart at P2-3 and betaPix is expressed in cardiomyocytes at E8.5, as well as being expressed in the mouse adult heart (Kim and Park, 2001; Pang *et al.*, 2011; Boczonadi *et al.*, 2014b). *Git1* knockout mice develop cardiac hypertrophy and subsequent heart failure, with increased cardiomyocyte apoptosis and defective cardiac maturation (Pang *et al.*, 2011). Little is known about betaPix/Rac1 interaction in cardiomyocytes, however other Rho GTPases have been shown to interact with

betaPix/Git1 in cardiomyocytes (Dickover *et al.*, 2014; Wilson *et al.*, 2014). In cardiomyocytes it is proposed that Rac1, Scrib and betaPix form a protein complex at the cell membrane, which is essential for early ventricular myocardial development (Boczonadi *et al.*, 2014b). FAK is a cytoplasmic tyrosine kinase that is activated and targeted to focal adhesions following cell attachment to ECM. FAK phosphorylates betaPix and enhances its binding to Rac1, which facilitates targeting of Rac1 to focal adhesions (Chang *et al.*, 2007). Cardiac specific deletion of *FAK* suggests an important role during heart development, particulary in OFT alignment (Hakim *et al.*, 2007). Affixin is an integrin-linked kinase-binding focal adhesion protein, which is highly expressed in skeletal and heart muscle. Affixin regulates cytoskeletal rearrangement by activating Rac1 through betaPix and alphaPix *in vitro* (Matsuda *et al.*, 2008) and activates Rac1 via betaPix in myoblasts in skeletal muscle (Matsuda *et al.*, 2008).

Vav2 is an exchange factor for Rho family GTPases and is ubiquitously expressed (Abe *et al.*, 2000). Vav2 is tyrosine phosphorylated upon VEGF treatment, which temporally correlates with Rac1 activation and requires VEGFR-2 signalling. Vav2 and Rac1 associate and form a complex after VEGF stimulation, to initiate lamellipodia formation and angiogenesis. Depleting endothelial cells of endogenous Vav2 with siRNA prevents VEGF-induced Rac1 activation, impairing endothelial cell migration (Garrett *et al.*, 2007).

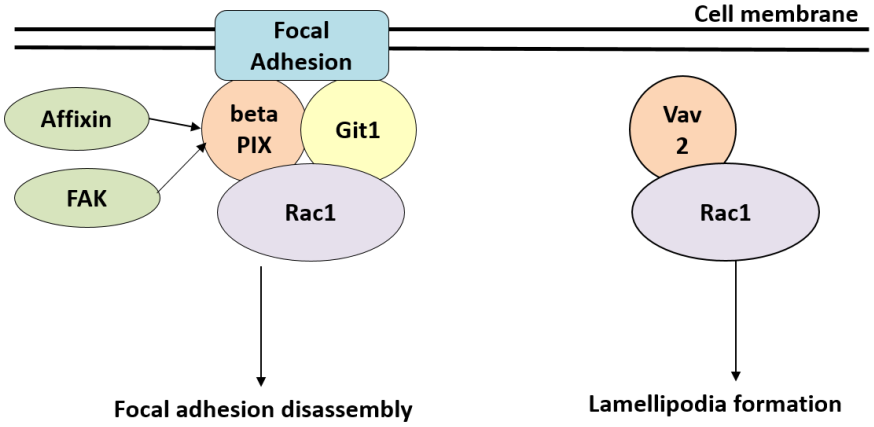

Figure 32: Rac1 Activators.
GEF betaPIX and GAP Git1 bind Rac1 at the cell membrane to initiate focal adhesion disassembly. Affixin and FAK both activate betaPIX and enhance its binding to Rac1. GEF Vav2 binds Rac1 to initiate lamellipodia formation leading to cell migration.

1.9 Aims and Objectives

The development of the myocardial wall requires proliferation and differentiation of FHF and SHF derived cardiomyocytes, as well as signals from epicardial cells and invasion of EPDCs. The role of *Rac1* in myocardial cells and epicardial cells during ventricular wall development has not been fully elucidated. Preliminary data suggested that deleting *Rac1* from the epicardium and myocardium, using *Gata5-Cre*, resulted in defects within the myocardial wall (personal communication from Dr Helen Phillips). Therefore, the aim of this thesis was to determine the role of *Rac1* within the epicardial and myocardial populations during ventricular development:

- Define the expression of Rac1 within the embyonic heart during development.
- Use the Cre-LoxP system to conditionally delete *Rac1* from myocardial and epicardial cells and determine the role of Rac1 in these populations.
    - Characterise myocardial and OFT defects due to deletion of *Rac1* in *Gata5-Cre*, *WT1-CreERT2*, *Mlc2v-Cre* and *TnT-Cre* Cre populations.
    - Investigate cellular processes associated with Rac1, including cell migration, proliferation, differentiation and polarity in the ventricular and OFT myocardium prior to the onset of defects.
    - Analyse expression of potential Rac1 interacting proteins in cardiomyocytes.
    - Define how the deletion of *Rac1* affects continued development and remodelling of ventricles and OFT during later stages of heart development.

1.10 Hypothesis

In the developing embryonic heart it is hypothesised that Rac1 is involved in epithelial and myocardial cell movements through cell polarity and cell organisation mechanisms which are crucial for the development of the complex structure of the myocardial wall.

Chapter 2. Materials and Methods

2.1 Statement of Ethics

Ethical approval of the animal work carried out in this study has been authorised by the Newcastle University Ethics Committee in compliance with Directive 2010/63/EU of the European Paliament and was covered by Project Licence PPL 70/7864 approved by the UK Home Office.

2.2 Materials

2.2.1 General

All reagents were purchased from Sigma Aldrich unless stated otherwise.

2.2.2 Animals

Mice were maintained in the Institute of Genetic Medicine animal facility according to the Animals (Scientific Procedures) Act 1986, United Kingdom. Wild type CD1 mice were supplied by Charles River. Several mouse lines were used to generate control and mutant embryos and are described briefly below.

2.2.2.1 Rac1^{flox}

Rac1^{flox} mice were generated by inserting *LoxP* sites flanking exons 4 and 5 of the *Rac1* gene. These *LoxP* sites are recombined by Cre recombinase, leading to a frame shift and as a result no functional Rac1 protein is produced (Walmsley *et al.*, 2003). *Rac1^{flox}* mice were maintained on the C57BL/6 background.

2.2.2.2 Reporter lines

The expression pattern of Cre was examined using either a *LacZ* or enhanced yellow fluorescent protein (*EYFP*) construct, introduced into the *Rosa26* locus. These constructs contain a transcriptional stop sequence flanked by *LoxP* sites, which is removed in the presence of Cre recombinase, therefore allowing the expression of the LacZ and EYFP constructs in these cells. *R26REYFP* reporter mice were crossed to *Rac1^{flox}* mice to allow for reporting of Cre activity in mutant embryos (Srinivas *et al.*, 2001). Recombination in *R26REYFP* embryos was visualised using GFP immunostaining. *R26RLacZ* mice were crossed to

TnT-Cre mice to allow for reporting of Cre activity. Cre activity was visualised by X-gal staining for the expression of the LacZ construct in the *R26RLacZ* allele.

2.2.2.3 TnT-Cre

Troponin-T (TnT)-Cre, gifted by Marina Campione, is a cardiomyocyte specific Cre line and drives Cre expression in cardiomyocytes by E7.5. An nls-Cre-hGH cassette was fused with the rat TnT promotor *(Jiao et al., 2003).*

2.2.2.4 Gata5-Cre

Gata5-Cre is a mouse line that drives Cre expression in epicardial cells and a subset of cardiomyocytes. A fragment of the Gata5 promoter was ligated to cDNA encoding phage P1 Cre-recombinase (Merki *et al.*, 2005).

2.2.2.5 Mlc2v-Cre

The *MLC2v* gene is expressed bilaterally in the embryo in the cardiac primordia from around E7.5 in the mouse and is restricted to ventricular precursors and ventricular tissue from the linear heart tube stage throughout the entire postnatal time window. *Mlc2v-Cre* is a knock-in Cre line that drives Cre expression in a subset of ventricular cardiomyocytes. *Mlc2v* exons 1 and 2 were removed and replaced by Cre recombinase cDNA (Chen *et al.*, 1998).

2.2.2.6 WT1-CreERT2

*Wilms Tumour (WT)1-CreERT*2 is tamoxifen inducible Cre line that drives Cre expression in epicardial cells. The targeting strategy removed exon 1 of WT1 (Zhou *et al.*, 2008).

2.3 Methods

2.3.1 General

All procedures were carried out at room temperature unless stated otherwise.

2.3.2 Timed Matings

Mouse matings were set up overnight and separated following successful mating, which was determined by the presence of a copulation plug. To allow embryonic staging, 12pm on the day of plug detection was assumed to be embryonic day (E) 0.5.

2.3.3 Substance injections

2.3.3.1 Tamoxifen Injections

Pregnant *Rac1*^{flox} female mice were given two consecutive intraperitoneal injections of 1mg tamoxifen. The tamoxifen was dissolved in 10µl 100% ethanol by shaking at 37° C and then added to 90µl of peanut oil (100µl total volume per injection).

2.3.3.2 BrdU injections

Pregnant *Rac1*^{flox} female mice were given one intraperitoneal injection of BrdU (25mg/ml). BrdU was dissolved in sterile water by shaking at 72° C.

2.3.4 Mouse Dissection

2.3.4.1 Embryo/embryonic heart dissection

At the required developmental stage (between E8.5 to E17.5) pregnant females where sacrificed by cerebral dislocation and embryos were dissected out into ice cold phosphate buffered saline (PBS), unless stated otherwise for individual protocols. PBS was prepared by adding 10 tablets (OXOID) to 1 litre of distilled water (dH_20) and was autoclaved before use. Embryo yolk sacs/limbs were collected for genotyping. Young embryonic hearts (E8.5-E12.5) were dissected by firstly removing the pericardium to reveal the heart and then by gently pulling the heart away from the embryo and snipping the outflow tract with forceps. Older embryonic hearts (E13.5-E17.5) were dissected by cutting open the thoracic cavity to reveal the heart and then pulling the heart and lungs away from the embryos by holding onto the lungs with forceps. The lung lobes were then removed leaving the heart intact. Hearts were then rinsed in PBS.

2.3.4.2 Neonatal and adult heart dissection

At the required age, neonates and adults were sacrificed by cervical dislocation. After cervical dislocation, adult hearts were injected with 1M potassium chloride into the left atrium causing diastolic arrest. Hearts were then dissected out as for older embryonic hearts and rinsed in PBS.

2.3.4.3 Somite matching

Embryos were somite counted and matched within 3 somites for all experiments. The somite ranges for the relevant stages are shown in Table 5.

Age	Somite number range	Volume of Lysis Buffer (µl) (type of sample)
E8.5	8-12	50 (yolk sac)
E9.5	21-29	50 (yolk sac)
E10.5	35-39	100 (yolk sac)
E11.5	45-47	100 (yolk sac)
E12.5	-	200 (limb)
E13.5	-	200 (limb)
E15.5	-	400 (limb)
E17.5	-	400 (limb)
P0	-	400 (limb)

Table 5: Somite ranges for stages of embryonic development including the type of sample taken for genotyping and volume of lysis buffer used.

2.3.5 Genotyping of Mice

For identification of transgenic adult mice and embryos, ear notches and embryo limbs/yolk sacs were taken respectively and subjected to DNA extraction followed by polymerase chain reaction (PCR) to amplify target genomic regions.

2.3.5.1 DNA lysis

DNA extraction of adult mouse ear Notches was carried out using the 'hot shot DNA lysis method'. Ear Notches were added to 75µl of 25mM sodium hydroxide, 0.2mM ethylenediamine tetra-acetic acid (EDTA), pH 12 and heated at 95˚C for 30 minutes. The lysed solution was then cooled to 4˚C for 10 minutes and neutralised by the addition 75µl 40 mM Tris-HCl pH 5. Samples were vortexed and centrifuged for 2 minutes at 1500rpm. 2-4µl of each genomic DNA sample was used in genotyping PCR reactions.

DNA extraction of embryo samples was carried out using proteinase K digestion. The lysis buffer was prepared by diluting proteinase K to a final concentration of 600 µg/ml in proteinase K buffer (50 mM potassium chloride (KCl), 1.5mM magnesium chloride (MgCl2), 10 mM Trizma base (tris) pH 8.5, 0.45% v/v Igepal® CA-630, 0.45% v/v Tween-20). This was added to the samples and incubated at 56°C for 2 hours, or until the sample had completely

lysed. The samples were vortexed intermittently to ensure complete breakdown of the tissues and release of the DNA. Proteinase K was heat inactivated by incubating at 95°C for 10 minutes. The lysed sample was centrifuged at 13,000rpm full speed for 1 minute to collect any debris and stored at 4°C until use. The sample type and volume of lysis buffer was dependent on the age of the embryos and are detailed in Table 5.

2.3.5.2 Polymerase Chain Reaction

PCR was carried out using GoTaq DNA polymerase (Promega). Primers were designed and optimised previously; primer sequences are listed in Table 6. Each reaction was prepared for PCR in 0.2ml PCR tubes (Thermo) as described in Table 7. PCR was carried out on a SensoQuest thermo cycler. Briefly, the temperature program consisted of an initial denaturising step at 94°C for 2 minutes, followed by 35 cycles of; 94°C, annealing temperature, and 72°C, followed by an extension step at 72°C for 10 min.The samples were held at 4°C before use. The annealing temperatures and cycling times were specific to primer sequences as detailed in Table 7.

Gene	Primer	Sequence (5' to 3')	Product size (bp)
Rac1	Rac1 1	ATT TTG TGC CAA GGA CAG TGA CAA GCT	333bp (flox) 300bp (WT)
	Rac1 2	GAA GGA GAA GAA GCT GAC TCC CAT C	
	Rac1 3	CAG CCA CAG GCA ATG ACA GAT GTT C	
EYFP	EYFP 316	GGA GCG GGA GAA ATG GAT ATG	320bp (flox) 600bp (WT)
	EYFP 883	AAA GTC GCT CTG AGT TGT TAT	
	EYFP 4982	AAG ACC GCG AAG AGT TTG TC	
Cre	S1X Cre A	GCA TAA CCA GTG AAA CAG CAT TGC TG	280bp
	S1X Cre B	GGA CAT GTT CAG GGA TCG CCA GGC G	

Table 6: Genotyping PCR primer sequences and product sizes for Rac1, EYFP and Cre.

Gene	Reaction	PCR cycling conditions
Rac1	1µl 10µM Rac1 1 1µl 10µM Rac1 2 1µl 10µM Rac1 3 0.25µl 25mM dNTP 4µl 5x buffer 0.5µl MgCl2 0.1µl taq polymerase 8.15µl dH2O 4µl sample	1. 94˚C - 4 minutes 2. 94˚C - 30 seconds 3. 60˚C - 30 seconds 4. 72˚C - 30 seconds 5. 72˚C - 10 minutes Held at 4˚C Cycling 4-2 x35
EYFP	1µl 10µM EYFP 1 1µl 10µM EYFP 2 1µl 10µM EYFP 3 0.25µl 25mM dNTP 4µl 5x buffer 0.1µl taq polymerase 10.65µl dH2O 2µl sample	94˚C - 3 minutes 94˚C - 30 seconds 58˚C - 1 minute 72˚C - 1 minute 72˚C - 10 minutes Held at 4˚C Cycling 4-2 x35
Cre	1µl 10µM S1XA 1µl 10µM S1XB 0.25µl 25mM dNTP 4µl 5x buffer 0.1µl taq polymerase 11.65µl dH2O 2µl sample	1. 95˚C - 2 minutes 2. 95˚C - 30 seconds 3. 55˚C - 30 seconds 4. 72˚C - 30 seconds 5. 72˚C - 10 minutes Held at 4˚C Cycling 4-2 x35

Table 7: Genotyping PCR reaction set up and cycling conditions for Rac1, EYFP and Cre.

2.3.5.3 Agarose gel electrophoresis

Following PCR, 10µl of each sample was ran on a 2% agarose gel made using agarose (NBS biologicals) and TAE buffer (40mM Tris, 20mM acetic acid, and 1mM EDTA) with 0.5µg/ml ethidium bromide. A 100bp DNA ladder (Promega) was ran alongside samples to determine PCR product sizes. Gel Electrophoresis was carried out in TAE buffer typically maintained at 125 volts for 30 minutes. The gel was visualised using a UVP transluminator and the image captured.

2.3.6 Processing of Embryos/Hearts

2.3.6.1 Paraffin Wax Embedding

Embryos/hearts were washed in PBS then fixed in 4% paraformaldehyde (PFA) in PBS, washed in PBS and dehydrated in an ethanol series. Tissues were then transferred to glass vials and shaken in histoclear before an equal volume of wax (VWR) was added and maintained at 60°C. Embryos/hearts were then

placed in paraffin wax moulds and heated forceps were used for positioning in the correct orientation for transverse sectioning. Timings for each step vary according to embryo/heart size and are listed in Table 8.

2.3.6.2 Wax sections

Wax embedded embryos and hearts were sectioned transversely at a thickness of 8µm using a rotary microtome. Serial or sister sections were placed on water-covered histobond positively charged slides (Merienfeld) at 37°C and allowed to expand and dry. Slides were then placed in an oven to dry overnight at 37°C.

2.3.6.3 Cryoembedding

Following dissection, hearts/embryos were shaken in ice cold sucrose at 4˚C to remove water and prevent tissue damage during freezing; 15% sucrose in PBS until hearts/embryos had sunk then 30% sucrose in PBS until hearts/embryos had sunk. The hearts were placed in plastic wells and the sucrose was removed by pipetting. The hearts were then covered in O.C.T embedding medium (Cell Path) and snap frozen on dry ice. Cryoembedded hearts were stored at -80˚C.

2.3.6.4 Cryosections

10µm serial or sister sections were sliced using a Leica cryostat and placed onto histobond positively charged glass slides. The sections were allowed to air dry for 1 hour, after which they were wrapped in tin foil and stored at -80°C or used immediately.

	E9.5	E10.5/embryonic hearts	E11.5	E12.5	E13.5	E14.5	E15.5	E16.5	E17.5	P0/adult hearts
4% PFA at 4˚C	1 night	1 night	1 night	1 night	1 nights	2 nights	2 nights	5 nights	5 nights	5 nights
Wash PBS	5 mins (x2)	5 mins (x2)	5 mins (x2)	5 mins (x2)	5 mins (x2)	5 mins (x2)	5 mins (x2)	5 mins (x2)	5 mins (x2)	5 mins (x2)
50% EtOH (shaking)	30 mins	30 mins	1 hour	2 hours	2 hours	3 hours	3 hours	4 hours	5 hours	6 hours
70% EtOH (shaking)	30 mins (x2)	30 mins (x2)	1 hour (x2)	2 hours (x2)	2 hours (x2)	3 hours (x2)	3 hours (x2)	4 hours, O/N	5 hours, O/N	6 hours, O/N
95% EtOH (shaking)	30 mins	30 mins	1 hour	2 hours	2 hours	3 hours	3 hours	4 hours	5 hours	6 hours
100% EtOH (shaking)	30 mins (x2)	30 mins, 1 hour	1 hour (x2)	2 hours, O/N	2 hours, O/N	3 hours, O/N	3 hours, O/N	4 hours, O/N	5 hours, O/N (x2)	6 hours, O/N (x2)
Histoclear (shaking)	10 mins (x2)	15 mins (x2)	20 mins (x2)	20 mins (x2)	20 mins (x2)	20 mins (x2)	30 mins (x2)	1 hour (x2)	1 hour (x2)	1 hour (x2)
Histoclear / Wax (60˚C)	15 mins	20 mins	20 mins	30 mins	30 mins	1 hour	1 hour	1 hour	2 hours	2 hours
Wax (60˚C)	20 mins (x3)	30 mins (x3)	40 mins (x3)	1 hour (x3)	1 hour (x3)	1 hour (x4)	1 hour (x4)	1 hour (x4), O/N	2 hours (x4), O/N	2 hours (x4) O/N)

Table 8: Processing timings for embedding embryos/hearts in paraffin wax.
PFA, paraformaldehyde; PBS, phosphate buffered saline.

2.3.7 Histology staining

For all histology stains paraffin sections were first treated as follows; paraffin sections were dewaxed in Histoclear (National Diagnostics) for 10 minutes, twice. The sections were then incubated in 100% ethanol for 3 minutes, twice, followed by rehydration through ethanol series (90%, 70% and 50% EtOH, 2 minutes each) and equilibrated in dH_20 for 2 minutes.

2.3.7.1 Haematoxylin and eosin staining

Haematoxylin and eosin staining was used to identify changes in heart morphology in the mutant embryos. Haematoxylin stains the cell nuclei purple, while eosin stains the cytoplasm pink.

After equilibration in dH_20 the sections were stained in Harris' haematoxylin solution for 5-10 minutes. Excess haematoxylin was washed away with running water for 5 minutes. Slides were then dipped in an acid alcohol solution (1% v/v hydrochloric acid (HCl), 70% ethanol) to remove the stain from all tissues except the nucleus and returned to the running water for a further 5 minutes. The slides were then incubated in eosin (Fisher Scientific) for 5 minutes, rinsed in running water and dehydrated by dipping in 50%, 70% and 90% ethanol. Following this, the slides were transferred to 100% ethanol for 3 minutes, twice, and incubated twice in Histoclear for 10 minutes. Slides were mounted in Histomount (National Diagnostics) and dried overnight. Sections were imaged using a Zeiss Axioplan2 microscope and associated Axiovision SE64 software.

2.3.7.2 Alcian blue staining

After equilibration in dH_20 the sections were stained in Alcian blue solution for 30 minutes. Excess alcian blue was washed away with running water for 1 minute. The slides were then incubated in nuclear fast red for 5 minutes. Excess solution was removed by rinsing in running water for 1 minute, followed by dehydration through an ethanol series (50%, 70%, 90%, and 100%, twice). The slides were then incubated twice in Histoclear for 10 minutes and mounted in Histomount and dried overnight. Sections were imaged using a Zeiss Axioplan2 microscope and associated Axiovision SE64 software.

2.3.7.3 Sirius red Staining

After equilibration in dH_20 the sections were incubated in 0.2% phosphomolybolic acid for 5 minutes. Slides were then rinsed in dH_20, twice, followed by staining in picro-sirius red for 2 hours. Slides were then rinsed, first in 0.01% HCl and then dH_20 followed by dehydration through an ethanol series (50%, 70%, 90%, and 100%, twice). The slides were then incubated twice in Histoclear for 10 minutes and mounted in Histomount and dried overnight.

2.3.7.4 Millers elastin Staining

After equilibration in dH_20 the sections were stained in Millers stain for 1 hour. Slides were then rinsed in dH_20 before incubation in 3 % ferric chloride for 10 mins. Slides were then rinsed again in dH_2 before a 5 minute incubation in Eosin. Slides were rinsed for a final time in dH_20 rinse followed by dehydration through an ethanol series (50%, 70%, 90%, and 100%, twice). The slides were then incubated twice in Histoclear for 10 minutes and mounted in Histomount and dried overnight.

2.3.7.5 Toluidine blue Staining

After equilibration in dH_20 the sections were stained in toluidine blue working solution (10% stock solution [1% toluidine blue O in 70% EtOH] in 1% NaCl pH2.0-2.5) for 2-3 minutes. After staining slides were washed in dH_20, three times then dehydrated quickly through 95% and 2 changes of 100% ethanol. The slides were then incubated twice in Histoclear for 10 minutes and mounted in Histomount and dried overnight.

2.3.7.6 β-galactosidase staining

For whole mount β-galactosidase staining, embryos were dissected and washed in ice-cold PBS followed by a light fixation in 4% PFA at 4˚C. The length of fixation was dependent on the size of the embryo; 5 minutes for E8.5-E9.5, 15 minutes for E10.5-E12.5 and 40 minutes for E15.5 hearts. After fixation, embryos were washed in PBS for 5 mins, three times. Embryos/hearts were incubated in x-gal staining solution (0.1% w/v X-Gal, 5 mM potassium ferricyanide, 5 mM potassium ferrocyanide, 2 mM MgCl2, 0.02% Igepal® CA-630, 0.01% sodium deoxycholate, 0.02 M Tris pH 7.3) in the dark, shaking at 37˚C for 4 hours to overnight. Once the stain had developed fully, the X-gal

staining solution was removed and embryos/hearts were washed in PBS, three times, and fixed in 4% PFA overnight at 4˚C. Following fixation, embryos were washed in PBS, photographed and dehydrated for normal wax embedding.

2.3.8 Immunostaining

2.3.8.1 Immuno-fluorescent (IF) staining of wax sections

Paraffin sections were dewaxed in Histoclear (National Diagnostics) (10 minutes, twice), rehydrated in an ethanol series (100%, 90%, 70% and 50% EtOH – 5 minutes each) and equilibrated in PBS for 5 minutes. Antigen retrieval was carried out using 1M citrate buffer (pH 6); sections were boiled in citrate buffer in a pressure cooker for 5 minutes, cooled for 20 minutes then rinsed in dH_20. Non-specific epitope binding was blocked by incubation of the sections in 10% foetal calf serum (FCS) in Tris buffered saline with 0.3% triton x (TBS-Tx) for 30 minutes. TBS-Tx, (Tris HCl, 0.2M NaCl, 0.3% Triton X, pH7.5) was prepared freshly. Primary antibodies were diluted in 2% FCS in TBS-Tx. Dilutions are listed in Table 9. 100µl was added to each slide and covered with parafilm (Fisher Scientific). Slides were then placed in a humidified chamber and incubated at 4°C overnight.

Sections were washed in TBS-Tx (5 minutes, 3 times). Fluorescently-conjugated secondary antibodies (listed in Table 10) were diluted 1:200 in TBS-Tx then 100µl was added to each slide and covered with parafilm (ThermoFisher Scientific). Slides were then placed in a dark humidified chamber and incubated at room temperature for 1 to 2 hours. Slides were then washed in TBS-Tx (5 minutes, 3 times) in the dark, mounted in Vectashield with DAPI with a glass coverslip (Cell Path) and left at 4°C overnight before viewing. Sections were imaged using either a Zeiss AxioImager or a Nikon Confocal microscope with associated Axiovision SE64 or Nikon Elements software, respectively.

2.3.8.2 Immunohistochemistry (IHC) staining of wax sections

Paraffin sections were initially treated as for fluorescence staining except endogenous peroxidise activity was inhibited using 3% H_2O_2 for 10 minutes after antigen retrieval, followed by additional washing in dH_20. Slides were incubated with biotinylated secondary antibodies (listed in Table 10) and then washed in

TBS-Tx (5 minutes, 3 times) before AB complex (VectorStain) was added for 30 minutes (250µl per slide). Slides were then washed in TBS-Tx (5 minutes, 3 times) before Diaminobenzine (DAB) was added until brown staining was observed, when the reaction was discontinued by placing in PBS. Slides were then counterstained in 0.5% methyl green for 10 minutes and washed in H_20 (2 times 5-10 dips, then 20-30 seconds) and butanol (2 times 2-5 dips, then 15-20 seconds). Slides were then placed in Histoclear (10 mins, twice), before mounting in Histomount and were left overnight to dry. Sections were imaged using a Zeiss Axioplan2 microscope and associated Axiovision SE64 software.

2.3.8.3 Signal amplification - Tyramide Signal Amplification (TSA)

Tyramide Signal Amplification (TSA) kit (PerkinEkmer) was used as per manufacturer's protocol for antibodies listed in Table 9. Briefly, slides were dewaxed, rehydrated, antigen retrieval and washed as for fluorescent staining (Chapter 2 Section 2.3.8.1) and then TSA-IF protocol was followed. Slides were blocked in TNB blocking buffer (0.1M Tris-HCl pH7.5, 0.15M NaCl, 0.5% Blocking reagent) for 30 mins. Primary antibodies were diluted in TNB buffer, dilutions listed in Table 9.100µl was added to each slide and covered with parafilm (Fisher Scientific). Slides were then placed in a humidified chamber and incubated at 4°C overnight. Sections were washed in TBS-Tx (3 times, 5 minutes). Biotinylated secondary antibodies (listed in Table 10) were diluted 1:300 in TNB then 100µl was added to each slide and covered with parafilm (Fisher Scientific). Slides were placed in a humidified chamber and incubated at room temperature for 1 hour. Following antibody incubation, slides were then washed in TBS-Tx (5 minutes, 3 times). Streptavidin-HRP diluted in TNB buffer 1:100, 100µl was added to each slide and covered with parafilm and incubated at room temperature for 30 minutes. Sections were washed again in TBS-Tx (5 minutes, 3 times), before Cyanide 3 Tyramide, diluted 1:50 in amplification diluent, was added to the slides. Slides were covered in parafilm and left in the dark for 10 mins. Slides were then washed a final time in TBS-Tx in the dark (5 minutes, 3 times), then mounted in Vectashield with DAPI with a glass coverslip (Cell Path) and left at 4°C overnight before viewing. Sections were imaged using either a Zeiss AxioImager or a Nikon Confocal microscope with associated Axiovision SE64 or Nikon Elements software, respectively.

2.3.8.4 Alternative antigen retrieval methods

Anti-α-SMA staining did not require antigen retrieval as stated in Table 9.

Anti-CD31 staining required proteinase K antigen retrieval as stated in Table 9. Following the 5 minutes PBS wash, 400µl Proteinase K (20µg/ml) in TE buffer was added to each slide and incubated for 30 minutes. The slides were then washed and then TSA-IF protocol was followed as described above in Chapter 2 Section 2.3.8.3.

2.3.8.4 Immuno-fluorescent staining of cryosections

Frozen sections were thawed to room temperature before fixation in 4% PFA for 10 minutes. Sections were then washed in PBS (5 minutes, twice), treated with detergent (0.5% Triton X in PBS, 10 minutes) before being washed again in PBS (5 minutes, twice). Slides were then treated as for wax sections (as described in Chapter 2 Section 2.3.8.1).

Primary Antibodies	**Supplier/Order number**	**Dilution**	**Targets**	**Method**
Mouse anti- α -actinin	GeneTex/GTX103219	1:500	Cardiomyocytes	IF
Rabbit anti-cardiac-actin	GeneTex/GTX101876	1:200	Cardiomyocytes	IF
Rabbit anti-ANF	Source BioSci/ GTX112698S	1:200	Trabeculae cardiomyocytes	IF
Mouse anti- α -smooth muscle actin	Sigma Aldrich /A5228	1:500	Cardiac smooth muscle cells	IHC (No antigen retrieval), IF
Mouse anti- β -catenin	BD Bioscience/ 610153	1:200	Adherens junctions	IF
Rat anti-BrdU	Abcam/Ab6326	1:200	Proliferating cells	IF
Rabbit anti-Ccn1	Santa Cruz/ Sc-13100	1:100	ECM	IF
Rat anti-CD31	BD Biosciences/ 553370	1: 300	Endothelial cells	IF (Proteinase K antigen retrieval, TSA)
Rabbit anti-cleaved caspase 3	Cell Signalling/ 9661	1: 100	Apoptosis	IF (TSA)
Goat anti-Cx-40	Santa Cruz sc-20466	1:50	Adherens junctions	IF
Rabbit anti-Cx-43	Sigma/C6219	1:100	Adherens junctions	IF
Rabbit anti-Delta4	Santa Cruz/sc-28915	1:100	Endothelial cells	IF

Rabbit anti-Desmin	Millipore 04-585	1:100	Desmosomes	IF
Mouse anti-E-cadherin	BD transduction/610181	1:100	Adherens junctions	IF
Rabbit anti-ENAH	Abcam/Ab124685	1:400	Rac1 interactor	IF
Rabbit anti-ERG	Abcam/Ab92513	1:1000	Endothelial cells	IF
Rat anti-endomucin	Santa Cruz/sc-65495	1:300	Endocardial cells	IF
Rabbit anti-FAK	Abcam/ab40794	1:100	Endocardial cell focal adhesions	IF
Mouse anti-fibronectin	Santa Cruz/sc8422	1:20	ECM	IF
Chicken anti-GFP	Abcam/Ab13970	1: 100	EYFP	IF,
Rabbit anti-GFP	Torrey Pines/TP401	1:100	EYFP	IHC
Mouse anti-Islet1	Hybridoma	1:5	SHF cells	IF
Rabbit anti-laminin	Sigma/L9393	1:50	ECM basement membrane	IF
Mouse anti-MF20	Dev Hyb Bank/1-2/21/13	1: 500	Cardiomyocytes	IF, IN+HC
Rabbit anti-N1ICD	Cell signalling/4147	1:400	Activated Notch	IF (TSA)
Mouse anti- Neuropilin 1	Sigma/PA5-23306	1:100	Endocardial signalling	IF
Mouse anti-NfatC1	BD Bioscience/556602	1:500	Endocardial signalling	IF
Mouse anti- N-cadherin	BD Bioscience/ 610920	1: 200	Adherens junctions	IF
Rabbit anti-phHH3	Millipore/06-570	1: 300	Proliferating cells	IF
Rabbit anti-PKCz	Santa Cruz sc-216	1:100	Apical Membrane	IF
Goat anti-scrib	Santa Cruz/ sc-11049	1:100	PCP signalling	IF
Rabbit anti- Sema3a	Abcam/Ab23393	1:100	Endocardial signalling	IF
Goat anti-Sfrp1	Abcam/Ab110113	1:100	ECM	IF
Rabbit Anti-SM22 α	Abcam/ab14106	1:200	Smooth muscle cells	IF
Goat anti-troponin I	Hytest	1:100	Cardiomyocytes	IF
Rabbit anti-acetylated tubulin	Sigma/ T6793	1:500	MTOC	IF
Rabbit anti-gamma-tubulin	Sigma/ T6557	1:100	MTOC	IF
Goat Anti-Vav2	Santa Cruz/Sc-8586	1:200	Rac1 interactor	IF
Rat anti-VE-cadherin	BD Bioscience/555289	1:50	Endocardial cell adherens junctions	IF (TSA)
Mouse anti-VEGFA	ThermoFisher//MA1 16629	1:100	VEGF signalling	IF
Rabbit anti-VEGFR2	ThermoFisher	1:100	VEGF signalling	IF

	/MA515157			
Chicken anti – Vimentin	Abcam/Ab24525	1: 100	Fibroblasts	IF
WGA 594 conjugate	ThermoFisher/ W11262	1:200	Binds to sialic acid and *N*-acetylglucosaminyl residues in cell and nuclear membranes	IF
Rabbit anti-ZO1	Abcam/ab59720	1:100	Tight junctions	IF

Table 9: Primary antibodies for immunostainng. All on paraffin sections unless otherwise stated.

Secondary Antibodies	Supplier/Order number	Animal raised in	Dilution
Alexa Fluor 594 anti-rabbit	Life Technologies/ A11012	Donkey	1 in 200
Alexa Fluor 594 anti-mouse	Life Technologies /A21203	Donkey	1 in 200
Alexa Fluor 594 anti-goat	Life Technologies /A11058	Donkey	1 in 200
Alexa Fluor 594 anti-chicken	Life Technologies /A11042	Goat	1 in 200
Alexa Fluor 488 anti-mouse	Life Technologies / A21201	Donkey	1 in 200
Alexa Fluor 488 anti-rabbit	Life Technologies/ A21201	Goat	1 in 200
Alexa Fluor 488 anti-rat	Life Technologies / A21208	Donkey	1 in 200
Alexa Fluor 488 anti-goat	Life Technologies /A11055	Donkey	1 in 200
anti-mouse biotinylated	Dako Denmark/E0354	Rabbit	1 in 300
anti-rabbit biotinylated	Dako Denmark/ E0432	Goat	1 in 300
anti-rat biotinylated	Dako Denmark E0	Rabbit	1 in 300

Table 10: Secondary antibodies for immunostaining.

2.3.9 RNA Isolation from hearts

2.3.9.1 Tissue collection

Embryonic, neonatal and adult hearts were dissected as described in Chapter 2 Section 2.3.4 using diethylpyrocarbonate (DEPC)-treated PBS and RNase free plastic wear and instruments. Hearts were transferred to RNase free eppendorf tubes, snap frozen in liquid nitrogen and stored at -80˚C.

2.3.9.2 RNA extraction

Hearts were allowed to thaw on ice before RNA extraction using the TRIzol® Plus RNA Purification System (Ambion) or Reliaprep RNA tissue miniprep system (Promega). The manufacturer's protocols were followed for both kits and are briefy described below.

The TRIzol® Plus RNA Purification System was used for RNA extraction of wild type hearts. Hearts were pooled as per Table 11. The heart tissue was homogenised in 500µl Trizol using a 2ml syringe with 21G and 27G needles. 0.2

volumes of chloroform were added and the sample was shaken vigorously by hand, then incubated at room temperature for 2-3 minutes. Samples were centrifuged at 12,000 x g for 15 minutes at 4°C to allow phase separation of the samples components. 200µl of the upper aqueous phase, containing nucleic acids, was transferred to a fresh tube and an equal volume of RNase-free 70% ethanol added. The samples were mixed and then transferred to a PureLink™ RNA mini kit spin column (Life Technologies) and centrifuged for 15 seconds at full speed to allow binding of RNA to the column. The spin column was washed once in the supplied wash buffer 1 before on-column DNaseI treatment to remove any genomic DNA within the sample. 10 units of DNaseI were diluted in 1x DNase buffer in DEPC-H2O to a total volume of 80 µl for each sample. The DNaseI mix was added to the spin column and incubated for 15 minutes at room temperature. The column was then washed again in wash buffer 1, followed by multiple washes in wash buffer 2 (contains ethanol). RNA was eluted in 30µl of the supplied RNase free water, by centrifugation at 13,000rpm for 2 minute, and stored at -80°C.

Embryo stage	No. of hearts pooled
E10.5	5
E13.5	3
E15.5	2
E17.5	2

Table 11: Number of embryonic hearts pooled for RNA extraction at each stages.

The Reliaprep RNA tissue miniprep system was used for RNA extraction of control and *Rac1*^{TnTCre} hearts. 100µl LBA buffer containing 1-Thioglycerol was added to E10.5 hearts and homogenisation was carried out by pipetting 7–10 times using a P200 pipettor. The homogenates were then centrifuged for 3 minutes at 13,000rpm and the supernatant was transferred to a clean tube. 34µl Isopropanol was added to the supernatant and the mixture was vortexed and then added to a ReliaPrep™ minicolumn inside a collection tube. The tube was centrifuged at 13,000rmp for 1 minute. The flowthrough was discarded and 500µl of RNA Wash Solution was added to the Minicolumn and centrifuged at 13,000rpm for 30 seconds. The flowthrough was again discarded and 30µl of DNase I mix was added to the Minicolumn membrane and incubated for 15

minutes. 200µl of Column Wash Solution (with ethanol) was added to the Minicolumn and centrifuged at 13,000 rpm for 15 seconds. 500µl of RNA Wash Solution (with ethanol) was then added and centrifuged at 13,000rpm for 30 seconds. The collection tube was discarded and the ReliaPrep™ Minicolumn was placed into a new collection tube. 300µl of RNA Wash Solution was added and the tube was centrifuged at high speed for 2 minutes. The ReliaPrep™ Minicolumn was then transferred to an Elution Tube. RNA was eluted in 15µl of Nuclease-Free Water, by centrifugation at 13,000rpm for 1 minute and stored at –80°C.

2.3.9.3 RNA quantification and quality assessment

Quantification of RNA samples was carried out using a NanoDrop spectrophotometer (Thermo Scientific). The NanoDrop channels were blanked using elution buffer and 1 µl of each sample was loaded onto the pedestals. Quantifications were given in ng/µl and quality was judged based on the absorbance at 260 nm divided by absorbance at 280 nm (260/280 value). A 260/280 value of 2.0 is considered high quality RNA. Quality was also tested by running the samples on a 1% agarose gel at 200 V for 15 minutes. Total RNA was then used to synthesise complementary DNA (cDNA).

2.3.10 cDNA synthesis

cDNA was produced from 1 µg of RNA using the high capacity cDNA reverse transcription kit (Invitrogen) according to the manufacturer's instruction. A 40 µl cDNA synthesis reaction contained: 1µg RNA, 1 x Reverse transcriptase buffer, 1 mM each dNTP, 1 x random primers and 100 units reverse transcriptase. The cDNA synthesis reaction was carried out in a thermocycler with the following cycling conditions: 25˚C for 10 minutes, 37˚C for 2 hours, 85˚C for 5 minutes, 4˚C for 10 minutes. Synthesized cDNA was stored at -20°C until required.

2.3.11 Semi-quantitative PCR

Semi-quantitative reverse transcriptase (RT)-PCR was carried out using primers listed in Table 12. The same reaction mix and PCR conditions were used for all genes and are listed in Table 13. The number of PCR cycles was selected such that both the target gene and housekeeping gene PCR amplification product was clearly visible on an agarose gel and could be quantified. Therefore, the

amplification needed to be in the exponential range but not yet at the reaction plateau.

Band intensities were analysed in Image J software. Target gene values were normalised to Glyceraldehyde 3-phosphate dehydrogenase (GAPDH) values for each individual sample.

Gene	Primer sequence	Product size (bp)	Reference
Rac1	CCC AAT ACT CCT ATC ATC CTC G	258	(Wells *et al.*, 2004)
	CAG CAG GCA TTT TCT CTT CC		
Rac2	CCA GCA CCC CCA TCA TCC TGG	248	(Wells *et al.*, 2004)
	GGG GCG CTT CTG CTG TCG TGT G		
Rac3	CAC ACA CCC ATC CTT CTG GTG	253	(Wells *et al.*, 2004)
	CAG TGC ACT TCT TGC CTG GC		
HOP	CGG GAC AGA CGT AAG GTC A	876	(Grego-Bessa *et al.*, 2007)
	TCA ACC ACC AGT GTG TTT AGT GAA		
PEG1	TGC TCC CTT CCG GCC CAA	627	(Grego-Bessa *et al.*, 2007)
	TCT GAA CAG CCA GCG GGA TGC		
Irx5	CCA CTC GCC ACC GCC ACC T	304	(Grego-Bessa *et al.*, 2007)
	GCC ATA GTT CGT GTA GCC CGG ATA		

Table 12: Primers used for semi-quantitative PCR.

Reaction (20µl)	PCR cycling conditions
1µl 10µM forward and reverse primer mix **0.25µl 25mM dNTP** **4µl 5x buffer** **0.1µl taq polymerase** **8.15µl dH2O** **2µl cDNA (100ng)**	1. 94˚C - 4 minutes 2. 94˚C - 30 seconds 3. 60˚C - 30 seconds 4. 72˚C - 1 minute (Cycling 2-4 x25) 5. 72˚C - 10 minutes Held at 4˚C

Table 13: Reaction and cycling conditions for semi-quantitative PCR.

2.3.12 Quantitative Real Time PCR (qPCR)

2.3.12.1 Primer Design for qPCR

Gene sequences were taken from the mouse database in ensembl. Primers were designed using Primer3 and Primer-BLAST according to parameters listed in Table 14.

2.3.12.2 Quantitative Real Time PCR

qPCR was carried out using SYBR Green Jumpstart Taq readymix kit (Sigma) or SYBR® Select Master Mix (Life Technologies). For both mixes, 10ng of cDNA was included in a 10µl reaction mix consisting of 1x SYBR green/select,

0.1x reference dye and 1µM primers (listed in Table 15) and remaining volume dH_20. Samples were prepared in triplicate with water controls for each gene of interest. GAPDH was used as a housekeeping gene after determining consistent expression throughout embryonic heart development.

For wild type gene expression analysis, quantitative real time PCR was carried out on at 7900HT Fast Real Time PCR system (Applied Biosystems) using SDS v2.4.1 software. The temperature program for the 7900HT instrument was as follows; 95˚C for 15 minutes, followed by 40 PCR cycles of; 95˚C for 30s (100% ramp rate), 60˚C for 30s (100% ramp rate) and 72˚C for 30s (100% ramp rate). This was followed by a melt curve of 80˚C for 10s (100% ramp rate), 68˚C for 10s (100% ramp rate) then to 99˚C (2% ramp rate). For expression analysis in control and *Rac1*^{TnTCre} hearts, a Quant Studio 7 (Life Technologies) system was used with Quant Studio 7 analysis software. The temperature program for the Quant Studio 7 was 95˚C for 20s (1.9˚C/s ramp rate), PCR cycling of 95˚C for 1s (1.9˚C/s ramp rate) and 60˚C for 20s (1.6˚C/s ramp rate), 40 times. This was followed by a melt curve of 95˚C for 15s (1.9˚C/s ramp rate), 60˚C for 1 minute (1.6˚C/s ramp rate) then to 95˚C for 15s (0.05˚C/s ramp rate). For both instruments the samples were added to 384 well plates (Greiner Bio One/Life Technologies).

Variable	Parameters
Primer length (bp)	18-22bp
Primer melting temperature (Tm)	Min: 57°C, Max: 70°C, Optimum: 60°C
Max Tm difference	1°C between primers
Primer GC content	40-60%
Primer details	No hairpin loops or secondary structures predicted using Sigma online software.
	No more than three contiguous nucleotides with the same base or repeats of sequences of three or more bases.
PCR product size	50-200bp
Exon junction span	Primer must span an exon-exon junction
Database	Refseq RNA (refseq_rna)
Organism	Mus musculus (taxid: 10090)
Splice variant handling	Allow primer to amplify

Table 14: Parameters for designing qPCR primers.

Gene	Primer sequence (5' to 3')	Product size (bp)	Spanning exons	Primer efficiency (%)
Gapdh **(Dr Simon Bamforth)**	TGTGCAGTGCCAGCCTCGTC	80	2-3	98.3
	TGACCAGGCGCCCAATACGG			
Rac1	AGGGATGATAAGGACACCAT	121	5-6	97.8
	GAGCTGAGCACTCCAGGTAT			
Rac1 Ex4-5	TTCCCTTGTGAGTCCTGCAT	164	4-5	99.7
	TGGGAGTCAGCTTCTTCTCC			
Ccn1 **(Mo and Lau, 2006)**	GCAGCAAGACCAAGAAATCC			88.0
	TTCTGGTCTGCAGAGGTGTG			
Sfrp1	GCCCGAGATGCTCAAATGTG	181	1-3	95.3
	CATCCTCAGTGCAAACTCGC			
Afp	TTTACCCAGTTTGTTCCGGAA	104	2-3	99.9
	CTTTCTAAACACCCATCGCCA			
Nrg1 **(D'Uva *et al.*, 2015)**	ATCGCCCTGTTGGTGGTCGG	-	-	87.7
	AGCTTCTGCCGCTGTTTCTTG			
ErbB2 **(D'Uva *et al.*, 2015)**	CGCTGCCCCAGTGGTGTGAA	-	-	92.0
	GCAGCCTCGTTCGTCCAGGT			
ErbB4 **(D'Uva *et al.*, 2015)**	GCCCCAAAGCCAACGTGGAG	-	-	86.5
	GCGGCATCAGCTGCGTAACC			
Vegf-a **(Dr Colin Miles)**	ATCTTCAAGCCGTCCTGTGT	-	-	88.8
	GCATTCACATCTGCTGTGCT			

Table 15: Primer sequences with their predicted product sizes, target exons and primer efficiency used for all qPCR analysis.

2.3.12.3 qPCR Analysis

Primer efficiencies were calculated using the DART-PCR program and are listed in Table 15. Primers with efficiencies less than 80% were discounted and redesigned.

Analysis was carried out using the comparative Ct method (Schmittgen and Livak, 2008). Briefly, triplicate Ct values were averaged with any values differing more than 0.5 Ct value from the other triplicates being excluded from the analysis. For each gene of interest, the average expression value for each sample was normalised to the average GAPDH expression value of that sample via subtraction. The ΔΔCt values were then calculated and an average for each

sample group was determined. Fold expression was determined and used for representation in a bar graph.

2.3.13 Microarray

2.3.13.1 Sample collection

All surfaces and dissecting equipment were cleaned with RNase away to remove contaminating RNase. Embryos were collected at E10.5 in ice cold DEPC PBS. Embryos were removed from yolk sacs and somites counted. Hearts were removed from the chest cavity and immediately snap frozen in liquid nitrogen. Hearts were then stored at -80°C until required for RNA extraction. Remaining embryonic tissue was used for genotyping.

2.3.13.2 RNA extraction

Samples were allowed to thaw on ice, followed by RNA extraction using the RNeasy Plus Micro kit (Qiagen). The protocol was carried out as per manufacturer's instructions. Briefly, four hearts were pooled in 350µl RLT-plus lysis buffer with 1% β-mercaptoethanol. Hearts were homogenised by pipetting 7–10 times using a P200 pipettor. The lysate was then centrifuged for 3 minutes at 13,000rpm. The supernatant was transferred to a gDNA eliminator spin column in a 2ml collection tube and centrifuged for 30 seconds at 13,000rpm. 1 volume of 70% RNase free ethanol was added to the flow through and mixed by pipetting. The mixture was then transferred to an RNeasy MinElute spin column and centrifuged for 15 seconds at 13,000rpm. The flow through was discarded and 700µl RW1 buffer was added to the columnand centrifuged for 15 seconds at 13,000rpm. 500µl of RPE buffer was added to the spin column, the column was inverted 3 times and left to stand for 2 minutes. 500µl of 80% RNase free ethanol was then added to the column and centrifuged for 2 minutes. The spin column was placed in a new collected tube and centrifuged with the lid open for 5 minutes, before finally being placed in an elution tube. RNA was eluted in 15µl RNase free water, by centrifugation at 13,000rpm, and stored at -80˚C.

2.3.13.3 Microarray Analysis

RNA samples from somite matched control and *Rac1*^{TnTCre} E10.5 embryonic hearts were sent on dry ice to Aros for quality control assessment. Microarray analysis was carried out on an Affymetrix Mouse Transcriptome Array 1.0.

Analysis was carried out using Transcriptome analysis console v3.0. Gene changes of ≥1.5 fold with a P-value of ≤0.05 were included.

2.3.14 In situ hybridisation

RNase free pipette tips and DEPC-treated solution were used to minimise probe degradation.

2.3.14.1 Luria Bertani broth and Agar plate preparation

Luria Bertani (LB) broth was prepared with 171 mM NaCl, 1% w/v Tryptone (Oxoid) and 0.5% w/v yeast extract (Fisher) in dH_2O and autoclaved.

Agar plates were prepared by the addition of 1.5% w/v of Agar (Fisher) to LB broth and autoclaving. Agar was then cooled to 50°C and ampicillin was added to a final concentration of 50 µg/ml. The agar was then poured into petri dishes (20-25 ml per dish) and allowed to set in the presence of a flame. Agar plates were made freshly and kept at 4˚C for no longer than 4 weeks.

2.3.14.2 Probe plasmid transformation

Probe plasmids donated by De la Pompa are listed in Table 18. Upon receipt, the probe plasmids were transformed, mini prepped and sent for sequencing. Transformations were carried out using 5-alpha subefficiency E-coli cells (NEB) according to the manufacturer's instructions. 1-10 ng of plasmid DNA was added to a 30 µl aliquot of competent cells and gently mixed, then incubated on ice for 30 minutes. Competent cells were heat-shocked for 20 seconds in a 42°C water bath to encourage uptake of the plasmid DNA, then returned to ice for a further 2 minutes. LB broth was preheated to room temperature and 970µl was added to each vial of competent cells. The competent cells were then incubated at 37°C in a thermomixer for 60 minutes with agitation. 100 µl of culture was spread onto an ampicillin containing LB agar plate and incubated at 37°C for 16 hours. After this time plates were stored at 4°C.

2.3.14.3 Miniprep of plasmid DNA

For miniprep of plasmid DNA, overnight cultures were prepared by inoculating 3ml of LB media containing ampicillin (50 µg/ml), with a single colony picked from an agar plate. Cultures were incubated at 37°C for 16 hours with agitation. The cultures were pelleted by centrifugation at 6,000 x g for 5 minutes at 4°C.

The miniprep protocol was then carried out using a QIAprep Spin Miniprep kit (QIAGEN) according to the manufacturer's instructions. Briefly, samples were resuspended in 250µl buffer P1, lysed in buffer P2 and then neutralised by the addition of buffer N3. The sample was centrifuged at 17,000 x g for 10 minutes to pellet cell debris and the supernatant was applied to a QIAprep spin column and centrifuged for 1 minute to allow binding of the plasmid DNA. The DNA was washed in buffer PB, then buffer PE, with centrifugation for 1 minute after each step. Plasmid DNA was eluted in 30µl buffer EB. The miniprep DNA was then measured of a nanodrop.

2.3.14.4 NanoDrop spectrophotometry

Quantification of DNA samples was carried out using a NanoDrop spectrophotometer (Thermo Scientific). The NanoDrop channels were blanked using elution buffer and 1µl of each sample was loaded onto the pedestals. Quantifications were given in ng/µl and quality was judged based on the absorbance at 260 nm divided by absorbance at 280nm (260/280 value). A 260/280 value of 1.8 is considered high quality DNA.

2.3.14.5 DNA sequencing

Sanger sequencing was performed to confirm that the correct plasmid DNA had been amplified. A 20µl volume containing between 30-100ng/µl of plasmid DNA was sent to GATC Biotech for sequence analysis. The sequence was returned in FASTA format and was analysed using a basic local alignment search tool (BLAST) (available online at: http://blast.ncbi.nlm.nih.gov/) to compare to all known sequences across the murine genome.

2.3.14.6 Linearization

All restriction enzymes, buffers and bovine serum albumen (BSA) were obtained from New England Biolabs. 4 µg plasmid DNA was digested in a 20 µl reaction mix containing: 20 units of restriction enzyme, 1x enzyme buffer, 1x BSA (not required for high fidelity enzymes). The digestion mix was incubated at 37°C for 2-4 hours. The restriction enzymes used for each probe are listed in Table 19.

2.3.14.7 PCR Purification

Purification of PCR and restriction digest reactions was carried out using a QIAquick PCR purification kit (QIAGEN), according to the manufacturer's instructions. Briefly, the sample to be purified was diluted in 5 volumes of the supplied buffer PB and then added to a QIAquick spin column and centrifuged at full speed to allow the DNA to adhere to the column surface. The column was washed by adding buffer PE, containing ethanol, and centrifuged again at full speed. The column was centrifuged a final time to ensure all of buffer PE had been removed then transferred to a fresh microcentrifuge tube for collection. The sample was eluted in 30µl of buffer EB. To confirm the size of the purified sample, 5µl was added to 1µl of 6x loading dye (Promega) for gel electrophoresis.

2.3.14.8 NanoDrop spectrophotometry

Quantification of DNA samples was carried out using a NanoDrop spectrophotometer (Thermo Scientific) as detailed in Chapter 2 Section 2.3.14.4.

2.3.14.9 Probe design – PCR amplification of Rac1 cDNA

Primers designed to amplify around a 400-500bp fragment of target gene (listed in Table 16). PCR amplification was carried out using E10.5 heart cDNA. Reaction and cycling conditions are described in Table 17.

Gene	Forward primer sequence	Reverse primer sequence	Product size (bp)	PCR/cloning
Afp	GCAGAGTGCTGCAAATTACCC	AATGTCGGCCATTCCCTCAC	540	Cloning
Apob	TTCTGGAGTATGCTTTAAAAGTTGT	TAGAAGCCTTGGGCACATTG	468	Cloning
Apoa1	CCAACAGCTGAACCTGAATCTCC	GTCTGGCTTTCTCGCCAAGT	503	Cloning
Ccn1	TCCTCTGTGTCCCCAAGAACTGTCTCTCCCCAATCTGGGC	TAATACGACTCACTATAGGGGGGCCGGTATTTCTTGACAC	535	PCR
Erbb2	GGCTGCTGGACATTGATGAGACTGAATACCATGCAGATGG	TAATACGACTCACTATAGGGTAGAAGGTGCTGTCCATGGG	412	PCR
Papss2	AGCAGGACTCCCGTTCTTTG	GTTGATGACTCCATCGTCCAGT	466	Cloning
Peg1	TATTTAGGTGACACTATAGCACATCCCGGTGCTTCTTCT	TAATACGACTCACTATAGGGCTGATGTGGTCTCGGCTTGT	627	PCR
Rac1	AGTGAATCTGGGCCTATGGG	ACAGCAGGCATTTTCTCTTCC	435	Cloning
Rac1 Ex4-5	TGCTTTTCCCTTGTGAGTCCTGCATCATTTGAAAATGTCCG	TAATACGACTCACTATAGGGGTCAGCTTCTTCTCCTTCAGC	164	PCR
Sema4c	AGCCTCAGTGCCGGGTAAG	GTGACCAGCTCCCCAGAAGATA	508	Cloning
Sfrp1	GTTCTTCGGCTTCTACTGGCCCGAGATGCTCAAATGTGAC	TAATACGACTCACTATAGGGGTACTGGCTCTTCACCTTGC	403	PCR
Trf	CAGGCCAGTGTGGTCTAGTG	GCAGGGTTCTTTCCTTCGGT	454	Cloning
Ttr	ATTCGCGGATGTGGTTTTCAC	CGGTTGGTCCACTCTGCTTT	479	Cloning

Table 16: Primers used to amplify mouse E10.5 cDNA for RNA probe synthesis.

Reaction (40µl)	PCR cycling conditions
2µl 10µM forward and reverse primer mix **0.5µl 25mM dNTP** **8µl 5x buffer (clear)** **0.2µl taq polymerase** **27.3µl dH2O** **2µl cDNA (100ng)**	1. 94˚C - 4 minutes 2. 94˚C - 30 seconds 3. 60˚C - 30 seconds 4. 72˚C - 1 minute (Cycling 2-4 x35) 5. 72˚C - 10 minutes Held at 4˚C

Table 17: Reaction and cycling conditions for semi-quantitative PCR.

Purification of PCR reaction was carried out using Qiagen PCR purification kit (QIAGEN), as described in Chapter 2 Section 2.3.14.7.

The purified PCR product was quantified using a nanodrop. 50ng PCR product was then ligated into PGEM-T plasmid using PGEM-T Easy Vectors System (Promega). The ligation reaction was as follows; 5µl 2x rapid ligation buffer, 1µl PGEM-T, 1µl T4 DNA ligase, made up to 10µl with 50ng pcr product and dH_2O. The reaction was incubated at 4˚C overnight.

The ligation reaction was then used in a transformation using 5-alpha subefficiency E-coli cells (NEB) according to the manufacturer's instructions as described in Chapter 2 Section 2.3.14.2.

Miniprep of Rac1-PGEM-T plasmid DNA was carried out using a QIAprep Spin Miniprep kit (QIAGEN) according to the manufacturer's instructions as described in Chapter 2 Section 2.3.14.3. 10 colonies were picked from the agar plate for mini prep.

To determine if the miniprep DNA contained the required probe-PGEM-T, a test digest with an appropriate restriction enzyme was carried out. EcoRI was chosen as there were 2 EcoRI restriction sites within the PGEM-T therefore this would cut the plasmid into 2 linear fragments of DNA. The digestion reaction was set up as follows; 2µl 10x sutsmart buffer, 2µl miniprep plasmid DNA, 15µl water and 1µl of EcoR1-high fidelity. The reaction was incubated at 37˚C for 2 hours. 5µl of digestion reaction was added to 1µl 6x loading dye and ran on a 1% agarose gel. The DNA containing the ligated probe-PGEM-T plasmid was confirmed by Sanger sequencing by GATC as described in Chapter 2 Section 2.3.14.5.

2.3.14.10 Probe design - PCR

Primers were designed to amplify a 400-500bp fragment of target gene. T7 binding site was added to the 5' end of the forward primer and T3 binding site was added to the 5' end of the reverse primer. This allows DIG labelling of both antisense and sense probes.

A 40µl PCR reaction was set up containing 50ng cDNA, 1µM primers, 1x clear buffer, 125µM dNTPs with 0.2µl taq polymerase and dH_2O. PCR was carried out under general cycling conditions; 94˚C 3 mins, 35 cycles of 94˚C 30 seconds, 60˚C 30 seconds and 72˚C 1 minute, 72˚C for 10 minutes and stored at 4˚C.

Purification of PCR reaction was carried out using Qiagen PCR purification kit (QIAGEN), according to the manufacturer's instructions as detailed in Chpater 2 Section 2.3.14.7.

Probe	Plasmid /PCP DNA	Restriction enzyme for linearisation	RNA polymerase	Donated/made
Bmp10	Plasmid	BamHI	T7	De la Pompa
Hey2	Plasmid	EcoRI	T3	De la Pompa
EphB4	Plasmid	EcoRI	T7	De la Pompa
ErbB2	PCR	-	T7	Made
Rac1	Plasmid	Sal1	T7	Made
Rac1 Ex4-5	PCR	-	T7	Made
Ccn1	PCR	-	T7	Made
Sfrp1	PCR	-	T7	Made
Neuregulin1	Plasmid	Xba1	T7	Anthony Firulli
Neuropilin 1	Plasmid	Xho1	T7	Anthony Firulli
Vegf-a	Plasmid	BamHI	T7	Anthony Firulli
Vegfr-2	Plasmid	EcoRI	Sp6	Simon Bamforth

Table 18: Probes used for in slide *in situ* hybridisation.

2.3.14.11 DIG labelling of probe

DIG labelling of the probe was carried out using DIG RNA labelling kit (Sp6/T7) (Roche) as per manufacturer's protocol. Briefly, 1µg of purified linearised plasmid/PCR product was included in a 20µl reaction containing 1xNTP labelling mix, 1x transcription buffer, 20 units of RNase inhibitor and 40 units of required RNA polymerase diluted in RNase free water. The reaction was mixed gently and centrifuged briefly to collect all of reaction then incubated at 37°C for 2 hours. DNaseI treatment was carried out to remove template DNA; 2µl

DNaseI was added and the reaction was incubated at 37°C for a further 15mins. The reaction was then stopped by adding 2µl 0.2M EDTA (pH8.0).

2.3.14.12 Probe extraction

The probe was extracted using Lithium Chloride. 80 µl DEPC TE, 10 µl 4M LiCl and 250µl 100% EtOH (ice cold) were added to the reaction and left in -80°C for 2 hours. The samples were then centrifuge at 4°C for 30mins (in a pre-cooled centrifuge). The supernatant was removed and the pellet was air-dried for 10 minutes before being redissolved in 100µl DEPC TE with 2µl RNase inhibitor. Probes were ran on agarose gel to check Add 5µl to 1µl loading dye and run on 1% agarose gel at 200V for 10 mins. Probes were stored at -80°C.

2.3.14.13 Embryo dissection and processing

Embryos were dissected, fixed and processed for wax embedding as described previously using DEPC treated solutions and RNase free plastic ware and instruments. PFA was prepared with DEPC-treated PBS and ethanol dilutions were prepared with DEPC-treated dH_2O.

Microtome sectioning was carried out as described previously using DEPC-treated dH_2O and RNase away spray to ensure microtome and hot plate were RNase free. Slides were kept at 4˚C until use.

2.3.14.14 Pre hybridation

All solutions, glassware and plastic ware were RNase free. Solutions were made with DEPC- treated dH_20 or PBS. Glass bottles were treated with DEPC dH_20 and autoclaved. Additional glassware and metal utensils were baked in an oven at 180˚C overnight. RNase away spray was used to wipe plastic ware and lab bench space. Slides were either placed in glass troughs containing solutions or in a humid chamber with on slide solutions. Slides were dewaxed using histoclear (10 minutes, twice) and dehydrated through an ethanol series; 100%, twice, 90%, 70% and 50% for 5 minutes each. Slides were placed in DEPC-PBS for 5 minutes, followed by a postfixation with 4% DEPC PFA for 20 minutes in a humid chamber. Slides were washed in DEPC PBS for 5 minutes, twice, before being incubated with 10µg/ml Proteinase K in DEPC PBS for 20 minutes at 37˚C. Slides were then washed in DEPC PBS for 5 minutes, twice, and fixed again in DEPC PFA for 5 minutes. Slides were washed in DEPC PBS

for 5 minutes followed by 15 minutes in 0.07N hydrochloric acid whist stirring. Slides were then washed in DEPC PBS for 5 minutes, twice, then 0.25% acetic anhydride in 0.1M triethanolamine pH8 for 10 minutes whilst stirring. Slides were then washed in DEPC PBS for 5 minutes, twice, then DEPC dH_2O. Finally, slides were equilibrated in hybridisation buffer (50% formamide, 0.75M NaCl, 0.075M Na-citrate) for 2 hours at 65°C in a hybridisation chamber.

2.3.14.15 Hybridisation

Probes were diluted 1:300 in hybridisation buffer and heated to 70˚C for 5 minutes before adding to slide. Slides were covered with a glass coverslip and incubated at 65°C overnight, in the dark.

2.3.14.16 Posthybridisation washes and antibody detection

Coverslips were washed from slides using prewarmed posthybridisation buffer 1 (50% formamide, 5X SSC, 1% SDS). Slides were washed in buffer 1 at 65˚C for 30 minutes, twice, then posthybridisation buffer 2 (50% formamide, 2X SSC, 0.1% SDS) at 65˚C for 30 minutes, twice. Slides were then washed in MABT (0.5M Maleic acid, 0.75M NaCl, 0.5% Tween 20, pH7.5) for 5 minutes, 3 times before blocking with 20% FCS, 10mg/ml BSA in MABT for 2 hours. Slides were incubated with anti-dig antibody, 1:1000 diluted in 1:5 blocking buffer, overnight, 4°C and covered with parafilm.

2.3.14.16 Developing

Slides were washed in MABT for 20 minutes, twice, and then for 1 hour, three times. Slides were then washed in AP-Buffer (0.1M Tris, 0.1M NaCl, 0.05M Mg2Cl, 0.1% Tween 20) for 10 minutes, three times. To develop, slides were incubated in NBT/BCIP (20µl/ml) in AP buffer and kept in the dark humid chamber until the required staining intensity was reached. Slides were washed in PBS for 5 minutes, twice and then postfixed with 4% PFA for 15 minutes washed again in PBS for 5 minutes, twice. Finally, slides were dehydratated through an ethanol series (50%, 70%, 90%, 100%, twice) for 5 minutes each then histoclear for 4 minutes, twice before being mounted in DPX. Sections were imaged using a Zeiss Axioplan2 microscope and associated software.

2.3.15 Western blotting

2.3.15.1 Protein extraction

E15.5 hearts were allowed to thaw on ice, then lysed using cell lytic MT cell lysis buffer containing 10µg/µl Proteinase inhibitors. For E15.5 hearts, 200µl buffer was added. The hearts were then homogenised using a 2ml syringe with 21G and 27G needles. After the tissue was fully homogenised, the samples were centrifuged for 5 seconds and then spun at 4°C for 1 hour. Finally, samples were centrifuged at 4˚C for 20 minutes at 12000rpm and stored at -20°C.

2.3.15.2 Bradford assay

Standards (2000, 1000, 500, 250, 125, 62.5, 31.25, O µg/µl) were prepared by a 1:1 serial dilution of BSA in cell lytic buffer with 10µg/µl protease inhibitors. 5µl of each standard and sample was added to clear 96 well plates, in duplicate. 250µl Bradford reagent (warmed to room temperature) was then added to each well and incubated for at least 5 minutes before being read of a Multiskan. Sample concentration was calculated using the standard curve produced from the data.

2.3.15.2 Sample preparation

10µg protein was diluted in laemmli buffer with 5% β-mercaptoethanol and heated at 95˚C for 5 minutes. The samples were then centrifuged at 12000rpm for 5 minutes and cooled to room temperature for 5 minutes.

2.3.15.3 Gel electrophoresis

4-12% Tris-Glycine gels (ThermoFisher Scientific) were clamped into a tank (ThermoFisher Scientific), which was then filled with running buffer (2.5mM Tris pH8.0, 19mM Glycine, 0.01% SDS). The gel combs were removed and 20-30µl of sample and 10µl of protein standard were added to individual wells. The gel was run at 90V until the protein moved out of wells and then at 180V for around 90 minutes, current set to 500mA.

2.3.15.4 Transfer

The membrane was prepared whilst the gel was running; membrane and blotting paper were dipped in methanol for 30 seconds, dH_2O for 5 minutes and

then ice-cold transfer buffer (48mM Tris, 39mM Glycine, 0.04% SDS, 20% Methanol) for at least 20 minutes. Transfer sponges were added to the transfer buffer. The transfer was carried out in a tank with transfer buffer, at 100V for 1 hour at 4°C with a magnetic stirrer.

2.3.15.5 Ponceau stain

The membrane was removed and then stained with ponceau S to check for successful transfer of proteins; the membrane was dipped in methanol for 30 seconds then stained with ponceau S for 5 minutes and washed in 5% acetic acid, twice, to remove background. The membrane was then rinsed in TBST and cut if necessary.

2.3.15.6 Blocking and antibodies

The membrane was blocked using 5% milk/TBST (TBS, 0.1% Tween 20) for 1 hour before incubating in primary antibody, diluted in 5% milk/TBST overnight at 4°C. To remove the primary antibody, the membrane was washed, firstly in 5% milk/TBST, for 10 minutes, 4 times, and secondly in TBST, for 10 minutes, 4 times. The secondary antibody was diluted 1:10,000 in 5% milk/TBST, added to the membrane and incubated for 1 hour, shaking. The secondary antibody was removed by washing, firstly in 5% milk/TBST, for 10 minutes, 4 times, and secondly in TBST, for 10 minutes, 4 times. Primary and secondary antibodies used are listed in Table 19.

Antibodies	Supplier/Order no.	Dilution used
Rabbit anti-GAPDH	Abcam/ab22555	1:10,000
Rabbit anti-Rac1	Millipore/ 05-389	1:10,000
Goat anti-Rabbit HRP	Dako/P0448	1:10,000

Table 19: Antibodies used in western blotting.

2.3.15.7 Developing

The membrane was incubated with SuperSignal west dura extended duration substrate (ThermoFisher Scientific) for 5 minutes. Following this, excess substrate was removed from the membrane and the membrane was placed in a clear plastic sheet inside the developing cassette. High performance chemiliminescence film (GE Healthcare) was exposed to the membrane for 1

minute before being placed in the developer. Exposure times were then adjusted accordingly.

2.3.15.8 Stripping for re-probing

To allow sequential blotting of proteins with similar molecular weight, the membrane was stripped after developing of the first protein blot and then reincubated with a second primary antibody. The membrane was incubated with mild stripping buffer (0.2M glycine, 0.1% SDS, 0.1% Tween 20, pH2.2) for 10 minutes, twice, followed by washes in PBS, for 10 minutes, twice, and TBST, for 10 minutes, twice. The membrane was then developed to check for effective striping, washed in TBST and blocked again before incubation with an additional primary antibody.

2.3.15.9 Western blot analysis

Blots were scanned and band intensities were analysed in Image J software. Target gene values were normalised to GAPDH values for each individual sample.

2.3.16 Magnetic Resonance Imaging (MRI)

2.3.16.1 Embryo dissection for MRI

Embryos were dissected in Hanks balanced salt solution with 5mM EDTA at 37°C. Embryos were bled out for up to 20 minutes on a heat mat. The umbicical cord was repeatedly clipped to encourage pumping out of blood. Embryos were washed twice in cold PBS then photographed. The left forelimb was removed to mark the left side of the embryo and used for genotyping. Slits were made on either side of the abdomen to allow penetration of fixative and contrast agent. Embryos were transferred to tubes and immersion fixed in 4% PFA + 4µl/ml Magnevist® (Gd-DTPA) on ice. Magnevist® (gadopentetate dimeglumine, Gd-DTPA) is a paramagnetic material which shortens the longitudinal relaxation time (T_1) of water protons enhancing the contrast of the MRI scan. Embryos were store at 4°C for at least 4 days to allow full penetration of fixative and Magnevist® before being sent to for MRI.

2.3.16.2 MRI tube preparation

MRI tubes were prepared as described previously (Bamforth *et al.*, 2012). The MRI tube consists of a nuclear magnetic resonance tube (outer diameter 28mm; Fluorochem, UK) containing a teflon disk attached to a nylon rod to allow the embryos to be removed from the tube after scanning. 32 embryos (8 layers, 4 embryos per layer) were loaded into the MRI tube by embedding in agarose (1% agarose w/v in dH2O, heated to dissolve) containing the contrast reagent Magnevist® (4µl/ml). The tube was sealed with a lid and parafilm to prevent the agarose from drying out and shipped on ice packs to Oxford for scanning. MRI scanning was carried out by Dr Jurgen Schneider (University of Oxford) and the embryos and images collected as a series of tagged image format (.tiff) files.

2.3.16.3 MRI data analysis and 3D reconstructions

The collected .tiff stacks can be analysed through AMIRA software (FEI Visualization Science Group). The voxel size used was: x-25.4, y-25.4, z-24.4. The .tiff stack for each layer of the MRI tube was opened separately and a transverse view through the embryos was analysed, using the removed left forelimb for orientation purposes. Embryos were analysed for morphological changes and 3D reconstructions were produced.

The .tiff stack was cropped to include only the region of interest for the reconstruction, in order to minimise the file size. The labelling tools within the program were then used to label each structure of the heart for reconstruction. The hue, saturation and value levels for the colours used for each structure are shown in Table 20. A 3D model of each structure was then produced using the 'SurfaceGen' option with unconstrained smoothing.

	Hue	**Saturation**	**Value**
Aorta	0.0000	0.859	0.859
Pulmonary artery	0.549	0.585	0.965
Outside surface of heart	0.500	0.127	0.800
Left ventricular lumen	0.041	0.804	0.800
Right ventricular lumen	0.667	0.506	1.000
Trachea	0.376	0.161	0.949

Table 20: Colouring for MRI 3D reconstructions using Amira.

2.3.17 High resolution episcopic microscopy (HREM)

2.3.17.1 Embryo dissection and processing for HREM

Embryos were harvested and dissected in Hanks buffer with 5mm EDTA at 37˚C. During the dissection embryos were continuously flipped to minimise pooling of blood on one side of the embryo and the umbilical vessels were repeatedly clipped to keep blood pumping out for as long as possible. After most of the blood had pumped out, embryos were transferred to PBS with 50mM KCL to ensure the heart arrested in diastole. Embryos were decapitated below the lower jaw and sliced around the liver region to remove the lower portion then left to bleed out at 37C for 5 minutes. Some of the pericardium was removed to reveal the heart. Torsos were then fixed in 4% PFA for 30 minutes, followed by several washes of dH_2O whilst shaking vigorously on a rocker. Torsos were left in dH_2O until the hearts turned completely white when all the blood was lysed (up to 1 hour). Torsos were transferred back to 4% PFA for overnight fixation and dehydrated to 70% as for normal wax embedding (Chapter 2 Section 2.3.6.1). Torsos were sent in 70% ethanol to Dr Tim Mohun for embedding, sectioning and imaging. HREM scanning was carried out by Dr Tim Mohun (The Francis Crick Institute) and images were collected as a series of .tiff files.

2.3.17.2 HREM data analysis and 3D reconstructions

The collected .tiff stacks can be analysed through AMIRA software (FEI Visualization Science Group) as detailed in Chapter 2 Section 2.3.16.1.

2.3.18 Embryonic heart dissection and processing for Transmission electron microscopy (TEM)

To look at the sarcomeric ultrastructure of E10.5 embryonic hearts, tissue was analysed by transmission electron microscopy (TEM).

Embryos were collected in ice-cold PBS and hearts were dissected as described in 2.3.4.1. The atria were removed to ensure only ventricle tissue was analysed. The hearts were then transferred to EM fixative (4% glutaraldehyde, 4% PFA, 0.1M sodium cacodylate, 3mM $CaCl_2$, pH7.4) and stored at 4˚C before being processed by the Newcastle University EM unit, sectioned and imaged using a Phillips TEM.

2.3.19 Cardiomyocyte cell counts

2.3.19.1 Dissociation and fixative of cardiomyocytes

E15.5 hearts were dissected in ice-cold DEPC-PBS at low-light intensity. Hearts were then added to 500µl of 0.28 Wunsch units/ml Liberase TM (Roche) and incubated for 20 minutes at 37˚C, shaking at 300rpm. Hearts were then manually dissociated by pipetting up and down. 500µl of 0.2M EDTA (0.1M final concentration) was added to inhibit the collagenase reaction. Cells were washed in FACs buffer (2% FCS in PBS) by spinning down at 1500rpm for 5 minutes. The supernatant was removed and the pellet was resuspended in 500µl PBS and fully disaggregated by pipetting up and down. An equal volume (500µl) of fixation buffer (4% Formaldehyde (Polysciences) in PBS) was added to give a final formaldehyde concentration of 2%. The cells were incubated at room temperature for at least 1 hour. Formaldehyde was then removed by spinning down at 1500rpm for 5 minutes and the cells were stored in FACs buffer in the dark. The fixed cells were incubated with 0.1% Triton X-100 and stained with 20µl Propidium Iodine (PI) solution (Abcam) for 30 minutes before analysis using a Tali image based cytometer (Invitrogen).

2.3.19.2 Cell count analysis

The number of PI-positive and EYFP-positive cells were counted using the Tali image based cytometer. Parameters were set for roundness and size of cells counted to include the cardiomyocyte population.

2.3.20 Measurements

2.3.20.1 Heart size and myocardial thickness measurements

Brightfield images were taken on a Zeiss Axioplan microscope with associated Axiovision SE64 software. Thoracic cavity and heart diameter were measured using the length tool in Axiovision SE64 software. At least 3 sections were measured per embryo and an average measurement was taken. For myocardial thickness measurements, 3 measurements were taken perpendicular to the outer myocardial surface of each ventricle and averaged. The myocardial thickness measurements were normalized for each section by dividing by the average heart width.

2.3.20.2 Trabeculae counts and directionality analysis

Trabeculae counts were carried out on histology stained transverse sections from E9.5-E17.5 control and mutant embryos. The number of trabeculae protrusions arising from the compact myocardial wall were counted in the left and right ventricle in at least 3 sections per embryo.

For measurement of the directionality of the developing trabeculae angles were measured from the perpendicular compact myocardium using imageJ software. HREM tiff images were used from E10.5 and E11.5 control and mutant embryos. All trabeculae arising from the compact myocardium were measured in at least 5 sections per embryos.

2.3.20.3 Cell migration measurements

Brightfield images were taken on a Zeiss Axioplan microscope with associated Axiovision SE64 software. Thoracic cavity and heart diameter were measured using the length tool in Axiovision SE64 software. At least 3 sections were measured per embryo and an average measurement was taken. For cell migration measurements, measurements were taken perpendicular to the outer myocardial surface of each ventricle to the furthest Cre-positive derived migrating cell. The cell migration measurements were normalized for each section by dividing by the average heart width.

2.3.20.4 Outflow tract length measurements

E10.5 embryos were dissected with the head and tail removed to reveal the outflow tract clearly. Brightfield images of the side view of embryos were taken on a Leica MZ6 microscope. OFT length was measured using ImageJ software.

2.3.20.5 Cell counts

Fluorescent images were taken on a Zeiss AxioImager using associated Axiovision LE64 software. Images of both left and right ventricles and the interventricular septum (IVS) were taken for at least 3 sections per embryo. Cell count analysis was carried out using ImageJ software. Cell counts of phHH3/caspase3/BrdU were expressed as a ratio of total number of cells (DAPI).

2.3.20.6 Cardiomyocyte cell area

To measure the area of cardiomyocytes the cell membrane was stained with wheat germ agglutinate (WGA) containing a fluorescent Alexa 594 conjugate (ThermoFisher W11262).

Slides were dewaxed, rehydrated and washed with PBS. WGA was diluted 1:200 in PBS and 95µl added to each slide before covering with a coverslip and incubated in a humidified chamber for 30 minutes in the dark. Slides were then washed 3 times for 5 minutes in PBS and mounted in DAPI containing Vectorshield (Vector).

Slides were then imaged using an AxioImager 2 (Zeiss). The area of individual cardiomyocytes was then measured using Image J, restricting measurements to cardiomyocytes in a transverse orientation found adjacent to transversely sectioned capillaries. The average area of cardiomyocytes was determined for the RV, and LV for control and mutant hearts (n=3, 3 sections per heart). Cardiomyocyte size was analysed in Microsoft excel and significance determined using a unpaired t-test ($p<0.05$).

2.3.21 Co-Immunoprecipitation (Co-IP)

2.3.21.1 Blocking beads for IP

Dynabeades in Slurry (Life Technologies 10006D) (50µl contains 1.5mg). Magnet used to remove supernatant. 1ml of 1% BSA/PBS added to beads and mixed for 1 hour using rotary shaker. Magnet used to remove the supernatant. Beads washed in PBS twice by pipetting up and down. Magnet used to remove the supernatant. 400µl of lysis buffer and proteinase inhibitors added. Stored at 4°C until required.

2.3.21.2 Preclearing lysates

Preclearing prevents non-specific binding of proteins to beads, removes proteins that bind to immunoglobulins non-specifically and lowers background and improves signal to noise ratio. 50µl of species specific serum added to 1ml of lysate. Incubated on ice for 1 hour. 100µl of bead slurry added to the lysate and incubated for 30 minutes at 4°C with gentle agitation. Supernatant removed using magnet and use for IP.

2.3.21.3 Immunoprecipitation with antibody-beads

100µl of prepared bead slurry added to an Eppendorf with 5µl of primary antibody (recommended dilution on data sheet). Antibody and beads incubated at 4°C with gentle mixing overnight. Supernatant removed and washed twice with lysis buffer. Pre-cleared cell lysate added (300µl) to block beads with antibody conjugate. Incubated at room temperature for 4 hours, rotary mixing. Beads washed three times in wash buffer, removing the supernatant between washes (using magnet). Buffer resuspended and transferred to a clean tube. 20µl elution buffer and 20µl of 2X laemelli buffer added and heated at 70°C for 10 minutes to remove beads. Followed by cooling at 4°C for 5 minutes and centrifugation. Supernatant protein kept and store at -20°C until required.

2.3.22 Statistics

2.3.22.1 Unpaired t-test

Statistical analysis was carried out using an unpaired student's t-test in Microsoft Excel. Variance analysis was carried out using the F-test in Microscoft Excel and the type of t-test was calculated accordingly (equal or un-equal variance). Statistical significance was assigned when $p \leq 0.05$, unless otherwise stated. Standard error of the mean (SEM) was used for all error bars.

2.3.22.2 Kruskal Wallis Test

Kruskal Wallis is a non-parametric test carried out in SPSS for statistical analysis of *Rac1* expression data from qRT-PCR.

2.3.22.3 Chi-sqaured

Chi-squared is a non-parametric test carried out in SPSS for statistical analysis of genotype frequency data and trabeulae angle measurements.

2.3.22.4 Two-way ANOVA

The two-way ANOVA is a non-parametic test carried out in SPSS for statistical analysis of multiple grouped data; myocardial thickness measurements, trabeculae numbers, cell counts and cell area measurements.

2.3.22.5 Power calculations

Power calculations were carried out for any data requiring statistical analysis using the unpaired t-test using the tool available at the following site;

http://biomath.info/power/ttest.htm. All experiments were sufficiently powered unless stated.

Chapter 3. Early myocardial deletion of Rac1 causes embryonic heart defects

3.1 Introduction

3.1.1 Rac1 in embryogenesis

Unlike the other members of the Rac family, *Rac1* is expressed ubiquitously early in mouse embryogenesis (Wang and Zheng, 2007). Rac1 is critical for embryogenesis as *Rac1* null mice die during gastrulation with extensive cell death observed in the space between the endoderm and ectoderm (Sugihara et al., 1998). Due to the embryonic lethality of *Rac1* deletion, tissue specific functions of Rac1 could not be investigated using this mouse model. Therefore, conditional inactivation of *Rac1* using Cre-LoxP technology has been employed in both previously published work and in this thesis.

3.1.2 Cre-LoxP technology

The Cre-LoxP recombination system was first described in 1992 and has since been extensively used throughout developmental biology (Lakso *et al.*, 1992). The technique utilises the enzyme Cre recombinase, produced by the bacteriophage P1, which acts on short sequences termed '*LoxP* sites'. These *LoxP* sites can be introduced into specific regions of DNA. The Cre recombinase can then cause recombination between two *LoxP* sites, removing the intervening sequence. This technology can be used to cause tissue specific gene inactivation, by removal of important functional regions, or gene activation, by insertion of a floxed (flanked by *LoxP* sites) 'stop' sequence upstream of a gene of interest which is expressed in a specific tissue. Cre recombinase is expressed under the control of a promoter, allowing specific spatial and temporal activation of the Cre enzyme, which therefore results in tissue-specific activation/inactivation of the gene of interest.

3.1.3 Rac1 in cardiac development

Using Cre-LoxP technology, *Rac1* has been shown to have critical roles in endothelial cells and neural crest cells during cardiac development (Tan *et al.*, 2008; Thomas *et al.*, 2010).

Recent studies published after the onset of this project have highlighted a role of Rac1 in cardiomyocytes during embryonic development (Abu-Issa, 2014; Leung *et al.*, 2014; Leung *et al.*, 2015). Abu-Issa reported cardiac defects in mice with *Rac1* deficiency in cardiac progenitors, using a precardiac mesoderm specific Cre line, *Nkx2.5-Cre*. *Rac1* deficient cardiomyocytes appear to have reduced adhesion and $Rac1^{Nkx2.5Cre}$ embryos are embryonic lethal by E12.5 with disorganised, thin ventricular walls and defective OFT alignment (Abu-Issa, 2014). The defects were attributed to defective cell adhesion as shown by disrupted β-catenin and FAK (Abu-Issa, 2014). Additionally, Leung and colleagues generated mice with *Rac1* deficiency in SHF progenitors using *Mef2c-Cre*. Rac1 deficient cardiomyocytes have impaired elongation and cytoskeleton organisation and $Rac1^{Mef2cCre}$ embryos have cardiac defects; VSD and ASD as well as a thinned RV myocardium and a bifid cardiac apex (Leung *et al.*, 2014). In the IVS of *Rac1* SHF mutant hearts, expression of the PCP protein Scrib was shown to be lost and apoptosis was significantly increased. An overall decrease in migratory markers WAVE and Arp2/3 was also shown, as well as a decrease in transcription factors Gata4, Tbx5, Nkx2.5 and Hand2 in the RV myocardium (Leung *et al.*, 2014). Furthermore, these mice have a spectrum of OFT defects ranging from OA to severe TGA with additional incidence of aortic atresia and abnormal right subclavian artery (ARSA). The OFT defects occur as a result of early defects in cell proliferation in the splanchnic mesoderm and reduced NCC and SHF cell migration into the developing OFT, leading to a shorted OFT (Leung *et al.*, 2015). Both Abu-Issa and Leung have shown *Rac1* is critical in cardiac progenitors and have suggested *Rac1* functions to regulate cardiomyocyte polarity and/or adhesion for normal cardiac development. Despite these investigations, the role of Rac1 in early myocardial development remains unclear. The findings of Abu-Issa rely on very limited phenotyping data and poor quality immunostaining in cultured cardiomyocytes. Isolated cardiomyocytes are not representative of the complex structure of the developing myocardium and do not distinguish between the different types of cardiomyocytes i.e compact and trabeculae cardiomyocytes display widely different properties including the maturation of the actin-cytoskeleton and cell-cell junctions. Also the genetic analysis of $Rac1^{Mef2cCre}$ hearts, by Leung and colleagues, was carried out at E13.5, at this time point the

phenotype was already established, therefore, any gene transcriptional changes detected may be secondary to the phenotype. Additionally, the expression of Rac1 and additional PCP protein Scrib is not consistent with previously reports of cell membrane localisation in cardiomyocytes (Boczonadi *et al.*, 2014b). Both Abu Issa and Leung and colleagues use conditional deletions of *Rac1* that include multiple cell types, leading to difficulties separating possible differential roles of Rac1 in specific cell types. Additionally, neither group has investigated the role of Rac1 in the formation of the trabeculae and subsequent development of the myocardium. Thus, the aim of this project was to investigate the role of *Rac1* in developing myocardium.

3.1.4 Rac1^{flox} mice

At least two separate strains of *Rac1^{flox}* mice have been generated to allow investigation of Rac1 in specific tissues using the Cre-LoxP system. Several investigators have used *Rac1^{flox}* mice generated by David J. Kwiatkowski and produced by Jackson Laboratories (stock 5550). These mice have LoxP sites flanking exon 1 of the *Rac1* gene (Tan *et al*., 2008; Thomas *et al*., 2010; Abu-Issa, 2014; Leung *et al*., 2014; Leung *et al*., 2015). Reduction of Rac1 protein has been confirmed in these mice by western blot analysis (Tan *et al*., 2008). In the heart, *Rac1* mRNA levels were reduced as well as Rac1 protein levels shown by western blot and immunostaining, although the immunostaining is inconsistent with previous reports of Rac1 localisation (Leung *et al*., 2014). In this study, *Rac1^{flox}* mice were used which were generated by insertion of LoxP sites flanking exons 4 and 5 of the *Rac1* gene (Walmsley *et al*., 2003). Cre-mediated recombination between these sites results in the excision of exons 4 and 5 and a subsequent frame shift and lack of a functional Rac1 protein in Cre expressing cells.

3.2 Aims of chapter

The primary aims of this chapter were to confirm and define *Rac1* expression in the developing heart and subsequently determine its role within the epicardial and myocardial populations during ventricular development.

The development of the myocardial wall requires proliferation and differentiation of FHF and SHF derived cardiomyocytes, as well as signals from epicardial

cells and invasion of epicardial derived cells. The role of Rac1 in myocardial cells and epicardial cells during ventricular wall development has not been fully elucidated. Preliminary data suggested that deleting *Rac1* from the epicardium and myocardium, using *Gata5-Cre*, resulted in defects within the myocardial wall (personal communication from Dr Helen Phillips). Therefore, the aim of this chapter was to characterise these defects in detail.

It was hypothesised that *Rac1* is required in both epicardial and myocardial cells for normal heart development and its differential roles could be determined by conditional deletion of *Rac1* from myocardial and epicardial cells using *Gata5-Cre*, *WT1-CreERT2*, *Mlc2v-Cre* and *TnT-Cre* transgenic mouse lines.

3.3 Results

3.3.1 Rac1 expression in the embryonic heart through development

3.3.1.1 Rac1 gene expression in the embryonic, postnatal and adult heart

Rac1 is known to be ubiquitously expressed throughout mouse tissues, including the heart (Wang and Zheng, 2007). However, the temporal expression of *Rac1* in the heart during cardiac development has not previously been reported. To attain a developmental series for cardiac *Rac1* expression, qPCR was carried out on dissected wild type hearts of a series of ages covering the main stages of heart development. At E10.5 the four chambered heart is formed, followed by continued myocardial and OFT development between E10.5-E17.5. At postnatal stages, structural and functional changes occur within the myocardium to adapt to the hyperoxic environment. The adult heart structure is achieved by 6 weeks of age. CD1 embryonic hearts were collected for RNA at E10.5, E13.5, E15.5, E17.5, postnatal day (P) 0, P2, P4 P6, P8, P10, P12, P15, P18 and 6 weeks (n=6 for each time point). RNA was extracted using the Trizol Plus RNA purification system (Ambion). qPCR analysis was carried out using the Comparative Ct method and gene expression values were normalised to housekeeping gene, *GAPDH*, values. qPCR analysis firstly confirmed that *Rac1* is expressed in the developing heart A). Secondly, it revealed that *Rac1* expression levels vary significantly throughout embryonic and postnatal development and in the adult (Kruskal Wallis, $p<0.01$). *Rac1* is consistently expressed throughout embryonic development. Kruskal Wallis

pairwise analysis revealed no significant changes during embryonic development. However, postnatally at P2 there is a significant increase in expression (~50%) that remains constant for 10 days. At P15 *Rac1* expression is significantly decreased (~30%) and returns to embryonic levels that are sustained in the adult heart. Kruskal Wallis pairwise analysis revealed significant differences between P2 and both E15.5 and E17.5. Additionaly, significant differences are seen between P15 (as well as 6 weeks) and postnatal stages P2, P4, P6 and P10. *GADPH* values remained constant in all samples (Figure 33B). The increase in *Rac1* at P2 suggests *Rac1* may have an important role in postnatal heart development. During postnatal heart development, cardiomyocytes undergo elongation into the characteristic rod-shaped structure, with fully aligned myofibrils and fully formed intercalated discs restricted to myofibril anchorage (Hirschy *et al.*, 2006; Martin-Puig *et al.*, 2008). Therefore, the increased expression of *Rac1* may have a role in the maturation of the cytoskeleton and polarisation of postnatal cardiomyocytes. Alternatively, following birth cardiomyocytes lose the ability to proliferate and withdraw from the cell cycle. There is a final round of karyokinesis without the accompanied cytokinesis, resulting in binucleated cardiomyocytes. At P4-P6, binucleation initiates and by P21, 85-90% of all cardiomyocytes are binucleated. Several studies have also proposed a wave of cardiomyocyte proliferation at P15 (Porrello *et al.*, 2011; Naqvi *et al.*, 2014). Since Rac1 has a role in cell cycle regulation, it is plausible that Rac1 may play a role in retaining cell proliferation during these early postnatal stages.

These results are in agreement with reports of ubiquitous embryonic expression of *Rac1* including in the heart (Wang and Zheng, 2007), however they do not allow interpretation of cell specific expression of *Rac1*.

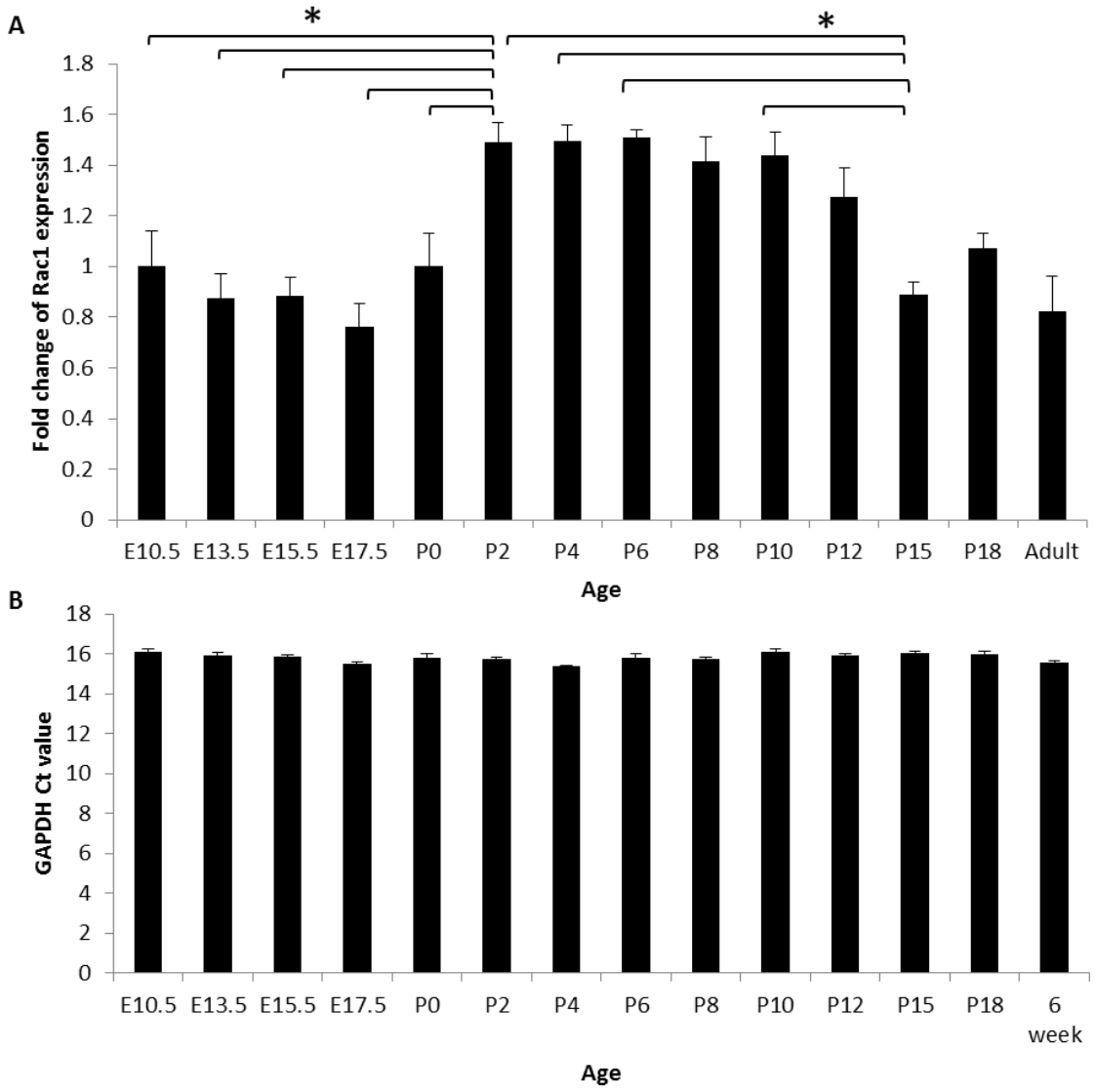

Figure 33: Cardiac expression of *Rac1* throughout embryonic and postnatal development, and in the adult by qPCR.
Quantitative real time PCR (qPCR) analysis shows that cardiac expression of *Rac1* remains relatively stable throughout embryonic development, however during postnatal development *Rac1* is upregulated (P2-P12) by around 50% then returns to embryonic levels by P15. Expression values are normalised to housekeeping gene *GAPDH* and are relative to E10.5 expression (n=6) (**A**). *GAPDH* expression is consistent across all ages in the samples used to determine *Rac1* cardiac expression by qPCR (**B**). *P<0.05. E embryonic day; P postnatal day. Statistical analysis carried out using the Krustal Wallis Method.

3.3.1.2 Rac1 gene expression in cardiomyocytes

To identify the cardiac cell type(s) that express *Rac1* during cardiac development, *in situ* hybridisation was carried out on E11.5, E13.5 and E15.5 embryonic sections. The *Rac1* RNA probe was designed to target the 5' UTR. The *Rac1* probe hybridisation showed strong expression across the whole

embryo section including the myocardium, endocardium and epicardium (Figure 34). The myocardial expression of *Rac1* is relatively similar at E11.5 and E13.5 but is reduced at E15.5 (asterisk and arrow head respectively in Figure 34, A', B' and C'). Strong expression was observed in endocardial cells (arrows in Figure 34, A' and A'') and in the sub-epicardial region (arrowheads in Figure 34, A' and A''). Within the myocardium, *Rac1* expression is seen in the cardiomyocytes and at E13.5 and E15.5 strong *Rac1* expression also appeared around intra-myocardial and septal vessels (arrows in Figure 34, B' and C''). A sense RNA probe was used as a negative control and did not show any non-specific hybridisation (Figure 34D-D'). These results confirm that *Rac1* is expressed in cardiomyocytes within the developing myocardium and highlight that *Rac1* is also expressed in additional cardiac cells including endocardial cell layers as well suggestive expression in endothelial cells and/or smooth muscle cells of the cardiac vessels.

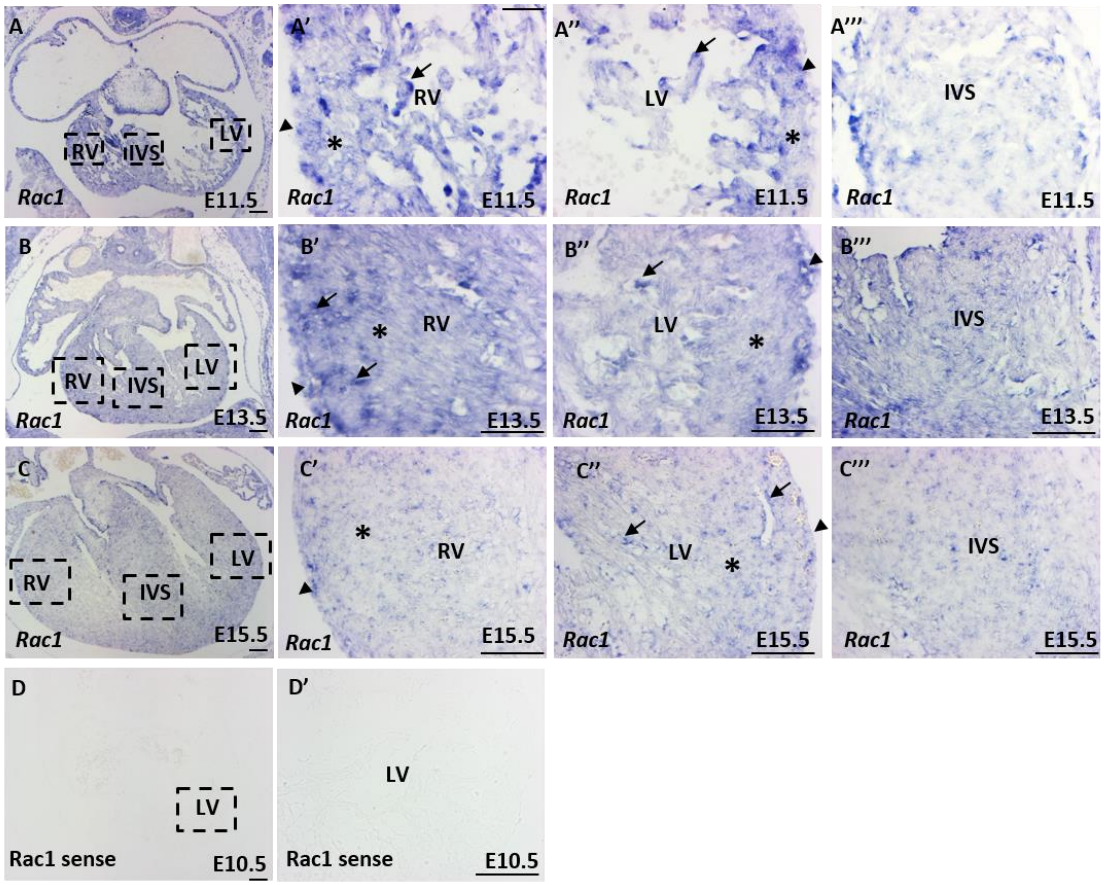

Figure 34: Cardiac expression of *Rac1* during development by slide *in situ* hybridisation.
Rac1 is expressed ubiquitously in the myocardium during embryonic heart development (asterisk in **A'**, **B'** and **C'**). High expression is observed in endocardial cells at E11.5 (arrows in **A'** and **A''**) and around intra-myocardial vessels at E13.5 and E15.5 (arrows in **B'** and **C''**). E; embryonic day, RV; right ventricle, LV; left ventricle, IVS; interventricular septum. Scale bars; A-D 100μm, A'-D' 50μm.

3.3.2 Targeted deletion of Rac1 from specific cell types in the developing heart

To determine the role of *Rac1* during ventricular development, *Rac1* was deleted from specific cardiac cell types using the Cre-LoxP system.

3.3.2.1 Cre mouse lines

The transgenic mouse Cre lines used in this study are listed in Table 21 and an example of the expression pattern of each Cre line at E15.5 is shown in Figure 35. *Gata5-Cre* was initially accepted as an epicardial specific Cre line but subsequently the Phillips' group established it is also expressed in the myocardium (Merki *et al.*, 2005). *Gata5-Cre* is expressed from E9.25 in all

epicardial cells and a proportion of myocardial cells, predominantly in the LV (Merki *et al.*, 2005). *WT1-CreERT2* is tamoxifen inducible and is expressed in epicardial cells only (Zhou *et al.*, 2008). *TnT-Cre* is expressed from E7.5 in all myocardial cells (Jiao *et al*., 2003). *Mlc2v-Cre* is expressed in a portion of ventricle myocardial cells from E7.5 and shows patchy expression during embryonic heart development (Chen *et al.*, 1998).

3.3.3.2 Mouse crosses

Rac1^{flox} mice (as described in Chapter 3 Section 3.1.4) contain *LoxP* sites flanking exons 4 and 5 of the *Rac1* gene (Walmsley *et al.*, 2003) (Figure 36B). *Rac1*^{flox} mice were firstly crossed to *R26REYFP* reporter mice to detect Cre activity and subsequent *Rac1* deletion. *R26REYFP* mice contain a 'floxed' transcriptional stop sequence, which is removed in the presence of *Cre*, therefore, allowing the expression of the *EYFP* construct in *Cre* expressing cells (Srinivas *et al.*, 2001) (Figure 36C). *Rac1*$^{flox;}$ *R26REYFP* mice were subsequently crossed to different Cre lines to generate *Rac1*$^{f+;}$*EYFP*$^{f+;}$*Cre* stud males. These stud males were then mated to *Rac1*^{ff}*;EYFP*^{ff} females to produce *Rac1*^{ff}*;EYFP*^{ff}*;Cre* mutant embryos (subsequently referred to as *Rac1*^{Cre}) (Figure 36D).

Rac1^{Cre} mutants are homozygous for *Rac1* deletion and controls are heterozygous or wild type for *Rac1* deletion in *Cre* expressing cells, combined with expression of EYFP (cross shown in Figure 36).

Cre Line	Age of onset	Expression	Reference
Gata5-Cre	E9.25	Epicardial and Myocardial	(Merki *et al*., 2005)
WT1-CreERT2	Tamoxifen inducible E8.5	Epicardial	(Zhou *et al*., 2008)
TnT-Cre	E7.5	Cardiomyocyte	(Jiao *et al*., 2003)
Mlc2v-Cre	E7.5	Patchy myocardial	(Chen *et al*., 1998)

Table 21: Summary of Cre lines used to delete *Rac1* from cardiac cell types.

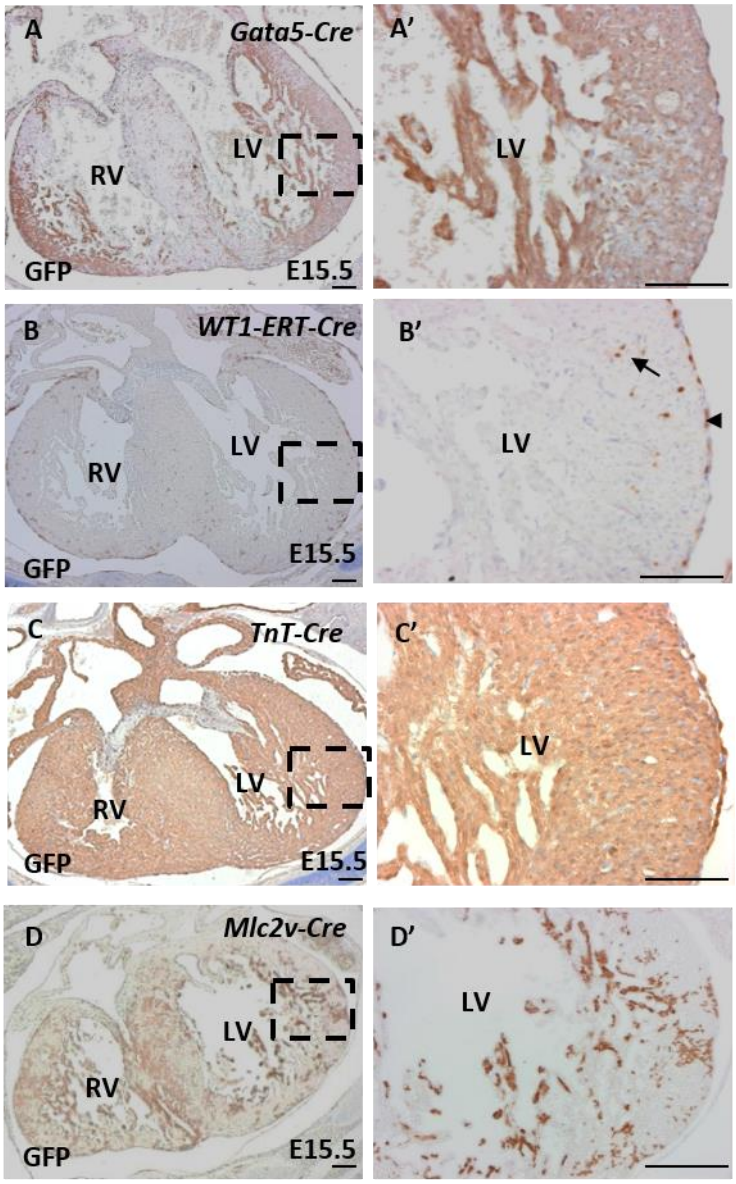

Figure 35: Cardiac expression of *Gata5-Cre*, *WT1-CreERT2*, *TnT-Cre* and *Mlc2v-Cre* at E15.5.

EYFP reporting of Cre expression using IHC. *Gata5-Cre* is expressed throughout the epicardium and patchy in myocardium (**A** and enlarged in **A'**). *WT1-CreERT2* is expressed in the epicardium only under the control of tamoxifen; injections were given at either E8.5-E10.5 or E9.5-E11.5 (**B** and enlarged in **B'**, arrow heads point to epicardial cells and arrows point to migrating epicardial derived cells). *TnT-Cre* is expressed in the myocardium only (**C** and enlarged in **C'**). *Mlc2v-Cre* is expressed in a population of ventricle myocardial cells (**D** and enlarged in **D'**). RV; right ventricle, LV; left ventricle, GFP; green fluorescent protein. Scale bars; A-D 100μm, A'-D' 50μm.

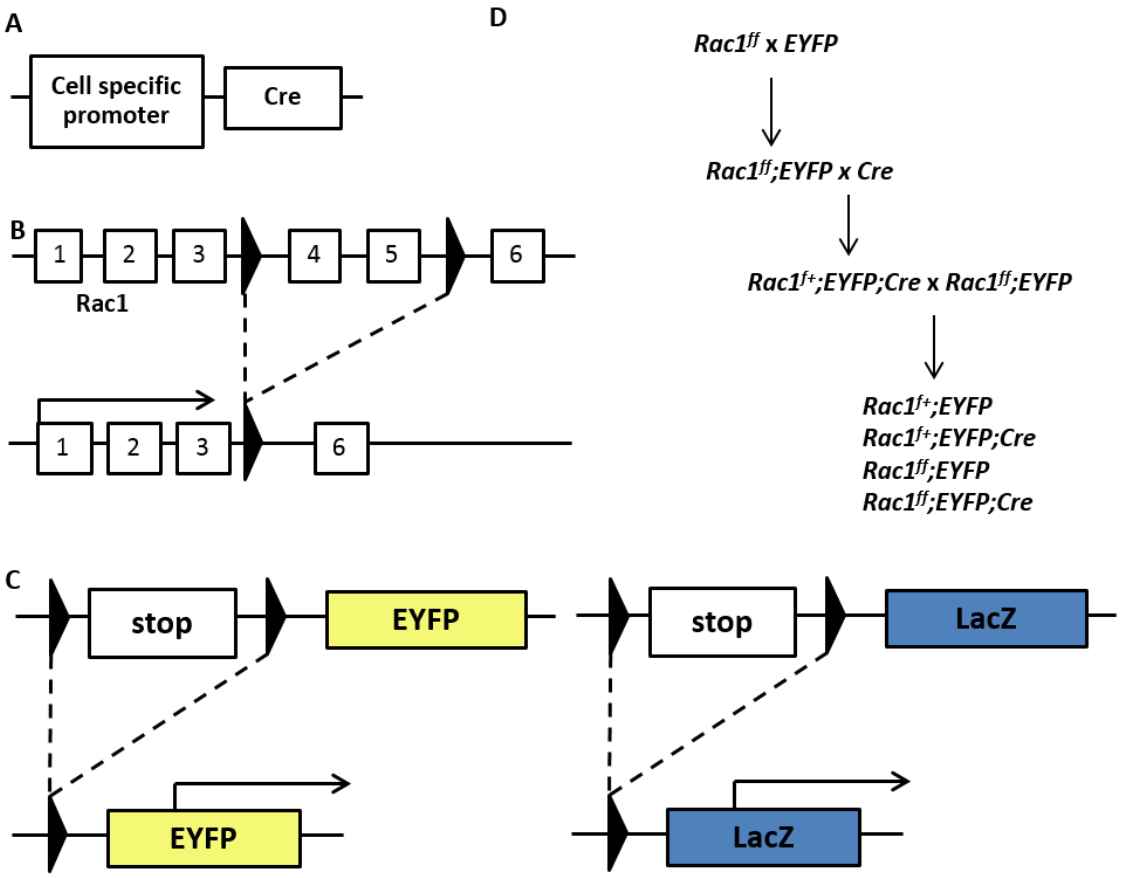

Figure 36: Cre-LoxP system utilised to generate cardiac cell specific deletion of *Rac1.*
Cre is expressed under the control of a cell-specific promoter (**A**). *Rac1*^{flox} mice contain *LoxP* sites flanking exons 4 and 5 of the *Rac1* gene; these sites are recombined out by *Cre* leading to a frame shift and subsequent lack of a functional Rac1 protein in Cre expressing cells (Walmsley *et al.*, 2003) (**B**). *R26REYFP* mice contain a transcriptional stop sequence flanked by *LoxP* sites, which is removed in the presence of *Cre*, therefore, allowing the expression of the EYFP construct in Cre expressing cells (Srinivas *et al.*, 2001) (**C**). *Rac1*^{flox} mice were firstly crossed to *R26REYFP* mice to allow reporting of Cre activity and consequent *Rac1* deficiency. *Rac1*$^{flox;}$ *R26REYFP* mice were crossed to Cre lines to generate *Rac1*$^{f+;}$*EYFP*$^{f+;}$*Cre* stud males. These stud males were then mated to *Rac1*^{ff}*;EYFP*^{ff} females to produce *Rac1*^{ff}*;EYFP*^{ff}*;Cre* mutant embryos (**D**). Black arrows represent *LoxP* sites, EYFP; yellow fluorescent protein.

3.3.3.3 Rac1 mRNA transcript expression in Rac1^{TnTCre} *hearts*

To confirm *Rac1* deletion in the mutant embryonic hearts the Rac1 transcript was first examined by semi-quantitative RT-PCR. In *Rac1*^{Cre} cells, the Cre recombinase should remove the *LoxP* flanked sequence containing *Rac1* exons 4 and 5, leading to production of 134bp fragment of mRNA that will be degraded by non-sense mediated decay. To test this principle, primers were designed

either side of the *LoxP* sites (the forward primer binding in exon 3 and the reverse primer binding in exon 6) to amplify a segment of cDNA containing the deleted sequence (Figure 37A). Control and *Rac1*^{TnTCre} E12.5 hearts were dissected for RNA and the cDNA synthesised was used in RT-PCR. In the control hearts the expected wild type *Rac1* band of 356bp was produced. In the *Rac1*^{TnTCre} E12.5 hearts, in addition to the expected wild type *Rac1*, a smaller product was also produced (134bp). The size of this PCR fragment is consistent with the size of the wild type *Rac1* fragment (356bp) without the deleted *LoxP* flanked fragment (222bp) (n=4) (Figure 37B). These results suggest that the recombined floxed mRNA is transcribed in the *Rac1*^{Cre} hearts with Rac1 exons 4-5 skipped and that the wild type Rac1 allele mRNA is also transcribed in the *Rac1*^{Cre} hearts. This is a novel finiding as it is not mentioned in the orignial publication or in any additional publications using this mouse model. Quantification of Rac1 deletion was confirmed on a protein level in the orginal publication (Walmsley *et al.*, 2003), therefore this was investigated in Chapter 3 Section 3.3.3.4.

To quantify the reduction in wild-type *Rac1* mRNA transcript in embryonic hearts, qPCR was carried out using primers designed to target the floxed exons 4 and 5 only (Figure 37D). RNA was extracted from E10.5 control and *Rac1*^{TnTCre} hearts using the Reliaprep RNA tissue miniprep system (Promega) and the cDNA synthesised was used in qPCR**.** qPCR analysis was carried out using the 'Comparative Ct method' and gene expression values were normalised to housekeeping gene, *GAPDH*, values. A 52% reduction in expression of *Rac1* exons 4 and 5 was confirmed in E10.5 *Rac1*^{TnTCre} hearts compared to control hearts (n=6, p-value 6.77×10^{-5}) (Figure 37C). It is hypothesised that the remaining 48% expression of *Rac1* in E10.5 *Rac1*^{TnTCre} hearts is from non-cardiomyocytes expressing wild type *Rac1*, including epicardial cells, smooth muscle cells and endothelial cells. However, these experiments do not confirm that Rac1 is deleted specifically and efficiently in Cre-positive derived cells (i.e. cardiomyocytes in *Rac1*^{TnTCre} hearts).

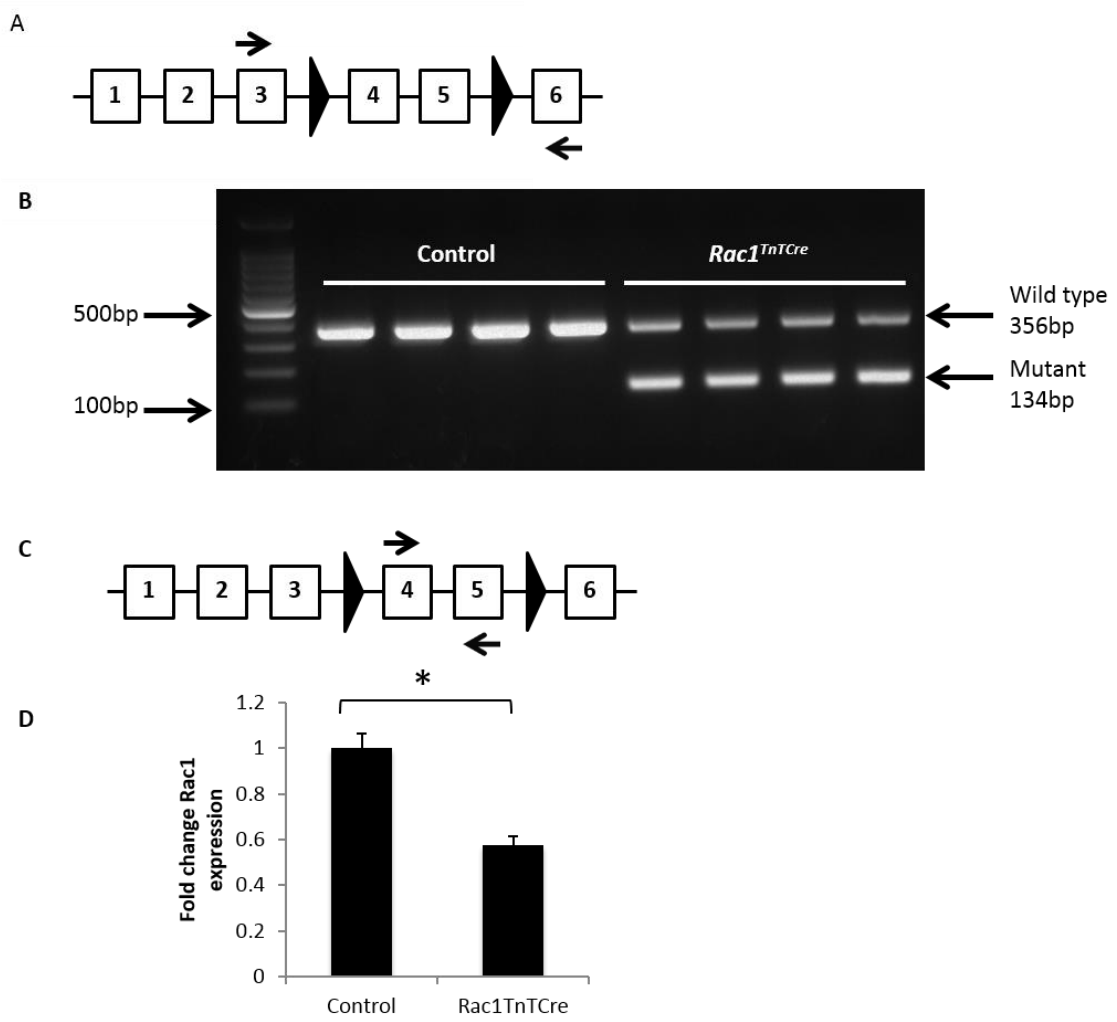

Figure 37: Analysis of *Rac1*^{flox} transcript expression in *Rac1*^{TnTCre} hearts. A shorter mRNA transcript (134bp) is observed in the *Rac1*^{TnTCre} E10.5 hearts in addition to the wild type band (356bp) as shown by RT-PCR (n=4) (**B**). RT-PCR primers bind either side of the LoxP sites in the *Rac1*^{flox} allele (**A**). qPCR analysis of wild-type *Rac1* mRNA in E10.5 embryonic hearts revealed a 52% reduction in *Rac1* expression in *Rac1*^{TnTCre} hearts compared to controls (n=4) (**D**). Primers target the floxed exons 4 and 5 only (**C**). qPCR analysis was carried out using the Comparative Ct method and gene expression values were normalised to housekeeping gene, *GAPDH*, values. *P<0.05. Statistical analysis carried out using the unpaired t-test.

To confirm if *Rac1* is deleted specifically in Cre-positive derived cells, slide *in situ* hybridisation was carried out using a *Rac1* probe designed to target the 'floxed' exons, 4 and 5, only. E12.5 control and *Rac1*^{TnTCre} embryos were embedded and sectioned for *in situ* hybridisation. Slide *in situ* hybridisation was carried out using a *Rac1* exon 4-5 antisense RNA probe. A sense RNA probe was used as a negative control and did not develop any non-specific hybridisation (data not shown). The antisense probe showed comparable

hybridisation staining to the *Rac1* probe exon 3-4 staining described in Figure 34 in control E12.5 hearts. In *Rac1*^{TnTCre} E12.5 hearts, reduced *Rac1* expression was observed in the myocardial layer (Figure 38, asterisk in A' compared to B'), however, *Rac1* expression in other cells appeared unchanged such as expression in endocardial cells (Figure 38, arrows in A' compared to arrows in B') and in mesenchymal cells of the cardiac OFT cushions (Figure 38, arrows in C' and D'). Staining intensity is also comparable in control tissues such as the oesophagus and trachea (Figure 38, arrows in C'' and D''). Therefore, it is suggested that *Rac1* mRNA is efficiently and selectively deleted from cardiomyocytes in the Rac1^{TnTCre} embryos.

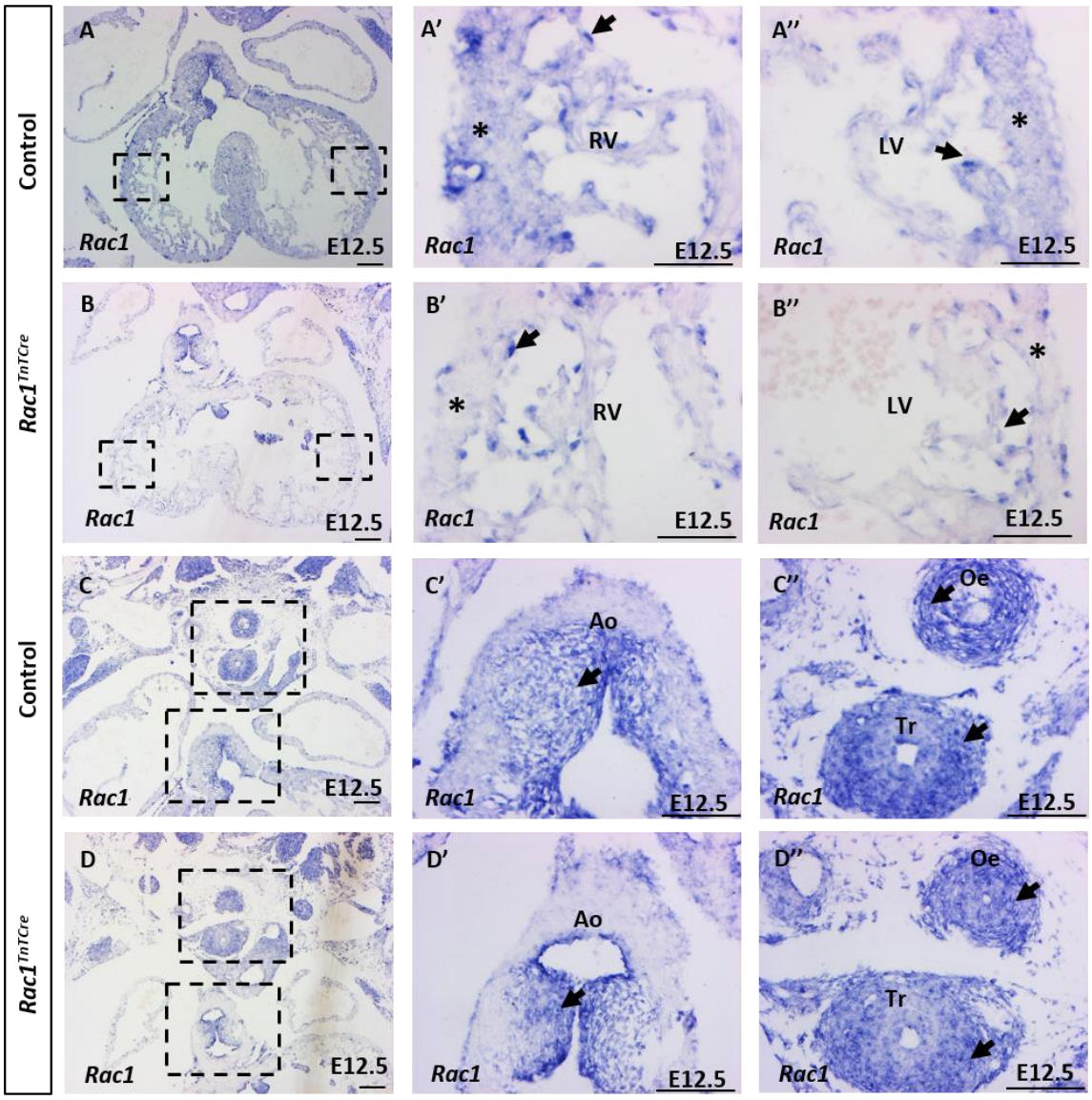

Figure 38: Specific myocardial deletion of *Rac1* shown by slide *in situ* hybridisation in E12.5 control and *Rac1*^{TnTCre} embryo sections.
Rac1 is expressed ubiquitously at E12.5 in control hearts with high expression in endocardial cells and in the OFT cushions (**A'**, **C'**). In *Rac1*^{TnTCre} hearts, *Rac1* expression is reduced in the myocardial layer (asterisk in **A'** and **B'**), however expression is retained in the endocardial layer of the developing myocardium (arrows in A' and B'). Additionally, staining intensity is comparable in the mesenchymal cells of the OFT cushions (arrows in **C'** and **D'**) and in the trachea/oesophagus (arrows in **C''** and **D''**). E; embryonic day, RV; right ventricle, LV; left ventricle, Ao; Aorta, Oe; oesophagus, Tr; Trachea. Scale bars; A-D 100μm, A'-D'' 50μm.

3.3.3.4 Rac1 protein expression in Rac1^{TnTCre} *hearts*

Western blotting was performed to determine if the recombined mRNA transcript is able to produce a protein in the i mutant hearts. Control and *Rac1*^{TnTCre} E15.5 hearts were dissected and extracted for total protein.

Polyclonal IgG Rac1 antibody (Millipore) was used to detect Rac1 C-terminal as this antibody would bind both wild type Rac1 and to the mutant Rac1 protein if it is produced from the mutant mRNA described in Chapter 3 Section 3.3.3.3. Band intensity was determined using ImageJ software and GADPH was used to normalise Rac1 protein expression. The western blot shown in Figure 39A shows that Rac1 is visually reduced in E15.5 *Rac1*^{TnTCre} hearts. Quantification of the band intensities confirms an 80.1% reduction in Rac1 protein in *Rac1*^{TnTCre} E15.5 hearts compared to controls (Figure 39B) (n=3, p-value 0.016). It is proposed that the remaining Rac1 protein is attributed to Rac1 expression in non-cardiomyocytes cardiac cells. Therefore, it is suggested that Rac1 protein is efficiently and selectively deleted from cardiomyocytes in the Rac1$^{TnT\text{-}Cre}$ embryos. These results suggest that mutant mRNA described in Chapter 3 Section 3.3.3.3 undergoes non-sence RNA medicated decay.

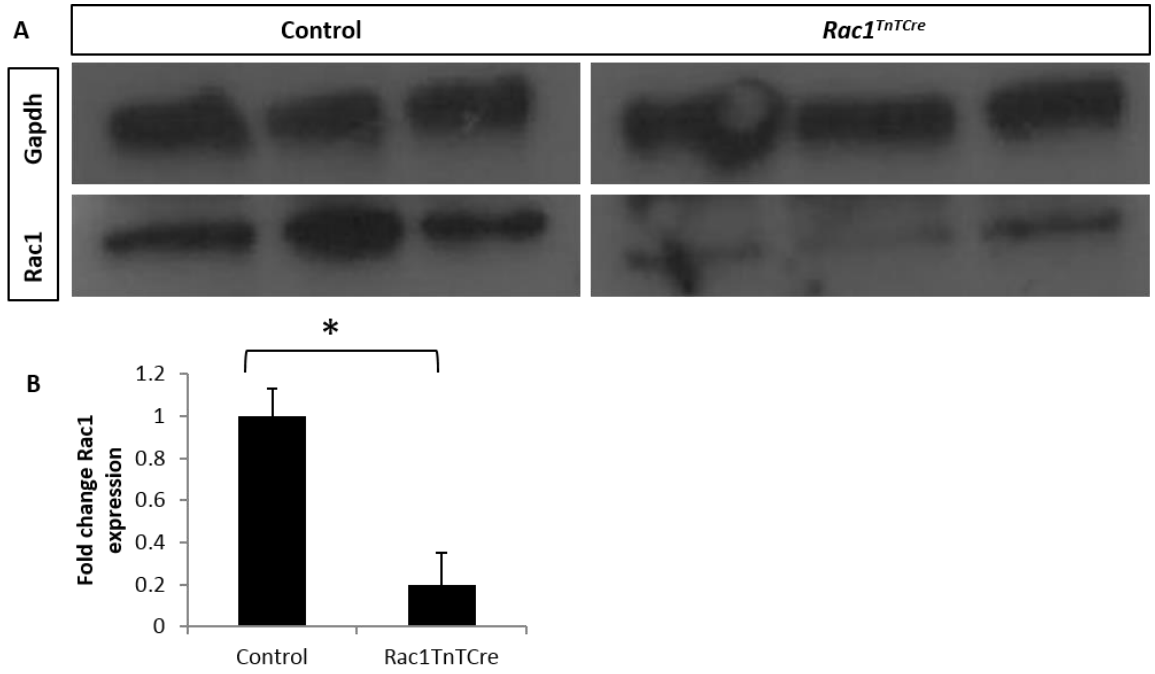

Figure 39: Western blot of Rac1 protein in *Rac1*^{TnTCre} hearts.
Western blotting for Rac1 in using protein from E15.5 hearts revealed a reduction in Rac1 in *Rac1*^{TnTCre} hearts compared to controls (n=3) (**A**). GAPDH was used as a loading control. Quantification of band intensity using ImageJ software showed an 80.1% reduction of Rac1 in *Rac1*^{TnTCre} E15.5 hearts compared to controls (n=3) (*P<0.05) (**B**). *P<0.05. Statistical analysis carried out using the unpaired t-test.

3.3.3.5 Rac gene expression in Rac1^{TnTCre} hearts

Rac family members *Rac1*, *Rac2* and *Rac3* are differentially expressed. *Rac1* is expressed ubiquitously, *Rac2* expression is limited to hematopoietic tissues and *Rac3* is predominanty expressed in the central nervous system. Therefore, *Rac1* is the only Rac family member that is expressed in the heart. It was postulated that the absence of *Rac1* in the heart could lead to compensatory ectopic expression of the other Rac family (*Rac2* and *Rac3*) genes in the heart. RT-PCR was carried out using primers for *Rac1*, *Rac2* and *Rac3* to determine gene expression in whole embryos and in E12.5 control and *Rac1*^{TnTCre} hearts (Figure 40) (Wells *et al.*, 2004). *Rac1*, *Rac2* and *Rac3* are all expressed in E12.5 whole embryo cDNA (Figure 40A). As previously shown, *Rac1* mRNA is expressed in E12.5 hearts in both controls and *Rac1*^{TnTCre} hearts. *Rac2* mRNA is weakly expressed in control E12.5 hearts but expression is comparable in *Rac1*^{TnTCre} hearts and *Rac3* mRNA is not expressed in either control or *Rac1*^{TnTCre} E12.5 hearts (Figure 40B). These results confirm that there is no compensatory change in Rac family member gene expression in the absence of *Rac1* in the heart.

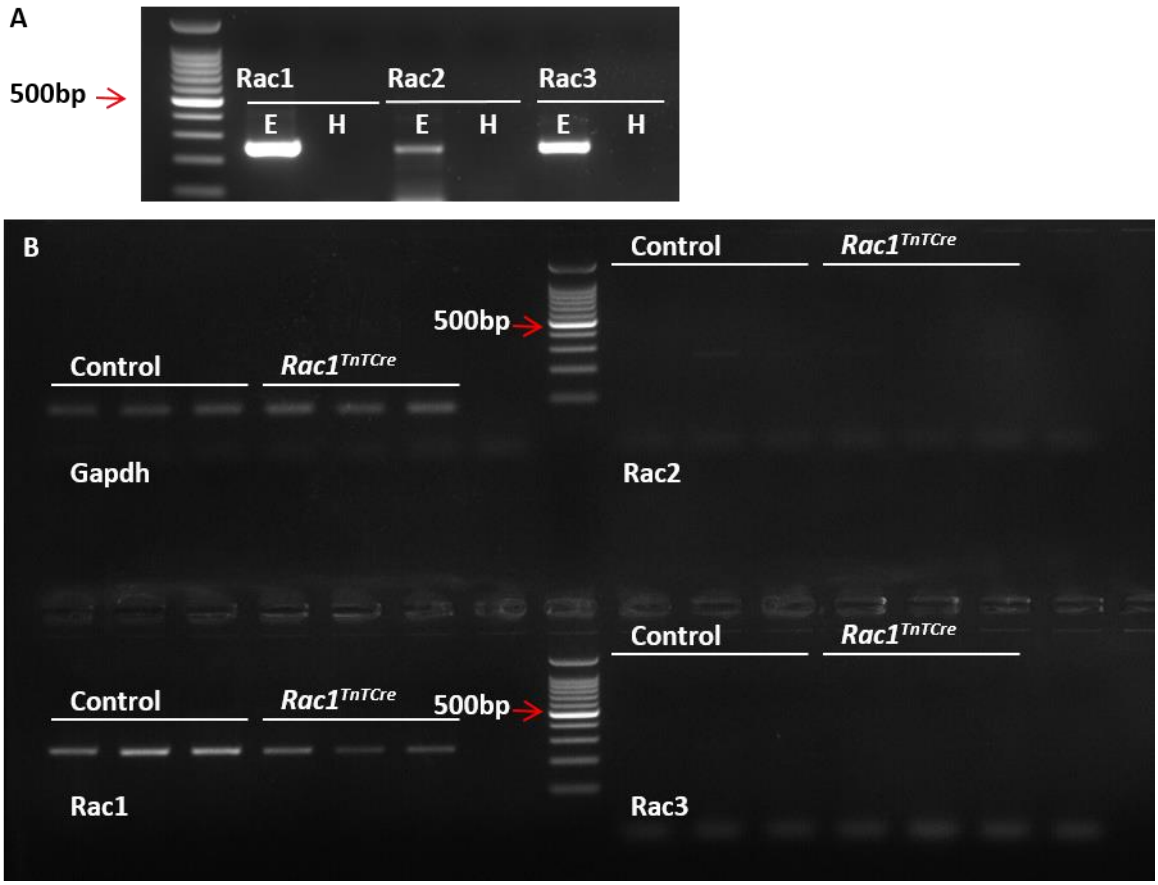

Figure 40: Expression of *Rac* family genes in E12.5 *Rac1*^{TnTCre} hearts.
Rac1, Rac2 and *Rac3* are all expressed in E12.5 whole embryo cDNA (n=3) (**A**). *Rac1* mRNA is expressed in E12.5 hearts in both controls and *Rac1*^{TnTCre} hearts (n=3) (**B**). *Rac2* is weakly expressed in both control and *Rac1*^{TnTCre} hearts. However, *Rac3* mRNA is not expressed in E12.5 hearts, in either control or *Rac1*^{TnTCre} hearts (n=3) (**B**).

Rac1 expression was only assessed at a transcript and protein level in *Rac1*^{TnTCre} hearts due to the previously mentioned issues with specific Rac1 antibodies. For the crosses of *Rac1flox* mice with additonal Cre lines, Rac1 deletion is assessed by the expression of EYFP in Cre positive dervived cells. It is assumed that specific *Rac1* knock out in Cre postive derived cells is consistent in the *Rac1flox* model, with no resulting increase in alternative *Rac* gene expression. However, recombination efficeincy of Cre lines can be variable, therefore this represents a limitation in the interpretation of the data from *Gata5Cre*, *WT1-CreERT2* and *Mlc2vCre* crosses and in comparisons between these crosses.

3.3.3 Combined myocardial and epicardial specific Rac1 deletion causes cardiac defects

To identify the role of *Rac1* in epicardial and myocardial cells during development, *Rac1*^{flox} mice were initially crossed with *Gata5-Cre* mice.

3.3.3.1 Gata5-Cre mice

Gata5-Cre mice were generated as an epicardial specific Cre line with Cre expression observed in the septum transversum at E9.25. At E12.5, expression was detected in the epicardium, pericardium and body wall (Merki *et al.*, 2005). Merki and colleagues also described *Gata5-Cre* expression in the liver and additional studies have shown *Gata5-Cre* is expressed in other tissues, including the lung epithelium and skin (Xing *et al.*, 2010).

3.3.3.2 Gata5-Cre expression

As mentioned, *Gata5-Cre* mice were initially generated as an epicardial specific Cre line. However, the Phillips' group have recently reported expression in the developing myocardium (Boczonadi *et al.*, 2014b). Anti-GFP IHC staining of E9.5-E15.5 *Gata5Cre;EYFP* sections confirmed expression in epicardial cells and also patchy Cre expression within the cardiomyocytes of the developing myocardium (Figure 41). The LV has a consistently higher proportion of *Gata5-Cre*-positive derived cells compared to the RV and *Gata5-Cre* cells mainly appear clustered together in large patches (Figure 41A-E). *Gata5-Cre* is also expressed in the pericardium and SHF cells of the developing OFT and pharyngeal region at E10.5 (Figure 41F-G).

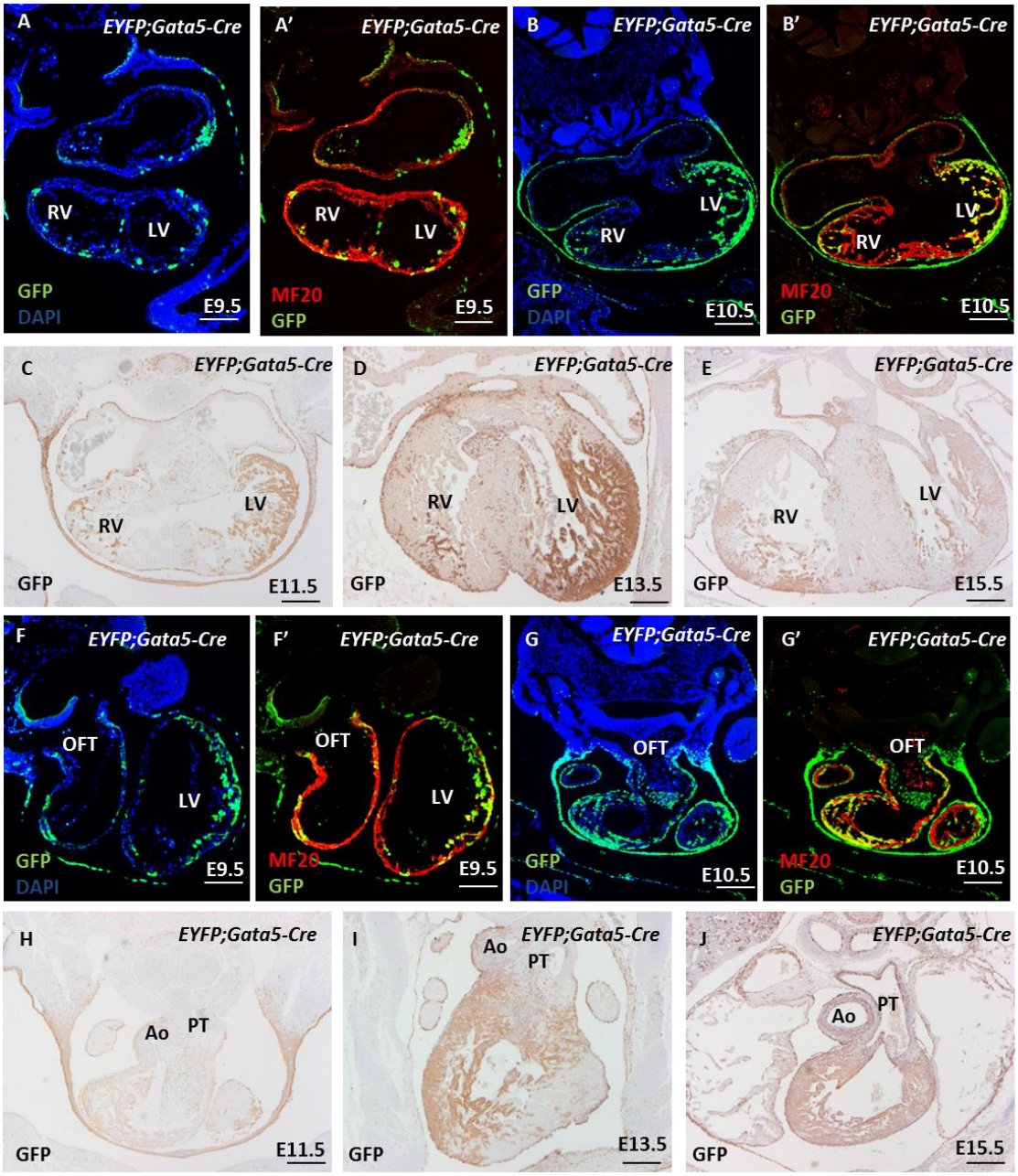

Figure 41: Gata5-Cre expression throughout cardiac development.
Gata5-Cre is expressed in a subset of myocardial cells from E9.5 (**A** and **A'**). From E10.5-E15.5, myocardial *Gata5-Cre* expression is predominately in the left ventricle (**B'**-**E**). *Gata5-Cre* is also detected in epicardial cells at E10.5 and onwards (**B**-**E**), and in the myocardial cells of the outflow tract from E9.5 (**F**-**J**). E; embryonic day, GFP; green fluorescent protein. MF20; myosin II heavy chain, LV; left ventricle, RV; right ventricle, OFT; outflow tract, Ao; aorta, PT; pulmonary trunk. Scale bars; 100µm.

3.3.3.3 Rac1^{flox} x Gata5-Cre mouse cross

Timed matings were set up between *Rac1^{flox}* mice and *Rac1$^{flox;+;}$Gata5-Cre* mice. *Rac1^{Gata5Cre}* embryos were collected across developmental stages E10.5-P0 and analysed using histological and IHC techniques.

The expected number of *Rac1^{Gata5Cre}* embryos were observed as predicted by Mendelian ratios across all ages (E9.5-P0), however some *Rac1^{Gata5Cre}* embryos were found dead *in utero*, from E14.5 onwards, and none survived at birth, therefore, the mutant embryos are embryonic lethal (Table 22). Table 23 shows a summary of the abnormalities observed in *Rac1^{Gata5Cre}* mutant embryos. No external or cardiac defects were observed in control embryos or in *Rac1$^{f+Gata5Cre}$* heterozygous mutants. The heterozygous mutants could therefore be used as Cre-positive controls.

3.3.3.4 Extracardiac defects in Rac1^{Gata5Cre} embryos

Rac1^{Gata5Cre} embryos presented with oedema, cranial haemorrhage, non-closure of the ribs and heart defects. A summary of the defects observed in *Rac1^{Gata5Cre}* embryos is detailed in (Table 23).

Oedema and cranial haemorrhage can be indicative of heart function failure and may result secondary to the heart defects. However, as *Gata5-Cre* is expressed in many tissues, including the lung epithelium and skin, the observed oedema and cranial haemorrhage could also result from Rac1 deficiency in non-cardiac tissues (Xing *et al.*, 2010).

At E11.5 *Gata5-Cre* is expressed in the pericardium (Figure 43, A and B). *Rac1^{Gata5Cre}* mutants display an abnormally thin body wall from E12.5 (Figure 43, C and D), leading to non-closure of the ribs later in development, at E15.5 (Figure 43, E' and F'). This suggests that *Rac1* has an important role in the maturation and thickening of the pericardium and ventral body wall.

Embryonic day (E)	Total embryos	*Rac1*^{Gata5Cre} embryos observed	*Rac1*^{Gata5Cre} embryos expected	% *Rac1*^{Gata5Cre} embryos alive	Chi-squared
E10.5	17	8	4.25	100%	ns
E11.5	70	16	17.5	100%	ns
E12.5	36	8	9	100%	ns
E13.5	64	22	16	100%	ns
E14.5	27	6	6.75	96.3%	ns
E15.5	124	32	31	97.6%	ns
E16.5	16	4	4	100%	ns
E17.5	33	7	8.25	94%	ns
P0	13	5	3.25	0%	ns

Table 22: *Rac1*^{Gata5Cre} embryos observed in expected Mendelian ratios.
The number of *Rac1*^{Gata5Cre} embryos observed at dissection was within the expected limits at each age. Some *Rac1*^{Gata5Cre} embryos were found dead at dissection from E14.5 onwards. Statistical analysis carried out using the Chi-squared test.

Embryonic day (E)	Total *Rac1*^{Gata5Cre} embryos	Oedema	Cranial Haemorrhage	Thin body wall/non closure of ribs	Heart Defect
E10.5	5	0%	0%	0%	0%
E11.5	5	0%	0%	0%	80%
E12.5	6	100%	0%	0%	100%
E13.5	6	100%	16.7%	100%	100%
E14.5	5	100%	20%	100%	100%
E15.5	25	100%	56%	100%	100%
E16.5	4	100%	100%	100%	100%
E17.5	5	100%	80%	100%	100%
P0	5	-	-	100%	100%

Table 23: Summary of the defects observed in *Rac1*^{Gata5Cre} mutant mice.
Rac1^{Gata5Cre} embryos display oedema, cranial haemorrhage and non closure of the ribs, as well as heart defects.

3.3.3.5 Gata5-Cre expression in Rac1^{Gata5Cre} *hearts*

Anti-GFP staining of E11.5, E13.5 and E15.5 control and *Rac1*^{Gata5Cre} sections showed similar expression of *Gata5-Cre* in controls and *Rac1*^{Gata5Cre} embryos (Figure 44). All epicardial cells expressed *Gata5-Cre* at E15.5. In the ventricle, *Gata5-Cre* was expressed in the majority of LV cardiomyocytes (~90%) as well as in some cardiomyocytes in the RV (~40%) and IVS (~20%) (Figure 44). In the OFT, *Gata5-Cre* was expressed in the wall of both the aorta and pulmonary trunk (Figure 45). The number of *Gata5-Cre*-positive derived cells appeared to be reduced in *Rac1*^{Gata5Cre} hearts from E13.5 (Figure 44, D compared to C).

Additionally, the *Gata5-Cre*-positive derived cells appeared more rounded in *Rac1*^{Gata5Cre} hearts compared to controls (Figure 44, D compared to C). These observations are indicative of altered cell survival/proliferation and/or cell polarity in the absence of *Rac1*, which will be discussed further in Chapter 5.

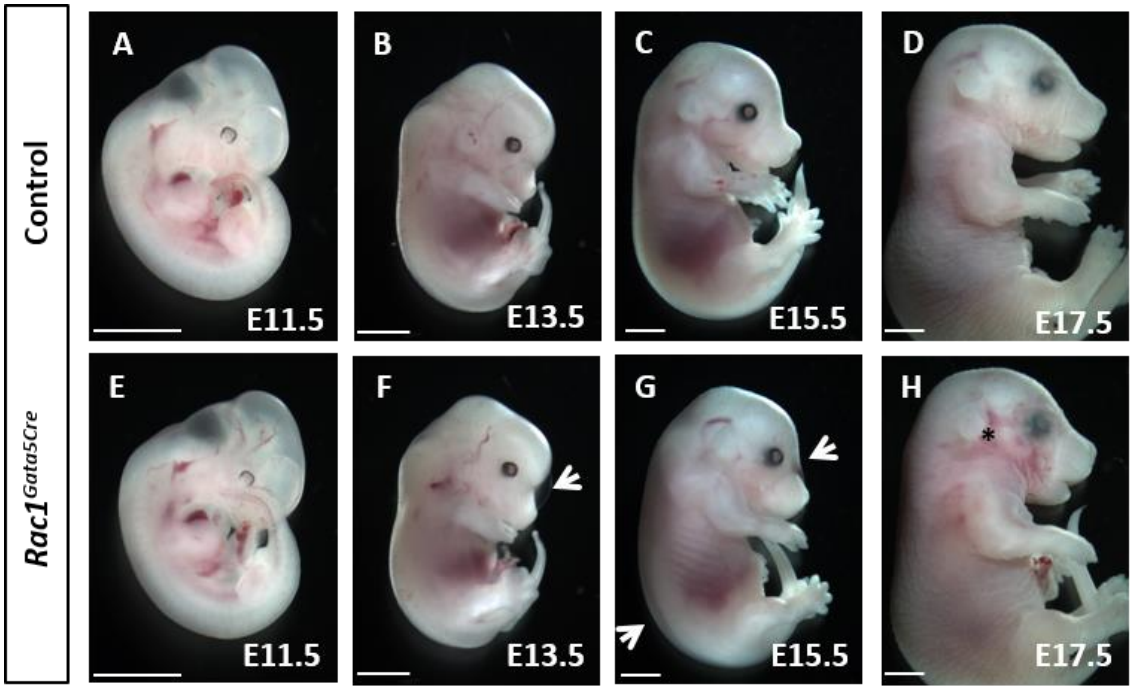

Figure 42: *Rac1*^{Gata5Cre} embryos during development.
Control embryos develop normally (**A**-**D**). Whereas, *Rac1*^{Gata5Cre} embryos develop oedema by E13.5 (white arrow in **F** and **G**) and haemorrhage by E17.5 (asterisk in). E; embryonic day. Scale bars; 2mm.

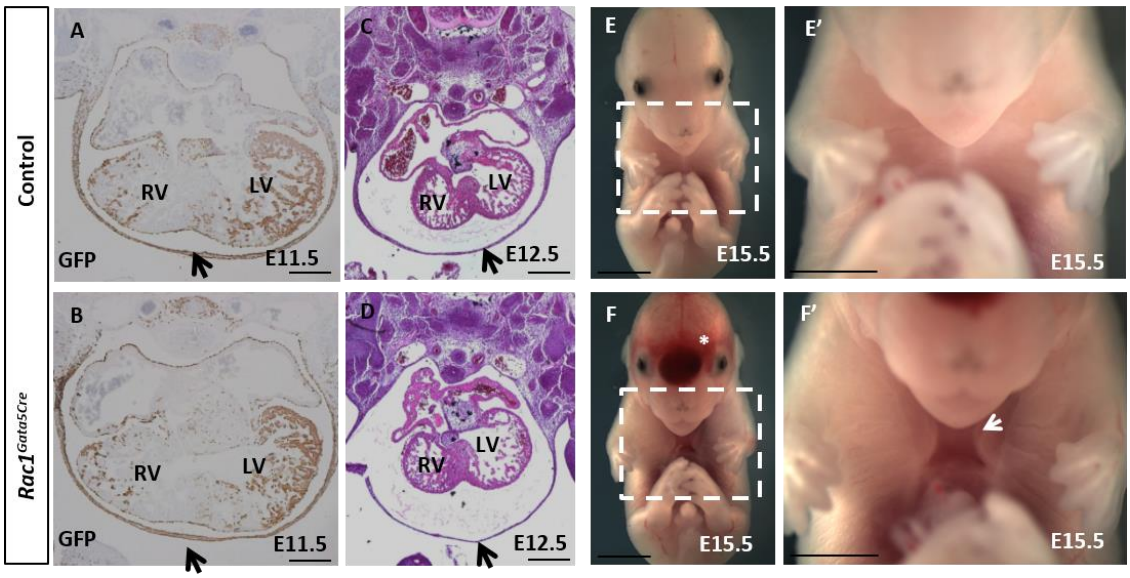

Figure 43: Body wall defects in *Rac1*^{Gata5Cre} embryos.
Gata5-Cre is expressed in the body wall at E11.5 (arrows in **A** and **B**). *Rac1*^{Gata5Cre} embryos have thin body wall from E12.5 (arrows in **C** and **D**) and non-closure of the ribs at E15.5 (**F** and white arrow in **F'**), as well as cranial haemorrhage (asterisk in F). LV; left ventricle, RV; right ventricle, E; embryonic day, GFP; green fluorescent protein. Scale bars; A-B 200µm, C-D 400µm, E-F' 1mm.

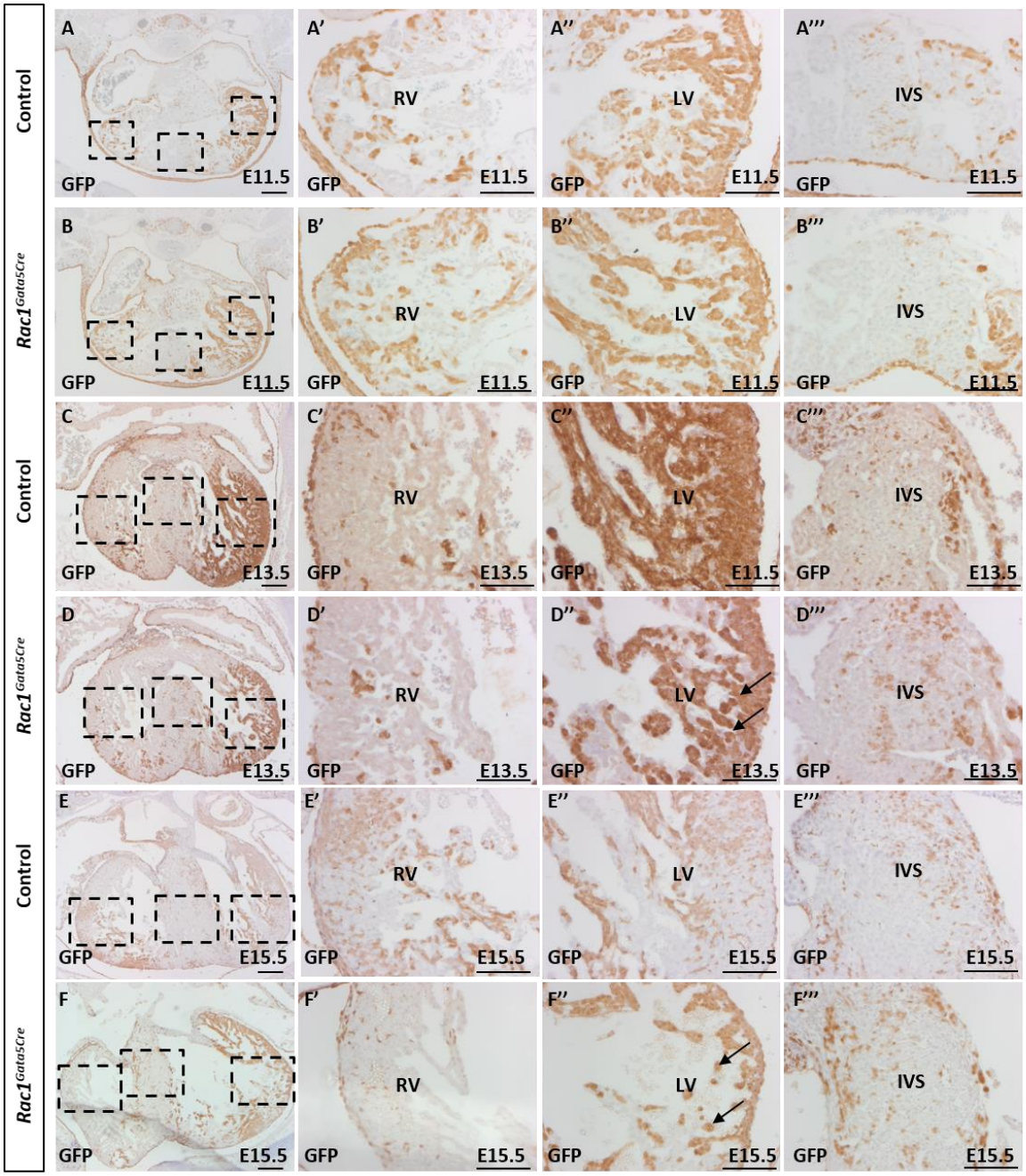

Figure 44: *Gata5-Cre* expression in control and *Rac1*^{Gata5Cre} ventricles.
Anti-GFP staining of E11.5, E13.5 and E15.5 control and *Rac1*^{Gata5Cre} ventricle sections showed similar expression of *Gata5-Cre* in both control and *Rac1*^{Gata5Cre} embryos (n=3). Additionally, the *Gata5-Cre*-positive derived cells appeared more rounded in *Rac1*^{Gata5Cre} hearts compared to controls (arrows in **D''** and **F''** compared to **C''** and **E''**). E; embryonic day, RV; right ventricle, LV; left ventricle, IVS; interventricular septum, GFP; green fluorescent protein. Scale bars; A-F 200µm, A'-F''' 100µm.

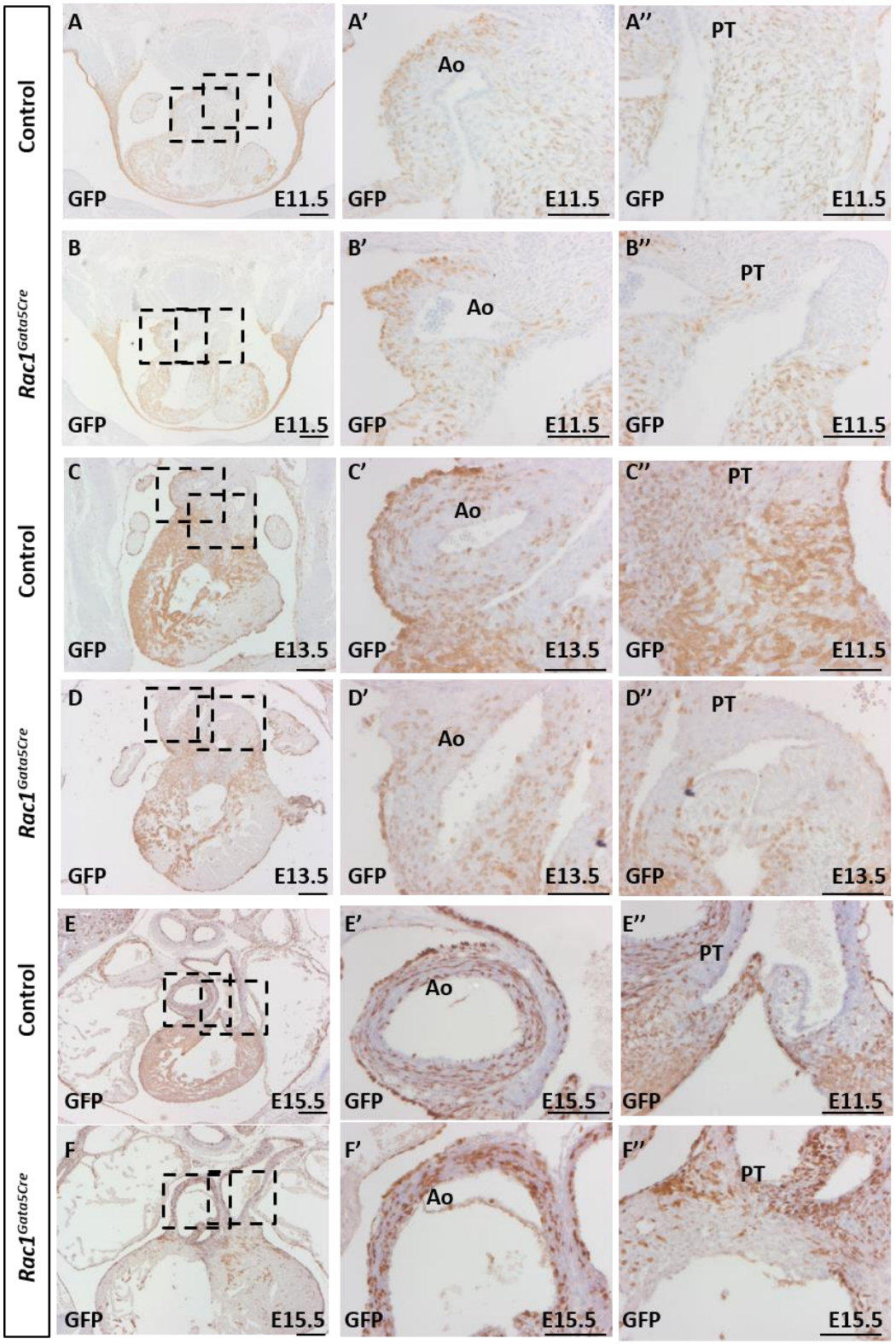

Figure 45: *Gata5-Cre* expression in control and *Rac1*^{Gata5Cre} OFT.
Anti-GFP staining of E11.5, E13.5 and E15.5 control and *Rac1*^{Gata5Cre} OFT sections showed similar expression of *Gata5-Cre* in the aorta and pulmonary trunk in both control and *Rac1*^{Gata5Cre} embryos (n=3) (**A**-**F**). E; embryonic day, Ao; aorta, PT; pulmonary trunk, GFP; green fluorescent protein. Scale bars; A-F 200μm, A'-F''' 100μm.

3.3.3.6 Cardiac defects in Rac1^{Gata5Cre} embryos

From E11.5 onwards, *Rac1*^{Gata5Cre} embryos display heart abnormalities (listed in Table 24). At E11.5 the *Rac1*^{Gata5Cre} hearts have notably sparse trabeculae (Figure 46, D' compared to C'). Later in development, *Rac1*^{Gata5Cre} hearts have a significantly thinned myocardial wall compared to controls (Figure 46E'-L'). Left and right myocardial measurements at E12.5, E13.5, E15.5 and E17.5 show the myocardium becomes increasingly thinner compared to controls from E13.5 onwards and does not recover during development (Figure 46N). In controls, the LV thickens more than the RV from E15.5 to E17.5. However, this difference is not seen in *Rac1*^{Gata5Cre} hearts; both ventricles are of a similar thickness at E17.5 (Figure 46N). The cross-sectional diameter of the heart diameter is unchanged in *Rac1*^{Gata5Cre} hearts compared to controls (Figure 46M). These results suggest the myocardium is not undergoing normal thickening and compaction in *Rac1*^{Gata5Cre} embryos as in the controls.

Occasional epicardial defects were also observed on the surface of the heart in some *Rac1*^{Gata5Cre} mutants from E12.5. These defects included areas of detached epicardial cells filled with blood, forming blisters on the surface of the heart (Figure 47A-C). In some areas, the epicardial surface appeared uneven with small epicardial blisters and invaginations of the myocardium (Figure 47C).

At E15.5, VSD were observed in all *Rac1*^{Gata5Cre} mutants (Figure 48, A and D). Additionally, the aorta remained connected to the RV in the form of OA and DORV (Figure 48, B and E). The aorta appeared dilated with a thinner muscular wall (Figure 48, C' and F').

The *Rac1*^{Gata5Cre} cardiac phenotype confirms that *Rac1* is required in the myocardium and/or epicardium for normal development of the ventricles and correct OFT alignment. It is hypothesised that the *Rac1*^{Gata5Cre} embryos die at/before birth due to the combination of lethal body wall and heart defects observed during development.

Embryonic day (E)	Total *Rac1*^{Gata5Cre} embryos	Epicardial blood blisters	Thin myocardium	Abnormal trabeculae	VSD	OA/ DORV
E10.5	5	0%	0%	0%	-	-
E11.5	5	20%	40%	60%	-	-
E12.5	6	83.3%	33.3%	100%	-	-
E13.5	5	40%	100%	100%	-	-
E14.5	5	60%	100%	100%	-	-
E15.5	8	100%	100%	100%	100%	100%
E16.5	4	50%	100%	100%	100%	100%
E17.5	5	20%	100%	100%	100%	100%

Table 24: Summary of the cardiac defects observed in *Rac1*^{Gata5Cre} mutant embryos.

No defects were observed in the control embryos/pups at any age. A visible reduction in the thickness of the myocardium was classed as a thin myocardium. Abnormal trabeculae was defined as a visibly reduced number of trabeculae or aberrant directionality of trabeculae. VSD; ventricular septal defect, OA; overriding aorta, DORV; double outlet right ventricle.

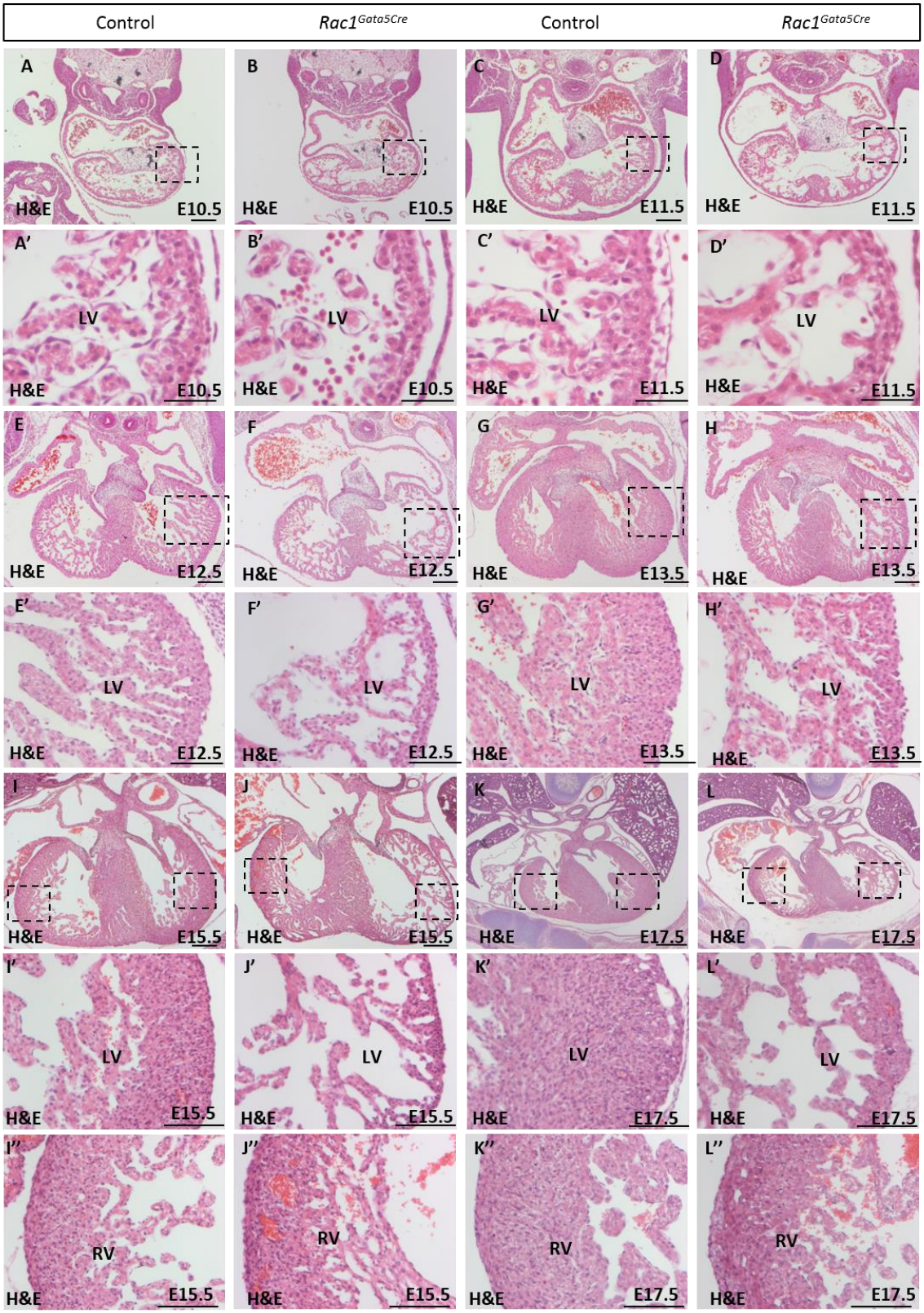
Control
Rac1Gata5Cre
Control
Rac1Gata5Cre
A
B
C
D
H&E
E10.5
E10.5
E11.5
E11.5
A'
B'
C'
D'
LV
LV
LV
LV
H&E
E10.5
E10.5
E11.5
E11.5
E
F
G
H
H&E
E12.5
E12.5
E13.5
E13.5
E'
F'
G'
H'
LV
LV
LV
LV
H&E
E12.5
E12.5
E13.5
E13.5
I
J
K
L
H&E
E15.5
E15.5
E17.5
E17.5
I'
J'
K'
L'
LV
LV
LV
LV
H&E
E15.5
E15.5
E17.5
E17.5
I''
J''
K''
L''
RV
RV
RV
RV
H&E
E15.5
E15.5
E17.5
E17.5

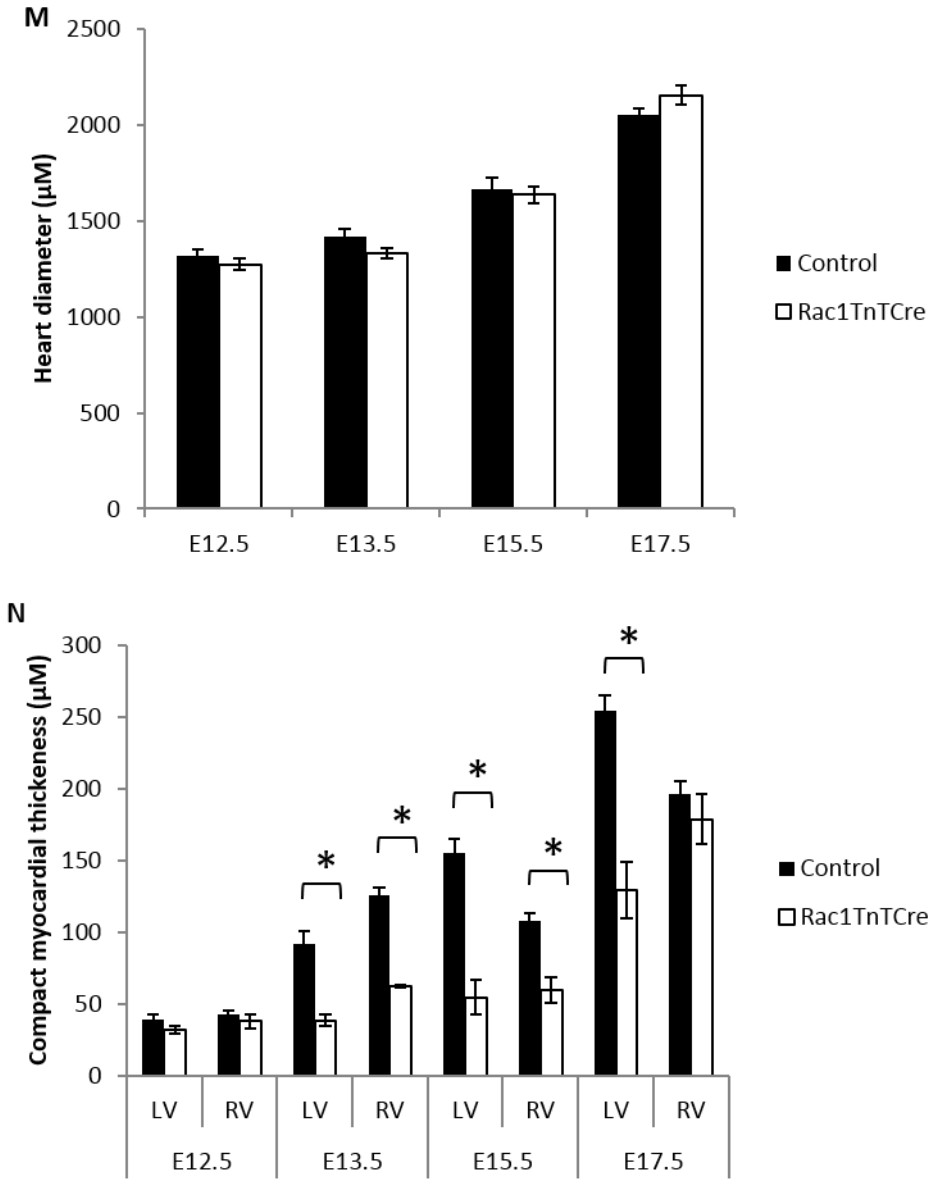

Figure 46: H&E staining and myocardial measurements of control and *Rac1*^{Gata5Cre} hearts.

Example images of H&E stained control and *Rac1*^{Gata5Cre} heart sections at E10.5 to E17.5 (n=5) (**A**-**L**). The heart diameter is unchanged in *Rac1* ^{Gata5Cre} hearts compared to controls (**M**). *Rac1*^{Gata5Cre} hearts have a significantly thinned compact myocardium compared to aged matched controls from E13.5 (**N**). In controls, the left ventricle is thicker than the right ventricle at E17.5, whereas the ventricles are of equal thickness in *Rac1*^{Gata5Cre} embryos (**N**). E; embryonic day, RV; right ventricle, LV; left ventricle. Scale bars; A-J 200µm, A'-H' 50µm, K-L 500µm, I'-L'' 100µm. *p<0.05. Statistical analysis carried out using a two-way ANOVA.

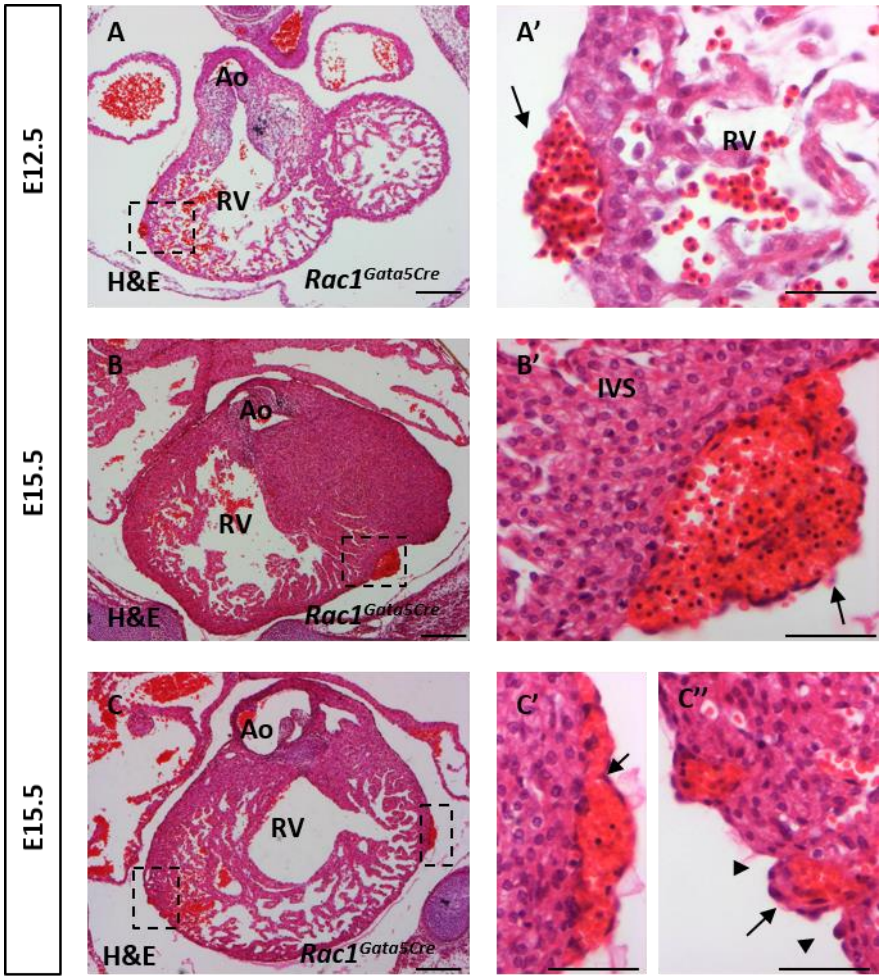

Figure 47: Epicardial defects in *Rac1*^{Gata5Cre} hearts.
Example images of epicardial blisters in *Rac1*^{Gata5Cre} hearts at E12.5 and E15.5. In some areas, the epicardium is detached from the surface of the heart and the gap is filled with red blood cells (**A'**, **B'** and **C'**). In other areas, the epicardial surface appears uneven with small epicardial blisters and invaginations of the myocardium (**C''**). RV; right ventricle, Ao; aorta. Scale bars; A-C 200µm, A'-C'' 100µm.

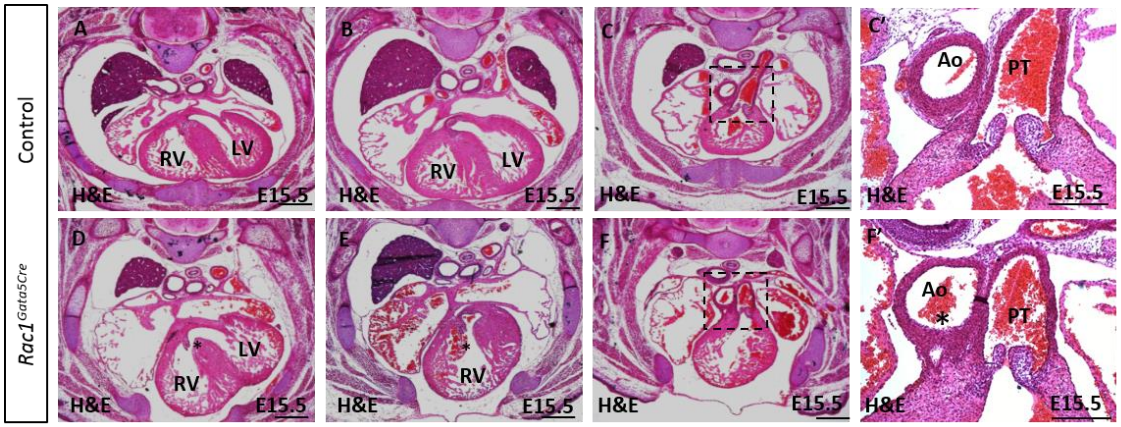

Figure 48: OFT defects in *Rac1*^{Gata5Cre} hearts.
Rac1^{Gata5Cre} hearts have ventricular septal defects (VSD) (asterisk in **D**), double outlet right ventricle (DORV) (asterisk in **E**) and dilated aorta (asterisk in **F'**) (n=5). E; embryonic day, LV; left ventricle, RV; right ventricle, Ao; aorta, PT; pulmonary trunk. Scale bars; A-F 500μm, C' and F' 100μm.

3.3.4 Epicardial specific deletion of Rac1 does not affect cardiac development

As both epicardial and myocardial cells were affected in the *Gata5-Cre* crosses, to dissect the roles of *Rac1* in the epicardium and myocardium during cardiac development, *Rac1* was first specifically deleted from epicardial cells by crossing *Rac1*^{flox} mice to a tamoxifen inducible *WT1-CreERT2* mouse line.

3.3.4.1 WT1-CreERT2 mice

The generation and validation of *WT1-CreERT2* mice has been described previously (Zhou *et al.*, 2008). Briefly, *GFPCre* complementary DNA was knocked into the endogenous *WT1* start codon. *WT1-Cre* expression was confined to proepicardium and epicardium from E9.5 to E15.5, and was not detected in the myocardium. To regulate Cre-labelling temporally, a cDNA encoding a Cre-modified oestrogen receptor ligand-binding domain (*CreERT2*) was also knocked into the *WT1* locus. CreERT2 fusion protein recombinase activity requires tamoxifen. Maternal injection of tamoxifen at E10.5 and E11.5 was found to induce Cre activity whereas no expression was detected in the absence of tamoxifen. The frequency of *WT1*^{CreERT2} labelled cells in epicardium was reduced compared to constitutive labelling by *WT1*^{GFPCre}, probably due to inefficient CreERT2 activation by tamoxifen concentrations compatible with maintenance of pregnancy (Zhou *et al.*, 2008).

3.3.4.2 Rac1^{flox} x WT1-CreERT2 mouse cross

Timed matings were set up between *Rac1^{flox}* mice and *Rac1$^{flox;+;}$WT1-CreERT2* mice. Cre recombinase was activated in *WT1-CreERT2*-expressing epicardial cells following an intraperitoneal dose of tamoxifen administered on 2 consecutive days at either E8.5 and E9.5 (n=4) or E9.5 and E10.5 (n=6). At this point in embryonic development epicardial cells are migrating from the pro-epicardium and attaching to the surface of the myocardium to form the single layered epicardium. Therefore, Rac1 should be deleted in the pro-epicardial cells as they form the epicardial layer. This is similar to when *Gata5-Cre* is expressed in the epicardium and hence allows the dissection of the *Rac1^{Gata5Cre}* phenotype using this model. *Rac1$^{WT1-CreERT2}$* embryos were collected at E15.5 and the expected numbers of embryos were observed as predicted by Mendelian ratios. All *Rac1$^{WT1-CreERT2}$* mice were alive and appeared to have developed normally compared to littermate controls at E15.5 (Figure 49, A and D). *Rac1$^{WT1-CreERT2}$* embryos were analysed using histological and IHC techniques. No external or cardiac defects were observed in control embryos or in *Rac1$^{f+WT1-CreERT2}$* heterozygous mutants. The heterozygous mutants could, therefore, be used as Cre-positive controls.

3.3.4.3 WT1-CreERT2 expression

IHC staining with an anti-GFP antibody confirmed Cre activation in epicardial cells and EPDCs exclusively at E15.5 (Figure 49G-L).

3.3.4.4 Cardiac phenotype in Rac1$^{WT1-CreERT2}$ embryos

H&E staining showed no observable defects in myocardial development in E15.5 *Rac1$^{WT1-CreERT2}$* hearts when Cre was induced at either E8.5-9.5 or E9.5-10.5 (Figure 49A-B, D-F). Measurements of left and right myocardial wall thickness confirmed no differences between control and *Rac1$^{WT1-CreERT2}$* hearts (Figure 49C). Additionally, no septal or OFT defects were observed in *Rac1$^{WT1-CreERT2}$* embryos.

3.3.4.4 Migration of epicardial and EPDCs in Rac1$^{WT1-CreERT2}$ embryos

IHC staining with anti-GFP identifies the Cre-positive epicardial cells and EPDCs in the *Rac1$^{WT1-CreERT2}$* hearts. Epicardial cells appear to have migrated from the proepicardium and spread over the outer surface of the heart in both

control and *Rac1*$^{WT1\text{-}CreERT2}$ embryos (Figure 49G-L). The number of Cre-positive derived epicardial cells is not significantly different in *Rac1*$^{WT1\text{-}CreERT2}$ compared to control hearts (Figure 49M). Furthermore, Cre-positive derived EPDCs are found migrating into the myocardial layer of the heart in *Rac1*$^{WT1\text{-}CreERT2}$ embryos as in controls (Figure 49, arrows in C and F). The number and distance of Cre-positive derived EDPCs is not significantly different in *Rac1*$^{WT1\text{-}CreERT2}$ embryos compared to controls (Figure 49M-N). However, there is a slight trend towards a reduced number/distance of migration of EPDCs, therefore analysis of additional hearts at E15.5 and additional ages, possibly E12.5 and E17.5, would be necessary to conclude that Rac1 has no role in EPDC migration. An epicardial explant and cell migration assay could also be carried out.

The lack of a cardiac phenotype in *Rac1*$^{WT1\text{-}CreERT2}$ embryos at E15.5, indicates that Rac1 is not required in epicardial cells for the normal thickening and maturation of the myocardium during embryonic development, up to this stage. Therefore, it was hypothesised that *Rac1* is essential in myocardial cells for the development of the myocardial wall.

Embryo stage	**Total embryos**	***Rac1*$^{WT1\text{-}CreERT2}$ expected embryos**	***Rac1*$^{WT1\text{-}CreERT2}$ observed embryos**	**% embryos alive**	**Chi-squared**
E15.5	59	14.75	14	100%	ns

Table 25: Expected and observed numbers and percentages for *Rac1*^{Mlc2vCre} embryos and pups.
The number of *Rac1*$^{WT1\text{-}CreERT2}$ embryos observed at dissection were within the expected limits E15.5. No *Rac1*$^{WT1\text{-}CreERT2}$ embryos were found dead at dissection. Statistical analysis carried out using the Chi-squared test.

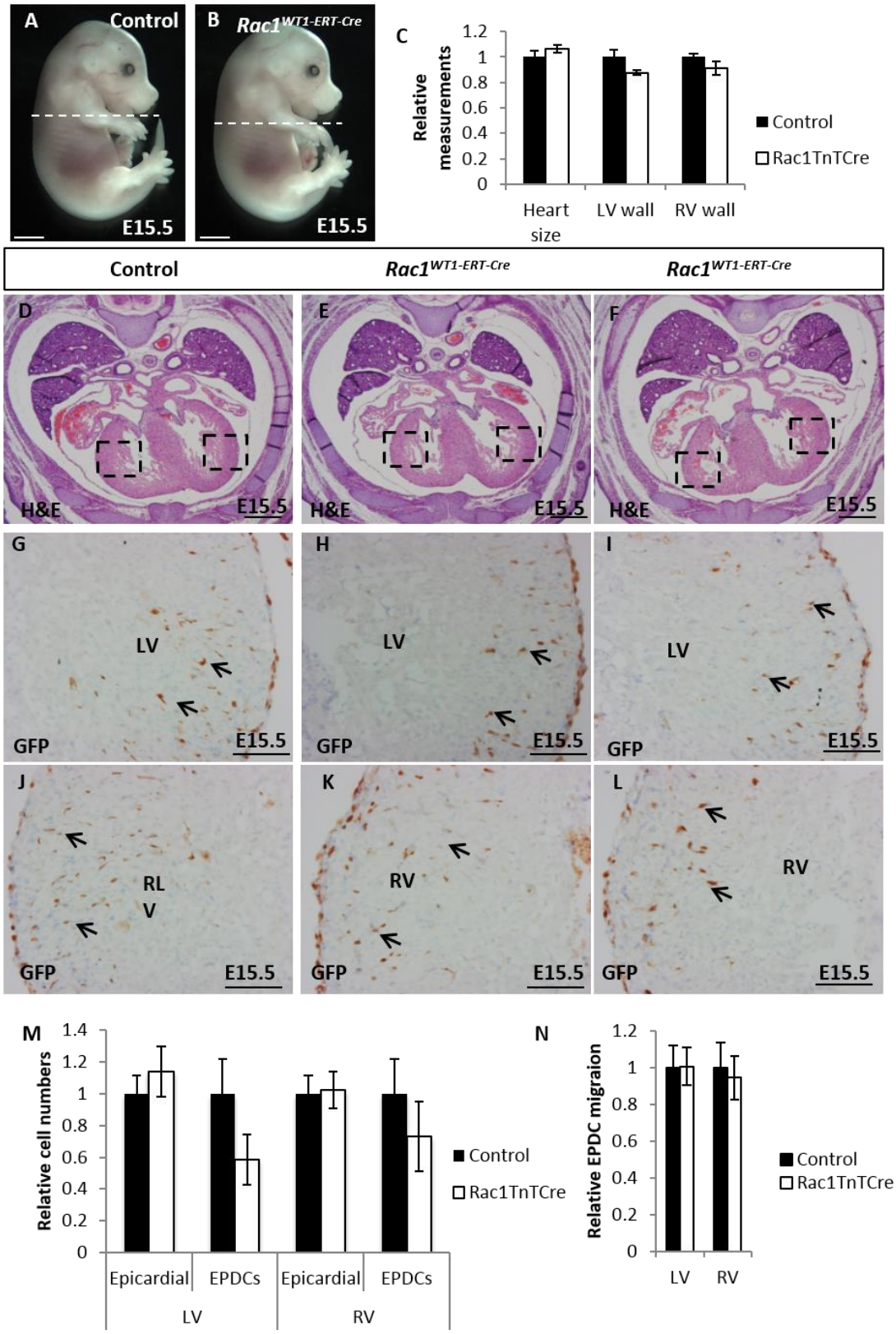
A
Control
E15.5
B
Rac1WT1-ERT-Cre
E15.5
C
Relative measurements
1.2
1
0.8
0.6
0.4
0.2
0
Heart size
LV wall
RV wall
Control
Rac1TnTCre
Control
Rac1WT1-ERT-Cre
Rac1WT1-ERT-Cre
D
E
F
H&E
E15.5
G
H
I
LV
GFP
E15.5
J
K
L
RL
V
RV
M
Relative cell numbers
1.4
1.2
1
0.8
0.6
0.4
0.2
0
Epicardial
EPDCs
Epicardial
EPDCs
LV
RV
Control
Rac1TnTCre
N
Relative EPDC migraion
1.2
1
0.8
0.6
0.4
0.2
0
LV
RV
Control
Rac1TnTCre

Figure 49: *Rac1*$^{WT1\text{-}CreERT2}$ phenotype.
Rac1$^{WT1\text{-}CreERT2}$ embryos do not have any external phenotype (**A** and **D**) (n=14). *Rac1*$^{WT1\text{-}CreERT2}$ hearts are normal compared to controls (**B** and **E**) (n=6). Statistical analysis carried out using an unpaired t-test. *Rac1*$^{WT1\text{-}CreERT2}$ epicardial cells correctly form the epicardium as in the control and the EPDCs successfully migrate into the myocardium as in the control (n=6) (**C** and **F**, arrows point to migrating EPDCs). RV; right ventricle, LV; left ventricle, EPDCs; epicardially derived cells, GFP; green fluorescent protein. Scale bars; A-B 2mm, D-F 500µm, G-L 100µm. Statistical analysis carried out using a two-way ANOVA.

3.3.5 Patchy myocardial deletion of Rac1 does not affect cardiac development

To further dissect the roles of Rac1 in the epicardium and myocardium during cardiac development, *Rac1* was specifically deleted from myocardial cells by crossing *Rac1*^{flox} mice to a *Mlc2v-Cre* mouse line.

3.3.5.1 Mlc2v-Cre mice

The *Mlc2v-Cre* mice have been generated by a gene knock-in approach, with *Cre recombinase* being inserted into exons 1 and 2 of the *Mlc2v* gene (Chen *et al.*, 1998).

3.3.5.2 Mlc2v-Cre expression

Mlc2v-Cre is exclusively expressed in cardiomyocytes, therefore, it allows investigation of gene function specifically in the myocardium without interference from extra-cardiac defects or additional cardiac cell functions (as in *Rac1*^{Gata5Cre} embryos). Dual IF staining of E9.5, E10.5 and E15.5 *EYFP;Mlc2v-Cre* embryo sections using anti-GFP and anti-MF20 confirmed patchy expression in cardiomyocytes of the developing ventricular myocardium (Figure 50, A, C and E). At E15.5, *Cre* expression was highest in the IVS (~80%), and less in the myocardium of the ventricles, at around 50% and 30% in the right and left ventricles, respectively. Expression was absent from the developing atria and OFT (Figure 50, B and D).

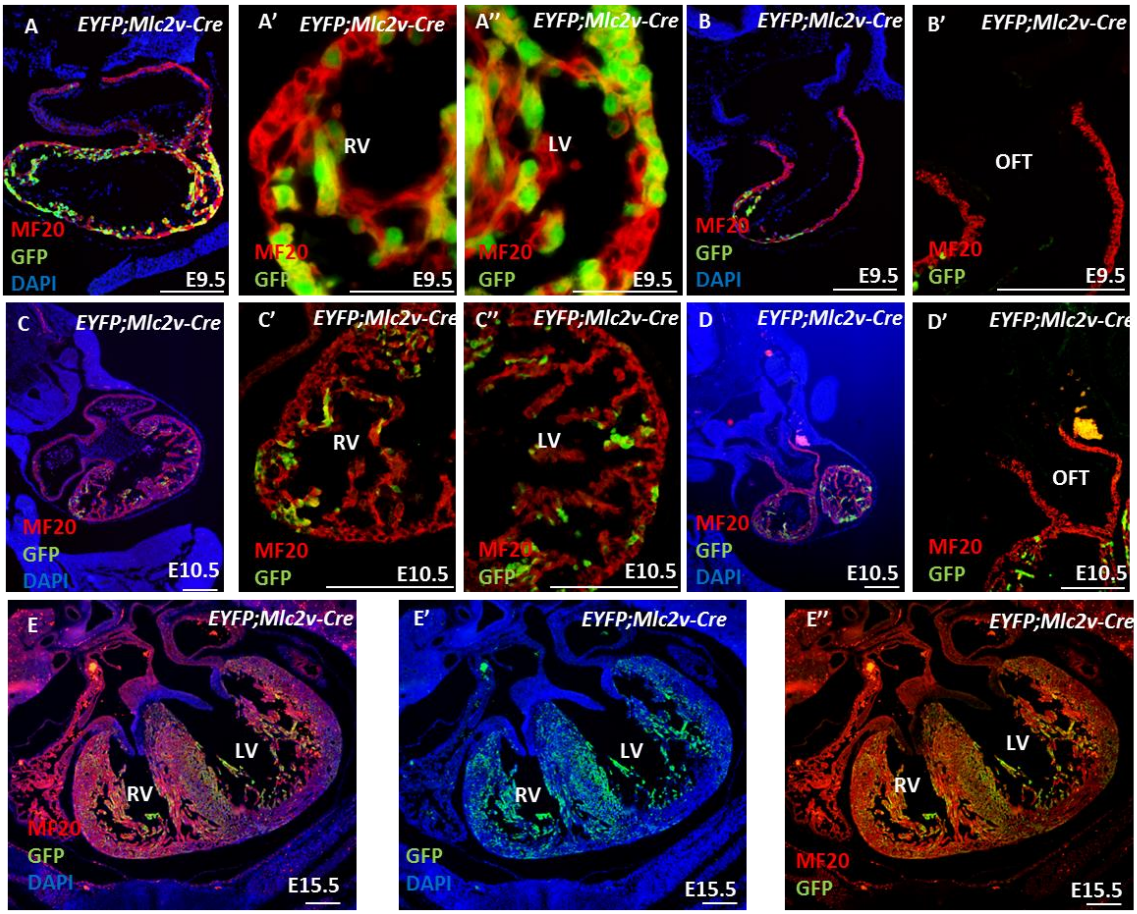

Figure 50: Mlc2v-Cre expression during cardiac development.
Dual IF staining of E9.5, E10.5 and E15.5 *EYFP;Mlc2v-Cre* sections using anti-GFP and anti-MF20 confirmed patchy expression in cardiomyocytes of the developing ventricular myocardium. Expression was absent from the developing atria and OFT. E; embryonic day. GFP; green fluorescent protein. LV; left ventricle, RV; right ventricle, OFT; outflow tract. Scale bars; A-E'' 200μm, except A'-A'' 50μm.

3.3.5.3 Rac1^{flox} x Mlc2v-Cre mouse cross

Rac1 and *Mlc2v* genes are found close together on Chromosome 5 (20.06cM apart) (Figure 51A), consequently, mutants could only be generated via genetic recombination (Figure 51C versus D). The frequency of mutant offspring observed was 20.7% and this is consistent with the predicted recombinant frequency of 20.06% (Figure 51B). Timed matings were set up between *Rac1^{flox}* mice and *Rac1$^{flox;+;}$Mlc2v-Cre* mice. All *Rac1^{Mlc2vCre}* mice survived to at least 21 days and appeared to develop normally compared to littermate controls (Figure 52A-B). *Rac1^{Mlc2vCre}* embryos were collected at E15.5 and analysed by histology and IHC techniques.

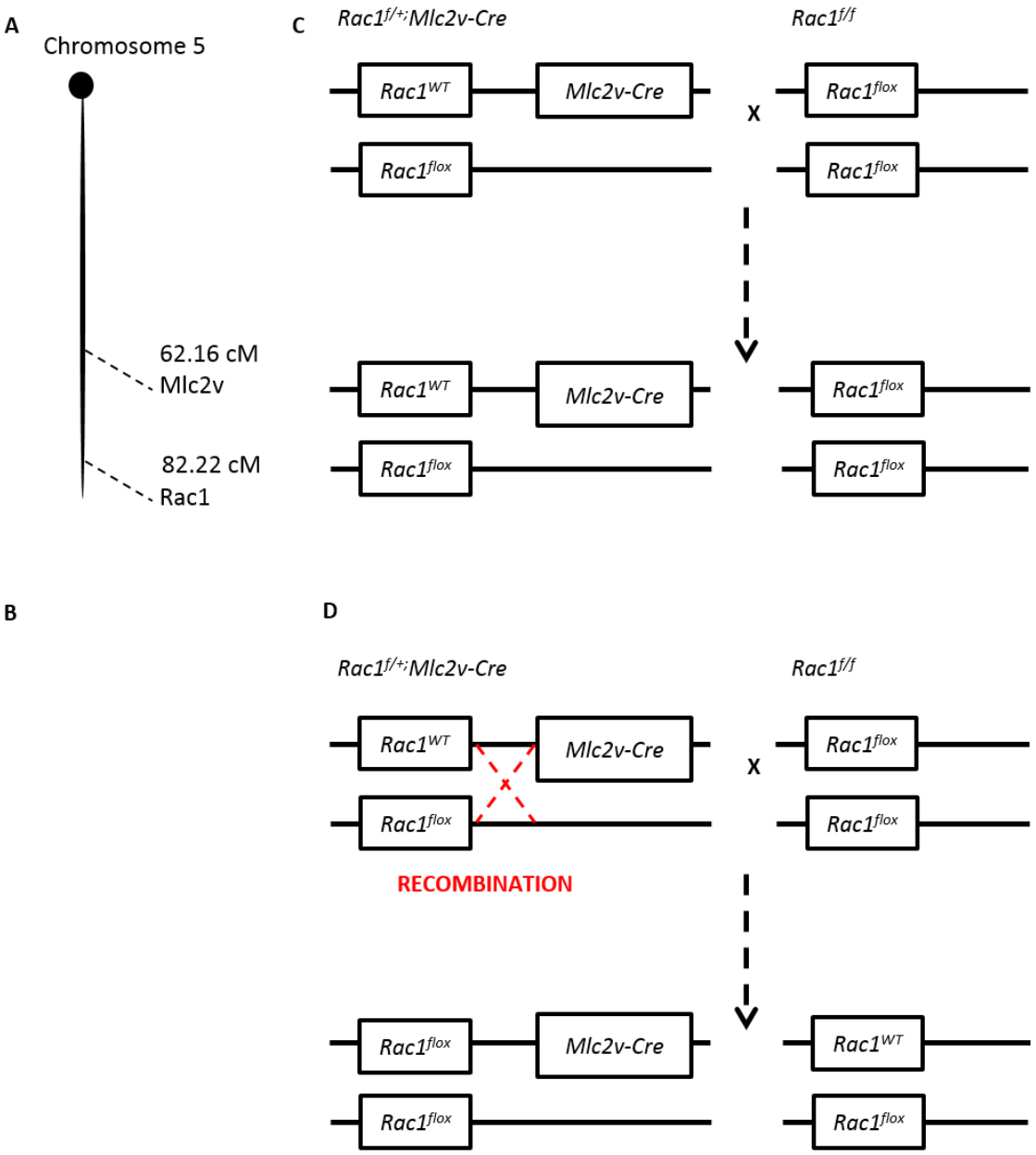

Figure 51: Recombination explanation of *Rac1^{flox}* x *Mlc2v-Cre* cross.
Rac1 and *Mlc2v* genes are found close together on Chromosome 5 (20.06cM apart) (**A**), consequently, mutants could only be generated via genetic recombination (**C** versus **D**). The frequency of mutant embryos and neonates observed was 20.7% and this is consistent with the predicted recombinant frequency between *Rac1^{flox}* and *Rac1^{WT};Mlc2v-Cre* alleles of 20.06% (**B**).

Embryo stage	Total embryos	*Rac1*^{Mlc2vCre} embryos expected		*Rac1*^{Mlc2vCre} embryos observed		% embryos alive	Chi-squared
		Number	Percentage	Number	Percentage		
E9.5	26	6.5	25%	1	3.8%	100%	0.013
E15.5	75	18.75	25%	8	10.6%	100%	1.01E-6
Weaned pups	15	3.75	25%	3	20%	100%	0.033

Table 26: Expected and observed numbers and percentages for *Rac1*^{Mlc2vCre} embryos and pups.

The number of *Rac1*^{Mlc2vCre} embryos observed at dissection were within the expected limits at each age. No *Rac1* ^{Mlc2vCre} embryos were found dead at dissection. Statistical analysis carried out using the Chi-squared test.

3.3.5.4 Cre expression in Rac1^{Mlc2vCre} *embryos*

IHC staining of E15.5 wax sections with anti-GFP antibody confirmed Cre activation in a subset of ventricle myocardial cells in both control and *Rac1*^{Mlc2vCre} embryos (Figure 53). Expression was patchy in both ventricles and IVS but was absent from the atria and OFT.

3.3.5.5 Cardiac phenotype in Rac1^{Mlc2vCre} *embryos*

E15.5 sections were stained with H&E to examine cardiac morphology in *Rac1*^{Mlc2vCre} embryos. *Rac1*^{Mlc2vCre} hearts were grossly normal with a thickened ventricle myocardium, confirmed by myocardial thickness measurements of the left and right ventricle (Figure 52C-D). The thickened and compact myocardium consisted of mostly unaffected wild type cells or Cre expressing Rac1 mutant cardiomyocytes which were interspersed with unaffected wild type cells. (Figure 53E-F). Interestingly, in 3 out of 8 *Rac1*^{Mlc2vCre} hearts, a small region of the compact myocardial wall appeared thinner and less compacted compared to the rest of the myocardial wall (Figure 53E-F). These areas of thin and less compact myocardium correlated with regions of densely packed Cre expressing Rac1 mutant cardiomyocytes. *Rac1*^{Mlc2vCre} embryos did not have any septal or OFT defects.

3.3.5.6 Cardiomyocyte maturation

E15.5 sections were immunostained using an anti-α-SMA antibody to examine cardiomyocyte maturation in *Rac1*^{Mlc2vCre} embryos. Reduction in α-SMA expression is associated with cardiomyocyte differentiation and therefore at

E15.5, α-SMA becomes restricted to the compact myocardium and is relatively absent from the trabeculated myocardium. α-SMA expression appeared normal in *Rac1*^{Mlc2vCre} hearts compared to controls, implying myocardial wall maturation is unaffected in *Rac1*^{Mlc2vCre} embryos (Figure 53E-F). In conclusion, deleting *Rac1* from a subset of cardiomyocytes leads to mild myocardial defects, but does not recapitulate the defects seen in *Rac1*^{Gata5Cre} embryo hearts. Therefore it was hypothesised that the high percentage of Rac1 expressing cardiomyocytes (50% and 70% in the right and left ventricles, respectively) are able to compensate for the lack of Rac1 in the interspersed mutant cells. In regions where mutant cells are clustered mild myocardial defects are observed, similar to that seen in the *Rac1*^{Gata5Cre} embryos (Figure 53F).

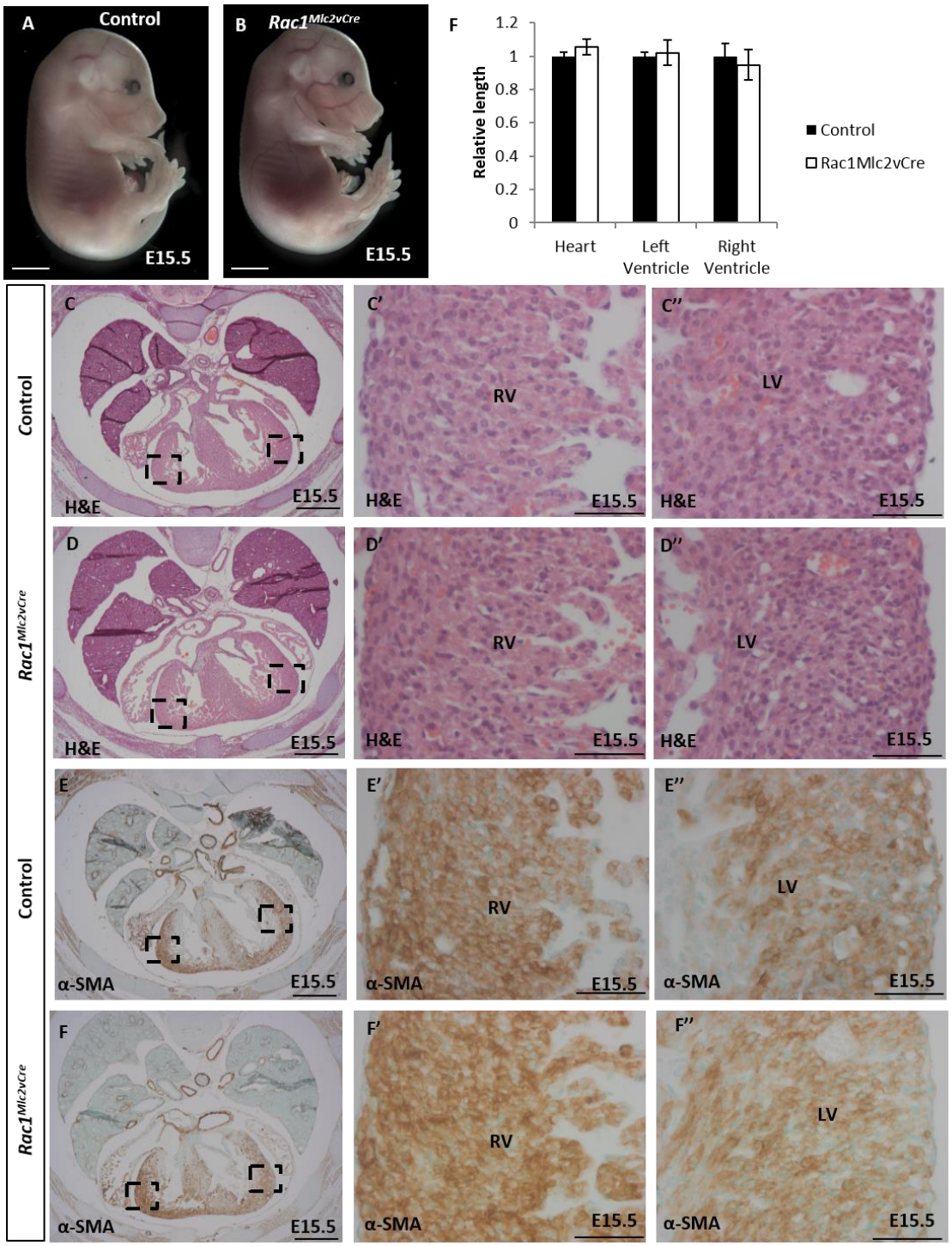

Figure 52: *Rac1*^{Mlc2vCre} embryos show no abnormal phenotype.
Rac1^{Mlc2vCre} embryos develop normally and do not show any external defects at E15.5 (n=8) (**A**-**B**). H+E staining of transverse sections shows that there are no structural heart defects in *Rac1*^{Mlc2vCre} hearts and myocardial development is normal compared to controls at E15.5 (n=6) (**C**-**D**) and α-SMA IHC staining reveals normal cardiomyocyte maturation compared to controls at E15.5 (n=6) (**E**-**F**). LV; left ventricle, RV; right ventricle. Scale bars; A-B 2mm, C-F 500μm, C'-F'' 50μm.

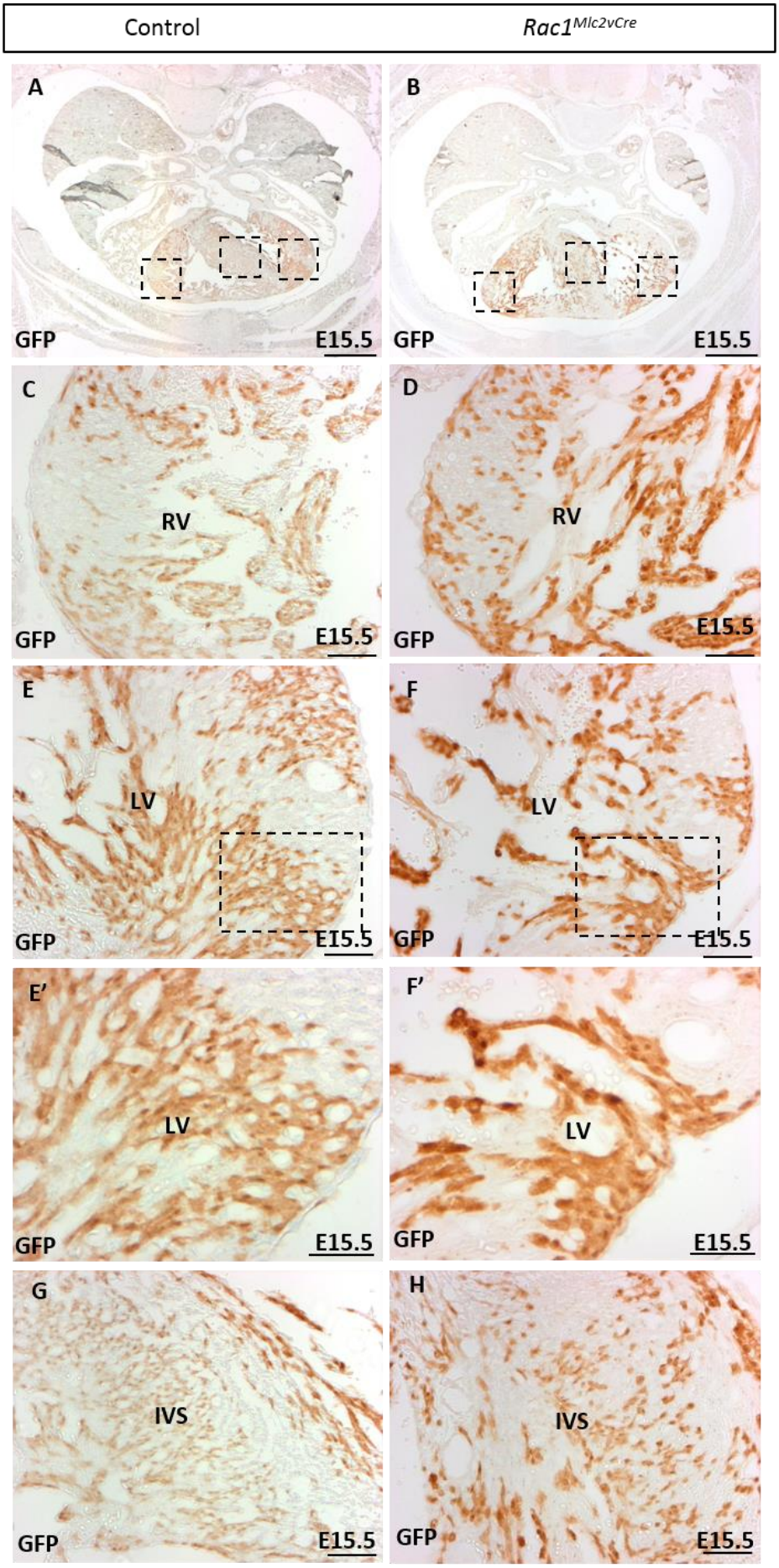
Control
Rac1Mlc2vCre
A
B
GFP
E15.5
C
D
RV
E
F
LV
E'
F'
G
H
IVS

Figure 53: IHC anti-GFP staining of E15.5 control and *Rac1*^{Mlc2vCre} heart sections.
IHC staining of E15.5 wax sections with anti-GFP antibody confirmed Cre activation in a subset of myocardial cells in both control and *Rac1*^{Mlc2vCre} embryos. Mlc2v-Cre expression was patchy in both ventricles and IVS (**A**-**D**, **G**-**H**). In regions of densely packed Cre expressing mutant cells, the compact myocardial wall appeared thinner and less compacted compared to the rest of the myocardial wall in *Rac1*^{Mlc2vCre} hearts. Whereas, wild type cells or interspersed Cre expressing mutant cells were found in areas of compacted ventricular wall (**E'**-**F'**). LV; left ventricle, RV; right ventricle, IVS; interventricular septum. Scale bars; A-B 500μm, C-H 200μm, E'-F' 50μm.

3.3.6 Rac1 is required in the myocardium for normal myocardial and outflow tract development

As shown in Chapter 3 Section 3.3.4 Rac1 is not required in the epicardium for ventricular wall development, therefore it was hypothesised that deletion of Rac1 in cardiomyocytes is the source of the myocardial phenotype observed in *Rac1*^{Gata5Cre} embryos. Therefore, *Mlc2v-Cre* was used to delete *Rac1* from cardiomyocytes. However, as discussed in Chapter 3 Section 3.3.5, the percentage of cardiomyocytes expressing *Mlc2v-Cre* was too low to give a myocardial phenotype and did not recapitulate the *Gata5-Cre* cardiomyocyte expression. Deletion of *Rac1* in ventricular wall myocardial cells (~30% of myocardial cells in LV and ~50% of myocardial cells in RV, calculated using % GFP IHC staining of *Mlc2v-Cre* derived cells at E15.5) did not recapitulate the myocardial and OFT defects seen in *Rac1*^{Gata5Cre} embryos (~90% of myocardial cells in LV and ~40% of myocardial cells in RV, calculated using % GFP IHC staining of *Gata5-Cre* derived cells at E15.5). It was therefore hypothesised that Rac1 deletion in the majority of ventricular cardiomyocytes may recapitulate the *Rac1*^{Gata5Cre} phenotype. To test this hypothesis, Rac1 was deleted from all developing cardiomyocytes by crossing *Rac1*^{flox} mice to a myocardial specific *TnT-Cre* line.

3.3.6.1 TnT-Cre mice

Similar to *Mlc2v-Cre*, *TnT-Cre* is exclusively expressed in cardiomyocytes, therefore it allows investigation of gene function specifically in the myocardium without interference from extra-cardiac defects or additional cardiac cell functions (as in *Rac1*^{Gata5Cre} embryos). However, *TnT-Cre* is expressed in all cardiomyocytes rather than a small subset (as in *Mlc2v-Cre)* (Jiao *et al.*, 2003).

In *TnT-Cre* mice, Cre recombinase is expressed under the control of Troponin-T promoter which is expressed in all differentiated cardiomyocytes from E7.5.

3.3.6.2 TnT-Cre expression

R26RLacZ and *R26REYFP* mice were crossed to *TnT-Cre* mice to allow for reporting of Cre activity (Figure 54K-M). Cre activity was visualised by X-gal staining for the expression of the LacZ construct in the *R26RLacZ* allele (Figure 54M). IF staining using anti-GFP was used to visualise EYFP expressing cells (Figure 54L). X-gal staining of *R26RLacZ;TnT-Cre* embryos confirms *TnT-Cre* expression is restricted to the cardiomyocytes in the heart at E8.5 and E10.5 (Figure 54A-B). The X-gal stained E10.5 embryos were sectioned and counterstained with eosin to confirm expression is restricted to the myocardial layer of the heart; expression is absent in epicardial, endocardial and mesenchymal regions (Figure 54E). At E13.5 and onwards, X-gal staining of *R26RLacZ;TnT-Cre* hearts shows *TnT-Cre* expression is restricted to heart and is absent in the OFT vessels (Figure 54C-D). Additionally, IHC staining of E13.5 and E15.5 *R26REYFP;TnT-Cre* using anti-GFP, confirmed expression in the myocardial layer and expression is absent in epicardial, endocardial and mesenchymal regions (Figure 54F-G).

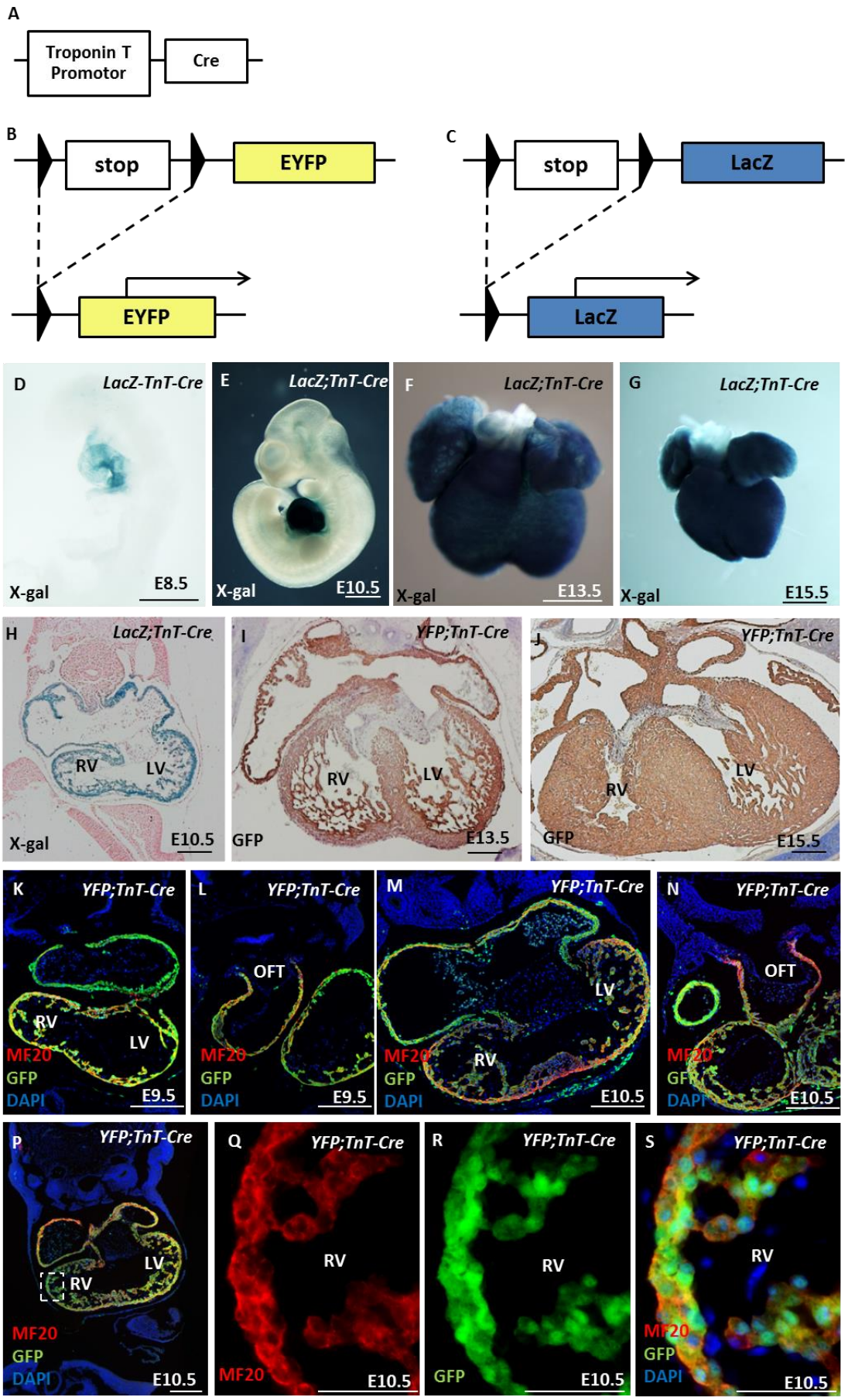
A
Troponin T Promotor
Cre
B
stop
EYFP
EYFP
C
stop
LacZ
LacZ
D
LacZ-TnT-Cre
X-gal
E8.5
E
LacZ;TnT-Cre
X-gal
E10.5
F
LacZ;TnT-Cre
X-gal
E13.5
G
LacZ;TnT-Cre
X-gal
E15.5
H
LacZ;TnT-Cre
RV
LV
X-gal
E10.5
I
YFP;TnT-Cre
RV
LV
GFP
E13.5
J
YFP;TnT-Cre
RV
LV
GFP
E15.5
K
YFP;TnT-Cre
RV
LV
MF20
GFP
DAPI
E9.5
L
YFP;TnT-Cre
OFT
MF20
GFP
DAPI
E9.5
M
YFP;TnT-Cre
LV
RV
MF20
GFP
DAPI
E10.5
N
YFP;TnT-Cre
OFT
MF20
GFP
DAPI
E10.5
P
YFP;TnT-Cre
LV
RV
MF20
GFP
DAPI
E10.5
Q
YFP;TnT-Cre
RV
MF20
E10.5
R
YFP;TnT-Cre
RV
GFP
E10.5
S
YFP;TnT-Cre
RV
MF20
GFP
DAPI
E10.5

Figure 54: *TnT-Cre* expression
TnT-Cre mice express Cre recombinase under the control of the Troponin-T promoter (**A**). EYFP and LacZ reporter mice have a lox-stop-lox site that allows the regulation of expression of EYFP and LacZ under the control of Cre recombinase (**B** and **C**, respectively). TnT-Cre is expressed in the heart at E8.5 and onwards as shown by X-gal staining (**D**-**G**). Transverse sections of E10.5 X-gal stained embryos show TnT-Cre is exclusively expressed in the myocardial cells and is absent from other cardiac cells such as the mesenchymal cells of the developing cardiac cushions (**H**). This data is confirmed by anti-GFP immunostaining at E13.5 and E15.5 (**I**-**J**). TnT-Cre is expressed exclusively in cardiomyocytes as shown by dual IF with GFP and MF20, a cardiomyocyte marker (**K**-**N**). LV; left ventricle, RV; right ventricle, OFT; outflow tract. Scale bars A-P; 200µm Q-S; 50µm.

3.3.6.3 Rac1^{flox} x TnT-Cre cross

Timed matings were set up between *Rac1^{flox}* mice and *Rac1$^{flox;+;}$TnT-Cre* mice. *Rac1^{TnTCre}* embryos were collected across developmental stages E9.5-P0 and analysed using histological and IHC techniques.

The expected numbers of *Rac1^{TnTCre}* embryos, as predicted by Mendelian ratios, were observed up to E17.5. However, some *Rac1^{TnTCre}* embryos were found dead *in utero*, from E12.5 onwards and none were alive at birth. Only 1 *Rac1^{TnTCre}* pup was collected at birth, and was deceased. Any additional *Rac1^{TnTCre}* pups were most likely cannibalised by the dam at birth, after the pups had died. *Rac1^{TnTCre}* embryos do not have an external phenotype (Figure 56A-B). No external or cardiac defects were observed in control embryos or in *Rac1$^{f+TnTCre}$* heterozygous mutants. The heterozygous mutants could therefore be used as Cre positive controls.

3.3.6.4 Cardiac phenotype in Rac1^{TnTCre} embryos

All *Rac1^{TnTCre}* embryos have visible heart abnormalities from E11.5 onwards; a summary of the heart defects is detailed in Table 28. The cardiac phenotype in *Rac1^{TnTCre}* embryos recapitulates that seen in the *Rac1^{Gata5Cre}* mutants. At E11.5 the *Rac1^{TnTCre}* hearts have notably sparse trabeculae (Figure 55, B' compared to A'), and from E13.5 the *Rac1^{TnTCre}* hearts have a significantly thinned myocardium (Figure 55, D' compared to C' and J). Poor septum formation is also observed from E11.5 onwards (Figure 55, B compared to A). *Rac1^{TnTCre}* hearts appear irregular in shape with large ventricular lumens compared to controls from E12.5 (Figure 55C-H). At E15.5, the *Rac1^{TnTCre}* hearts are

significantly increased in diameter compared to controls (Figure 55, G, H and J) and appear to be positioned at an abnormal angle within the thoracic cavity. At E15.5 all *Rac1*^{TnTCre} embryos have a muscular VSD (Figure 56E). Additionally, the aorta remains associated with the RV and displays DORV/OA (Figure 56F).

Embryo stage	Total embryos	*Rac1*^{TnTCre} embryos observed	*Rac1*^{TnTCre} embryos expected	Alive (%) *Rac1*^{TnTCre} embryos	Chi-squared
E9.5	208	43	52	100%	ns
E10.5	336	96	84	100%	ns
E11.5	183	44	45.75	100%	ns
E12.5	164	40	41	85%	ns
E13.5	98	20	24.5	80%	ns
E14.5	23	8	5.75	100%	ns
E15.5	141	27	35.25	88.89%	ns
E17.5	25	7	6.25	85.71%	ns
P0	34	1	8.5	0%	1.75E-07

Table 27: *Rac1*^{TnTCre} embryos observed in expected Mendelian ratios.
The number of *Rac1*^{TnTCre} embryos observed at dissection were within the expected limits at each age. Some *Rac1* ^{TnTCre} embryos were found dead at dissection from E12.5 onwards. Statistical analysis carried out using the Chi-squared test.

Embryo stage	Total *Rac1*^{TnTCre} embryos	Thinned myocardium	Abnormal trabeculae	VSD	DORV/ OA	Abnormal position of heart
E9.5	3	0/3	0/3	-	-	-
E10.5	3	0/3	3/3	-	-	-
E12.5	2	2/2	2/2	-	-	2/2
E15.5	6	6/6	6/6	6/6	6/6	6/6
E17.5	4	4/4	4/4	4/4	4/4	4/4
P0	0	-	-	-	-	-

Table 28: Summary of the cardiac defects in *Rac1*^{TnTCre} embryos.
Rac1^{TnTCre} embryos display thinned myocardium, abnormal trabeculae, VSD, DORV/OA and abnormal position of the heart. No defects were noted in the control embryos at any age. VSD; ventricular septal defect, DORV; double outlet right ventricle, OA; overriding aorta.

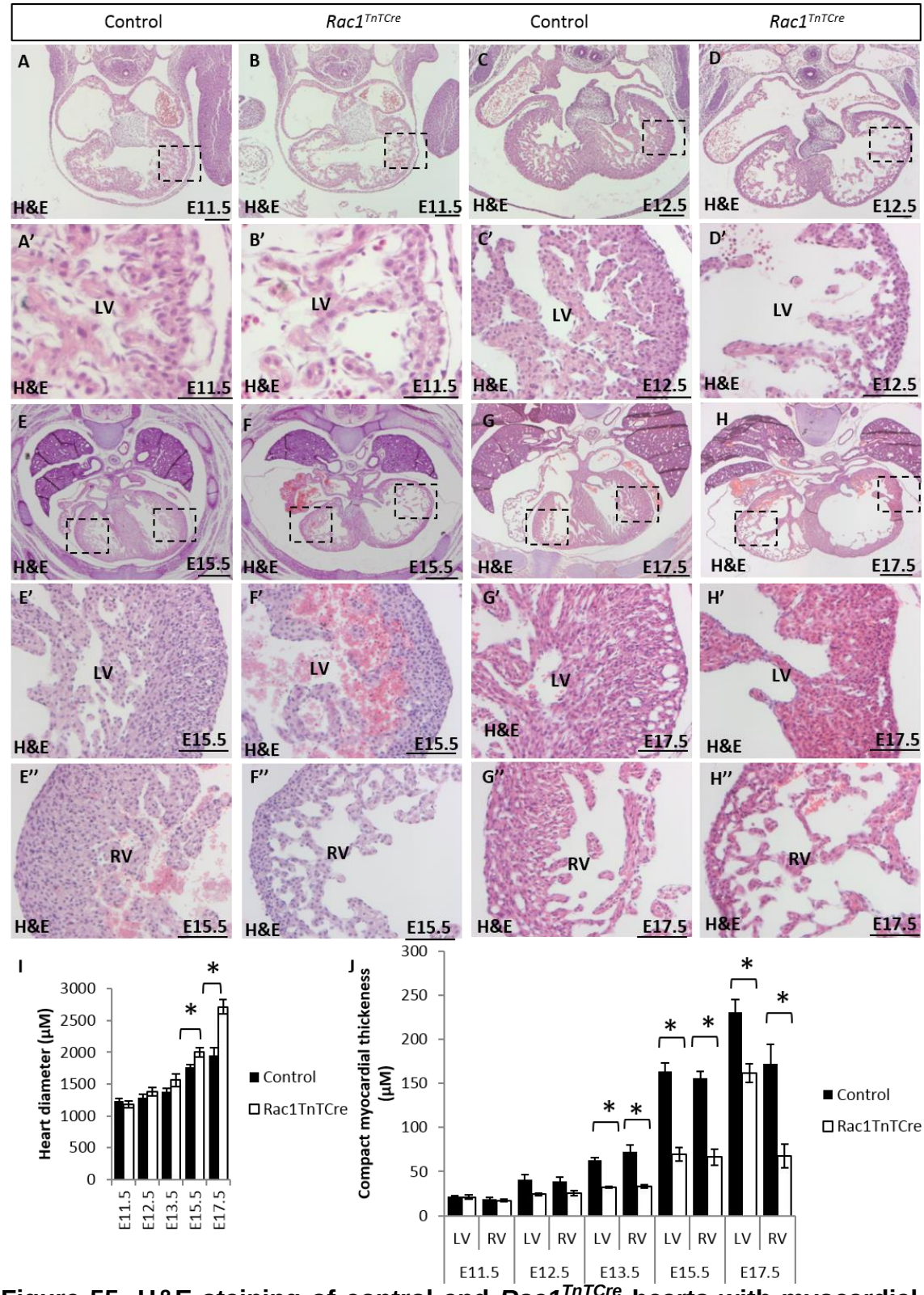

Figure 55: H&E staining of control and *Rac1*^{TnTCre} hearts with myocardial measurements.

Myocardial abnormalities are observed from E11.5 including thin compact myocardium and irregular trabeculae (**A**-**B**). *Rac1*^{TnTCre} hearts have a significantly thinned compact myocardial layer compared to controls at E13.5 (n=4), E15.5 (n=4) and E17.5 (n=4) (**J**). At E17.5 in *Rac1*^{TnTCre} hearts, the left ventricle is more compacted compared to the right ventricle, whereas the

thickness is similar between left and right ventricles in controls. The diameter of the *Rac1*^{TnTCre} hearts is significantly increased compared to controls at E15.5 (**I**). LV; left ventricle, RV; right ventricle. Scale bars; A-F 200µm, G-H 500µm, A'-F'' 50µm, G'-H'' 100µm. *p<0.05. Statistical analysis carried out using a two-way ANOVA.

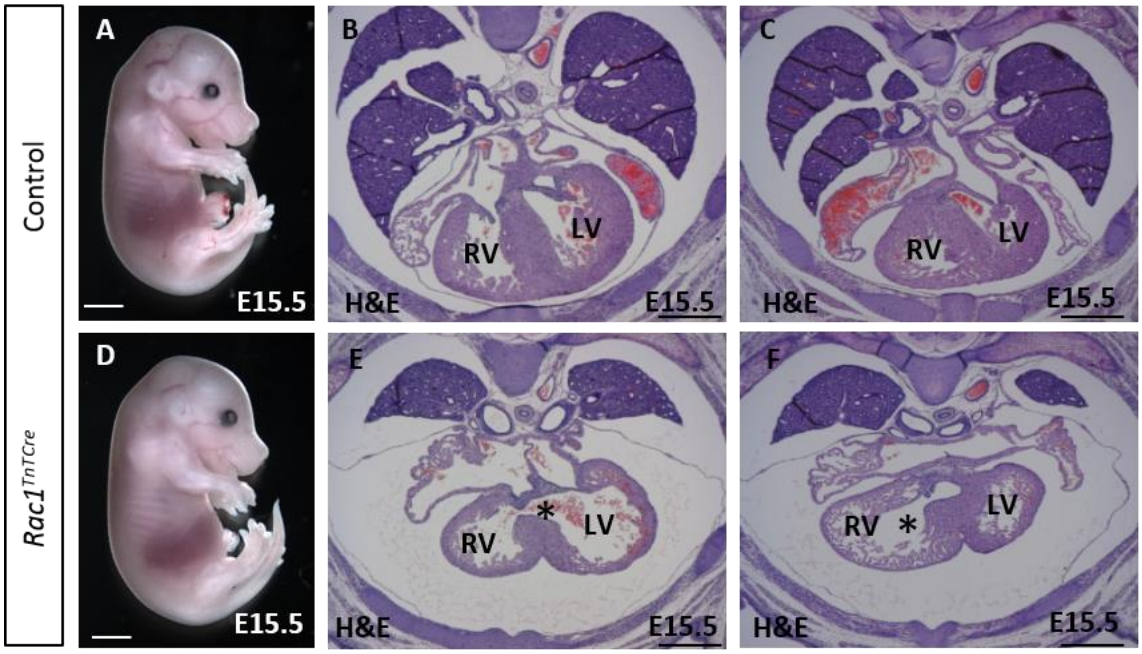

Figure 56: OFT defects in *Rac1*^{TnTCre} embryos.
Rac1^{TnTCre} embryos do not have an external phenotype (**A**-**B**). At E15.5 all *Rac1*^{TnTCre} embryos have a muscular VSD (Asterisk (*) in **E**) and the aorta remains associated with the right ventricle causing displays DORV/overriding aorta (OA) (Asterisk (*) in **F**) (n=4). LV; left ventricle, RV; right ventricle. Scale bars; A and D 2mm, B-C, E-F 500µm.

3.3.7 The epicardium forms normally in Rac1^{TnTCre} *hearts.*

To confirm that the epicardium is unaffected in *Rac1*^{TnTCre} hearts, immunostaining using an anti-WT1 antibody marker of epicardial cells was carried out. At E11.5 the epicardium has completely enveloped the myocardium, this can be seen in both control and *Rac1*^{TnTCre} hearts (arrows point to WT1-postive epicardial cells in Figure 57).

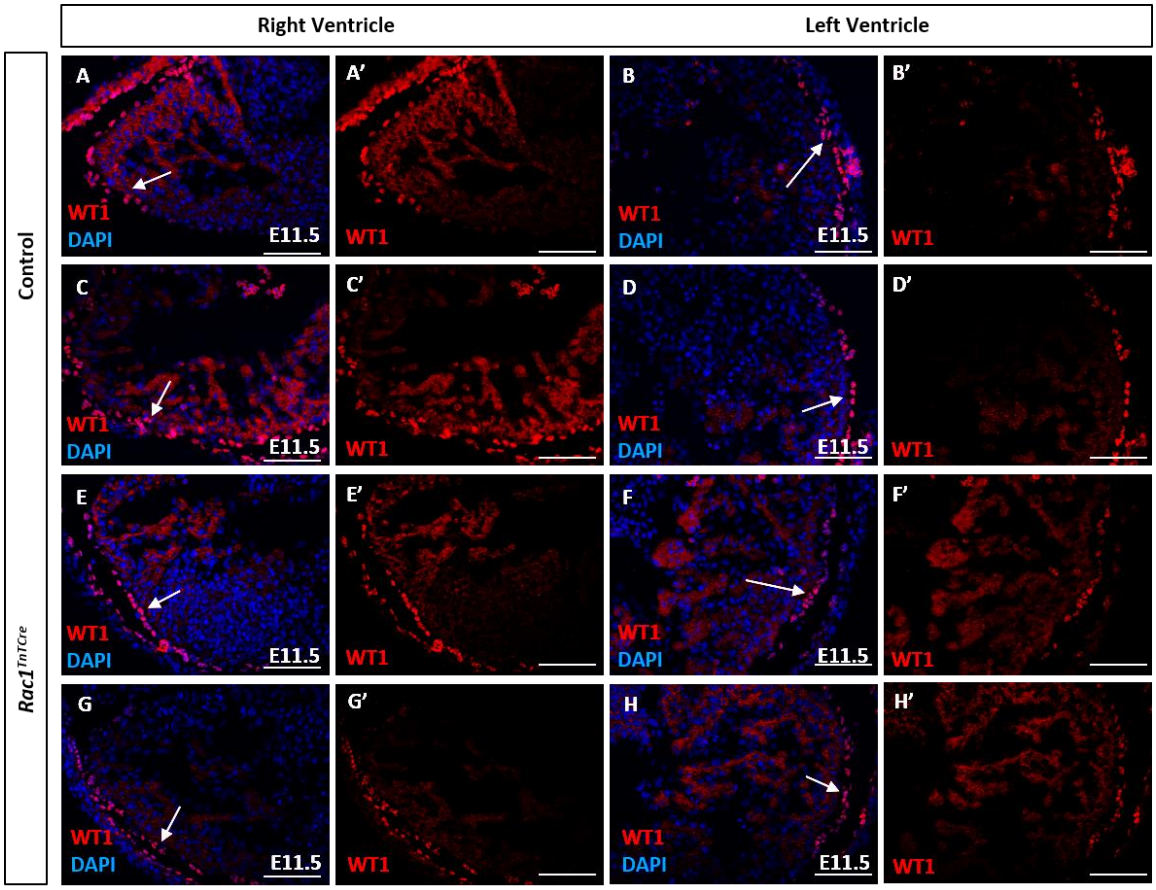

Figure 57: Epicardium forms normally in *Rac1*^{TnTCre} hearts.
Immunostaining using an anti-WT1 antibody marker of epicardial cells shows the epicardium is formed by E11.5 in both control (**A**-**D'**) and *Rac1*^{TnTCre} hearts (**E**-**H'**) (n=3) (arrows point to WT1-postive epicardial cells).

To summarise, deletion of *Rac1* from all myocardial cells during development results in severe and lethal myocardial and OFT defects during embryonic development. This suggests that *Rac1* is crucial in the development of the myocardial wall and in the alignment of the OFT. Further analysis of the OFT and ventricular cardiomyocytes in *Rac1*^{TnTCre} and *Rac1*^{Gata5Cre} will help elucidate the specific role of *Rac1* in these tissues during cardiac development in Chapters 4 and 5 respectively.

3.4 Discussion

This chapter aimed to firstly confirm expression of *Rac1* in the developing heart and secondly to dissect its role within the development of the myocardium. Preliminary data suggested that deleting Rac1 from the epicardium and myocardium, using *Gata5-Cre*, resulted in defects within the myocardial wall (personal communication Dr Helen Phillips). Therefore, the aim was to characterise these defects in detail and dissect the role of Rac1 in the

epicardium and myocardium during myocardial development, using additional Cre lines.

3.4.1 Rac1 expression

In this chapter Rac1 expression was confirmed within the developing embryonic heart at both the mRNA transcript level and protein level and this is consistent with previous studies (Wang and Zheng, 2007). It was shown through slide *in situ* hybridisation that *Rac1* mRNA is expressed in the myocardium and epicardium as well as being strongly expressed in the endocardium. Confirmation of these *in situ* hybridisation results at the protein level was tried through immunostaining, however non-specificity of the Rac1 antibodies tested within the heart meant this was not possible. Several alternative immunostaining techniques were tried but none of the three Rac1 antibodies tested gave specific staining for Rac1. Rac1 is known to be expressed in the heart and previous reported expression of Rac1 in the heart shows Rac1 antibody staining at the cell membrane of cardiomyocytes (Boczonadi *et al.*, 2014b). The three antibodies tested all gave different staining patterns, one was the same as the secondary antibody only control showing specific expression within the heart. This may be attributed to the nature of myocardial tissue which is particularly susceptible to non-specific binding of antibodies. The other two gave ubiqutous expression which was unchanged in Rac1 deleted cells, i.e cardiomyocytes in $Rac1^{TnTCre}$ sections.

3.4.2 Role of Rac1 in cardiac development

Using Cre-LoxP technology it was demonstrated that Rac1 can be deleted within specific cell types during cardiac development. This tool has allowed investigation of the role of Rac1 in the epicardium and/or myocardium, and consequently it was shown that Rac1 is required in myocardial cells for normal cardiac development. Combined deletion of Rac1 in epicardial cells and myocardial cells, using *Gata5-Cre,* resulted in lethal myocardial and OFT defects. Dissection of the $Rac1^{Gata5\text{-}Cre}$ phenotype using epicardial and myocardial specific Cre lines revealed that Rac1 is critical in myocardial cells but may not be required in epicardial cells for normal myocardial thickening and subsequent OFT alignment during embryonic development.

3.4.2.1 Rac1 in the ventral body wall

Extra-cardiac defects were observed in *Rac1*^{Gata5Cre} mutants including non-closure of the ribs and an open ventral body wall. Both Rac1 and *Gata5-Cre* are expressed in the developing ventral body wall mesenchyme and *Rac1*^{Gata5Cre} embryos have a thin body wall from E12.5. This data suggests that Rac1 is deleted from the body wall at an early stage in embryonic development and has a role in the thickening of the body wall mesenchyme. Ventral body wall defects have been observed in other *Gata5-Cre* mutants. For example, *Alk5;Gata5Cre* mutants have a body wall closure defect with extrusion of visceral organs through the ventral body wall (Sridurongrit *et al.*, 2008). Alk5 is one of the co-receptors for TGF-β signalling and this signalling pathway is known to be involved in regulation of numerous cellular processes. Additionally, secretion of Wnt ligands from the developing ventral body wall mesenchyme play a critical role in fusion of the sternum and closure of the secondary body wall (Snowball *et al.*, 2015). Since these developmental processes are affected in *Rac1*^{Gata5Cre} mutants, Rac1 deletion may disrupt TGF-β or Wnt signalling in the ventral body wall mesenchyme. Rac1 is downstream of non-canonical Wnt signalling and is also linked with canonical Wnt signalling. Alternatively, cadmium exposure induces ventral body wall defects in the chick and is associated with an increase in Rac1 causing dissociation of cadherin-mediated AJs (Doi *et al.*, 2011). Therefore, deregulated AJ in Rac1 deficient mesenchymal cells represents a potential cause of the ventral body wall defects in *Rac1*^{Gata5Cre} embryos. The primary cause of the body wall defects in *Rac1*^{Gata5Cre} embryos was not the focus of this thesis, however determining the role of Rac1 in cardiomyocytes during development may help elucidate its role in body wall development.

3.4.2.2 Rac1 in the epicardium

Rac1 is expressed in migrating cells and is required for the formation of the lamelipodia and filopodia that are necessary for cell movement (Duquette and Lamarche-Vane, 2014). Thus it was surprising that deletion of *Rac1* in the epicardium, using *WT1-CreERT2,* did not result in any significant defects in epicardial cell migration. In normal development, epicardial cells form an uninterrupted epicardial layer over the surface of the myocardium and EPDCs

migrate into the compact layer. The *Rac1* deficient epicardial cells in *Rac1*$^{WT1\text{-}CreERT2}$ hearts were not significantly reduced in number or in average compact myocardial migration distance, however additional ages would be useful in drawing conclusions from this result. Additionally, epicardium explants and epicardial cell migration assays could be used to confirm that the loss of Rac1 does not affect epicardial cell migration. These results may suggest that epicardial Rac1 is not required in epicardial cells for the formation of the epicardium, epicardial cell migration or for the normal thickening of the compact layer during early heart development. However, some defects seen in *Rac1*^{Gata5Cre} hearts are suggestive of an epicardial phenotype, particularly the epicardial blisters consisting of a detached epicardial cell layer filled with blood, and an uneven epicardial surface. Since no significant defects were observed in the epicardial specific *Rac1* knock-out, it may suggest that the epicardial phenotype observed in *Rac1*^{Gata5Cre} is secondary to the myocardial phenotype, or alternatively that the efficiency of *Rac1* knock-out is reduced in *WT1-CreERT2* compared to *Gata5-Cre*. This cannot be determined from the work in this thesis since *Rac1* knock-out was only validated in the *TnT-Cre* model.

Additionally, Rac1 may be required for the later migration and differentiation of epicardial cells and development of the myocardium. This would be similar to the role of Rac1 in NCC's where no migration defect was observed, however, differentiation defects were apparent. EPDCs migrate into the compact myocardium and differentiate into smooth muscle cells and endothelial cells of the coronary vessels, as well as fibroblasts (Mikawa and Gourdie, 1996; Dettman *et al.*, 1998; Perez-Pomares *et al.*, 2002). Defective EPDC differentiation is known to affect coronary vasculature development and therefore may possibly lead to defective cardiovascular development during later embryonic and postnatal developmental stages (Rhee *et al.*, 2009). However, in the context of this thesis, *Rac1* in epicardial cells is not required for the normal maturation of the ventricular myocardium or OFT alignment.

3.4.2.3 Rac1 in the myocardium

The phenotype observed in the different *Cre* line crosses suggests that Rac1 is required in the myocardium for the normal maturation of the ventricles. The cellular and molecular mechanism by which cardiomyocyte specific Rac1

deficiency leads to OFT and myocardial defects are discussed in Chapter 4 and Chapter 5, respectively. The role of Rac1 in other cell types suggests that Rac1 could be regulating many processes during development such as cell proliferation and/or survival, cell adhesion, cell polarity and cytoskeletal arrangement.

Previous work suggests that Rac1 is required for normal polarity in cardiac progenitors (Abu-Issa, 2014). *Nkx2.5-Cre* specific deletion of *Rac1* results in heart failure at E12.5-E13.5 due to thin disorganised myocardial walls and OFT alignment defects similar to $Rac1^{TnTCre}$ and $Rac1^{Gata5Cre}$ mutants. *Nkx2-5-Cre* expressing progenitors are shown to primarily give rise to the cardiomyocyte lineage, therefore, it is not surprising that our $Rac1^{TnTCre}$ hearts closely model the *Nkx2.5-Cre* phenotype. However, there is additional but infrequent contribution to the endothelial lineage (Moses *et al.*, 2001; Stanley *et al.*, 2002) and *Nkx2.5-Cre* deletes *Rac1* from early cardiac progenitors. Additionally, Rac1 is thought to be required for polarity in SHF progenitors (Leung *et al.*, 2014). $Rac1^{Mef2Cre}$ embryos exhibited ventricular and atrial septal defects, a thinner RV myocardium, and a bifid cardiac apex. Markers of the SHF include *Islet1* and *Mef2c* and hence *Islet1-Cre* and *Mef2c-Cre* are commonly used for targeted SHF gene deletion. *Islet1-Cre* progenitors were found to contribute to SHF cardiomyocytes as well as SMCs, and endothelial cells (Cai *et al.*, 2003; Moretti *et al.*, 2006; Yang *et al.*, 2006; Sun *et al.*, 2007). *Mef2c-Cre* progenitors represent a more restricted population than *Islet1-Cre* progenitors, but also contribute to SHF cardiomyocytes, SMCs and ECs. Specifically, *Mef2c-Cre* progenitors also contribute to the endocardial cells of the RV, the smooth muscle of the pulmonary trunk and the endothelium of the OFT (Verzi *et al.*, 2005). Similar to $Rac1^{Mef2Cre}$ hearts, our $Rac1^{TnTCre}$ mutants display thin myocardial walls and VSD. Taking this into consideration, our $Rac1^{TnTCre}$ model is more appropriate for investigating the role of *Rac1* in cardiomyocytes as it specifically targets cardiomyocytes during myocardial development and is not affected by the deletion of *Rac1* in additional cell types.

Therefore, despite the investigations discussed above, the role of Rac1 in early myocardial development remains unclear. Both Abu Issa and Leung and colleagues use conditional deletions of Rac1 which include multiple cell types, leading to difficulties separating possible differential roles of Rac1 in specific cell

types. Additionally, neither group have investigated the role of Rac1 in the formation of the trabeculae and subsequent development of the myocardium. Therefore the aim was to investigate the role of Rac1 specifically in the cardiomyocytes during myocardial trabeculation and thickening.

Our *Rac1*^{Mlc2vCre} hearts did not display any major myocardial defects. *Mlc2v-Cre* is expressed in a subpopulation of ventricle cardiomyocytes, often surrounded by unaffected cardiomyocytes. These findings suggest that interactions between cardiomyocytes and/or other cell types are important for myocardial development and can be compensated for by the majority of unaffected cardiomyocytes in *Rac1*^{Mlc2vCre} hearts, compared to severe defects when Rac1 is deleted from all cardiomyocytes. The observations of subtle myocardial defects in areas highly populated by Cre-positive derived cardiomyocytes supports this hypothesis. However, since the effciency of the *Cre* recombination in the *Rac1*^{Mlc2vCre} cross was not assessed, it can not be directly compared to that of the *Rac1*^{TnTCre} model.

Our *Rac1*^{TnTCre} model allows analysis of a more restricted population of cardiomyocytes during ventricular development compared to published *Rac1*$^{Nkx2.5Cre}$ and *Rac1*^{Mef2cCre} mutants and also our *Rac1*^{Gata5Cre} mutants. Therefore, further analysis of Rac1 function in cardiomyocytes descibed in this thesis was carried out in *Rac1*^{TnTCre} hearts and occasionally complemented by analysis of *Rac1*^{Gata5Cre} cardiomyocytes.

Both *Rac1*^{TnTCre} and *Rac1*^{Gata5Cre} mutants display an apparent reduction in ventricular cardiomyocytes and disrupted cardiomyocyte morphology. Therefore, cardiomyocyte cell cycle and polarity were primarily investigated in mutant hearts, to determine if similar mechanisms were occurring to that which have been reported in the alternative Rac1 mutant models. These are discussed in Chapters 4 and 5 in relation to the OFT defects and myocardial defects, respectively.

3.4.3 Conclusions

In conclusion, in this chapter expression of *Rac1* in the developing heart was confirmed and deletion of *Rac1* within epicardial and myocardial populations using Cre-LoxP technology was validated. Using various Cre lines it was

determined that *Rac1* is crucial within the developing myocardium for normal maturation of the ventricles and for correct OFT alignment.

Chapter 4. Outflow tract alignment defects in Rac1 mutants

4.1 Introduction

4.1.1 Overview of OFT development

The cardiac OFT forms at the arterial pole of the heart and connects the embryonic ventricles to the aortic sac. During heart looping, myocardial cells are added to the arterial pole from the SHF progenitor population in the pharyngeal mesoderm (Kelly and Buckingham, 2002; Cai *et al.*, 2003; Buckingham *et al.*, 2005). The OFT undergoes remodeling, consisting of OFT rotation, septation into the aorta and the pulmonary trunk and subsequent alignment of the two vessels with left and right ventricles, respectively. Deployment of SHF cells and cardiac NCC and subsequent remodeling of the OFT are critical for correct vessel formation and alignment and are regulated by various signalling pathways.

4.1.2 OFT formation

The OFT elongates by addition of SHF progenitor cells from the pharyngeal mesoderm to the myocardial and endocardial layers of the distal OFT (Kelly and Buckingham, 2002; Cai *et al.*, 2003; Buckingham *et al.*, 2005). The SHF cells migrate together forming an epithelial-like sheet. SHF cells remain in their precursor state for a longer duration, with a differentiation delay and higher level of proliferation, compared to FHF cells. Additionally, SHF cells have prolonged expression of Islet1 whereas Islet1 is expressed only transiently in the FHF (Cai *et al.*, 2003). The processes regulating remodeling of the OFT are critical for correct OFT septation and alignment.

4.1.3 OFT remodelling

The OFT is septated into the base of the ascending aorta and base of the pulmonary trunk while both outflow vessels remain associated with the RV. OFT septation is accompanied by retraction and rotation of the truncal myocardium in an anticlockwise direction, resulting in alignment of the aorta with the LV and pulmonary trunk with the RV (Bajolle *et al.*, 2006). The septation process is completed by convergence of the OFT septum with AV and ventricular septa, separating the systemic and pulmonary circulation. The movement of the aorta

behind the pulmonary trunk, between the AV valves during OFT alignment and septation is known as ‘wedging’, and without ‘wedging’ the aorta overrides the ventricular septum. As the OFT cushions fuse, a process of invasive myocardialisation leads to muscularisation of the OFT cushions and produces smooth muscular walls at the base of the pulmonary trunk and ascending aorta (van den Hoff *et al.*, 2001; Sugishita *et al.*, 2004; Waldo *et al.*, 2005b; Rana *et al.*, 2007).

4.1.4 Cell polarity in the OFT

Cell polarity regulates both collective and individual cell movements during embryonic development (Munoz-Soriano *et al.*, 2012). Epithelial cells exhibit apical-basolateral polarity and PCP, both of which are required for normal embryonic development. Cardiomyocytes are not an epithelial cell, however they display features of epithelial cell polarity, including PCP signalling and apical-basal polarity (ABP). Adult cardiomyocytes are highly polarised with cell-cell junctions localised at ICD with attachment to the ECM on their lateral surface. The role of the two types of polarity in cardiomyocytes during development has been investigated but requires further studies.

4.1.5 Apical basal polarity in the OFT

Like epithelial cells, cardiomyocytes display ABP. The apical side is at the luminal side of the cell. The basal side of the cell is attached to the basement membrane and the lateral side of the cell is where it is attached to adjoining cells. The apical, lateral and basal sides of the cell are regulated by the presence of AJ and TJ (Kaplan *et al.*, 2009) (Figure 14). MTOC are polarised cell organelles and are apically expressed (Magdalena *et al.*, 2003) (Figure 14). ECM proteins such as laminin are present at the basal side of the cell in the basal lamina of the basement membrane and are involved in adhesion and cell migration (Timpl *et al.*, 1979) (Figure 14).

4.1.6 PCP signalling in the OFT

Disruptions in PCP signalling components can lead to OFT defects (Murdoch *et al.*, 2003; Phillips *et al.*, 2005; Henderson *et al.*, 2006; Phillips *et al.*, 2007; Phillips *et al.*, 2008; Gibbs *et al.*, 2016). Polarisation and organisation of

cardiomyocytes in the outflow myocardium is disrupted in both *Scrib* and *Vangl2* mutants.

4.1.7 Conotruncal congenital heart defects

Coordinated migration, proliferation and differentiation of multiple cell lineages is required for correct OFT morphogenesis. Disruption in either SHF or NCC cell populations contributes to a spectrum of OFT defects in humans and animal developmental models (Yelbuz *et al.*, 2002; Abu-Issa and Kirby, 2007; Ramsbottom *et al.*, 2014). Myocardial and endocardial populations have also been shown to be important during OFT rotation and alignment (Bamforth *et al.*, 2001; Bajolle *et al.*, 2006; Zhang *et al.*, 2009), as well as cellular processes essential for remodeling such as programmed cell death and myocardialisation (Bartram *et al.*, 2001; Watanabe *et al.*, 2001).

4.2 Aims of Chapter 4

As identified in Chapter 3, myocardial deletion of *Rac1* during embryonic development results in OFT defects including DORV and OA with VSD. These phenotype data suggests that *Rac1* plays an important role within the development of the myocardium, which is critical for normal ventricular septation and alignment of the OFT. The aim of this chapter was therefore to dissect the cellular mechanism which is disrupted in the absence of *Rac1*, during the formation and remodelling of the OFT.

It can be hypothesised that defective OFT development and/or OFT remodelling causes the DORV/OA phenotype observed in both the $Rac1^{Gata5Cre}$ and $Rac1^{TnTCre}$ embryos. The aim was, therefore, to investigate each stage of OFT development to identify the primary defect in *Rac1* myocardial mutant hearts, focussing on $Rac1^{TnTCre}$ mutants.

Firstly, the expression of *Gata5-Cre* and *TnT-Cre* will be examined to define the boundary of affected cardiomyocytes within the OFT myocardium. Secondly, early development of the OFT will be studied in $Rac1^{TnTCre}$ heart, including addition of SHF cells, myocardial cell proliferation and cell polarity. Thirdly, OFT remodelling will be analysed, looking at OFT myocardialisation and wedging of the aorta in $Rac1^{TnTCre}$ hearts.

Rac1 is implicated in the regulation of cell proliferation and cell polarity in cardiomyocytes as well as additional cell types. Thus, it is additionally hypothesised that alterations in these cellular processes within the developing OFT myocardium is the primary defect in *Rac1* myocardial mutant hearts. Therefore, the aim was to focus on analysis of cell proliferation and polarity in Rac1 deficient OFT cardiomyocytes, using the *Rac1*^{TnTCre} model.

4.3 Results

Rac1 is expressed in the developing OFT myocardium (Figure 38) and myocardial deletion of *Rac1*, as well as published SHF and cardiac progenitor deletion of *Rac1*, has been shown to result in OFT defects, suggesting a role of *Rac1* in OFT formation and/or remodelling.

4.3.1 Early OFT formation and cellular morphology in Rac1^{TnTCre} mutant hearts

The key processes in OFT formation were examined in *Rac1*^{TnTCre} embryos with an aim to ascertain the primary defect causing the observed DORV/OA phenotype.

4.3.1.1 Addition of SHF progenitors and OFT lengthening

The OFT elongates by addition of SHF progenitor cells from the pharyngeal mesoderm to the myocardium of the distal OFT. To assess this process in the *Rac1*^{TnTCre} embryos, analysis of SHF progenitor addition and also OFT length was carried out.

To determine if addition of SHF progenitor cells occurs normally in the *Rac1*^{TnTCre} embryos, immunostaining for a SHF specific marker, Islet1, was carried out on E10.5 sections. At E10.5, the OFT is undergoing elongation by addition of SHF cells at the arterial pole. In controls, Islet1 expression appeared strong in the nucleus of distal OFT cells (arrows in Figure 58) and was decreased in a gradient towards the ventricular myocardium (Figure 58A-A''). No expression was observed in ventricular cardiomyocytes (arrow heads). The *Rac1*^{TnTCre} hearts showed comparable expression pattern of Islet1 (n=3) (Figure 58B-B''). From these results, it was concluded that SHF progenitors correctly

migrate from the pharyngeal mesoderm and contribute to the arterial pole of the OFT in *Rac1*^{TnTCre} hearts.

To analyse OFT length, E10.5 *Rac1*^{TnTCre} embryos were dissected and the hearts and OFT were imaged (Figure 59A-B). OFT length was measured using ImageJ software in control (n=6, average somite number 33.8) and *Rac1*^{TnTCre} (n=6, average somite number 34.1) embryos. There was no significant difference in OFT length between the control and *Rac1*^{TnTCre} embryos (Figure 59C).

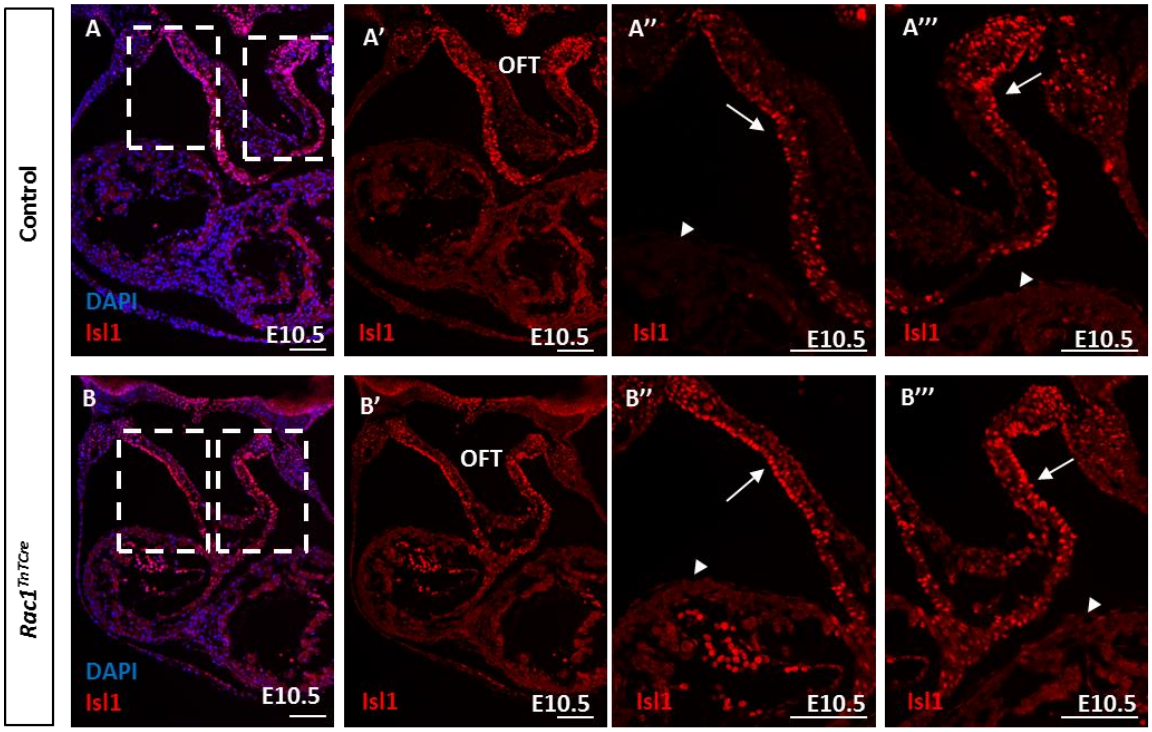

Figure 58: Islet1 expression in control and *Rac1*^{TnTCre} OFT at E10.5.
In controls, Islet1 expression appears strong in the nucleus of distal OFT cells (arrows in **A''** and **A'''**) and is decreased in a gradient towards the ventricular myocardium. No Islet1 expression was observed in ventricular cardiomyocytes (arrow heads in **A''** and **A'''**). The *Rac1*^{TnTCre} hearts showed equivalent expression of Islet1 compared to controls (n=3). OFT; outflow tract. Scale bars; 100µm.

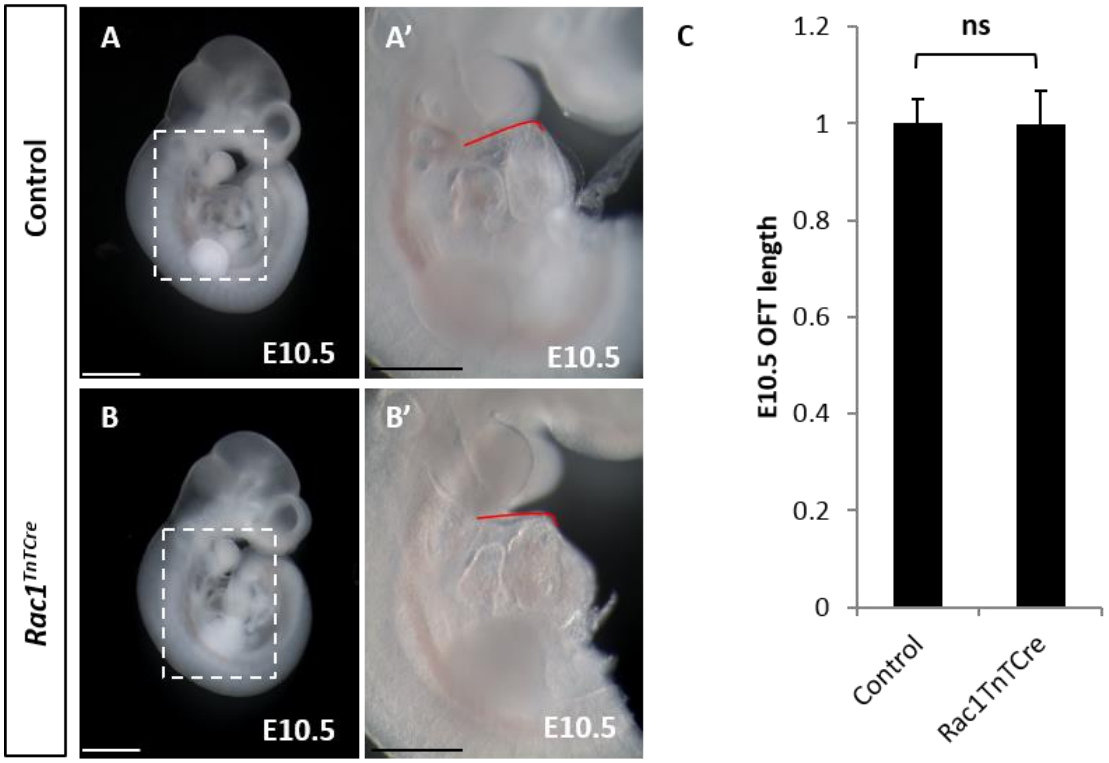

Figure 59: *Rac1*^{TnTCre} OFT length is normal at E10.5.
E10.5 control and *Rac1*^{TnTCre} embryos were dissected and the hearts and OFT were imaged (**A**-**B**). OFT length was measured using ImageJ software and found to be in equivalent in *Rac1*^{TnTCre} embryos compared to controls (**C**) (n=6). Scale bars 1mm. Statistical analysis carried out using the unpaired t-test.

4.3.1.2 OFT morphology

The shape and angle of the OFT was also investigated using 3D Amira reconstructions of heart sections and HREM data.

E9.5 (n=3) and E10.5 (n=3) hearts were reconstructed from section images using Amira software. These 3D models indicate that the overall morphology of the OFT is normal in *Rac1*^{TnTCre} hearts at E9.5 (Figure 60A-B) and E10.5 (Figure 60C-D).

Additionally, E10.5 (n=6) and E11.5 (n=5) embryos were sent for HREM imaging. This allowed visualisation of the OFT in the form of tiff videos and 3D erosion models that were produced from the HREM images by Dr Tim Mohun, Francis Crick Institute. Figure 61 and Figure 62 show example stills of tiff videos and 3D erosion videos respectively. Analysis of the HREM data confirmed that the OFT morphology is normal in *Rac1*^{TnTCre} embryos at E10.5 and E11.5. In addition, the OFT cushions appeared to have formed normally at E11.5 (Figure 61E-J). At E11.5 the RV appears smaller in the HREM tiffs of the *Rac1*^{TnTCre}

hearts (Figure 61H-J) compared to controls (Figure 61E-G), however this is due to the angle of the section and was not noted in the 3D reconstructed hearts (Figure 62).

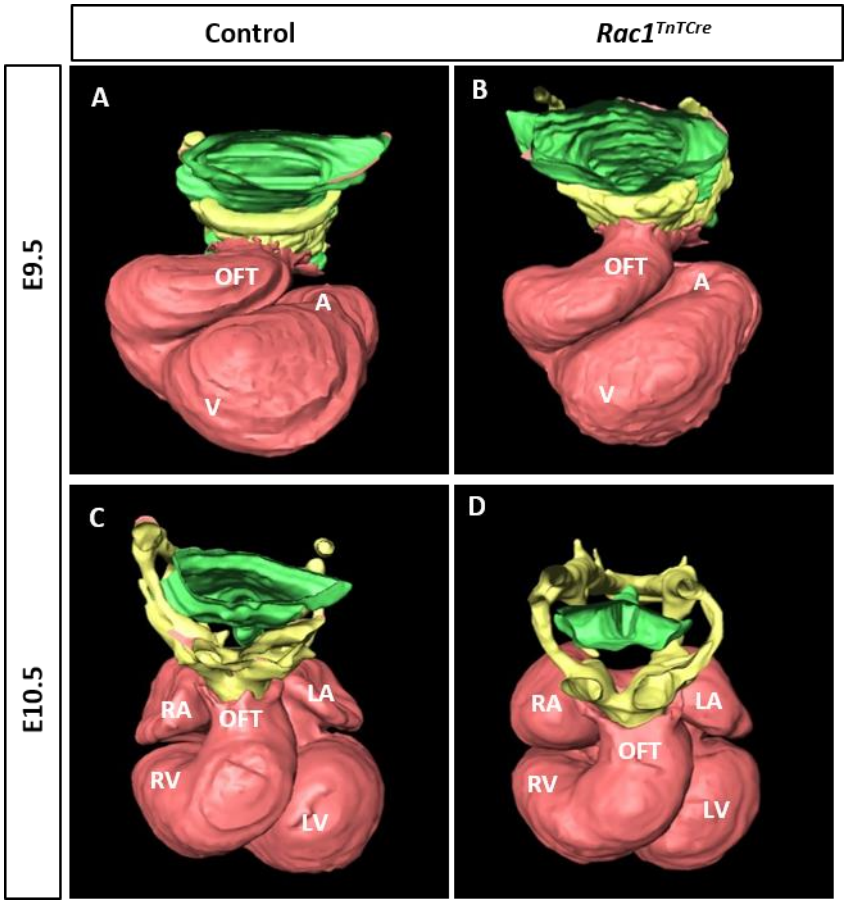

Figure 60: 3D Amira reconstructions of E9.5 and E10.5 control and *Rac1*^{TnTCre} hearts.
The size and shape of the OFT and ventricles is normal in *Rac1*^{TnTCre} hearts compared to controls at E9.5 (**B**) and E10.5 (**D**) (n=3). OFT; outflow tract, A; atria, V; ventricle, RA; right atria, LA; left atria, RV; right ventricle and LV; left ventricle. Red; myocardium, yellow; PAA and green; pharynx.

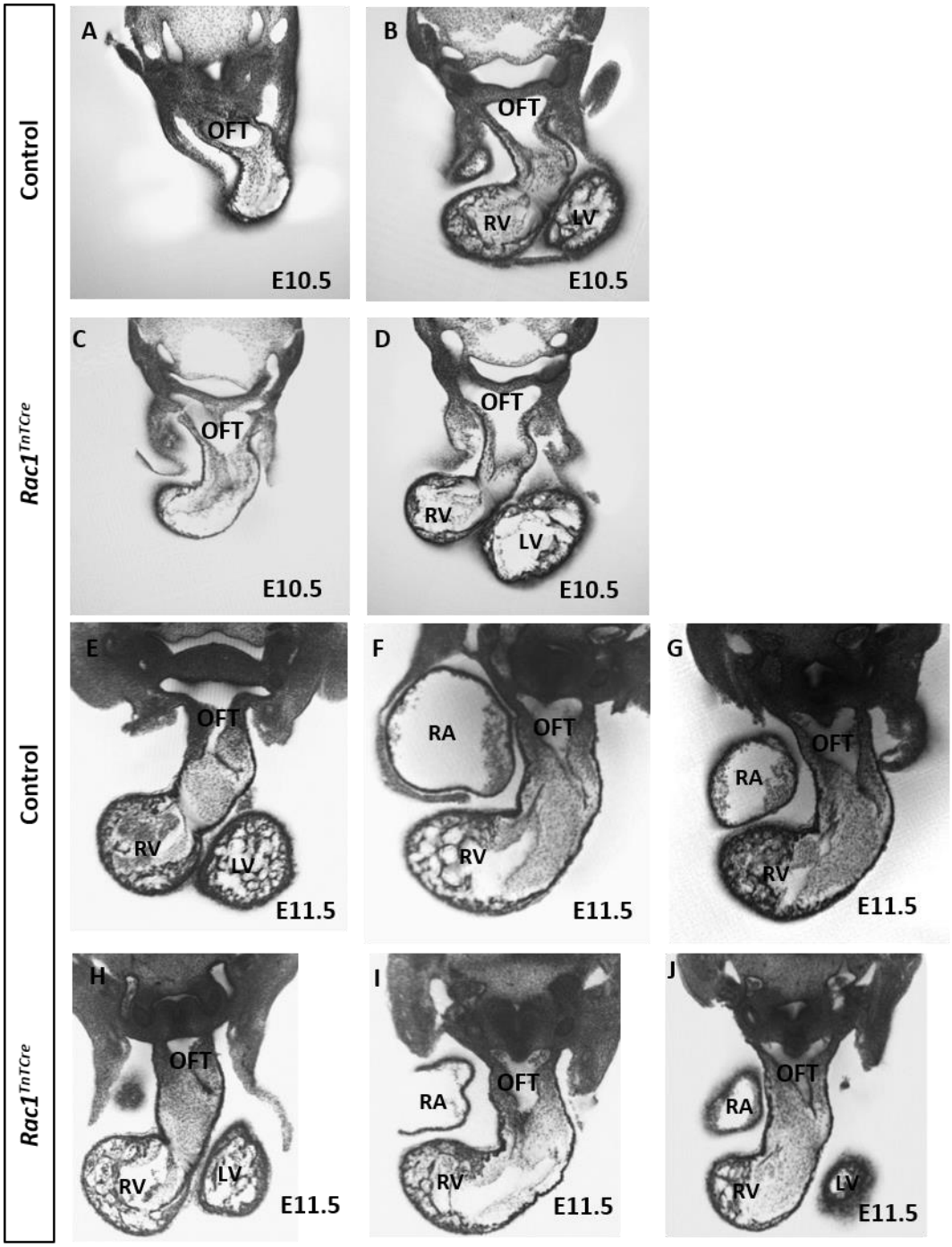

Figure 61: HREM images of E10.5 and E11.5 control and *Rac1*^{TnTCre} hearts. The size and shape of the OFT is normal in *Rac1*^{TnTCre} hearts compared to controls at E10.5 (**C**-**D**) (n=6) and E11.5 (**H**-**J**) (n=5). In addition, the OFT cushions appeared to have formed normally at E11.5 (**E**-**J**). OFT; outflow tract, RA; right atria, RV; right ventricle and LV; left ventricle.

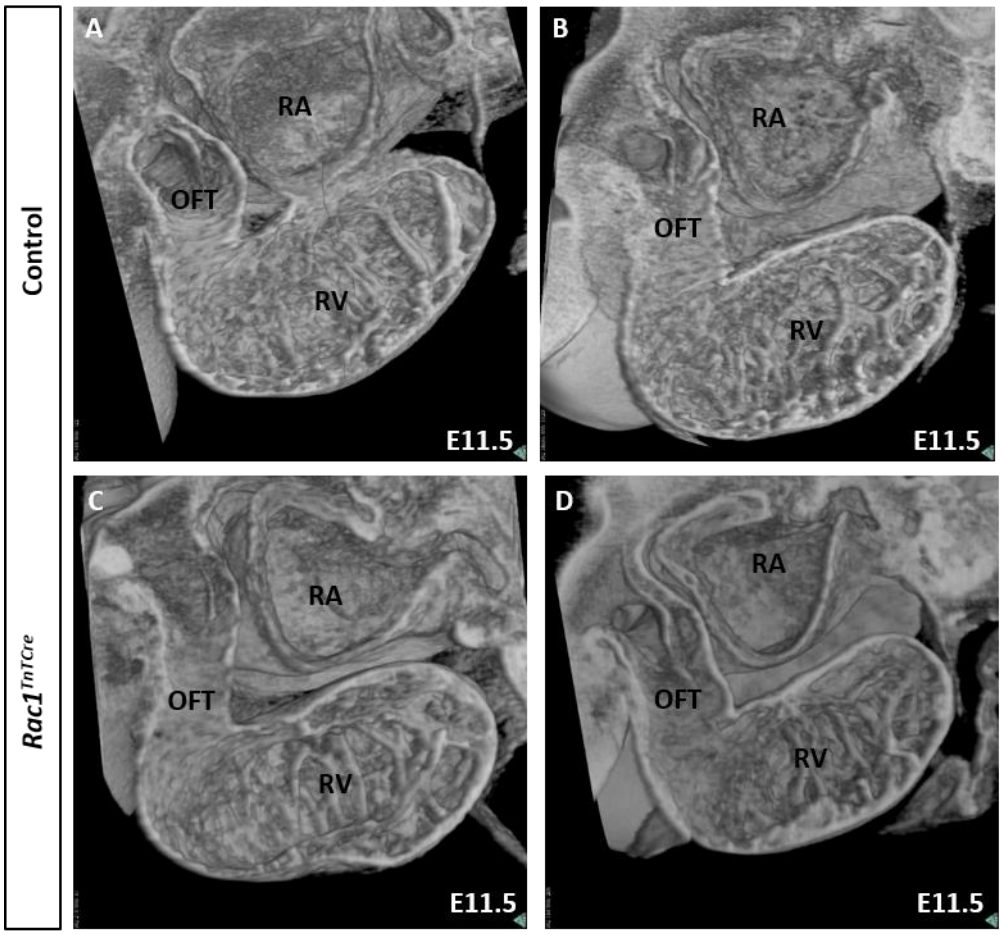

Figure 62: Cut-ventricle view of 3D reconstructions of E11.5 control and *Rac1*^{TnTCre} hearts.
The size and shape of the OFT is normal in *Rac1*^{TnTCre} hearts (**C**-**D**) compared to controls E11.5 (**A**-**B**) (n=5). OFT; outflow tract, RA; right atria and RV; right ventricle.

Taken together, Islet1 staining of SHF cells and 3D models of *Rac1*^{TnTCre} hearts suggest that deficiency of *Rac1* does not affect the addition of SHF cells to the developing OFT or the subsequent OFT lengthening.

4.3.1.3 Rac1 deficient cardiomyocytes in the OFT 'transition zone'

As SHF progenitor cells are incorporated into the OFT myocardium, they progressively differentiate into cardiomyocytes. The region of the OFT where this differentiation process initiates is called the 'transition zone' (Ramsbottom *et al.*, 2014). Both *Gata5-Cre* and *TnT-Cre* are expressed in differentiated cardiomyocytes and therefore are expected to be expressed in the developing OFT myocardium. Since *Rac1*^{Gata5Cre} and *Rac1*^{TnTCre} embryos display OFT defects similar to those seen in SHF mutants, it was hypothesised that *Gata5-*

Cre and *TnT-Cre* may be more widely expressed in SHF cells outside of the differentiated myocardium. Consequently, investigation of the boundaries of *Gata5-Cre* and *TnT-Cre* expression in the OFT in relation to the transition zone was carried out.

The transition zone can be marked by the gradual reduction in SHF-specific gene, Islet-1, expression and the initiation of myosin heavy chain (MF20) expression. As described earlier, at both E9.5 and E10.5, Islet-1 is strongly expressed in the nucleus of the distal OFT SHF cells. Islet1 expression is reduced as cells differentiate into cardiomyocytes, creating a gradient of Islet-1 expression in the OFT (Figure 58). Islet-1 is not expressed in the ventricular myocardium. MF20 is a component of the actin-myosin cytoskeleton and is specifically expressed in the myocardium. At E9.5 and E10.5, MF20 expression is initiated in differentiated cardiomyocytes of the distal OFT and is strongly expressed in the ventricular myocardium. This myocardial expression is retained throughout development.

E9.5 and E10.5 embryos *EYFP;Gata5-Cre* and *EYFP;TnTCre* embryos were dissected, embedded in paraffin and sectioned. Dual staining with anti-GFP, to label Cre expressing cells, and a cardiomyocyte marker, MF20 or SHF marker, Islet-1, was carried out.

Dual staining with GFP and Islet1 or MF20 shows *TnT-Cre* becomes active as cardiomyocytes begin to differentiate. The expression of *TnT-Cre*, as marked by GFP, shows an overlapping expression pattern with MF20 in the OFT at E9.5 and E10.5 (Figure 63, B and D). Additionally, as *TnT-Cre* expression is initiated, Islet1 expression is reduced in a gradient towards the ventricular myocardium (Figure 64, B and D).

Similar to *TnT-Cre*, dual staining with GFP and MF20 shows *Gata5-Cre* is active in differentiated cardiomyocytes, since GFP shows an overlapping expression pattern with MF20 in the OFT at E9.5 and E10.5. However, *Gata5-Cre* also appears to be active in the pharyngeal mesenchyme and SHF progenitors before they begin to differentiate into cardiomyocytes and prior to the onset of MF20 expression (arrows in Figure 63, A and C). The GFP expression overlaps with some SHF progenitors (arrows in Figure 64, A and C).

These results highlight that *Gata5-Cre* is more widely expressed within the SHF compared to *TnT-Cre*. Therefore, the extent of *Rac1* deletion within the

developing OFT varies between *Rac1*^{Gata5Cre} and *Rac1*^{TnTCre} mutants. However, despite this the OFT phenotype observed in the *Rac1*^{Gata5Cre} and *Rac1*^{TnTCre} is comparable. Therefore, it is suggested that the expression of *Gata5-Cre* within the SHF derived cells of the pharyngeal mesoderm does not contribute to the observed phenotype in *Rac1*^{Gata5Cre} embryos. Consequently, it can be hypothesised that *Rac1* deletion in differentiated cardiomyocytes is responsible for the OFT defects observed in *Rac1*^{Gata5Cre} and *Rac1*^{TnTCre} mutants.

Gata5-Cre and *TnT-Cre* lineage tracing overlaps within the 'transition zone' (Figure 65) therefore, the aim was to assess the characteristics of the *Rac1* deficient cardiomyocytes in this region including cardiomyocyte differentiation, proliferation, polarity and adhesion.

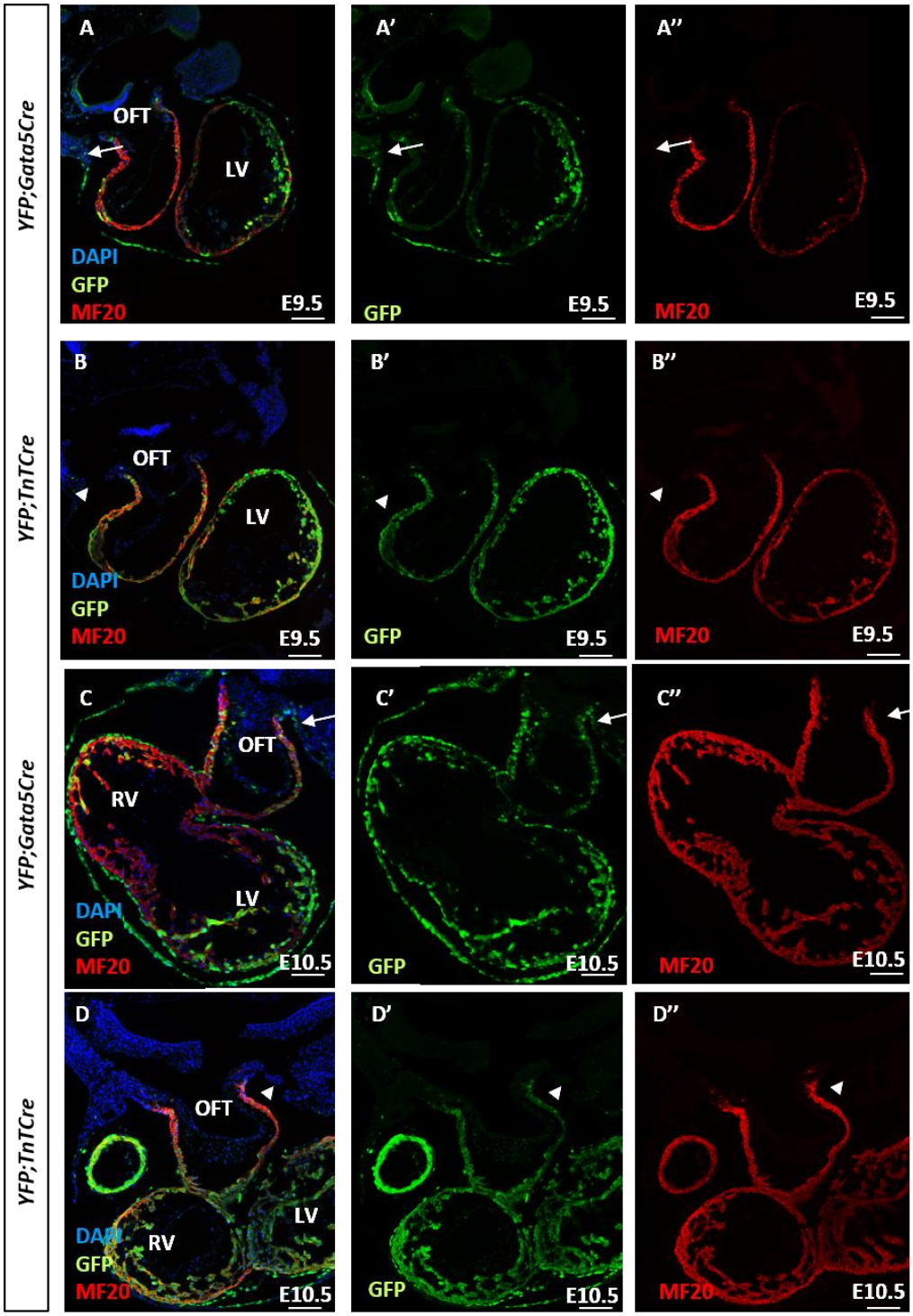

Figure 63: *Gata5-Cre* and *TnT-Cre* expression in the OFT in relation to cardiomyocyte marker, MF20.
Dual staining with GFP and MF20 shows *TnT-Cre* becomes active as cardiomyocytes begin to differentiate. The expression of *TnT-Cre*, as marked by GFP, shows an overlapping expression pattern with MF20 in the OFT at E9.5 and E10.5 (**B** and **D**). However, *Gata5-Cre* is also active in the pharyngeal mesenchyme and SHF progenitors before they begin to differentiate into cardiomyocytes and prior to the onset of MF20 expression (arrows in **A** and **C**). LV; left ventricle, RV; right ventricle, OFT; outflow tract. Scale bars; 100μm.

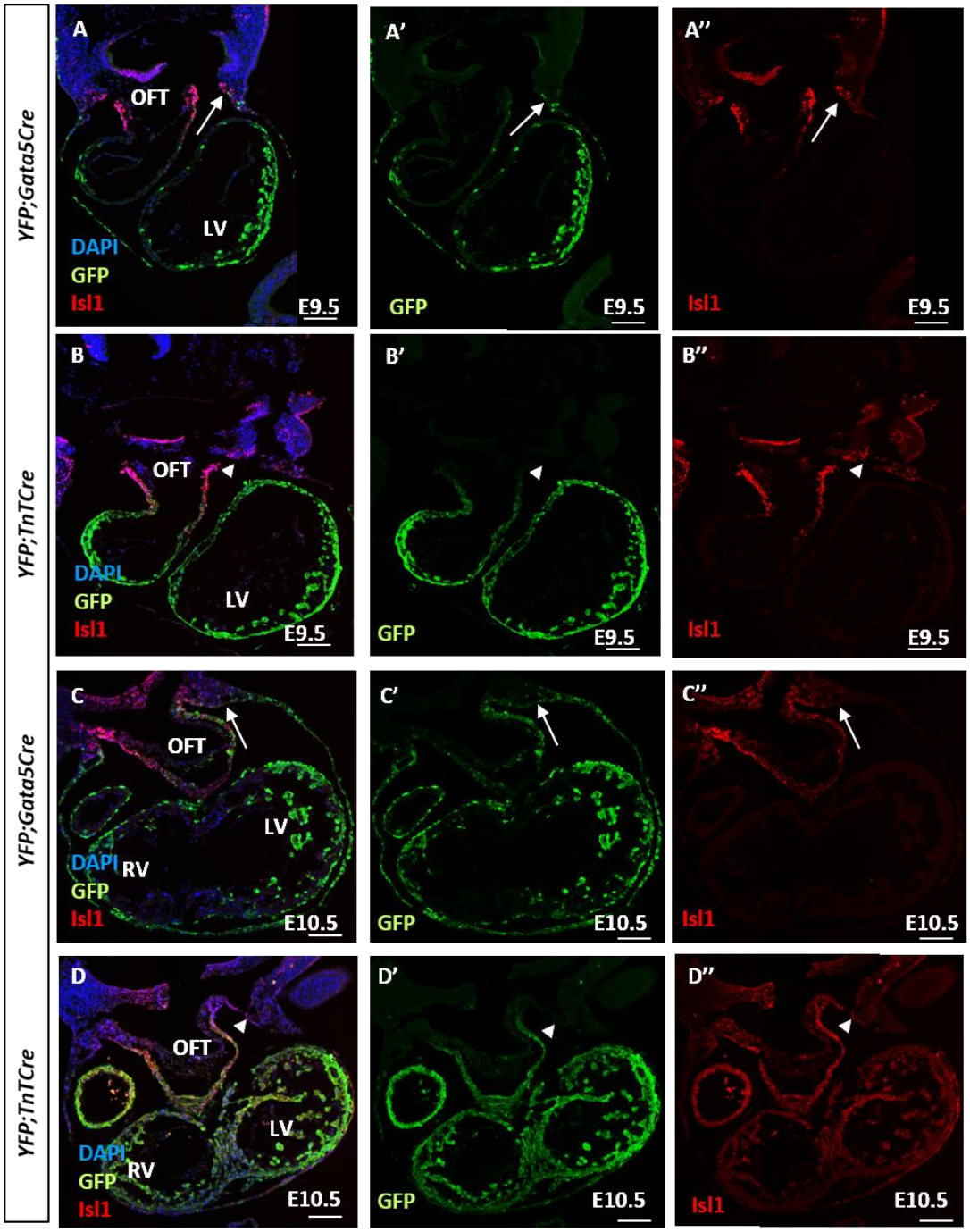

Figure 64: *Gata5-Cre* and *TnT-Cre* expression in the OFT in relation to SHF marker, Iselt1.

Dual staining with GFP and Islet1 shows *TnT-Cre* becomes active as cardiomyocytes begin to differentiate. As *TnT-Cre* expression is initiated, Iselt1 expression is reduced in a gradient towards the ventricular myocardium (**B** and **D**). However, *Gata5-Cre* is also active in the pharyngeal mesenchyme and SHF progenitors before they begin to differentiate into cardiomyocytes and prior to the onset of MF20 expression (arrows in **A** and **C**). The GFP expression overlaps with SHF progenitors (arrows in **A** and **C**). LV; left ventricle, RV; right ventricle, OFT; outflow tract Scale bars; 100µm.

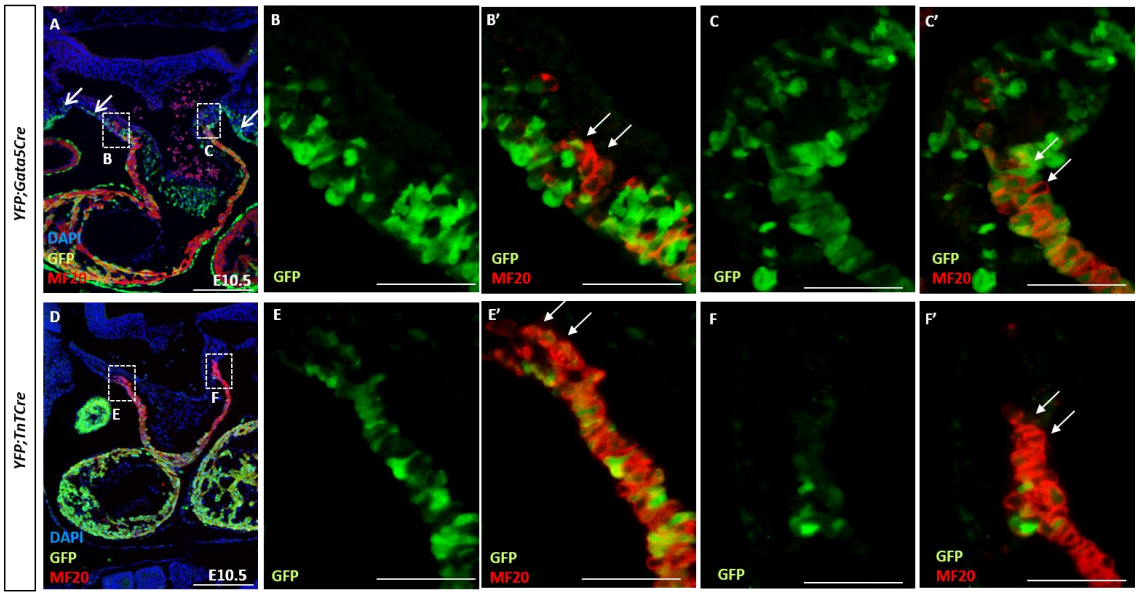

Figure 65: *Gata5-Cre* and *TnT-Cre* expression in the OFT in relation to cardiomyocyte marker, MF20.
Dual staining with GFP and MF20 shows *TnT-Cre* becomes active as cardiomyocytes begin to differentiate (**D**). The expression of *TnT-Cre*, as marked by GFP, shows an overlapping expression pattern with MF20 in the OFT at E10.5 (**D**). However, *Gata5-Cre* shows a wider expression pattern than MF20 expression, with additional expression in the pharyngeal mesoderm (arrows in **A**). *Gata5-Cre* is more widely expressed within SHF compared to *TnT-Cre*, *Gata5-Cre* and *TnT-Cre* expression overlaps within in the 'transition zone' (**B** and **C** compared to **E** and **F**).

4.3.1.4 OFT cardiomyocyte differentiation

As shown in Figure 64 and Figure 66, SHF cells begin to express Cre as they are undergoing cardiomyocyte differentiation, and it was hypothesised that this process could be altered in the absence of Rac1. To determine if cardiomyocyte differentiation occurs normally in the transition zone in *Rac1*^{TnTCre} hearts, immunostaining with MF20 was carried out on E9.5 and E10.5 sections. In controls, MF20 expression appeared strong in the myocardial cells of the OFT. The *Rac1*^{TnTCre} hearts had normal expression pattern of MF20 in the OFT compared to controls (E9.5 n=3, E10.5 n=3) (Figure 66). These results suggest that deficiency of *Rac1* does not affect the differentiation of SHF cells into cardiomyocytes in the transition zone.

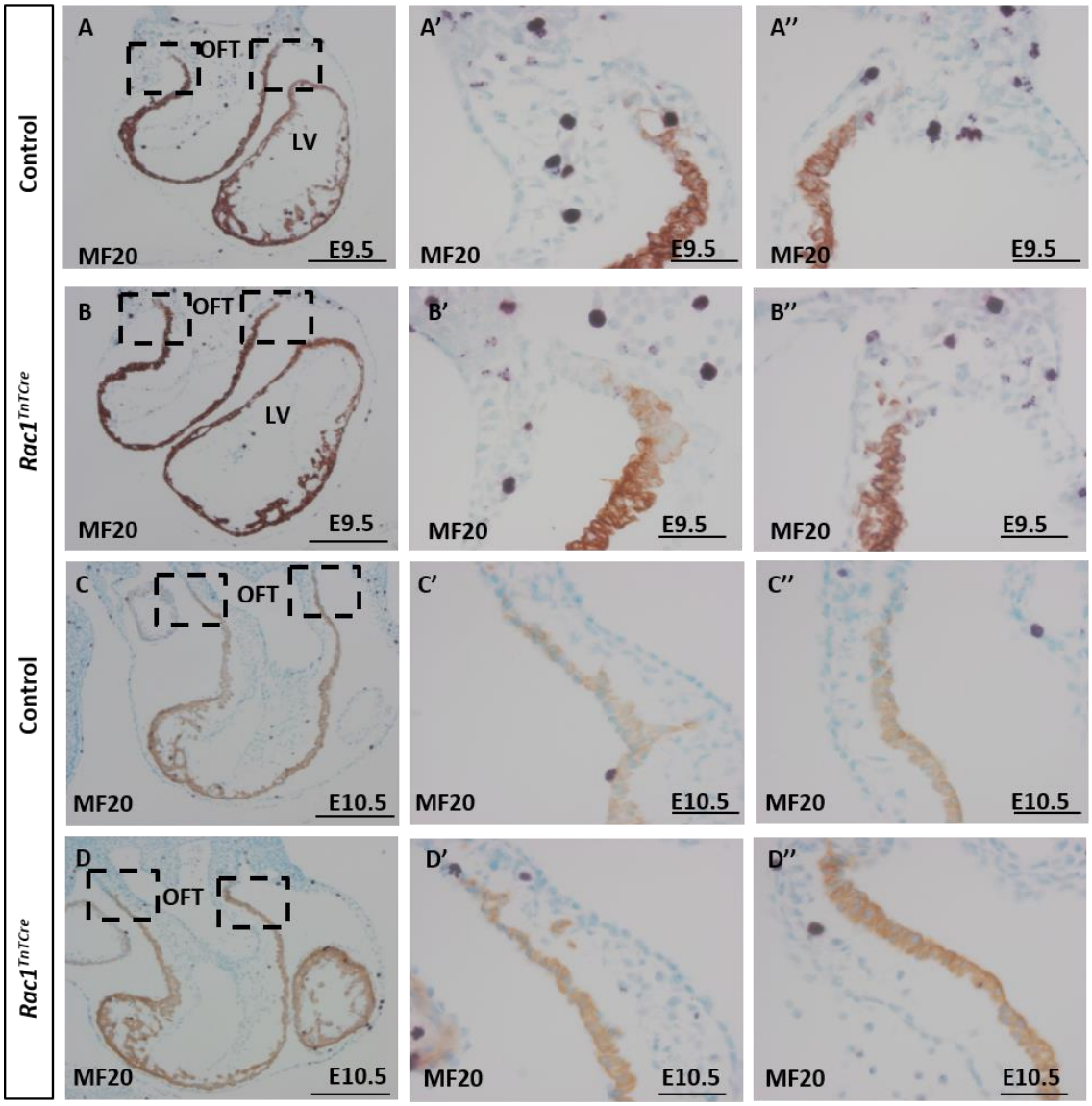

Figure 66: MF20 IHC on E9.5 and E10.5 control and *Rac1*^{TnTCre} heart sections.
Anti-MF20 IHC staining shows that cardiomyocyte differentiation within the OFT is normal in *Rac1*^{TnTCre} hearts compared to controls at E9.5 (**A**-**B**) and E10.5 (**C**-**D**) (n=4). LV; left ventricle, OFT; outflow tract. Scale A-B 200μm, A'-D'' 50μm.

4.3.1.5 OFT cardiomyocyte proliferation and apoptosis

Since regulated cell proliferation and apoptosis is crucial for normal OFT development, it can be hypothesised that either increased cell death or reduced proliferation in the developing OFT following its initial formation could explain the OFT defects observed later in development. Therefore, cell death and proliferation was examined in the OFT myocardial cells in control and *Rac1*^{TnTCre} hearts, by IF with apoptosis marker, caspase-3 and proliferation marker, BrdU.

To analyse proliferation in the developing OFT, BrdU incorporation was utilised to identify cells undergoing DNA synthesis. Administration of BrdU into pregnant females results in BrdU incorporation into all embryonic cells that are undergoing DNA synthesis (S phase) during the exposure time. E9.5 embryos were exposed to BrdU for 1 hour prior to dissection. Embryos were then dissected, processed and sectioned. Dual immunostaining staining using anti-MF20 and anti-BrdU allowed identification of proliferating cardiomyocytes. Cell count analysis revealed proliferation levels in the OFT myocardium was relatively high, however was not altered in *Rac1*^{TnTCre} hearts (n=5) (Figure 67B). Similarly, immunostaining with anti-caspase 3 was utilised to identify cells undergoing apoptosis. Dual staining with anti-caspase-3 and anti-MF20 was carried out on E9.5 sections of control and *Rac1*^{TnTCre} hearts. Cell count analysis revealed the level of apoptosis in the developing OFT in controls was minimal and was unchanged in the *Rac1*^{TnTCre} hearts (n=5) (Figure 67C). Furthermore, the number of cells in the OFT was equivalent between controls and *Rac1*^{TnTCre}embryos (Figure 67A). Therefore, *Rac1* deficiency does not affect OFT cardiomyocyte apoptosis or proliferation and hence there is no difference in cell number.

It can be proposed from these results that SHF progenitors are undergoing progressive differentiation into cardiomyocytes and the subsequent cardiomyocytes are undergoing regulated proliferation and cell death.

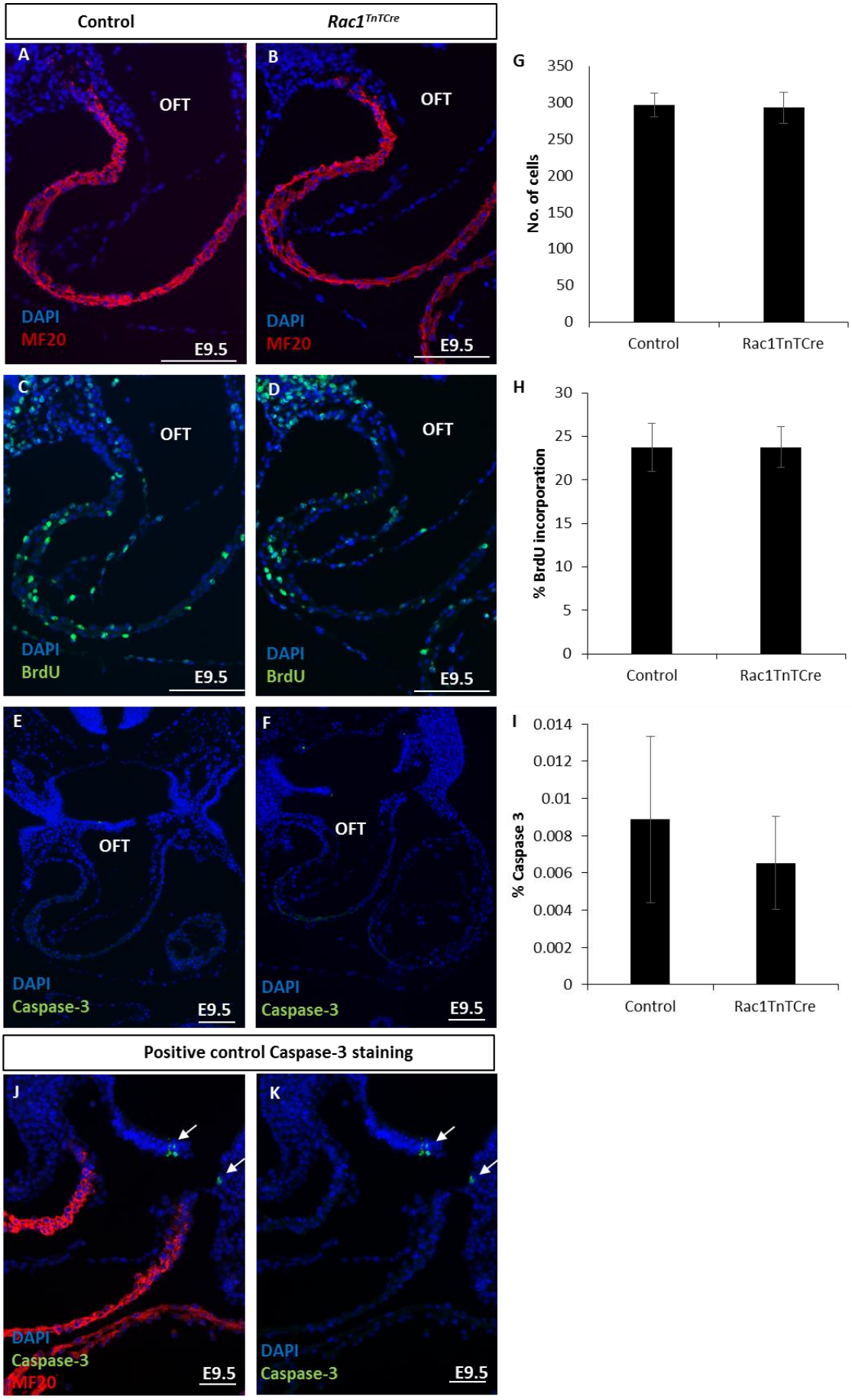
Control
Rac1TnTCre
A
OFT
DAPI
MF20
E9.5
B
OFT
DAPI
MF20
E9.5
G
No. of cells
350
300
250
200
150
100
50
0
Control
Rac1TnTCre
C
OFT
DAPI
BrdU
E9.5
D
OFT
DAPI
BrdU
E9.5
H
% BrdU incorporation
30
25
20
15
10
5
0
Control
Rac1TnTCre
E
OFT
DAPI
Caspase-3
E9.5
F
OFT
DAPI
Caspase-3
E9.5
I
% Caspase 3
0.014
0.012
0.01
0.008
0.006
0.004
0.002
0
Control
Rac1TnTCre
Positive control Caspase-3 staining
J
DAPI
Caspase-3
MF20
E9.5
K
DAPI
Caspase-3
E9.5

Figure 67: Cell proliferation and apoptosis analysis of E9.5 control and *Rac1*^{TnTCre} OFT sections.
No significant differences were observed in the total cardiomyocyte cell number (**A**-**B**, **G**), BrdU detected cardiomyocyte proliferation (**C**-**D**, **H**) or caspase-3 detected cardiomyocyte apoptosis (**E**-**F**, **I**) (n=6). Positive control for caspase-3 immunofluorescent staining in OFT (**J**-**K**). OFT; outflow tract. Scale bar 100μm. Statistical analysis carried out using the unpaired t-test. Large SEM is seen in the caspase analysis, in both the control and *Rac1*^{TnTCre} hearts. Statistical power calculations suggest the experiment may be underpowered.

4.3.1.6 Outflow tract cardiomyocyte adhesion and polarity

In addition to cardiomyocyte differentiation and proliferation, continued OFT development requires regulated cardiomyocyte adhesion and polarity (Ramsbottom *et al.*, 2014). Therefore, some of the main markers of cardiomyocyte adhesion and polarity were investigated in *Rac1*^{TnTCre} mutant hearts.

E9.5 and E10.5 embryos were dissected, embedded in paraffin and sectioned. Immunostaining for AJ, desmosome, gap junction, and TJ markers were carried out in control and *Rac1*^{TnTCre} hearts. Images of left and right sides of the OFT at the transition zone were taken as shown in Figure 68 and analysed for Figure 69 to Figure 75.

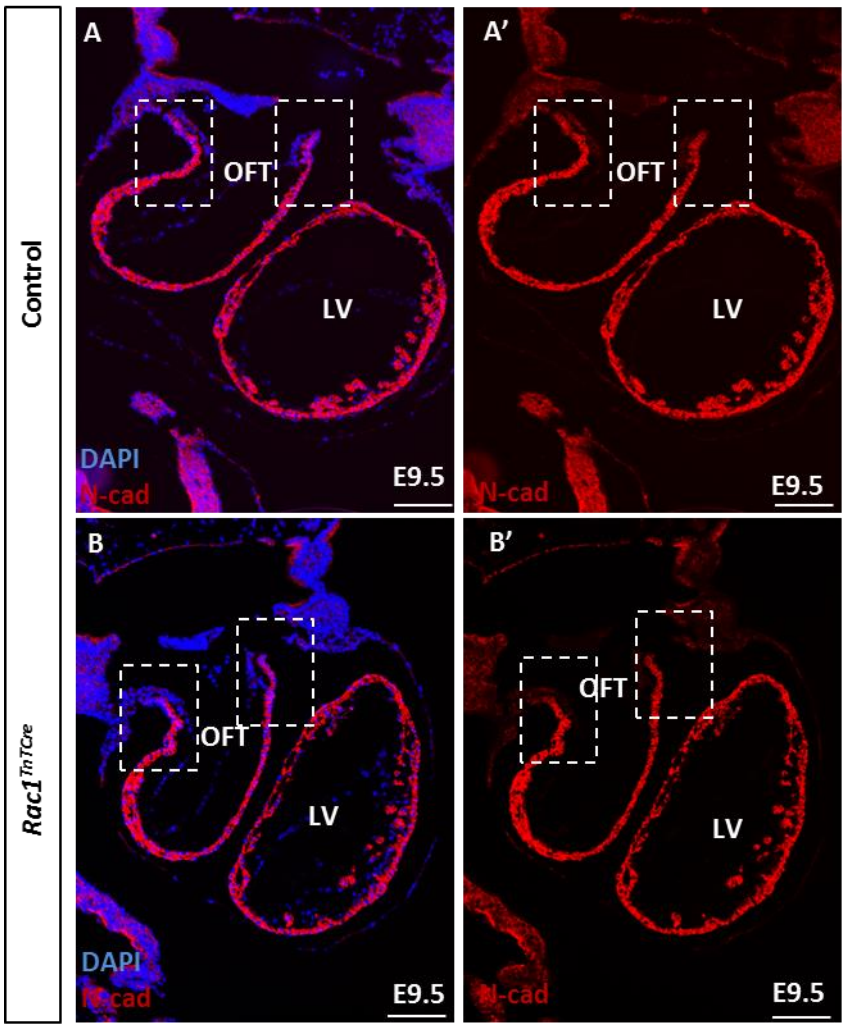

Figure 68: Transition zone in OFT investigated for markers of cardiomyocyte adhesion and polarity.
Example of N-cadherin staining in E9.5 control (**A**-**A'**) and *Rac1*^{TnTCre} (**B**-**B'**) transverse sections. Images of left and right sides of the OFT at the transition zone were taken and analysed for Figure 69 to Figure 75. LV; left ventricle, OFT; outflow tract. Scale bar 100µm.

AJ markers, β-catenin and cadherins were all restricted to the membrane as expected in both controls and *Rac1*^{TnTCre} hearts (Figure 69 and Figure 70). E9.5 expression of β-catenin (n=4) and N-cadherin E9.5 (n=4) are normal (Figure 69 and Figure 70 respectively) as well as expression of E-cadherin at both E9.5 (n=3) and E10.5 (n=3) (Figure 70). Desmosome marker, desmin, appeared to be normally expressed in the *Rac1*^{TnTCre} OFT compared to controls at E9.5 (n=4) (Figure 71). TJ have restricted expression at apical membranes, therefore are a useful indicator of cell polarity. TJ marker, PKC-ζ appeared to be normally expressed in the *Rac1*^{TnTCre} OFT compared to controls at both E9.5 (n=3) and E10.5 (n=3) (Figure 72A-H). Additional TJ marker, ZO-1 also appeared normally

expressed at cell-cell junctions in E10.5 control and *Rac1*^{TnTCre} OFT cardiomyocytes (n=3) (Figure 72I-L).

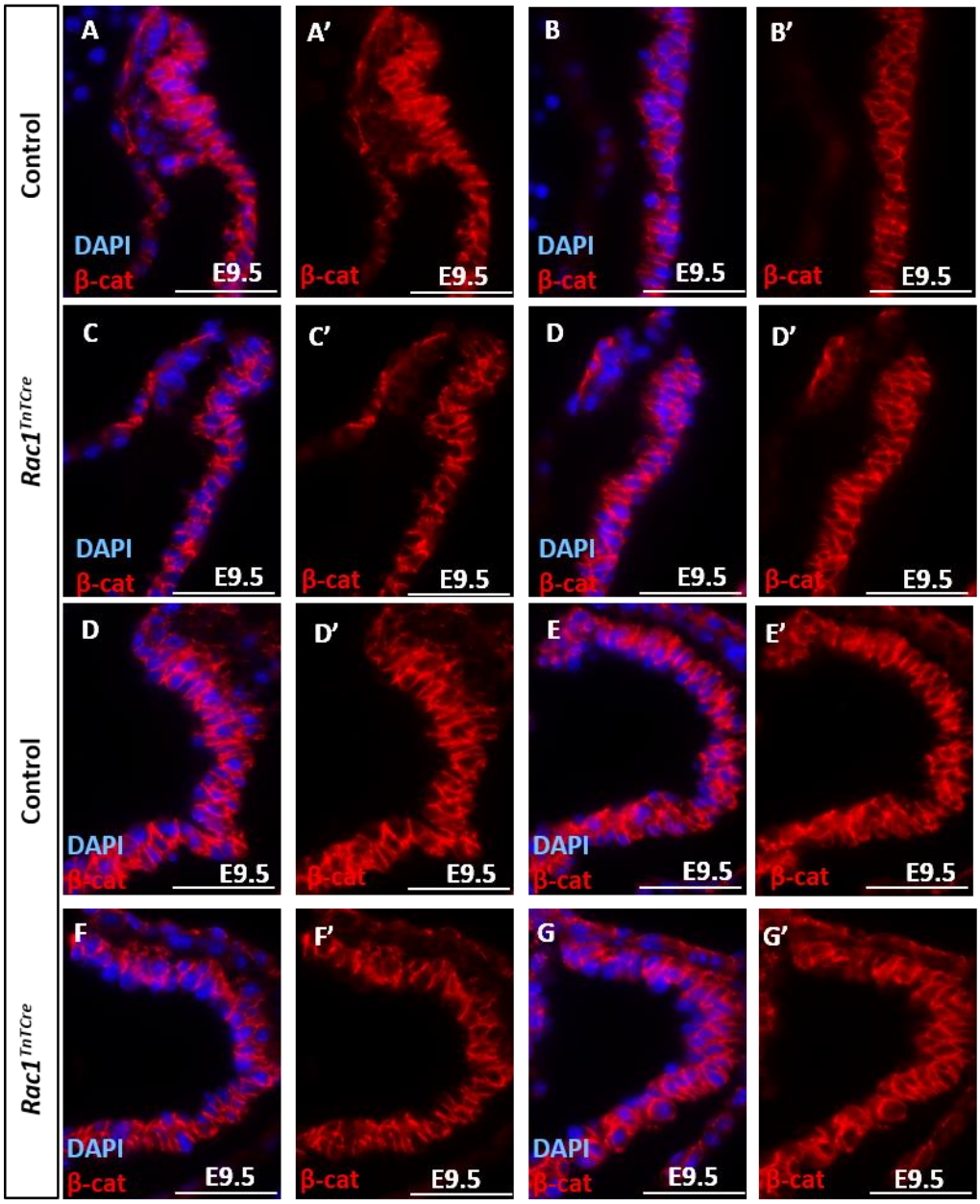

Figure 69: β-catenin IF in OFT cardiomyocytes in control and *Rac1*^{TnTCre} hearts.
Adherens junction marker, β-catenin is restricted to the membrane as expected in both controls and *Rac1*^{TnTCre} hearts at E9.5 (n=4). Scale bars; 50µm.

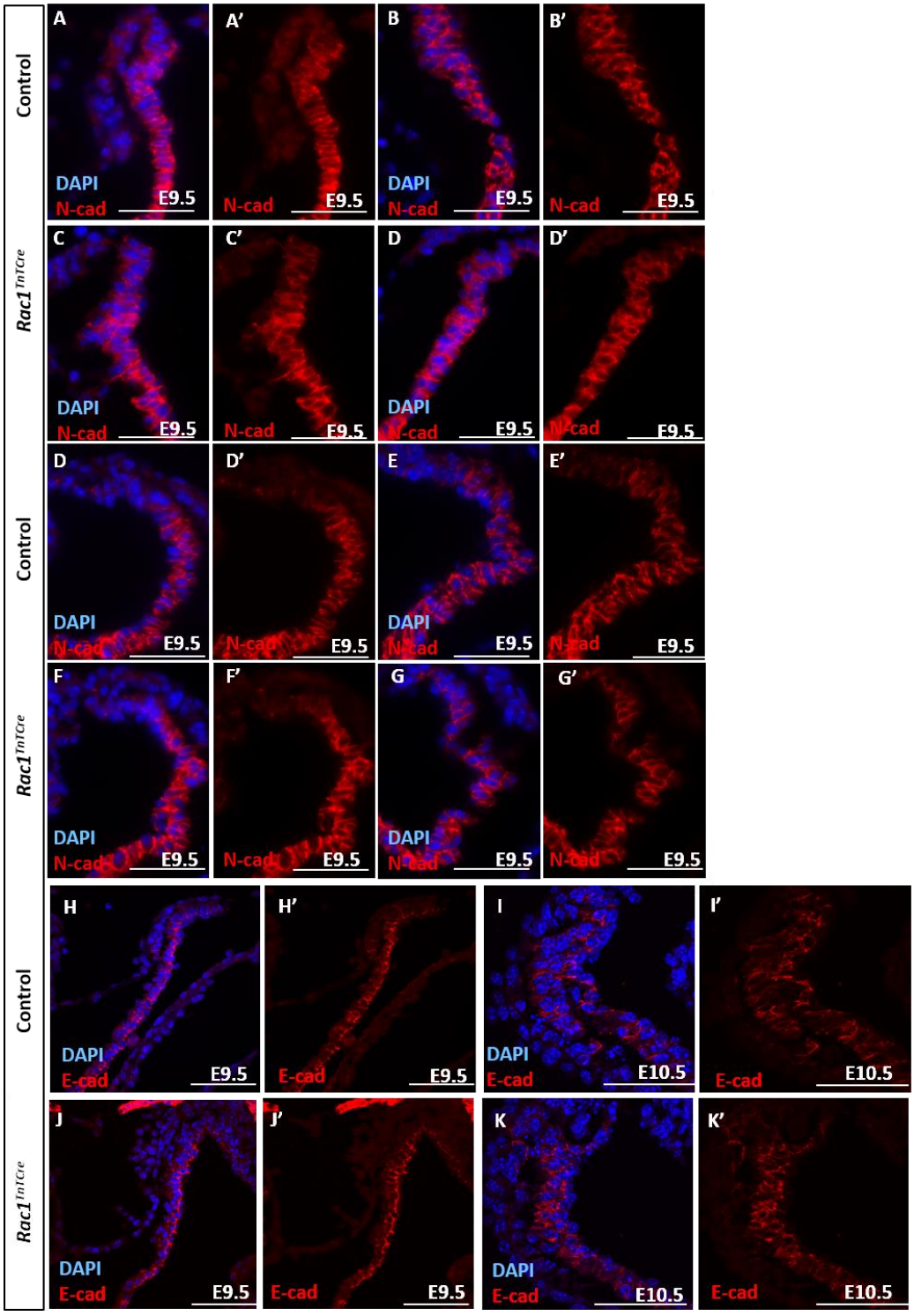

Figure 70: N-cadherin and E-cadherin IF in OFT cardiomyocytes in control and *Rac1*^{TnTCre} hearts.

Adherens junction marker, N-cadherin is restricted to the membrane as expected in both controls and *Rac1*^{TnTCre} hearts at E9.5 (n=4) (**A-G'**). Adherens junction marker, E-cadherin expression is restricted to the membrane in both controls and *Rac1*^{TnTCre} hearts at both E9.5 (n=3) and E10.5 (n=3) (**H-K'**). Scale bars; A-G' 50μm, H-K' 100μm.

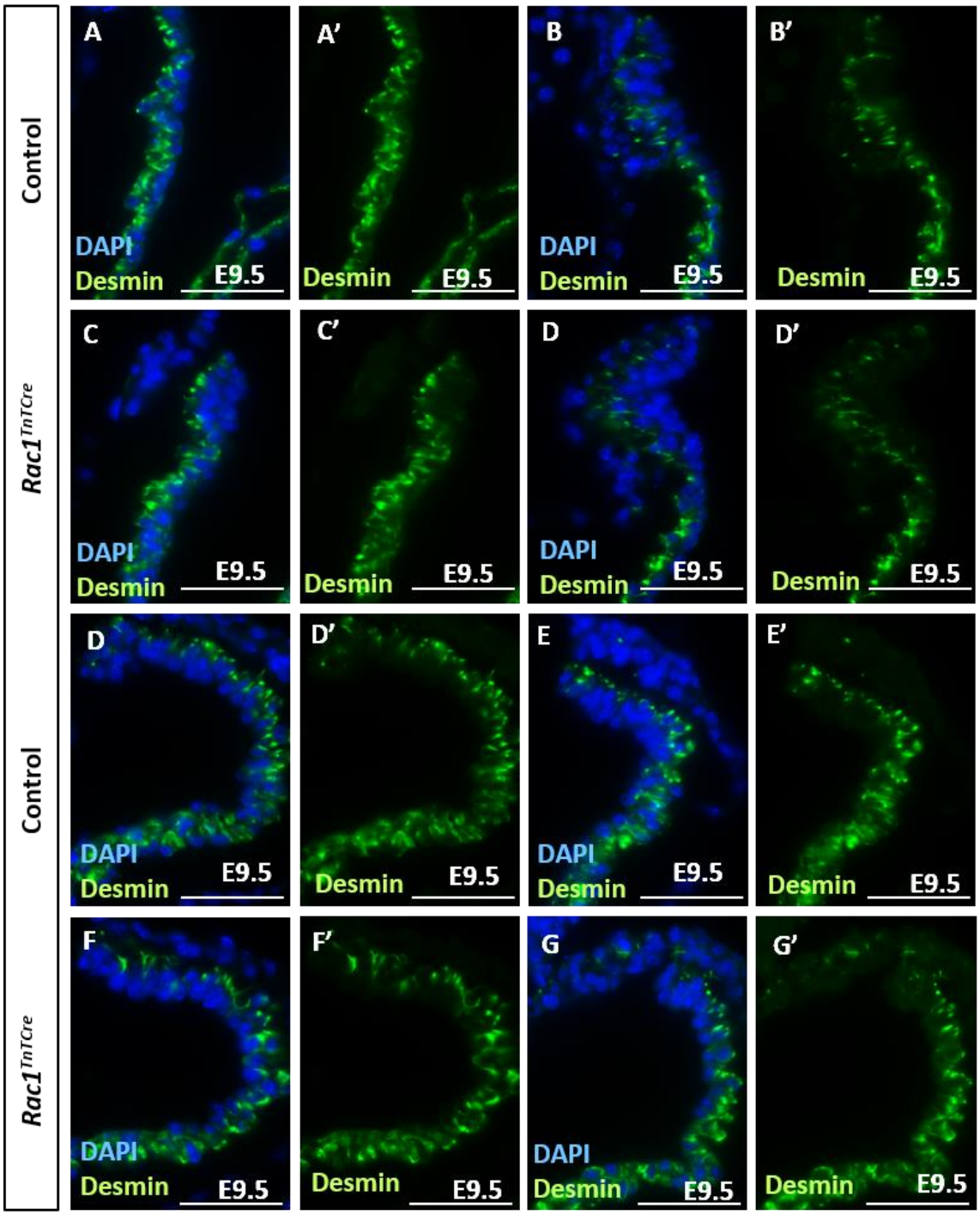

Figure 71: Desmin IF in OFT cardiomyocytes in control and *Rac1*^{TnTCre} hearts.
Desmosome marker, Desmin, is normally expressed in the *Rac1*^{TnTCre} OFT compared to controls at E9.5 (n=4). Scale bars; 50µm.

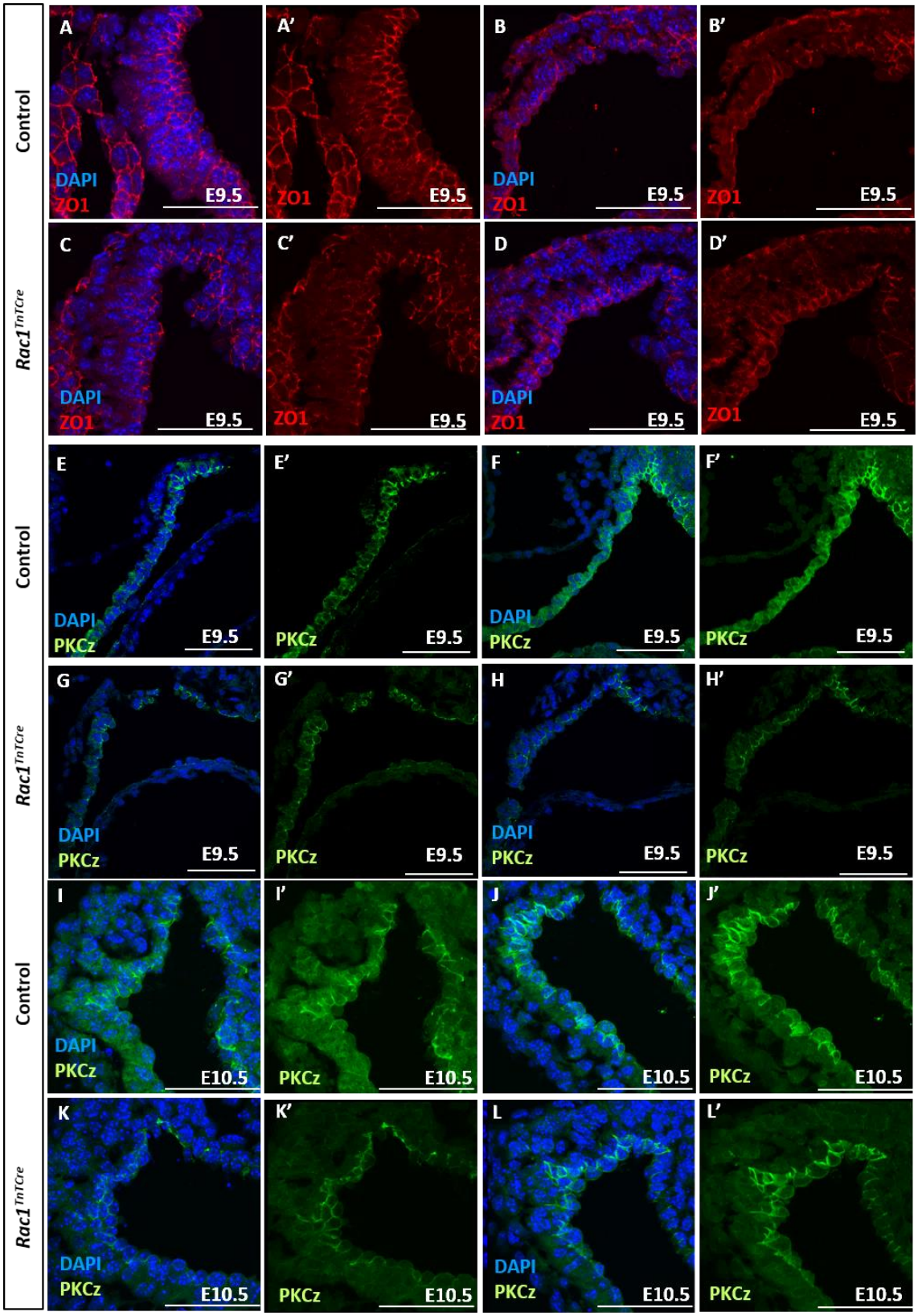

Figure 72: PKCk and ZO-1 IF in OFT cardiomyocytes in control and *Rac1*^{TnTCre} hearts.

Tight junction marker, PKC-z appeared to be normally expressed in the *Rac1*^{TnTCre} OFT compared to controls at both E9.5 (n=3) and E10.5 (n=3) (**A**-**H**). Additional tight junction marker, ZO-1 also appeared normally expressed at cell-

cell junctions in E10.5 control and *Rac1*^{TnTCre} OFT cardiomyocytes (n=3) (**I**-**L**). Scale bars; 100µm.

Microtubule protein, acetylated gamma (γ)-tubulin appeared normally expressed within the OFT cardiomyocytes in controls and *Rac1*^{TnTCre} hearts (n=3) (Figure 73).

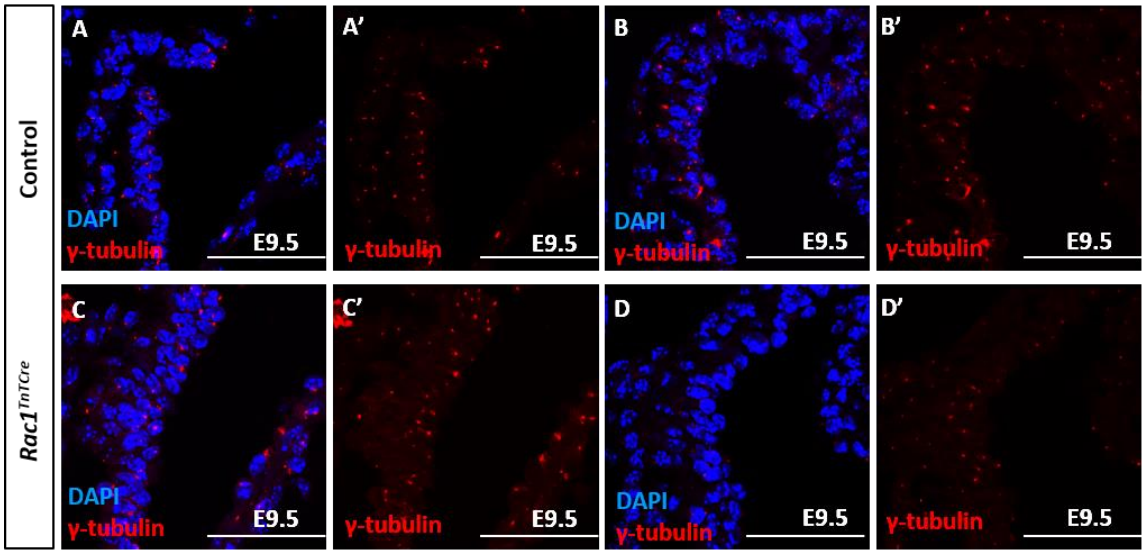

Figure 73: Gamma (γ)-tubulin IF in OFT cardiomyocytes in control and *Rac1*^{TnTCre} hearts.
Microtubule protein, acetylated gamma (γ)-tubulin appeared normally expressed within the OFT cardiomyocytes in controls and *Rac1*^{TnTCre} hearts (n=3). Scale bars; 100µm.

4.3.1.7 Extracellular matrix (ECM)

ECM protein laminin is expressed in the basal lamina within the basement membrane in both controls and *Rac1*^{TnTCre} hearts at E9.5 (n=3) (Figure 74).

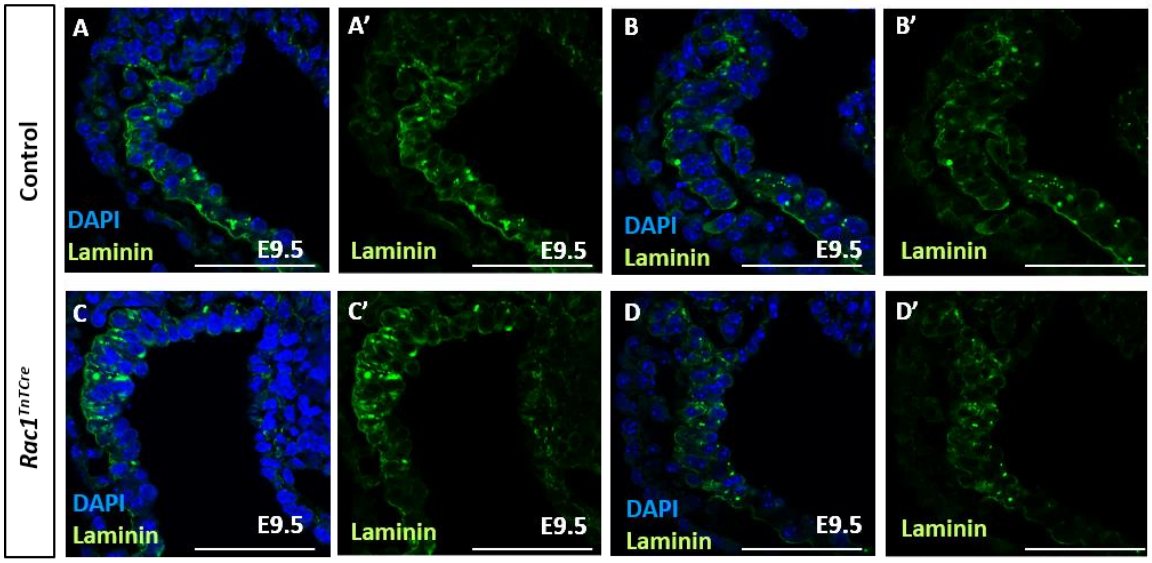

Figure 74: Laminin IF in OFT cardiomyocytes in control and *Rac1*^{TnTCre} hearts.
ECM protein laminin is expressed in the basal lamina within the basement membrane in both controls and *Rac1*^{TnTCre} hearts at E9.5 (n=3). Scale bars; 100µm.

4.3.1.8 Planar cell polarity signalling

Scrib is a component of PCP signalling and is thought to interact with Rac1 within embryonic cardiomyocytes (Boczonadi *et al.*, 2014b). Scrib expression was restricted to cardiomyocyte cell membrane in controls and *Rac1*^{TnTCre} hearts at both E9.5 (n=3) and E10.5 (n=3), suggesting deficiency of Rac1 does not affect Scrib membrane binding (Figure 75).

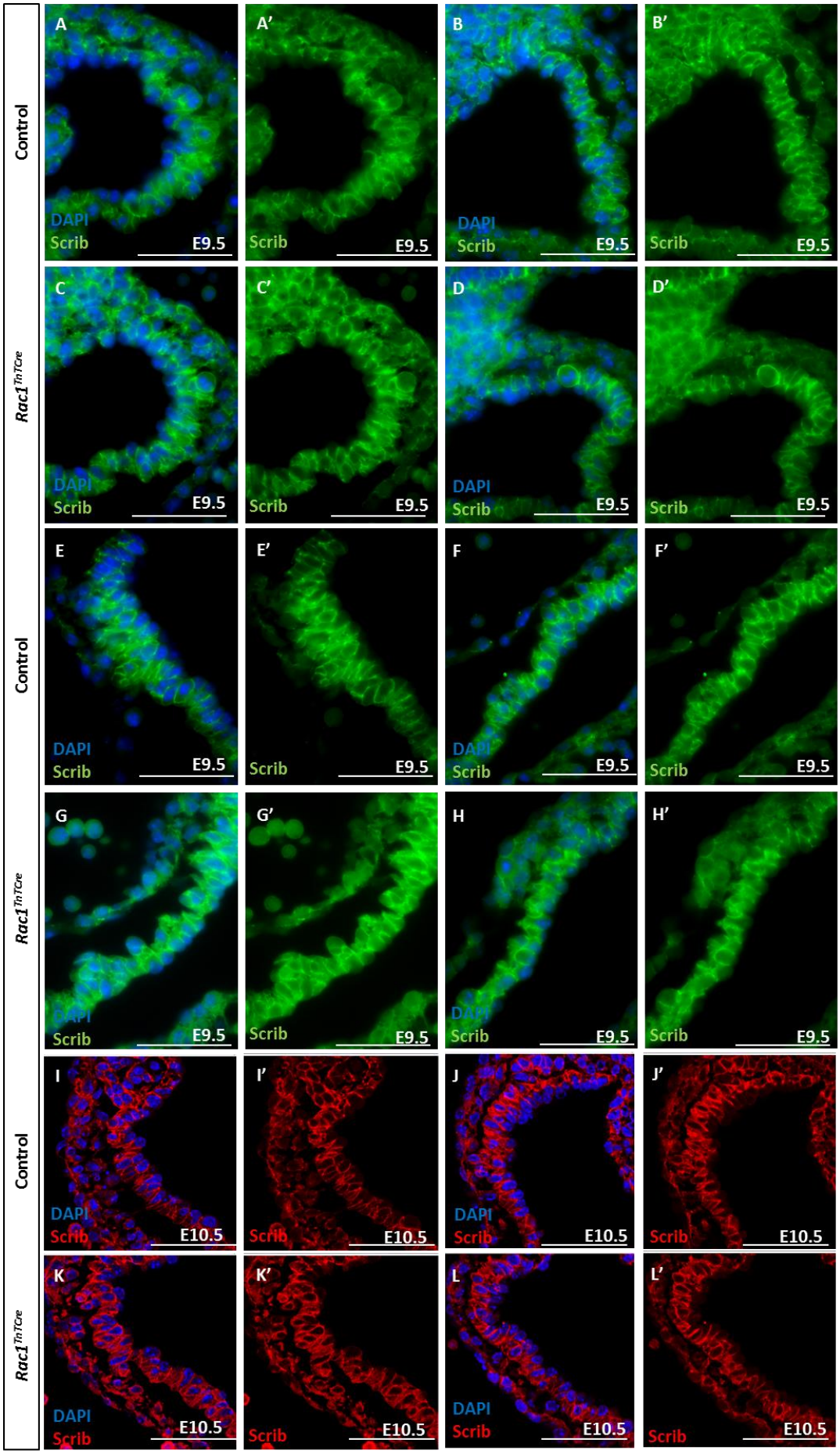
Control
Rac1TnTCre
Control
Rac1TnTCre
Control
Rac1TnTCre
A
A'
B
B'
C
C'
D
D'
E
E'
F
F'
G
G'
H
H'
I
I'
J
J'
K
K'
L
L'
DAPI
Scrib
E9.5
E10.5

Figure 75: Scrib IF in OFT cardiomyocytes in control and *Rac1^{TnTCre}* hearts.
PCP signalling protein scrib was restricted to cardiomyocyte cell membrane in controls and *Rac1^{TnTCre}* hearts at E9.5 (n=3) and E10.5 (n=3). Scale bars; A-H' 50μm, I-L' 100μm.
Immunostaining for indicators of cell polarisation such as cell-cell junction proteins, MTOCs and ECM proteins reveal that OFT cardiomyocyte adhesion and polarity is unaffected during early OFT formation in *Rac1^{TnTCre}* hearts.

4.3.2 OFT remodelling in Rac1^{TnTCre} hearts

OFT morphology in the early stages of heart development appears unaffected in *Rac1^{TnTCre}* hearts, at both a tissue and cellular level. Therefore, it was hypothesised that the OFT alignment defects arise from abnormalities in later OFT remodelling.

4.3.3.1 OFT rotation and wedging of the aorta

Later in development, at around E12.5, the OFT septates into the aorta and pulmonary trunk. The OFT rotates and these vessels spiral around each other. 'Wedging' then occurs where the aorta moves behind the pulmonary trunk and positions itself between the AV valves, to allow for OFT alignment into the correct ventricular chambers. This process is dependent on the retraction and rotation of the truncal myocardium (Watanabe *et al.*, 2001) and without wedging, the aorta overrides the ventricular septum.
To visualise OFT development in *Rac1^{TnTCre}* embryos and define the developmental stage when the OFT defects arise, E11.5-E15.5 embryos were dissected with the pericardium/body wall removed to allow visualisation of the heart and OFT. Images were taken of control and *Rac1^{TnTCre}* embryo hearts and OFTs and analysed (n=3 for each time point). The shape of both the heart and OFT appears normal at E11.5 and E12.5 (Figure 76A-D). However, by E13.5 the heart appears to be ballooned in shape with the OFT at an aberrant angle (Figure 76E-F). This abnormality becomes more pronounced at E14.5 and E15.5 (Figure 76G-J'). Therefore, it was hypothesised that the DORV/OA defect in *Rac1^{TnTCre}* and *Rac1^{Gata5Cre}* embryos arises from a defect in the maturation and/or rotation of the OFT. To investigate this, the embryonic stage when the OFT defects become apparent will be determined and IF will be used to look at the process of OFT myocardialisation.

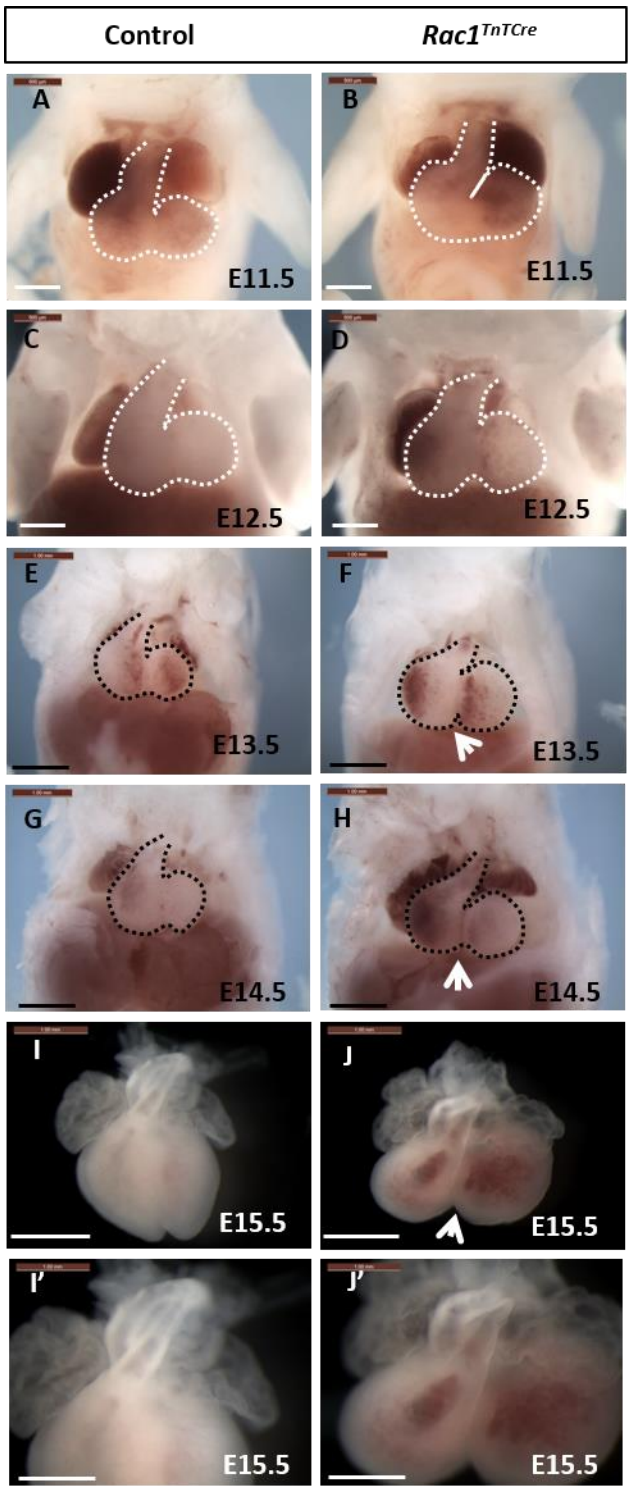

Figure 76: Images of control and *Rac1*^{TnTCre} dissected hearts during development. The shape of both the heart and OFT appears normal at E11.5 and E12.5 (**A**-**D**). However, by E13.5 the heart appears to be ballooned in shape with the OFT at an aberrant angle (**E** and **F**). This abnormality becomes more pronounced at E14.5 and E15.5 (**G**-**J'**). The heart appears bifid in shape with a prominent interventricular groove (arrows in **F**, **H** and **J**). Scale bars; A-J 500μm, I'-J' 1mm.

4.3.2.2 3D visualisation of Rac1^{Gata5Cre} *and Rac1*^{TnTCre} *hearts*

Histology sections of mutant hearts revealed fully penetrant DORV/OA. To allow 3D visualisation of the OFT defects in mutant hearts, *Rac1*^{Gata5Cre} and *Rac1*^{TnTCre} and stage matched control embryos were sent for magnetic resonance imaging (MRI). E15.5 *Rac1*^{Gata5Cre} and *Rac1*^{TnTCre} embryos were dissected, bled out and incubated with fixative and contrast agent for optimal

MRI imaging. Embryos were then embedded within agarose inside a MRI tube and sent to Dr Jurgen Schneider, University of Oxford, for imaging (Bamforth *et al.*, 2012). 3D models were created from MRI image stacks using Amira software (*Rac1*^{Gata5Cre}; n=15, controls; n=8, *Rac1*^{TnTCre}; n=4, controls; n=4). MRI reconstructions highlight the abnormal shape of both *Rac1*^{Gata5Cre} and *Rac1*^{TnTCre} hearts, with severely dilated and rounded ventricular chambers. The reconstructions also show thin myocardial walls and OFT alignment defects (Figure 77).

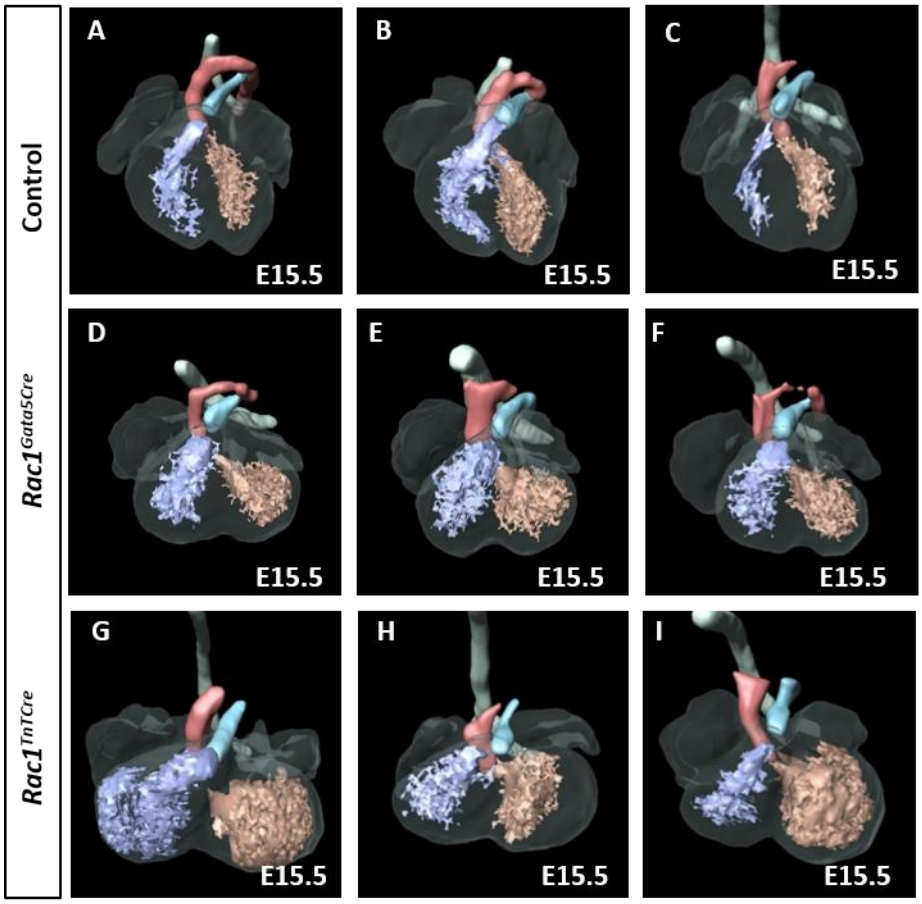

Figure 77: 3D reconstructions of E15.5 *Rac1*^{Gata5Cre} and *Rac1*^{TnTCre} hearts MRI data.
Example images of 3D models created from MRI image stacks using Amira software. Orange; left ventricle, purple; right ventricle, red; aorta, blue; pulmonary trunk, white; trachea.

4.3.2.3 OFT myocardialisation

At E12, myocardialisation initiates and leads to a muscularisation of the base of the aorta and pulmonary trunk. To determine if myocardialisation of the OFT

cushions occurs normally in *Rac1*^{TnTCre} embryos, staining for ECM and myocardial specific proteins was carried out on E11.5-E14.5 control and *Rac1*^{TnTCre} wax sections (n=3). Alcian blue stains ECM in blue and was counterstained with eosin. IHC staining for myocardial markers, anti-α-SMA and anti-MF20, with DAB was counterstained with methyl green. Alcian blue staining confirms a high density of ECM within the endocardial and OFT cushions at E12.5 and E13.5 as expected (Figure 78A-D). By E14.5, the majority of ECM is confined to the AV and semilunar valves (Figure 78E-F). The composition of the endocardial and OFT cushions appears normal in *Rac1*^{TnTCre} hearts from E12.5-E14.5 (Figure 78A-F). Also, initial cushion formation is unaffected in *Rac1*^{TnTCre} hearts, shown at E12.5. However, the positioning of the OFT cushions appears to be disrupted from E13.5 onwards. The complete fusion of the endocardial cushions, OFT and IVS is not seen in *Rac1*^{TnTCre} hearts as in controls. It was hypothesised that this could be as a result of the shortened IVS and dilated ventricle chambers.

Anti-α-SMA and anti-MF20 immunostaining highlights the myocardial cells migrating into the OFT cushions and confirms that the OFT cushions are undergoing myocardialisation in both controls and in *Rac1*^{TnTCre} hearts (Figure 79A-D, Figure 80A-D). By E14.5 the cushions have fully myocardialised (Figure 80E-F). At E12.5 these invading myocardial cells are projecting inwards, into the OFT cushions, in the *Rac1*^{TnTCre} hearts as in controls (Figure 81).

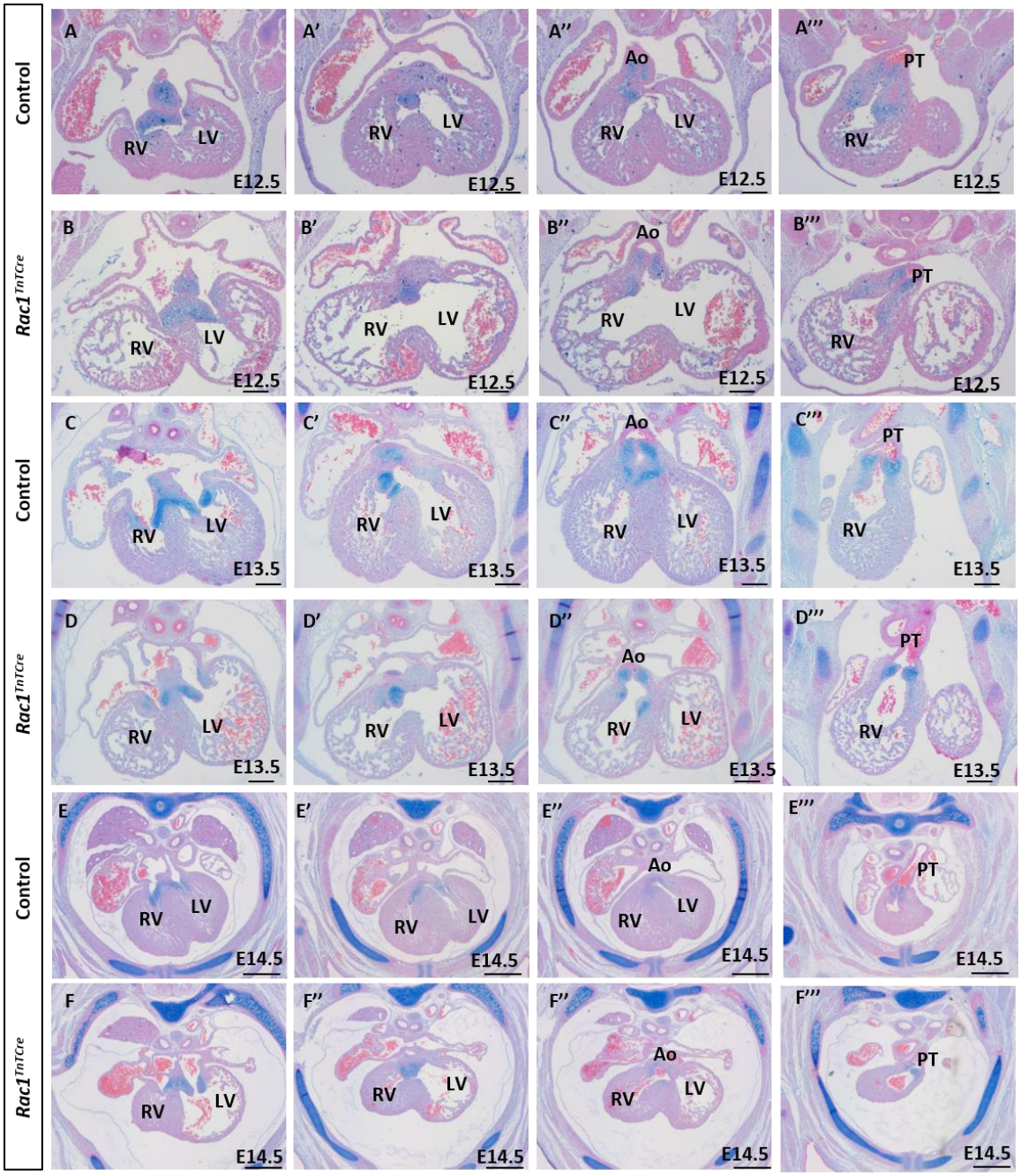

Figure 78: Alcian blue staining of E12.5, E13.5 and E14.5 control and *Rac1*^{TnTCre} heart sections.

Alcian blue staining confirms a high density of ECM within the endocardial and OFT cushions at E12.5 and E13.5 as expected (**A**-**D**) (n=4). By E14.5, the majority of ECM is confined to the AV and semilunar valves (**E**-**F**) (n=3). The composition of the endocardial and OFT cushions appears normal in *Rac1*^{TnTCre} hearts from E12.5-E14.5 (**A**-**F**). Also, initial cushion formation is unaffected in *Rac1*^{TnTCre} hearts, shown at E12.5. However, the positioning of the OFT cushions appears to be disrupted from E13.5 onwards. The complete fusion of the endocardial cushions, OFT and IVS is not seen in *Rac1*^{TnTCre} hearts as in controls (**C**-**D**). LV; left ventricle, RV; right ventricle, Ao; aorta, PT;pulmonary trunk. Scale bars; A-D''' 200μm, E-F''' 500μm.

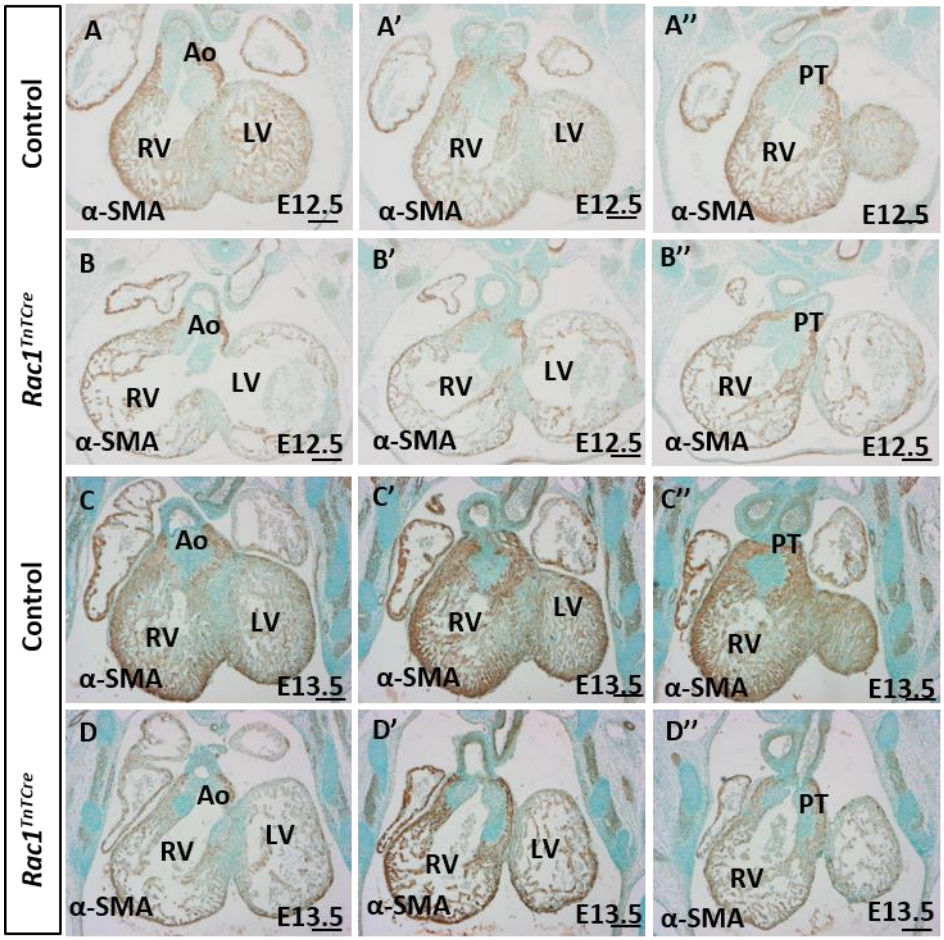

Figure 79: α-SMA IHC on E12.5 and E13.5 control and *Rac1*^{TnTCre} hearts. Anti-α-SMA IHC staining highlights the myocardial cells migrating into the OFT cushions and confirms that the OFT cushions are undergoing myocardialisation in both controls and in *Rac1*^{TnTCre} hearts (**A**-**D**) (n=4). LV; left ventricle, RV; right ventricle, Ao; aorta, PT;pulmonary trunk. Scale bars 200μm.

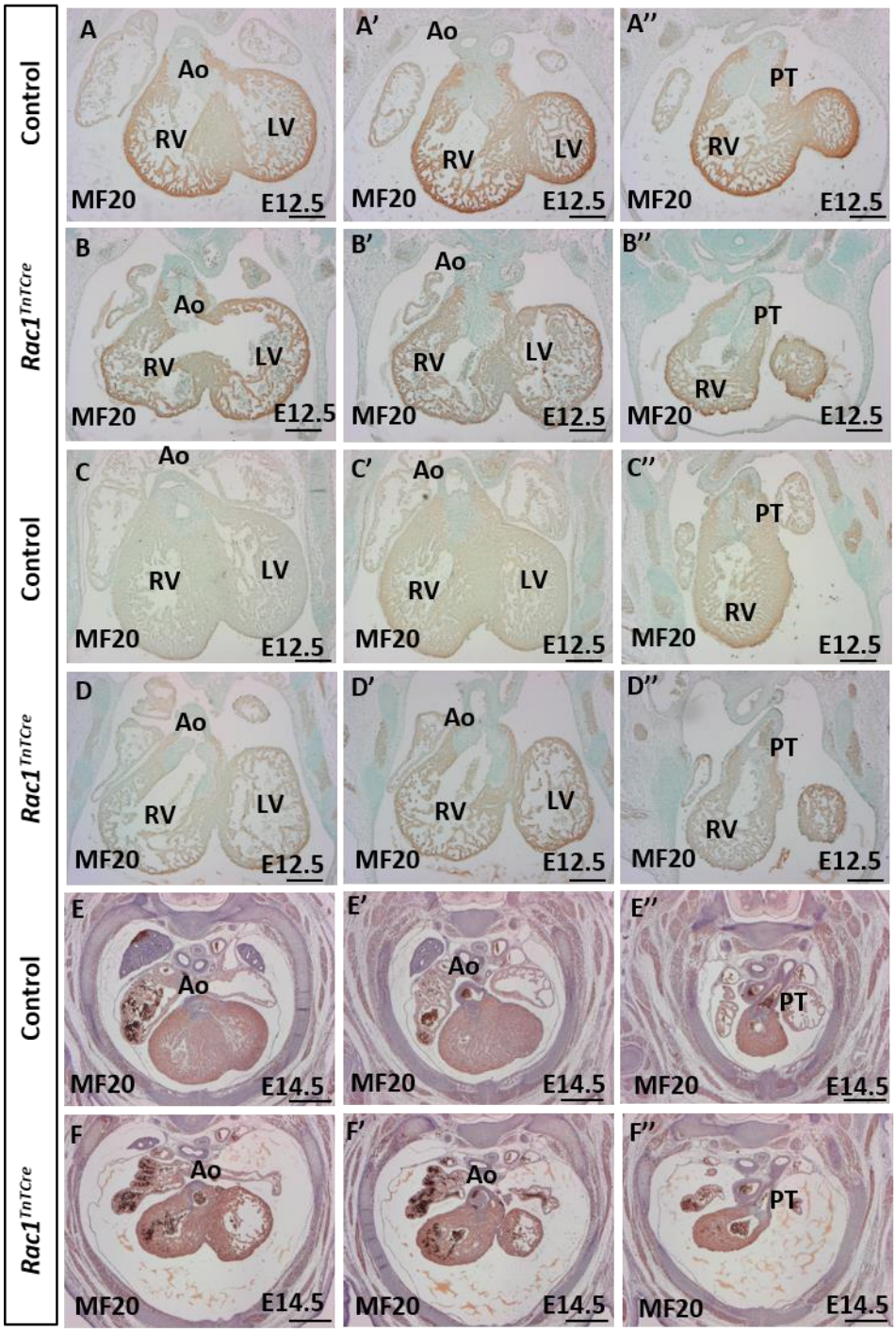

Figure 80: MF20 IHC on E12.5, E13.5 and E14.5 control and *Rac1*^{TnTCre} hearts.

Anti-MF20 IHC staining highlights the myocardial cells migrating into the OFT cushions and confirms that the OFT cushions are undergoing myocardialisation in both controls and in *Rac1*^{TnTCre} hearts (**A**-**D**) (n=4). By E14.5 the cushions have fully myocardialised (**E** and **F**) (n=3). LV; left ventricle, RV; right ventricle, Ao; aorta, PT;pulmonary trunk. Scale bars; A-D'' 200μm, E-F'' 500μm.

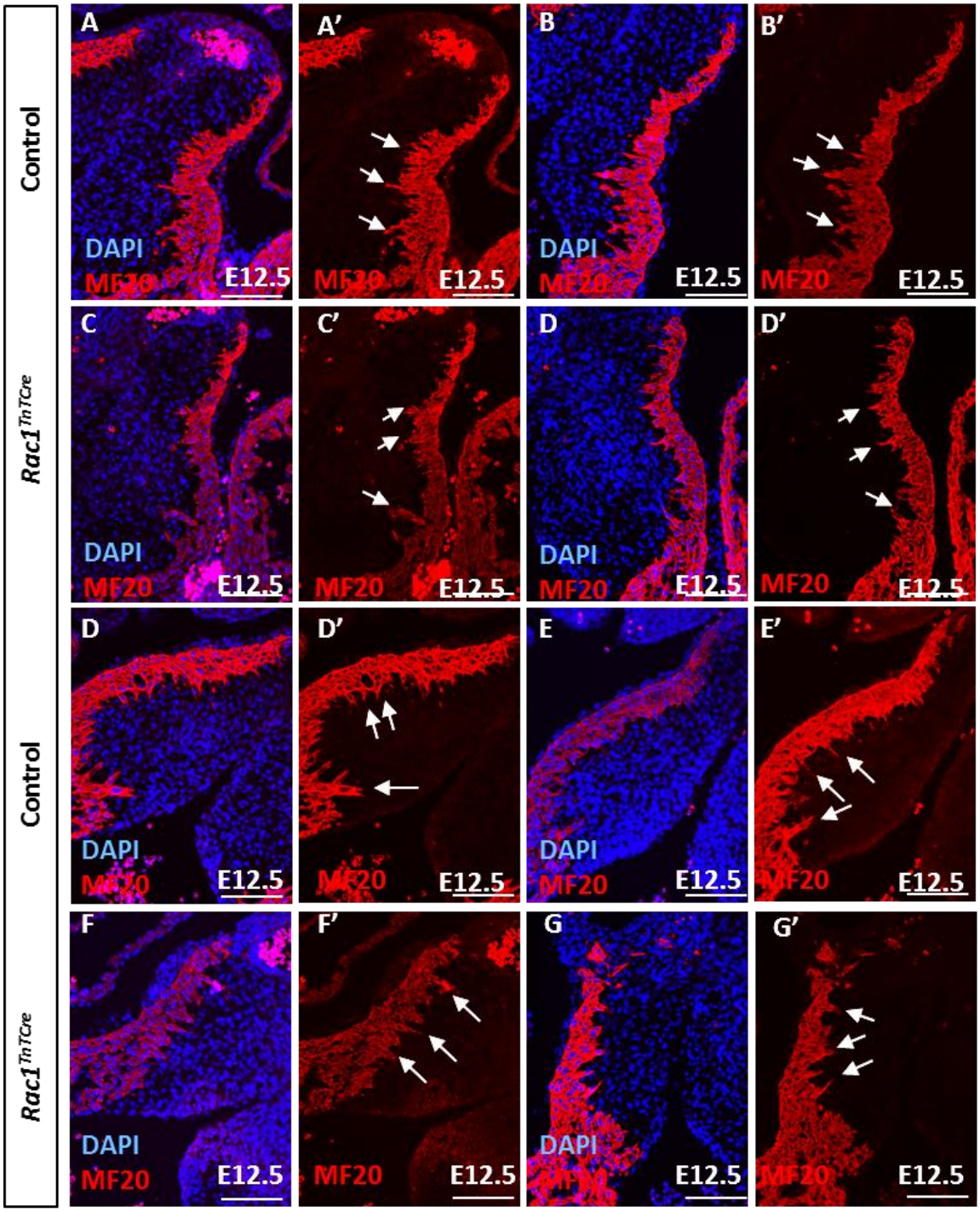

Figure 81: MF20 IFon E12.5 control and *Rac1*^{TnTCre} hearts sections.
Anti-MF20 IHC staining shows the invading myocardial cells are projecting inwards, into the OFT cushions at E12.5, in the *Rac1*^{TnTCre} hearts as in controls (white arrows) (n=4). Scale bars; 100µm.

4.4 Discussion

This chapter aimed to dissect the cellular mechanism(s) which is/are disrupted in the absence of Rac1 in cardiomyocytes, during the formation and/or

remodelling of the OFT. Myocardial deletion of Rac1 during embryonic development results in OFT defects including DORV and OA with VSD, suggesting that Rac1 plays an important role within the development of the myocardium, which is critical for normal ventricular septation and alignment of the OFT.

In summary, it was shown that both *Gata5-Cre* and *TnT-Cre* are expressed in the distal OFT at the 'transition zone' at E9.5, however early OFT formation is unaffected in $Rac1^{TnTCre}$ hearts, with normal addition of SHF cells and OFT lengthening, cardiomyocyte differentiation and proliferation. Additionally, $Rac1^{TnTCre}$ cardiomyocytes in the OFT appear correctly polarised with regular cell-cell junctions. Interesting, despite the lack of OFT formation defects, later in cardiac development the OFT is positioned at an aberrant angle to the ventricles and leads to misalignment of the OFT vessels resulting in DORV/OA with VSD.

4.4.1 Cre expression in the OFT

Firstly the aim was to characterise the expression boundary of both *Gata5-Cre* and *TnT-Cre* within the OFT myocardium. Both *Gata5-Cre* and *TnT-Cre* are expressed in the transition zone between Islet-1-expressing SHF progenitors and MF20-expressing differentiated cardiomyocytes. *TnT-Cre* becomes active as cardiomyocytes begin to differentiate and shows an exclusive overlapping expression pattern with MF20 and coincides with reduced Islet-1 expression in the OFT myocardium. In addition to the 'transition zone', *Gata5-Cre* is also active in the pharyngeal mesenchyme, in Islet-1-expressing SHF progenitors before the onset of MF20 expression. However, despite the expanded expression of *Gata5-Cre* in the developing OFT compared to *TnT-Cre*, the OFT phenotype observed in the $Rac1^{Gata5Cre}$ and $Rac1^{TnTCre}$ is comparable. Therefore, it can be implied that the expression of *Gata5-Cre* within the SHF derived cells of the pharyngeal mesoderm does not contribute to the observed OFT phenotype in $Rac1^{Gata5Cre}$ embryos. Hence subsequent analysis focussed on the deletion of Rac1 in differentiated myocardium.

4.4.2 OFT development in Rac1^{TnTCre} hearts

Next each stage of OFT development in *Rac1^{TnTCre}* hearts was characterised and investigation of the key regulatory cellular processes involved at each stage was carried out. It was hypothesised that defective OFT development and/or OFT remodelling causes the DORV/OA phenotype observed in both the *Rac1^{Gata5Cre}* and *Rac1^{TnTCre}* embryos.

4.4.2.1 OFT formation

Early development of the OFT was investigated in *Rac1^{TnTCre}* hearts, including addition of SHF cells, myocardial cell differentiation, proliferation and cell polarity.

Expectedly, SHF addition and OFT lengthening was normal in *Rac1^{TnTCre}* hearts. Additionally, cardiomyocyte differentiation was unchanged.

Rac1 is implicated in the regulation of cell proliferation and cell polarity in cardiomyocytes as well as additional cell types (Abu-Issa, 2014; Leung *et al.*, 2014). Hence it was surprising that these cellular processes appeared to be occurring as normal within the developing OFT myocardium in *Rac1^{TnTCre}* hearts. The levels of cell proliferation and apoptosis was unchanged in *Rac1^{TnTCre}* hearts, along with total cardiomyocyte number. Polarised cell-cell junctions including AJ, desmosomes and TJ were expressed and localised at the cell membrane in *Rac1^{TnTCre}* hearts as in controls. Additional markers of cell polarity, MTOCs and ECM proteins, were also unaffected.

The absence of early OFT defects is contrasting to observations in SHF Rac1 mutants. *Rac1;Mef2cCre* mice develop a spectrum of OFT defects ranging from OA to severe TGA with additional incidence of aortic atresia and ARSA. In this study it was proposed that the OFT defects occur as a result of early defects in cell proliferation in the splanchnic mesoderm and reduced cardiac NCCs and SHF cell migration into the developing OFT, leading to a shorted OFT (Leung *et al.*, 2015). *Mef2c-Cre* progenitors contribute to SHF cardiomyocytes, SMCs and ECs including endocardial cells of the RV, the smooth muscle of the pulmonary trunk and the endothelium of the OFT (Verzi *et al.*, 2005). *Gata5-Cre* and *TnT-Cre* expression is restricted to SHF-derived cardiomyocytes and Rac1 mutant hearts do not display early OFT defects. The phenotypic differences between these mutants highlights the importance of defining Cre expression within the

OFT and reveals that different regions of the OFT are required for OFT lengthening, OFT septation and OFT rotation and alignment.

It is interesting that the OFT malformations observed in both *Rac1*^{TnTCre} and *Rac1*^{Gata5Cre} embryos later in development are similar to classic SHF mutants where all SHF derived cardiac cells are affected, suggesting that it is the cardiomyocytes of the OFT which are required for OFT rotation and remodelling and supports evidence that OFT malformations can have multiple causes and origins (Neeb *et al.*, 2013).

4.4.2.2 OFT remodelling

Finally, OFT remodelling was then analysed, including OFT myocardialisation and wedging of the aorta, in *Rac1*^{TnTCre} hearts.

Visualisation of the OFT throughout embryonic development in *Rac1*^{TnTCre} hearts revealed abnormalities arising from E13.5. The rotation and alignment of the OFT is disrupted in Rac1 myocardial mutants. OFT cushion formation and composition appears normal in *Rac1*^{TnTCre} hearts. Additionally, subsequent myocardialisation of the cushions is unaffected with myocardial cells observed invading and replacing the ECM in the underlying cushions.

The ventricle myocardium is severely thinned in both *Rac1*^{TnTCre} and *Rac1*^{Gata5Cre} hearts from E12.5. Interestingly, the OFT myocardium and IVS is relatively thick in both *Rac1*^{TnTCre} and *Rac1*^{Gata5Cre} mutants compared to control hearts. This suggests possible differences between ventricular cardiomyocytes and those in the OFT myocardium and IVS. *In situ* hybridisation for Rac1 did not reveal any differences in Rac1 expression between these areas, suggesting this difference does not occur as a result of increased or decreased expression of Rac1 but possibly due to differences in cardiomyocyte morphology and development in the IVS and OFT myocardium. This theory is supported by the fact that cardiomyocytes in these regions have a different origin. The IVS is known to form as the trabeculae coalesce during early cardiac development and regulatory pathways include the absence of Hand2 signalling in the IVS region (Togi *et al.*, 2006). In addition, the OFT myocardium is involved in myocardialisation of the OFT cushions. This suggests that Rac1 is not required for the processes occurring in the IVS or OFT myocardium, however is crucial for development of the ventricular free wall myocardium.

It has been shown that correct alignment of the OFT requires rotation of the OFT myocardium. Failure of rotation of the OFT myocardial wall during OFT remodeling results in alignment defects, including TGA, DORV and OA (Bamforth *et al.*, 2001; Watanabe *et al.*, 2001; Bajolle *et al.*, 2006).

In *Rac1*^{TnTCre} and *Rac1*^{Gata5Cre} hearts, the combination of a thinned ventricle myocardium with a thick developed OFT myocardium could lead to defective OFT positioning later in development - without the support of the ventricle myocardium, the OFT myocardium cannot correctly rotate to facilitate OFT alignment.

At E10.5 the shape and structure of the *Rac1*^{TnTCre} heart is comparable to controls (Figure 82). By E13.5 the myocardium is significantly thinned and the ventricles are slightly ballooned in shape in *Rac1*^{TnTCre} embryos, however OFT positioning is unaffected (Figure 82). By E15.5 the myocardium is severely thinned, and the heart is significantly dilated and ballooned in shape and significantly increased in size (Figure 82). The ballooned shape of the ventricles interrupts cardiac rotation and prevents AV septation, meaning the aorta remains associated with the RV (Figure 82).

These results suggest Rac1 has a specific role in ventricle cardiomyocytes during embryonic development and the severe myocardial defects result in defective OFT positioning later in development.

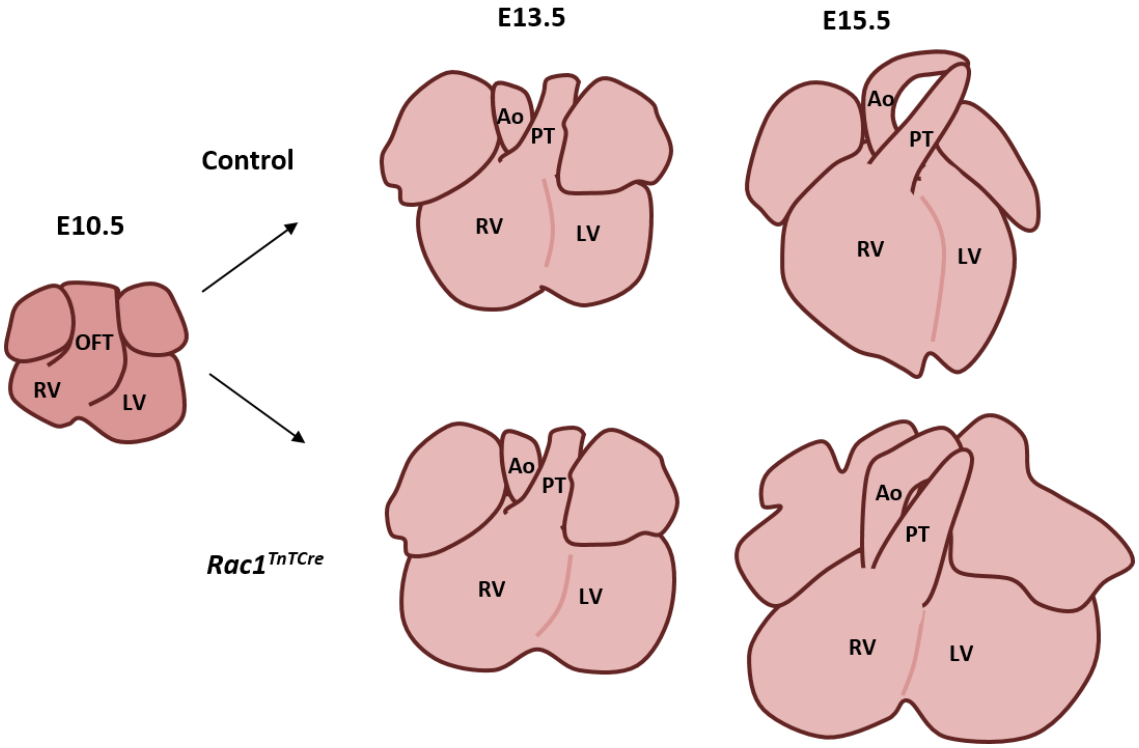

Figure 82: The shape of the ventricles affects the alignment of the OFT at E15.5.
At E10.5 the shape and structure of the *Rac1*^{TnTCre} heart is comparable to controls. By E13.5 the myocardium is significantly thinned and the ventricles are slightly ballooned in shape in *Rac1*^{TnTCre} embryos, however OFT positioning is unaffected. By E15.5 the myocardium is severely thinned and significantly ballooned in shape and significantly increased in size. The ballooned shape of the ventricles interrupts cardiac rotation and prevents atrioventricular septation, meaning the aorta remains associated with the RV.

4.4.3 Conclusions

In this chapter, it is concluded that myocardial deletion of *Rac1* does not affect initial OFT formation but leads to defects in OFT remodelling and alignment. It is proposed that DORV/OA defects arise as a consequence of the severe abnormalities in ventricular chamber maturation and disrupted ventricular septation, rather than from direct defects in the OFT. These defects in the ventricle myocardium cause cardiac dilation with rounded ventricles and abnormal positioning of the aorta above the IVS. The underdeveloped IVS is not sufficient to complete ventricular septation; therefore, the aorta overrides the septum. This is an example of early myocardial defects causing later OFT defects without disruption of the OFT formation.

Chapter 5. Trabeculation and compaction is disrupted in *Rac1* mutants

5.1 Introduction

5.1.1 Ventricular development

As discussed in Chapter 1 Section 1.6.1, the development of a mature thickened myocardial wall requires signalling and interaction between cells in all three cardiac layers, as well as interactions within the ECM surrounding the myocardium.

After the formation of the linear heart tube, the myocardium undergoes trabeculation and compaction which requires proliferation and differentiation of cardiomyocytes (Sedmera *et al.*, 2000; Harvey, 2002; Hirschy *et al.*, 2006; Henderson and Chaudhry, 2011; Samsa *et al.*, 2013) (Figure 11). Regulated cardiomyocyte differentiation, proliferation, polarity and cytoskeletal organisation is essential for correct ventricular wall development, and these can be influenced by interactions with the ECM and signalling to and from the endocardium. Rac1 is known to play a role in many of these key developmental processes involved in ventricular development.

5.1.2 Cardiomyocyte differentiation

Cardiomyocytes of both the FHF and SHF can be identified by expression of differentiation markers, including MF20, α-SMA and SM22α. As the ventricle wall undergoes maturation, both α-SMA and SM22α are increasingly restricted to the compact layer and become completely restricted by E15.5. At birth, both α-SMA and SM22α are absent from cardiomyocytes and are expressed exclusively within the smooth muscle cells of the coronary vessels. However, MF20 remains expressed in cardiomyocytes throughout development and postnatally. The trabeculae cardiomyocytes are more differentiated than compact myocytes; therefore can be distinguished by the markers previously described, α-SMA and SM22α, as well as additional markers such as ANF, BMP10 and PEG1.

5.1.3 Cardiomyocyte cytoskeleton

The contractile sarcomeric cytoskeleton consists of thin actin filaments, which are attached to Z-discs, and thick myosin filaments interspersed between them (Figure 13). One of the main roles of Rac1 is regulation of the actin cytoskeleton. Rac1 controls cytoskeletal dynamics and is a key regulator of cell adhesion and migration, mediated by signalling through effector proteins such as p21 activated kinase (PAK), Extracellular signal-related kinase (ERK) and Mena . PAK1 is a serine threonine kinase which can be directly activated by Rac1 and plays a key role in cytoskeletal reorganisation and cell spreading downstream of Rac1 (Sussman *et al.*, 2000; Parrini *et al.*, 2002; ten Klooster *et al.*, 2006; Sheehan *et al.*, 2007). ERK/mitogen activated protein kinase (MAPK) activation has been shown to be both upsteam and downstream of Rac1 and is involved in cytoskeletal reorganization and hypertrophy in the heart (Clerk *et al.*, 2001; Yanazume *et al.*, 2002; Kawamura *et al.*, 2003; Ray *et al.*, 2007; Elnakish *et al.*, 2012). In cardiomyocytes, active Rac1 is associated with Mena (Ram *et al.*, 2014). Mena, a member of the Ena/VASP family of actin regulatory proteins, increases actin filament assembly by its intrinsic polymerase and anti-capping activities. Mena is localised at the ICD and Z-disc, and co-localises with numerous cytoskeletal proteins in addition to Rac1 (Benz *et al.*, 2013). Mena co-localises with CapZ at the Z-disc; CapZ acts as a barbed end capping protein for F-actin and is localised at the end of thin filaments in the Z-disc. At the ICD Mena co-localised with Cx-43, cadherin and vinculin. RNAi knockdown of *Mena* led to significantly increased Rac1 activity, as shown by increased GTP-bound Rac1 protein as well as altered localisation of Cx-43 at the ICD, resulting in faster intercellular communication (Ram *et al.*, 2014). In mice overexpressing constitutively active Rac1, left ventricular Mena expression was increased significantly, and this was associated with lateral redistribution of Cx-43. Similar to Rac1, Mena is highly expressed during heart development but its expression is downregulated in the adult heart. However, Mena is upregulated in CVD, associated with heart failure, and is a critical regulator of cardiac function. Mice overexpressing Mena in the cardiomyocytes develop exacerbated hypertrophy, fibrosis and contractile dysfunction following TAC compared to controls (Belmonte *et al.*, 2013). *Mena* KO mice have reduced cardiac performance and there are structural alterations at the ICD (Aguilar *et*

al., 2011). This suggests that Mena is a critical regulator of the ICD, in part via interactions with Rac1 (Ram *et al.*, 2014). Cardiomyocytes expressing a mutant version of Mena remain in the compact myocardial layer, suggesting Mena is required for the migration of cardiomyocytes into the trabeculae layer (Toyofuku *et al.*, 2004b).

5.1.4 Cardiomyocyte polarity and adhesion

Cardiomyocytes display features of epithelial cell polarity including PCP and ABP. The apical side and the basolateral side of the cell regulated by the presence of AJ and TJ (Kaplan *et al.*, 2009). MTOC are polarised cell organelles and are apically expressed (Magdalena *et al.*, 2003).

Adult cardiomyocytes are highly polarised with cell-cell junctions localised at ICD with attachment to the ECM on their lateral surface (Borg *et al.*, 1983). ICD allow connection and communication between cardiomyocytes and consist of desmosomes, AJ and gap junctions (Figure 14). TJ join epithelial cells near the apical membrane (Hartsock and Nelson, 2008) and the PAR-PKCζ complex co-localizes with TJ protein ZO-1 and is required for the establishment of epithelial cell polarity (Ohno, 2001; Suzuki *et al.*, 2001).

Rac1 is implicated in both apicobasal polarity and PCP signalling pathways as a regulator of actin cytoskeleton, cell shape and morphology (Henderson and Chaudhry, 2011; Mack and Georgiou, 2014). The role of Rac1 in cell polarity has been demonstrated in convergent extension cellular movement, orientation of hair cells in the cochlea and anterior-posterior body axis specification during development (Bosco *et al.*, 2009; Grimsley-Myers *et al.*, 2009; Roszko *et al.*, 2009).

PCP signalling has been shown to regulate cytoskeleton organisation and stimulate cardiogenesis through polymerization of actin (Afouda et al., 2008). Studies investigating the role of PCP proteins in ventricular development have shown expression within the developing myocardium and several PCP mutant mice display ventricular myocardial defects (Murdoch *et al*., 2003; Phillips *et al*., 2005; Henderson *et al*., 2006; Phillips *et al*., 2007; Phillips *et al*., 2008). Polarisation and organisation of cardiomyocytes in the ventricular myocardium is disrupted in both Scrib and Vangl2 mutant mice (Murdoch *et al*., 2003; Phillips *et al*., 2005; Henderson *et al*., 2006; Phillips *et al*., 2007; Phillips *et al*.,

2008) (Figure 20). Rac1 and fellow PCP signalling protein, Scrib, interact in cardiomyocytes and their combined role is linked with ventricular maturation (Boczonadi *et al*., 2014b). Scrib is a scaffolding protein that is essential for cell polarisation and orientation, and interacts with known Rac1 GEFs, betaPix and Git1 (Audebert *et al*., 2004; Osmani *et al*., 2006; Momboisse *et al*., 2009). Scrib controls recruitment of betaPix to the leading edge of migrating cells, to promote cell polarisation (Osmani *et al*., 2006). Global deletion of Scrib using PGK-Cre and cardiac specific deletion of Scrib using Nkx2.5-Cre resulted in myocardial defects, including a thinned myocardium, stunted trabeculae, VSD and poor formation of the IVS (Boczonadi *et al*., 2014b). The defects in the Scrib;Nkx2.5-Cre embryos were attributed to an increase in cardiomyocyte apoptosis and a reduction in cell proliferation (Boczonadi *et al*., 2014b). Boczonadi and colleagues found that Scrib co-localises with Rac1 and betaPix at the cell membrane at E8.5, and that in Scrib deficient cardiomyocytes, Rac1 and betaPix are absent from the cell membrane. Rac1;Scrib;Nkx2.5-Cre double heterozygous embryos display DORV and VSD with disrupted cell adhesion as shown by mislocalised N-cadherin and absent Cx-43 (Boczonadi *et al*., 2014a). Additionally, Scrib is shown to be absent from the IVS in Rac1;Mef2c-Cre hearts (Leung *et al*., 2014).

5.1.5 Signalling pathways in ventricular development

As described in Chapter 1.6.6 there are many signalling pathways which have been shown to regulate the development of the ventricle wall, including Notch, VEGF and Semaphorin (Toyofuku *et al*., 2004b; Grego-Bessa *et al*., 2007; Nagy *et al*., 2010; Wu *et al*., 2012).

5.1.5.1 VEGF signalling during ventricular development

VEGF signalling is one of the major signalling pathways between the myocardium and endocardium important for both myocardial development and coronary vessel formation (Bruns *et al*., 2010; Jopling *et al*., 2011; Shalaby *et al.*, 1995; Miquerol *et al.*, 2000; Milgrom-Hoffman *et al.*, 2011; Wu *et al.*, 2012). Rac1 interacts with the VEGF signalling pathway in endothelial cells and promotes VEGF-induced endothelial cell migration by stimulating the formation of lamellipodia and membrane ruffles. Inhibiting Rac1 in human endothelial cells

led to reduced VEGFR-2 mRNA and protein expression (Meissner *et al.*, 2009) and inhibition of VEGFR-2 signalling blocks VEGF-induced Rac1 activation (Garrett *et al.*, 2007). VEGF signalling promotes Rac1 initiated lamellipodia formation and angiogenesis via Rac GEF Vav2 (Garrett *et al.*, 2007).

Therefore, Vav2 acts downstream of VEGF to activate Rac1 and VEGF signalling to VEGFR-2 is upstream of the Rac1-Vav2 interaction in endothelial cells (Garrett *et al.*, 2007). *Vav2* knockout adult mice develop cardiovascular defects, including an increase in collagen fibrosis, arterial pressure and heart rate, due to deregulation of the renin-angiotensin II system (Sauzeau *et al.*, 2007). Overexpression of either wild-type or constitutively active Vav2 results in prominent membrane ruffles and enhanced stress fibres in cells with elevated rates of cell migration and Rac1 activity (Liu and Burridge, 2000).

VE-cadherin mediates adhesion between endothelial cells and is an important regulator of angiogenesis and blood vessel permeability. Rac1 controls VE-cadherin adhesion by acting downstream of several growth factors, including Ang-1 and VEGF (Abe *et al.*, 2000; Noren *et al.*, 2000; Del Valle-Perez *et al.*, 2010; Jones *et al.*, 2013; Liao *et al.*, 2014).

5.1.5.2 Semaphorin signalling during ventricular development

Plexins are the first known transmembrane receptors that interact directly with Rho small GTPases. On binding to GTPases, the plexin receptor regulates the remodelling of the actin cytoskeleton and alters cell movement in response to semaphorin guidance cues (Tong *et al.*, 2007). Mutations in the GTPase activation domain of PlexinD1 recapitulates the phenotype of *PlexinD1* null mice (Worzfeld *et al.*, 2014). PTA was also found in a patient with a mutation in the intracellular region of PlexinD1, which is predicted to perturb its membrane anchoring and catalytic GTPase-activation (Gay *et al.*, 2011; Hota and Buck, 2012; Ta-Shma *et al.*, 2013). Rac1 is known to interact directly with the intracellular domain of PlexinA and PlexinB family members, to both regulate receptor activity and propagate downstream signalling processes (Vikis *et al.*, 2000; Vikis *et al.*, 2002; Turner *et al.*, 2004; Tong and Buck, 2005; Bell *et al.*, 2011). Additionally, over expression of Rac1 increases cell surface expression of Plexins and their interaction with semaphorins. Similarly, the amount of

Rac1.GTP is increased in the presence of PlexinA1 (Turner *et al.*, 2004). Moreover, it has been proposed that Plexin sequesters Rac1 away from PAK, an effector protein that stimulates actin polymerization and forward movement of the cell front (Vikis *et al.*, 2002). Plexins appear to have preferential binding affinity for certain GTPases and thus can modulate different downstream activities. Rho GTPase binding may also destabilize dimerization of Plexin effector domains (Tong *et al.*, 2007). It appears that Rac1 plays a slightly different role in PlexinA signalling compared to PlexinB signalling (Vikis *et al.*, 2000; Vikis *et al.*, 2002; Toyofuku *et al.*, 2005; Tong *et al.*, 2007). Early reports suggested that PlexinC1 and D1 do not bind Rho-GTPases in vitro.

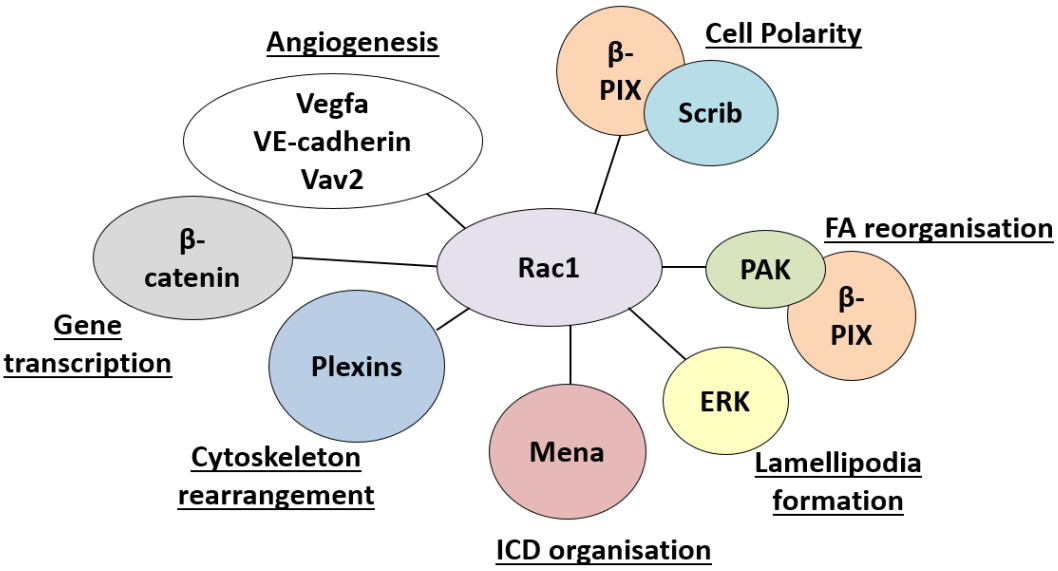

Figure 83: Active Rac1 interacts with numerous proteins to regulate several cellular processes.
Rac1 directly interacts with Plexins and ERK in cytoskeleton rearrangement, as well as PAK in FA reorganisation and Mena in ICD organisation. As part of the PCP pathway, Rac1 interacts with Scrib to regulate cell polarity. Rac1 interacts with VEGFA, VE-cadherin, Vav2 and p120-catenin in the formation of lamellipodia during angiogenesis. Additionally, Rac1 stabilises β-catenin, increasing its translocation to the nucleus leading to gene transcription of Wnt targets.

Rac1 is involved in various cellular processes, such as cell migration, polarity, survival, morphology, proliferation, differentiation, and regulation of the various phases of the cell cycle. Although the role of Rac1 in several cell types, particularly in endothelial cells and neurones, has been extensively

investigated, its role in the maturation and movement of cardiomyocytes is unknown.

5.2 Aims of the Chapter

As identified in Chapter 3, myocardial deletion of *Rac1* during embryonic development results in myocardial defects including a thin myocardial wall and sparse trabeculae formation. This data suggests that *Rac1* plays a crucial role in the development of the myocardium.

The aim of this chapter is to dissect the cellular mechanism of *Rac1* during the development of the ventricular myocardium. The maturation of the myocardium is a complex process involving regulated cardiomyocyte differentiation and the formation and subsequent remodelling of a trabeculated myocardial layer. Rac1 plays a role in many of the cellular processes that are required during myocardial development including cell migration, proliferation and differentiation. In order to dissect the main function of *Rac1* in embryonic cardiomyocytes, and to determine the primary cause of the cardiovascular defects in $Rac1^{TnTCre}$ hearts, first the hearts were characterised at the onset of myocardial defects and the examined the key regulatory cellular processes involved at this stage of embryonic development. The expression of potential Rac1 interactors during the onset of cardiac abnormalities was also analysed in $Rac1^{TnTCre}$ hearts. Additionally, how the deletion of *Rac1* affected continued development and remodelling of ventricles during later stages of heart development was examined.

It is hypothesised that disrupted cell polarity/cellular organisation leads to defective trabeculae formation and reduced compact myocardial proliferation.

5.3 Results

5.3.1 Trabeculation is disrupted in $Rac1^{TnTCre}$ hearts

5.3.1.1 3D modelling of $Rac1^{TnTCre}$ hearts shows reduced trabeculae network from E10.5

Both $Rac1^{TnTCre}$ and $Rac1^{Gata5Cre}$ hearts display abnormal, sparse trabeculae and defective myocardial thickening (Section 3.3.6.4). However, 2D images are a poor representation of the complex 3D trabeculae network that develops in the ventricles from E9.5 onwards. To analyse the abnormal trabeculae in the

Rac1^{TnTCre} hearts in 3D, E10.5 and E11.5 embryos were sent to Dr Tim Mohun at the Francis Crick Institute for HREM imaging (Weninger *et al.*, 2006; Captur *et al.*, 2014). HREM imaging allows reconstruction of embryos and hearts using 3D modelling software. The embryos were dehydrated in ethanol and sent for further processing and imaging by Dr Mohun. Tiff images, videos and 3D reconstructions were produced by Dr Mohun (Figure 84 and Figure 85).

Analysis of the tiff images, videos and 3D reconstructions revealed distinct differences in the formation of the trabeculae in *Rac1*^{TnTCre} hearts compared to controls, at E11.5 (n=6), with a subtle phenotype evident at E10.5 (n=5). At E10.5, initial trabeculae protrusions are regularly spaced on the inner layer of the ventricle free wall (Figure 84A-D) and form a luminal network, this can be seen clearly in the control 3D hearts (Figure 85A-B). In the *Rac1*^{TnTCre} hearts, there appears to be slightly fewer trabeculae protrusions at E10.5 (Figure 84D-F and Figure 85C-D). At E11.5, the trabeculae continue to develop into a highly organised network and trabeculae coalesce to form the developing IVS. Again, this can be seen in the control E11.5 hearts (Figure 84G-L and Figure 85E-F). Whereas the trabeculae network is markedly reduced in the *Rac1*^{TnTCre} hearts, with some areas of smooth compact myocardium completely lacking in trabeculae formation (arrows in Figure 84, J and K), including an underdeveloped IVS compared to controls (arrow heads in Figure 84G-L). In 3D, the trabeculae network in *Rac1*^{TnTCre} hearts remains simplified and disorganised with fewer, larger trabeculae present (Figure 85G-H). Again, areas of smooth compact myocardium completely lacking in trabeculae formation can be identified (arrows in Figure 85, G compared with H).

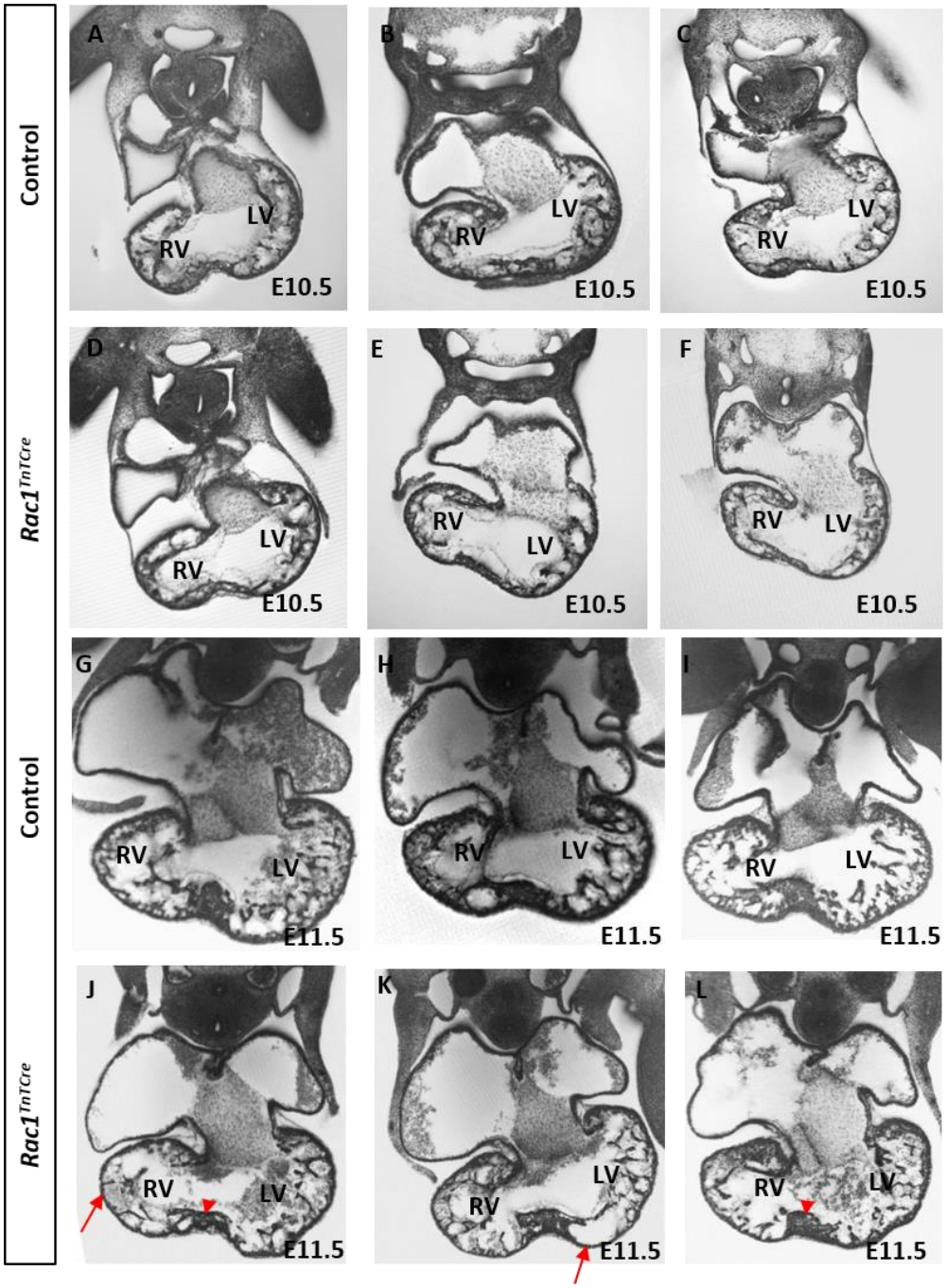

Figure 84: Trabeculae formation is visibly disrupted from E10.5 in *Rac1*^{TnTCre} hearts.
Example HREM images of E10.5 (n=6) and E11.5 (n=5) control and *Rac1*^{TnTCre} hearts. At E10.5 the trabeculae appear reduced in number and disorganised (**D**-**F**, compared to **A**-**C**). At E11.5, there appears to be fewer trabeculae protrusions in the *Rac1*^{TnTCre} hearts with some areas of smooth compact myocardium completely lacking in trabeculae formation (arrows in **J** and **K**). The IVS appears underdeveloped in *Rac1*^{TnTCre} hearts compared to controls by E11.5 (arrow heads in **J** and **L**). LV; left ventricle, RV; right ventricle.

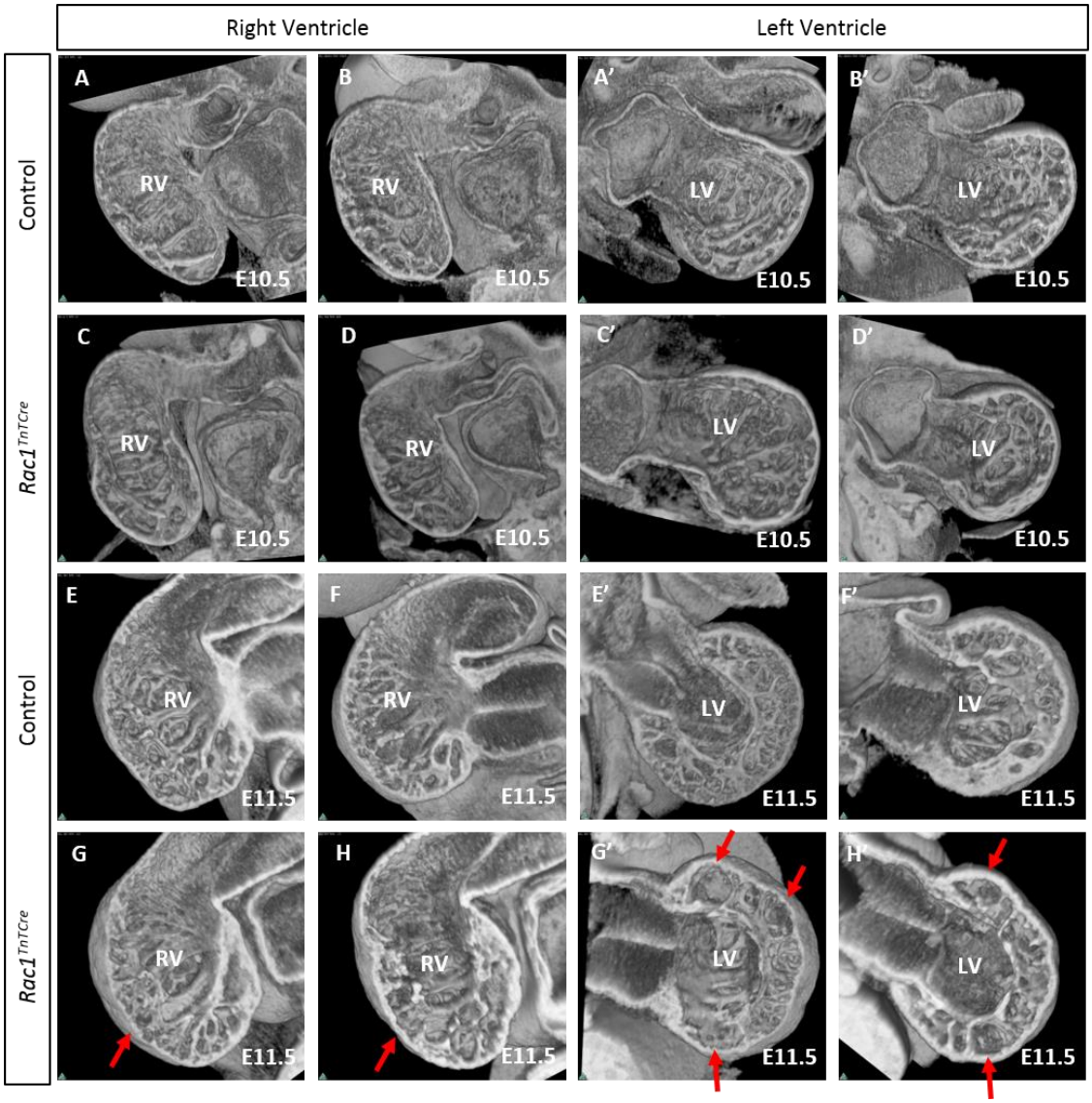

Figure 85: Trabeculae network formation is visibly disrupted by E11.5 in *Rac1*^{TnTCre} hearts.
3D reconstructions of HREM images from E10.5 and E11.5 control and *Rac1*^{TnTCre} embryos. At E10.5 in controls, initial trabeculae protrusions are regularly spaced on the inner layer of the ventricle free wall and form a luminal network (**A-B**). In the *Rac1*^{TnTCre} hearts, there appears to be fewer and less organised trabeculae protrusions (**C-D**) (n=2). At E11.5, the trabeculae continue to develop into a highly organised network and trabeculae coalesce to form the developing IVS (**E-F**). Whereas the trabeculae network is markedly reduced in the *Rac1*^{TnTCre} hearts, with some areas of smooth compact myocardium completely lacking in trabeculae formation compared to controls (arrows in **G-H**) (n=2). LV; left ventricle, RV; right ventricle.

5.3.1.2 Angle of trabeculae formation is disrupted from E10.5 in Rac1^{TnTCre} *hearts*

As observed from HREM 3D models, ventricle free wall trabeculae protrusions typically develop perpendicular to the myocardial wall, forming a complex

myocardial network within the ventricular lumen. Analysis of trabeculae angle projections in E10.5 *Rac1*^{TnTCre} control and mutant section images revealed that mutant trabeculae form at aberrant angles to the myocardial wall compared to controls. The data spread for the angles of trabeculae projections from the compact myocardium was significantly increased in *Rac1*^{TnTCre} hearts compared to controls (n=5, Figure 86). In controls, the data spread was greater in the LV as compared to the RV, whereas it was comparable between left and right ventricle in *Rac1*^{TnTCre} hearts (Figure 86, B compared to C). Chi squared statistical analysis revealed significant differences in the spread of trabeculae angles between controls and *Rac1*^{TnTCre} hearts at 30°-39°, 40°-49°, 60°-69° and 80°-89° ($p<0.05$).

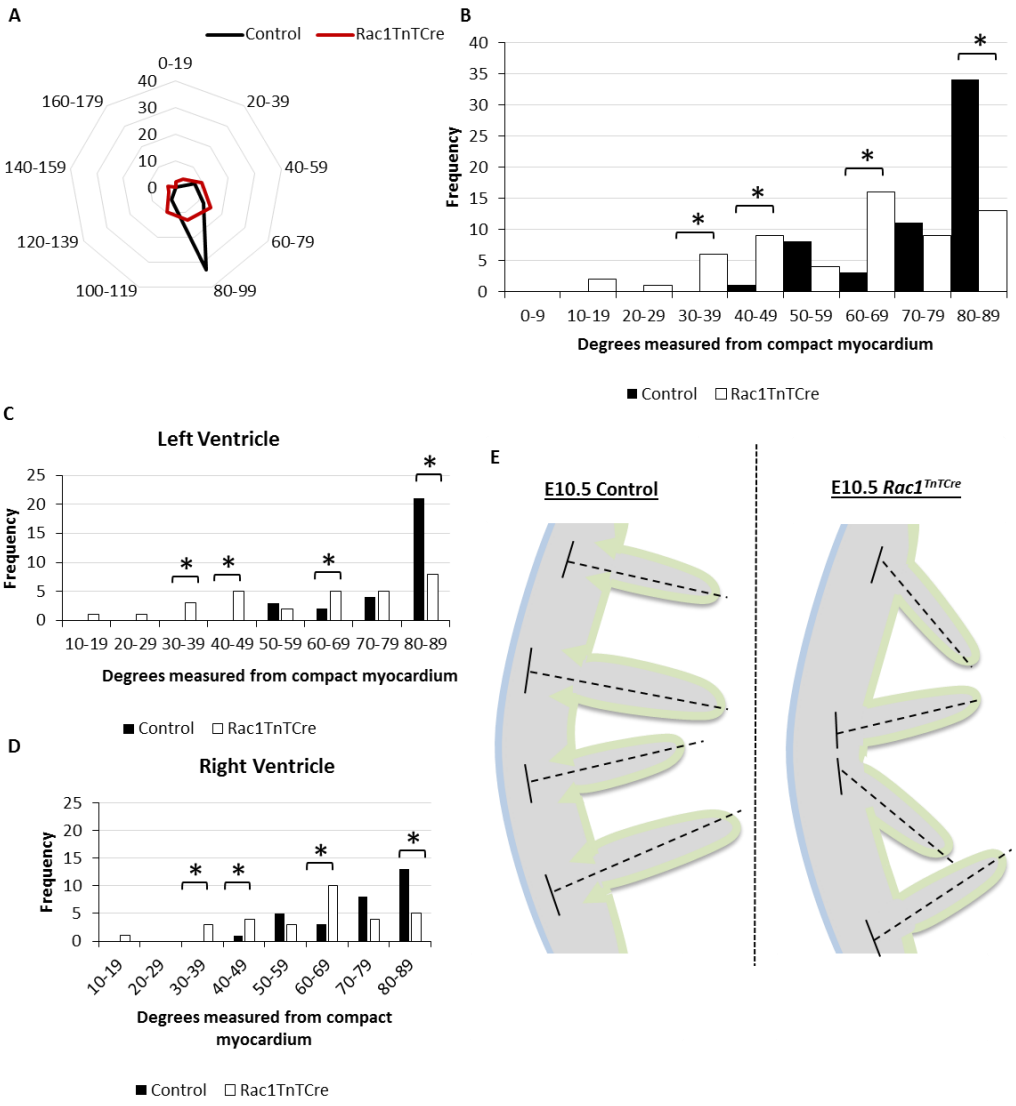

Figure 86: Trabeculae formation angle is disrupted in *Rac1*^{TnTCre} hearts at E10.5.
Trabeculae projection angle measured from the compact myocardium in control and *Rac1*^{TnTCre} E10.5 hearts (**A** and **B**) (n=5). Data separated into left and right ventricle (**C** and **D**, respectively). The data spread for the angles of trabeculae projections from the compact myocardium was significantly increased in *Rac1*^{TnTCre} hearts compared to controls (n=5, **A** and **B**). In controls, the data spread was greater in the left ventricle as compared to the right ventricle, whereas it was comparable between left and right ventricle in *Rac1*^{TnTCre} hearts (**C** compared to **D**). Schematic representation of the angles of trabeculae in control and *Rac1*^{TnTCre} hearts (**E**). Statistical analysis carried out using the Chi-squared test in SPSS. *P<0.05.

5.3.1.3 Number of trabeculae reduced from E10.5 in Rac1^{TnTCre} *hearts*

To quantify the reduction in trabeculae, projections from the myocardium were counted in 10 sections per embryo using the E10.5 and E11.5 HREM data sets, and E9.5 H&E sections. The number of trabeculae was found to have a trend

for a reduction in *Rac1*^{TnTCre} hearts compared to controls from E10.5, but not statistically significant (Figure 87A). From E12.5 the trabeculae begin to remodel and contribute to the IVS, papillary muscles and moderator band whilst the ventricular myocardium becomes thickened with fewer trabeculae. In the *Rac1*^{TnTCre} hearts it appeared that the number of trabeculae remains high in the RV, while becoming markedly reduced in the LV during later stages of heart development, at E12.5-E17.5. To quantify this, trabeculae numbers were counted from H&E staining of E12.5, E15.5 and E17.5 embryos (Figure 87C). The total number of trabeculae is significantly higher in E15.5 *Rac1*^{TnTCre} hearts compared to controls (Figure 87C). This suggests that the trabeculae in the RV do not undergo compaction as in controls, whereas the trabeculae in the LV possibly undergo abnormal compaction. These results highlight that the left and right ventricles may remodel in diverse ways during normal ventricular development and is investigated further in Chapter 5 Section 5.3.9.

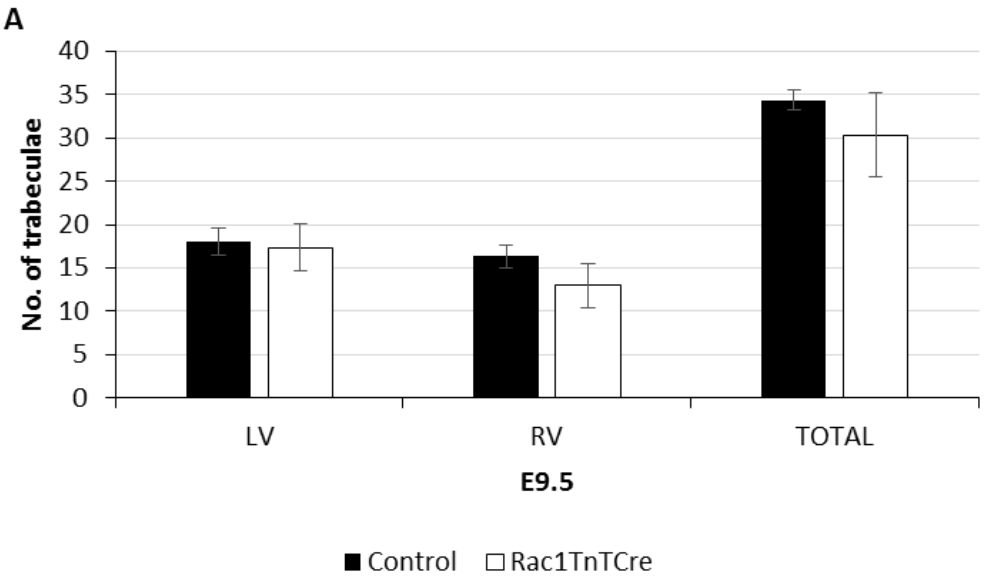
A
No. of trabeculae
40
35
30
25
20
15
10
5
0
LV
RV
TOTAL
E9.5
Control
Rac1TnTCre

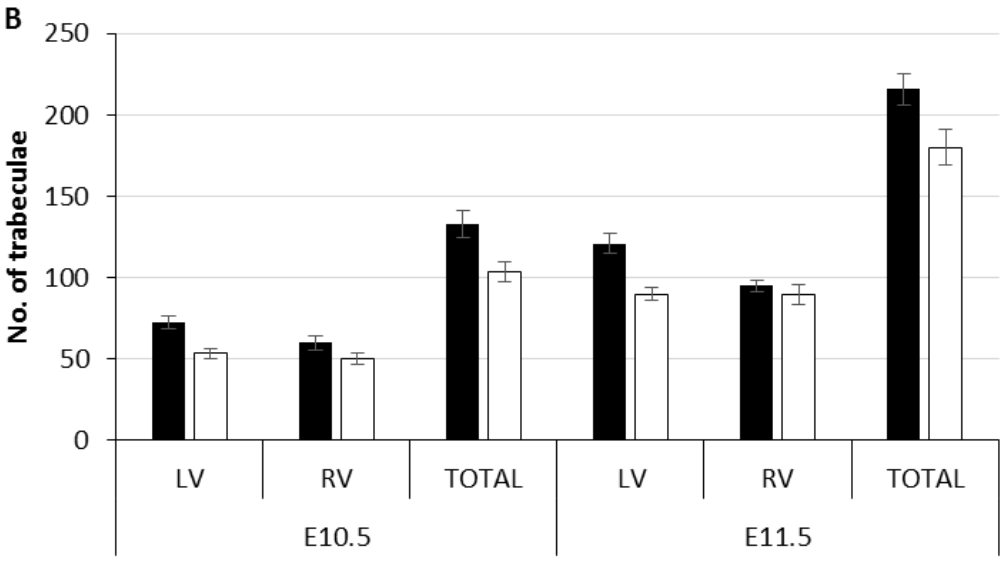
B
No. of trabeculae
250
200
150
100
50
0
LV
RV
TOTAL
LV
RV
TOTAL
E10.5
E11.5
Control
Rac1TnTCre

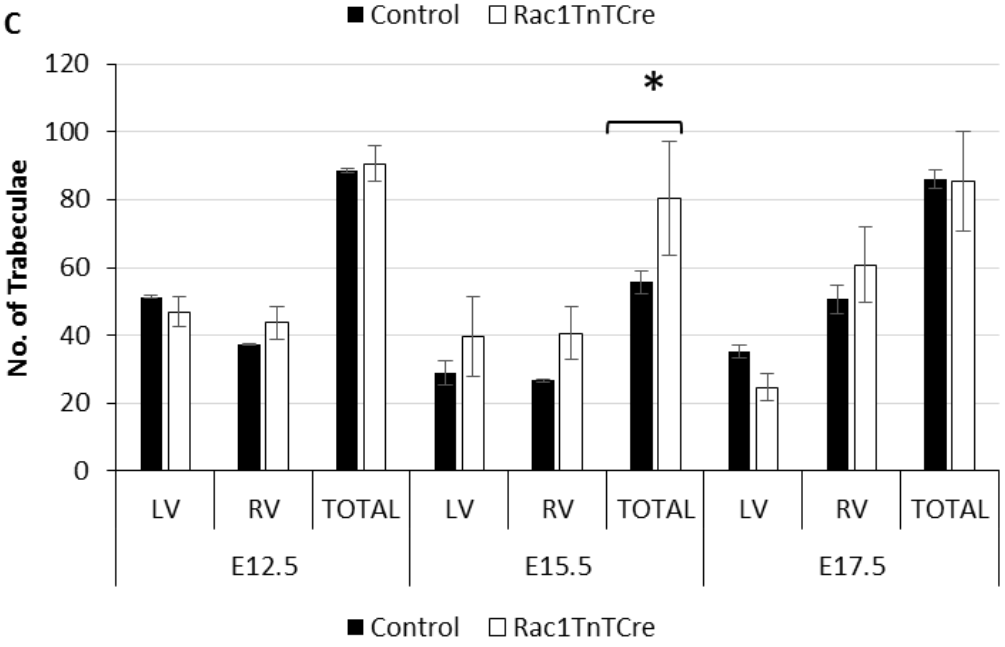
C
No. of Trabeculae
120
100
80
60
40
20
0
*
LV
RV
TOTAL
LV
RV
TOTAL
LV
RV
TOTAL
E12.5
E15.5
E17.5
Control
Rac1TnTCre

Figure 87: Decreased number of ventricular trabeculae projections in *Rac1^{TnTCre}* hearts from E10.5.
Counts of ventricular trabeculae projections in E9.5-E17.5 control and *Rac1^{TnTCre}* hearts (n=4). Counts are separated into right ventricle (RV), left ventricle (LV) and the combined total for each ages (TOTAL). The number of trabeculae was unchanged in the *Rac1^{TnTCre}* hearts compared to controls at E9.5 (**A**), however a trend for a reduction in trabeculae was seen in the left ventricle from E10.5-E11.5, but this was not statistically significant (**B**). The myocardium begins to compact at E15.5 in controls, as shown by a trend for a reduction in the number of trabeculae (**C**), this trend is not seen in the *Rac1^{TnTCre}* hearts and conversely shows a significant increase in the total number of trabeculae at E15.5 (**C**). In the *Rac1^{TnTCre}* hearts, the number of trabeculae remains high in the right ventricle, becoming markedly reduced in the left ventricle during later stages of heart development, at E17.5 (**C**). Statistical analysis carried out using a two-way ANOVA, *p<0.05.

From the HREM data and trabeculae analysis it can be concluded that the development of the trabeculated myocardium is disrupted from E10.5 onwards, consisting of reduced formation and directionality of the trabeculae. The development and maturation of the ventricular myocardium is a complex and poorly defined process, involving regulated cardiomyocyte differentiation, proliferation and maturation. Each of these processes were investigated in *Rac1^{TnTCre}* (and some *Rac1^{Gata5Cre}*) hearts to determine the primary defect in myocardial development.

5.3.2 Early cardiomyocyte markers are expressed in Rac1 deficient cardiomyocytes

To investigate early cardiomyocyte differentiation in *Rac1^{TnTCre}* embryos, immunostaining using antibodies against early cardiomyocyte markers was carried out. MF20 and SM22α markers are both expressed in differentiated cardiomyocytes in the early developing heart at E9.5 and E10.5. As shown in Figure 88, at E9.5 MF20 is uniformly expressed in the myocardial wall in *Rac1^{TnTCre}* hearts as in controls (Figure 88A-F). Normal expression of MF20 is continued at E10.5 and additionally, SM22α is expressed as expected in the myocardial wall, developing trabeculae and IVS in *Rac1^{TnTCre}* hearts (Figure 88G-J). These results suggest that Rac1 is not required for the initial differentiation of cardiomyocytes during embryogenesis.

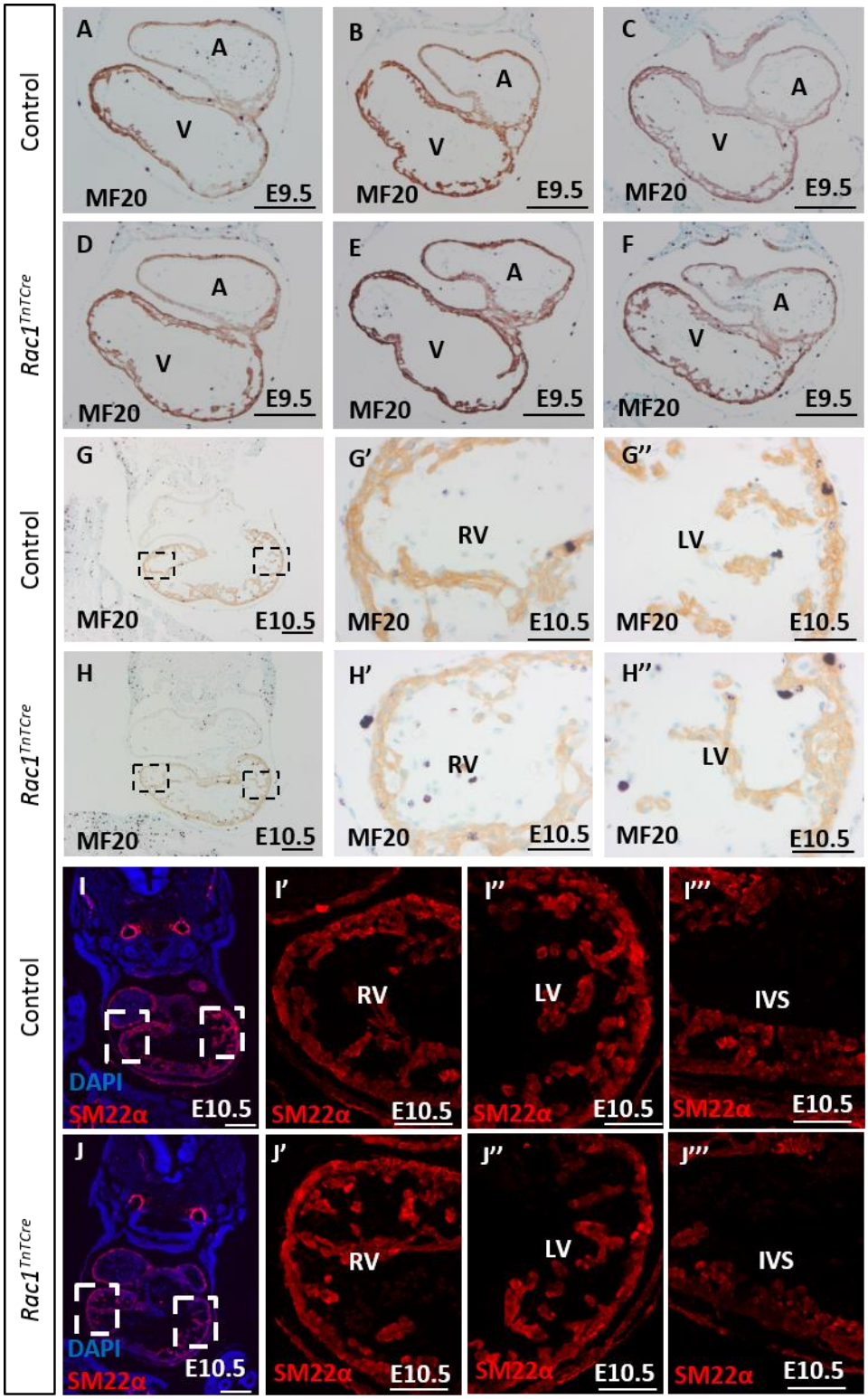

Figure 88: Normal expression of cardiomyocyte markers, MF20 and SM22α, in E9.5 and E10.5 *Rac1*^{TnTCre} hearts.
Immunostaining using anti-MF20 (**A**-**H**) and anti-SM22α (**I**-**J**) shows expression of these differentiated cardiomyocyte proteins in the myocardial layer of the heart in controls and *Rac1*^{TnTCre} hearts (n=4). LV; left ventricle, RV; right ventricle. Scale bars; A-J 200μm, A'J'' 100μm.

5.3.3 Cell cycle is not altered in E10.5 Rac1^{TnTCre} hearts

As previous analysis has shown, *Rac1^{TnTCre}* mutant hearts have fewer trabeculae and a thinner myocardial wall, implying that cell proliferation or cell survival may be affected.

Rac1 is known to play a role in cell cycle regulation and has been shown to delay entry into M phase (Moore *et al.*, 1997; Mamidipudi *et al.*, 2004). Therefore, to determine if cell cycle is affected in *Rac1^{TnTCre}* hearts, analysis of key cell cycle genes and markers of proliferation was carried out by qPCR and IF, respectively.

5.3.3.1 Key cell cycle genes CIP/KIP group proteins; p21, p27 and p53 are unchanged in Rac1^{TnTCre} hearts

p21, p27 and p53 are CIP/KIP group proteins which are selectively expressed during different phases of the cell cycle (Ahuja *et al.*, 2007). p21 prevents cells from entering the S-phase by blocking cyclin/CDK-complex activity, resulting in an accumulation of cells in G0/G1, altering cell morphology and differentiation, without triggering apoptosis. In addition, p21 mediates the p53-induced G1 cell cycle arrest resulting from DNA damage. p53 tumour-suppressor gene activity results in cell cycle arrest in G1 and initiation of DNA repair. If repair fails, p53 induces Bax gene apoptosis. p27 regulates cell progression from the G1- to S-phase by mediating G1 arrest through inhibiting cyclin/CDK-complex activities, in response to a variety of growth inhibitory cytokines including transformation growth factor. Overexpression of p27 leads to apoptotic cell death in all cell types (Wang *et al.*, 1997).

qPCR analysis of key cell cycle gene expression was carried out in E10.5 hearts as this time point is before the onset of myocardial defects (n=6). There was no change in expression of p21, p27 and p53 in E10.5 *Rac1^{TnTCre}* hearts compared to controls (Figure 89).

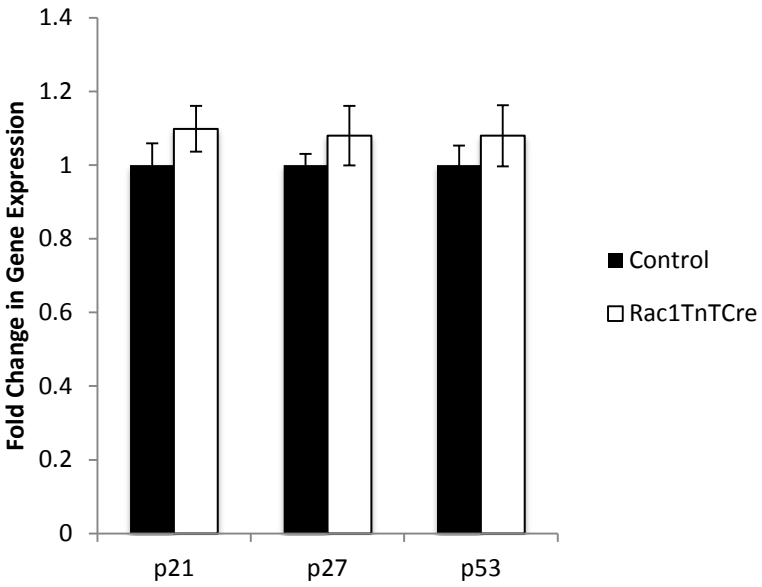

Figure 89: Cell cycle gene p21, p27 and p53 have unchanged expression in E10.5 *Rac1*^{TnTCre} whole hearts.
qPCR analysis of cell cycle gene expression in E10.5 control and *Rac1*^{TnTCre} whole hearts. p21, p27 and p53 no significant differences in expression in *Rac1*^{TnTCre} hearts compared to controls (n=6). Expression was normalised to housekeeping gene, GAPDH. Statistical analysis carried out using the unpaired t-test.

5.3.3.2 Cell proliferation is not significantly altered in Rac1^{TnTCre} *hearts*

To investigate proliferation in *Rac1*^{TnTCre} compact and trabeculae cardiomyocytes, BrdU *in utero* injection combined with immunostaining of embryonic sections was carried out. Administration of BrdU in pregnant females results in BrdU incorporation into all embryonic cells that are undergoing DNA synthesis (S phase) during the exposure time. E9.5, E10.5, E11.5, E12.5 and E13.5 embryos were exposed to BrdU *in utero* for 1 hour before dissection. Embryos were then dissected, processed and sectioned. Dual immunofluorescence staining using anti-MF20 and anti-BrdU allowed identification of proliferating cardiomyocytes. Cell counts were carried out and the data is presented in Figure 90 and Figure 91. Cell counts were separated into compact layer and trabeculae layer cardiomyocytes and left and right ventricles were analysed separately, except at E9.5 when the whole ventricle was included due to small numbers of cells and lack of a clear boundary between ventricles. At E9.5 and E10.5 the number of cells in the compact layer and trabeculae layer is comparable between control and *Rac1*^{TnTCre} hearts (n=5)

(Figure 90A-F). At E11.5 there is a reduction in trabeculae cardiomyocytes in the LV, as well as in IVS, with the RV unchanged (n=5) (Figure 90G-I). At E12.5 there is a reduction in trabeculae and total cardiomyocytes in the LV, as well as the total cardiomycytes in the RV (Figure 90J-L). From E13.5 the first significant reduction in compact cardiomyocyte number is observed, as well as a decrease in total cell numbers in both the right and left ventricles (n=3) (Figure 90M-O). Additionally at E13.5, cell number is decreased in the trabeculae layer in the LV (n=3) (Figure 90M-O). This data suggests that the *Rac1* deficient trabeculae cardiomyocytes in the left ventricle are either unable to survive or have a slower proliferation rate compared to control cells.

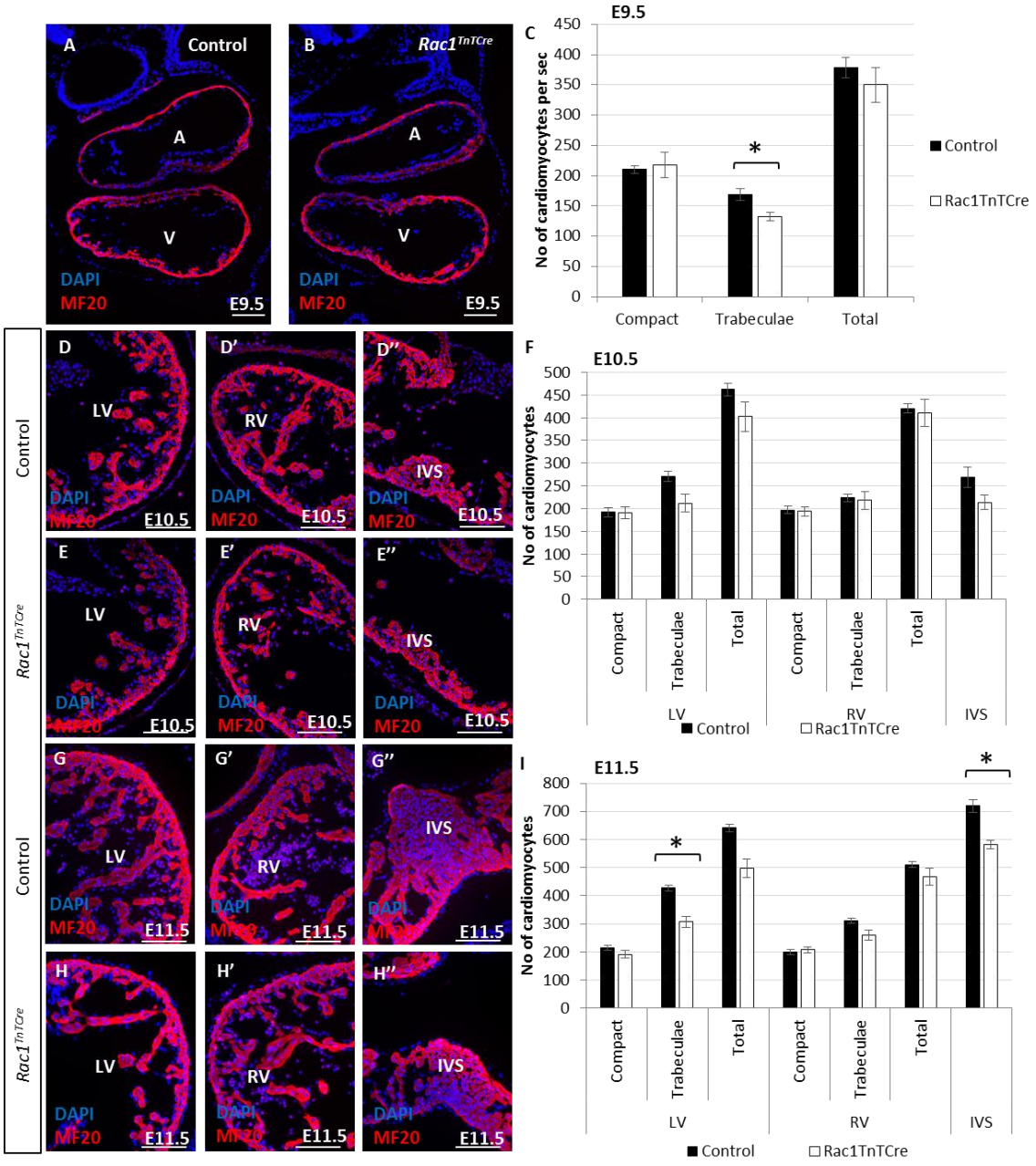

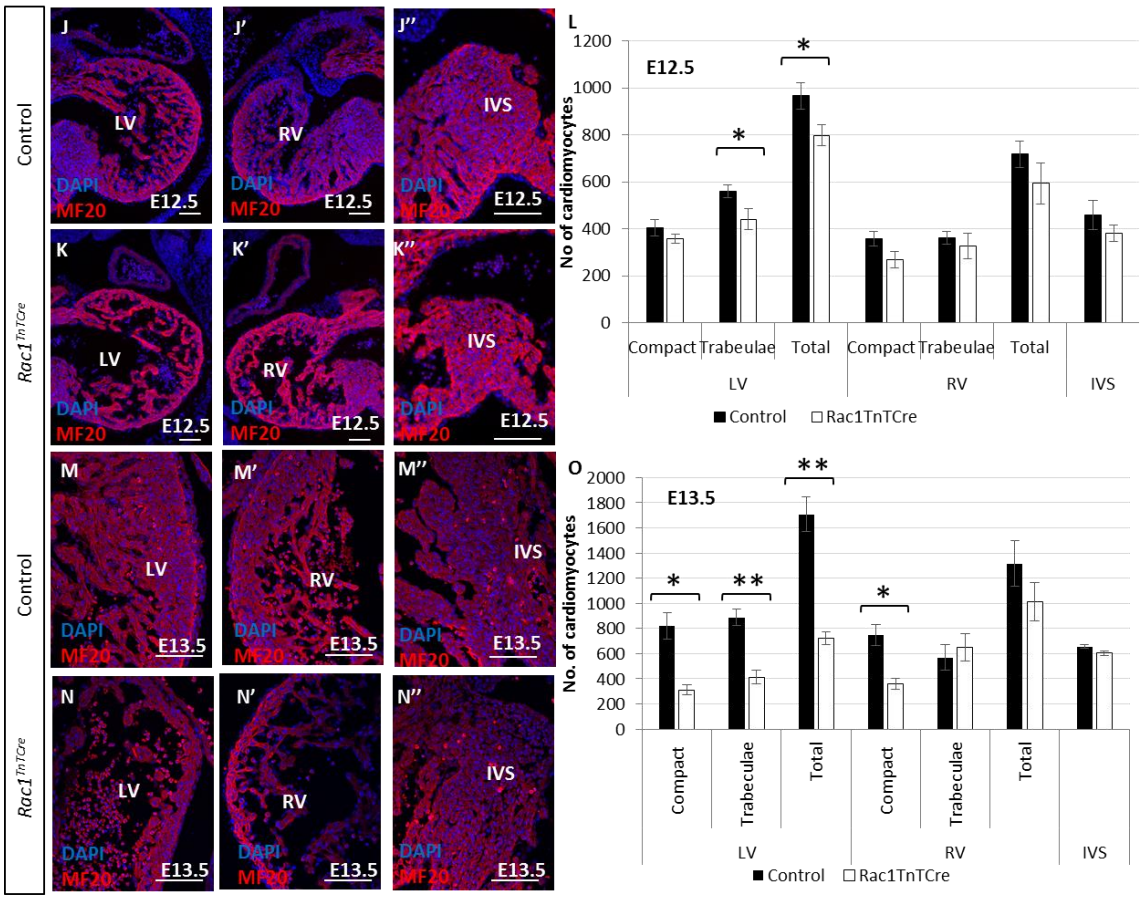

Figure 90: Cardiomyocyte cell number is reduced in *Rac1*^{TnTCre} ventricles compared to controls in transverse heart sections.
Immunostaining with anti-MF20 for cardiomyocytes (red) and DAPI nuclear stain (blue). Cells were counted in at least 3 sections per embryo and separated into left and right ventricle and IVS, and for the ventricle myocardium the counts were also separated into trabeculae, compact and total. At E9.5 and E10.5 the number of cells in the compact layer and trabeculae layer is comparable between control and *Rac1*^{TnTCre} hearts (n=5) (**A-F**). At E11.5 there is a reduction in trabeculae cardiomyocytes in the LV, as well as in IVS, with the RV unchanged (n=5) (**G-I**). At E12.5 there is a reduction in trabeculae and total cardiomyocytes in the LV, as well as the total cardiomyocytes in the RV (**J-L**). From E13.5 the first significant reduction in compact cardiomyocyte number is observed, as well as a decrease in total cell numbers in both the right and left ventricles (n=3) (**M-O**). Additionally at E13.5, cell number is decreased in the trabeculae layer in the LV (n=3) (**M-O**). LV; left ventricle, RV; right ventricle, IVS; interventricular septum. Scale bars; 100µm. Statistical analysis carried out using a two-way ANOVA.

Suprisingly, no significant differences were observed in the percentage of cardiomyocytes which had incorporated BrdU, therefore cells undergoing DNA synthesis during the 1 hour incubation period, at E9.5-E12.5 (Figure 91A-L, n=4). Unexpectedly at E13.5, there was an increase in the percentage of BrdU expressing LV trabeculae cardiomyocytes in *Rac1*^{TnTCre} hearts, in comparison

with LV compact layer and trabeculae cardiomyocytes in control hearts (n=3, p-0.0003). This may be occurring as a compensatory mechanism in response to the severely thinned myocardium and reduced contraction potential.

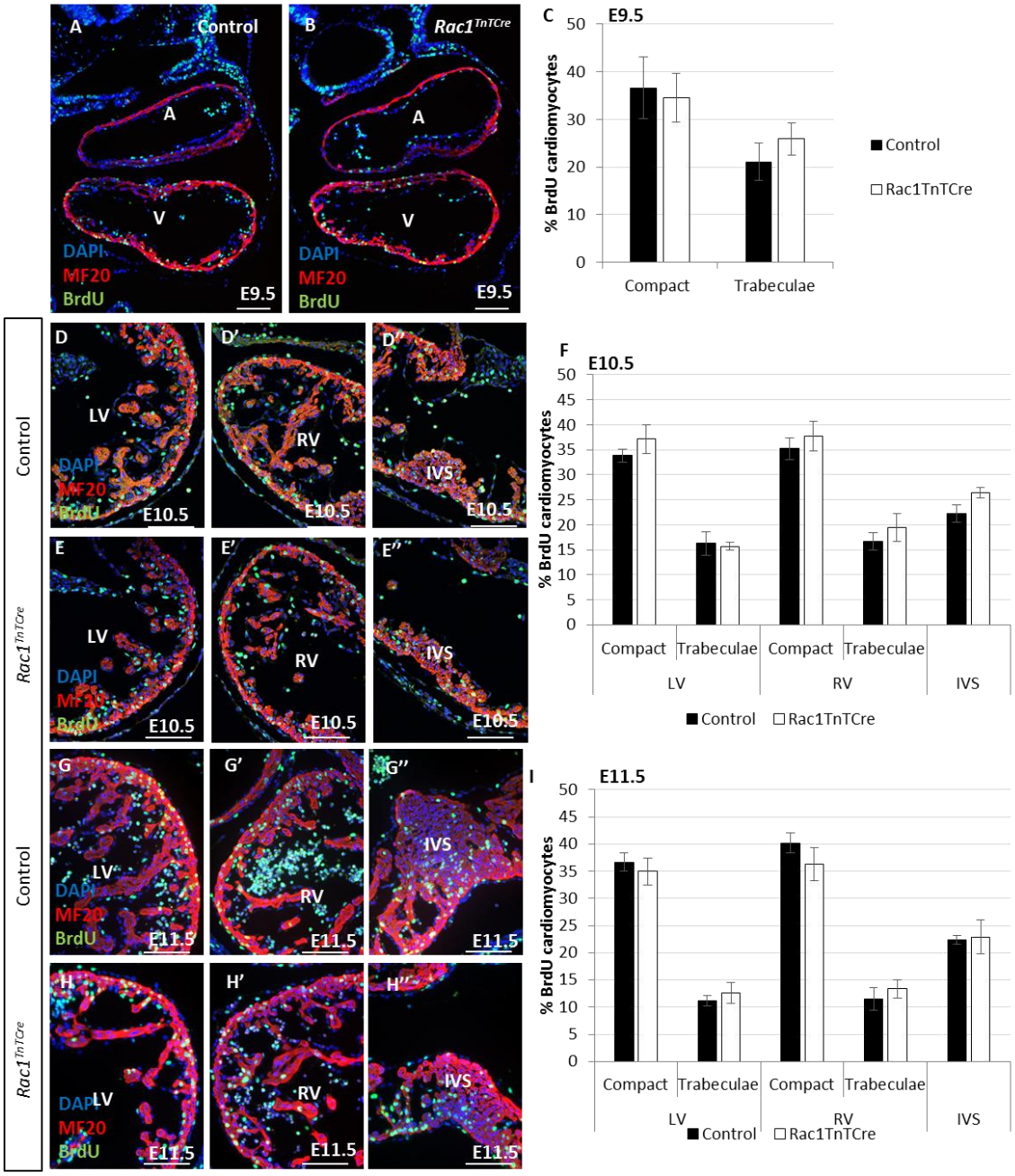

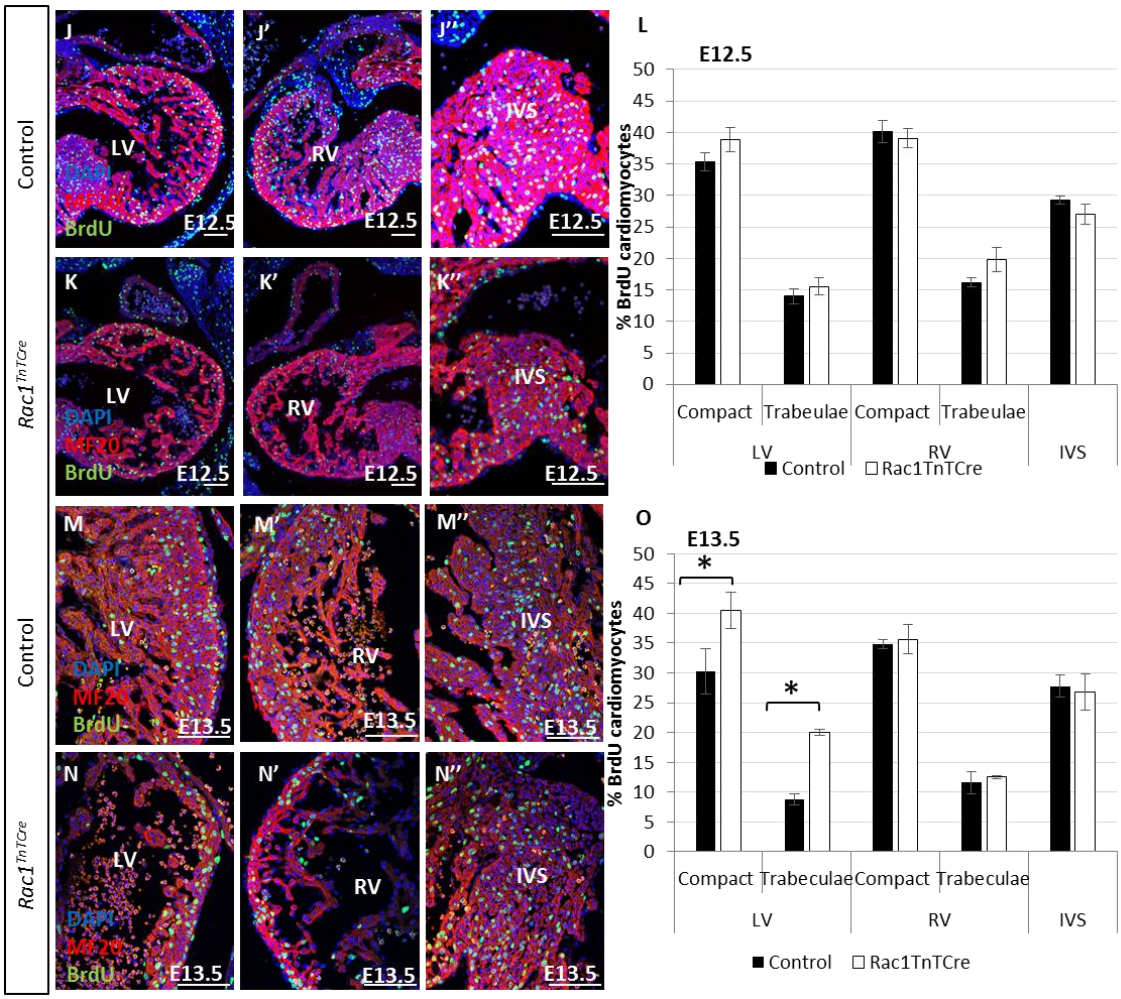

Figure 91: BrdU incoporation, as a marker of cell proliferation, is not altered in *Rac1*^{TnTCre} ventricular cardiomyocytes compared to controls. Immunostaining with anti-BrdU for proliferating cells (green), anti-MF20 for cardiomyocytes (red) and DAPI nuclear stain (blue). Cells were counted in at least 3 sections per embryo and separated into left and right ventricle and IVS, and for the ventricle myocardium the counts were also separated into trabeculae, compact and total. No significant differences were observed in the percentage of cardiomyocytes that had incorporated BrdU at E9.5-E12.5 (**A**-**L**, n=5). Unexpectedly at E13.5, there was an increase in the percentage of BrdU expressing left ventricle compact layer and trabeculae cardiomyocytes in *Rac1*^{TnTCre} hearts in comparison with left ventricle trabeculae cardiomyocytes in control hearts (n=3, p-0.0003) (**M**-**O**). LV; left ventricle, RV; right ventricle, IVS; interventricular septum. Scale bars; 100µm. Statistical analysis carried out using the two-way ANOVA. *P<0.05.

Since cardiomyocyte cell number is reduced from E9.5 but no differences in BrdU incorporation were detected, it was hypothesised that *Rac1* deficient cardiomyocytes may be undergoing DNA synthesis and incorporating BrdU without undergoing cytokinesis and cell division. Phospho-histone H3 (phHH3) immunostaining is an additional tool for analysing cell proliferation. phHH3 is

selectively expressed during the G2 and M phase of the cell cycle and thus represents a more selective window of cell proliferation during later stages of the cell cycle compared to BrdU incorporation. Dual immunostaining with anti-phHH3 was carried out in E11.5, E12.5 and E13.5 embryos to address this hypothesis. Again, MF20 was used as a marker to identify cardiomyocytes. In *Rac1*^{TnTCre} hearts, similar to BrdU incorporation analysis, there was no significant change in percentage expression of phHH3 in *Rac1* deficient cardiomyocytes at E11.5 or E12.5 (n=3) (Figure 92).

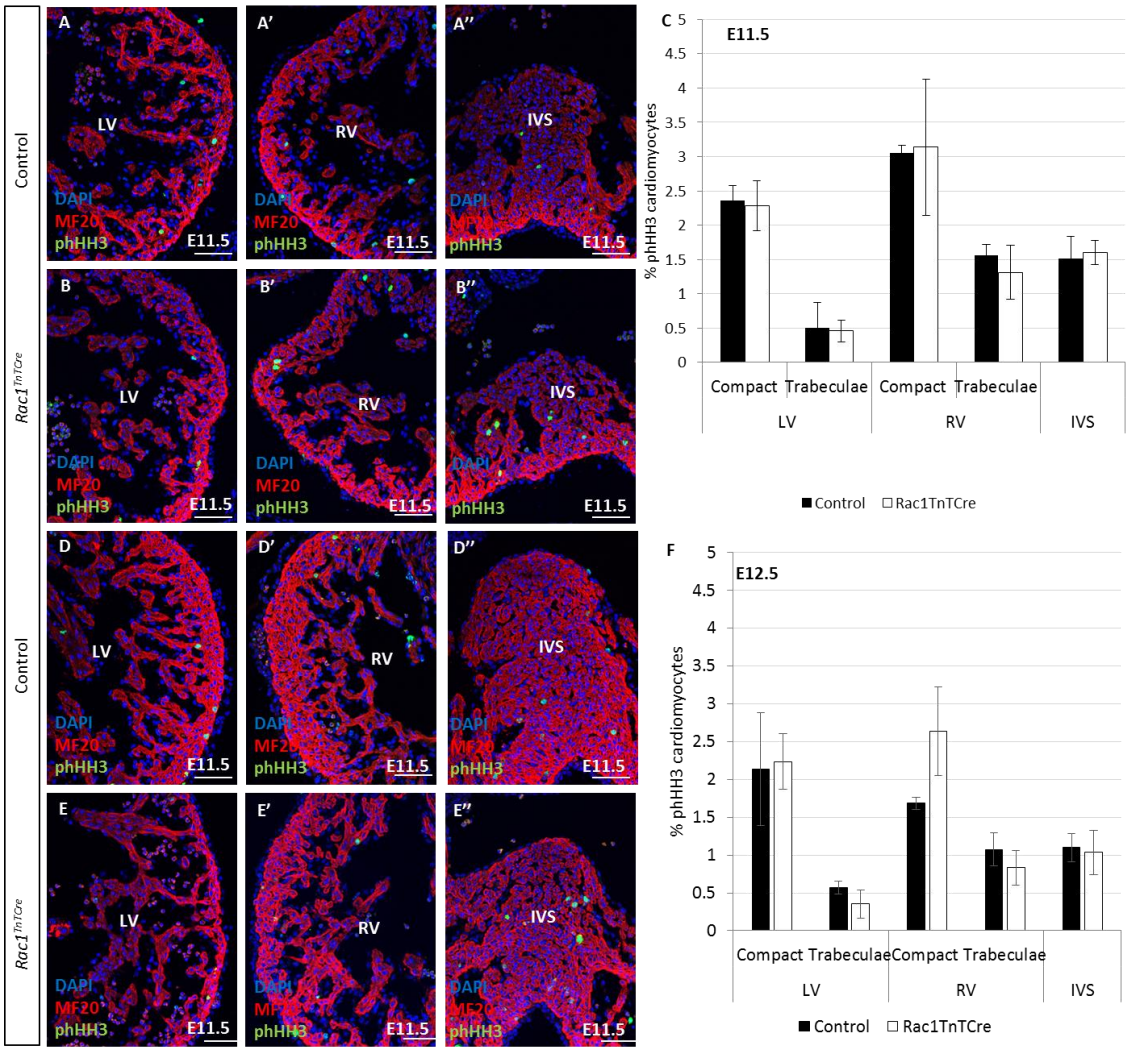

Figure 92: phHH3 expression is unchanged in cardiomyocytes in *Rac1*^{TnTCre} hearts compared to controls.
Immunostaining with anti-phHH3 for proliferating cells (green), anti-MF20 for cardiomyocytes (red) and DAPI nuclear stain (blue). Cells were counted in at least 3 sections per embryo and separated into left and right ventricle and IVS, and for the ventricle myocardium the counts were also separated into trabeculae, compact and total. In *Rac1*^{TnTCre} hearts, similar to BrdU incorporation analysis, there was no significant change in percentage expression of phHH3 in *Rac1* deficient cardiomyocytes at E11.5 or E12.5 (**A**-**F**) (n=3). Scale bars; 100µm. Statistical significance carried out using the two-way ANOVA.

The combined data from BrdU and phHH3 proliferation analysis in *Rac1*^{TnTCre} hearts shows no significant differences in the proliferation rate of cardiomyocytes during early cardiac development (E9.5-E13.5). It is possible that a small reduction in rate or a delay in proliferation may result in increasingly reduced cell numbers over the course of heart development. However, since there is no significant change in proliferation, it is likely that the cause of the

severe myocardial phenotype is another developmental process, such as cell apoptosis.

5.3.3.3 Cell death is normal in Rac1^{TnTCre} hearts

To investigate if the reduction in trabeculae cell numbers was due to increased cell death in *Rac1* deficient hearts, dual immunofluorescent staining with anti-caspase 3 was carried out and again MF20 was used as a marker to identify cardiomyocytes in *Rac1^{TnTCre}* hearts.

Caspase 3 is activated by auto-proteolytic cleavage or cleavage by another caspase protease to initiate cellular apoptosis. During cardiac development, cell death is relatively rare but is required for some developmental processes, such as outflow tract remodelling (Watanabe *et al.*, 1998; Watanabe *et al.*, 2001). Other embryonic tissues such as the neural tube display relatively high levels of apoptosis and therefore were used as a positive control for anti-Caspase-3 staining.

In *Rac1^{TnTCre}* hearts, levels of Caspase-3 positive cell death was low and not significantly changed compared to controls at E9.5 (n=5) (Figure 93A-C), E11.5 (n=4, Figure 93, A and D-E) and E12.5 (n=4, Figure 93, A and F-I). These results show that *Rac1* deficient cardiomyocytes are not undergoing abnormal apoptosis during the early stages of heart development. It is therefore proposed that the myocardial phenotype is not due to aberrant cardiomyocyte apoptosis.

Combined results from phHH3, BrdU and Caspase-3 staining confirm that cell proliferation and apoptosis is unaffected in *Rac1^{TnTCre}* hearts. These results are surprising since *Rac1^{TnTCre}* hearts display a severely thinned myocardial wall and reduced trabeculae. However, from heart dissections, MRI 3D reconstructions and cross-sectional measurements it was noted that *Rac1^{TnTCre}* hearts are dilated and larger compared to control hearts (Figure 94, C compared to B) (n=4). Therefore, as the cell number was counted and averaged in 3 transverse sections, this may not be representative of the whole heart. It was therefore hypothesised that *Rac1^{TnTCre}* hearts may contain equivalent numbers of cardiomyocytes compared to control hearts but spread over a larger surface area, thus appears less in individual heart sections. To test this hypothesis, E15.5 hearts were dissociated, propidium iodide (PI) was added to label cell nuclei and YFP was used to identify cardiomyocytes. Control and

Rac1^{TnTCre} hearts had comparable numbers of cardiomyocytes (n=4), however the SEM error bars suggest high variability between *Rac1*^{TnTCre} hearts (Figure 94A). Statistical power calculations suggest the experiment is underpowered. Due to time constraints further whole hearts cell counts were not possible in ths project but this is the focus of ongoing work and will be necessary to confirm equal cell numbers in *Rac1*^{TnTCre} hearts. From this preliminary data, it is proposed that the decreased cell numbers counted from sections may not be representative of total numbers of cardiomyocytes within a whole heart and hence no differences were observed in proliferation, apoptosis or cell cycle gene expression.

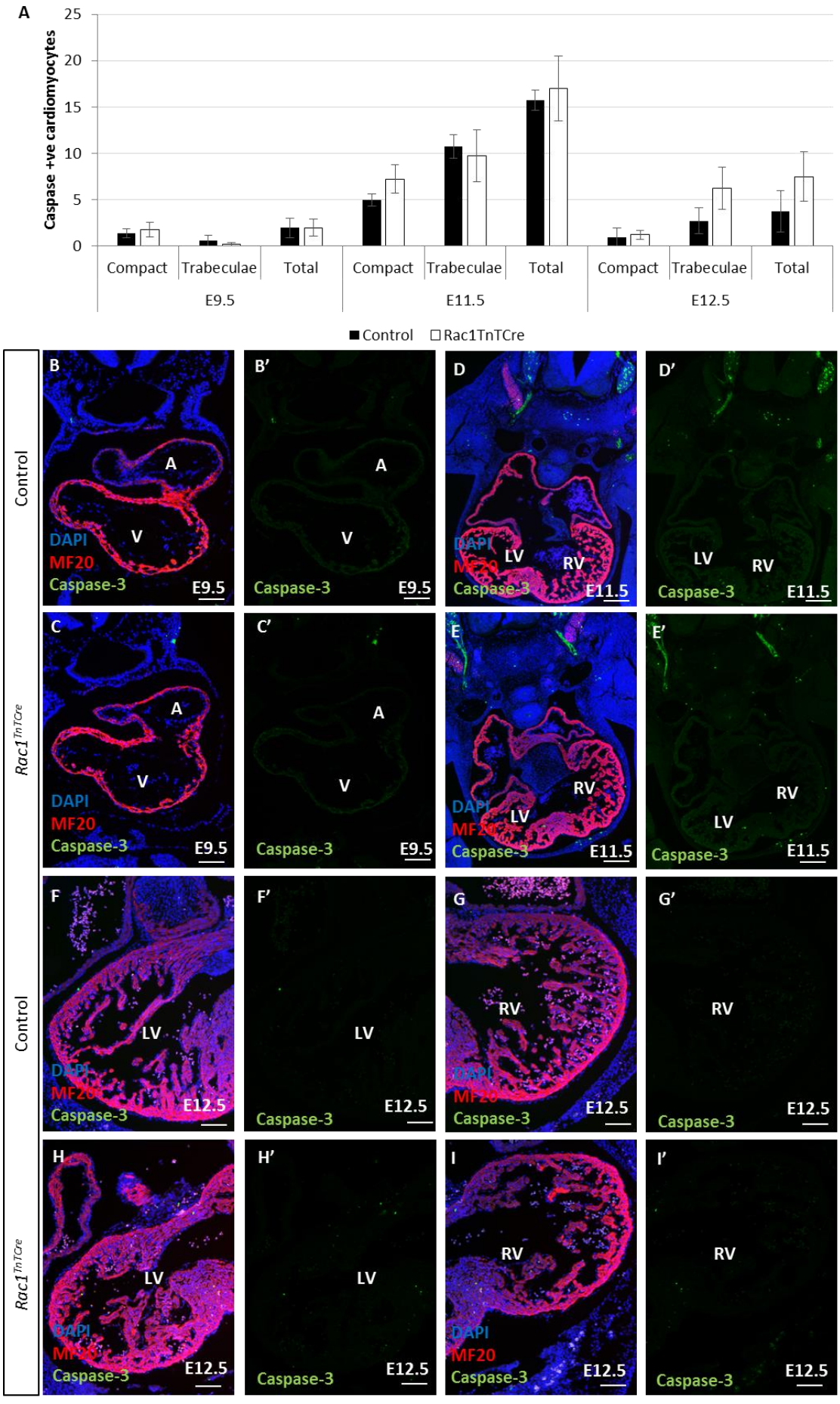
A
Caspase +ve cardiomyocytes
25
20
15
10
5
0
Compact
Trabeculae
Total
Compact
Trabeculae
Total
Compact
Trabeculae
Total
E9.5
E11.5
E12.5
Control
Rac1TnTCre
B
B'
D
D'
C
C'
E
E'
F
F'
G
G'
H
H'
I
I'
A
V
LV
RV
DAPI
MF20
Caspase-3
E9.5
E11.5
E12.5
Control
Rac1TnTCre

Figure 93: Cell death is normal in *Rac1*^{TnTCre} cardiomyocytes.
Immunostaining with anti-caspase-3 to mark apoptosis (green), anti-MF20 for cardiomyocytes (red) and DAPI nuclear stain (blue). Cells were counted in 3 sections per embryo and separated into trabeculae, compact and total cardiomyocytes. The level of Caspase-3 positive cell death was low and not significantly changed compared to controls at E9.5 (n=5, **A**-**C**), E11.5 (n=4, **A**, **D**-**E**) and E12.5 (n=4, **A**, **F**-**I**). Scale bars; 100µm. Statistical analysis carried out using the two-way ANOVA.

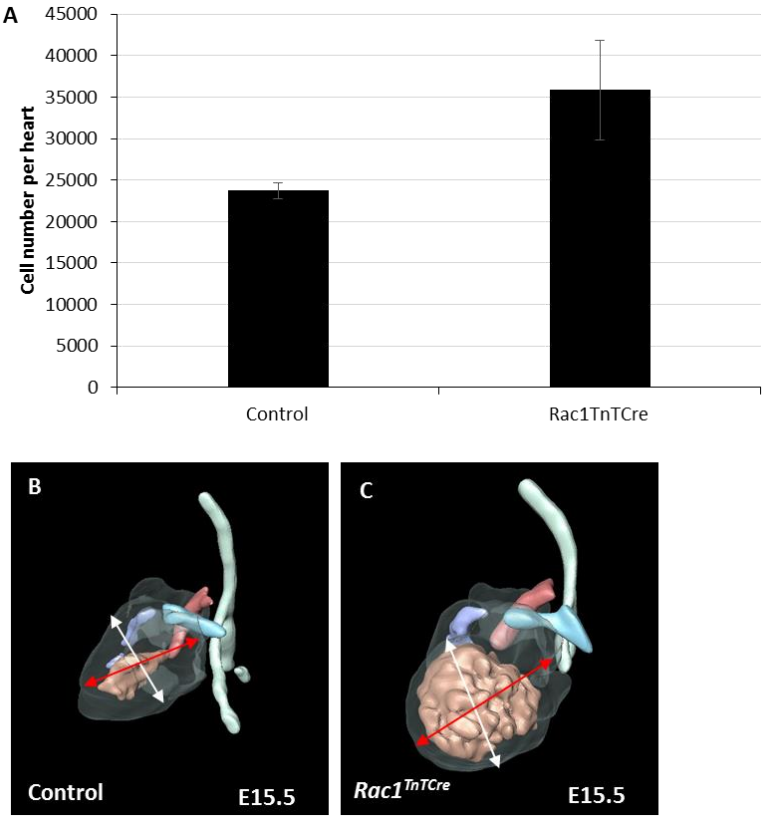

Figure 94: Cardiomyocyte number in control and *Rac1*^{TnTCre} hearts.
No significant difference in cell number was observed between E15.5 control and *Rac1*^{TnTCre} hearts (**A**) (n=4). However the ventricles are ballooned and increased in size (**C** compared to **B**) (n=4). Statistical analysis carried out using the unpaired t-test. Large SEM is seen in the *Rac1*^{TnTCre} hearts. Statistical power calculations suggest the experiment is underpowered.

5.3.4 Cardiomyocyte maturation is altered in Rac1^{TnTCre} *hearts*

During myocardial development, cardiomyocytes undergo maturation to become elongated and contractile with fully formed cell-cell junctions. Several markers of cardiomyocyte maturation have been identified and investigated in previous studies, including specific markers of compact and trabeculae myocardium maturation. Immunostaining and semi-quantificative PCR analysis

was used to investigate some of these markers in *Rac1*^{TnTCre} hearts and some *Rac1*^{Gata5Cre} hearts.

α-SMA is expressed in all myocardial and smooth muscle cells during early embryonic development, as demonstrated in Figure 88. However later in development, as the cardiomyocytes differentiate, they gradually switch off α-SMA expression. Trabeculae cardiomyocytes are most differentiated whilst the compact cardiomyocytes remain in a more immature proliferative state, as a result, expression is gradually restricted to the compact myocardium from E12.5 and is mostly absent from the trabeculae by E15.5. As the compact cardiomyocytes undergo maturation, α-SMA expression is restricted to the SMCs of the coronary vessels and great vessels, with some expression in the OFT myocardium, which can be seen at E17.5. Anti- α-SMA IHC staining was carried out in *Rac1*^{TnTCre} hearts at a range of ages (E11.5 to E17.5) to determine if cardiomyocyte maturation is affected in the absence of *Rac1* (Figure 95). In *Rac1*^{TnTCre} embryos, α-SMA was expressed normally compared to controls at E11.5 (n=4, Figure 95A-B), and E13.5 (n=6, Figure 95C-D). The α-SMA expressing compact myocardium is thinner in the *Rac1*^{TnTCre} E13.5 (Figure 95C-D), E15.5 (Figure 95E-F) and E17.5 (Figure 95G-H), mutants compared to controls (Figure 46, n=6). The expression of α-SMA appears disrupted from E15.5, when it is aberrantly retained strongly in the trabeculae cardiomyocytes compared to reduced expression in controls (n=4) (arrows in Figure 95F' and F''). Additionally, the left compact cardiomyocytes retain strong expression from E15.5, which continues to E17.5 (n=4) (Figure 95F'' and H''). The retained expression in the trabeculae cardiomyocytes suggests that the trabeculae cardiomyocytes are not fully maturing.

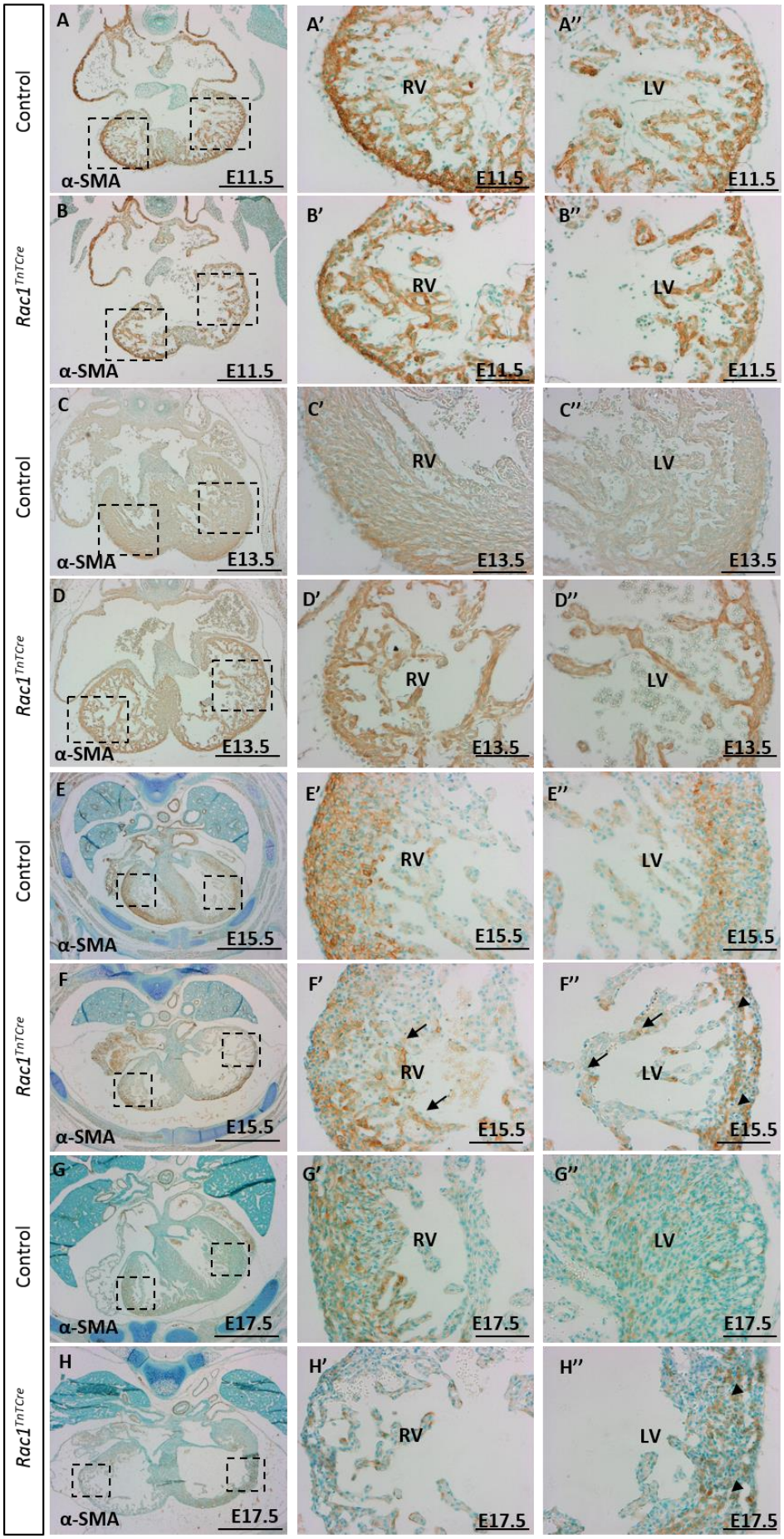
Control
Rac1TnTCre
Control
Rac1TnTCre
Control
Rac1TnTCre
Control
Rac1TnTCre
A
A'
A''
B
B'
B''
C
C'
C''
D
D'
D''
E
E'
E''
F
F'
F''
G
G'
G''
H
H'
H''
α-SMA
RV
LV
E11.5
E13.5
E15.5
E17.5

Figure 95: α-SMA expression is disrupted at E15.5 in *Rac1*^{TnTCre} hearts.
IHC staining using anti-α-SMA on E11.5-E17.5 transverse sections of control and *Rac1*^{TnTCre} embryos. α-SMA expression appears normal in the *Rac1*^{TnTCre} hearts compared to controls at E11.5 (**A**-**B**) (n=4). The α-SMA expressing compact myocardium is thinner in the *Rac1*^{TnTCre} E13.5 (**C**-**D**) (n=6), E15.5 (**E**-**F**) (n=4) and E17.5 (**G**-**H**) (n=4) mutants compared to controls. The expression of α-SMA appears disrupted from E15.5, when it is aberrantly retained strongly in the trabeculae cardiomyocytes compared to reduced expression in controls (arrows in **F'** and **F''**) (n=4). Additionally, the left compact cardiomyocytes retain strong expression from E15.5 that continues to E17.5 (arrow heads in **F''** and **H''**) (n=4). E; embryonic day, LV; left ventricle, RV; right ventricle. Scale bars; A-H 500μm, A'-H'' 100μm.

Similar to α-SMA, SM22α is expressed in all cardiomyocytes early in development, with expression being restricted to smooth muscle cells later in development. As previously shown in Figure 88, SM22α is expressed normally in E10.5 *Rac1*^{TnTCre} mutants compared to controls, with varying expression throughout the myocardium.

E12.5 and E15.5 *Rac1*^{TnTCre} embryos were dissected and processed for fluorescent IHC. Anti-SM22α antibody staining was carried out on control and *Rac1*^{TnTCre} heart sections (Figure 96). At E12.5, strong expression of SM22α is restricted to the compact layer in controls with variation in the strength of expression between cells (Figure 96A-B). However, in *Rac1*^{TnTCre} hearts, SM22α remains strongly expressed in some trabeculae cardiomyocytes (Figure 96C-D). This pattern is continued at E15.5, when SM22α is strongly expressed around the edges of trabeculae in the *Rac1*^{TnTCre} hearts (Figure 97C-D) and is mostly absent in controls (Figure 97A-B). Dual staining with endomucin, an endocardial and coronary vein marker, and SM22α in E12.5 and E15.5 sections reveals strong SM22α expression in the outer layer of the trabeculae myocardium, underneath the endomucin-positive endocardial layer (Figure 96 and Figure 97). CD31, is another endothelial marker expressed in both coronary arteries and veins and shows reduced expression within the compact myocardium in *Rac1*^{TnTCre} hearts. However, expression is increased around the trabeculae, corresponding to the areas of increased SM22α expression (Figure 98, B compared to D). The reduced expression of CD31 within the compact myocardium implies defective coronary vessel formation in *Rac1*^{TnTCre} hearts and is discussed further in Chapter 5 Section 5.3.9.

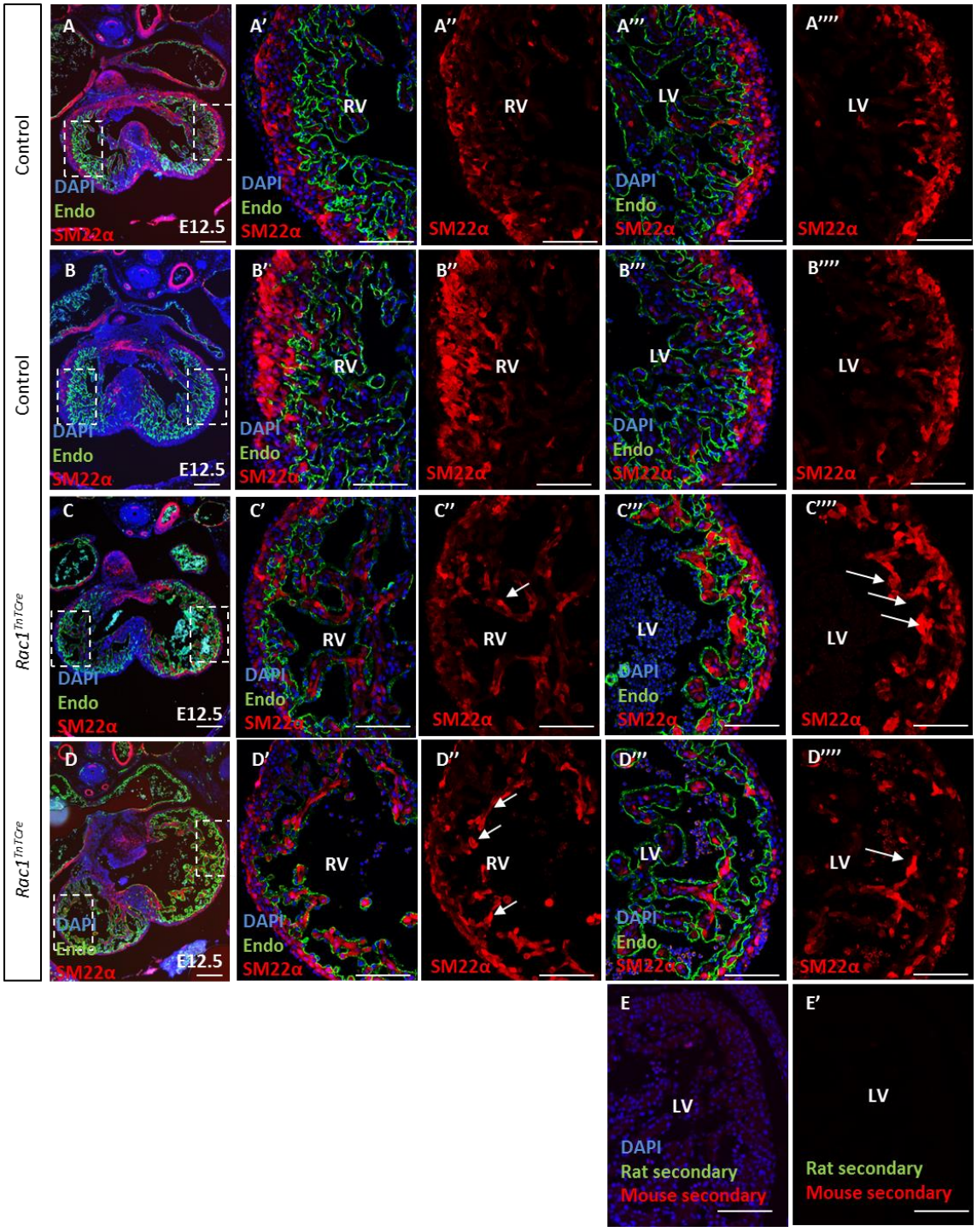

Figure 96: Aberrant expression of SM22α in the trabeculae cardiomyocytes in E12.5 *Rac1*^{TnTCre} hearts.
IF staining with anti-SM22α, an early embryonic cardiomyocyte and smooth muscle marker and anti-endomucin, an endocardial marker to distinguish trabeculae myocardium from the compact myocardium. SM22α expression shows increased retention in *Rac1*^{TnTCre} trabeculae cardiomyocytes compared to controls, particularly in the left ventricle (arrows in **C** and **D**) (n=4). Secondary only controls (**E**). E; embryonic day, LV; left ventricle, RV; right ventricle. Scale bars; A-D 200μm, A'-D''' 100μm.

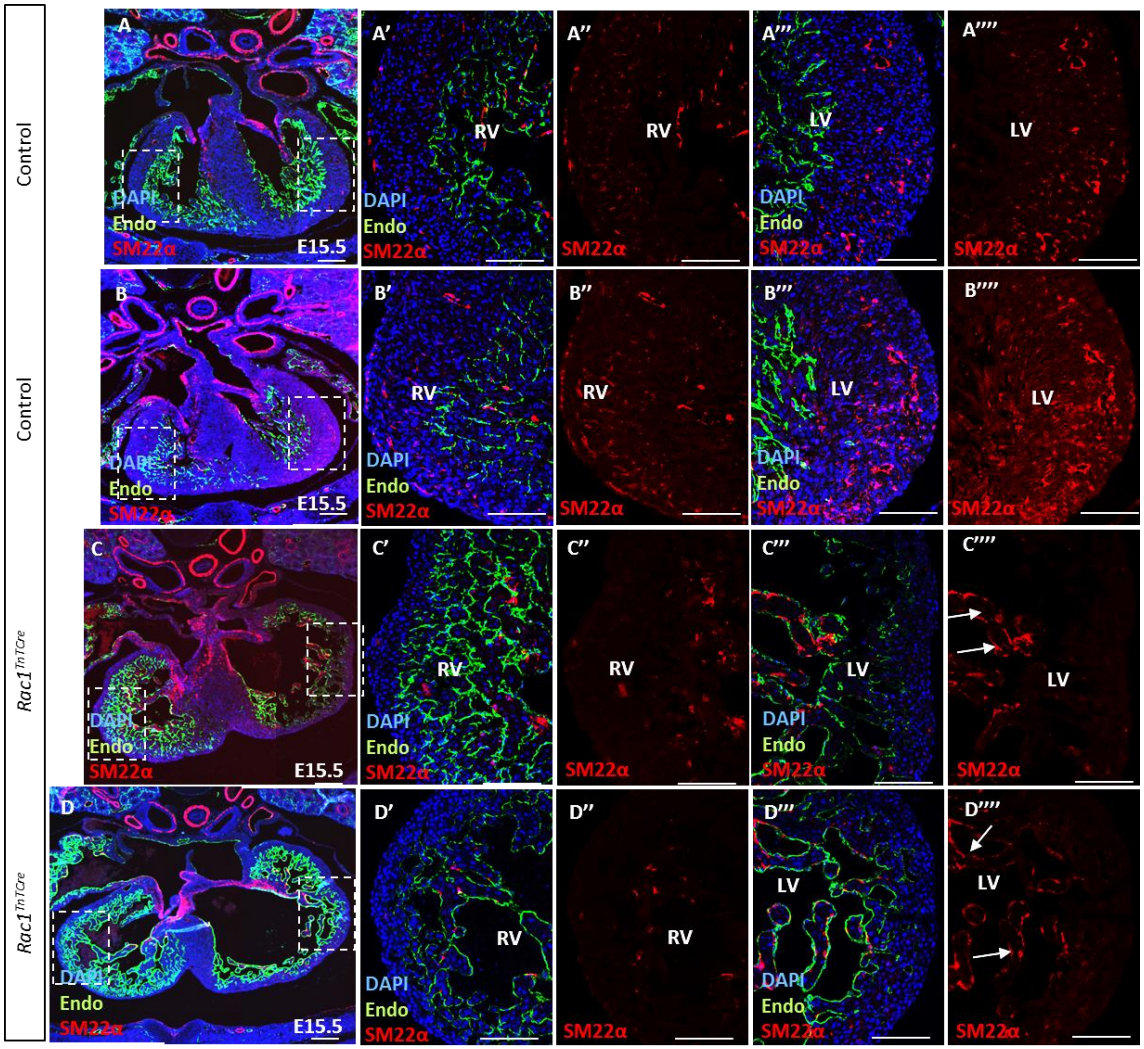

Figure 97: Continued aberrant retention of embryonic cardiomyocyte markers in the trabeculae cardiomyocytes in E15.5 *Rac1*^{TnTCre} hearts.
IF staining with anti-SM22α, an early embryonic cardiomyocyte and smooth muscle marker and anti-endomucin, an endocardial marker to distinguish trabeculae myocardium from the compact myocardium. SM22α expression shows increased retention in *Rac1*^{TnTCre} trabeculae cardiomyocytes compared to controls, particularly in the left ventricle (arrows in **C'''** and **D''''**) (n=4). E; embryonic day, LV; left ventricle, RV; right ventricle. Scale bars; A-D 200μm, A'-D''' 100μm.

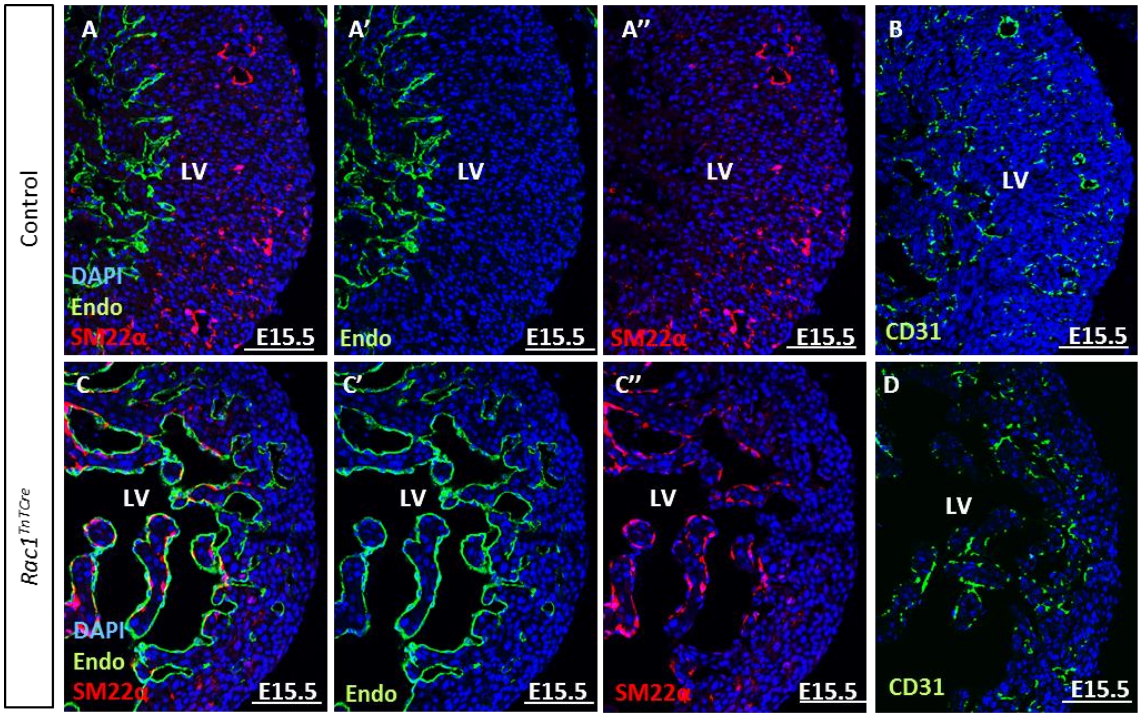

Figure 98: Disrupted localisation of SM22α and endothelial markers, endomucin and CD31, within the developing ventricular wall.
IF staining with anti-SM22α, an early embryonic cardiomyocyte and smooth muscle marker, anti-endomucin, an endocardial marker, and CD31, an endothelial marker. SM22α expression shows increased retention in trabeculae cardiomyocytes and decreased expression within the compact myocardium in *Rac1*^{TnTCre} compared to controls (arrows in **C''** compared to **A''**) (n=4). CD31 expression is also reduced within the compact myocardium (**D** compared to arrows in **B**). Endomucin positive staining is aberrantly detected within the compact myocardium (arrows in **C'** compared to **A'**). E; embryonic day, LV; left ventricle, RV; right ventricle. Scale bars; 100μm.

Since trabeculae cardiomyocytes appear to be retaining early cardiomyocyte markers, semi-quantitative PCR and immunofluorescent staining for some additional compact and trabeculae markers, *Peg1*, *Hop* and *Irx3/5*, was carried out in younger control and *Rac1*^{TnTCre} hearts.

Peg1 is initially expressed uniformly throughout the linear heart tube, but is then subsequently restricted to the developing myocardial trabeculae of both the atria and ventricles into late development. Mice lacking the *Peg1* gene are viable and grossly normal with subtle alterations in trabeculation; an increase in thickness and reduction in density of the compact myocardium (King *et al.*, 2002).

Hop is a small unusual homeodomain protein that is highly expressed in the developing heart, regulated by *Nkx2.5* expression. *Hop* expression initiates in

early cardiogenesis and continues in cardiomyocytes throughout embryonic and postnatal development. *Hop* inactivation in mice results in severe myocardial abnormalities (Chen *et al.*, 2002; Shin *et al.*, 2002). Hop physically interacts with serum response factor (SRF) and modulates its activity by inhibiting its binding to DNA. SRF transcriptional regulation is involved in balancing cardiomyocyte proliferation and differentiation.

Iroquois homeobox (Irx) 5 is important for postnatal cardiomyocyte repolarisation. In mice, *Irx3* and *Irx5* have redundant functions in the endocardium to regulate AV canal morphogenesis and OFT formation. Direct transcriptional repression of *Bmp10* by Irx3 and Irx5 in the endocardium is required for ventricular septation. A postnatal deletion of Irx3 and Irx5 in the myocardium leads to prolongation of AV conduction, due in part to activation of expression of the Na(+) channel protein Nav1.5 (Gaborit *et al.*, 2012).

RNA was extracted from E10.5 control and $Rac1^{TnTCre}$ hearts and the synthesised cDNA was used in RT-PCR. In $Rac1^{TnTCre}$ hearts, expression of trabeculae marker *Peg1* was significantly increased ($p<0.05$) (Figure 99, B and E). Additional trabeculae marker, *Hop*, also had a trend for increased expression but was not significant (Figure 99, C and E). *Irx5* expression was unchanged in $Rac1^{TnTCre}$ hearts (Figure 99D-E). Peg1 and Hop are both myocardial markers whereas, Irx5 is an endocardial marker, suggesting that the maturation of the myocardium is altered in $Rac1^{TnTCre}$ hearts. *In situ* hybridisation for *Peg1* in E10.5 control and $Rac1^{TnTCre}$ hearts revealed *Peg1* is strongly expressed in the trabeculated myocardium, and to a lesser extent in the compact myocardium (Figure 99F-G). $Rac1^{TnTCre}$ hearts show subtle increases in expression of *Peg1* within the myocardium, particularly in the compact layer of the LV (arrows in Figure 99, G'' compared to F''). This suggests the development of the compact myocardium is altered in $Rac1^{TnTCre}$ hearts from E10.5.

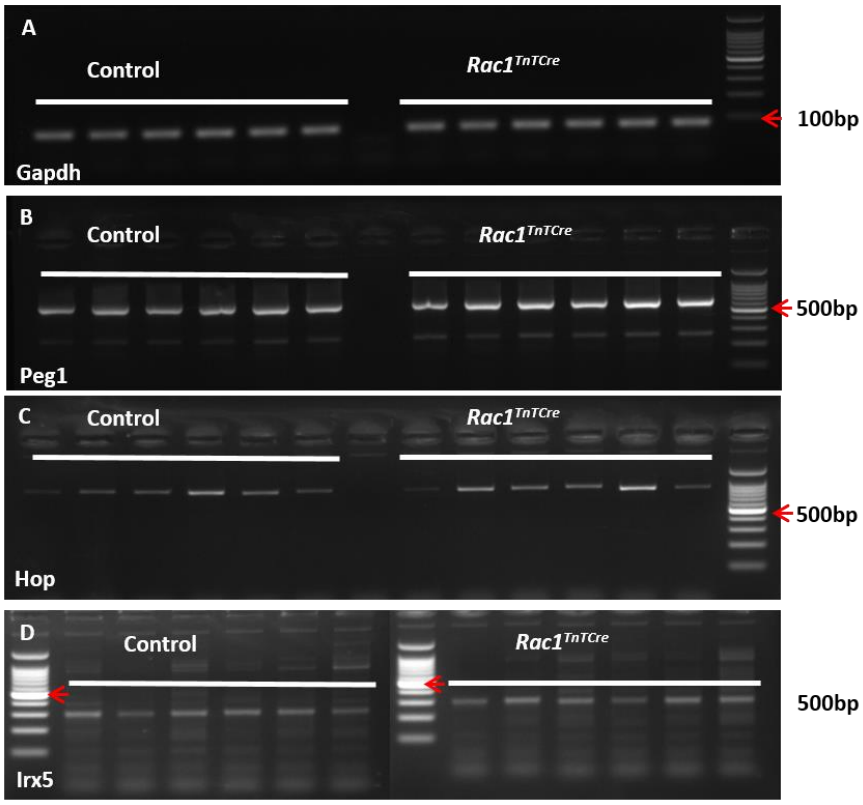
A
Control
Rac1TnTCre
100bp
Gapdh
B
Control
Rac1TnTCre
500bp
Peg1
C
Control
Rac1TnTCre
500bp
Hop
D
Control
Rac1TnTCre
500bp
Irx5

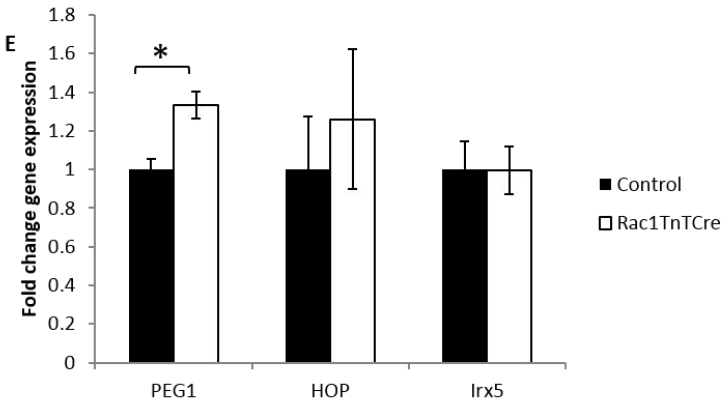
E
Fold change gene expression
1.8
1.6
1.4
1.2
1
0.8
0.6
0.4
0.2
0
*
PEG1
HOP
Irx5
Control
Rac1TnTCre

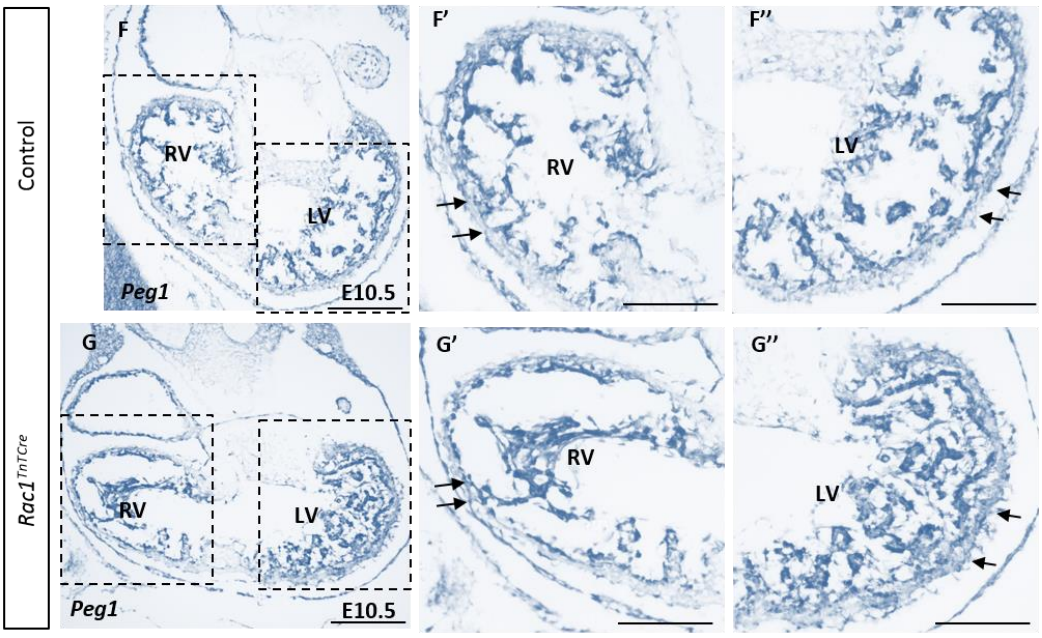
Control
Rac1TnTCre
F
RV
LV
Peg1
E10.5
F'
RV
F''
LV
G
RV
LV
Peg1
E10.5
G'
RV
G''
LV

Figure 99: Trabeculae myocardial specific gene *Peg1* is upregulated in *Rac1*^{TnTCre} hearts.
Semi-quantitative PCR of compact and trabeculae marker gene expression in control and *Rac1*^{TnTCre} E10.5 hearts. Semi-quantitative PCR gel (**A**-**D**) and densitometry analysis (**E**) reveal increased expression of *Peg1* in *Rac1*^{TnTCre} hearts compared to controls, P<0.05 (n=6). Statistical analysis carried out using the unpaired t-test. Large SEM error bars in both control and *Rac1*^{TnTCre} groups for HOP analysis suggest sample variability. Statistical power calculations suggest this experiment is underpowered and additional samples may be beneficial to assigning statistical significance to the trend for increased HOP expression in *Rac1*^{TnTCre} hearts. *Peg1 in situ* hybridisation on E10.5 control and *Rac1*^{TnTCre} sections (**F**-**G**). Increased expression of *Peg1* in the compact layer of the left ventricle in *Rac1*^{TnTCre} hearts compared to controls (arrows in **G''** compared to **F''**) (n=3). LV; left ventricle, RV; right ventricle. Scale bars; F-G 200μm, F'-G'' 100μm.

Atrial natriuretic factor (ANF) is a marker of cardiomyocyte growth and differentiation, and is regulated spatially, developmentally and hormonally (Temsah and Nemer, 2005). *ANF* is not expressed in the early linear heart tube; expression is initiated at E8.25 on the ventral side of the early looping heart tube. During early chamber development, *ANF* is more strongly expressed in the LV compared to RV, becoming restricted to the LV and absent from the RV later in development. ANF is not expressed in the AVC, OFT or the inner curvature of the ventricles (Christoffels *et al.*, 2000) and is completely restricted to the atria after birth. E15.5 embryos were dissected, embedded and sectioned for immunostaining. Anti-ANF immunofluorescent staining revealed ventricular ANF expression is restricted to the trabeculae in both control and *Rac1*^{TnTCre} hearts (Figure 100). Expression was most prominent in the atria and LV, particularly along the LV luminal edge of the IVS (Figure 100A-D). Substantially weaker expression was observed in the trabeculae of the RV in controls, (Figure 100E) however this remained prominent in *Rac1*^{TnTCre} hearts (Figure 100F). Expression appeared comparable between the LV of control and *Rac1*^{TnTCre} hearts (Figure 100C-D). These results provide further evidence that the RV trabeculae are not maturing as in controls (as described in Figure 100).

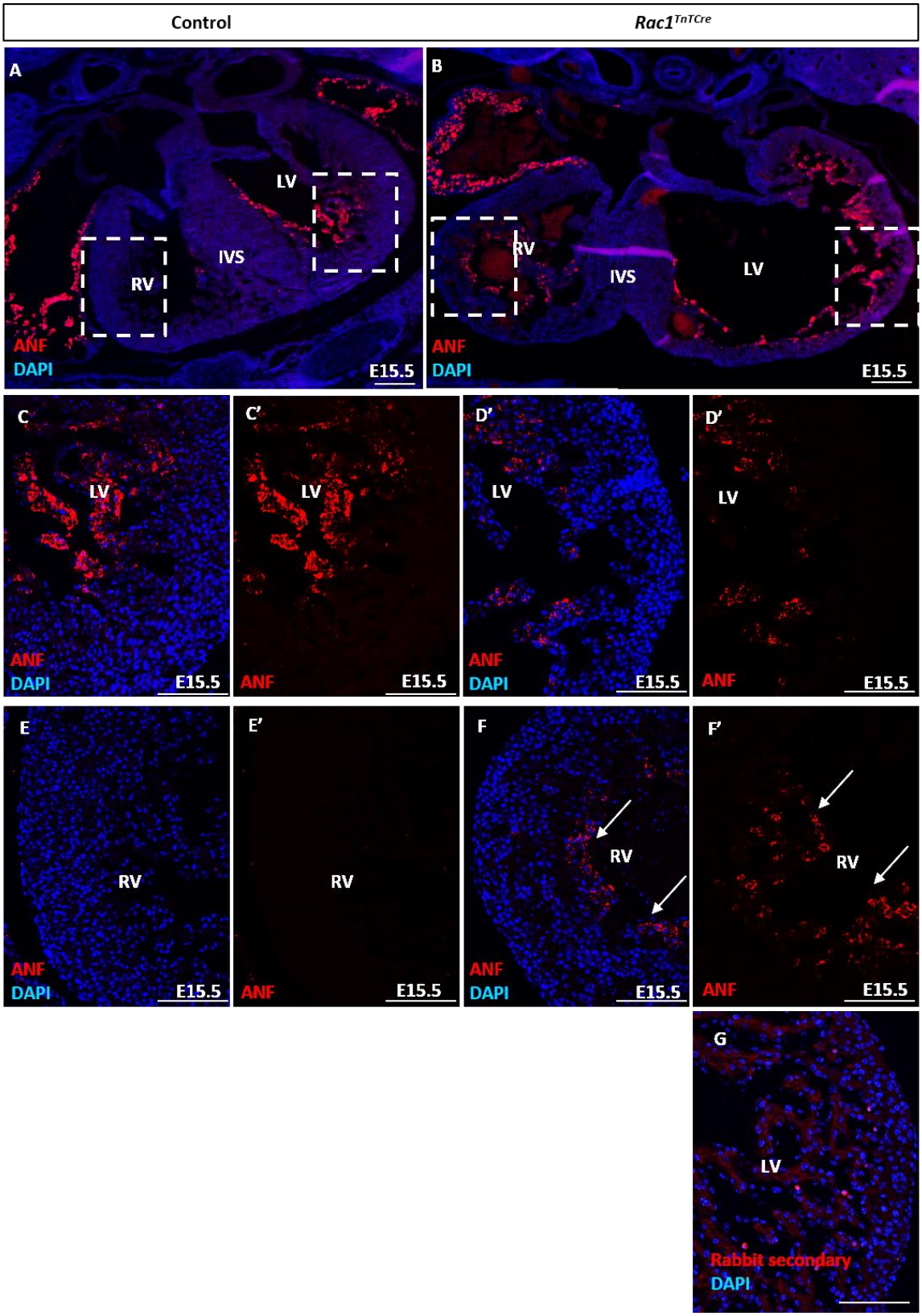

Figure 100: Aberrant expression of ANF in the right ventricle in *Rac1*^{TnTCre} hearts.

IF staining with anti-ANF antibody (red) in E15.5 control and *Rac1*^{TnTCre} transverse heart sections. *Rac1*^{TnTCre} hearts display strong expression of ANF in the trabeculae layer of the right ventricle (arrows in **F-F'**) compared with no

expression in control hearts (**E**-**E'**) (n=4). Expression appeared comparable between the left ventricle of control and *Rac1*^{TnTCre} hearts (**C**-**D**) (n=4). Secondary only control (**G**). LV; left ventricle, RV; right ventricle, IVS; interventricular septum. Scale bars; A-B 200µm, C-F' 100µm.

The abnormal trabeculae and compact myocardium development in *Rac1*^{TnTCre} hearts highlights possibly differential development mechanisms of the right and left ventricles. Trabeculae formation and directionality is particularly affected in the LV, as is expanded trabeculae specific Peg1 expression within the compact myocardium. However, ANF expression is upregulated in the RV. Additonally, remodelling of the trabeculae appears to be absent in the RV whereas remodelling is abnormal in the LV. Taken together, the increase in trabeculae specific gene expression by qPCR, *in situ* hybridisation and immunostaining suggests that the maturation of the trabeculae myocardium is disrupted, in addition to the initial trabeculae formation in *Rac1*^{TnTCre} hearts. Maturation of cardiomyocytes involves changes in cell morphology including establishment of the mature cytoskeleton and cell-cell adhesion junction, as well as polarisation of the cell. Therefore, these features were investigated in *Rac1*^{TnTCre} hearts.

5.3.5 Cytoskeleton in Rac1 deficient cardiomyocytes

The cytoskeleton provides structural and functional integrity to the cell and is essential for cell contraction and also for some cellular processes, such as cell migration. To investigate the formation of the actin cytoskeleton in *Rac1* deficient cardiomyocytes, IF staining for multiple components of cytoskeleton was carried out along with TEM imaging.

E10.5 and E11.5 embryos were dissected and processed for immunostaining. IF was carried out using antibodies against cardiac-actin, α-actinin and cardiac-Tn-I. Expression of these sarcomeric proteins was unchanged in *Rac1*^{TnTCre} myocardium compared to controls (Figure 101 and Figure 102). In cardiomyocytes, cardiac actin is present as a component of the thin actin filaments, as well as actin microfilaments. Tn-I is also a component of the thin actin filaments, which are connected and stabilised in the Z-disc, through actin binding protein, α-actinin (Sjoblom *et al.*, 2008). α-actinin shows expression within the Z-disc of cardiomyocytes at E11.5 (Figure 101A-F). Expression of α-actinin appears unchanged in *Rac1*^{TnTCre} cardiomyocytes compared to controls

(Figure 101D-F compared to A-C). Cardiac actin and Tn-I show similar expression patterns, within the thin actin filaments (Figure 101G-L and Figure 102). Expression of Tn-I appears unchanged between control and *Rac1*^{TnTCre} cardiomyocytes at E11.5 (Figure 101G-L). Additionally, cardiac actin expression is normal at E10.5 and E11.5 in *Rac1*^{TnTCre} hearts (Figure 102). Therefore the actin cytoskeleton appears normal in *Rac1*^{TnTCre} hearts by IF.

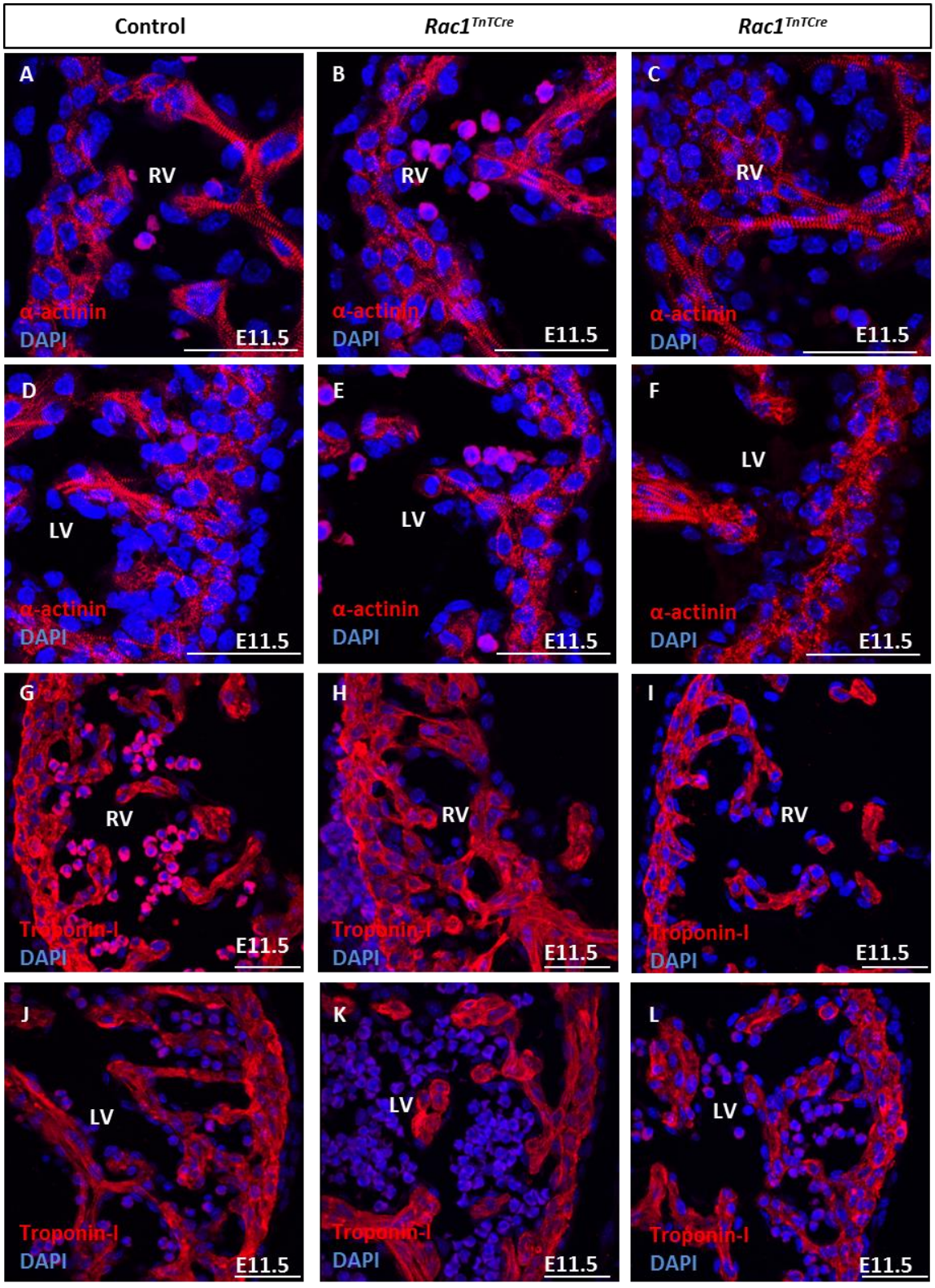

Figure 101: Sarcomeric proteins, α-actinin and troponin-I are expressed normally in *Rac1*^{TnTCre} hearts.

IF staining with anti-α-actinin and anti-troponin I antibodies in E11.5 control and *Rac1*^{TnTCre} transverse heart sections. Control and *Rac1*^{TnTCre} hearts display strong expression of both α-actinin (**A**-**F**) and troponin-I (**G**-**L**) within the cardiomyocytes of the developing myocardium at E11.5 (n=3). LV; left ventricle, RV; right ventricle. Scale bars; 50μm.

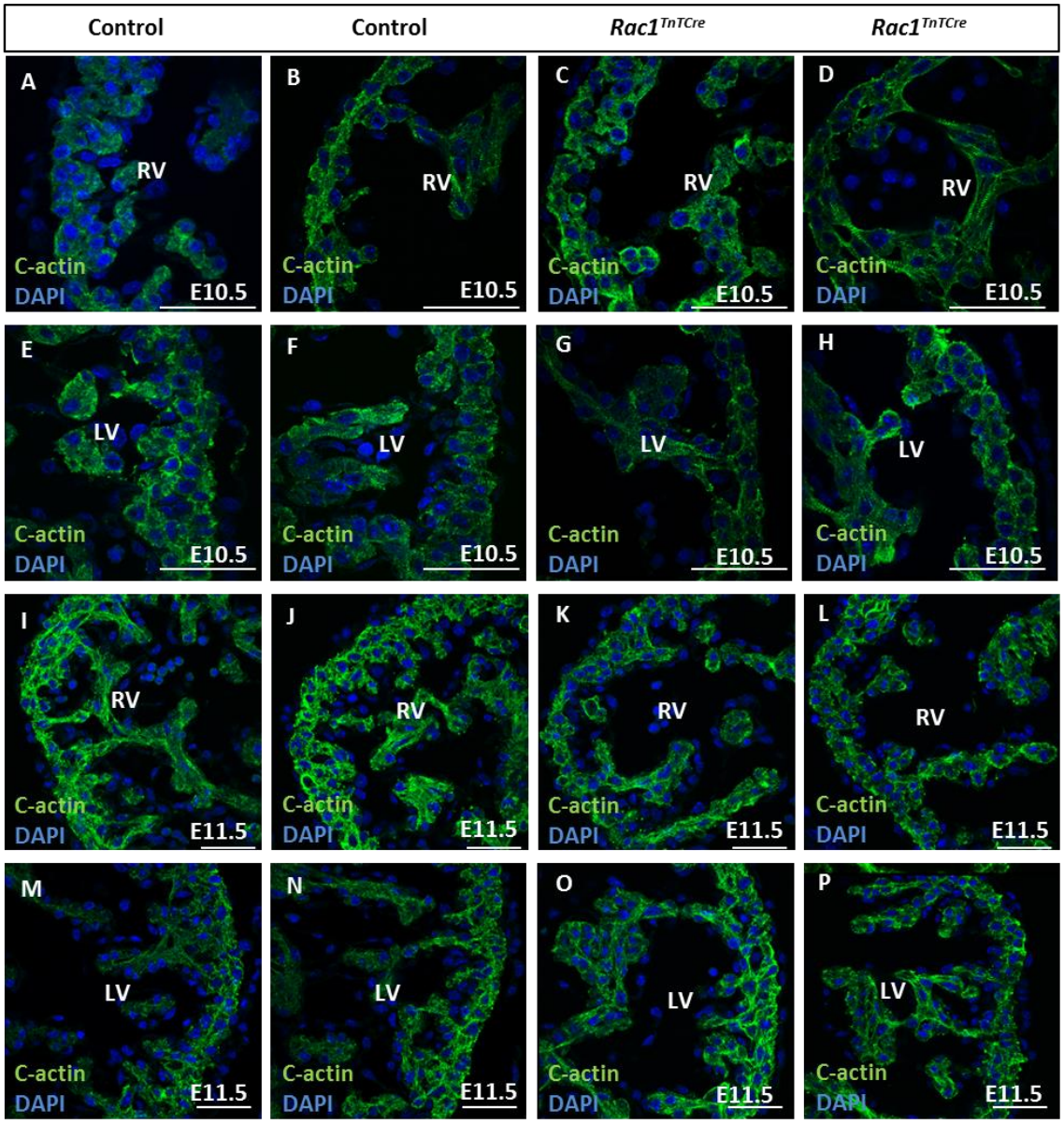

Figure 102: Sarcomeric protein cardiac-actin is expressed normally in *Rac1*^{TnTCre} hearts.
IF staining with anti-c-actin antibody in E10.5 and E11.5 control and *Rac1*^{TnTCre} transverse heart sections. Control and *Rac1*^{TnTCre} hearts display strong expression of c-actin within the cardiomyocytes of the developing myocardium at both E10.5 and E11.5 (n=3). LV; left ventricle, RV; right ventricle. Scale bars; 50µm.

E10.5 control and *Rac1*^{TnTCre} hearts were dissected and fixed for TEM imaging. Hearts were processed, sectioned and stained by the Newcastle University Electron Microscopy Research Facility. Images were taken from the compact and trabeculae regions of the myocardium in one section from each heart (n=6). Analysis of the control TEM images revealed differences in the myofibril

formation in compact versus trabeculae cardiomyocytes. This is unsurprising since trabeculae cardiomyocytes are more differentiated than compact cardiomyocytes and thus have a more developed cytoskeletal structure. In the *Rac1*^{TnTCre} hearts, the myofibrils appeared to be less well formed compared to controls in both the compact and trabeculae regions. The mutant myofibrils tended to be thinner and more fragmented (arrows in Figure 103). This suggests that Rac1 is involved in myofibril formation during embryonic cardiomyocyte maturation.

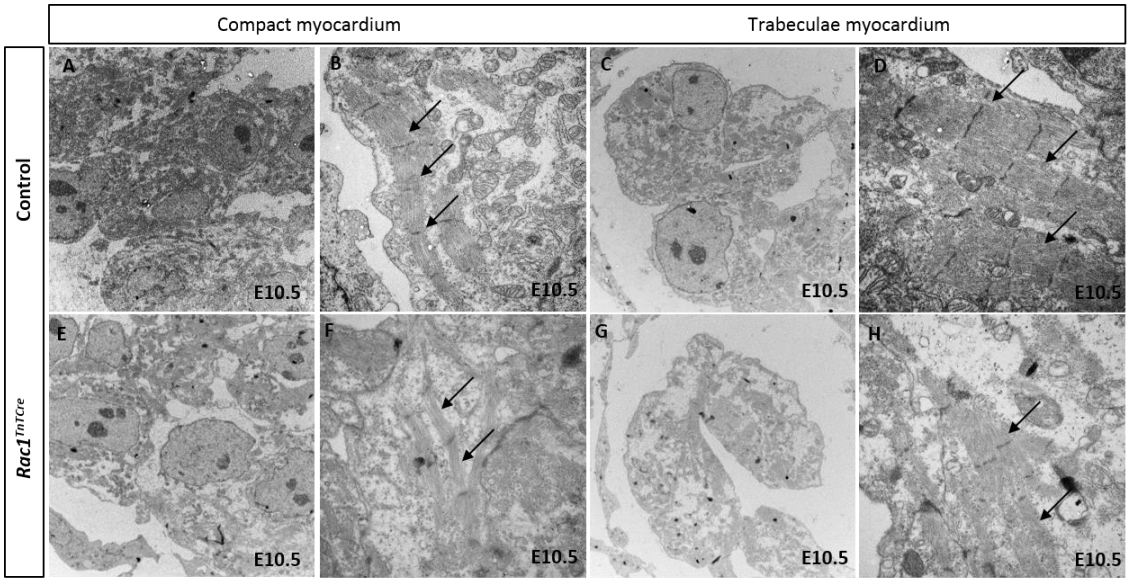

Figure 103: Disrupted sarcomere formation in *Rac1*^{TnTCre} hearts compared to controls.
TEM images of trabeculae and compact myocardium regions in E10.5 control and *Rac1*^{TnTCre} hearts. *Rac1*^{TnTCre} hearts display disrupted formation of sarcomeres compared to controls (arrows in **F** and **H**, compared to arrows in **B** and **D**) (n=6).

5.3.6 Cardiomyocyte Polarity

Cardiomyocyte polarisation and adhesion are intrinsically linked and are essential for myocardial development. Like epithelial cells, cardiomyocytes display ABP and adhesion through AJ, TJ and desmosomes. Cardiomyocytes also display properties of PCP, however the role of PCP signalling in cardiomyocytes is not fully understood.

To investigate if cardiomyocyte polarity is affected in *Rac1*^{TnTCre} hearts, immunofluorescence staining was carried out for proteins associated with PCP

signalling and cell polarisation, as well as cell membrane staining to analyse cell shape and size.

Scrib is a fellow member of the PCP signalling pathway and has been shown to interact with Rac1 in cardiomyocytes previously (Boczonadi *et al.*, 2014b), and was therefore selected to investigate the effect of the loss of Rac1 on the PCP pathway. E9.5 and E12.5 embryos were dissected and processed for immunofluorescence. Staining using an anti-Scrib antibody confirmed that Scrib is expressed at the cell membrane as expected (shown in Figure 104). Surprisingly, Scrib expression was unchanged in *Rac1*^{TnTCre} mutants at both E9.5 (n=3, Figure 104A-D) and E12.5 (n=3, Figure 104E-H). These results suggest that Scrib does not require interaction with Rac1 for localisation at the membrane and is unaffected in the absence of Rac1.

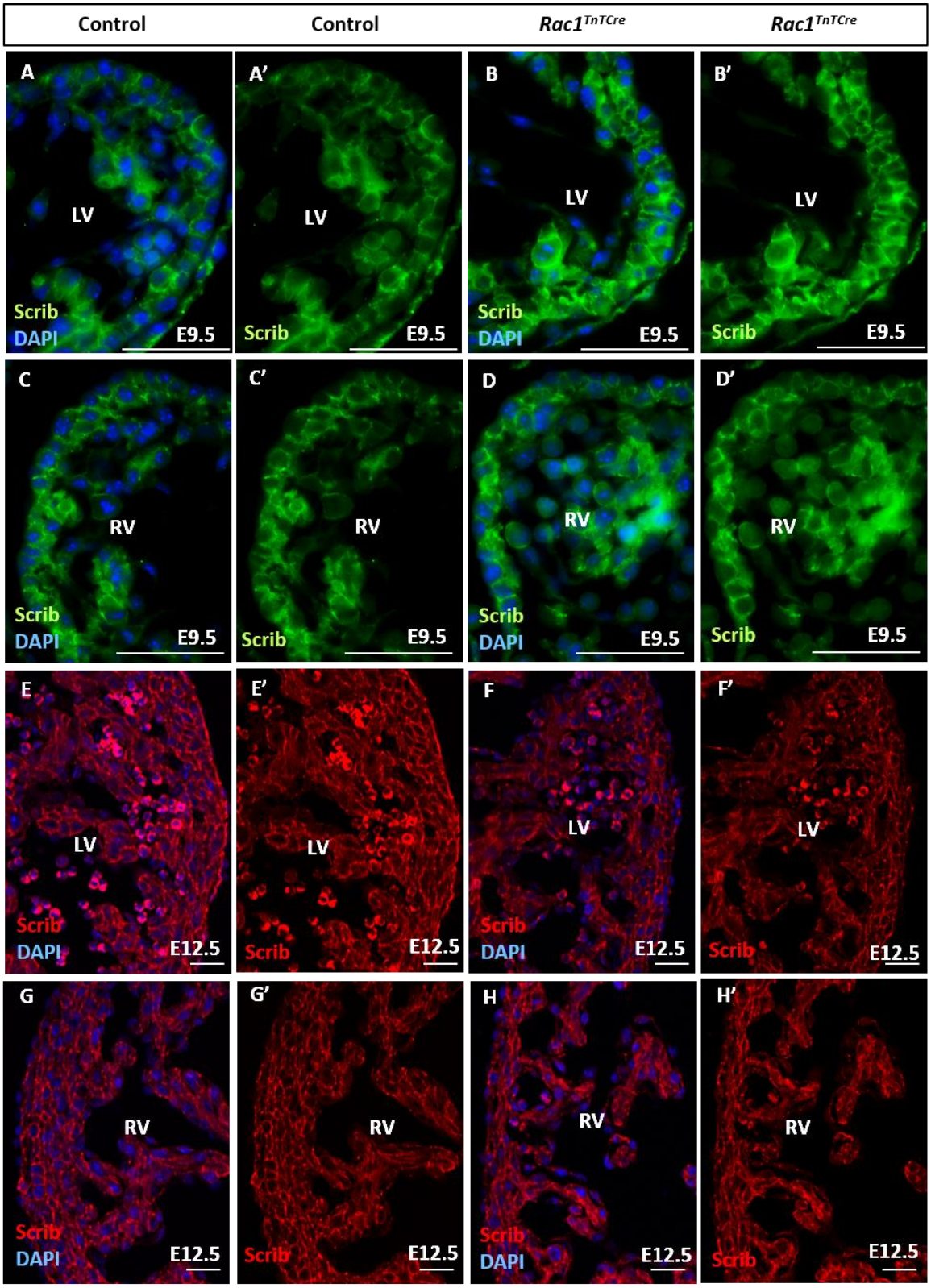

Figure 104: PCP protein, Scrib is unaffected in *Rac1*^{TnTCre} hearts.
IF staining with anti-Scrib antibody in E9.5 (**A**-**D**) and E12.5 (**E**-**H**) control and *Rac1*^{TnTCre} transverse heart sections. Control and *Rac1*^{TnTCre} hearts display membrane localisation of Scrib within the cardiomyocytes of the developing myocardium at both E9.5 (**A**-**D**) and E12.5 (**E**-**H**) (n=3). LV; left ventricle, RV; right ventricle. Scale bars; 50µm.

Wheat germ agglutinin (WGA) binds to sialic acid and *N*-acetylglucosaminyl residues both cell and nuclear membranes. Staining using an Alexa Fluor 594 conjugate was carried out on E10.5-17.5 sections (Figure 105A-H) (n=4). WGA membrane staining was used to draw around cell membranes using Nikon elements confocal software, in order to calculate cell circularity and cell size. The analysis revealed that *Rac1*^{TnTCre} cardiomyocytes were significantly larger in size compared to controls from E10.5 (Figure 105A, B and I) and remained consistently larger at E17.5 (Figure 105F-H, I). From E10.5 to E15.5 the cardiomyocytes of *Rac1*^{TnTCre} ventricles have significantly increased cell area compared to controls, in both left and right ventricles (Figure 105I) (except at E12.5 the increase in cell area is only significant in the LV of *Rac1*^{TnTCre} hearts, with no differences in the RV). For E17.5 cell area measurements, compact and trabeculae regions were separated. In both ventricles, b compact and trabeculae cardiomyocytes had significantly increased cell areas compared to controls (Figure 105J). No differences in cell shape were detected, as calculated by circularity measurements (Figure 105K). These results suggest that the *Rac1* deficient cardiomyocytes undergo a hypertrophic response in the absence of *Rac1*.

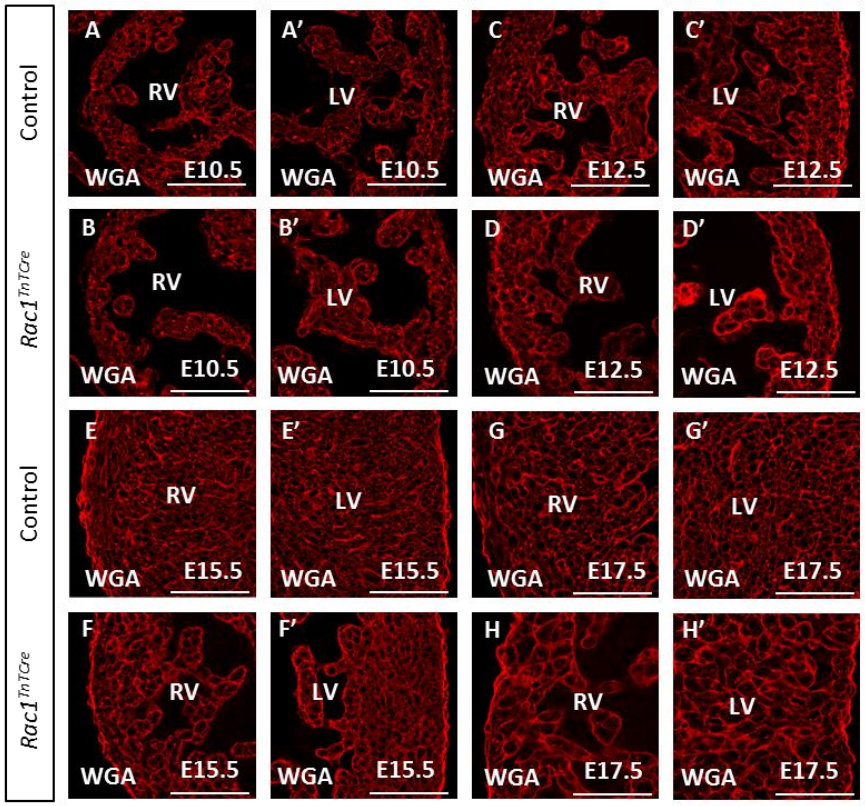
Control
Rac1TnTCre
Control
Rac1TnTCre
A
RV
WGA
E10.5
A'
LV
WGA
E10.5
C
RV
WGA
E12.5
C'
LV
WGA
E12.5
B
RV
WGA
E10.5
B'
LV
WGA
E10.5
D
RV
WGA
E12.5
D'
LV
WGA
E12.5
E
RV
WGA
E15.5
E'
LV
WGA
E15.5
G
RV
WGA
E17.5
G'
LV
WGA
E17.5
F
RV
WGA
E15.5
F'
LV
WGA
E15.5
H
RV
WGA
E17.5
H'
LV
WGA
E17.5

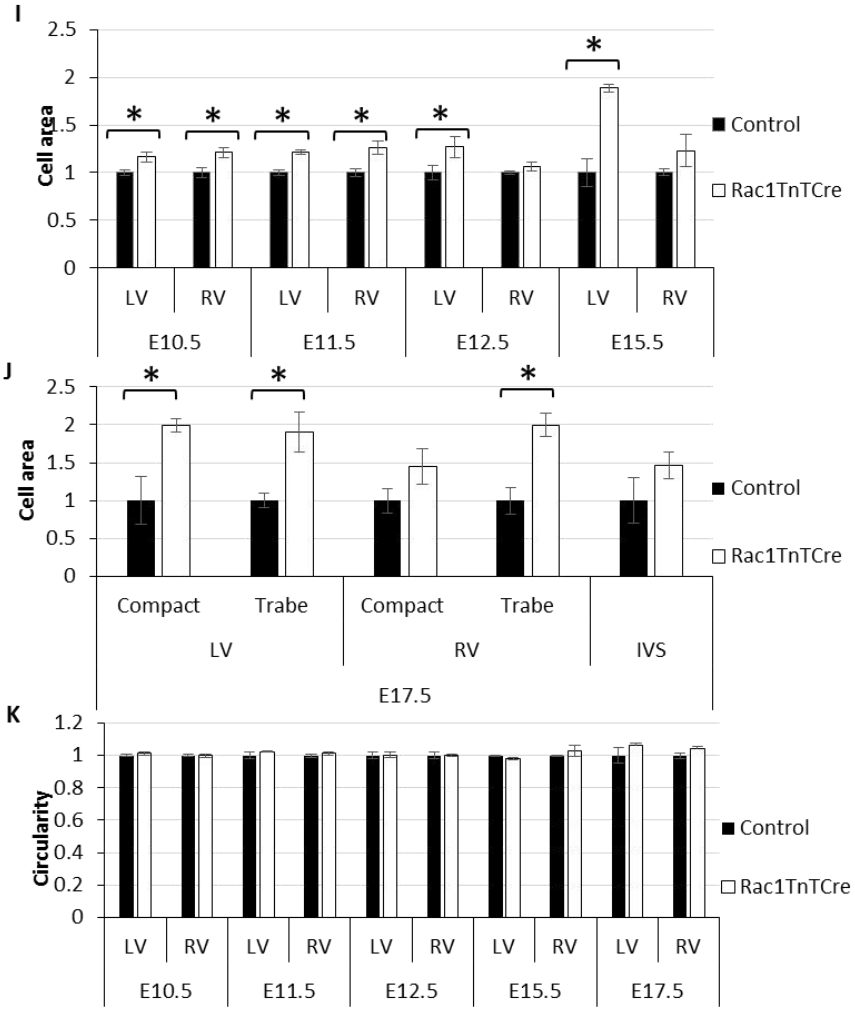
I
Cell area
2.5
2
1.5
1
0.5
0
*
Control
Rac1TnTCre
LV
RV
E10.5
E11.5
E12.5
E15.5
J
Cell area
Compact
Trabe
LV
RV
IVS
E17.5
K
Circularity
1.2
1
0.8
0.6
0.4
0.2
0
E10.5
E11.5
E12.5
E15.5
E17.5

Figure 105: Cardiomyocyte hypertrophy observed from E10.5 in *Rac1*^{TnTCre} hearts.
E10.5-E17.5 control and *Rac1*^{TnTCre} heart sections were stained with wheat germ agglutinin (WGA) to label the cell membrane (**A**-**H**) (n=4). Cardiomyocyte area and shape measurements were carried out using ImageJ. From E10.5 to E15.5 the cardiomyocytes of *Rac1*^{TnTCre} ventricles have significantly increased cell area compared to controls, in both left and right ventricles (**I**) (except at E12.5 the increase in cell area is only significant in the left ventricle of *Rac1*^{TnTCre} hearts, with no differences in the right ventricle). For E17.5 cell area measurements, compact and trabeculae regions were separated. In both ventricles, compact and trabeculae cardiomyocytes had significantly increased cell areas compared to controls (**J**). No differences in cell shape were detected, as calculated by circularity measurements (**K**). LV; left ventricle, RV; right ventricle, IVS; interventricular septum. Scale bars; 100μm. Statistical analysis carried out using a two-way ANOVA, *p<0.05.

5.3.7 Cardiomyocyte adhesion

Cardiomyocytes are attached to adjacent cardiomyocytes through the ICD, which are exclusive to cardiomyocytes (Borg *et al.*, 1983). ICD allow connection and communication between cardiomyocytes and consist of desmosomes, AJ and gap junctions. Via immunostaining, each type of ICD component was investigated in *Rac1*^{TnTCre} hearts, as well as additional cell-cell junctions, TJ.

5.3.7.1 Adherens junctions

The main proteins of the AJ in embryonic cardiomyocytes include N-cadherin and the cytoplasmic proteins, α- and β-catenin, to which thin actin filaments are attached. IF with anti-N-cadherin and anti-β-catenin antibodies revealed expression of both proteins at the cell membrane from E9.5. Expression of N-cadherin in *Rac1*^{TnTCre} ventricles is comparable to controls at E10.5 (n=4) and E11.5 (n=4) (Figure 106A-H). However, by E12.5, N-cadherin expression is visibly reduced in *Rac1*^{TnTCre} ventricles, in both the compact and trabeculae myocardium (n=3) (Figure 106I-L). Expression of β-catenin in *Rac1*^{TnTCre} ventricles is comparable to controls at E10.5 (n-4) (Figure 107A-H). However, at E11.5, β-catenin expression is visibly reduced and disorganised in *Rac1*^{TnTCre} ventricles, in both the compact and trabeculae myocardium (n=4) (Figure 107I-P).

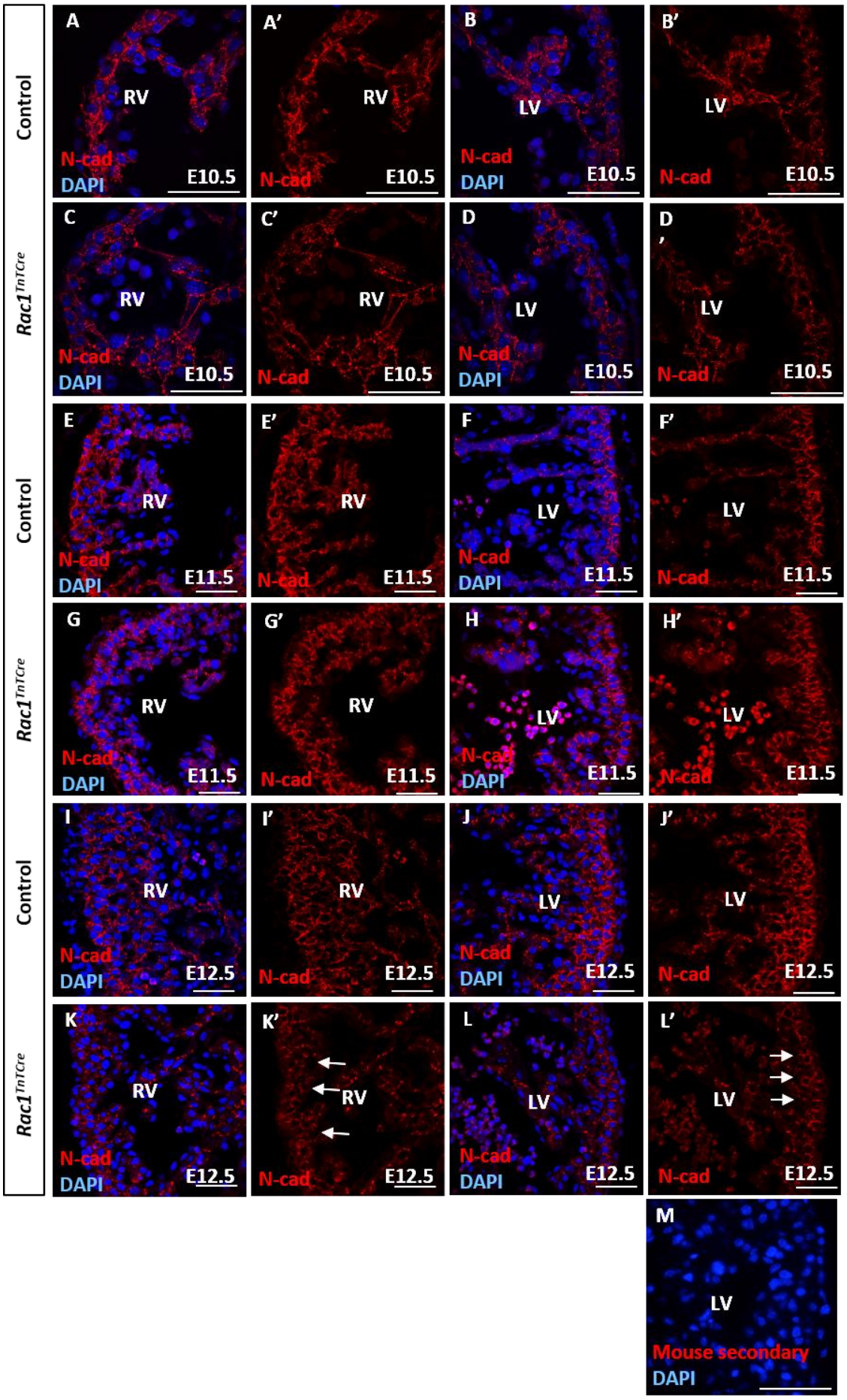
Control
Rac1TnTCre
Control
Rac1TnTCre
Control
Rac1TnTCre
A
A'
B
B'
C
C'
D
D'
E
E'
F
F'
G
G'
H
H'
I
I'
J
J'
K
K'
L
L'
M
RV
LV
N-cad
DAPI
E10.5
E11.5
E12.5
Mouse secondary

Figure 106: Adherens junction protein, N-cadherin is disrupted at E11.5 in *Rac1*^{TnTCre} hearts.

IF staining with anti-N-cadherin antibody in E10.5 and E11.5 control and *Rac1*^{TnTCre} transverse heart sections. Control hearts display strong expression of N-cadherin in the adherens junctions in cardiomyocytes of the developing myocardium at all ages. Expression of N-cadherin in *Rac1*^{TnTCre} ventricles is comparable to controls at E10.5 and E11.5 (n=3). However, by E12.5, N-cadherin expression is visibly disrupted in *Rac1*^{TnTCre} ventricles, in both the compact and trabeculae myocardium (arrows in **K'** and **L'** compared to **I'** and **J'**) (n=3). Secondary only control (**M**). LV; left ventricle, RV; right ventricle. Scale bars; 50μm.

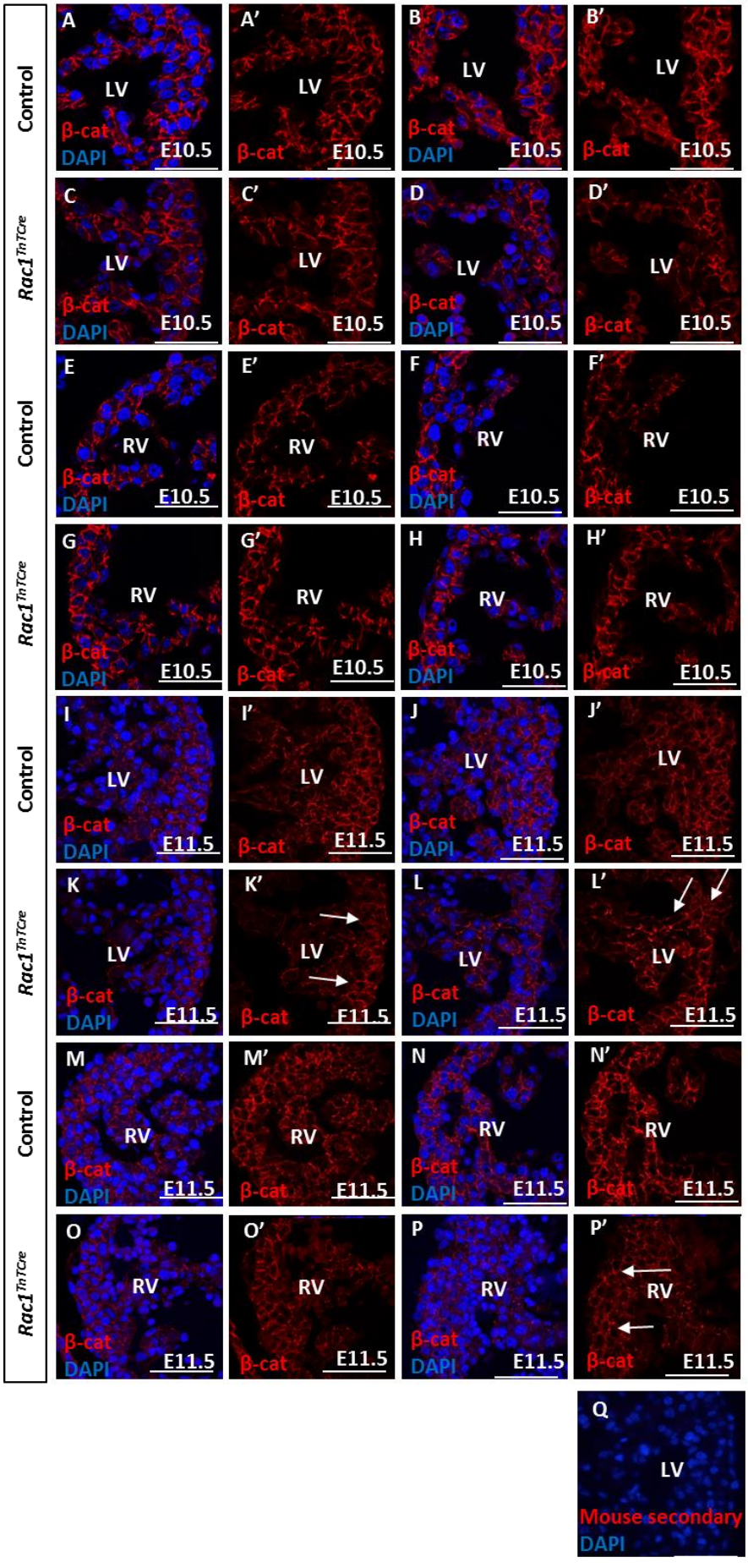
Control
Rac1TnTCre
Control
Rac1TnTCre
Control
Rac1TnTCre
Control
Rac1TnTCre
A
A'
B
B'
C
C'
D
D'
E
E'
F
F'
G
G'
H
H'
I
I'
J
J'
K
K'
L
L'
M
M'
N
N'
O
O'
P
P'
Q
LV
RV
β-cat
DAPI
E10.5
E11.5
Mouse secondary

Figure 107: Adherens junction protein, β-catenin is disrupted in *Rac1*^{TnTCre} hearts.
IF staining with anti-β-catenin antibody in E10.5 and E11.5 control and *Rac1*^{TnTCre} transverse heart sections. Control hearts display strong expression of β-catenin in the adherens junctions in cardiomyocytes of the developing myocardium at all ages. Expression of β-catenin in *Rac1*^{TnTCre} ventricles is comparable to controls at E10.5 (n=3). However at E11.5, β-catenin expression is visibly reduced and disorganised in *Rac1*^{TnTCre} ventricles, in both the compact and trabeculae myocardium (arrows in **K'**, **L'** and **P'** compared to **I', J'** and **N'**) (n=3). Secondary only control (**Q**). LV; left ventricle, RV; right ventricle. Scale bars; 50μm.

5.3.7.2 Gap junctions

Cx-40 is expressed in the common ventricular chamber, particularly in the trabeculae at E9.5. By E10.5 there is strong Cx-40 expression in the LV in both trabeculae and compact layer cardiomyocytes, with no expression in the RV. Cx-40 is expressed in the RV at E11.5 and from E11.5-E14.5 Cx-40 is strongly expressed in the trabeculae layer whilst absent from the compact myocardium (Delorme *et al.*, 1997). From E14.5 onwards, ventricular expression of Cx-40 fades and it is restricted to the atria and His-Purkinje cardiac conduction system (Severs *et al.*, 2001).

Cx-43 is expressed in the compact myocardium cardiomyocytes at E9.5. From E11.5-E14.5 Cx-43 is strongly expressed in the trabeculae layer whilst reduced in the compact myocardium and co-localsises with Cx-40 (Delorme *et al.*, 1997). Neither Cx-40 nor Cx-43 are expressed in the cardiac OFT at any stage of development. In the adult heart, Cx-43 is the main connexin that makes up the gap junctions of the ventricular myocardium and is essential for cell-cell coupling and normal cardiac function (Kolcz *et al.*, 2002; Heinzel *et al.*, 2005; Boengler *et al.*, 2006; Boengler *et al.*, 2007).

IF staining was carried out with an anti-Cx-40 antibody in E9.5 and E10.5 control and *Rac1*^{TnTCre} transverse heart sections. Control and *Rac1*^{TnTCre} hearts display strong Cx-40 in the LV trabeculae at E9.5 and throughout the LV myocardium at E10.5, with some expression in the RV trabeculae (Figure 108). Expression is comparable between control and *Rac1*^{TnTCre} ventricles (n=3) (Figure 108).

IF with an anti-Cx-43 antibody confirmed expression within the ICD at the cell membrane from E9.5. Expression of Cx-43 in *Rac1*^{TnTCre} ventricles is

comparable to controls at E9.5 (n=3) and E10.5 (n=4) (Figure 109A-J). However, by E11.5 Cx-43 expression is disrupted in *Rac1*^{TnTCre} ventricles, in both the compact and trabeculae myocardium (n=4) (Figure 109K-V).

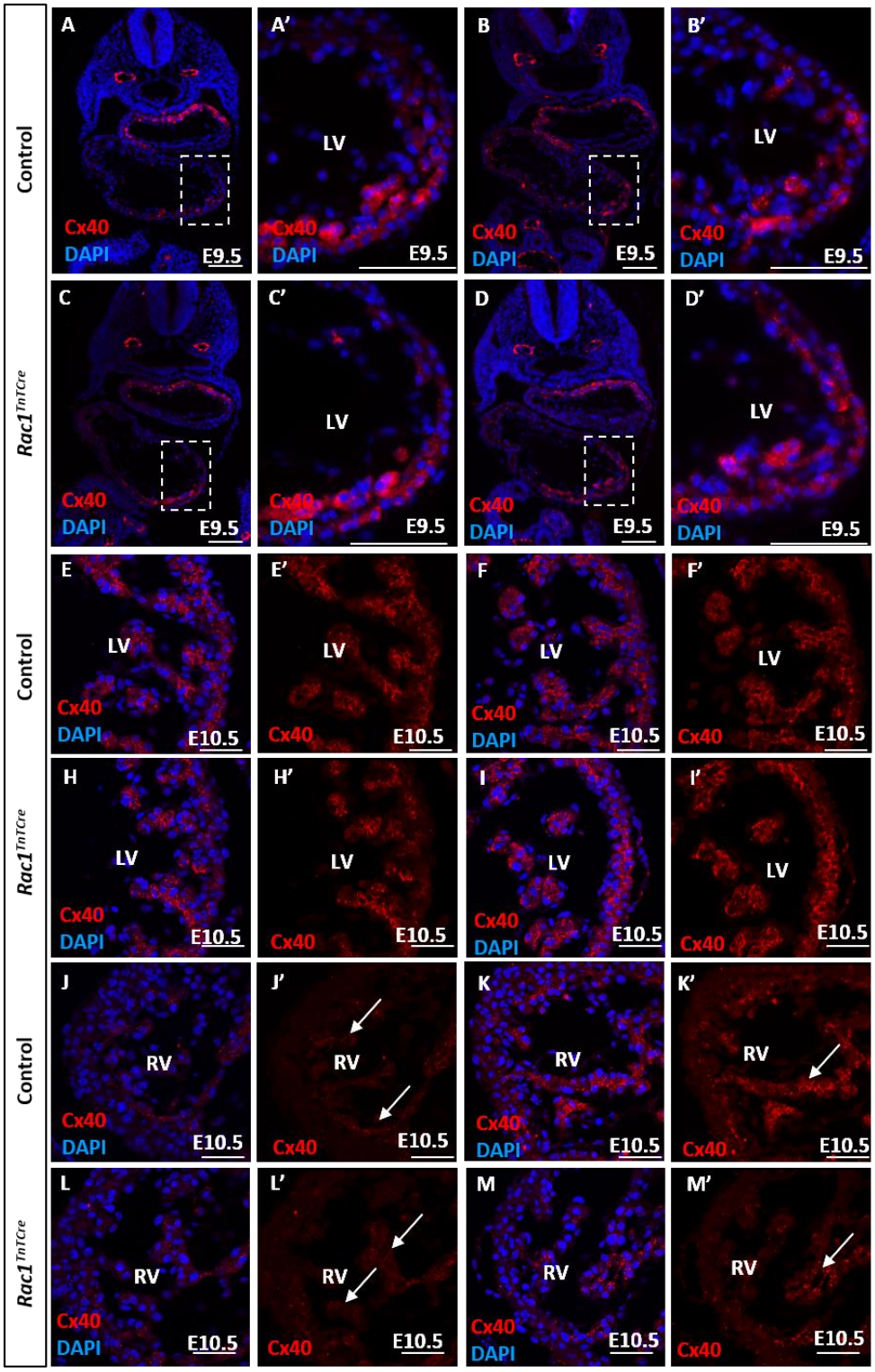

Figure 108: Gap junction protein, Cx-40 is expressed normally in *Rac1*^{TnTCre} hearts.

IF staining with anti-Cx-40 antibody in E9.5 and E10.5 control and *Rac1*^{TnTCre} transverse heart sections. Control and *Rac1*^{TnTCre} hearts display strong Cx-40 expression in the left ventricle trabeculae at E9.5 and throughout the left ventricle myocardium at E10.5 (arrows **A**-**I**) with some expression in the right ventricle trabeculae (arrows in **J**-**M**) (n=3). LV; left ventricle, RV; right ventricle. Scale bars; A-D 200μm, A'-M' 50μm.

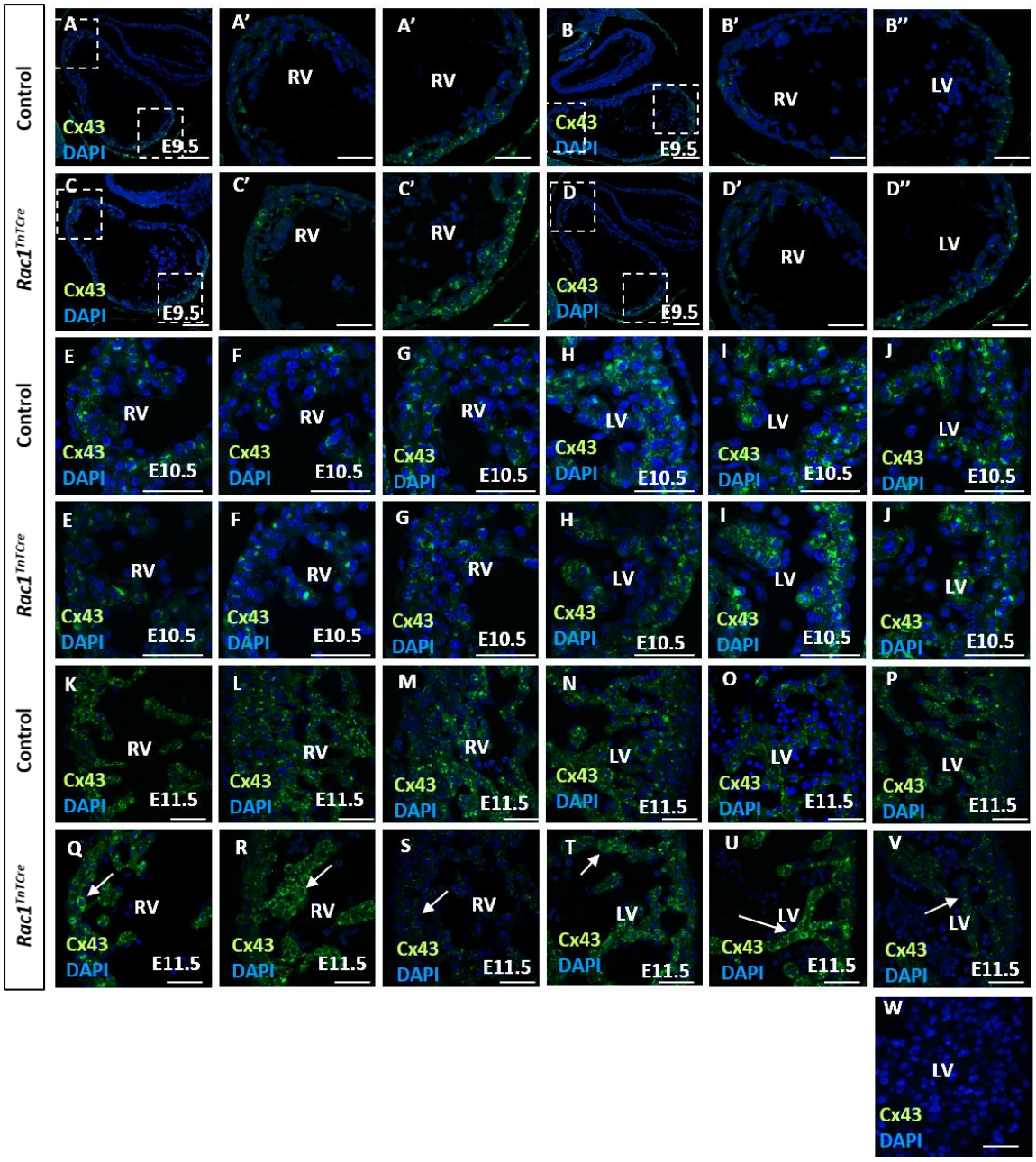

Figure 109: Gap junction protein, Cx-43 expression is disrupted at E11.5 in *Rac1*^{TnTCre} hearts.

IF staining with anti-Cx-43 antibody in E9.5, E10.5 and E11.5 control and *Rac1*^{TnTCre} transverse heart sections. *Rac1*^{TnTCre} hearts display strong expression of Cx-43 in the gap junctions in cardiomyocytes of the developing myocardium at E9.5 and E10.5, which is comparable to controls (**A**-**J**) (n=4). At E11.5, expression of Cx-43 appears disrupted with reduced or odd expression in both the compact and trabeculae myocardium (arrows in **Q**-**V** compared to **K**-**P**) (n=4). Secondary only control (**W**). LV; left ventricle, RV; right ventricle. Scale bars; A-D 100µm, A'-V 50µm.

5.3.7.3 Desmosomes

Desmin is part of the desmosome complex, as well as the main protein in desmin intermediate filaments. IF staining was carried out with an anti-Desmin antibody in E9.5-E12.5 control and *Rac1*^{TnTCre} transverse heart sections. At E9.5 (n=3) and E10.5 (n=4) control and *Rac1*^{TnTCre} hearts display comparably strong expression of Desmin in the cell-cell junctions between cardiomyocytes (Figure 110). At E11.5 (n=4) and E12.5 (n=3), control hearts display strong expression of Desmin in cardiomyocytes of the developing myocardium. Whereas, in *Rac1*^{TnTCre} hearts, Desmin expression is strongest within the trabeculae and appears clumpy, compared to uniform expression throughout the myocardium in control hearts (Figure 111).

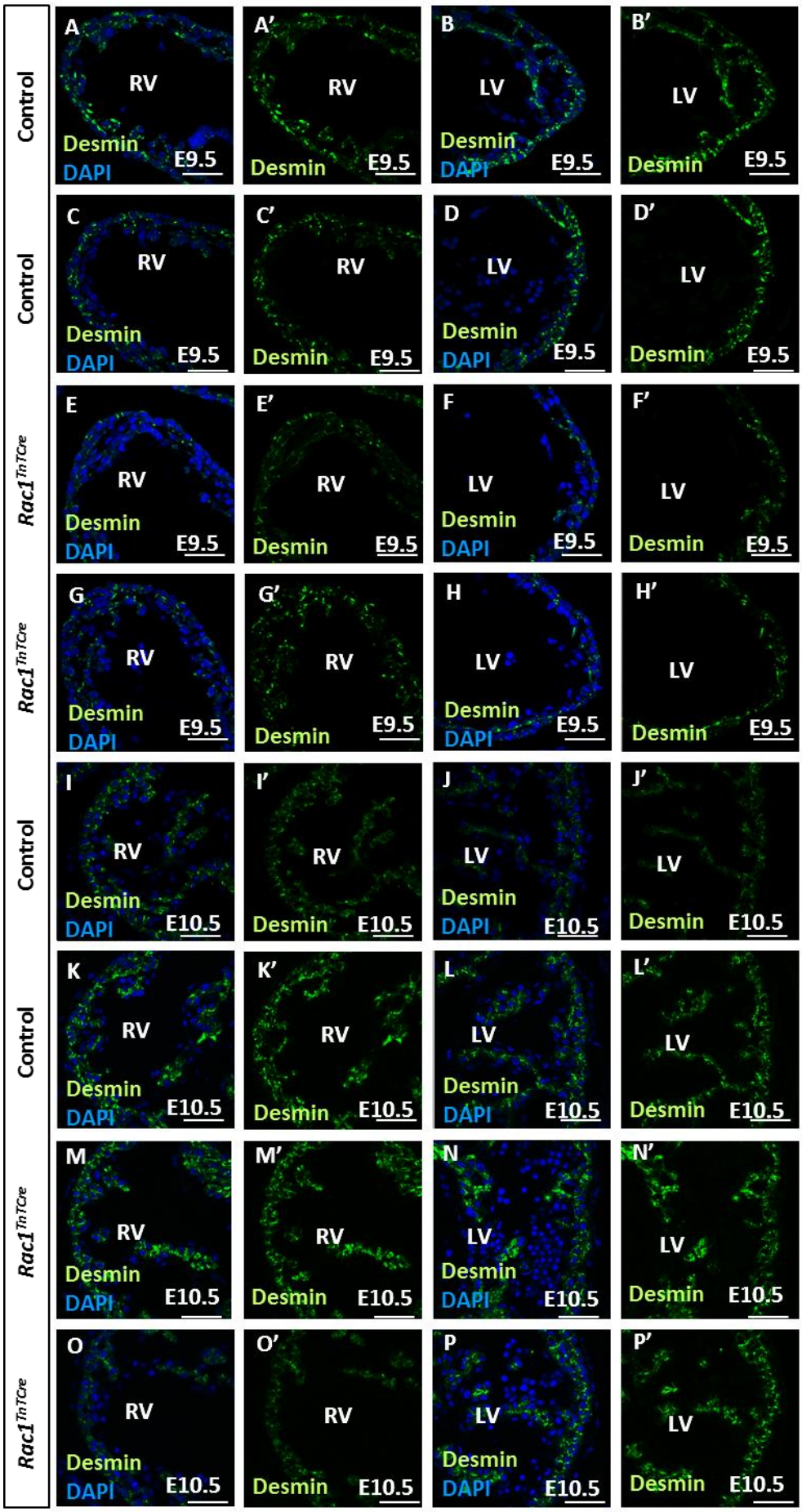
Control
Control
Rac1 TnTCre
Rac1 TnTCre
Control
Control
Rac1 TnTCre
Rac1 TnTCre
A
RV
Desmin
DAPI
E9.5
A'
RV
Desmin
E9.5
B
LV
Desmin
DAPI
E9.5
B'
LV
Desmin
E9.5
C
RV
Desmin
DAPI
E9.5
C'
RV
Desmin
E9.5
D
LV
Desmin
DAPI
E9.5
D'
LV
Desmin
E9.5
E
RV
Desmin
DAPI
E9.5
E'
RV
Desmin
E9.5
F
LV
Desmin
DAPI
E9.5
F'
LV
Desmin
E9.5
G
RV
Desmin
DAPI
E9.5
G'
RV
Desmin
E9.5
H
LV
Desmin
DAPI
E9.5
H'
LV
Desmin
E9.5
I
RV
Desmin
DAPI
E10.5
I'
RV
Desmin
E10.5
J
LV
Desmin
DAPI
E10.5
J'
LV
Desmin
E10.5
K
RV
Desmin
DAPI
E10.5
K'
RV
Desmin
E10.5
L
LV
Desmin
DAPI
E10.5
L'
LV
Desmin
E10.5
M
RV
Desmin
DAPI
E10.5
M'
RV
Desmin
E10.5
N
LV
Desmin
DAPI
E10.5
N'
LV
Desmin
E10.5
O
RV
Desmin
DAPI
E10.5
O'
RV
Desmin
E10.5
P
LV
Desmin
DAPI
E10.5
P'
LV
Desmin
E10.5

Figure 110: Desmosomal protein, Desmin is expressed normally in *Rac1*^{TnTCre} hearts during early heart development.
IF staining with anti-Desmin antibody in E9.5 (n=3) and E10.5 (n=4) control and *Rac1*^{TnTCre} transverse heart sections. Control and *Rac1*^{TnTCre} hearts display strong expression of Desmin in the cell-cell junctions in cardiomyocytes of the developing myocardium at all ages. LV; left ventricle, RV; right ventricle. Scale bars; 50µm.

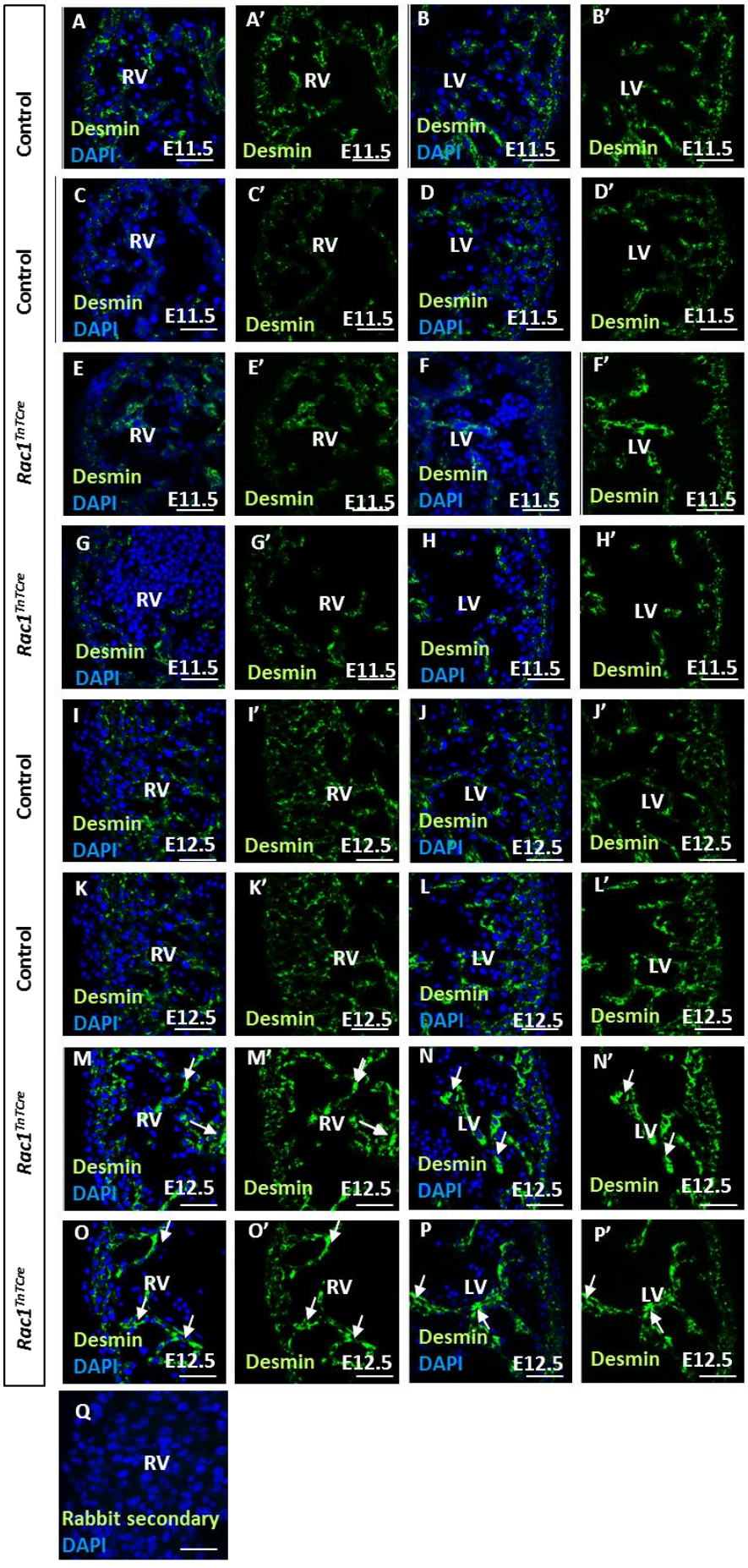
Control
Control
Rac1 TnTCre
Rac1 TnTCre
Control
Control
Rac1 TnTCre
Rac1 TnTCre
A
A'
B
B'
C
C'
D
D'
E
E'
F
F'
G
G'
H
H'
I
I'
J
J'
K
K'
L
L'
M
M'
N
N'
O
O'
P
P'
Q
RV
LV
Desmin
DAPI
E11.5
E12.5
Rabbit secondary

Figure 111: Desmonsomal protein, Desmin expression is altered later in cardiac development in *Rac1^{TnTCre}* hearts.
IF staining with anti-Desmin antibody in E11.5 (n=4) and E12.5 (n=3) control and *Rac1^{TnTCre}* heart sections. Control and *Rac1^{TnTCre}* hearts display strong expression of Desmin in cardiomyocytes of the developing myocardium at all ages. In *Rac1^{TnTCre}* hearts Desmin expression is strong and clumpy within the trabeculae, compared to uniform expression throughout the myocardium in control hearts (arrows in **M**-**P** compared to **I**-**L**). Secondary only control (**Q**). LV; left ventricle, RV; right ventricle. Scale bars; 50μm.

5.3.7.4 Tight junctions

ZO-1 is a crucial part of the TJ and is expressed normally in *Rac1^{TnTCre}* hearts. IF staining with anti-ZO1 antibody was carried out on E9.5 and E10.5 control and *Rac1^{TnTCre}* transverse heart sections. Control and *Rac1^{TnTCre}* hearts display expression of ZO1 within the cell-cell junctions in cardiomyocytes of the developing myocardium (n=4) (Figure 112). Strong expression of ZO1 was seen in cell-cell junctions of the endocardium and epicardium (Figure 112).

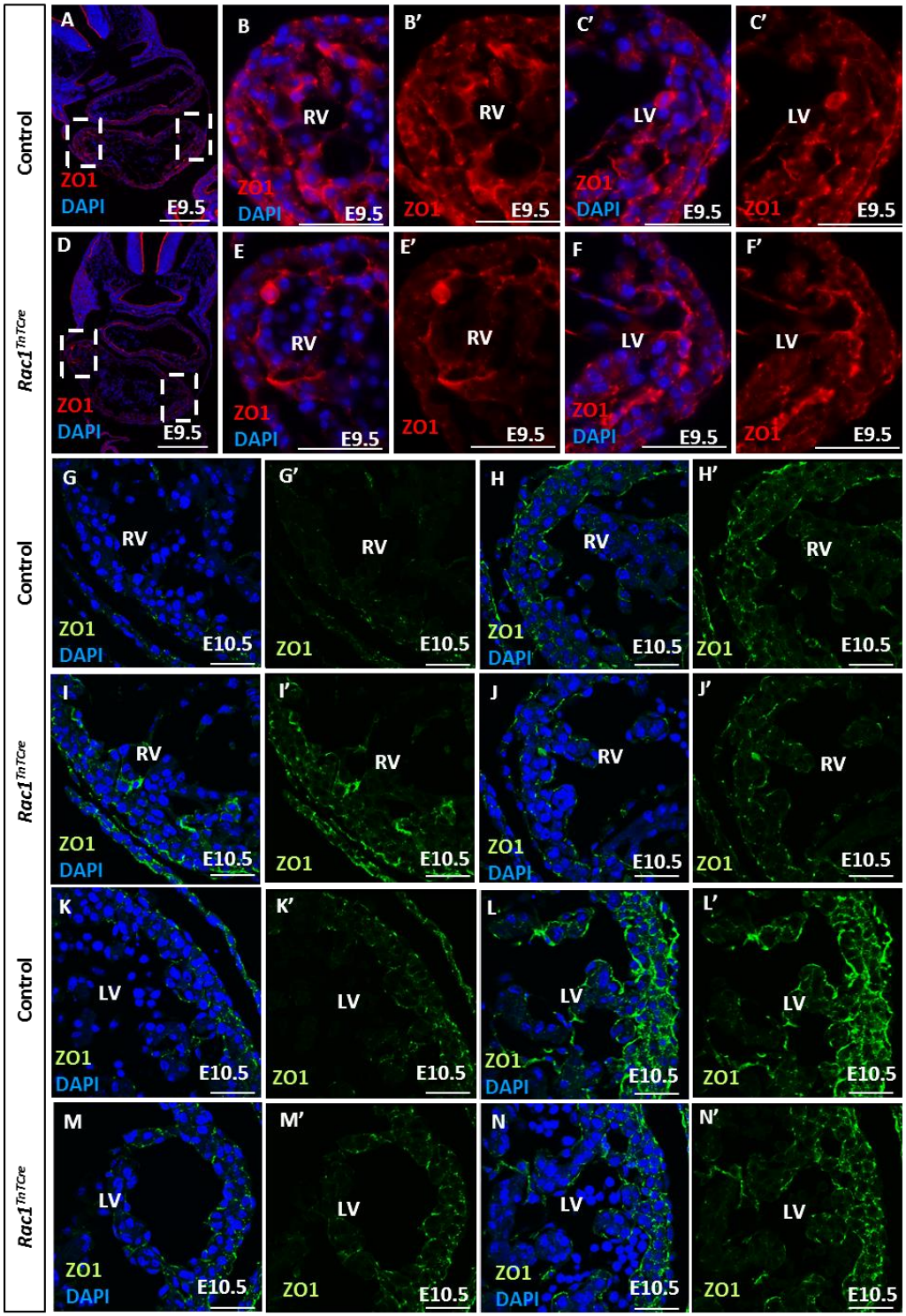

Figure 112: Tight junction protein, ZO1 is expressed normally in *Rac1*^{TnTCre} hearts.

IF staining with anti-ZO1 antibody in E9.5 and E10.5 control and *Rac1*^{TnTCre} transverse heart sections. Control and *Rac1*^{TnTCre} hearts display expression of ZO1 within the cell-cell junctions in cardiomyocytes of the developing myocardium and no differences were observed between them (n=4). Strong expression of ZO1 was seen in cell-cell junctions of the endocardium and epicardium. LV; left ventricle, RV; right ventricle. Scale bars; A and D 200μm, B-C', E-N' 50μm.

5.3.7.5 Microtubules

γ-tubulin is a main component of the MTOC, which are apically expressed polarised cell organelles. IF staining with anti-γ-tubulin antibody was carried out on E11.5 control and *Rac1*^{TnTCre} transverse heart sections. Control and *Rac1*^{TnTCre} hearts display localised expression of γ-tubulin in the MTOCs in cardiomyocytes of the developing myocardium (Figure 113A-G). Quantification of the number of γ-tubulin positive MTOCs did not show any difference between controls and *Rac1*^{TnTCre} hearts (n=4) (Figure 113H).

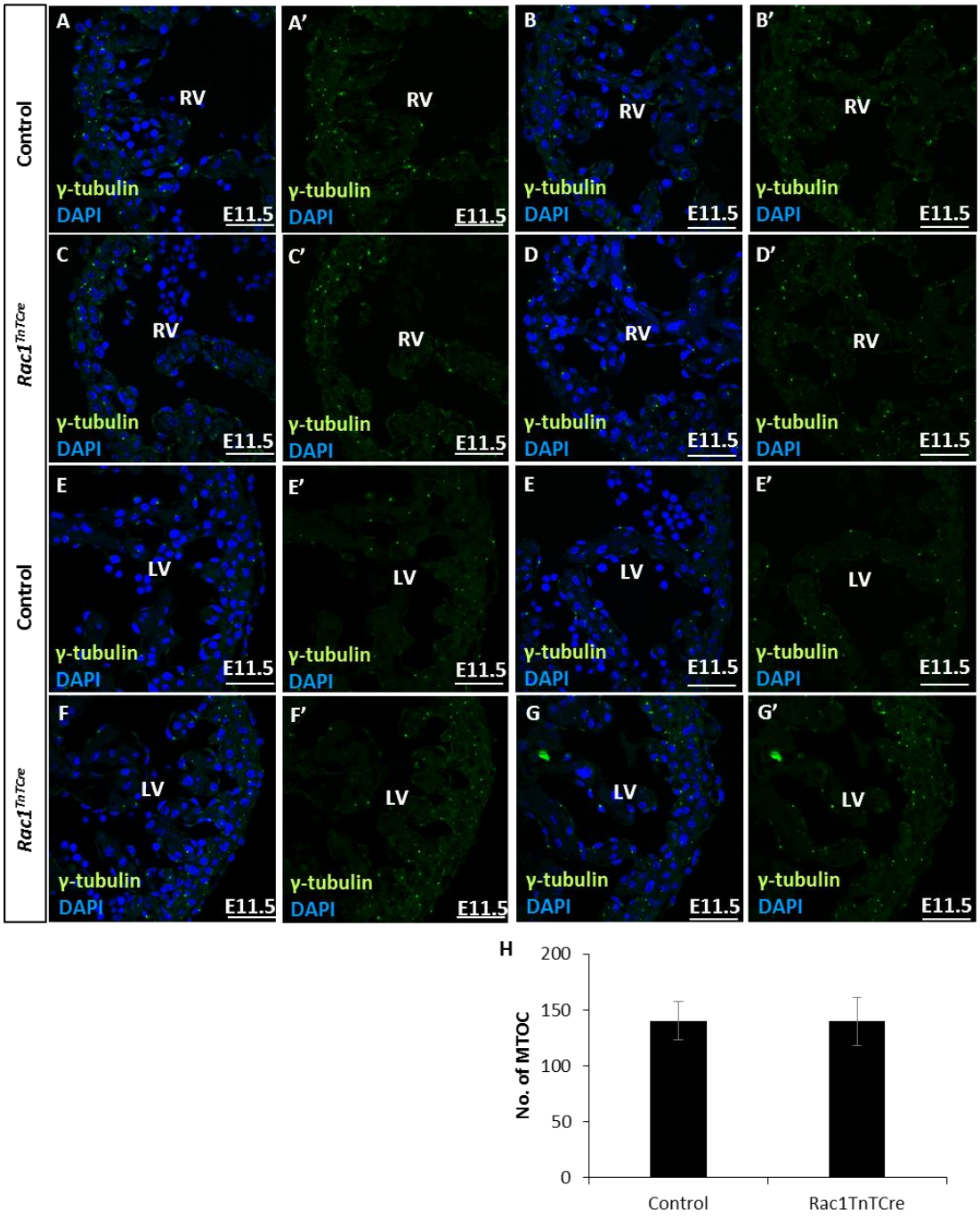

Figure 113: MTOC protein, γ-tubulin is expressed normally in *Rac1*^{TnTCre} hearts.

IF staining with anti-γ-tubulin antibody in E11.5 control and *Rac1*^{TnTCre} transverse heart sections. Control and *Rac1*^{TnTCre} hearts display localised expression of γ-tubulin in the MTOCs in cardiomyocytes of the developing myocardium (n=4). Quantification of the number of γ-tubulin positive MTOCs did not show any difference between controls and *Rac1*^{TnTCre} hearts. LV; left ventricle, RV; right ventricle. Scale bars; 50μm. Statistical analysis carried out using the unpaired t-test.

These data suggest that cell polarity and adhesion are disrupted in *Rac1*^{TnTCre} hearts. However, this disruption was observed at E11.5 and older stages of embryonic heart development, at a time when the compact myocardial and trabeculae defects are already apparent. This implies that the polarity and adhesion defects occur secondary to an unknown primary defect within the cardiomyocytes. Possible causes of this defect include altered gene expression and abnormal signalling within the myocardium and are investigated in Chapter 5 Sections 5.3.8 and 5.3.9, respectively.

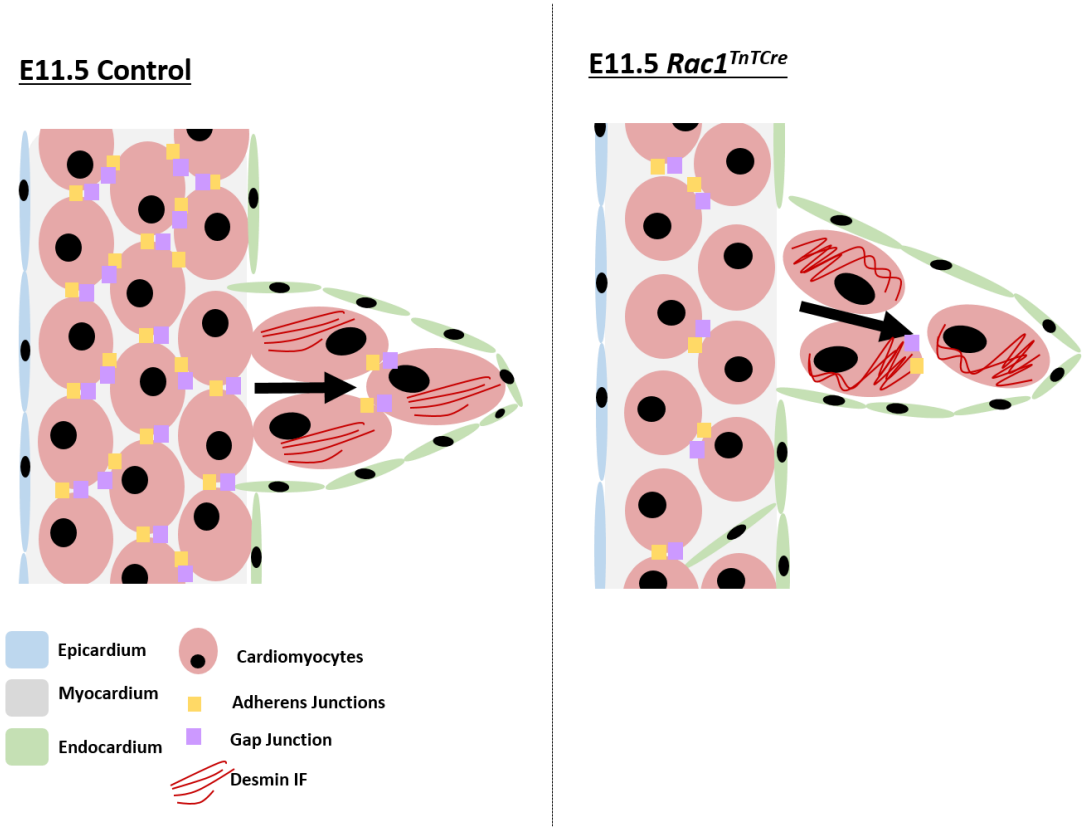

Figure 114: *Rac1*^{TnTCre} cardiomyocytes display disrupted cell-cell adhesion and desmin intermediate filaments from E11.5.
Proteins of both AJ (yellow) and Gap junctions (purple) show reduced ICD expression at E11.5 in *Rac1* deficient cardiomyocytes and Desmin intermediate filaments (red) appear clumpy in the trabecular layer of *Rac1*^{TnTCre} hearts at E11.5.

5.3.8 Gene expression in Rac1^{TnTCre} *hearts*

As discussed in Chater 5 Section 5.3.1 embryonic deletion of *Rac1* in cardiomyocytes disrupts the development of the myocardium, particularly the formation and maturation of the trabeculae. The cardiomyocyte cytoskeleton

appears immature and trabeculae maturation markers are aberrantly expressed. However, the mechanism of how the lack of *Rac1* leads to these disruptions remains unknown. Rac1 has many cellular functions including regulation of pathways controlling gene transcription, such as NFkB, JNK and MAPK signalling pathways (Perona *et al.*, 1997; Bosco *et al*., 2009).

As a result, investigation of transcriptional changes in *Rac1*^{TnTCre} hearts using a microarray was carried out. Changes in gene expression would be expected to occur before phenotypic changes. Since myocardial defects in *Rac1*^{TnTCre} hearts can be detected from E11.5, E10.5 was selected to investigate gene level changes. RNA was extracted from E10.5 *Rac1*^{TnTCre} hearts and sent to Aros for analysis on an Affymetrix Mouse Transcriptome 1.0 microarray chip (n=3, 4 hearts pooled per sample). The data was analysed using the Transcriptome analysis console v3.0. Genes with a significant fold change of 1.5 or more are listed in Table 29.

Gene Symbol	Gene	Fold Change	P-value	Function
Afp	alpha fetoprotein	6.53	0.003	Foetal form of plasma albumin
Apob	apolipoprotein B	2.61	0.044	Component of LDL in plasma
Apoa1	apolipoprotein A-I	1.85	0.040	Component of HDL in plasma
Sfrp1	secreted frizzled-related protein 1	1.73	0.015	Modulator of Wnt signalling
Papss2	3-phosphoadenosine 5-phosphosulfate synthase 2	1.72	0.017	Involved in sulphation
Trf	transferrin	1.67	0.004	Plasma glycoprotein, binds iron
Ttr	transthyretin	1.66	0.028	Plasma protein , transports thyroxine and retinol
Cyr61/ Ccn1	cysteine rich protein 61	1.59	0.002	ECM-associated signalling
LOC101055909	protein transport protein Sec61 subunit beta-like	1.56	0.016	Necessary for protein translocation in the ER
Gm3893	predicted gene 3893	-1.53	0.027	-
Gm15171	predicted gene 15171	-1.53	0.019	-
Igkv17-121	immunoglobulin kappa variable 17-121	-1.61	0.012	-
Gm13432	predicted gene 13432	-1.74	0.031	-

Table 29: Differentially expressed genes in E10.5 *Rac1^{TnTCre}* hearts vs controls.
Microarray analysis of E10.5 control and *Rac1^{TnTCre}* hearts was carried out (n=3, 4 hearts pooled per sample). Genes with a significant fold change of 1.5 or more ($p<0.05$).

In order to validate the gene changes detected in *Rac1^{TnTCre}* hearts, qPCR analysis was carried out on the RNA used for microarray analysis and additional RNA from E10.5 single heart samples. cDNA was synthesised from the RNA and primers were designed to amplify a region of the gene, spanning exons. Three genes were selected for validation via qPCR; alphafetoprotein (*Afp*), secreted frizzled related protein 1 (*Sfrp1*) and cysteine rich protein 61 (*Ccn1*). *Afp* had the largest fold change of 6.53, and therefore represented a good target for validation. Additional genes, *Sfrp1* and *Ccn1* are expressed in the developing heart, associated with the ECM (Jaspard *et al.*, 2000; Mo and Lau, 2006). qPCR analysis using the cDNA from the microarray samples showed *Afp*, *Sfrp1* and *Ccn1* were all significantly increased in *Rac1^{TnTCre}* hearts compared to controls (n=3, 4 hearts pooled) (Figure 115). However, in the additional E10.5 single hearts, the expression of all three genes showed a trend

for increase but were not significant (n=6, single hearts) (Figure 115). These results could be due to variability amongst the single E10.5 hearts, such as slight differences in developmental stage/somite number. Pooling of 4 hearts together averages any potential outliers and allows subtle gene expression changes to be detected. Statistical power calculations suggest that the single E10.5 heart experiment is underpowered and may benefit from additional samples to assign statistical significance to the trend for increased expression of Afp, Sfrp1 and Ccn1 in *Rac1*^{TnTCre} hearts. However, the large number of extra samples required to demonstate these differences is both impractible and unethical.

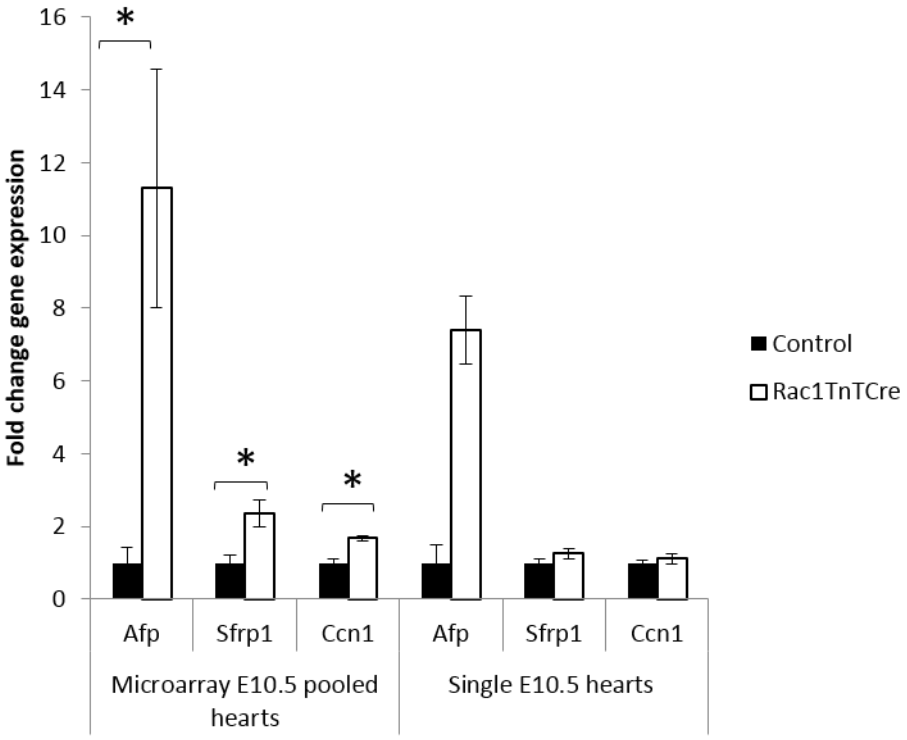

Figure 115: qPCR analysis of microarray target gene expression in E10.5 *Rac1*^{TnTCre} hearts.
qPCR analysis of microarray E10.5 pooled hearts; *Afp*, *Sfrp1* and *Ccn1* were all significantly increased in *Rac1*^{TnTCre} hearts compared to controls (n=3, 4 hearts pooled). However, in the additional E10.5 single hearts, the expression of all 3 genes showed a trend for increase but were not significant (n=6, single hearts). Significance determined by unpaired t-test. *P<0.05. Statistical power calculations suggest the single E10.5 heart experiment is underpowered and may benefit from additional samples to assign statistical significance to the trend for increased expression of Afp, Sfrp1 and Ccn1 in *Rac1*^{TnTCre} hearts. Expression normalised to housekeeping gene *Gapdh*. E; embryonic day.

Since the qPCR results using additional samples were inconclusive, slide *in situ* hybridisation was carried out to investigate gene expression patterns within the heart. All the known microarray targets were included in this analysis. *In situ* probes were designed to hybridise to a 400bp region of RNA. E10.5 embryos were dissected and processed in RNA free conditions. Hybridisation was carried out on control E10.5 heart sections to determine expression within the heart (Figure 116). No expression of *Afp* (Figure 116A), *Apoa1* (Figure 116B), *Apob* (Figure 116C), *Papss2* (Figure 116D), *Trt* (Figure 116E) or *Ttr* (Figure 116F) was shown within the heart, therefore no further analysis of these genes was carried out.

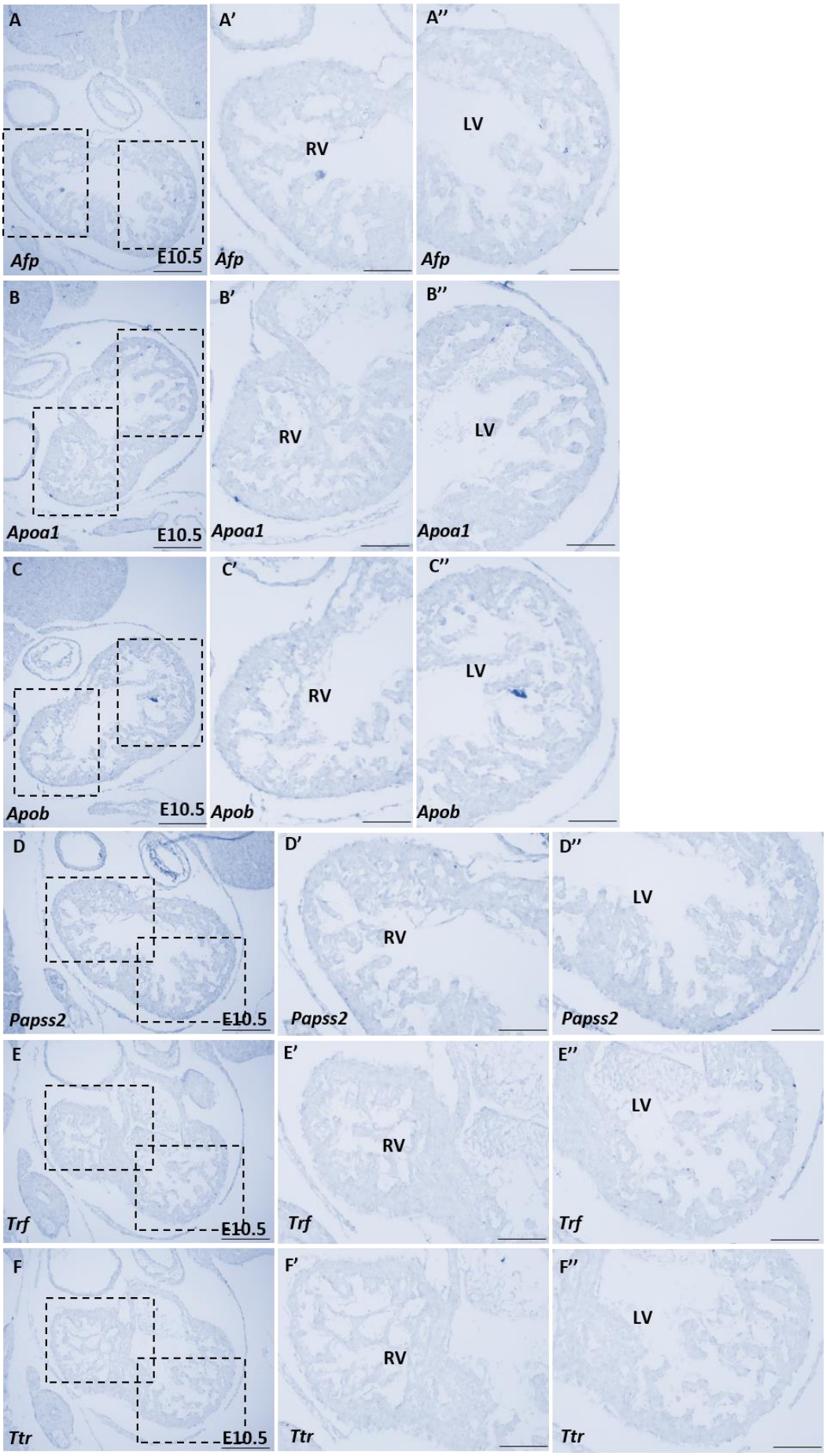
A
A'
A''
RV
LV
Afp
E10.5
B
B'
B''
Apoa1
C
C'
C''
Apob
D
D'
D''
Papss2
E
E'
E''
Trf
F
F'
F''
Ttr

Figure 116: In situ hybridisation of microarray targets in control E10.5 heart sections.
Slide *in situ* hybridisation using antisense probes for *Afp* (**A**), *Apoa1* (**B**), *Apob* (**C**), *Papss2* (**D**), *Trf* (**E**) and *Ttr* (**F**). No expression of any probe was observed within the myocardium of the ventricles at E10.5. E; embryonic day, LV; left ventricle, RV; right ventricle. Scale bars; A-F 200μm, A'-F'' 100μm.

Since expression of *Sfrp1* and *Ccn1* within the heart has previously been published (Jaspard *et al.*, 2000; Mo and Lau, 2006), expression of these genes in $Rac1^{TnTCre}$ hearts was investigated. Slide *in situ* hybridisation was carried out on control and $Rac1^{TnTCre}$ E10.5 heart sections (n=3) using probes designed to hybridise to a 400bp region of RNA. Images were taken and analysed. In controls, *Sfrp1* is expressed uniformly within the ventricular myocardium (Figure 117), whereas *Ccn1* shows punctate expression within the ventricular myocardium (Figure 118). $Rac1^{TnTCre}$ hearts appear to have increased expression of both *Sfrp1* and *Ccn1* within the myocardium (Figure 117 and Figure 118 respectively). Expression of both transcripts is comparable between left and right ventricles (Figure 117 and Figure 118).

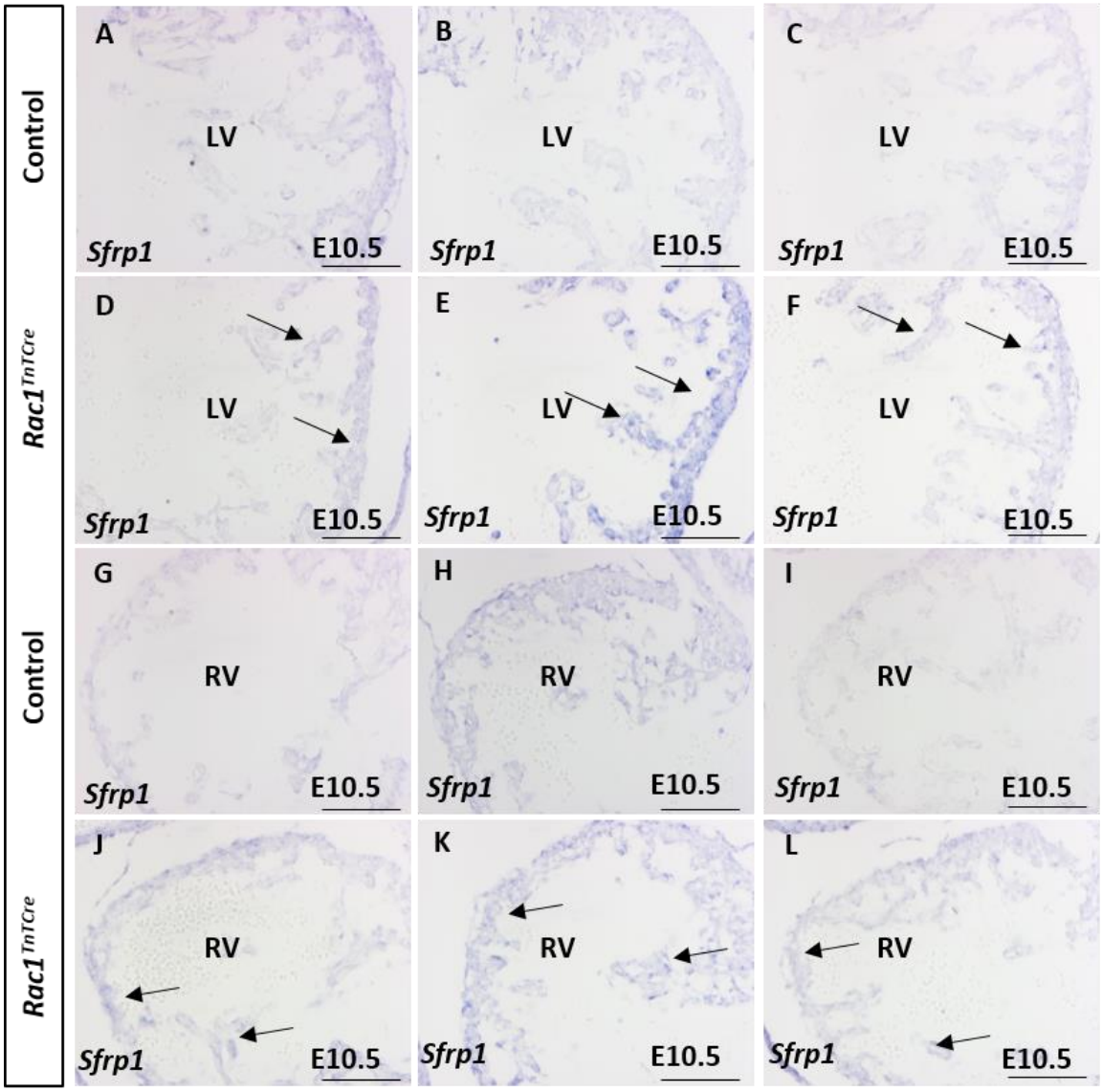

Figure 117: *In situ* hybridisation of *Sfrp1* probe in control and *Rac1*^{TnTCre} E10.5 heart sections.

Slide *in situ* hybridisation using *Sfrp1* antisense probe shows strong uniform expression within the myocardium of the ventricles at E10.5 (**A**-**C**, **G**-**I**). Expression of *Sfrp1* appears to be upregulated in *Rac1*^{TnTCre} hearts (**D**-**F**, **J**-**L**) (n=3). Expression between left and right ventricles is comparable in both controls and in *Rac1*^{TnTCre} hearts. E; embryonic day, LV; left ventricle, RV; right ventricle. Scale bars; 100µm.

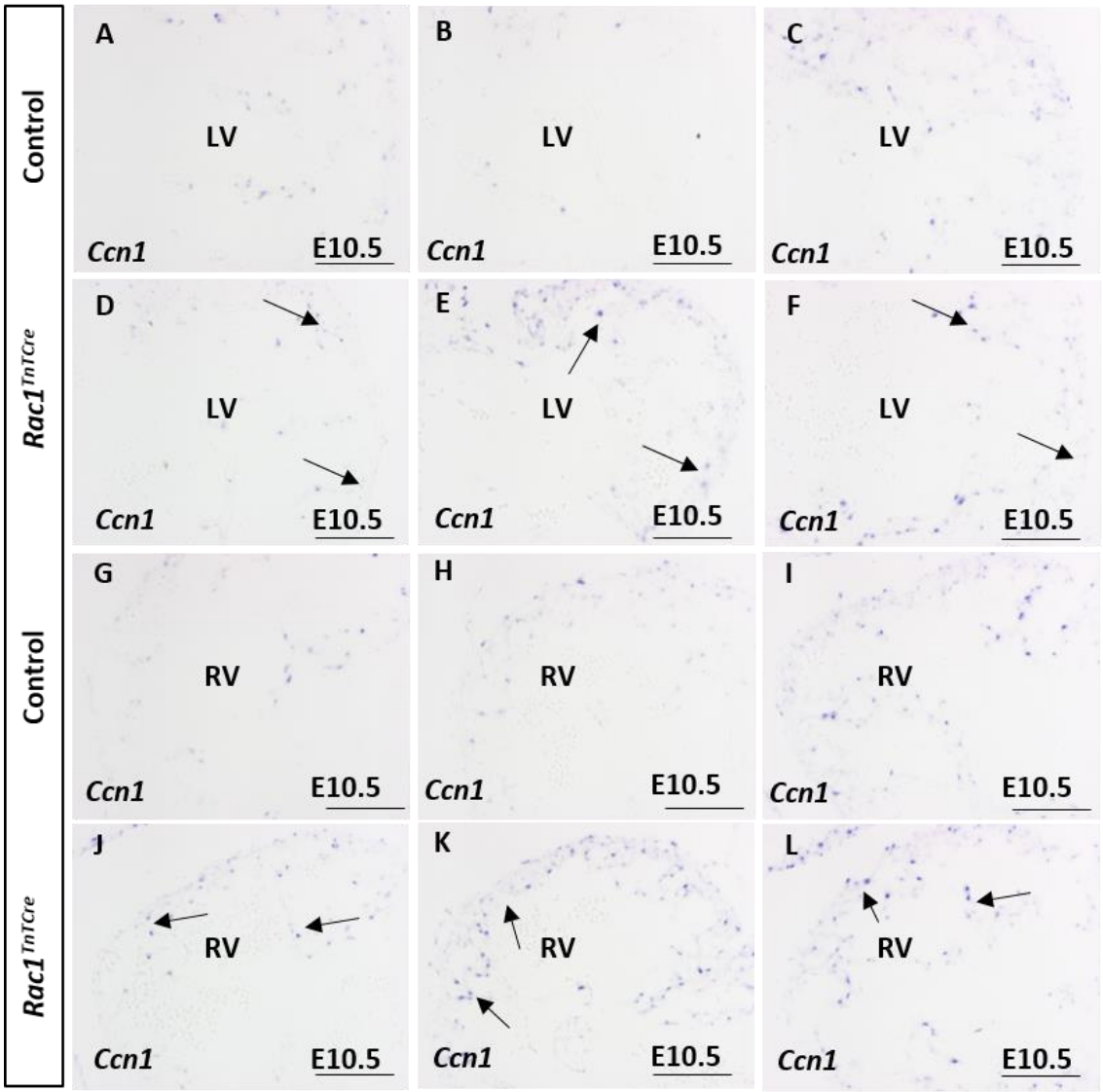

Figure 118: *In situ* hybridisation of *Ccn1* probe in control and *Rac1*^{TnTCre} E10.5 heart sections.
Slide *in situ* hybridisation using *Ccn1* antisense probe shows strong punctate expression within the myocardium of the ventricles at E10.5 (**A**-**C**, **G**-**I**). Expression of *Ccn1* appears to be upregulated in *Rac1*^{TnTCre} hearts (**D**-**F**, **J**-**L**) (n=3). Expression between left and right ventricles is comparable in both controls and in *Rac1*^{TnTCre} hearts. E; embryonic day, LV; left ventricle, RV; right ventricle. Scale bars; 100µm.

Furthermore, in order to determine if the protein expression correlated with the transcript expression IF staining using antibodies against Sfrp1 and Ccn1 on E10.5 control and *Rac1*^{TnTCre} transverse sections was carried out. Ccn1 expression appears to be localised to both the endocardium and epicardium, with little to no expression within the ventricular myocardium (Figure 119A-D). This is in contrast to the mRNA expression pattern shown by *in-situ*

hybridisation (Figure 118). Sfrp1 appears to be expressed in all three layers of the developing myocardium, with strongest expression in the epicardium (Figure 119E-J), correlating to the mRNA expression pattern shown by *in situ* hybridisation (Figure 117). Both Ccn1 and Sfrp1 protein expression appears comparable in *Rac1*^{TnTCre} ventricles compared to controls (Figure 119).

Through X-gal staining Mo *et al.* show speckled expression of *Ccn1* within the compact myocardium similar to our *in situ* hybridisation analysis (Figure 118), however they also show intense staining on *Ccn1* within the AV cushions and OFT cushions at E10.5 (Mo and Lau, 2006). From Figure 119 Sfrp1 is shown to be strongly expressed within the myocardium at E10.5, which is in support of previous published data showing strong myocardial expression through antibody staining at E9.5 and E11.5 (Jaspard *et al.*, 2000).

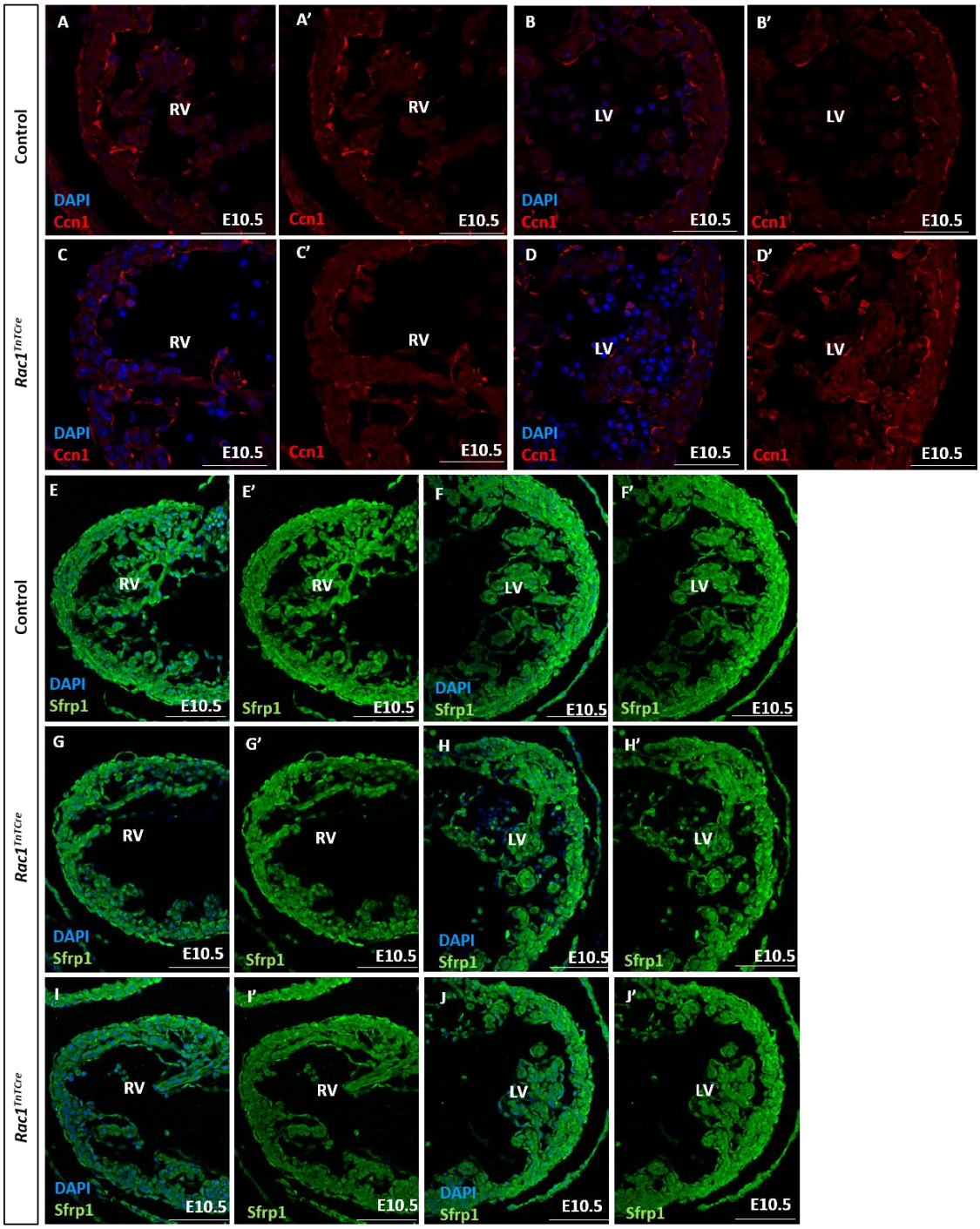

Figure 119: Ccn1 and Sfrp1 IF staining of E10.5 control and *Rac1*^{TnTCre} transverse sections.

Ccn1 expression appears to be localised to both the endocardium and epicardium, with little to no expression within the ventricular myocardium (**A**-**D**). Sfrp1 appears to be expressed in all three layers of the developing myocardium and is strongest in the epicardium (**E**-**J**). Both Ccn1 (**C**-**D** compared to **A**-**B**) and Sfrp1 (**G**-**J** compared to **E**-**F**) protein expression appears comparable in *Rac1*^{TnTCre} ventricles compared to controls (n=4). Scale bars; A-D 100µm, E-J 50µm.

The microarray analysis reveals several changes in gene expression in *Rac1*^{TnTCre} hearts compared to controls. Investigation of expression of these genes in the heart excluded all but two genes from further analysis. Expression of *Sfrp1* and *Ccn1* appeared to be increased in *Rac1*^{TnTCre} hearts as shown by slide *in situ* hybridisation. However, Sfrp1 and Ccn1 protein expression appeared unaltered in *Rac1*^{TnTCre} hearts using IF. Furthermore, the microarray results could not be confirmed in additional E10.5 heart samples by qPCR. These results suggest that the small changes in gene expression initially detected in *Rac1*^{TnTCre} hearts may be due to the nature of microarray data analysis and the associated false positve rate (Hariharan, 2003). This suggests that that deletion of *Rac1* in cardiomyocytes has little effect on gene expression, however due to variation in RNA samples it is possible that significant differences may not have been detected.

5.3.9 The endocardium is disrupted in Rac1 myocardial mutants

The endocardium is essential for normal myocardial development and interactions between the endocardium and myocardium act to regulate processes such as cardiomyocyte proliferation, trabeculation and coronary vessel formation. As shown in Section 5.3.3 proliferation and cell number is unchanged in *Rac1*^{TnTCre} mutants, however trabeculae formation is disrupted. Therefore, it was hypothesised that myocardial-endocardium interactions may be disrupted leading to defective trabeculation, and that coronary vessel formation may also be disrupted in *Rac1* mutant hearts. To assess this hypothesis, the role of the endocardium and coronary vessel formation was investigated in *Rac1*^{TnTCre} hearts.

To visualise the endocardium in *Rac1*^{TnTCre} hearts, IF staining was carried out using antibodies against endocardial/endothelial markers, CD31 and endomucin. CD31 is expressed in all endothelial cells, including endocardial cells, whereas endomucin is restricted to endocardial cells and some coronary vein endothelial cells during embryonic cardiac development. E10.5 to E17.5 *Rac1*^{TnTCre} embryos were dissected and processed for immunostaining.

At E12.5, CD31 expression can be seen in the endocardial cells, with the highest expression in the endocardium at the base of the trabeculae, as well as in the endothelium of sub-epicardial veins (Figure 120A). There is little to no

expression of CD31 within the compact myocardium at E12.5. By E15.5, CD31 marks the endothelium of the developing coronary vessels and microvasculature within the compact myocardium, but also remains expressed in the endocardial cells covering the trabeculae (Figure 120C). The distribution of CD31-positive endothelial cells appeared comparable to controls at E12.5 in the *Rac1*^{TnTCre} hearts (Figure 120, B compared to A). However, at E15.5 there was a marked reduction in the number of CD31-positive endothelial cells within the compact myocardium in *Rac1*^{TnTCre} hearts compared to controls (Figure 120, D compared to C). No large CD31-positive coronary vessels were detected in *Rac1*^{TnTCre} hearts and the CD31-positive microvascular in the compact layer of E15.5 *Rac1*^{TnTCre} hearts appeared reduced. Additionally, the vessels that have formed appeared to be developing in aberrant directions compared to controls (Figure 120, D compared to C). In control hearts, the CD31-positive endocardial cells were uniformly distributed around the trabeculae, however in *Rac1*^{TnTCre} hearts, the CD31-positive endocardial cells appeared to be more concentrated at the base of the trabeculae (Figure 120, D compared to C).

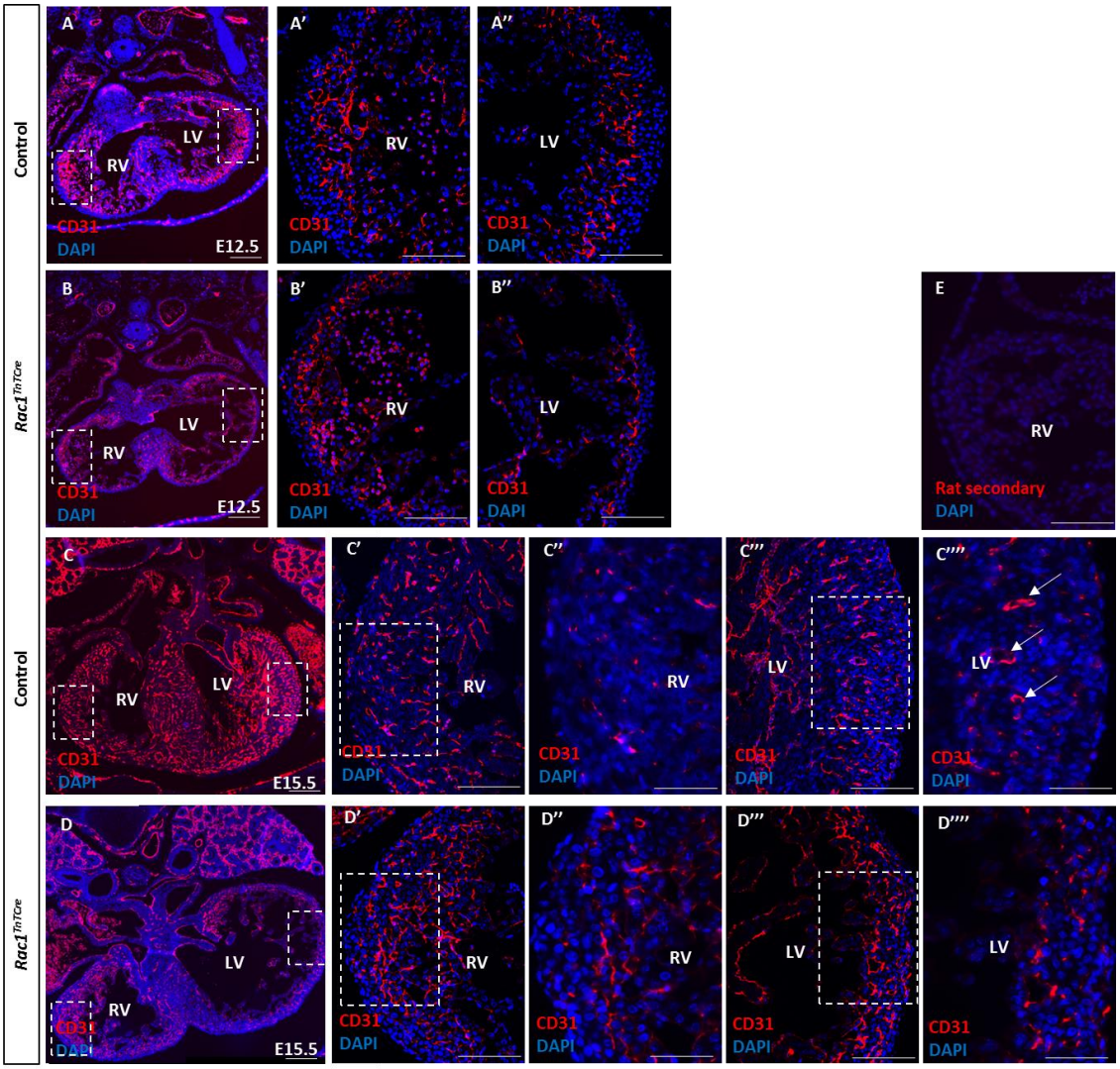

Figure 120: CD31 IF staining of E12.5 and E15.5 control and *Rac1*^{TnTCre} transverse sections.
The pattern of CD31+ endothelial cells is disrupted in the *Rac1*^{TnTCre} hearts (**B** and **D**) compared to controls (**A** and **C**), with less CD31+ vessels forming in the mutants compared to controls and more endothelial cells at the base of the trabeculae in the mutants compared to controls (n=4). Secondary only control (**E**). LV; left ventricle, RV; right ventricle. Scale bars; A-D 200μm, A'-D''' 100μm, C''-D'''' 50μm.

From E10.5 to E17.5, endomucin-positive endocardial cells line the trabeculae and highlight the distinct regions of the compact and trabeculae myocardium (Figure 121 and Figure 122). At E10.5 and E11.5, trabeculae form uniformly along the compact myocardium, and at the base of the trabeculae endocardial cells project into the compact myocardium (Figure 121). It has previously been suggested that these cells migrate into the compact myocardium and contribute to coronary vessel endothelium, however sufficient evidence is lacking (Wu *et*

al., 2012) and recent data suggests this may not be the case (Zhang *et al.*, 2016). Compared to controls, in *Rac1*^{TnTCre} hearts the number of these projecting endocardial cells at the base of trabeculae is significantly fewer at E11.5 (arrows in Figure 121G-L) and shows a trend at E10.5 (arrows in Figure 121A-F). In controls, endocardial cells at the base of the trabeculae project into the compact layer in between individual cardiomyocytes. As previously mentioned, in *Rac1*^{TnTCre} hearts this was observed less often and occasionally endocardial cells appeared completely surrounded in compact myocardium (arrows in Figure 121O-P). This mutant phenotype was continued in E12.5 *Rac1*^{TnTCre} hearts, when the compact myocardial wall is significantly thinned and the border between compact and trabeculae myocardial is less well defined (Figure 122A-B). In *Rac1*^{TnTCre} hearts, the trabeculae appear to undergo compensatory remodelling between E12.5 to E17.5 (Figure 122A-F). This is striking at E15.5 (Figure 122C-D) and E17.5 (Figure 122E-F), with endomucin positive cells appearing ‘trapped’ within the compact myocardial layer (arrows in Figure 122, D’’ and F’’). Additionally, the difference between the right and left ventricle walls from E15.5 onwards suggests there is differential remodelling between the two ventricles in mutant hearts. The RV remains thin with relatively large numbers of trabeculae compared to controls (Figure 122, D’ and F’), whereas the LV thickens and becomes smooth on the inner surface with relatively few trabeculae (Figure 122, D’’ and F’’). However, this thickened left ventricular wall is less densely packed than in controls and contains ‘trapped’ endomucin positive endocardial cells arrows in Figure 122, D’’ and F’’.

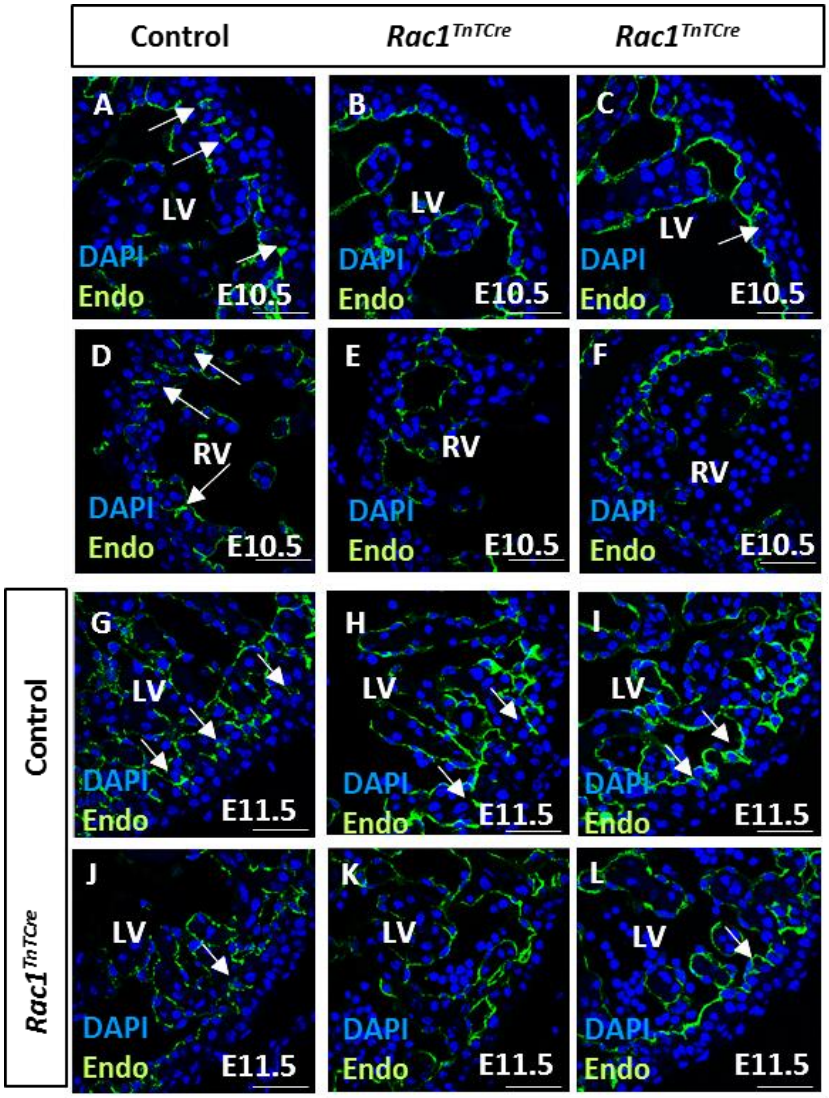

Figure 121: Endomucin IF staining of E10.5 and E11.5 control and *Rac1*^{TnTCre} transverse sections.
Immunostaining with anti-endomucin for endothelial cells with DAPI nuclear stain (blue) (**A**-**P**). From E10.5, endomucin positive endocardial cells line the trabeculae and highlight the distinct compact and trabeculae myocardial regions. At E10.5 and E11.5, trabeculae form uniformly along the compact myocardium and at the base of the trabeculae, endocardial cells project into the compact myocardium. Compared to controls, in *Rac1*^{TnTCre} hearts the number of these projecting endocardial cells at the base of trabeculae is significantly fewer at E11.5 (arrows in **G**-**L**) and shows a trend at E10.5 (arrows in **A**-**F**) (n=4). In controls, endocardial cells at the base of the trabeculae project into the compact layer in between individual cardiomyocytes. As previously mentioned, in *Rac1*^{TnTCre} hearts, this is observed less often and occasionally, endocardial cells appear surrounded in the compact myocardium (arrows in **O**-**P**). Scale bars; 50µm.

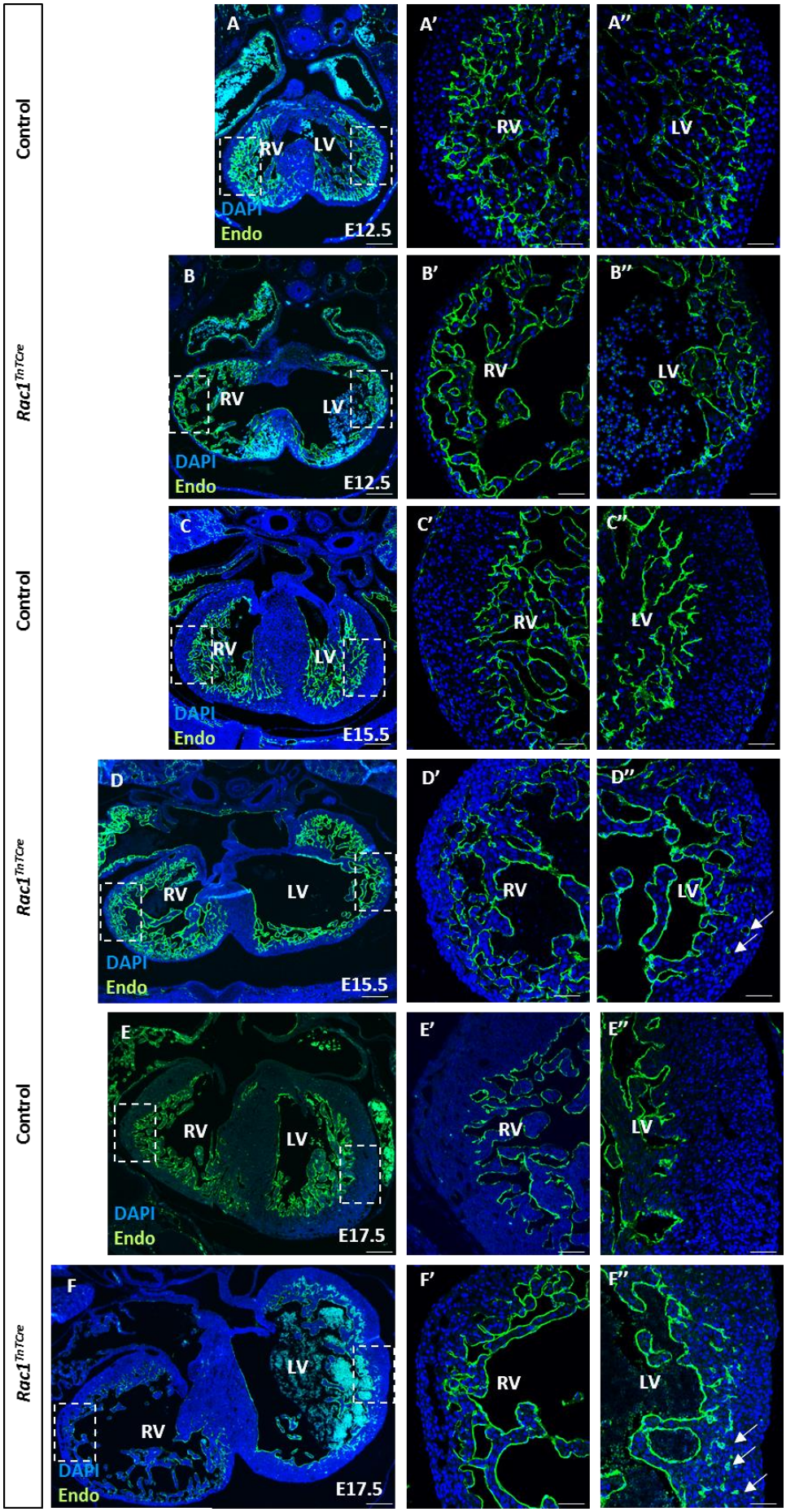
Control
Rac1TnTCre
Control
Rac1TnTCre
Control
Rac1TnTCre
A
A'
A''
RV
LV
DAPI
Endo
E12.5
B
B'
B''
RV
LV
DAPI
Endo
E12.5
C
C'
C''
RV
LV
DAPI
Endo
E15.5
D
D'
D''
RV
LV
DAPI
Endo
E15.5
E
E'
E''
RV
LV
DAPI
Endo
E17.5
F
F'
F''
RV
LV
DAPI
Endo
E17.5

Figure 122: Endomucin IF staining of E12.5, E15.5 and E17.5 control and *Rac1*^{TnTCre} transverse sections.

Immunostaining with anti-endomucin for endothelial cells with DAPI nuclear stain (blue) (**A**-**P**). In mutant *Rac1*^{TnTCre} hearts the trabeculae appear to undergo compensatory remodelling between E12.5 to E17.5 (**A**-**F**) (n=4). This is striking at E15.5 (**C**-**D**) and E17.5 (**E-F**), with endomucin positive cells appearing 'trapped' within the compact myocardial layer (arrows in **D''** and **F''**). The right ventricle remains thin with relatively large numbers of trabeculae compared to controls (**D'** and **F'**), whereas the left ventricle thickens and becomes smooth on the inner surface with relatively few trabeculae (**D''** and **F''**), but is less densely packed than in controls and contains 'trapped' endomucin positive endocardial cells (arrows in **D''** and **F''**). LV; left ventricle, RV; right ventricle. Scale bars; A-F 200μm, A'-F'' 50μm.

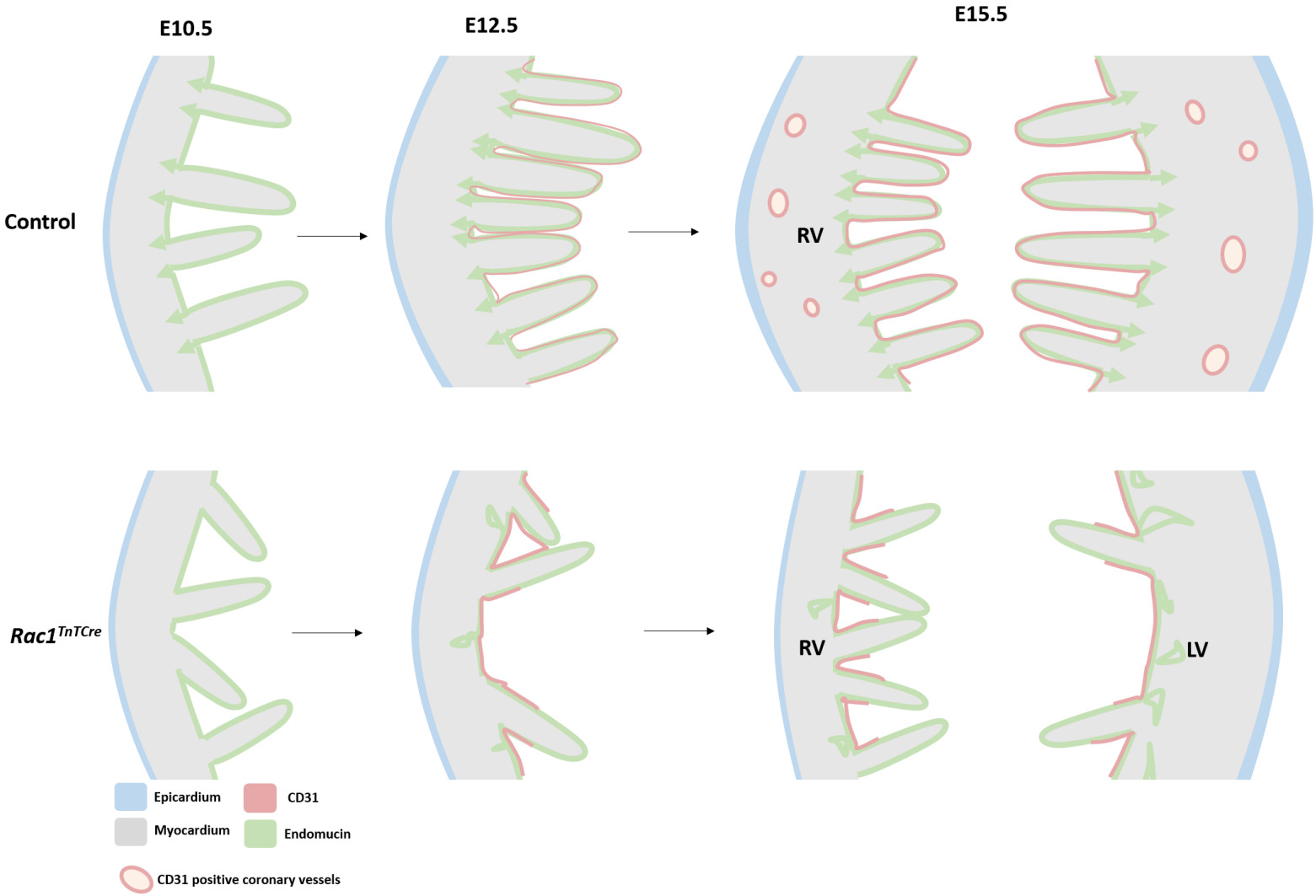
E10.5
E12.5
E15.5
Control
RV
Rac1TnTCre
RV
LV
Epicardium
CD31
Myocardium
Endomucin
CD31 positive coronary vessels

Figure 123: Endocardial abnormalities in *Rac1*^{TnTCre} hearts.
In controls, endocardial cells at the base of the trabeculae project into the compact layer in between individual cardiomyocytes. In *Rac1*^{TnTCre} hearts this is observed less often. This mutant phenotype was continued in E12.5 *Rac1*^{TnTCre} hearts, when the compact myocardial wall is significantly thinned and the border between compact and trabeculae myocardial is less well defined, additionally some endocardial cells appear trapped within the myocardial wall. In *Rac1*^{TnTCre} hearts, the trabeculae appear to undergo compensatory remodelling between E12.5 to E17.5. This is striking at E15.5, with endomucin positive cells again appearing 'trapped' within the compact myocardial layer, particularly in the LV. Additionally, the difference between the right and left ventricle walls from E15.5 onwards suggests there is differential remodelling between the two ventricles in mutant hearts. In *Rac1*^{TnTCre} hearts the RV remains thin with relatively large numbers of trabeculae compared to controls, whereas the LV thickens and becomes smooth on the inner surface with relatively few trabeculae. However, this thickened left ventricular wall is less densely packed than in controls and contains 'trapped' endomucin positive endocardial cells. At E12.5, CD31 expression can be seen in the endocardial cells, with the highest expression in the endocardium at the base of the trabeculae, as well as in the endothelium of sub-epicardial veins. There is little to no expression of CD31 within the compact myocardium at E12.5. By E15.5, CD31 marks the endothelium of the developing coronary vessels and microvasculature within the compact myocardium, but also remains expressed in the endocardial cells covering the trabeculae. However, at E15.5 there was a marked reduction in the number of CD31-positive endothelial cells within the compact myocardium in *Rac1*^{TnTCre} hearts compared to controls. No large CD31-positive coronary vessels were detected in *Rac1*^{TnTCre} hearts and the CD31-positive microvascular in the compact layer of E15.5 *Rac1*^{TnTCre} hearts appeared reduced. In control hearts, the CD31-positive endocardial cells were uniformly distributed around the trabeculae, however in *Rac1*^{TnTCre} hearts, the CD31-positive endocardial cells appeared to be more concentrated at the base of the trabeculae from E12.5.

CD31 and endomucin immunostaining revealed reduced coronary endothelial cells and aberrant ‘trapped’ endocardial cells in the myocardium of *Rac1*^{TnTCre} hearts during late stages of embryonic heart development. This phenotype suggests that the myocardium is undergoing abnormal compaction. Additionally, the number of projecting endocardial cells was reduced early in development. This suggests that the endocardial cells behaviour is altered during early myocardial development. It was therefore hypothesised that, in *Rac1*^{TnTCre} hearts, endocardial cells are not migrating into the compact myocardium, as in controls, to give rise to the endothelial cells of the coronary vessels and hence the lack of coronary vessel formation later in development. However, the contribution of endocardial cells to the coronary vessels is currently debatable (Wu *et al.*, 2012), and recent evidence suggests it may only be a small proportion of coronary endothelial cells which arise from the endocardium (Zhang *et al.*, 2016). Therefore, this area of research requires further investigation. Since the endocardium appears disrupted during early myocardial development, and myocardial-endocardial interactions are known to be important for this process, further investigatation of endocardial cells in *Rac1*^{TnTCre} mutants was carried out by using immunostaining for characteristic endothelial markers, including VE-cadherin, ERG and Nfatc1.

VE-cadherin is found clustered at cell-cell contacts, in AJ and interacts with β-catenin, plakoglobin and p120-catenin. VE-cadherin is required for interaction with the cytoskeleton and junctional strength, but can also regulate endothelial cell differentiation, growth, and migration. VE-cadherin appears selectively expressed in endocardial cells, with increased density at cell-cell junctions and is unaffected in *Rac1*^{TnTCre} hearts (E9.5; n=3, E10.5; n=7 E11.5, n=6) (Figure 124 and Figure 125).

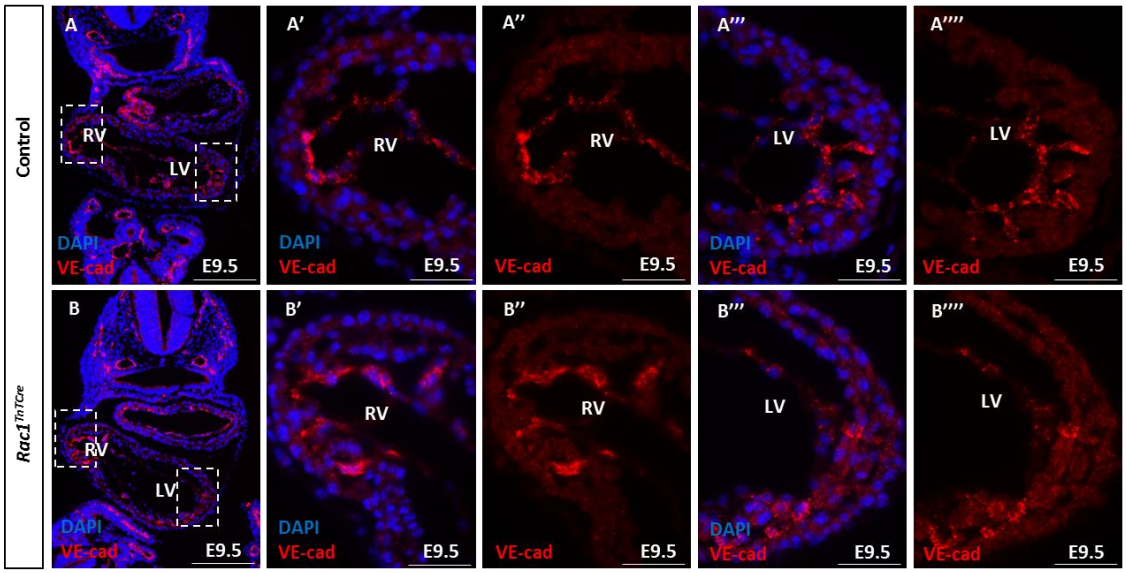

Figure 124: VE-cadherin IF staining of E9.5 control and *Rac1*^{TnTCre} transverse sections.
IF staining shows strong VE-cadherin expression within the endocardium at E9.5, expression was comparable between controls and *Rac1*^{TnTCre} hearts in both the left and right ventricle (n=4). LV; left ventricle, RV; right ventricle. Scale bars; A-B 200μm, A'-B'''' 50μm.

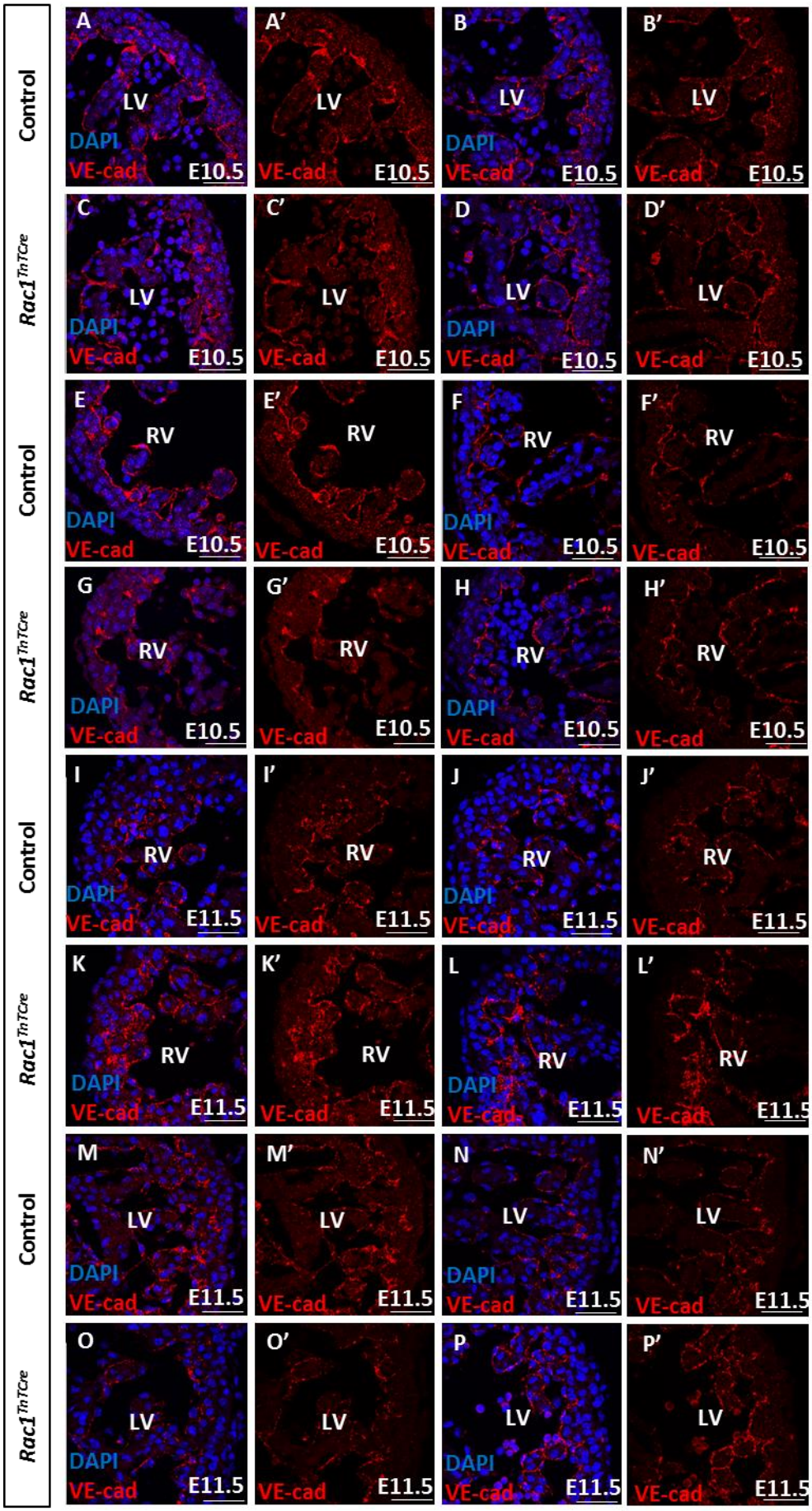
Control
Rac1TnTCre
Control
Rac1TnTCre
Control
Rac1TnTCre
Control
Rac1TnTCre
A
A'
B
B'
C
C'
D
D'
E
E'
F
F'
G
G'
H
H'
I
I'
J
J'
K
K'
L
L'
M
M'
N
N'
O
O'
P
P'
LV
RV
DAPI
VE-cad
E10.5
E11.5

Figure 125: VE-cadherin IF staining of E10.5 and E11.5 control and *Rac1*^{TnTCre} transverse sections.
IF staining shows strong VE-cadherin expression within the endocardium at E10.5 and E11.5, expression was comparable between controls and *Rac1*^{TnTCre} hearts in both the left and right ventricle (E10.5, n=4) (E11.5, n=3). LV; left ventricle, RV; right ventricle. Scale bars; 50µm.

Nfatc1 is active in the nucleus of endocardial cells during cardiac development and is 'switched off' in migratory endocardial cells as they enter the compact myocardium (Ajima *et al.*). Staining of E10.5, E11.5 and E13.5 hearts sections with anti-Nfatc1 confirmed expression of Nfatc1 in all endocardial cells in both controls and *Rac1*^{TnTCre} hearts, however there was no difference between the two groups (E10.5; n=3, E11.5; n=4, E13.5 n=3) (Figure 126).

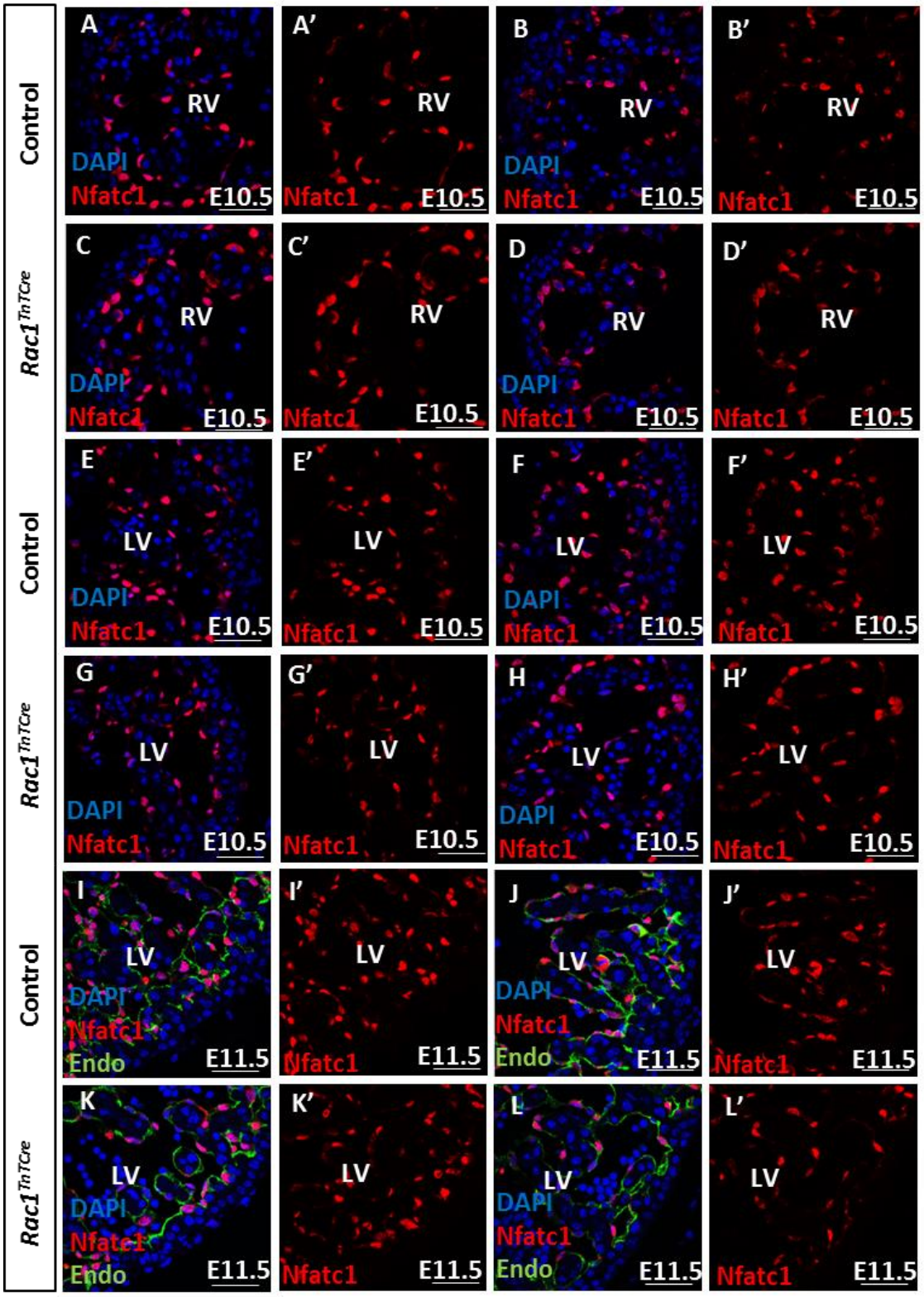

Figure 126: Nfatc1 IF staining of E10.5 and E11.5 control and *Rac1*^{TnTCre} transverse sections.

IF staining shows strong Nfatc1 expression within the nucleus of endocardial cells at E10.5 and E11.5, expression was comparable between controls and *Rac1*^{TnTCre} hearts in both the left and right ventricle (n=4). LV; left ventricle, RV; right ventricle. Scale bars; 50µm.

ERG, an ETS family transcription factor, is known to be expressed in endothelial cells. Staining of E11.5 hearts sections with anti-ERG and anti-endomucin confirmed expression of ERG within all endomucin-positive endocardial cells (Figure 127). In *Rac1*^{TnTCre} hearts, as previously seen with endomucin IF staining (Figure 96), endocardial cells do not appear to be protruding into the compact myocardium as in controls and endocardial cells appear to be gathered at the base of trabeculae (arrows in Figure 127, C-D and F) and also at the ends of the trabeculae (arrows in Figure 127E) (n=4).

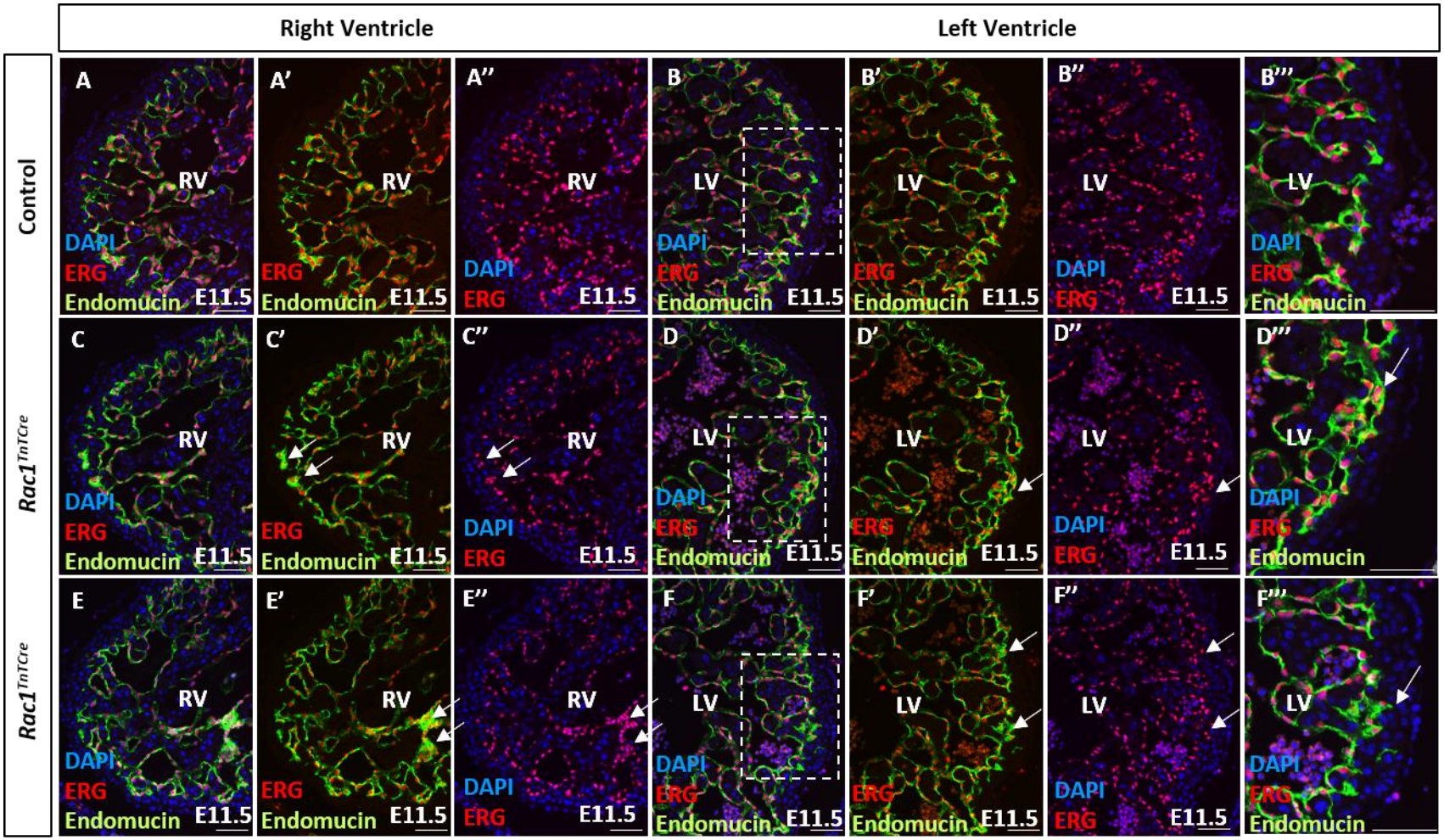

Figure 127: ERG and endomucin IF staining of E11.5 control and *Rac1*^{TnTCre} transverse sections.
IF staining shows strong ERG expression within the nucleus of endocardial cells (also stained with endomucin) at E11.5. Endocardial cells do not appear to be protruding into the compact myocardium as in controls and endocardial cells appear to be gathered at the base of trabeculae (arrows in **C**, **D** and **F**) and also at the ends of the trabeculae (arrows in **E**) (n=4). LV; left ventricle, RV; right ventricle. Scale bars 50µm/

5.3.10 Signalling between myocardium and endocardium

As discussed earlier, signalling between the myocardium and endocardium is vital for normal myocardial development. Some of the main signalling pathways which are active in the myocardium and endocardium during myocardial development include Notch signalling and VEGF signalling, and semaphorin signalling has also recently been implicated (Toyofuku *et al.*, 2004b; Grego-Bessa *et al.*, 2007; Wu *et al.*, 2012; D'Amato *et al.*, 2016). It is hypotheised that these signalling pathways may be perturbed in *Rac1* myocardial mutants. To investigate this some of the main proteins in these signalling pathways were examined in *Rac1*^{TnTCre} hearts, using IF staining, *in situ* hybridisation and qPCR.

5.3.10.1 Notch Signalling

Notch 1 is activated in endocardial cells through binding of ligands delta4 and jagged1. Previous studies have reported that N1ICD is most strongly expressed in endocardial cells at the base of trabeculae. IF staining using anti-N1ICD shows strong staining in the endocardium at E11.5. The expression of N1ICD is comparable in *Rac1*^{TnTCre} hearts (Figure 128, B-C compared to A).

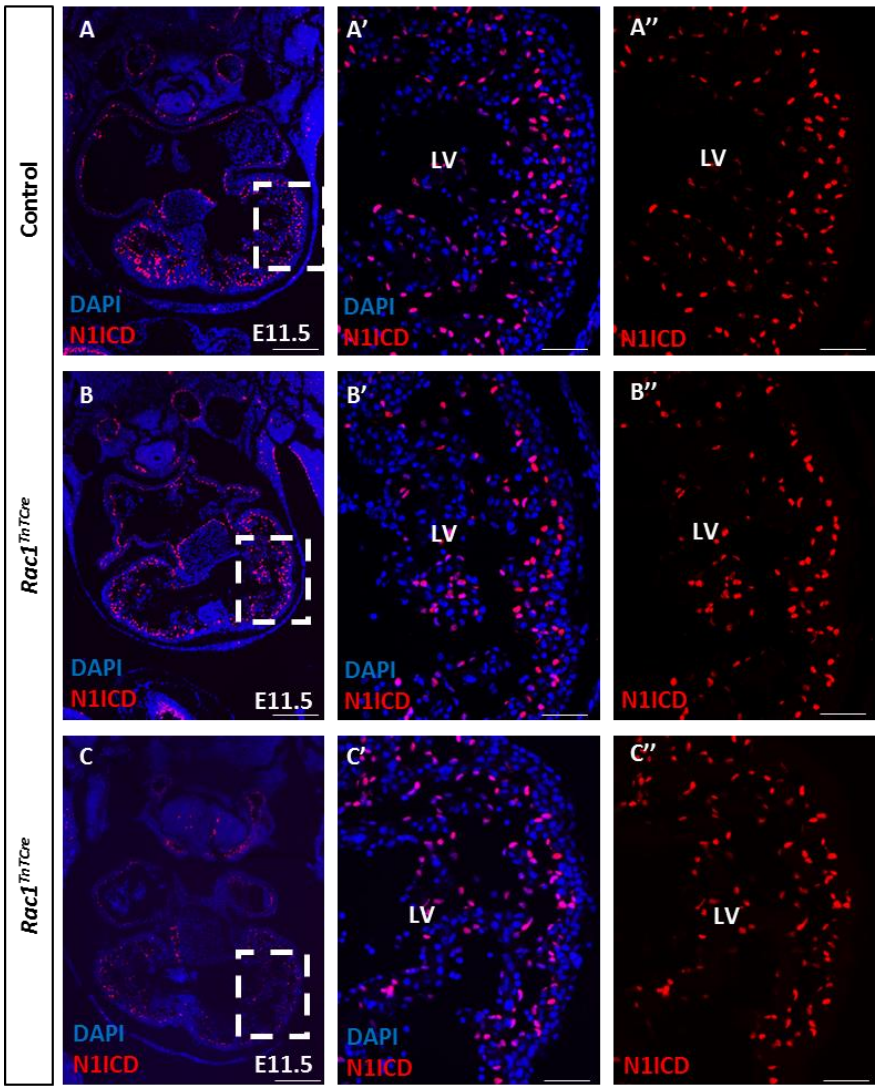

Figure 128: N1ICD IF staining of E11.5 control and *Rac1*^{TnTCre} transverse sections.
IF staining shows strong N1ICD expression within the nucleus of endocardial cells at E11.5, expression was comparable between controls and *Rac1*^{TnTCre} hearts in both the left and right ventricle (n=4). LV; left ventricle, RV; right ventricle. Scale bars; A-C 200μm, A'-C'' 50μm.

Hey2 is a downstream target of Notch signalling and provides a readout of Notch signalling in the myocardium. *Hey2* expression is restricted to the compact myocardium within the ventricle (Leimeister *et al.*, 1999). *In situ* hybridisation using a Hey2 probe confirmed expression of *Hey2* within the compact myocardium with little to no expression in the trabeculae myocardium, at both E10.5 and E12.5. In *Rac1*^{TnTCre} hearts, *Hey2* expression was similarly limited to the compact myocardium at E10.5 (n=4) (Figure 129, B compared with A) and E12.5 (n=4) (Figure 129, D compared with C).

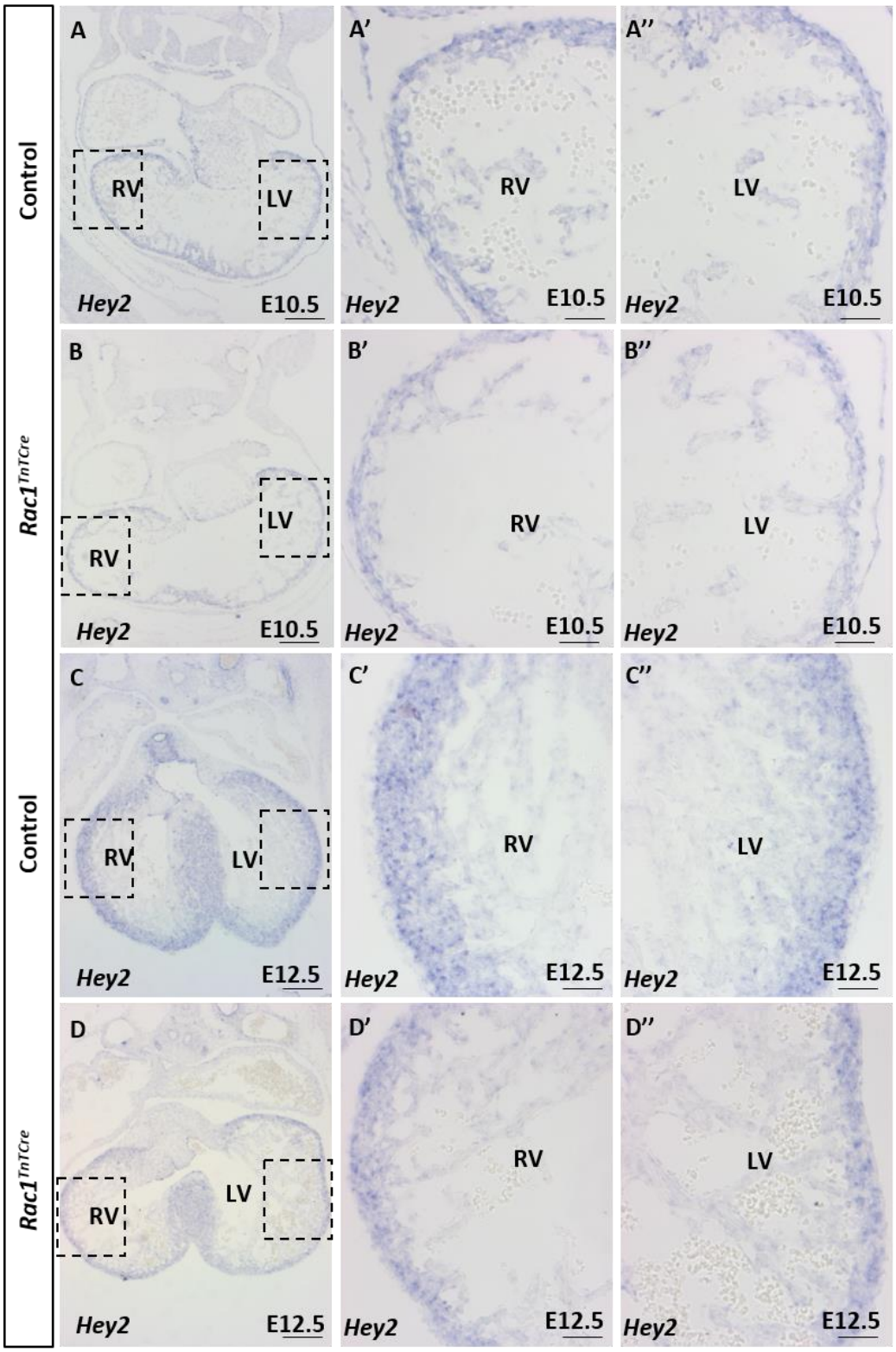

Figure 129: *In situ* hybridisation of *Hey2* in E10.5 and E12.5 control and *Rac1*^{TnTCre} hearts.
In control hearts *Hey2* expression is restricted to the compact myocardium at both E10.5 (**A**) and E12.5 (**C**), the expression appears unchanged in *Rac1*^{TnTCre} hearts at both E10.5 (**B**) and E12.5 (**D**) (n=3). RV; right ventricle, LV; left ventricle. Scale bars; A-D 200μm, A'-D'' 50μm.

These results suggest that Notch signalling between the endocardium and myocardium is normal in *Rac1*^{TnTCre} hearts, with activated Notch expressed in endocardial cells, and signalling effector *Hey2* expressed in the compact myocardium. However, as Notch signalling is known to play several roles during cardiac development, additional indicators of Notch signalling were investigated. During trabeculation, there are two parallel Notch dependent cardiac developmental processes. The first is the transition of primitive myocardial epithelium to trabeculae and compact myocardium, mediated by EphrinB2-Nrg signalling in the endocardium. The second involves maintenance of BMP-dependent proliferation of trabeculae cardiomyocytes. These processes were investigated in *Rac1*^{TnTCre} hearts.

5.3.10.2 EphrinB2 - Neuregulin signalling pathway

Notch signals to the EphrinB2/EphB4 ligand-receptor pair in the endocardium and activates expression of Nrg within the endocardium. Nrg can then signal to the myocardium by binding to ErbB2/4 receptors expressed in cardiomyocytes.

qPCR was carried out on E10.5 heart cDNA to assess gene transcription changes in the ErbB/Nrg signalling pathway. There were no significant changes in *Nrg*, *ErbB2* or *ErbB4* in *Rac1*^{TnTCre} hearts compared to controls (n=6) (Figure 130).

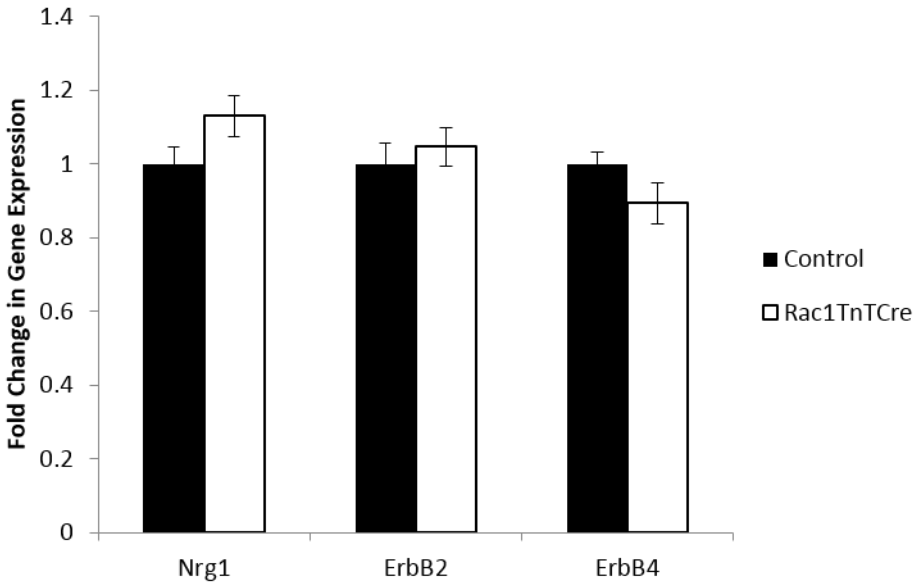

Figure 130: qPCR analysis of *Nrg/ErbB* signalling genes in E10.5 *Rac1*^{TnTCre} hearts.
There were no significant changes in expression of *Nrg, ErbB2* or *ErbB4* (n=6). Housekeeping gene G*APDH*. Statistical analysis carried out using the unpaired t-test.

Additionally, slide *in situ* hybridisation was carried out to assess localisation of *EphB4* and *Nrg1* within the endocardium and *ErbB2* within the myocardium. As expected, *EphB4* and *Nrg1* are highly expressed in the endocardium at E10.5 and E12.5, whereas *ErbB2* is highly expressed in the myocardium. Expression of *Nrg1*, *EphB4* and *ErbB2* is unchanged in *Rac1*^{TnTCre} hearts compared to controls (Figure 131, Figure 132 and Figure 133) (E10.5; n=3, E12.5; n=3).

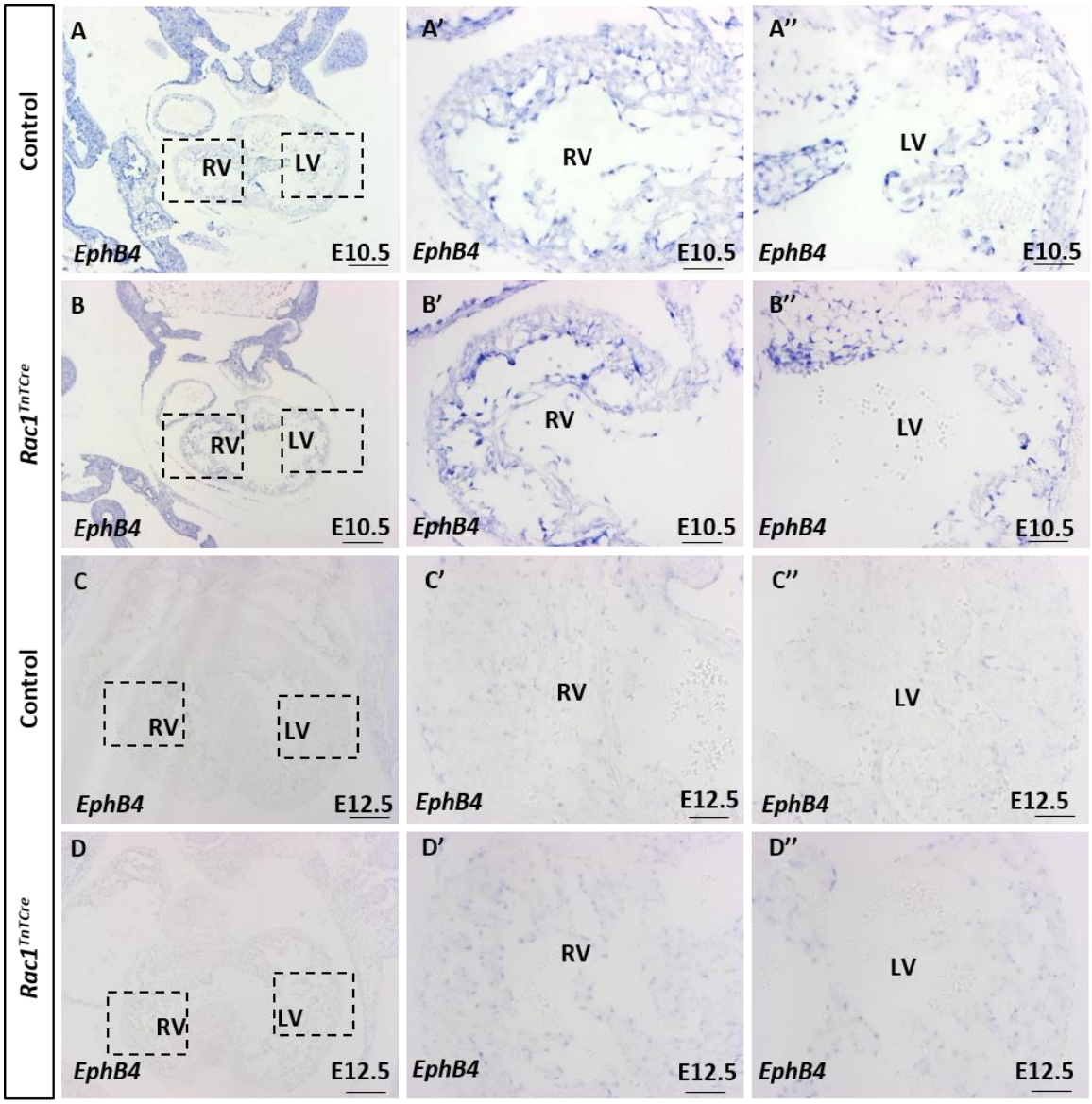

Figure 131: *In situ* hybridisation of *EphB4* in E10.5 and E12.5 control and *Rac1*^{TnTCre} hearts.

Within the ventricles, expression of *EphB4* is observed in endocardial cells at E10.5 (arrows in **A'** and **A''**) and E12.5 (arrows in **C'** and **C''**). Expression of *EphB4* in *Rac1*^{TnTCre} hearts is comparable to controls at E10.5 (arrows in **B'** and **B''**) and E12.5 (arrows in **D'** and **D''**) (n=3). E; embryonic day, RV; right ventricle, LV; left ventricle. Scale bars; A-D 200μm, A'-D'' 50μm.

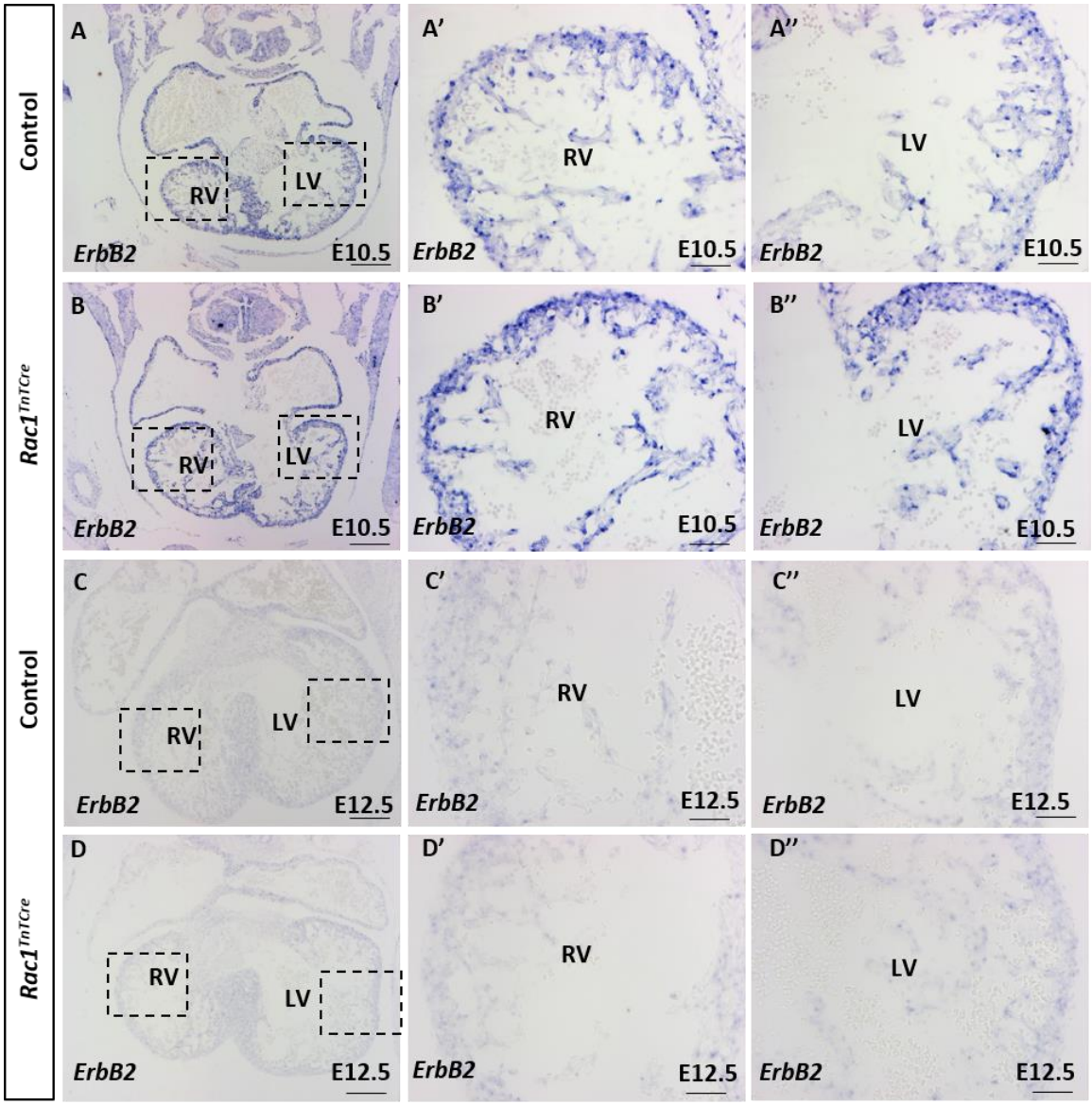

Figure 132: *In situ* hybridisation of *ErbB2* in E10.5 and E12.5 control and *Rac1*^{TnTCre} hearts.

Within the ventricles, expression of *ErbB2* is observed in the myocardium at E10.5 (arrows in **A'** and **A''**) and E12.5 (arrows in **C'** and **C''**). Expression of *ErbB2* in *Rac1*^{TnTCre} hearts is comparable to controls at E10.5 (arrows in **B'** and **B''**) and E12.5 (arrows in **D'** and **D''**) (n=3). E; embryonic day, RV; right ventricle, LV; left ventricle. Scale bars; A-D 200μm, A'-D'' 50μm.

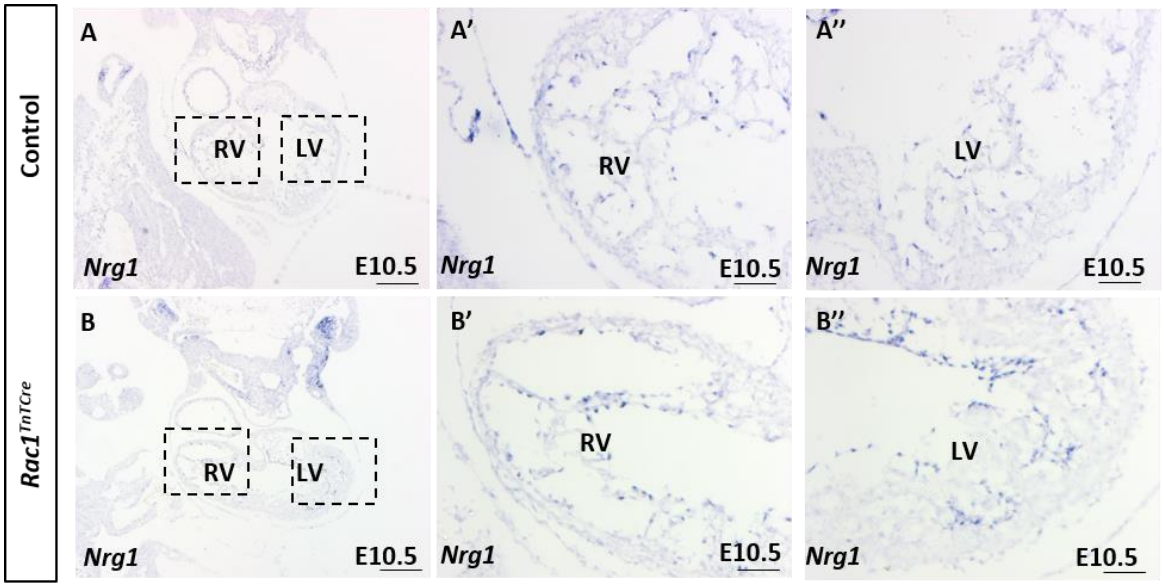

Figure 133: *In situ* hybridisation of *Nrg1* in E10.5 control and *Rac1*^{TnTCre} hearts.
Within the ventricles, expression of *Nrg1* is observed in the endocardium at E10.5 (arrows in **A'** and **A''**). Expression of *Nrg1* in *Rac1*^{TnTCre} hearts is comparable to controls at E10.5 (arrows in **B'** and **B''**) (n=3). E; embryonic day, RV; right ventricle, LV; left ventricle. Scale bars; A-D 200μm, A'-D'' 50μm.

5.3.10.3 Maintenance of BMP10 in trabeculae myocardium

BMP10 is required to maintain cardiomyocyte proliferative capacity after the onset of trabeculae cardiomyocyte differentiation and is therefore expressed transiently from E9.0 to E13.5, and is restricted to trabeculae cardiomyocytes (Neuhaus *et al.*, 1999).

Slide *in situ* hybridisation was carried out on E10.5 and E12.5 sections to investigate *Bmp10* expression in *Rac1*^{TnTCre} hearts. *Bmp10* was expressed strongly in the trabeculae cardiomyocytes at E10.5, with weak expression in compact cardiomyocytes in both control hearts and *Rac1*^{TnTCre} hearts. At E12.5 *Bmp10* expression remains restricted to trabeculae cardiomyocytes with no expression in the compact myocardium in both control and *Rac1*^{TnTCre} hearts (Figure 134).

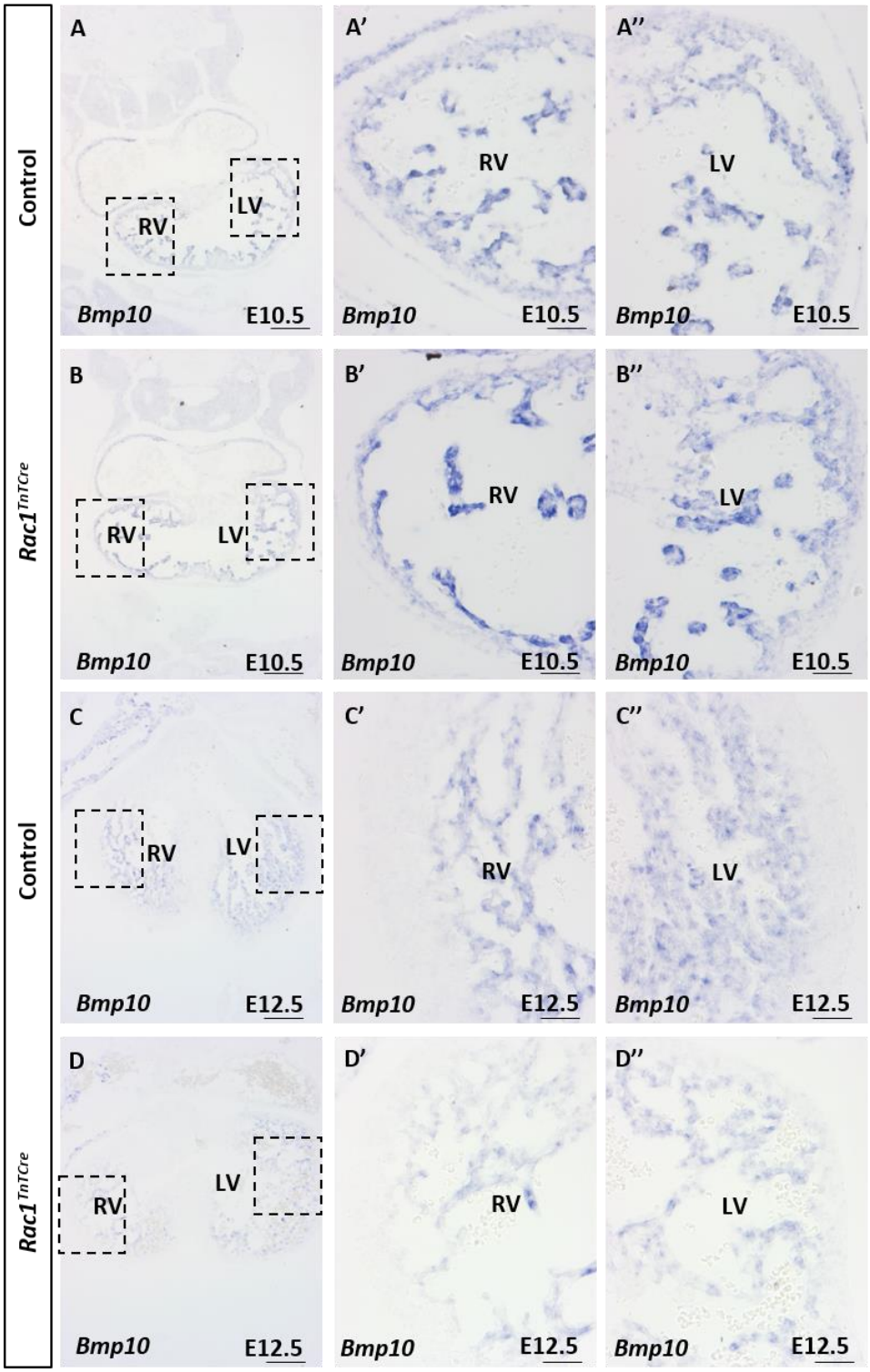

Figure 134: *In situ* hybridisation of *Bmp10* in E10.5 and E12.5 control and *Rac1*^{TnTCre} hearts.

Within the ventricles, expression of *Bmp10* is restricted to the trabeculated myocardium at E10.5 (arrows in **A'** and **A''**) and E12.5 (arrows in **C'** and **C''**). Expression of *Bmp10* in *Rac1*^{TnTCre} hearts is comparable to controls at E10.5 (arrows in **B'** and **B''**) and E12.5 (arrows in **D'** and **D''**) (n=3). E; embryonic day, RV; right ventricle, LV; left ventricle. Scale bars; A-D 200μm, A'-D'' 50μm.

5.3.10.4 VEGF signalling

Myocardial VEGF binds to VEGF receptors expressed in endocardial cells to regulate angiogenesis; the main VEGF receptor expressed in the endocardium during cardiac development is VEGFR-2. To determine if VEGF-a signalling in the myocardium is affected in the absence of Rac1, qPCR, slide *in situ* hybridisation and IF analysis of VEGF-a was carried out in control and *Rac1*^{TnTCre} hearts.

E10.5 and E12.5 hearts were dissected for RNA extraction, cDNA synthesis was carried out and used in qPCR reactions. There was no change in *Vegf-a* expression in *Rac1*^{TnTCre} hearts compared to controls at either E10.5 or E12.5 (n=6 and n=4, respectively) (Figure 135).

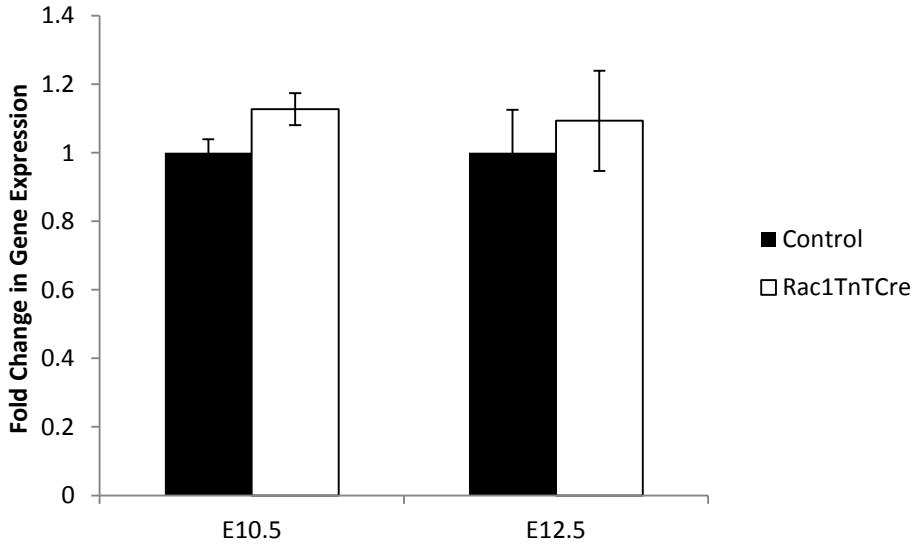

Figure 135: qPCR analysis of *Vegf-a* gene expression in *Rac1*^{TnTCre} hearts. qPCR analysis shows cardiac expression of *Vegf-a* at E10.5 (n=6) and E12.5 (n=3). No significant differences in expression were detected in *Rac1*^{TnTCre} hearts compared to controls ($P<0.05$). Expression values are normalised to housekeeping gene *GAPDH* and are relative to control expression. E; embryonic day. Statistical analysis carried out using the unpaired t-test.

Additionally, both *Vegf-a* and *Vegfr-2* expression was analysed by slide *in situ* hybridisation in E10.5 hearts. As expected, *Vegfr-2* is expressed solely in the endocardial cells of the ventricle at E10.5 (Figure 136A). Conversely, *Vegf-a* shows a varied expression pattern throughout the three main layers of the ventricle at E10.5 (Figure 136C). Expression of both the *Vegf-a* ligand and *Vegfr-2* receptor is comparable to controls in *Rac1*^{TnTCre} hearts (Figure 136, B and D, respectively).

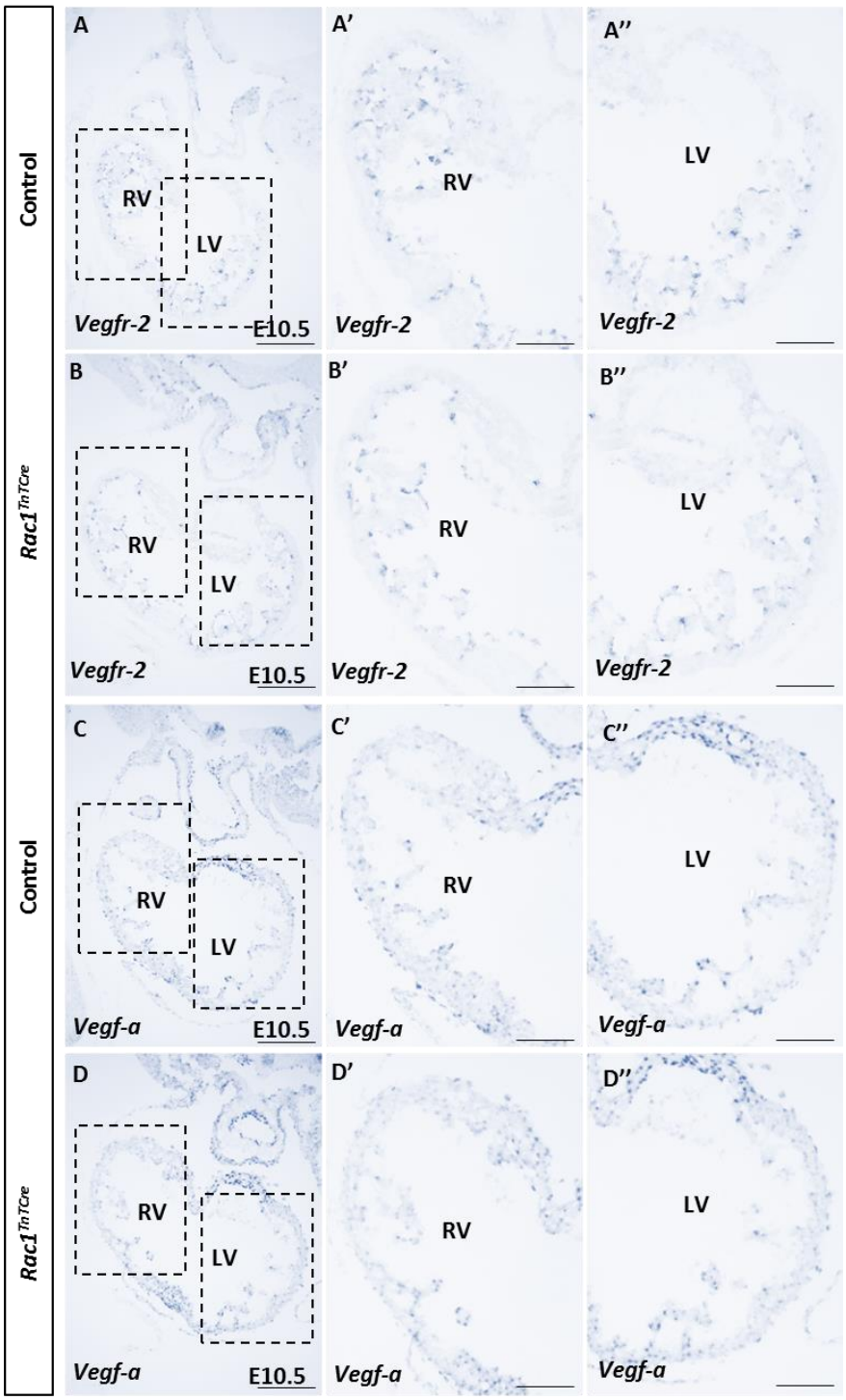

Figure 136: *In situ* hybridisation of *Vegf-a* and *Vegfr-2* in E10.5 control and *Rac1*^{TnTCre} hearts.
Within the ventricles, *Vegfr-2* is expressed solely in the endocardial cells at E10.5 (**A**). Conversely, *Vegf-a* shows a varied expression pattern throughout the three main layers of the ventricle at E10.5 (**C**). Expression of both the *Vegf-a* ligand and *Vegfr-2* receptor is comparable to controls in *Rac1*^{TnTCre} hearts (**B** and **D**, respectively) (n=3). E; embryonic day, RV; right ventricle, LV; left ventricle. Scale bars; A-D 200μm, A'-D'' 100μm.

To further asses VEGFR-2 at the protein level, IF staining using an anti-VEGFR-2 antibody was carried out. At E11.5 VEGFR-2 expression is restricted to endocardial cells within the developing ventricles. The receptor displays expression throughout the endocardial cell, with punctate expression in one region per cell. VEGFR-2 expression appeared normal in the majority of endocardial cells of the developing ventricles in *Rac1*^{TnTCre} hearts compared to controls, with the exception of the endocardial cells on the surface of the compact myocardium, where no trabeculae have formed. In these areas the VEGFR-2 expression appears reduced (arrows in Figure 137D-F). This observation is most striking in the RV and expression in the LV is more comparable between controls and *Rac1*^{TnTCre} hearts (arrows in Figure 137J-L).

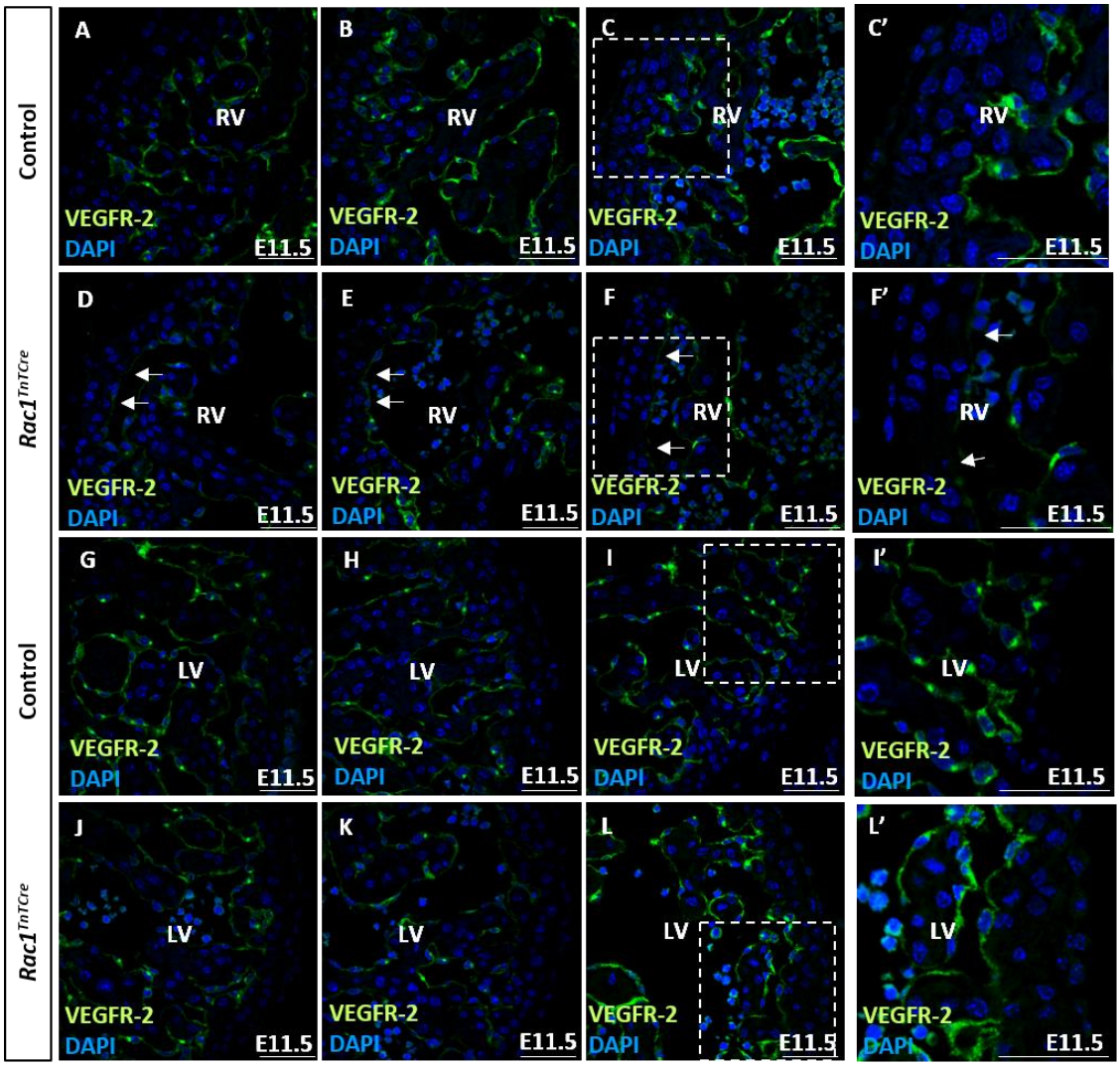

Figure 137: VEGFR-2 IF staining of E11.5 control and *Rac1*^{TnTCre} transverse sections.
At E11.5, VEGFR-2 expression appears reduced in the endocardial cells on the surface of the compact myocardium where no trabeculae are forming. This observation is most striking in the RV (shown by arrows in **D**-**F'**) and expression in the LV is more comparable between controls and *Rac1*^{TnTCre} hearts (**J**-**K**) (n=4). LV; left ventricle, RV; right ventricle. Scale bars; 50µm.

5.3.10.4 Semaphorin signalling

Plexin transmembrane receptors and their semaphorins ligands as well as co-receptors, including Nrp1, VEGFR-2 and ErbB2, are emerging as key regulatory proteins during development (Gu *et al.*, 2003; Gitler *et al.*, 2004; Toyofuku *et al.*, 2004a; Liu *et al.*, 2010; Epstein *et al.*, 2015). Chick and mouse KO studies have highlighted possible roles during cardiac development and trabeculae formation. It is, therefore, hypothesised that semaphorin signalling may be disrupted in *Rac1* mutant hearts. Based on literature research and reanalysis of microarray

data, ligands Sema3a and Sema4c, and receptor Nrp-1, represented good candidates to investigate in *Rac1*^{TnTCre} hearts (Gu *et al.*, 2003; Ko *et al.*, 2005; Perala *et al.*, 2005; Ieda *et al.*, 2007). E10.5 embryos were dissected and processed for slide *in situ* hybridisation or immunostaining.

Within the ventricles, *Sema4c* is expressed throughout the myocardium but is strongly expressed in the epicardium and some endocardial cells (Figure 138A). In *Rac1*^{TnTCre} hearts, *Sema4c* expression is substantially and specifically reduced in the myocardium, however the expression is retained in the epicardium and endocardium (Figure 138B and C). This expression pattern is similar to that seen with *Rac1* Exon4-5 probe (Figure 34). *Nrp1* shows a similar expression pattern to *Sema4c* in controls (Figure 138D) and also appears reduced in the myocardium of *Rac1*^{TnTCre} hearts (Figure 138E).

Sema3A is strongly expressed in subendocardial regions of the trabeculae myocardium early in development, and is then restricted to the purkinje fibres later in development (Behar *et al.*, 1996; Ieda *et al.*, 2007). At E10.5, *Sema3a* expression appears to be restricted to endocardial cells and some epicardial cells (Figure 139). Expression of *Sema3a* is comparable between controls and *Rac1*^{TnTCre} hearts (Figure 139).

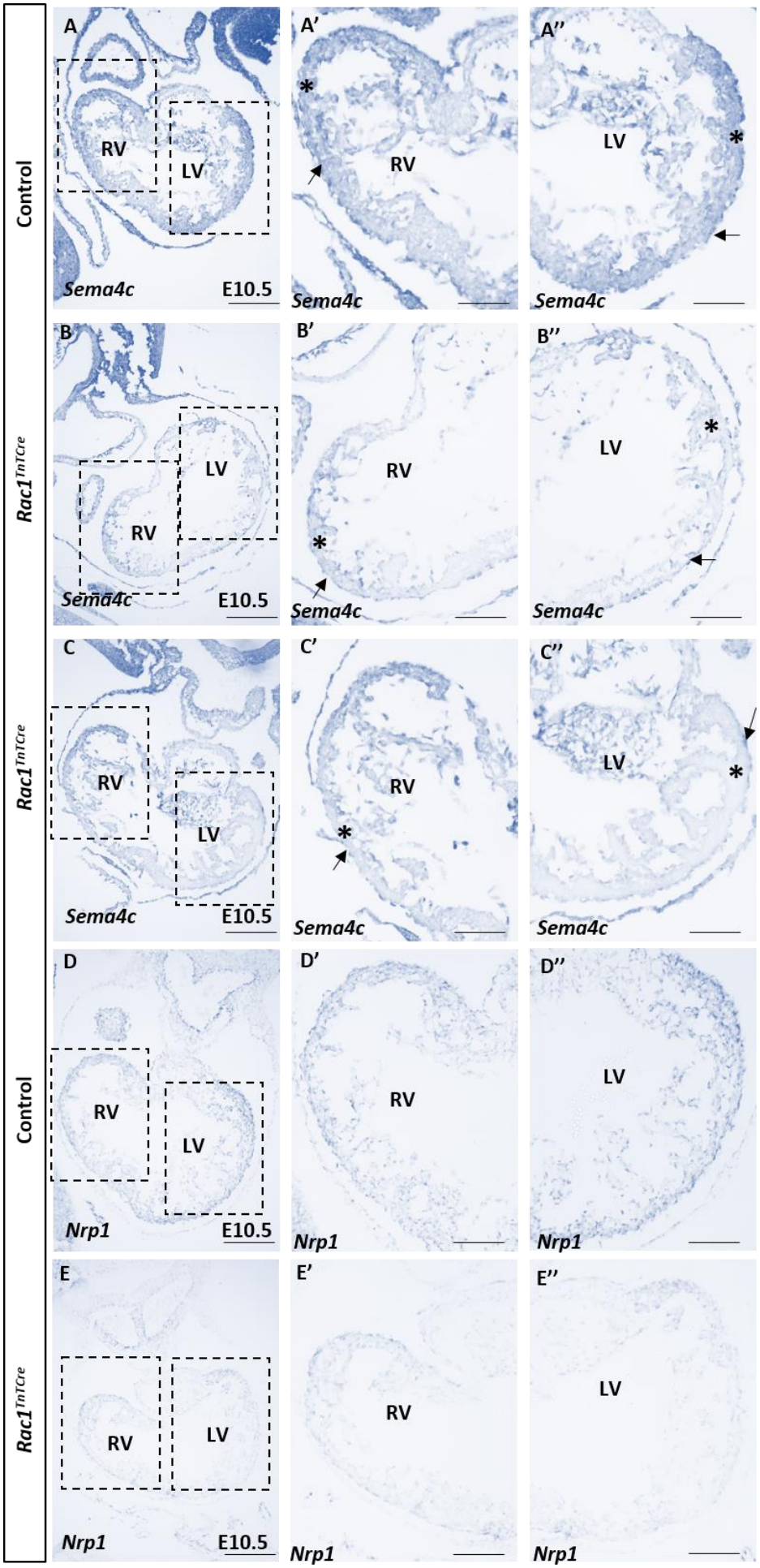
Control
Rac1 InTCre
Rac1 InTCre
Control
Rac1 InTCre
A
A'
A''
RV
LV
Sema4c
E10.5
B
B'
B''
C
C'
C''
D
D'
D''
Nrp1
E
E'
E''

Figure 138: *In situ* hybridisation of *Sema4c* and *Nrp1* in E10.5 control and *Rac1*^{TnTCre} hearts.
Within the ventricles, *Sema4c* is expressed throughout the myocardium but is strongly expressed in the epicardium and some endocardial cells (**A**). In *Rac1*^{TnTCre} hearts, *Sema4c* expression is reduced in the myocardium (asterisk in **B** and **C,** compared to asterisk in **A**) but the expression is retained in the epicardium and endocardium (arrows in **B** and **C,** compared to arrows in **A**) (n=3). *Nrp1* shows a similar expression pattern to *Sema4c* in controls (**D**) and also appears reduced in the myocardium of *Rac1*^{TnTCre} hearts (**E**) (n=3). E; embryonic day, RV; right ventricle, LV; left ventricle. Scale bars; A-D 200µm, A'-D'' 100µm.

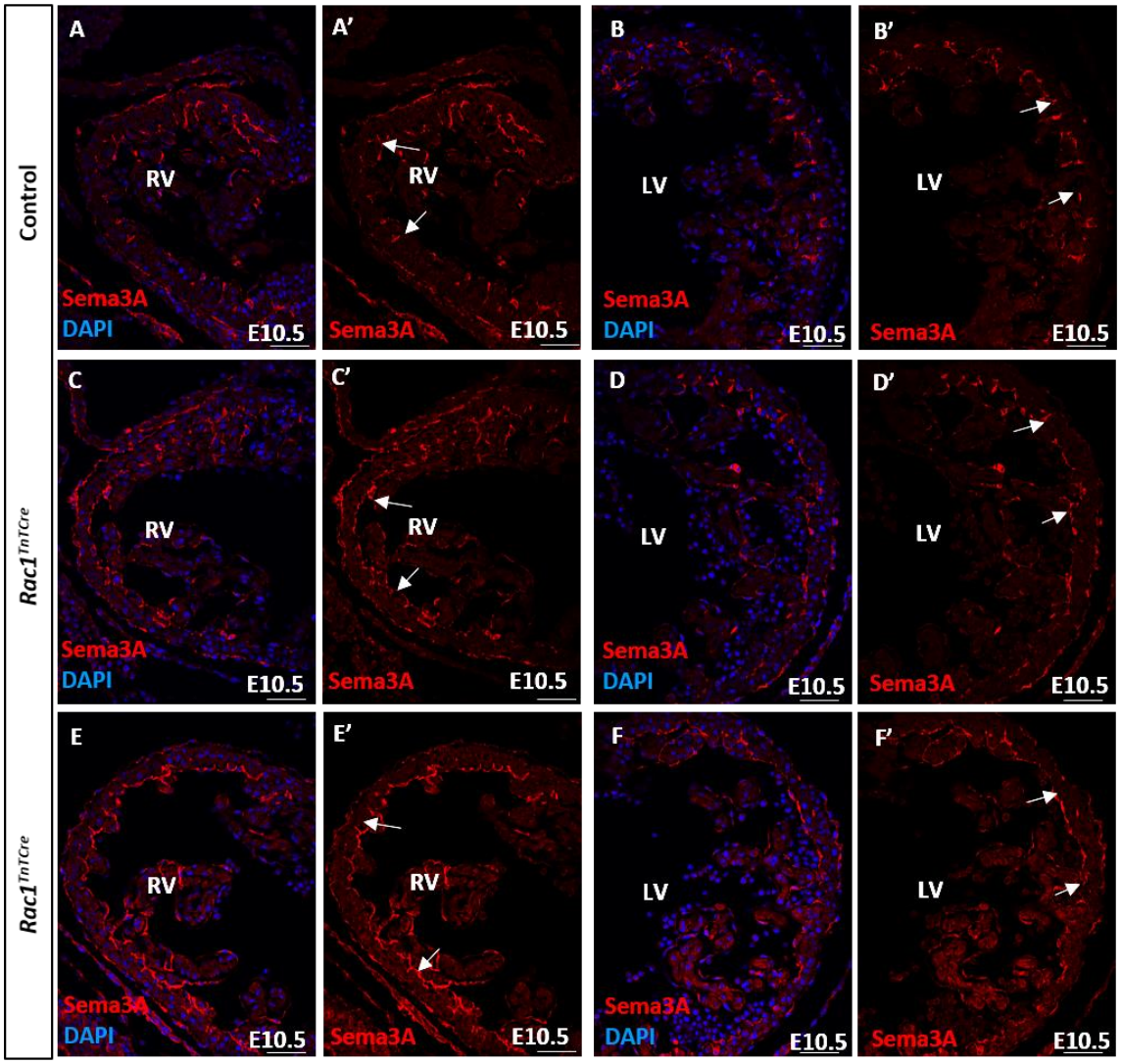

Figure 139: Sema3a IF staining of E10.5 control and *Rac1*^{TnTCre} transverse sections.
At E10.5, Sema3a expression appears to be restricted to endocardial cells and some epicardial cells. Expression of Sema3a is comparable between controls and *Rac1*^{TnTCre} hearts (arrows in **C**-**F** compared to arrows in **A**-**B**) (n=3). LV; left ventricle, RV; right ventricle. Scale bars; 50µm.

5.3.11 Extracellular matrix

In the heart, ECM is produced by cardiomyocytes and myocardial fibroblasts and consists of mainly type I, III and IV-type collagen, laminin, fibronectin and proteoglycans. One of the many functions of the ECM is a structural and signalling role during the formation and remodelling of the trabeculae. Mice lacking in ECM proteins fail to form trabeculae (Yamamura *et al.*, 1997; Camenisch *et al.*, 2000). It was therefore hypothesised that the composition of the ECM may be disrupted during trabeculae formation in *Rac1*^{TnTCre} hearts. To investigate the composition of the ECM in *Rac1*^{TnTCre} hearts, histology and immunofluorescent staining for main ECM proteins was carried out.

Histology stains including Alcian blue, Sirius red, Toluidine blue and Miller's elastin allow visual localisation of ECM proteins and were carried out on control and *Rac1*^{TnTCre} wax sections (n=4).

Miller's elastin stains elastin in blue and counterstaining with eosin allows contrast imaging. Staining of E12.5 sections did not reveal any elastin in the developing myocardium in either controls or *Rac1*^{TnTCre} hearts (Figure 140A-B). Toluidine blue is a basic thiazine metachromatic dye which stains nuclei in blue and proteoglycans and GAGs in purple. Staining of E12.5 sections did not reveal any GAGs in the developing myocardium in either controls or *Rac1*^{TnTCre} hearts (Figure 140C-D). Alcian blue stains the alcianophilic proteoglycans of the ECM in a blueish stain and counterstaining with nuclear fast red allows contrast imaging. Staining of E12.5 sections showed proteoglycans within the subepicardial and subendocardial spaces, however there was no difference in expression between controls and *Rac1*^{TnTCre} hearts (Figure 140E-F). Sirius red stains collagen I and collagen III red. Staining of E12.5 sections showed the collagen matrix surrounding the cardiomyocytes of the myocardium (Figure 140G-H). In *Rac1*^{TnTCre} hearts, the collagen matrix appeared disrupted and compared to controls (Figure 140G-H).

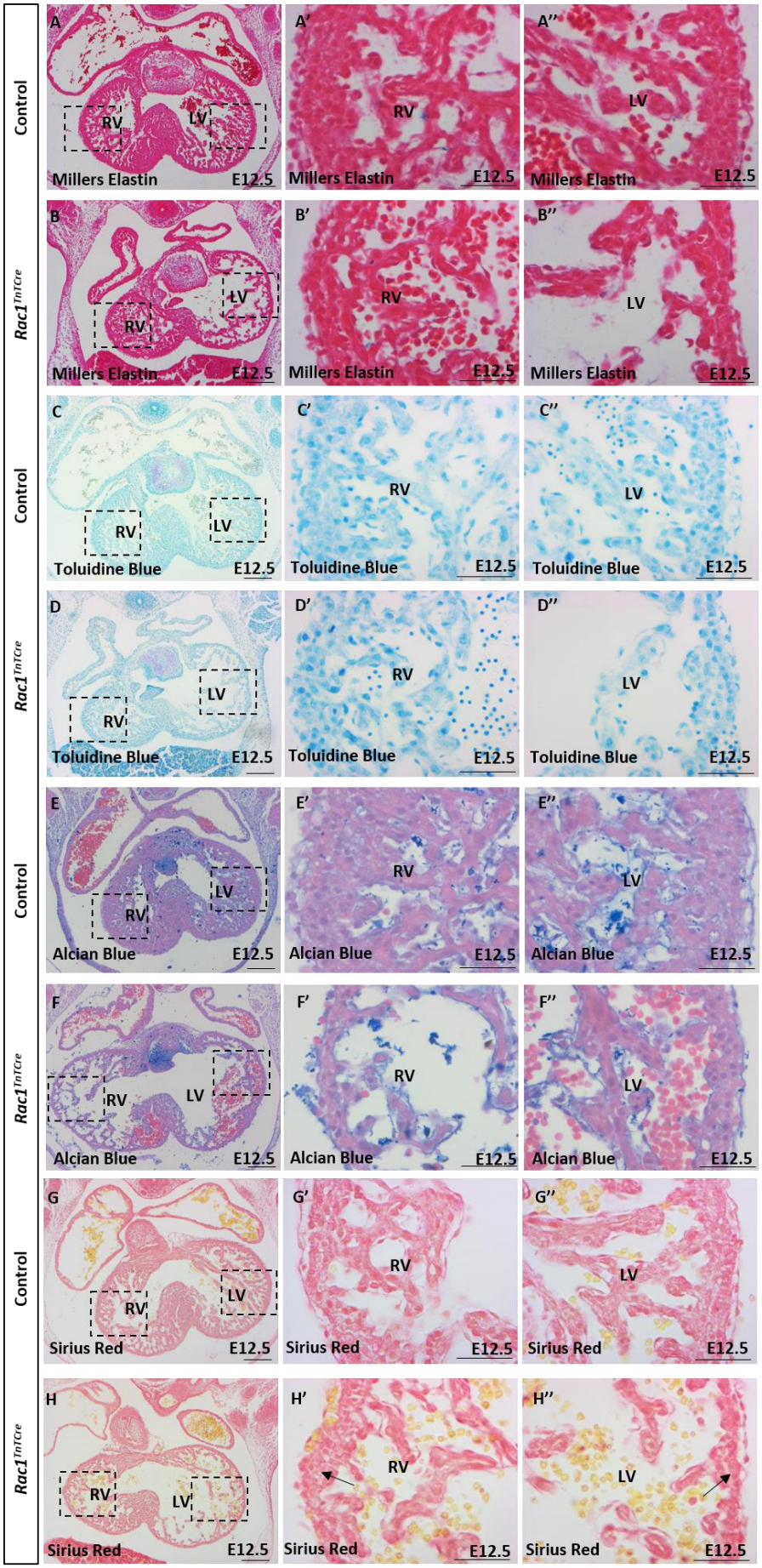
Control
Rac1InTCre
Control
Rac1InTCre
Control
Rac1InTCre
Control
Rac1InTCre
A
A'
A''
B
B'
B''
C
C'
C''
D
D'
D''
E
E'
E''
F
F'
F''
G
G'
G''
H
H'
H''
RV
LV
Millers Elastin
Toluidine Blue
Alcian Blue
Sirius Red
E12.5

Figure 140: Miller's Elastin, Toluidine Blue, Alcian blue and Sirius red histology staining of E12.5 control and *Rac1*^{TnTCre} transverse sections.
Miller's elastin stains elastin blue and counterstaining with eosin allows contrast imaging (**A**-**B**). Staining of E12.5 sections did not reveal any elastin in the developing myocardium in either controls or *Rac1*^{TnTCre} hearts (**A**-**B**) (n=4). Toluidine blue is a basic thiazine metachromatic dye that stains nuclei in blue and proteoglycans and GAGs in purple (**C**-**D**). Staining of E12.5 sections did not reveal any GAGs in the developing myocardium in either controls or *Rac1*^{TnTCre} hearts (**C**-**D**) (n=4). Alcian blue stains the alcianophilic proteoglycans of the ECM in a blueish stain and counterstaining with nuclear fast red allows contrast imaging (**E**-**F**). Staining of E12.5 sections did not reveal any differences in proteoglycan expression within the ventricle wall in *Rac1*^{TnTCre} hearts compared to controls (**E**-**F**) (n=4). Sirius red stains collagen I and collagen III red (**G**-**H**). Staining of E12.5 sections revealed disrupted collagen matrix within the myocardium in *Rac1*^{TnTCre} hearts compared to controls (**G**-**H**) (n=4). LV; left ventricle, RV; right ventricle. Scale bars; A-H 200μm, A'-H'' 50μm.

The main components of the ECM include collagens, laminins and fibronectins. Since the Sirius Red histology staining revealed aberrant collagen expression within the myocardial wall at E12.5, collagen expression was investigated earlier at E11.5, as well as expression of crucial components of the ECM during cardiac development; laminin (Beck *et al.*, 1990). and fibronectin(Astrof *et al.*, 2007).

Laminin is expressed on the basal membrane of cardiomyocytes early in ventricular development (Figure 141). Laminin IF staining within the myocardium appears normal at E9.5 and E10.5 in *Rac1*^{TnTCre} hearts compared to controls (n=4) (Figure 141A-O). However, at E11.5 laminin is aberrantly expressed around cardiomyocytes of the compact myocardium (n=4) (Figure 141P-W). This aberrant expression of laminin appears to correlate with disrupted collagen expression at E11.5 (n=4) (Figure 142, C compared to A). The disrupted ECM, could explain why endomucin-positive endocardial cells become 'trapped' within the compact myocardium in *Rac1*^{TnTCre} hearts (arrow in Figure 142, D compared to B).

Fibronectin is expressed in the sub-epicardial matrix during early ventricular development (Figure 143). Fibronectin IF staining within the myocardium is expanded in *Rac1*^{TnTCre} hearts compared to controls (n=4), with fibronectin expression aberrantly located in-between cardiomyocytes on the epicardial side of the compact myocardium (arrows in Figure 143, C-D and G-H).

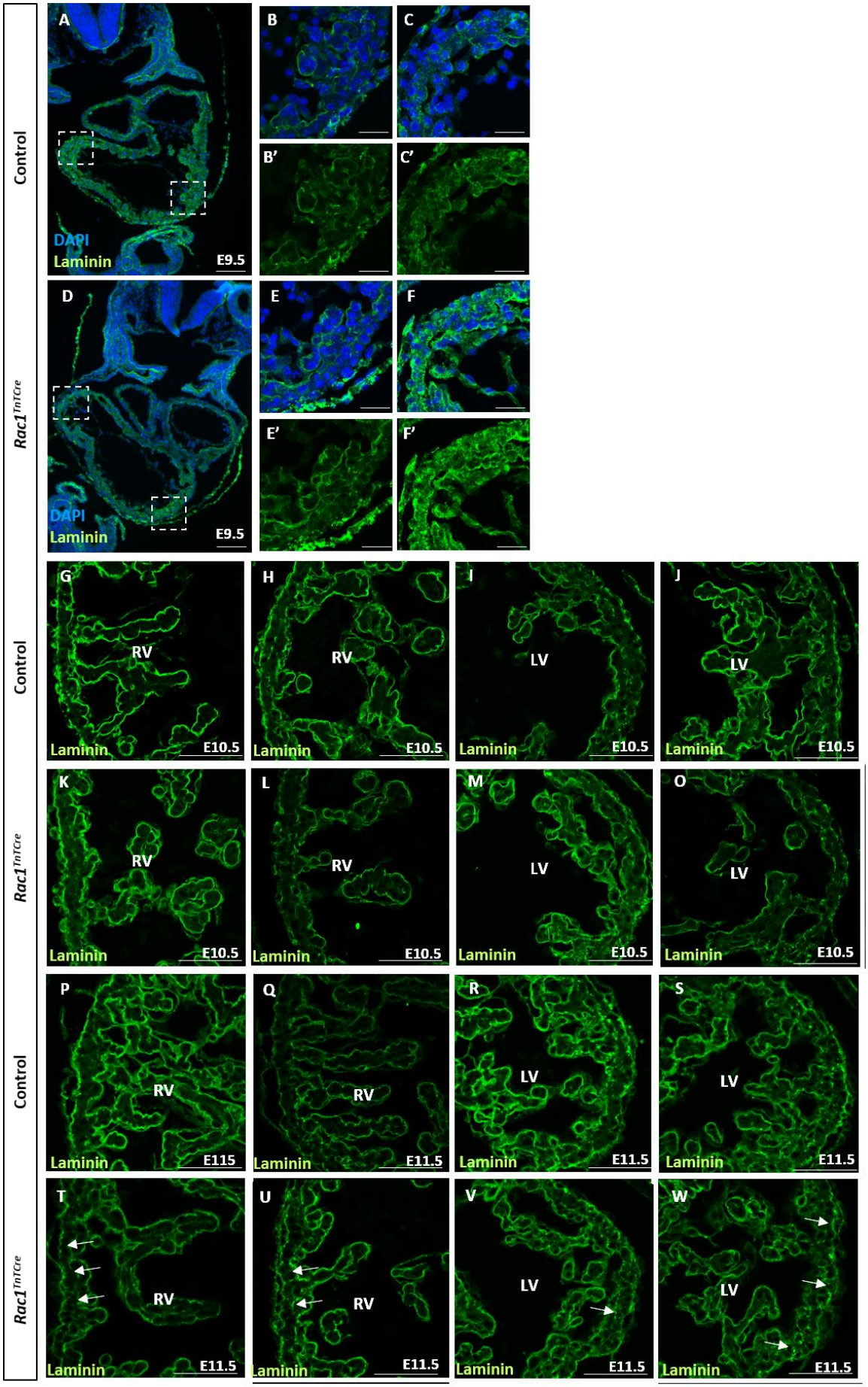
Control
Rac1TnTCre
Control
Rac1TnTCre
Control
Rac1TnTCre
A
B
C
B'
C'
DAPI
Laminin
E9.5
D
E
F
E'
F'
DAPI
Laminin
E9.5
G
H
I
J
RV
RV
LV
LV
Laminin
E10.5
K
L
M
O
RV
RV
LV
LV
Laminin
E10.5
P
Q
R
S
RV
RV
LV
LV
Laminin
E115
E11.5
E11.5
E11.5
T
U
V
W
RV
RV
LV
LV
Laminin
E11.5

Figure 141: Laminin IF staining of E9.5-11.5 control and *Rac1*^{TnTCre} transverse sections.
IF staining shows strong laminin expression in the sub-endocardium and sub-epicardium at E9.5 (**A**-**F**) and E10.5 (**G**-**O**) in both control and *Rac1*^{TnTCre} hearts. This expression pattern is continued at E11.5 in control hearts (**P**-**S**), however in *Rac1*^{TnTCre} hearts, laminin appeared to be aberrantly expressed around individual cardiomyocytes within the compact myocardium (**A**-**W**). Expression was comparable in both the left and right ventricles (n=4). LV; left ventricle, RV; right ventricle. Scale bars; A and D 100µm, all others 50µm.

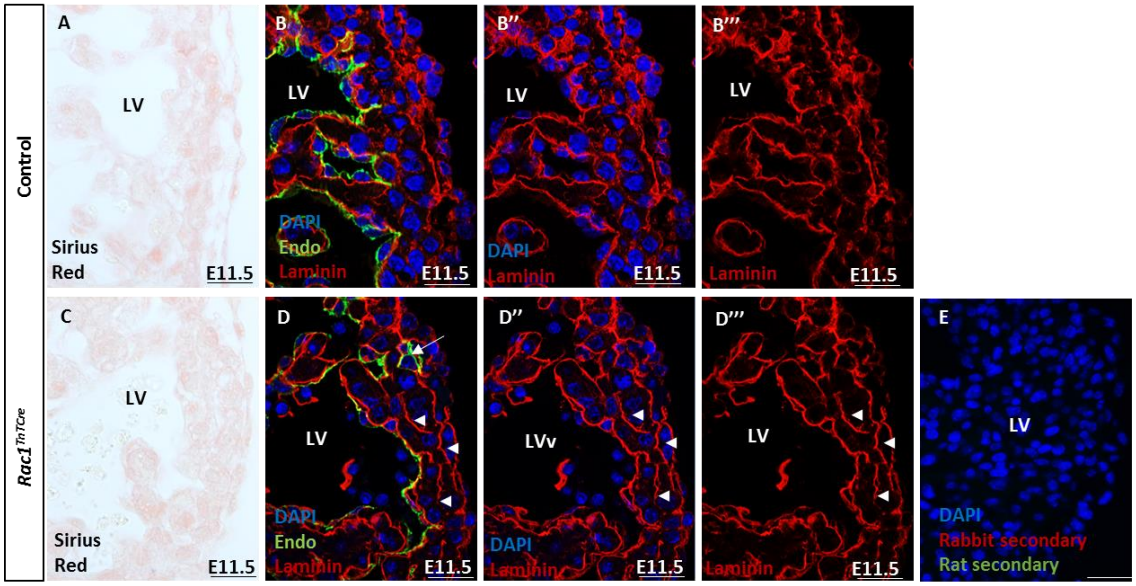

Figure 142: Sirius red and Laminin IF staining of E11.5 control and *Rac1*^{TnTCre} transverse sections.
In *Rac1*^{TnTCre} hearts, laminin is aberrantly expressed around individual cardiomyocytes within the compact myocardium (arrow heads in **D** compared to **B**) and endomucin appeared trapped within the compact myocardium (arrows in **D** compared to **B**) (n=4). Secondary only control (**E**). LV; left ventricle. Scale bars 50µm.

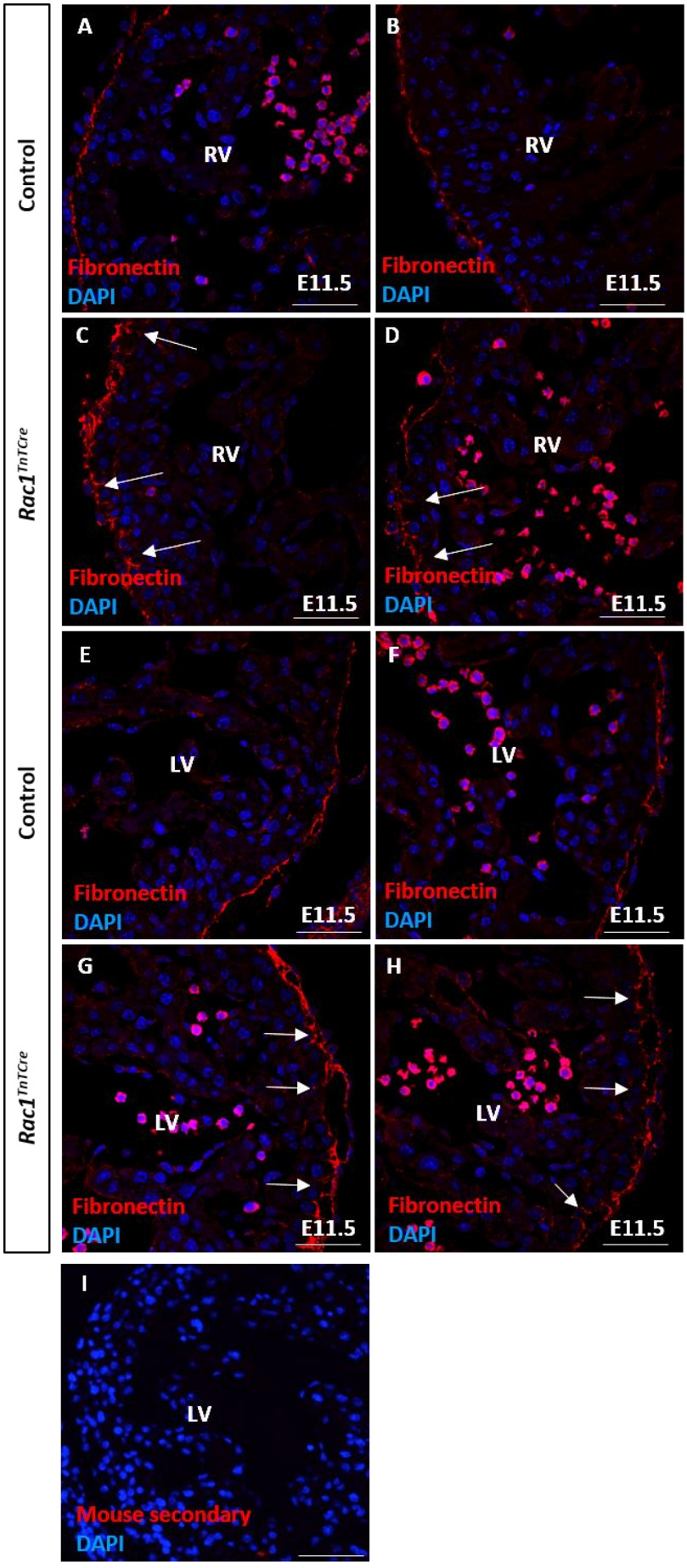
Control
Rac1 TnTCre
Control
Rac1 TnTCre
A
RV
Fibronectin
DAPI
E11.5
B
RV
Fibronectin
DAPI
E11.5
C
RV
Fibronectin
DAPI
E11.5
D
RV
Fibronectin
DAPI
E11.5
E
LV
Fibronectin
DAPI
E11.5
F
LV
Fibronectin
DAPI
E11.5
G
LV
Fibronectin
DAPI
E11.5
H
LV
Fibronectin
DAPI
E11.5
I
LV
Mouse secondary
DAPI

Figure 143: Fibronectin IF staining of E11.5 control and *Rac1*^{TnTCre} transverse sections.
Fibronectin is expressed in the sub-epicardial matrix during early ventricular development. Fibronectin IF staining within the myocardium is expanded in *Rac1*^{TnTCre} hearts compared to controls (n=4), with fibronectin expression aberrantly located inbetween cardiomyocytes on the epicardial side of the compact myocardium (arrows in **C**-**D** and **G**-**H**). Secondary only control (**I**). LV; left ventricle, RV; right ventricle. Scale bars 50µm.

5.3.12 Rac1 interactors

Since Mena is known to interact with Rac1 in cardiomyocytes and a previous study suggests Mena is required for the migration of cardiomyocytes into the trabeculae layer (Toyofuku *et al.*, 2004b; Ram *et al.*, 2014), investigatation of Mena expression in *Rac1*^{TnTCre} hearts was carried out. IF using an anti-Mena antibody was carried out on E10.5 transverse sections to determine if Mena expression was altered in *Rac1*^{TnTCre} hearts. At E10.5, Mena expression appears to across all cell layers of the developing ventricle, including cardiomyocytes (Figure 144A-I'). In controls, expression of Mena is significantly greater in the trabeculae myocardium compared to the compact myocardium (Figure 144A-D'). This pattern is lost in *Rac1*^{TnTCre} hearts as the expression of Mena in the trabeculae myocardium is similar to that of the compact myocardium (Figure 144E-I'). Overall expression of Mena is reduced in *Rac1*^{TnTCre} hearts compared to controls (Figure 144, G-H compared to A-D). Intensity analysis using ImageJ software revealed that Rac1 is significantly increased in the trabeculae of control ventricles compared to the compact layer, however in *Rac1*^{TnTCre} ventricles this difference in staining intensity is unchanged between the two layers of the ventricles ($P<0.05$) (Figure 144J). Therefore Mena expression in the trabeculae layer is significanly reduced in *Rac1*^{TnTCre} hearts as compared to controls ($P<0.05$) (Figure 144J). Overall intensity in the compact layer is reduced in *Rac1*^{TnTCre} ventricles but this difference is not significant (Figure 144J).

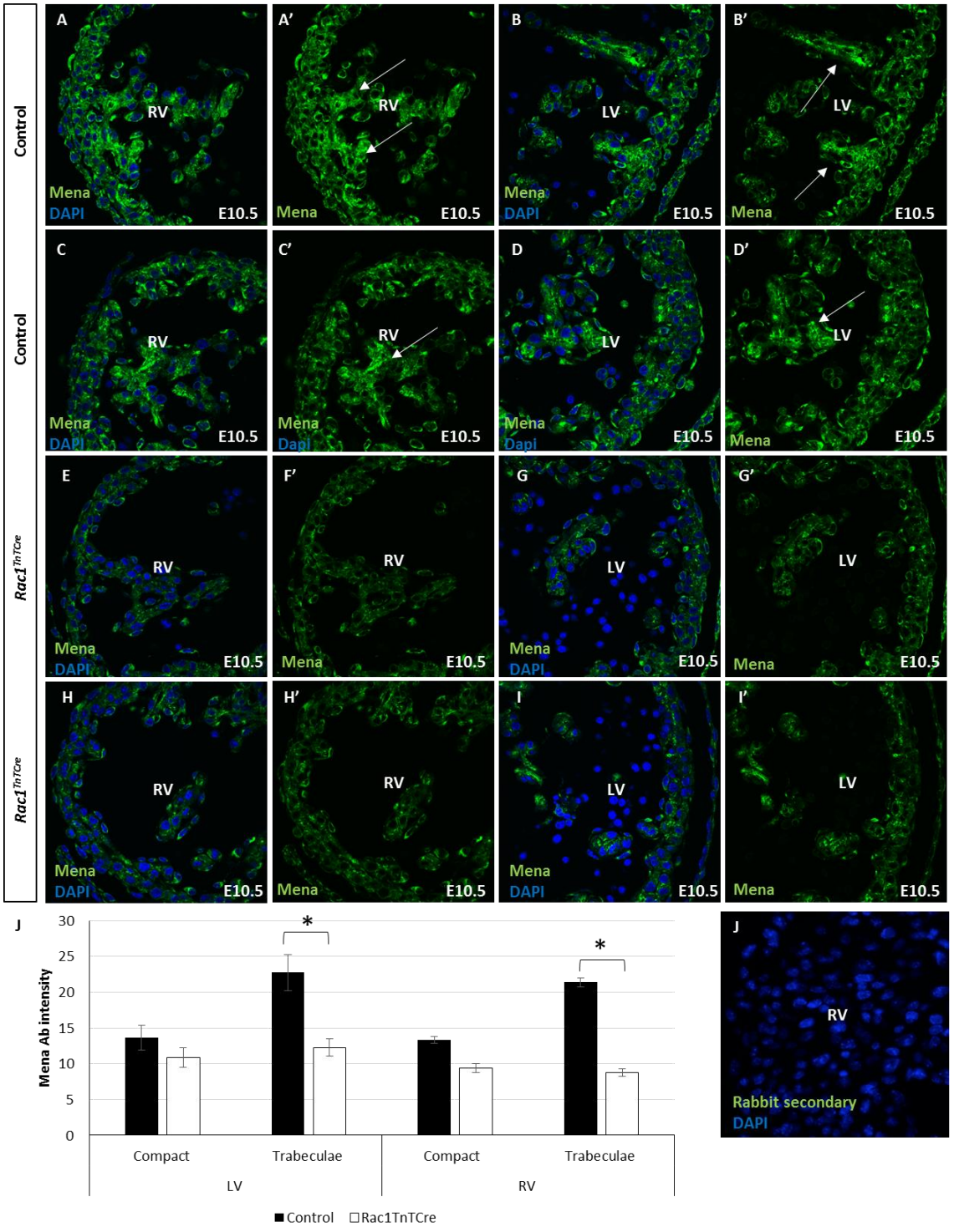

Figure 144: Mena IF staining of E10.5 control and *Rac1*^{TnTCre} transverse sections.

In controls, expression of Mena is greater in the trabeculae myocardium compared to the compact myocardium (**A**-**D**). This pattern is lost in *Rac1*^{TnTCre} hearts as the expression of Mena in the trabeculae myocardium is similar to that of the compact myocardium (**F**-**H**) (n=4). Staining intensity analysis (**J**). Expression of Mena is significantly reduced in the trabeculae layer of *Rac1*^{TnTCre} hearts compared to controls (* P<0.05). LV; left ventricle, RV; right ventricle. Scale bars 50µm. Secondary only control (**K**). Statistical analysis carried out using a two-way ANOVA.

Additionally, Vav2 is a ubiquitously expressed GEF for Rho family GTPases (Abe *et al.*, 2000). At E10.5, Vav2 expression appears across all cell layers of the developing ventricle but is strongest in the myocardium (Figure 145). In controls, expression of Vav2 is organised on the luminal side of the cardiomyocytes, resulting in a visible line of expression through the compact myocardium (arrows in Figure 145A-B). The expression pattern of Vav2 is disrupted in *Rac1*^{TnTCre} hearts with Vav2 being expressed throughout the cardiomyocytes, and the observed polarity of the normal staining pattern is lost within the compact myocardium (Figure 145C-F).

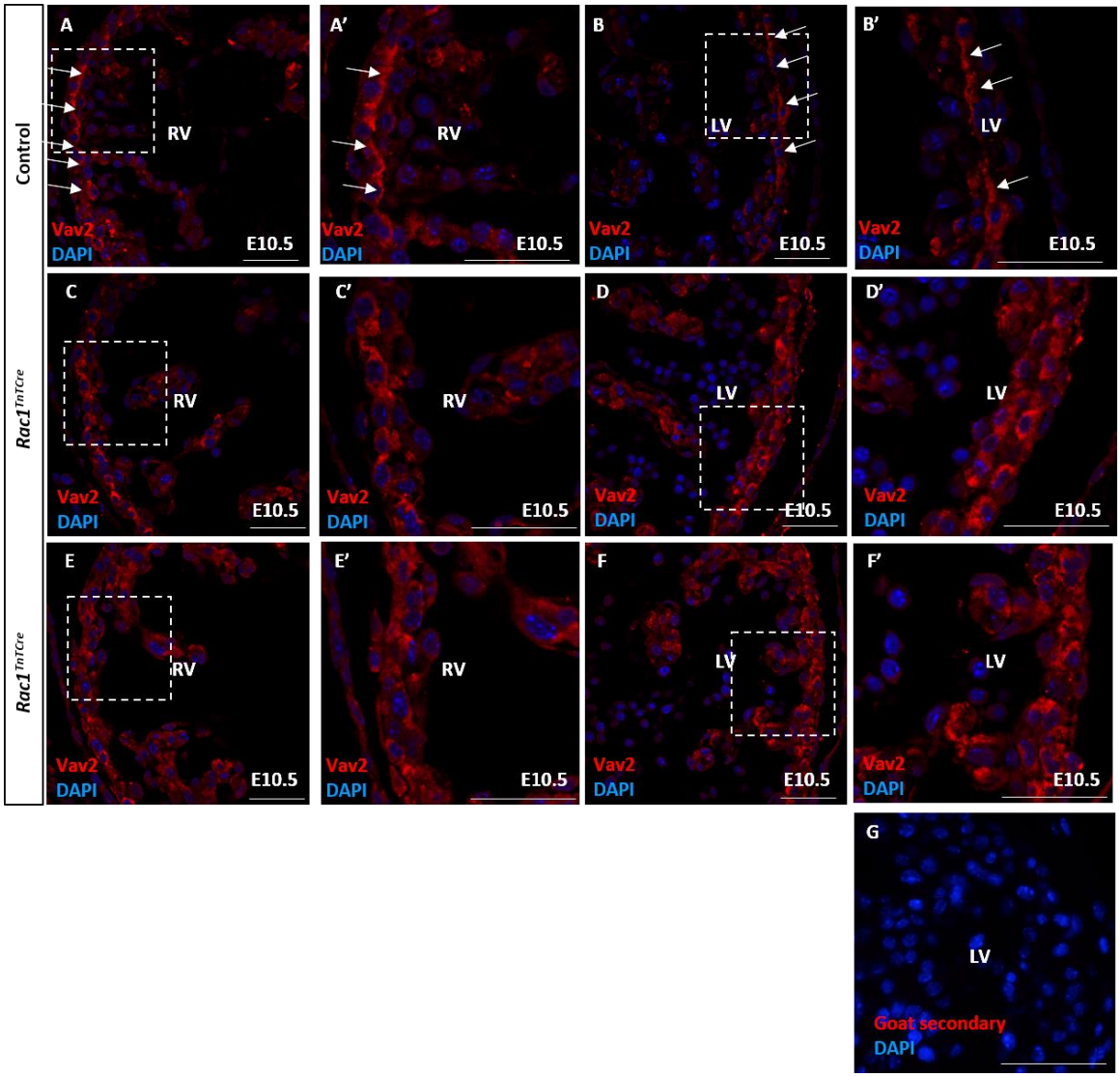

Figure 145: Vav2 IF staining of E10.5 control and *Rac1*^{TnTCre} transverse sections.
At E10.5, Vav2 expression appears across all cell layers of the developing ventricle but is strongest in the myocardium. In controls, expression of Vav2 is organised on the luminal side of the cell, resulting in a line of expression observed through the compact myocardium. The expression pattern of Vav2 is disrupted in *Rac1*^{TnTCre} hearts with Vav2 expressed throughout the cell and the line pattern is lost within the compact myocardium (n=4). Secondary only control (**G**). LV; left ventricle, RV; right ventricle. Scale bars 50µm.

Co-immunoprecipitation (Co-IP) was carried out to confirm that Rac1 interacts with Vav2 in the embryonic heart. IP was performed on CD1 E15.5 whole heart lysate with anti-Rac1 and anti-Vav2 antibodies. The enriched protein lysates were run on a gel along with total heart lysate and blotted for Rac1 and Vav2 antibodies (assistance from Kate Bailey). Expected protein size for Rac1 is 21kDa and for Vav2 is 101kDa. The Co-IP shown in Figure 146 demonstrates that Rac1 and Vav2 interact in the embryonic heart. However, a negative

control (no antibody or a non-specific antibody) was not included in this experiment and therefore, a limitation of the result interpretation is that Rac1/Vav2 binding to the Co-IP beads rather than a physical interaction between the proteins cannot be ruled out.

Rac1 and Mena Co-IP was also tried but this did not work on E15.5 hearts, possibly due to the Mena antibody not detecting at a low level.

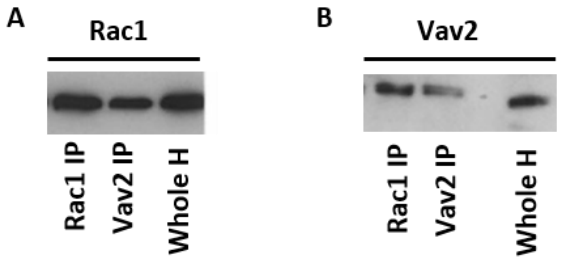

Figure 146: Co-IP analysis shows Rac1 and Vav1 interact in embryonic hearts.
IP performed on CD1 E15.5 whole heart lysate with anti-Rac1 and anti-Vav2 antibodies. The enriched protein lysates were run on a gel along with total heart lysate and blotted for Rac1 and Vav2 antibodies (assistance from Kate Bailey). Expected protein size for Rac1 is 21kDa and for Vav2 is 101kDa.

These results suggest that Rac1 interacts with both Mena and Vav2 in cardiomyocytes to regulate trabeculation and compact myocardial thickening (Figure 147). Vav2 and Mena expression is altered at E10.5 in the absence of Rac1. In controls Vav2 is expressed on the luminal edge of cardiomyocytes, however in *Rac1*^{TnTCre} hearts Rac1 is aberrantly expressed around all sides of the cardiomyocytes. Mena expression is strongest in the trabeculae layer in controls but is reduced to similar levels to the compact layer in *Rac1*^{TnTCre} mutants.

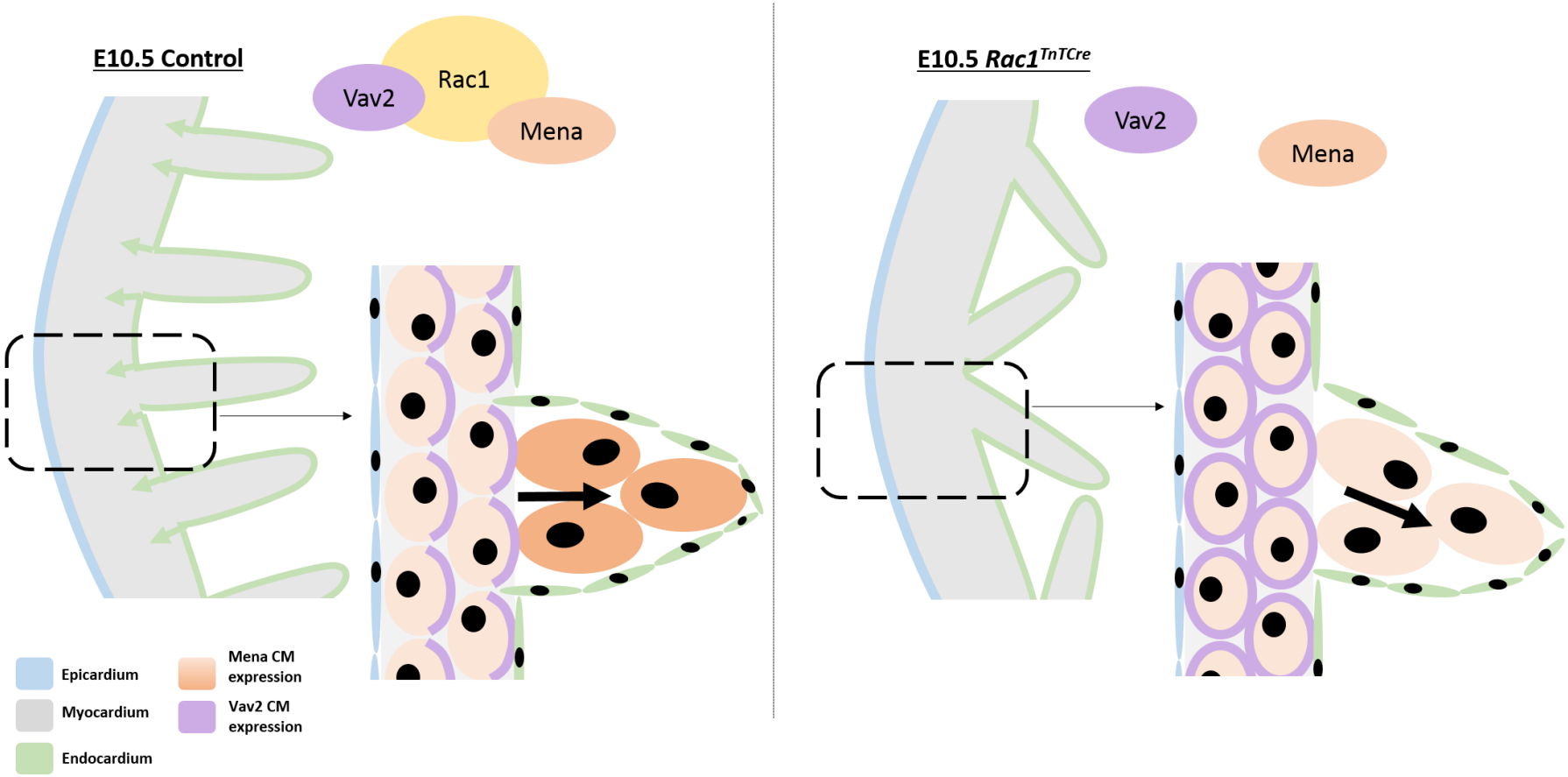

Figure 147: Rac1 interacts with Mena and Vav2 to regulate early ventricular development. Vav2 and Mena expression is altered at E10.5 in the absence of *Rac1*.
In controls Vav2 is expressed on the luminal edge of cardiomyocytes, however in *Rac1*^{TnTCre} hearts Rac1 is aberrantly expressed around all sides of the cardiomyocytes, suggesting loss of cell polarity. Mena expression is strongest in the trabeculae layer in controls but is reduced to similar levels to the compact layer in *Rac1*^{TnTCre} mutants.

5.4 Discussion

The aim of this chapter was to dissect the cellular mechanisms of Rac1 in cardiomyocytes during the maturation of the ventricular myocardium, and to identify the primary cause of the myocardial defects in *Rac1*^{TnTCre} hearts, as described in Chapter 3.

Myocardial deletion of *Rac1* during embryonic development resulted in severe myocardial defects including a thinned myocardial wall and sparse trabeculae formation. This data suggested that Rac1 plays a crucial role in the trabeculae development and thickening of the myocardium. It was hypothesised that disrupted cell polarity and/or cellular organisation leads to defective trabeculae formation and reduced compact myocardial proliferation. To investigate this hypothesis the *Rac1*^{TnTCre} hearts were characterised the at the onset of myocardial defects and the key regulatory cellular processes involved at this stage of embryonic development were examined.

Early in development, at around E9.5, trabeculae formation initiates. Trabeculae are found in all vertebrates and are a landmark in the initiation of ventricular chamber formation (Christoffels *et al.*, 2000). In *Rac1*^{TnTCre} hearts initial trabeculae formation appears unaffected, with trabeculae forming between E9.5-E10.5. This introduces a novel idea of different waves of trabeculae formation, and therefore it is hypothesised that Rac is involved in the ‘second’ wave of trabeculae formation. From E10.5, trabeculae formation is disrupted, with fewer trabeculae forming and large gaps in the compact myocardium that are lacking in trabeculation. The processes involved in trabeculation include cardiomyocyte proliferation, maturation, adhesion and migration and these can be regulated by changes in gene expression, cytoskeletal arrangements and signalling between the myocardium and endocardium. Since Rac1 is known to be involved in many of these processes, each of them were investigated in *Rac1*^{TnTCre} hearts by various methods. In addition, the expression of two potential Rac1 interactors during the onset of the defects in ventricular myocardial development was analysed.

5.4.1 Rac1 deletion does not affect cardiomyocyte proliferation

Cell cycle progression occurs normally in *Rac1*^{TnTCre} cardiomyocytes compared to control cardiomyocytes. Cell cycle gene expression within whole hearts was unchanged and the percentage of cardiomyocytes undergoing proliferation and apoptosis was comparable between control and *Rac1*^{TnTCre} cardiomyocytes. *Rac1*^{TnTCre} hearts display a severely thinned myocardium and fewer trabeculae in a cross-sectional view through the ventricle, however, *Rac1*^{TnTCre} hearts are significantly increased in size compared to control hearts and hence the total cell number is equal between control and *Rac1*^{TnTCre} hearts at E15.5. It is therefore proposed that in *Rac1*^{TnTCre} hearts normal levels of cardiomyocyte proliferation is leading to continued ballooning in the ventricles, with little contribution to increasing the thickness of the myocardial wall and trabeculation. This conclusion suggests that cardiomyocytes have disrupted proliferation directionality in *Rac1*^{TnTCre} hearts.

The lack of changes in either proliferation or cell death in *Rac1*^{TnTCre} hearts is in agreement with *Abu-Issa et al.,* who did not show any changes in proliferation or cell death in the myocardium of *Rac1;Nkx2.5-Cre* mice at E11.5, as determined by BrdU and TUNEL analysis respectively (Abu-Issa, 2014). However, they did not comment on the development of a severely thinned myocardium in the absence of proliferation or apoptosis differences. *Leung et al.* attributed the thinned RV myocardium in *Rac1;Mef2c-Cre* hearts to an increase in apoptosis in cardiomyocytes, with no change in cardiomyocyte proliferation (Leung *et al.*, 2014). Although this analysis was carried out in E11.5 hearts, when the cardiac phenotype was already established. Additionally, deletion of fellow PCP protein Scrib in cardiac progenitors caused a significantly thinned myocardium without any changes in pHHH3 or caspase-3 expression, at E10.5, before the onset of cardiac abnormalities (Boczonadi *et al.*, 2014b).

Rac1 is known to be involved in cell cycle regulation, for example, the expression of a dominant negative form of Rac1 in rat fibroblasts causes growth arrest in the G2/M phase of the cell cycle (Moore *et al.*, 1997). Although this is the case in various cell types, Rac1 does not appear to regulate the cell cycle in embryonic cardiomyocytes.

5.4.2 Rac1 deletion disrupts cardiomyocyte maturation

Early cardiomyocyte differentiation occurs normally in *Rac1*^{TnTCre} hearts; the myocardium expresses classic cardiomyocyte differentiation markers α-SMA, MF20, α-actinin, cardiac-actin and SM22α at E9.5 and E10.5. This is similar to *Notch1* mutants where defects in the endocardium and trabeculae myocardium were observed despite early ventricular myocardial differentiation being unaffected (Grego-Bessa *et al.*, 2007). However, later in development, the maturation of the cardiomyocytes appears affected, with disrupted expression of SM22α and α-SMA within the compact myocardium and trabeculae myocardium. *Rac1*^{TnTCre} cardiomyocytes fail to downregulate the expression of these proteins as the myocardium matures. It is speculated that the altered expression of SM22α and α-SMA is secondary to the abnormal development of the heart. Additionally, divergent maturation of the cardiomyocytes within the compact and trabeculae myocardium compartments is altered. Trabeculae marker *Peg1* is abnormally expressed in the compact myocardium at E10.5. *Peg1,* a paternally imprinted gene, is preferentially expressed in the trabeculae cardiomyocytes and is absent from the compact myocardium, OFT and AVJ during cardiac development stages E9-E12 (King *et al.*, 2002). *Peg1* knockout mice develop subtle but consistent abnormalities in the pattern of trabeculae; the trabeculae are fewer, and appear thicker and more irregular (King *et al.*, 2002). This phenotype is a subtle version of the abnormalities that have been described in this thesis in *Rac1*^{TnTCre} hearts. These similarities suggest that alterations in *Peg1* expression may contribute to the abnormal trabeculae phenotype in *Rac1*^{TnTCre} hearts. *Peg1* expression was also reduced in *Notch* mutants (Grego-Bessa *et al.*, 2007). However, a link between Rac1 and Peg1 is lacking, therefore altered Peg1 expression may be a downstream secondary effect of *Rac1* deletion. An additional trabeculae marker which is disrupted in *Rac1*^{TnTCre} hearts later in ventricular development is ANF. Expression of ANF, a marker of cardiomyocyte growth and differentiation, normally declines in the ventricle rapidly near birth whereas expression in the atrium is maintained (Temsah and Nemer, 2005). During early chamber development, ANF is more strongly expressed in the LV compared to RV, becoming restricted to the LV and absent from the RV later in development (Christoffels *et al.*, 2000). Expression of ANF was retained in the RV of E15.5 *Rac1*^{TnTCre} hearts.

Disrupted ANF has been reported in several other mutants with myocardial phenotypes. E17 *Jumonji* mutants exhibited a higher expression level of ANF than the wild type, suggesting a defect in downregulation of ANF (Lee *et al.*, 2000). *Jumonji* mutants display cardiac defects similar to *Rac1*^{TnTCre} embryos; DORV with abnormal development of the ventricular walls. Jumonji is a nuclear protein that regulates proliferation and is expressed in the myocardium of the ventricles and OFT (Toyoda *et al*., 2003). ANF was also aberrantly expressed in *Hey2* cardiomyocyte mutants and increased in *Hand2* endocardial mutants that display VSD and hypotrabeculated ventricles (Togi *et al.*, 2006; Xin *et al.*, 2007). The retained ANF expression gives further evidence of perturbed maturation of the myocardium.

5.4.3 Rac1 deficient cardiomyocytes are less adhesive

Cardiomyocyte adhesion is affected from E11.5 in the myocardium of *Rac1*^{TnTCre} hearts. Expression of ICD proteins, including AJ proteins, gap junction proteins and desmosomal proteins, is reduced in between cardiomyocytes, suggesting reduced adhesiveness and connectivity within the myocardium of *Rac1*^{TnTCre} hearts. Tight junctions are highly expressed in endothelial cells of the developing endocardium; however they are relatively absent in the embryonic cardiomyocytes that were investigated. Therefore, it was not possible to fully consider the effect of Rac1 deletion on tight junction formation and localisation, which may be disrupted later in embryonic development. The junctions of the ICD are affected subsequent to the onset of disrupted protein expression which contributes to the phenotype at E10.5. Mutations in ICD proteins can lead to cardiovascular defects (Li *et al.*, 1996; Linden *et al.*, 2001; Zhao *et al.*, 2005), therefore the alterations observed in the ICD may lead to further disruption of myocardial development. This is in agreement with *Leung et al*, and *Abu Issa* that described altered β-catenin expression at E13.5 in *Rac1;Mef2c-Cre* hearts and at E11.5 in *Rac1;Nkx2.5-Cre* cardiomyocytes in culture respectively (Abu-Issa, 2014; Leung *et al.*, 2014).

5.4.4 Gene expression changes are minimal in Rac1^{TnTCre} *hearts*

As determined by microarray analysis of E10.5 hearts, there were very few changes in gene expression levels in *Rac1*^{TnTCre} hearts compared to controls. In

addition, the small number of changes that were detected were not able to be confirmed in additional hearts or at a protein level. This is unsurprising since Rac1 is not a transcription factor and although Rac1 is known to regulate gene expression through its activation of JNK and SRF (Hill *et al.*, 1995; Minden *et al.*, 1995), this may not be applicable to its role in cardiomyocytes during development.

5.4.5 Cytoskeleton arrangements are disrupted in Rac1^{TnTCre} hearts

Rac1^{TnTCre} cardiomyocytes have disrupted sarcomere formation; actin myofibrils are thin and disorganised, and Rac1 is known to regulate the actin cytoskeleton; *Rac1* is essential in endothelial cells for regulation of the actin cytoskeleton and lamellipodia protrusion formation that is necessary for endothelial cell migration (Tan *et al.*, 2008). Immunostaining for cardiac-actin and α-actinin did not reveal any visible changes in the actin cytoskeleton. However, TEM imaging detected thin myofibrils forming in aberrant directions in *Rac1^{TnTCre}* cardiomyocytes. TEM is capable of significantly higher resolution images compared to fluorescent microscopy and therefore allows a more in-depth analysis of the actin cytoskeleton. Additionally, since actin myofibrils are only just beginning to form and align at E10.5, some cardiomyocytes displayed less developed actin myofibrils than others, dependent on their position in the compact and trabeculae myocardium. It was, therefore, difficult to investigate any disruptions by IF and TEM images of comparable regions of control and *Rac1^{TnTCre}* ventricles was necessary. Similar to our findings, *Leung et al.* found a deficiency in long actin filaments in PO hearts using phallodin staining of F-actin (Leung *et al.*, 2014). Disruptions of the actin filaments causes myocardial defects. For example, mice lacking *α-tropomyosin-1*, a regulatory protein of the actin thin filaments, develop enlarged, misshapen and non-beating hearts, with a thinned myocardium and fewer trabeculae (McKeown *et al.*, 2014). This phenotype is similar to the *Rac1^{TnTCre}* hearts and similarities within the myocardium include reduced striated myofibrils and smaller adherens junctions (McKeown *et al.*, 2014).

5.4.6 Disruptions to the endocardium and epicardium as a result of Rac1 myocardial deletion

The changes observed in myocardial maturation, adhesion and cytoskeleton, and directionality of compact myocardium proliferation and trabeculation appear to affect the development of the endocardium. Early in ventricular development, endocardial cells were observed trapped within the compact myocardium and the endocardial cells at the base of the trabeculae did not project into the compact myocardium as in controls. Additionally, coronary vessel formation is affected, with no large vessels present in the compact myocardium of *Rac1*^{TnTCre} hearts and smaller blood vessels appear to be forming in aberrant directions.

Signalling pathways between the endocardium and myocardium are crucial for the development of both layers during ventricular development. Some of the main signalling pathways, Notch, VEGF and Semaphorin, were investigated, however any changes in these pathways appeared secondary to the myocardial defects.

The Notch signalling pathway is the main pathway thought to be responsible for the initiation of trabeculation, with many Notch mutants displaying severe trabeculation defects (Grego-Bessa *et al.*, 2007). However, the Notch signalling pathway was unaffected in *Rac1*^{TnTCre} hearts. *N1ICD* was expressed in the endocardium and downstream effector *Hey2* was expressed in the myocardium as in controls. Additional Notch signalling pathway genes *Nrg1/ErbB2/4* and *Bmp10* were also unaffected. This is not surprising since initial trabeculae formation appears unaffected. These results therefore highlight that there is a novel pathway of trabeculation involving Rac1 during the second phase of trabeculation.

VEGF signalling appeared normal at E10.5 with both the ligand and receptor expressed in the myocardium and endocardium respectively. However at E11.5, VEGFR-2 was reduced in the endocardium where no trabeculae were forming. Rac1 promotes VEGF-induced endothelial cell migration by stimulating the formation of lamellipodia and membrane ruffles. Inhibiting Rac1 in human endothelial cells using a dominant negative approach led to reduced *Vegfr-2* mRNA and protein expression (Meissner *et al.*, 2009). In developing ventricles, movement and differentiation of the cardiomyocyte forming a trabeculae may

trigger VEGFR-2 expression in the adjacent endocardium. Therefore, VEGFR-2 expression may be downregulated as a consequence of the lack of trabeculae in *Rac1*^{TnTCre} hearts.

There was no difference in the expression of Sema3a or receptor Nrp1. However, *Sema4c* was strikingly reduced in the compact myocardium, similar to the targeted reduction of *Rac1* in the myocardium. Little has been published about Sema4c in the heart, but it is known to be required for myogenic terminal differentiation (Ko *et al.*, 2005; Wu *et al.*, 2007). Rac1 and Sema4C are not known to interact however Sema4C is linked with Rac1 GEF, Git1, in non-small-cell lung cancer (Li *et al.*, 2015) and expression of active Rac enhances the ability of Plexin-B1 to interact with fellow Sema4D, by stimulating the localisation of Plexin-B1 to the cell surface (Vikis *et al.*, 2002). Rac1 is known to interact directly with the intracellular domain of PlexinA and PlexinB family members, to both regulate receptor activity and propagate downstream signalling processes (Vikis *et al.*, 2000; Vikis *et al.*, 2002; Turner *et al.*, 2004; Tong and Buck, 2005; Bell *et al.*, 2011). These studies suggest that Rac1 deficiency affects Sema4c expression,

In addition to the signalling pathways mentioned above, the ECM also supports both the endocardium and myocardium, and is crucial to signalling between the two layers. Several components of the ECM are disrupted in *Rac1*^{TnTCre} hearts. Collagen, laminin and fibronectin expression all appear disturbed and increased inbetween cardiomyocytes. The expression pattern of collagen is altered within the myocardial layer, laminin is aberrantly expressed between cardiomyocytes of the compact layer and fibronectin expression is expanded into the compact layer from the subepicardium and is expressed between cardiomyocytes. In fibroblasts, Rac1 facilitates MMP mediated matrix remodelling and Rac1 inhibitor prevented matrix degradation (Tovell *et al.*, 2012). The deletion of Rac1 could lead to the upregulation or increased secretion of ECM proteins or the downregulation or decreased secretion of ECM degradation proteins in cardiomyocytes. However, in the absence of transcriptional changes, it is proposed that altered cardiomyocytes cytoskeleton and adhesion leads to disrupted organisation of the myocardium and its surrounding ECM. The increased fibronectin between the myocardial and epicardial layer is indicative of epicardial disfunction. This along with the absence of coronary vessels in

Rac1^{TnTCre} and *Rac1*^{Gata5Cre} hearts and the presense of epicardial blisters in *Rac1*^{Gata5Cre} hearts is suggestive of a secondary epicardial phenotype due to defects in the myocardium.

5.4.7 Rac1 interactors

Mena, a regulator of actin filament assembly and ICD composition, is localised at the ICD and Z-discs where it co-localises with numerous cytoskeletal proteins (Benz *et al.*, 2013). At the ICD Mena co-localised with Cx-43, cadherin and vinculin. Mena associates with active Rac1 in cardiomyocytes and is increased in cardiomyocytes overexpressing Rac1 (Ram *et al.*, 2014). It was shown that Mena is reduced in the myocardium of *Rac1*^{TnTCre} hearts compared to controls at E10.5 and that Cx-43 expression at the ICD is altered from E11.5. These results imply that Rac1 and Mena interact in cardiomyocytes and that Mena expression is altered in the absence of Rac1. αII-Spectrin is part of the Mena/VASP complex and is important for formation and stability of actin networks in the heart. αII-spectrin KO embryos die *in utero* and develop abnormal cardiac shape, cardiac dilation and thinning of the myocardium similar to Rac1 myocardial mutants (Benz *et al.*, 2013). Cardiomyocytes expressing a mutant version of Mena were shown to remain in the compact myocardial layer, suggesting Mena is required for the migration of cardiomyocytes into the trabeculae layer (Toyofuku *et al.*, 2004b). It was shown that Mena is more highly expressed in the trabeculae cardiomyocytes as compared to those in the compact layer. This distinction between the expression of Mena in the trabeculae compared to compact myocardium is lost in the *Rac1*^{TnTCre} hearts. These findings suggest that Mena is required for trabeculae specification and migration from the compact layer. In *Rac1*^{TnTCre} hearts, cardiomyocytes appear to have lost their directionality, with less migration into the trabeculae layer and fewer trabeculae formed. It is concluded that Rac1-Mena interactions are required for the directionality of cardiomyocyte movement, both in the thickening of the compact layer and in the process of trabeculation.

Vav2, an exchange factor for Rho family GTPases (Abe *et al.*, 2000), is associated with active Rac1 in endothelial cells (Liu and Burridge, 2000), and this thesis presents novel data to show that Vav2 and Rac1 are both expressed in cardiomyocytes. Vav2 is known to be required for the formation of actin

filaments and in this Chapter it is shown that Vav2 interacts with Rac1 in the embryonic heart. Our analysis using IF revealed that the localisation of Vav2 is disrupted in E10.5 *Rac1*^{TnTCre} hearts. In controls Vav2 is expressed on the luminal edge of cardiomyocytes, however in *Rac1*^{TnTCre} hearts Vav2 is aberrantly expressed around all sides of the cardiomyocytes, suggesting disrupted cardiomyocyte polarity.

5.4.8 Myocardial disorganisation in Rac1^{TnTCre} is due to altered Rac1-Mena-Vav2 interactions

The alterations in Mena and Vav2 expression suggests a role of both of these proteins in the disruption of the actin cytoskeleton and disorganisation of the compact myocardium seen in *Rac1*^{TnTCre} hearts. At E9.5 there are no abnormalities in *Rac1*^{TnTCre} mutants. The changes in Mena and Vav2 expression appear at E10.5, which is at the onset of subtle cardiac abnormalities; number and directionality of trabeculae begin to be affected and actin myofibril formation is disrupted. Therefore, it is proposed that Rac1-Mena/Vav2 interactions in cardiomyocytes are involved in regulation of the actin filaments and ICD assembly. In the absence of these interactions, the actin myofibrils are disrupted; TEM imaging highlighted disrupted actin filaments at E10.5 (Figure 148).

Unsurprisingly, since Mena-Rac1 interactions regulate the ICD, cardiomyocyte adhesion is affected at later stages of myocardial development with reduced ICD junctions; adhesion junctions (β-catenin, N-cadherin) and gap junctions (Cx-43) from E11.5. In addition, the myocardium appears disorganised with ECM protein expression expanded within the compact myocardium. The altered ECM most likely occurs as a consequence to altered cardiomyocyte adhesion and organisation due to disrupted Rac1/Mena interaction (Figure 148).

The disruption of the myocardium affects the endocardium from early in ventricular development. As mentioned, the ECM between these two layers is affected with altered laminin, fibronectin and collagen expression. The endocardium shows reduced VEGFR-2 expression, and endocardial cells appear pooled at the base of the trabeculae and appeared trapped within the compact layer at E11.5. It is proposed that this is due to the altered ECM composition and reduced adhesion between cardiomyocytes. Additionally, the

endocardial cells do not protrude into the compact myocardium at the base of the trabeculae as in controls. This again could be due to the increased ECM surrounding the cardiomyocytes and reduced adhesion. It is hypothesised that the lack of these projecting endocardial cells further contribute to the altered directionality of the trabeculae as these endocardial cells appear to be supporting the trabeculae at the base. Later in development, at E15.5, the compact myocardium is lacking in CD31-positive coronary vessels and is scattered with endomucin positive cells (Figure 148). The trabeculae seem to undergo aberrant remodelling, possibly in order to compensate for the severely thinned myocardium, leading to trapping of endocardial cells within the compact myocardium.

Mena appears to be required for movement of cardiomyocytes into the trabeculae layer through actin regulation; hence, in the absence of Rac1-Mena interaction in *Rac1*^{TnTCre} cardiomyocytes there is reduced Mena and fewer trabeculae formed. The trabeculae that do form appear aberrant in shape and size and display altered gene expression including ANF, α-SMA and SM22α (Figure 148).

In *Rac1*^{TnTCre} hearts, lack of Rac1-Mena/Vav2 interaction leads to disorganisation of the myocardial wall, disrupting the directionality of growth of the myocardium. Therefore, the heart balloons in size but the compact layer is does not undergo thickening and trabeculae formation is reduced. Regulated oriented cell division may be required for the initiation or trabeculation, compact layer expansion and maintenance of heart shape and size, and is altered in the absence of Rac1-Mena-Vav2 interactions.

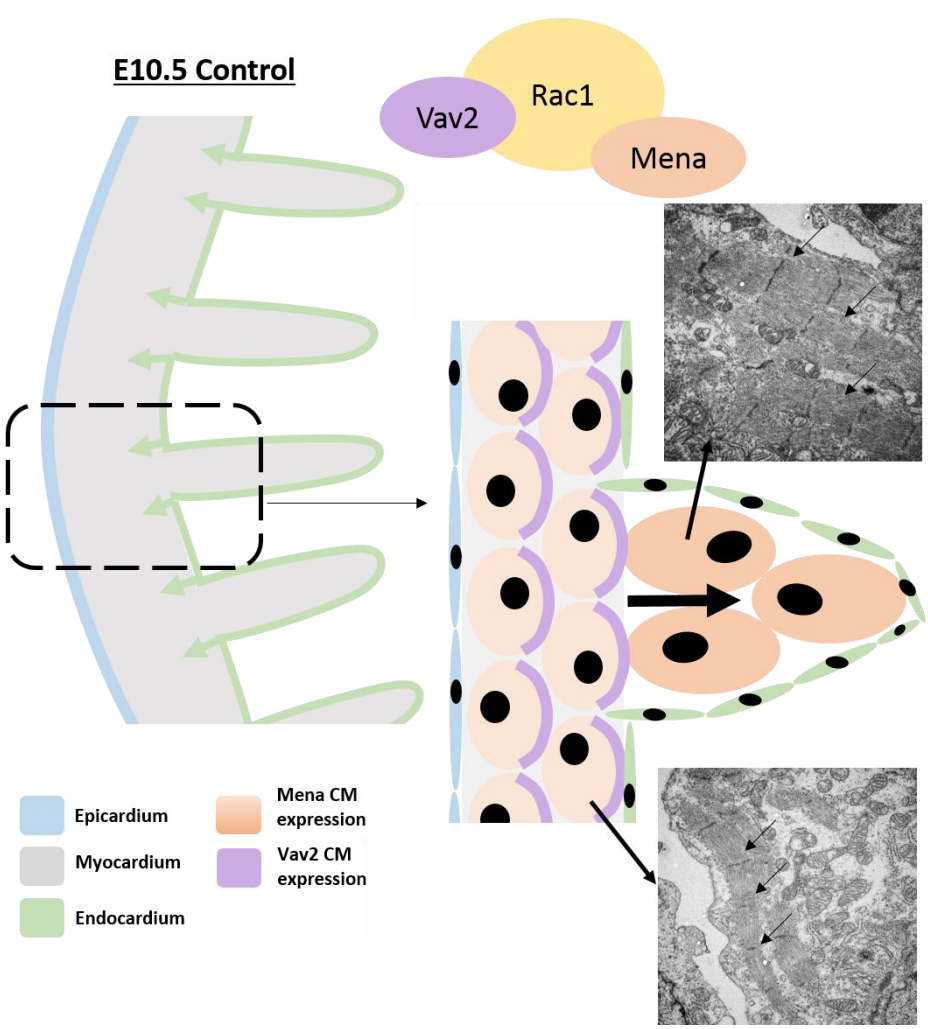
E10.5 Control
Vav2
Rac1
Mena
Epicardium
Myocardium
Endocardium
Mena CM expression
Vav2 CM expression

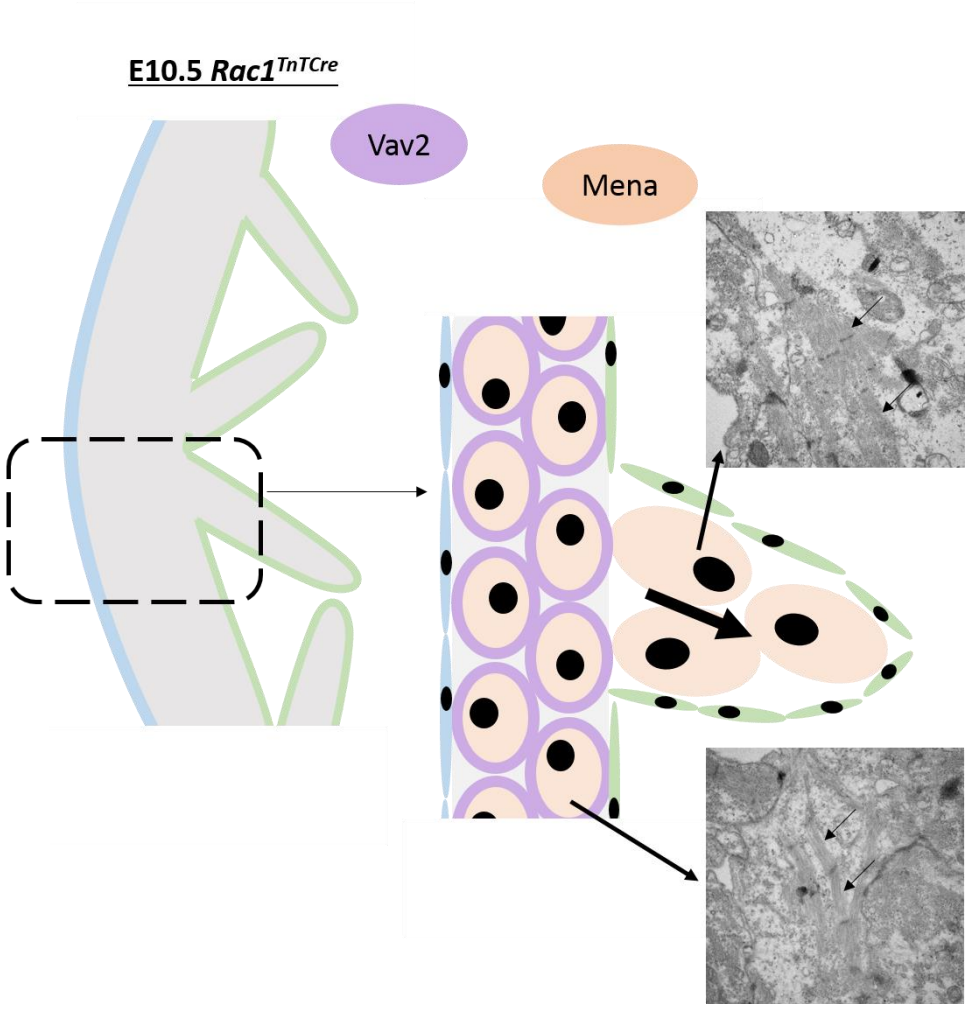
E10.5 Rac1TnTCre
Vav2
Mena

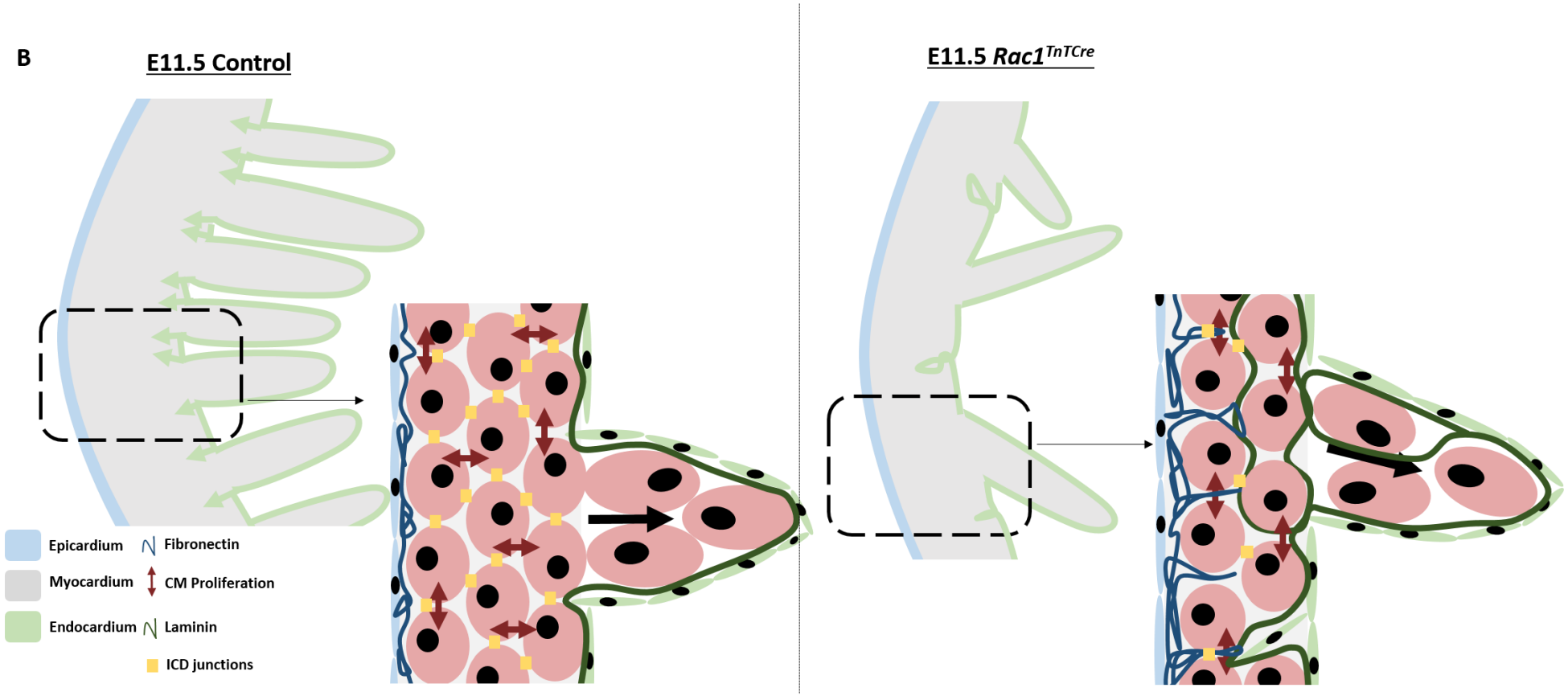
B
E11.5 Control
E11.5 Rac1TnTCre
Epicardium
Myocardium
Endocardium
Fibronectin
CM Proliferation
Laminin
ICD junctions

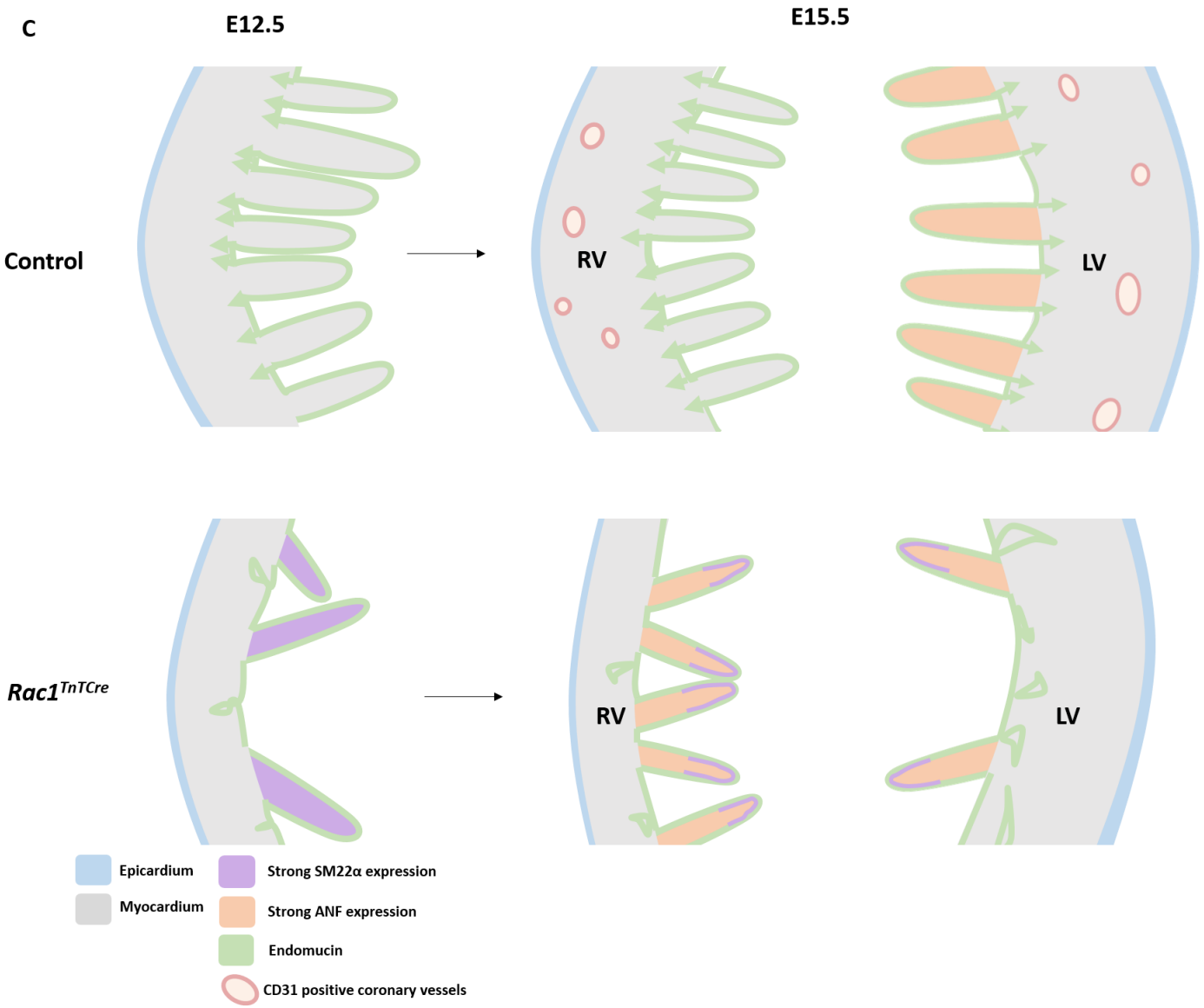
C
E12.5
E15.5
Control
RV
LV
Rac1TnTCre
RV
LV
Epicardium
Myocardium
Strong SM22α expression
Strong ANF expression
Endomucin
CD31 positive coronary vessels

Figure 148: Rac1 interacts with Mena and Vav2 to regulate early ventricular development, which leads to disruption of cardiomyocyte cytoskeletion and ICD, in addtion to alterations in the endocardium and coronary vessel formation later in development.

At E10.5 (**A**) Vav2 and Mena expression is altered in the absence of Rac1. In controls Vav2 is expressed on the luminal edge of cardiomyocytes, however in *Rac1*^{TnTCre} hearts, Vav2 is aberrantly expressed around all sides of the cardiomyocytes, suggesting loss of cell polarity. Mena expression is strongest in the trabeculae layer in controls but is reduced to similar levels to the compact layer in *Rac1*^{TnTCre} mutants. As a result of this actin myofibril disruption appears at E10.5 in both compact and trabeculae cardiomyocytes. At E11.5 (**B**), Rac1 deficient cardiomyocytes display altered ICD expression (yellow) and Desmin intermediate filaments (red) appear clumpy in the trabecular layer. In addition, ECM proteins laminin (blue) and fibronectin (green) are expanded within the compact myocardium. At E12.5 (**C**), some endomucin-positive cells become trapped within the myocardium (green) and trabeculae cardiomyocytes retain strong SM22α expression. Later in development, at E15.5 (**C**), the compact myocardium is lacking in CD31-positive coronary vessels (pink) and is scattered with endomucin positive cells (green), and the right ventricle trabeculae retain strong expression of ANF (orange).

The trabeculae seem to undergo aberrant remodelling, possibly in order to compensate for the severely thinned myocardium, leading to trapping of endocardial cells within the compact myocardium. Additionally, the difference between the right and left ventricle walls from suggests there is differential remodelling between the two ventricles in mutant hearts. The RV remains thin with relatively large numbers of trabeculae compared to controls, whereas the LV thickens and becomes smooth on the inner surface with relatively few trabeculae. However, this thickened left ventricular wall is less densely packed than in controls and contains ‘trapped’ endomucin positive endocardial cells.

Chapter 6. Final Discussion

6.1 Summary

Heart development in mammals is a very complex and highly regulated process. When heart development is disrupted CHDs can arise. CHDs are the most common form of birth abnormalities and in the majority of cases the cause is unknown. Evidence suggests that abnormalities occurring *in utero* can predispose individuals to heart disease in adult life. Therefore, investigating the genetic causes of CHD is relevant to treatment of both CHD and adult CVD.

Rac1, a member of the Rho family of small GTPases, is involved in a variety of cellular processes, such as cell migration, polarity, survival, morphology, proliferation and differentiation. Rac1 has been shown to play a critical role during embryonic development (Sugihara *et al.*, 1998) and appears to be reactivated during CVD (de las Fuentes *et al.*, 2012).

During heart development, the FHF forms the linear heart tube, consisting of a myocardial layer with an inner endocardial layer. Over the course of embryonic development, the linear tube loops and septates to form the four-chambered heart. This process requires the addition of extra-cardiac populations including the PE, NCC and SHF. At the onset of this thesis, the role of Rac1 in endothelial cells and NCC had been investigated in previous publications (Tan *et al.*, 2008; Thomas *et al.*, 2010). The role of Rac1 in adult cardiomyocytes during CVD had been studied in many publications (Higuchi *et al.*, 2003; Buscemi *et al.*, 2005; Satoh *et al.*, 2006). However, studies investigating the role of Rac1 in epicardial cells and cardiomyocytes during embryonic development were lacking. Therefore, genetically modified mice were used to delete *Rac1* from these cell populations and investigate the role of Rac1 during cardiovascular development. Since the onset of this project however, two papers have been published investigating the role of Rac1 within cardiomyocytes by conditionally deleting Rac1 from cardiac mesoderm progenitors and SHF progenitors (Abu-Issa, 2014; Leung *et al.*, 2014). These papers use *Mef2c-Cre* and *Nkx2.5-Cre* transgenic mouse lines to conditionally delete Rac1, which differ from our *TnT-Cre* mediated deletion as the Cre lines

include additional cell types as well as cardiomyocytes. These studies suggested that Rac1 is critical for cardiomyocyte polarity and adhesion during heart development. However, Abu-Issa provides very limited phenotyping data and poor quality immunostaining in cultured cardiomyocytes (Abu-Issa, 2014) and Leung *et al.* investigated gene transcriptional changes in hearts with a severe phenotype at E13.5, therefore the altered gene expression quantified could to be secondary to cellular changes (Leung *et al.*, 2014). Additionally, both Abu Issa and Leung and colleagues use conditional deletions of Rac1 which include multiple cell types, and are therefore, unable to identify the role of Rac1 solely in cardiomyocytes during myocardial development. Thus the role of Rac1 in early myocardial development remains unclear, particularly during the formation of the trabeculae and compaction of the myocardium. The work in this thesis confirms the findings of both Leung *et al.* and Issa; that Rac1 is required in cardiomyocytes for normal heart development and deletion of Rac1 results in cardiac abnormalities. In addition, as outlined below, this thesis gives an in depth evaluation of the role of Rac1 in pure epicardial and myocardial populations during embryonic heart development and identifies primary changes in cell morphology and protein expression at the onset of cardiac defects.

Work in this thesis confirmed that *Rac1* is expressed in the embryonic heart, within the myocardium, endocardium and epicardium layers. It was shown through several genetic mouse crosses that *Rac1* is crucial in cardiomyocytes for myocardial development, whilst expression in the epicardium may not be required. Myocardial deletion of *Rac1* resulted in reduced trabeculation, myocardial thinning and OFT alignment defects.

Although *TnT-Cre* is expressed from E7.5 in *Troponin-T* expressing cardiomyocytes, early cardiomyocyte differentiation is unaffected in *Rac1* myocardial mutants. Additionally, linear heart tube formation and initial trabeculae formation are unaltered. These findings suggest that *Rac1* is not required before E10.5 for cardiomyocytes differentiation and heart morphology. This is consistent with reports from Abu-Issa, where despite early activation of *Nkx2.5-Cre, c*ardiac mesoderm specification and heart tube formation and looping is unaffected in $Rac1^{Nkx2.5Cre}$ embryos (Abu-Issa, 2014).

In this project the role of Rac1 has been investigated specifically in cardiomyocytes during early ventricular development and two key proteins have been identified that interact with Rac1 and show altered expression in the absence of Rac1. Unlike the recent publications described, in this thesis primary defects have been identified at the point of onset of cardiac abnormalities and are separated from the defects which are secondary to the original defects but also contribute to the phenotype in later in development. *Rac1* deficient cardiomyocytes display aberrant expression of Rac1 interacting proteins, Vav2 and Mena, as well as disruption of the actin cytoskeleton at E10.5. At this time, subtle abnormalities begin to appear in the myocardium, including reduced trabeculae formation and altered directionality of trabeculae. Subsequently, at E11.5, cardiomyocyte adhesion is affected with reduced expression of ICD proteins. Therefore, it is proposed from the results in this thesis, that Rac1-Mena/Vav2 interactions in cardiomyocytes are involved in regulation of the actin filaments and ICD composition. Additionally the disruption of these proteins in *Rac1* myocardial mutants leads to the myocardial disorganisation and altered expression of ECM proteins observed within the compact myocardium. The altered Rac1-Mena/Vav2 interactions and disorganisation of the myocardium in *Rac1* myocardial mutants leads to several morphological disruptions as the hearts develop.

After E10.5, trabeculae formation is affected with trabeculae forming in aberrant directions and large portions of smooth compact myocardium appear where no trabeculae have formed. The migration mechanisms of cardiomyocytes into the trabeculae layer remains controversial, however, Rac1 is required in endothelial cells for cell migration and Rac1 deficient cells displayed reduced focal adhesion and lamellipodia formation with unorganised cell adhesion (Tan *et al.*, 2008). Therefore, it is proposed that Rac1 is also required for the migration of cardiomyocytes into the trabeculae layer, as in endothelial cells, possibly through interactions with Mena. Mena has been shown to be required for movement of cardiomyocytes into the trabeculae layer (Toyofuku *et al.*, 2004b), therefore reduced trabeculation may result from the observed reduction of Mena in Rac1 deficient cardiomyocytes. The trabeculae that do form appear aberrant in shape and size and display altered gene expression including ANF, α-SMA and SM22α.

It is proposed that the disorganisation of the myocardial wall disrupts the directionality of growth of the myocardium. The compact layer does not undergo thickening and trabeculae formation is reduced, resulting in a dilated/ballooning heart. Regulated oriented cell division may be required for the initiation or trabeculation, compact layer expansion and maintenance of heart shape and size. Analysis of this using antibodies against oriented expressed proteins such as Aurora B should be investigated to determine if this is altered in the absence of Rac1-Mena-Vav2 interactions.

The disruption of the myocardium affects the development of the endocardium from E11.5. Endocardial cells are gathered at the base of the trabeculae and are trapped within the compact layer at E11.5. Additionally, the endocardial cells do not protrude into the compact myocardium at the base of the trabeculae as in controls. Later in development, the trabeculae undergo aberrant remodelling, in order to compensate for the severely thinned myocardium, leading to trapping of endocardial cells within the compact myocardium. No coronary vessels are seen in *Rac1*^{TnTCre} hearts. The orgin of coronary endothelium is still controversial, however several populations have been documented, including the SV, epicardium and endocardium. It is hypothesied that Rac1 is required in cardiomyocytes to produce a thickening compact layer which allows migration of endocardial cells and also formation of coronary vessels from the contributing sources.

Myocardial deletion of *Rac1* does not affect initial OFT formation but leads to defects in OFT remodelling and alignment. The DORV/OA defects arise as a consequence of the severe abnormalities in ventricular chamber development and disrupted ventricular septation. The ventricle myocardium is severely thinned in *Rac1* myocardial mutants from E12.5, whereas, the OFT myocardium and IVS is relatively thick compared to control hearts. This suggests that Rac1 is not required in cardiomyocytes for the processes occurring in the IVS or OFT myocardium, however it is crucial for development of the ventricular free wall myocardium. This also suggests, in agreement with previous data, that these myocardial populations develop differently (Togi *et al.*, 2006). *Mlc2v-Cre* is highly expressed in the IVS; however there is no disruption of IVS formation in *Rac1*$^{Mlc2v\text{-}Cre}$ embryos, and *Gata5-Cre* is not expressed in the IVS but results in VSD similar to *Rac1*^{TnTCre} hearts. Combination of results from all Cre line

crosses suggests Rac1 is selectively required for myocardial maturation in the ventricular free wall and is not required for the development of the IVS or OFT myocardium. Since Rac1 is expressed ubiquitously throughout the heart, this again suggests that these myocardial populations developed differently and Rac1 is specifically involved in processes in the free wall ventricular myocardium. In *Rac1* myocardial mutants, the combination of a thinned ventricle myocardium with a thick developed OFT myocardium leads to abnormal heart shape and defective OFT positioning later in development. As correct alignment of the OFT requires compaction and rotation of the OFT myocardium (Bamforth *et al.*, 2001; Watanabe *et al.*, 2001; Bajolle *et al.*, 2006), without the support of the ventricle myocardium, the OFT myocardium cannot correctly rotate to facilitate OFT alignment in Rac1 myocardial mutants. Additionally, the dilated and ballooned shape of the ventricles is likely to impact on atrioventricular septation, meaning the aorta remains associated with the RV.

6.2 Conclusion

Rac1 and interacting partners Vav2 and Mena are required for actin cytoskeleton organisation and ICD arrangement. Thus, Rac1 is required to maintain cardiomyocyte organisation within the compact layer of the myocardium, which allows orientated cell proliferation required for compact myocardial thickening and for the migration of cardiomyocytes into the trabeculae layer.

6.3 Future work

6.3.1 Rac1 interactions with Mena and Vav2

The interaction between Rac1 and Mena/Vav2 in cardiomyocytes requires further investigation. Absence of gene expression changes from microarray analysis suggests that Mena and Vav2 are disrupted on a protein level. Mena is significantly reduced in the trabeculae layer and is subtly reduced in the compact layer and the cellular localisation of Vav2 is altered. Through the use of Co-IP, interactions between Rac1 and Vav2 within the embryonic heart has been confirmed. Rac1-Mena interactions were investigated using Co-IP, however this was unsuccessful. Since it has been published previously in cardiomyocytes, it is possible that this may have been due to the amount of

protein analysed and age of tissue investigated (Ram *et al.*, 2014). Mena expression is reduced as the heart develops, therefore this analysis should be carried out on younger E10.5 hearts; however obtaining enough protein for a Co-IP can be technically difficult from such a small amount of tissue. Additionally, the same analysis could be carried out in isolated cardiomyocytes to confirm the interaction between the proteins in cardiomyocytes alone.

Since Rac1 has a pivotal role in focal adhesion assembly, possible disruptions in focal adhesions in embryonic cardiomyocytes could be analysed by carrying out IF staining using focal adhesion protein antibodies such as vinculin, paxillin and PAK. The lack of reliability of the antibodies tested did not allow for investigation of these proteins in this thesis.

6.3.2 Role of Rac1 in endocardial cells during ventricular development

Using endothelial specific Cre line *Tie2-Cre*, Rac1 was deleted from endothelial cells. These embryos die at E9.5 due to developmental delay, with defective development of major vessels and complete lack of smaller branched vessels (Tan *et al.*, 2008). Since endocardial cells represent a small sub-population of endothelial cell, endocardial specific deletion of Rac1 would isolate the role of Rac1 in the endocardium. A potential Cre mouse for this experiment is *Nrp3-Cre,* as this Cre line is specific to endocardial cells and does not include additional endothelial sources such as the SV and epicardium (Zhang *et al*., 2016).

6.3.3 Role of Rac1 in epicardial cells during epicardium formation and migration of EDPCs

The deletion of *Rac1* in epicardial cells using *WT1-CreERT2* did not affect myocardial development during embryonic development. Histology analysis did not reveal any cardiac abnormalities at E15.5, specifically myocardial thickening is not affected. Additionally the formation of the epicardium and migration of EPDCs was not significantly altered as observed by GFP IHC staining. However, this deletion may be detrimental to further myocardial and coronary vessel development, postnatally, or in the adult heart. Since EPDCs migrate into the compact myocardium and differentiate into SMC and endothelial cells of the coronary vessels, as well as fibroblasts, these cell populations may be

affected in the absence of Rac1. Differentiation markers such as SM22α for smooth muscle cells, CD31 for coronary endothelial cells and vimentin for cardiac fibroblasts, could be analysed in GFP-positive cells to determine if any of these differentiation processes are affected by the loss of *Rac1*.

Some of the defects seen in *Rac1*^{TnTCre} and *Rac1*^{Gata5Cre} hearts are typical of an epicardial phenotype. Further studies could aim to confirm the cause of the epicardial defects. The work presented in this thesis suggests the epicardial defects are secondary to myocardial defects. However, since Rac1 delection was assessed indirectly with EYFP expression in *Rac1*^{Gata5Cre} and *Rac1*$^{WT1\text{-}CreERT2}$, a role of Rac1 in epicardial cells cannot be excluded.

6.3.4 Additional signalling pathways between the endocardium and myocardium

Additional signalling pathways which may be affected between the myocardium and endocardium include FGF, TGF-β and Ang/Tie2 signalling. FGF ligands binds to FGF receptors in either a cell autonomous or non-cell autonomous manner. In mice, the FGF ligands are expressed in endocardial cells and FGF receptors are expressed in endocardial cells as well as in myocardial cells. Gene inactivation studies have determined that FGF signalling from endocardial to myocardial cells regulates proliferation of the compact myocardium and trabeculation, therefore FGF signalling may be reduced in *Rac1*^{TnTCre} ventricles (Mima *et al.*, 1995; Lavine *et al.*, 2005; Lu *et al.*, 2008). TGF-β signalling is mediated via a heterotetrameric receptor complex, composed of two TGF-β type II (TGFβRII) receptors and two type I (Alk5) receptors. Genetic disruptions of this signalling in mice has highlighted a role in ventricular development, and results in similar defects to those seen in *Rac1*^{TnTCre} mutants; *Alk5-Gata5-Cre* mutants have a thinned myocardium with reduced cell-cell adhesion in epicardial cells (Sridurongrit *et al.*, 2008; Snider *et al.*, 2014). FKBP12 is associated with BMP/TGF-β signalling (Wang *et al.*, 1996) and is expressed at high levels in the endocardium, myocardium, and septum. FKBP12 deficient mice die between E14.5 and birth due to severe dilated cardiomyopathy and VSD. FKBP12 hearts had thinner left ventricular walls, hypertrophic trabeculae, and deep intertrabecular recesses which resembled LVNC (Shou *et al.*, 1998). Angiopoietin-1 (Ang-1) is a ligand produced in the myocardium and signals to

the Tie2 receptor in the endocardium. This signalling is essential for coronary vein formation and normal ventricular maturation (Shalaby *et al.*, 1995; Suri *et al.*, 1996). Angiopoietin-1 mutants are embryonic lethal at E12.5, with an immature endocardium. The mutants display a ventricular phenotype similar to Nrg1/ErbB2/4 mutants. Cardiomyocyte-specific Ang-1 deletion results in defective formation of subepicardial coronary veins, but had no significant effect on the formation of intramyocardial coronary arteries. Ang-1 regulates proliferation, migration and differentiation of immature ECs derived from the SV (Arita *et al.*, 2014). These signalling pathways could be investigated by the techniques used in this thesis; immunostaining, qPCR and *in situ* hybridisation.

6.3.5 Rac1 mutations in Patients

Patients with abnormal ventricular walls and/or DORV could be screened for mutations in *Rac1* or interacting partners *Mena* and *Vav2*.

6.4 Final Remarks

In this thesis, it is shown that Rac1 interactions with Mena and Vav2 act to regulate crucial processes that underlie initial trabeculation and compact myocardial thickening. This thesis also highlights the differences between the development of the left and right ventricles, and therefore should be taken into consideration in research and clinical evaluation of the two ventricles.

References

Abe, K., Rossman, K.L., Liu, B., Ritola, K.D., Chiang, D., Campbell, S.L., Burridge, K. and Der, C.J. (2000) 'Vav2 is an activator of Cdc42, Rac1, and RhoA', *J Biol Chem*, 275(14), pp. 10141-9.

Abraham, S., Yeo, M., Montero-Balaguer, M., Paterson, H., Dejana, E., Marshall, C.J. and Mavria, G. (2009) 'VE-Cadherin-mediated cell-cell interaction suppresses sprouting via signaling to MLC2 phosphorylation', *Curr Biol*, 19(8), pp. 668-74.

Abu-Issa, R. (2014) 'Rac1 modulates cardiomyocyte adhesion during mouse embryonic development', *Biochem Biophys Res Commun*.

Abu-Issa, R. and Kirby, M.L. (2007) 'Heart field: from mesoderm to heart tube', *Annu Rev Cell Dev Biol*, 23, pp. 45-68.

Adam, O., Frost, G., Custodis, F., Sussman, M.A., Schafers, H.J., Bohm, M. and Laufs, U. (2007) 'Role of Rac1 GTPase activation in atrial fibrillation', *J Am Coll Cardiol*, 50(4), pp. 359-67.

Afouda, B.A., Martin, J., Liu, F., Ciau-Uitz, A., Patient, R. and Hoppler, S. (2008) 'GATA transcription factors integrate Wnt signalling during heart development', *Development*, 135(19), pp. 3185-90.

Aguilar, F., Belmonte, S.L., Ram, R., Noujaim, S.F., Dunaevsky, O., Protack, T.L., Jalife, J., Todd Massey, H., Gertler, F.B. and Blaxall, B.C. (2011) 'Mammalian enabled (Mena) is a critical regulator of cardiac function', *Am J Physiol Heart Circ Physiol*, 300(5), pp. H1841-52.

Ahuja, P., Sdek, P. and MacLellan, W.R. (2007) 'Cardiac myocyte cell cycle control in development, disease, and regeneration', *Physiol Rev*, 87(2), pp. 521-44.

Ajima, R., Bisson, J.A., Helt, J.C., Nakaya, M.A., Habas, R., Tessarollo, L., He, X., Morrisey, E.E., Yamaguchi, T.P. and Cohen, E.D. 'DAAM1 and DAAM2 are co-required for myocardial maturation and sarcomere assembly. LID - S0012-1606(15)30049-X [pii] LID - 10.1016/j.ydbio.2015.10.003 [doi]', (1095-564X (Electronic)).

Anderson, R.H., Webb, S., Brown, N.A., Lamers, W. and Moorman, A. (2003a) 'Development of the heart: (2) Septation of the atriums and ventricles', *Heart*, 89(8), pp. 949-58.

Anderson, R.H., Webb, S., Brown, N.A., Lamers, W. and Moorman, A. (2003b) 'Development of the heart: (3) formation of the ventricular outflow tracts, arterial valves, and intrapericardial arterial trunks', *Heart*, 89(9), pp. 1110-8.

Angst, B.D., Khan, L.U., Severs, N.J., Whitely, K., Rothery, S., Thompson, R.P., Magee, A.I. and Gourdie, R.G. (1997) 'Dissociated spatial patterning of gap junctions and cell adhesion junctions during postnatal differentiation of ventricular myocardium', *Circ Res*, 80(1), pp. 88-94.

Arita, Y., Nakaoka, Y., Matsunaga, T., Kidoya, H., Yamamizu, K., Arima, Y., Kataoka-Hashimoto, T., Ikeoka, K., Yasui, T., Masaki, T., Yamamoto, K., Higuchi, K., Park, J.S., Shirai, M., Nishiyama, K., Yamagishi, H., Otsu, K., Kurihara, H., Minami, T., Yamauchi-Takihara, K., Koh, G.Y., Mochizuki, N., Takakura, N., Sakata, Y., Yamashita, J.K. and Komuro, I. (2014) 'Myocardium-derived angiopoietin-1 is essential for coronary vein formation in the developing heart', *Nat Commun*, 5, p. 4552.

Artigiani, S., Conrotto, P., Fazzari, P., Gilestro, G.F., Barberis, D., Giordano, S., Comoglio, P.M. and Tamagnone, L. (2004) 'Plexin-B3 is a functional receptor for semaphorin 5A', *EMBO Rep*, 5(7), pp. 710-4.
Astrof, S., Crowley, D. and Hynes, R.O. (2007) 'Multiple cardiovascular defects caused by the absence of alternatively spliced segments of fibronectin', *Dev Biol*, 311(1), pp. 11-24.
Audebert, S., Navarro, C., Nourry, C., Chasserot-Golaz, S., Lecine, P., Bellaiche, Y., Dupont, J.L., Premont, R.T., Sempere, C., Strub, J.M., Van Dorsselaer, A., Vitale, N. and Borg, J.P. (2004) 'Mammalian Scribble forms a tight complex with the betaPIX exchange factor', *Curr Biol*, 14(11), pp. 987-95.
Bajolle, F., Zaffran, S., Kelly, R.G., Hadchouel, J., Bonnet, D., Brown, N.A. and Buckingham, M.E. (2006) 'Rotation of the myocardial wall of the outflow tract is implicated in the normal positioning of the great arteries', *Circ Res*, 98(3), pp. 421-8.
Bajolle, F., Zaffran, S., Meilhac, S.M., Dandonneau, M., Chang, T., Kelly, R.G. and Buckingham, M.E. (2008) 'Myocardium at the base of the aorta and pulmonary trunk is prefigured in the outflow tract of the heart and in subdomains of the second heart field', *Dev Biol*, 313(1), pp. 25-34.
Bamforth, S.D., Braganca, J., Eloranta, J.J., Murdoch, J.N., Marques, F.I., Kranc, K.R., Farza, H., Henderson, D.J., Hurst, H.C. and Bhattacharya, S. (2001) 'Cardiac malformations, adrenal agenesis, neural crest defects and exencephaly in mice lacking Cited2, a new Tfap2 co-activator', *Nat Genet*, 29(4), pp. 469-74.
Bamforth, S.D., Schneider, J.E. and Bhattacharya, S. (2012) 'High-throughput analysis of mouse embryos by magnetic resonance imaging', *Cold Spring Harb Protoc*, 2012(1), pp. 93-101.
Bartram, U., Molin, D.G., Wisse, L.J., Mohamad, A., Sanford, L.P., Doetschman, T., Speer, C.P., Poelmann, R.E. and Gittenberger-de Groot, A.C. (2001) 'Double-outlet right ventricle and overriding tricuspid valve reflect disturbances of looping, myocardialization, endocardial cushion differentiation, and apoptosis in TGF-beta(2)-knockout mice', *Circulation*, 103(22), pp. 2745-52.
Beck, K., Hunter, I. and Engel, J. (1990) 'Structure and function of laminin: anatomy of a multidomain glycoprotein', *Faseb j*, 4(2), pp. 148-60.
Behar, O., Golden, J.A., Mashimo, H., Schoen, F.J. and Fishman, M.C. (1996) 'Semaphorin III is needed for normal patterning and growth of nerves, bones and heart', *Nature*, 383(6600), pp. 525-8.
Bell, C.H., Aricescu, A.R., Jones, E.Y. and Siebold, C. (2011) 'A dual binding mode for RhoGTPases in plexin signalling', *PLoS Biol*, 9(8), p. e1001134.
Belmonte, S.L., Ram, R., Mickelsen, D.M., Gertler, F.B. and Blaxall, B.C. (2013) 'Cardiac overexpression of Mammalian enabled (Mena) exacerbates heart failure in mice', *Am J Physiol Heart Circ Physiol*, 305(6), pp. H875-84.
Benz, P.M., Merkel, C.J., Offner, K., Abesser, M., Ullrich, M., Fischer, T., Bayer, B., Wagner, H., Gambaryan, S., Ursitti, J.A., Adham, I.M., Linke, W.A., Feller, S.M., Fleming, I., Renne, T., Frantz, S., Unger, A. and Schuh, K. (2013) 'Mena/VASP and alphaII-Spectrin complexes regulate cytoplasmic actin networks in cardiomyocytes and protect from conduction abnormalities and dilated cardiomyopathy', *Cell Commun Signal*, 11, p. 56.

Boczonadi, V., Gillespie, R., Keenan, I., Ramsbottom, S.A., Donald-Wilson, C., Al Nazer, M., Humbert, P., Schwarz, R.J., Chaudhry, B. and Henderson, D.J. (2014a) 'Scrib:Rac1 interactions are required for the morphogenesis of the ventricular myocardium', *Cardiovasc Res*.
Boczonadi, V., Gillespie, R., Keenan, I., Ramsbottom, S.A., Donald-Wilson, C., Al Nazer, M., Humbert, P., Schwarz, R.J., Chaudhry, B. and Henderson, D.J. (2014b) 'Scrib:Rac1 interactions are required for the morphogenesis of the ventricular myocardium', *Cardiovasc Res*, 104(1), pp. 103-15.
Boengler, K., Heusch, G. and Schulz, R. (2006) 'Connexin 43 and ischemic preconditioning: effects of age and disease', *Exp Gerontol*, 41(5), pp. 485-8.
Boengler, K., Konietzka, I., Buechert, A., Heinen, Y., Garcia-Dorado, D., Heusch, G. and Schulz, R. (2007) 'Loss of ischemic preconditioning's cardioprotection in aged mouse hearts is associated with reduced gap junctional and mitochondrial levels of connexin 43', *Am J Physiol Heart Circ Physiol*, 292(4), pp. H1764-9.
Borg, T.K., Johnson, L.D. and Lill, P.H. (1983) 'Specific attachment of collagen to cardiac myocytes: in vivo and in vitro', *Dev Biol*, 97(2), pp. 417-23.
Bosco, E.E., Mulloy, J.C. and Zheng, Y. (2009) 'Rac1 GTPase: a "Rac" of all trades', *Cell Mol Life Sci*, 66(3), pp. 370-4.
Botrugno, O.A., Paris, S., Za, L., Gualdoni, S., Cattaneo, A., Bachi, A. and de Curtis, I. (2006) 'Characterization of the endogenous GIT1-betaPIX complex, and identification of its association to membranes', *Eur J Cell Biol*, 85(1), pp. 35-46.
Brickner, M.E., Hillis, L.D. and Lange, R.A. (2000) 'Congenital heart disease in adults. First of two parts', *N Engl J Med*, 342(4), pp. 256-63.
Brown, C.B., Boyer, A.S., Runyan, R.B. and Barnett, J.V. (1996) 'Antibodies to the Type II TGFbeta receptor block cell activation and migration during atrioventricular cushion transformation in the heart', *Dev Biol*, 174(2), pp. 248-57.
Brown, C.B., Feiner, L., Lu, M.M., Li, J., Ma, X., Webber, A.L., Jia, L., Raper, J.A. and Epstein, J.A. (2001) 'PlexinA2 and semaphorin signaling during cardiac neural crest development', *Development*, 128(16), pp. 3071-80.
Bruneau, B.G. (2008) 'The developmental genetics of congenital heart disease', *Nature*, 451(7181), pp. 943-8.
Bruns, A.F., Herbert, S.P., Odell, A.F., Jopling, H.M., Hooper, N.M., Zachary, I.C., Walker, J.H. and Ponnambalam, S. (2010) 'Ligand-stimulated VEGFR2 signaling is regulated by co-ordinated trafficking and proteolysis', *Traffic*, 11(1), pp. 161-74.
Buckingham, M., Meilhac, S. and Zaffran, S. (2005) 'Building the mammalian heart from two sources of myocardial cells', *Nat Rev Genet*, 6(11), pp. 826-35.
Buikema, J.W., Mady, A.S., Mittal, N.V., Atmanli, A., Caron, L., Doevendans, P.A., Sluijter, J.P. and Domian, I.J. (2013) 'Wnt/beta-catenin signaling directs the regional expansion of first and second heart field-derived ventricular cardiomyocytes', *Development*, 140(20), pp. 4165-76.
Buscemi, N., Murray, C., Doherty-Kirby, A., Lajoie, G., Sussman, M.A. and Van Eyk, J.E. (2005) 'Myocardial subproteomic analysis of a constitutively active Rac1-expressing transgenic mouse with lethal myocardial hypertrophy', *Am J Physiol Heart Circ Physiol*, 289(6), pp. H2325-33.
Cai, C.L., Liang X Fau - Shi, Y., Shi Y Fau - Chu, P.-H., Chu Ph Fau - Pfaff, S.L., Pfaff Sl Fau - Chen, J., Chen J Fau - Evans, S. and Evans, S. (2003) 'Isl1 identifies a cardiac progenitor

population that proliferates prior to differentiation and contributes a majority of cells to the heart', (1534-5807 (Print)).
Cai, C.L., Martin, J.C., Sun, Y., Cui, L., Wang, L., Ouyang, K., Yang, L., Bu, L., Liang, X., Zhang, X., Stallcup, W.B., Denton, C.P., McCulloch, A., Chen, J. and Evans, S.M. (2008) 'A myocardial lineage derives from Tbx18 epicardial cells', *Nature*, 454(7200), pp. 104-8.
Cai, G.J., Sun, X.X., Zhang, L. and Hong, Q. (2014) 'Association between maternal body mass index and congenital heart defects in offspring: a systematic review', *Am J Obstet Gynecol*, 211(2), pp. 91-117.
Camelliti, P., Borg, T.K. and Kohl, P. (2005) 'Structural and functional characterisation of cardiac fibroblasts', *Cardiovasc Res*, 65(1), pp. 40-51.
Camenisch, T.D., Spicer, A.P., Brehm-Gibson, T., Biesterfeldt, J., Augustine, M.L., Calabro, A., Jr., Kubalak, S., Klewer, S.E. and McDonald, J.A. (2000) 'Disruption of hyaluronan synthase-2 abrogates normal cardiac morphogenesis and hyaluronan-mediated transformation of epithelium to mesenchyme', *J Clin Invest*, 106(3), pp. 349-60.
Captur, G., Lopes, L.R., Patel, V., Li, C., Bassett, P., Syrris, P., Sado, D.M., Maestrini, V., Mohun, T.J., McKenna, W.J., Muthurangu, V., Elliott, P.M. and Moon, J.C. (2014) 'Abnormal cardiac formation in hypertrophic cardiomyopathy: fractal analysis of trabeculae and preclinical gene expression', *Circ Cardiovasc Genet*, 7(3), pp. 241-8.
Captur, G., Syrris, P., Obianyo, C., Limongelli, G. and Moon, J.C. (2015) 'Formation and Malformation of Cardiac Trabeculae: Biological Basis, Clinical Significance, and Special Yield of Magnetic Resonance Imaging in Assessment', *Can J Cardiol*.
Captur, G., Wilson, R., Bennett, M.F., Luxan, G., Nasis, A., de la Pompa, J.L., Moon, J.C. and Mohun, T.J. (2016) 'Morphogenesis of myocardial trabeculae in the mouse embryo', *J Anat*, 229(2), pp. 314-25.
Carmeliet, P., Ferreira, V., Breier, G., Pollefeyt, S., Kieckens, L., Gertsenstein, M., Fahrig, M., Vandenhoeck, A., Harpal, K., Eberhardt, C., Declercq, C., Pawling, J., Moons, L., Collen, D., Risau, W. and Nagy, A. (1996) 'Abnormal blood vessel development and lethality in embryos lacking a single VEGF allele', *Nature*, 380(6573), pp. 435-9.
Carver, W., Price, R.L., Raso, D.S., Terracio, L. and Borg, T.K. (1994) 'Distribution of beta-1 integrin in the developing rat heart', *J Histochem Cytochem*, 42(2), pp. 167-75.
Chang, F., Lemmon, C.A., Park, D. and Romer, L.H. (2007) 'FAK potentiates Rac1 activation and localization to matrix adhesion sites: a role for betaPIX', *Mol Biol Cell*, 18(1), pp. 253-64.
Chen, F., Kook, H., Milewski, R., Gitler, A.D., Lu, M.M., Li, J., Nazarian, R., Schnepp, R., Jen, K., Biben, C., Runke, G., Mackay, J.P., Novotny, J., Schwartz, R.J., Harvey, R.P., Mullins, M.C. and Epstein, J.A. (2002) 'Hop is an unusual homeobox gene that modulates cardiac development', *Cell*, 110(6), pp. 713-23.
Chen, H., Shi, S., Acosta, L., Li, W., Lu, J., Bao, S., Chen, Z., Yang, Z., Schneider, M.D., Chien, K.R., Conway, S.J., Yoder, M.C., Haneline, L.S., Franco, D. and Shou, W. (2004) 'BMP10 is essential for maintaining cardiac growth during murine cardiogenesis', *Development*, 131(9), pp. 2219-31.
Chen, H.I., Sharma, B., Akerberg, B.N., Numi, H.J., Kivela, R., Saharinen, P., Aghajanian, H., McKay, A.S., Bogard, P.E., Chang, A.H., Jacobs, A.H., Epstein, J.A., Stankunas, K., Alitalo, K. and Red-Horse, K. (2014) 'The sinus venosus contributes to coronary

vasculature through VEGFC-stimulated angiogenesis', *Development*, 141(23), pp. 4500-12.
Chen, J., Kubalak, S.W. and Chien, K.R. (1998) 'Ventricular muscle-restricted targeting of the RXRalpha gene reveals a non-cell-autonomous requirement in cardiac chamber morphogenesis', *Development*, 125(10), pp. 1943-9.
Cheng, G., Wessels, A., Gourdie, R.G. and Thompson, R.P. (2002) 'Spatiotemporal and tissue specific distribution of apoptosis in the developing chick heart', *Dev Dyn*, 223(1), pp. 119-33.
Cherfils, J. and Zeghouf, M. (2013) 'Regulation of small GTPases by GEFs, GAPs, and GDIs', *Physiol Rev*, 93(1), pp. 269-309.
Christoffels, V.M., Habets, P.E., Franco, D., Campione, M., de Jong, F., Lamers, W.H., Bao, Z.Z., Palmer, S., Biben, C., Harvey, R.P. and Moorman, A.F. (2000) 'Chamber formation and morphogenesis in the developing mammalian heart', *Dev Biol*, 223(2), pp. 266-78.
Clerk, A., Pham, F.H., Fuller, S.J., Sahai, E., Aktories, K., Marais, R., Marshall, C. and Sugden, P.H. (2001) 'Regulation of mitogen-activated protein kinases in cardiac myocytes through the small G protein Rac1', *Mol Cell Biol*, 21(4), pp. 1173-84.
Cohen, E.D., Miller, M.F., Wang, Z., Moon, R.T. and Morrisey, E.E. (2012) 'Wnt5a and Wnt11 are essential for second heart field progenitor development', *Development*, 139(11), pp. 1931-40.
Cohen, E.D., Tian, Y. and Morrisey, E.E. (2008) 'Wnt signaling: an essential regulator of cardiovascular differentiation, morphogenesis and progenitor self-renewal', *Development*, 135(5), pp. 789-98.
Conrotto, P., Valdembri, D., Corso, S., Serini, G., Tamagnone, L., Comoglio, P.M., Bussolino, F. and Giordano, S. (2005) 'Sema4D induces angiogenesis through Met recruitment by Plexin B1', *Blood*, 105(11), pp. 4321-9.
Contreras-Ramos, A., Sanchez-Gomez, C., Fierro-Pastrana, R., Gonzalez-Marquez, H., Acosta-Vazquez, F. and Arellano-Galindo, J. (2009) 'Normal development of the muscular region of the interventricular septum. II. The importance of myocardial proliferation', *Anat Histol Embryol*, 38(3), pp. 219-28.
D'Amato, G., Luxan, G., del Monte-Nieto, G., Martinez-Poveda, B., Torroja, C., Walter, W., Bochter, M.S., Benedito, R., Cole, S., Martinez, F., Hadjantonakis, A.K., Uemura, A., Jimenez-Borreguero, L.J. and de la Pompa, J.L. (2016) 'Sequential Notch activation regulates ventricular chamber development', *Nat Cell Biol*, 18(1), pp. 7-20.
D'Uva, G., Aharonov, A., Lauriola, M., Kain, D., Yahalom-Ronen, Y., Carvalho, S., Weisinger, K., Bassat, E., Rajchman, D., Yifa, O., Lysenko, M., Konfino, T., Hegesh, J., Brenner, O., Neeman, M., Yarden, Y., Leor, J., Sarig, R., Harvey, R.P. and Tzahor, E. (2015) 'ERBB2 triggers mammalian heart regeneration by promoting cardiomyocyte dedifferentiation and proliferation', *Nat Cell Biol*, 17(5), pp. 627-38.
Dabiri, G.A., Turnacioglu, K.K., Sanger, J.M. and Sanger, J.W. (1997) 'Myofibrillogenesis visualized in living embryonic cardiomyocytes', *Proc Natl Acad Sci U S A*, 94(17), pp. 9493-8.
Danowski, B.A., Imanaka-Yoshida, K., Sanger, J.M. and Sanger, J.W. (1992) 'Costameres are sites of force transmission to the substratum in adult rat cardiomyocytes', *J Cell Biol*, 118(6), pp. 1411-20.

de las Fuentes, L., Yang, W., Davila-Roman, V.G. and Gu, C. (2012) 'Pathway-based genome-wide association analysis of coronary heart disease identifies biologically important gene sets', *Eur J Hum Genet*, 20(11), pp. 1168-73.
Del Monte, G., Grego-Bessa, J., Gonzalez-Rajal, A., Bolos, V. and De La Pompa, J.L. (2007) 'Monitoring Notch1 activity in development: evidence for a feedback regulatory loop', *Dev Dyn*, 236(9), pp. 2594-614.
Del Valle-Perez, B., Martinez, V.G., Lacasa-Salavert, C., Figueras, A., Shapiro, S.S., Takafuta, T., Casanovas, O., Capella, G., Ventura, F. and Vinals, F. (2010) 'Filamin B plays a key role in vascular endothelial growth factor-induced endothelial cell motility through its interaction with Rac-1 and Vav-2', *J Biol Chem*, 285(14), pp. 10748-60.
Delorme, B., Dahl, E., Jarry-Guichard, T., Briand, J.P., Willecke, K., Gros, D. and Theveniau-Ruissy, M. (1997) 'Expression pattern of connexin gene products at the early developmental stages of the mouse cardiovascular system', *Circ Res*, 81(3), pp. 423-37.
DeRuiter, M.C., Poelmann, R.E., VanderPlas-de Vries, I., Mentink, M.M. and Gittenberger-de Groot, A.C. (1992) 'The development of the myocardium and endocardium in mouse embryos. Fusion of two heart tubes?', *Anat Embryol (Berl)*, 185(5), pp. 461-73.
Desai, A. and Mitchison, T.J. (1997) 'Microtubule polymerization dynamics', *Annu Rev Cell Dev Biol*, 13, pp. 83-117.
Dettman, R.W., Denetclaw, W., Jr., Ordahl, C.P. and Bristow, J. (1998) 'Common epicardial origin of coronary vascular smooth muscle, perivascular fibroblasts, and intermyocardial fibroblasts in the avian heart', *Dev Biol*, 193(2), pp. 169-81.
Dickover, M., Hegarty, J.M., Ly, K., Lopez, D., Yang, H., Zhang, R., Tedeschi, N., Hsiai, T.K. and Chi, N.C. (2014) 'The atypical Rho GTPase, RhoU, regulates cell-adhesion molecules during cardiac morphogenesis', *Dev Biol*, 389(2), pp. 182-91.
Doi, T., Puri, P., Bannigan, J. and Thompson, J. (2011) 'Alteration of gene expression of IQGAP1 and Rho-family GTPases in the cadmium-induced ventral body wall defects in the chick model', *Reprod Toxicol*, 32(1), pp. 124-8.
Duquette, P.M. and Lamarche-Vane, N. (2014) 'Rho GTPases in embryonic development', *Small GTPases*, 5.
Eisenberg, L.M. and Markwald, R.R. (1995) 'Molecular regulation of atrioventricular valvuloseptal morphogenesis', *Circ Res*, 77(1), pp. 1-6.
Eldadah, Z.A., Hamosh, A., Biery, N.J., Montgomery, R.A., Duke, M., Elkins, R. and Dietz, H.C. (2001) 'Familial Tetralogy of Fallot caused by mutation in the jagged1 gene', *Hum Mol Genet*, 10(2), pp. 163-9.
Elnakish, M.T., Awad, M.M., Hassona, M.D., Alhaj, M.A., Kulkarni, A., Citro, L.A., Sayyid, M., Abouelnaga, Z.A., El-Sayed, O., Kuppusamy, P., Moldovan, L., Khan, M. and Hassanain, H.H. (2011) 'Cardiac remodeling caused by transgenic overexpression of a corn Rac gene', *Am J Physiol Heart Circ Physiol*, 301(3), pp. H868-80.
Elnakish, M.T., Hassanain, H.H., Janssen, P.M., Angelos, M.G. and Khan, M. (2013a) 'Emerging role of oxidative stress in metabolic syndrome and cardiovascular diseases: important role of Rac/NADPH oxidase', *J Pathol*, 231(3), pp. 290-300.
Elnakish, M.T., Hassona, M.D., Alhaj, M.A., Moldovan, L., Janssen, P.M., Khan, M. and Hassanain, H.H. (2012) 'Rac-induced left ventricular dilation in thyroxin-treated

ZmRacD transgenic mice: role of cardiomyocyte apoptosis and myocardial fibrosis', *PLoS One*, 7(8), p. e42500.
Elnakish, M.T., Moldovan, L., Khan, M., Hassanain, H.H. and Janssen, P.M. (2013b) 'Myocardial Rac1 Exhibits Partial Involvement in Thyroxin-Induced Cardiomyocyte Hypertrophy and its Inhibition is Not Sufficient to Improve Cardiac Dysfunction or Contractile Abnormalities in Mouse Papillary Muscles', *J Cardiovasc Pharmacol*.
Epstein, J.A., Aghajanian, H. and Singh, M.K. (2015) 'Semaphorin signaling in cardiovascular development', *Cell Metab*, 21(2), pp. 163-73.
Etheridge, S.L., Ray, S., Li, S., Hamblet, N.S., Lijam, N., Tsang, M., Greer, J., Kardos, N., Wang, J., Sussman, D.J., Chen, P. and Wynshaw-Boris, A. (2008) 'Murine dishevelled 3 functions in redundant pathways with dishevelled 1 and 2 in normal cardiac outflow tract, cochlea, and neural tube development', *PLoS Genet*, 4(11), p. e1000259.
Etienne-Manneville, S. and Hall, A. (2002) 'Rho GTPases in cell biology', *Nature*, 420(6916), pp. 629-35.
Fansa, E.K., Dvorsky, R., Zhang, S.C., Fiegen, D. and Ahmadian, M.R. (2013) 'Interaction characteristics of Plexin-B1 with Rho family proteins', *Biochem Biophys Res Commun*, 434(4), pp. 785-90.
Feiner, L., Webber, A.L., Brown, C.B., Lu, M.M., Jia, L., Feinstein, P., Mombaerts, P., Epstein, J.A. and Raper, J.A. (2001) 'Targeted disruption of semaphorin 3C leads to persistent truncus arteriosus and aortic arch interruption', *Development*, 128(16), pp. 3061-70.
Ferrara, N., Carver-Moore, K., Chen, H., Dowd, M., Lu, L., O'Shea, K.S., Powell-Braxton, L., Hillan, K.J. and Moore, M.W. (1996) 'Heterozygous embryonic lethality induced by targeted inactivation of the VEGF gene', *Nature*, 380(6573), pp. 439-42.
Fischer, A., Schumacher, N., Maier, M., Sendtner, M. and Gessler, M. (2004) 'The Notch target genes Hey1 and Hey2 are required for embryonic vascular development', *Genes Dev*, 18(8), pp. 901-11.
Francou, A., Saint-Michel, E., Mesbah, K., Theveniau-Ruissy, M., Rana, M.S., Christoffels, V.M. and Kelly, R.G. (2013) 'Second heart field cardiac progenitor cells in the early mouse embryo', *Biochim Biophys Acta*, 1833(4), pp. 795-8.
Frank, D., Kuhn, C., Katus, H.A. and Frey, N. (2006) 'The sarcomeric Z-disc: a nodal point in signalling and disease', *J Mol Med (Berl)*, 84(6), pp. 446-68.
Fuchs, S., Herzog, D., Sumara, G., Buchmann-Moller, S., Civenni, G., Wu, X., Chrostek-Grashoff, A., Suter, U., Ricci, R., Relvas, J.B., Brakebusch, C. and Sommer, L. (2009) 'Stage-specific control of neural crest stem cell proliferation by the small rho GTPases Cdc42 and Rac1', *Cell Stem Cell*, 4(3), pp. 236-47.
Furuse, M., Fujita, K., Hiiragi, T., Fujimoto, K. and Tsukita, S. (1998) 'Claudin-1 and -2: novel integral membrane proteins localizing at tight junctions with no sequence similarity to occludin', *J Cell Biol*, 141(7), pp. 1539-50.
Gaborit, N., Sakuma, R., Wylie, J.N., Kim, K.H., Zhang, S.S., Hui, C.C. and Bruneau, B.G. (2012) 'Cooperative and antagonistic roles for Irx3 and Irx5 in cardiac morphogenesis and postnatal physiology', *Development*, 139(21), pp. 4007-19.
Garg, V., Muth, A.N., Ransom, J.F., Schluterman, M.K., Barnes, R., King, I.N., Grossfeld, P.D. and Srivastava, D. (2005) 'Mutations in NOTCH1 cause aortic valve disease', *Nature*, 437(7056), pp. 270-4.

Garrett, T.A., Van Buul, J.D. and Burridge, K. (2007) 'VEGF-induced Rac1 activation in endothelial cells is regulated by the guanine nucleotide exchange factor Vav2', *Exp Cell Res*, 313(15), pp. 3285-97.
Gassmann, M., Casagranda, F., Orioli, D., Simon, H., Lai, C., Klein, R. and Lemke, G. (1995) 'Aberrant neural and cardiac development in mice lacking the ErbB4 neuregulin receptor', *Nature*, 378(6555), pp. 390-4.
Gautel, M. and Djinovic-Carugo, K. (2016) 'The sarcomeric cytoskeleton: from molecules to motion', *J Exp Biol*, 219(Pt 2), pp. 135-45.
Gay, C.M., Zygmunt, T. and Torres-Vazquez, J. (2011) 'Diverse functions for the semaphorin receptor PlexinD1 in development and disease', *Dev Biol*, 349(1), pp. 1-19.
Geiger, B. and Bershadsky, A. (2001) 'Assembly and mechanosensory function of focal contacts', *Curr Opin Cell Biol*, 13(5), pp. 584-92.
Gerety, S.S., Wang, H.U., Chen, Z.F. and Anderson, D.J. (1999) 'Symmetrical mutant phenotypes of the receptor EphB4 and its specific transmembrane ligand ephrin-B2 in cardiovascular development', *Mol Cell*, 4(3), pp. 403-14.
Gibbs, B.C., Damerla, R.R., Vladar, E.K., Chatterjee, B., Wan, Y., Liu, X., Cui, C., Gabriel, G.C., Zahid, M., Yagi, H., Szabo-Rogers, H.L., Suyama, K.L., Axelrod, J.D. and Lo, C.W. (2016) 'Prickle1 mutation causes planar cell polarity and directional cell migration defects associated with cardiac outflow tract anomalies and other structural birth defects', *Biol Open*, 5(3), pp. 323-35.
Gitler, A.D., Lu, M.M. and Epstein, J.A. (2004) 'PlexinD1 and semaphorin signaling are required in endothelial cells for cardiovascular development', *Dev Cell*, 7(1), pp. 107-16.
Goddeeris, M.M., Schwartz R Fau - Klingensmith, J., Klingensmith J Fau - Meyers, E.N. and Meyers, E.N. (2007) 'Independent requirements for Hedgehog signaling by both the anterior heart field and neural crest cells for outflow tract development', (0950-1991 (Print)).
Goldfarb, L.G., Park, K.Y., Cervenakova, L., Gorokhova, S., Lee, H.S., Vasconcelos, O., Nagle, J.W., Semino-Mora, C., Sivakumar, K. and Dalakas, M.C. (1998) 'Missense mutations in desmin associated with familial cardiac and skeletal myopathy', *Nat Genet*, 19(4), pp. 402-3.
Goldstein, M.A. and Entman, M.L. (1979) 'Microtubules in mammalian heart muscle', *J Cell Biol*, 80(1), pp. 183-95.
Gould, R.A., Yalcin, H.C., MacKay, J.L., Sauls, K., Norris, R., Kumar, S. and Butcher, J.T. (2016) 'Cyclic Mechanical Loading Is Essential for Rac1-Mediated Elongation and Remodeling of the Embryonic Mitral Valve', *Curr Biol*, 26(1), pp. 27-37.
Grego-Bessa, J., Luna-Zurita, L., del Monte, G., Bolos, V., Melgar, P., Arandilla, A., Garratt, A.N., Zang, H., Mukouyama, Y.S., Chen, H., Shou, W., Ballestar, E., Esteller, M., Rojas, A., Perez-Pomares, J.M. and de la Pompa, J.L. (2007) 'Notch signaling is essential for ventricular chamber development', *Dev Cell*, 12(3), pp. 415-29.
Grimsley-Myers, C.M., Sipe, C.W., Geleoc, G.S. and Lu, X. (2009) 'The small GTPase Rac1 regulates auditory hair cell morphogenesis', *J Neurosci*, 29(50), pp. 15859-69.
Gu, C., Rodriguez, E.R., Reimert, D.V., Shu, T., Fritzsch, B., Richards, L.J., Kolodkin, A.L. and Ginty, D.D. (2003) 'Neuropilin-1 conveys semaphorin and VEGF signaling during neural and cardiovascular development', *Dev Cell*, 5(1), pp. 45-57.

Gupta, V. and Poss, K.D. (2012) 'Clonally dominant cardiomyocytes direct heart morphogenesis', *Nature*, 484(7395), pp. 479-84.
Haataja, L., Groffen, J. and Heisterkamp, N. (1997) 'Characterization of RAC3, a novel member of the Rho family', *J Biol Chem*, 272(33), pp. 20384-8.
Habas, R., Kato, Y. and He, X. (2001) 'Wnt/Frizzled activation of Rho regulates vertebrate gastrulation and requires a novel Formin homology protein Daam1', *Cell*, 107(7), pp. 843-54.
Hakim, Z.S., DiMichele, L.A., Doherty, J.T., Homeister, J.W., Beggs, H.E., Reichardt, L.F., Schwartz, R.J., Brackhan, J., Smithies, O., Mack, C.P. and Taylor, J.M. (2007) 'Conditional deletion of focal adhesion kinase leads to defects in ventricular septation and outflow tract alignment', *Mol Cell Biol*, 27(15), pp. 5352-64.
Hamblet, N.S., Lijam, N., Ruiz-Lozano, P., Wang, J., Yang, Y., Luo, Z., Mei, L., Chien, K.R., Sussman, D.J. and Wynshaw-Boris, A. (2002) 'Dishevelled 2 is essential for cardiac outflow tract development, somite segmentation and neural tube closure', *Development*, 129(24), pp. 5827-38.
Hariharan, R. (2003) 'The analysis of microarray data', *Pharmacogenomics*, 4(4), pp. 477-97.
Harmon, R.M. and Green, K.J. (2013) 'Structural and functional diversity of desmosomes', *Cell Commun Adhes*, 20(6), pp. 171-87.
Hartsock, A. and Nelson, W.J. (2008) 'Adherens and tight junctions: structure, function and connections to the actin cytoskeleton', *Biochim Biophys Acta*, 1778(3), pp. 660-9.
Harvey, R.P. (2002) 'Patterning the vertebrate heart', *Nat Rev Genet*, 3(7), pp. 544-56.
Heinzel, F.R., Luo, Y., Li, X., Boengler, K., Buechert, A., Garcia-Dorado, D., Di Lisa, F., Schulz, R. and Heusch, G. (2005) 'Impairment of diazoxide-induced formation of reactive oxygen species and loss of cardioprotection in connexin 43 deficient mice', *Circ Res*, 97(6), pp. 583-6.
Henderson, D.J. and Chaudhry, B. (2011) 'Getting to the heart of planar cell polarity signaling', *Birth Defects Res A Clin Mol Teratol*, 91(6), pp. 460-7.
Henderson, D.J., Phillips, H.M. and Chaudhry, B. (2006) 'Vang-like 2 and noncanonical Wnt signaling in outflow tract development', *Trends Cardiovasc Med*, 16(2), pp. 38-45.
Hertig, C.M., Kubalak, S.W., Wang, Y. and Chien, K.R. (1999) 'Synergistic roles of neuregulin-1 and insulin-like growth factor-I in activation of the phosphatidylinositol 3-kinase pathway and cardiac chamber morphogenesis', *J Biol Chem*, 274(52), pp. 37362-9.
High, F.A. and Epstein, J.A. (2008) 'The multifaceted role of Notch in cardiac development and disease', *Nat Rev Genet*, 9(1), pp. 49-61.
Higuchi, Y., Otsu, K., Nishida, K., Hirotani, S., Nakayama, H., Yamaguchi, O., Hikoso, S., Kashiwase, K., Takeda, T., Watanabe, T., Mano, T., Matsumura, Y., Ueno, H. and Hori, M. (2003) 'The small GTP-binding protein Rac1 induces cardiac myocyte hypertrophy through the activation of apoptosis signal-regulating kinase 1 and nuclear factor-kappa B', *J Biol Chem*, 278(23), pp. 20770-7.
Hilenski, L.L., Ma, X.H., Vinson, N., Terracio, L. and Borg, T.K. (1992) 'The role of beta 1 integrin in spreading and myofibrillogenesis in neonatal rat cardiomyocytes in vitro', *Cell Motil Cytoskeleton*, 21(2), pp. 87-100.
Hill, C.S., Wynne, J. and Treisman, R. (1995) 'The Rho family GTPases RhoA, Rac1, and CDC42Hs regulate transcriptional activation by SRF', *Cell*, 81(7), pp. 1159-70.

Hingtgen, S.D., Tian, X., Yang, J., Dunlay, S.M., Peek, A.S., Wu, Y., Sharma, R.V., Engelhardt, J.F. and Davisson, R.L. (2006) 'Nox2-containing NADPH oxidase and Akt activation play a key role in angiotensin II-induced cardiomyocyte hypertrophy', *Physiol Genomics*, 26(3), pp. 180-91.
Hirschy, A., Schatzmann, F., Ehler, E. and Perriard, J.C. (2006) 'Establishment of cardiac cytoarchitecture in the developing mouse heart', *Dev Biol*, 289(2), pp. 430-41.
Hota, P.K. and Buck, M. (2012) 'Plexin structures are coming: opportunities for multilevel investigations of semaphorin guidance receptors, their cell signaling mechanisms, and functions', *Cell Mol Life Sci*, 69(22), pp. 3765-805.
Huber, A.B., Kolodkin, A.L., Ginty, D.D. and Cloutier, J.F. (2003) 'Signaling at the growth cone: ligand-receptor complexes and the control of axon growth and guidance', *Annu Rev Neurosci*, 26, pp. 509-63.
Hurlstone, A.F., Haramis, A.P., Wienholds, E., Begthel, H., Korving, J., Van Eeden, F., Cuppen, E., Zivkovic, D., Plasterk, R.H. and Clevers, H. (2003) 'The Wnt/beta-catenin pathway regulates cardiac valve formation', *Nature*, 425(6958), pp. 633-7.
Ieda, M., Kanazawa, H., Kimura, K., Hattori, F., Ieda, Y., Taniguchi, M., Lee, J.K., Matsumura, K., Tomita, Y., Miyoshi, S., Shimoda, K., Makino, S., Sano, M., Kodama, I., Ogawa, S. and Fukuda, K. (2007) 'Sema3a maintains normal heart rhythm through sympathetic innervation patterning', *Nat Med*, 13(5), pp. 604-12.
Ilagan, R., Abu-Issa, R., Brown, D., Yang, Y.P., Jiao, K., Schwartz, R.J., Klingensmith, J. and Meyers, E.N. (2006) 'Fgf8 is required for anterior heart field development', *Development*, 133(12), pp. 2435-45.
Itoh, M., Furuse, M., Morita, K., Kubota, K., Saitou, M. and Tsukita, S. (1999) 'Direct binding of three tight junction-associated MAGUKs, ZO-1, ZO-2, and ZO-3, with the COOH termini of claudins', *J Cell Biol*, 147(6), pp. 1351-63.
Itoh, M., Nagafuchi, A., Moroi, S. and Tsukita, S. (1997) 'Involvement of ZO-1 in cadherin-based cell adhesion through its direct binding to alpha catenin and actin filaments', *J Cell Biol*, 138(1), pp. 181-92.
Jaffe, A.B. and Hall, A. (2005) 'Rho GTPases: biochemistry and biology', *Annu Rev Cell Dev Biol*, 21, pp. 247-69.
Jaspard, B., Couffinhal, T., Dufourcq, P., Moreau, C. and Duplaa, C. (2000) 'Expression pattern of mouse sFRP-1 and mWnt-8 gene during heart morphogenesis', *Mech Dev*, 90(2), pp. 263-7.
Jiang, X., Rowitch, D.H., Soriano, P., McMahon, A.P. and Sucov, H.M. (2000) 'Fate of the mammalian cardiac neural crest', *Development*, 127(8), pp. 1607-16.
Jiao, K., Kulessa, H., Tompkins, K., Zhou, Y., Batts, L., Baldwin, H.S. and Hogan, B.L. (2003) 'An essential role of Bmp4 in the atrioventricular septation of the mouse heart', *Genes Dev*, 17(19), pp. 2362-7.
Jiao, K., Langworthy, M., Batts, L., Brown, C.B., Moses, H.L. and Baldwin, H.S. (2006) 'Tgfbeta signaling is required for atrioventricular cushion mesenchyme remodeling during in vivo cardiac development', *Development*, 133(22), pp. 4585-93.
Jones, M.C., Machida, K., Mayer, B.J. and Turner, C.E. (2013) 'Paxillin kinase linker (PKL) regulates Vav2 signaling during cell spreading and migration', *Mol Biol Cell*, 24(12), pp. 1882-94.

Jopling, H.M., Howell, G.J., Gamper, N. and Ponnambalam, S. (2011) 'The VEGFR2 receptor tyrosine kinase undergoes constitutive endosome-to-plasma membrane recycling', *Biochem Biophys Res Commun*, 410(2), pp. 170-6.
Kaplan, N.A., Liu, X. and Tolwinski, N.S. (2009) 'Epithelial polarity: interactions between junctions and apical-basal machinery', *Genetics*, 183(3), pp. 897-904.
Katz, T.C., Singh, M.K., Degenhardt, K., Rivera-Feliciano, J., Johnson, R.L., Epstein, J.A. and Tabin, C.J. (2012) 'Distinct compartments of the proepicardial organ give rise to coronary vascular endothelial cells', *Dev Cell*, 22(3), pp. 639-50.
Kawamura, S., Miyamoto, S. and Brown, J.H. (2003) 'Initiation and transduction of stretch-induced RhoA and Rac1 activation through caveolae: cytoskeletal regulation of ERK translocation', *J Biol Chem*, 278(33), pp. 31111-7.
Kawasaki, T., Kitsukawa, T., Bekku, Y., Matsuda, Y., Sanbo, M., Yagi, T. and Fujisawa, H. (1999) 'A requirement for neuropilin-1 in embryonic vessel formation', *Development*, 126(21), pp. 4895-902.
Kelly, R.G., Brown, N.A. and Buckingham, M.E. (2001) 'The arterial pole of the mouse heart forms from Fgf10-expressing cells in pharyngeal mesoderm', *Dev Cell*, 1(3), pp. 435-40.
Kelly, R.G. and Buckingham, M.E. (2002) 'The anterior heart-forming field: voyage to the arterial pole of the heart', (0168-9525 (Print)).
Kim, T. and Park, D. (2001) 'Molecular cloning and characterization of a novel mouse betaPix isoform', *Mol Cells*, 11(1), pp. 89-94.
King, T., Bland, Y., Webb, S., Barton, S. and Brown, N.A. (2002) 'Expression of Peg1 (Mest) in the developing mouse heart: involvement in trabeculation', *Dev Dyn*, 225(2), pp. 212-5.
Kirby, M.L., Gale, T.F. and Stewart, D.E. (1983) 'Neural crest cells contribute to normal aorticopulmonary septation', *Science*, 220(4601), pp. 1059-61.
Kirby, M.L. and Hutson, M.R. (2010) 'Factors controlling cardiac neural crest cell migration', *Cell Adh Migr*, 4(4), pp. 609-21.
Klaus, A., Muller, M., Schulz, H., Saga, Y., Martin, J.F. and Birchmeier, W. (2012) 'Wnt/beta-catenin and Bmp signals control distinct sets of transcription factors in cardiac progenitor cells', *Proc Natl Acad Sci U S A*, 109(27), pp. 10921-6.
Klewer, S.E., Krob, S.L., Kolker, S.J. and Kitten, G.T. (1998) 'Expression of type VI collagen in the developing mouse heart', *Dev Dyn*, 211(3), pp. 248-55.
Ko, J.A., Gondo, T., Inagaki, S. and Inui, M. (2005) 'Requirement of the transmembrane semaphorin Sema4C for myogenic differentiation', *FEBS Lett*, 579(10), pp. 2236-42.
Kokubo, H., Miyagawa-Tomita, S. and Johnson, R.L. (2005a) 'Hesr, a mediator of the Notch signaling, functions in heart and vessel development', *Trends Cardiovasc Med*, 15(5), pp. 190-4.
Kokubo, H., Miyagawa-Tomita, S., Nakazawa, M., Saga, Y. and Johnson, R.L. (2005b) 'Mouse hesr1 and hesr2 genes are redundantly required to mediate Notch signaling in the developing cardiovascular system', *Dev Biol*, 278(2), pp. 301-9.
Kokubo, H., Miyagawa-Tomita, S., Tomimatsu, H., Nakashima, Y., Nakazawa, M., Saga, Y. and Johnson, R.L. (2004) 'Targeted disruption of hesr2 results in atrioventricular valve anomalies that lead to heart dysfunction', *Circ Res*, 95(5), pp. 540-7.

Kolcz, J., Rajwa, B., Drukala, J., Dobrucki, J., Korohoda, W. and Malec, E. (2002) 'Three-dimensional visualization of connexin 43 on the human cardiomyocytes', *Appl Immunohistochem Mol Morphol*, 10(3), pp. 247-52.
Komiyama, M., Ito, K. and Shimada, Y. (1987) 'Origin and development of the epicardium in the mouse embryo', *Anat Embryol (Berl)*, 176(2), pp. 183-9.
Kopan, R. and Goate, A. (2002) 'Aph-2/Nicastrin: an essential component of gamma-secretase and regulator of Notch signaling and Presenilin localization', *Neuron*, 33(3), pp. 321-4.
Kozma, R., Ahmed, S., Best, A. and Lim, L. (1995) 'The Ras-related protein Cdc42Hs and bradykinin promote formation of peripheral actin microspikes and filopodia in Swiss 3T3 fibroblasts', *Mol Cell Biol*, 15(4), pp. 1942-52.
Krantz, I.D., Smith, R., Colliton, R.P., Tinkel, H., Zackai, E.H., Piccoli, D.A., Goldmuntz, E. and Spinner, N.B. (1999) 'Jagged1 mutations in patients ascertained with isolated congenital heart defects', *Am J Med Genet*, 84(1), pp. 56-60.
Kruithof, B.P., Kruithof-De-Julio, M., Poelmann, R.E., Gittenberger-De-Groot, A.C., Gaussin, V. and Goumans, M.J. (2013) 'Remodeling of the myocardium in early trabeculation and cardiac valve formation; a role for TGFbeta2', *Int J Dev Biol*, 57(11-12), pp. 853-63.
Kruithof, B.P., van den Hoff, M.J., Wessels, A. and Moorman, A.F. (2003) 'Cardiac muscle cell formation after development of the linear heart tube', *Dev Dyn*, 227(1), pp. 1-13.
Lagopoulos, M.E., Manlhiot, C., McCrindle, B.W., Jaeggi, E.T., Friedberg, M.K. and Nield, L.E. (2010) 'Impact of prenatal diagnosis and anatomical subtype on outcome in double outlet right ventricle', *Am Heart J*, 160(4), pp. 692-700.
Lai, D., Liu, X., Forrai, A., Wolstein, O., Michalicek, J., Ahmed, I., Garratt, A.N., Birchmeier, C., Zhou, M., Hartley, L., Robb, L., Feneley, M.P., Fatkin, D. and Harvey, R.P. (2010) 'Neuregulin 1 sustains the gene regulatory network in both trabecular and nontrabecular myocardium', *Circ Res*, 107(6), pp. 715-27.
Lakso, M., Sauer, B., Mosinger, B., Jr., Lee, E.J., Manning, R.W., Yu, S.H., Mulder, K.L. and Westphal, H. (1992) 'Targeted oncogene activation by site-specific recombination in transgenic mice', *Proc Natl Acad Sci U S A*, 89(14), pp. 6232-6.
Lampugnani, M.G., Zanetti, A., Breviario, F., Balconi, G., Orsenigo, F., Corada, M., Spagnuolo, R., Betson, M., Braga, V. and Dejana, E. (2002) 'VE-cadherin regulates endothelial actin activating Rac and increasing membrane association of Tiam', *Mol Biol Cell*, 13(4), pp. 1175-89.
Laugwitz, K.L., Moretti A Fau - Caron, L., Caron L Fau - Nakano, A., Nakano A Fau - Chien, K.R. and Chien, K.R. (2008) 'Islet1 cardiovascular progenitors: a single source for heart lineages?', (0950-1991 (Print)).
Lavine, K.J., Yu, K., White, A.C., Zhang, X., Smith, C., Partanen, J. and Ornitz, D.M. (2005) 'Endocardial and epicardial derived FGF signals regulate myocardial proliferation and differentiation in vivo', *Dev Cell*, 8(1), pp. 85-95.
Layland, J., Solaro, R.J. and Shah, A.M. (2005) 'Regulation of cardiac contractile function by troponin I phosphorylation', *Cardiovasc Res*, 66(1), pp. 12-21.
Lee, K.F., Simon, H., Chen, H., Bates, B., Hung, M.C. and Hauser, C. (1995) 'Requirement for neuregulin receptor erbB2 in neural and cardiac development', *Nature*, 378(6555), pp. 394-8.

Lee, L.J. and Lupo, P.J. (2013) 'Maternal smoking during pregnancy and the risk of congenital heart defects in offspring: a systematic review and metaanalysis', *Pediatr Cardiol*, 34(2), pp. 398-407.
Lee, Y., Song, A.J., Baker, R., Micales, B., Conway, S.J. and Lyons, G.E. (2000) 'Jumonji, a nuclear protein that is necessary for normal heart development', *Circ Res*, 86(9), pp. 932-8.
Leimeister, C., Externbrink, A., Klamt, B. and Gessler, M. (1999) 'Hey genes: a novel subfamily of hairy- and Enhancer of split related genes specifically expressed during mouse embryogenesis', *Mech Dev*, 85(1-2), pp. 173-7.
Leung, C., Liu, Y., Lu, X., Kim, M., Drysdale, T.A. and Feng, Q. (2015) 'Rac1 Signaling Is Required for Anterior Second Heart Field Cellular Organization and Cardiac Outflow Tract Development', *J Am Heart Assoc*, 5(1).
Leung, C., Lu, X., Liu, M. and Feng, Q. (2014) 'Rac1 signaling is critical to cardiomyocyte polarity and embryonic heart development', *J Am Heart Assoc*, 3(5), p. e001271.
Li, D., Hallett, M.A., Zhu, W., Rubart, M., Liu, Y., Yang, Z., Chen, H., Haneline, L.S., Chan, R.J., Schwartz, R.J., Field, L.J., Atkinson, S.J. and Shou, W. (2011) 'Dishevelled-associated activator of morphogenesis 1 (Daam1) is required for heart morphogenesis', *Development*, 138(2), pp. 303-15.
Li, F., Zhao, H., Liao, Y., Takashima, S., Asano, Y., Shintani, Y., Hori, M. and Kitakaze, M. (2008) 'Higher mortality in heterozygous neuropilin-1 mice after cardiac pressure overload', *Biochem Biophys Res Commun*, 370(2), pp. 317-21.
Li, J., Wang, Q., Wen, R., Liang, J., Zhong, X., Yang, W., Su, D. and Tang, J. (2015) 'MiR-138 inhibits cell proliferation and reverses epithelial-mesenchymal transition in non-small cell lung cancer cells by targeting GIT1 and SEMA4C', *J Cell Mol Med*, 19(12), pp. 2793-805.
Li, L., Krantz, I.D., Deng, Y., Genin, A., Banta, A.B., Collins, C.C., Qi, M., Trask, B.J., Kuo, W.L., Cochran, J., Costa, T., Pierpont, M.E., Rand, E.B., Piccoli, D.A., Hood, L. and Spinner, N.B. (1997) 'Alagille syndrome is caused by mutations in human Jagged1, which encodes a ligand for Notch1', *Nat Genet*, 16(3), pp. 243-51.
Li, Z., Colucci-Guyon, E., Pincon-Raymond, M., Mericskay, M., Pournin, S., Paulin, D. and Babinet, C. (1996) 'Cardiovascular lesions and skeletal myopathy in mice lacking desmin', *Dev Biol*, 175(2), pp. 362-6.
Liao, Z., Cao, C., Wang, J., Huxley, V.H., Baker, O., Weisman, G.A. and Erb, L. (2014) 'The P2Y Receptor Interacts with VE-Cadherin and VEGF Receptor-2 to Regulate Rac1 Activity in Endothelial Cells', *J Biomed Sci Eng*, 7(14), pp. 1105-1121.
Lincoln, J., Florer, J.B., Deutsch, G.H., Wenstrup, R.J. and Yutzey, K.E. (2006) 'ColVa1 and ColXIa1 are required for myocardial morphogenesis and heart valve development', *Dev Dyn*, 235(12), pp. 3295-305.
Linden, M., Li, Z., Paulin, D., Gotow, T. and Leterrier, J.F. (2001) 'Effects of desmin gene knockout on mice heart mitochondria', *J Bioenerg Biomembr*, 33(4), pp. 333-41.
Liu, B.P. and Burridge, K. (2000) 'Vav2 activates Rac1, Cdc42, and RhoA downstream from growth factor receptors but not beta1 integrins', *Mol Cell Biol*, 20(19), pp. 7160-9.
Liu, J., Bressan, M., Hassel, D., Huisken, J., Staudt, D., Kikuchi, K., Poss, K.D., Mikawa, T. and Stainier, D.Y. (2010) 'A dual role for ErbB2 signaling in cardiac trabeculation', *Development*, 137(22), pp. 3867-75.

Liu, W., Sato, A., Khadka, D., Bharti, R., Diaz, H., Runnels, L.W. and Habas, R. (2008) 'Mechanism of activation of the Formin protein Daam1', *Proc Natl Acad Sci U S A*, 105(1), pp. 210-5.
Lockhart, M., Wirrig, E., Phelps, A. and Wessels, A. (2011) 'Extracellular matrix and heart development', *Birth Defects Res A Clin Mol Teratol*, 91(6), pp. 535-50.
Loomes, K.M., Taichman, D.B., Glover, C.L., Williams, P.T., Markowitz, J.E., Piccoli, D.A., Baldwin, H.S. and Oakey, R.J. (2002) 'Characterization of Notch receptor expression in the developing mammalian heart and liver', *Am J Med Genet*, 112(2), pp. 181-9.
Lowery, J., Kuczmarski, E.R., Herrmann, H. and Goldman, R.D. (2015) 'Intermediate Filaments Play a Pivotal Role in Regulating Cell Architecture and Function', *J Biol Chem*, 290(28), pp. 17145-53.
Lu, S.Y., Sheikh, F., Sheppard, P.C., Fresnoza, A., Duckworth, M.L., Detillieux, K.A. and Cattini, P.A. (2008) 'FGF-16 is required for embryonic heart development', *Biochem Biophys Res Commun*, 373(2), pp. 270-4.
Luxan, G., Casanova, J.C., Martinez-Poveda, B., Prados, B., D'Amato, G., MacGrogan, D., Gonzalez-Rajal, A., Dobarro, D., Torroja, C., Martinez, F., Izquierdo-Garcia, J.L., Fernandez-Friera, L., Sabater-Molina, M., Kong, Y.Y., Pizarro, G., Ibanez, B., Medrano, C., Garcia-Pavia, P., Gimeno, J.R., Monserrat, L., Jimenez-Borreguero, L.J. and de la Pompa, J.L. (2013) 'Mutations in the NOTCH pathway regulator MIB1 cause left ventricular noncompaction cardiomyopathy', *Nat Med*, 19(2), pp. 193-201.
Mack, N.A. and Georgiou, M. (2014) 'The interdependence of the Rho GTPases and apicobasal cell polarity', *Small GTPases*, 5(2), p. 10.
Magdalena, J., Millard, T.H. and Machesky, L.M. (2003) 'Microtubule involvement in NIH 3T3 Golgi and MTOC polarity establishment', *J Cell Sci*, 116(Pt 4), pp. 743-56.
Mamidipudi, V., Zhang, J., Lee, K.C. and Cartwright, C.A. (2004) 'RACK1 regulates G1/S progression by suppressing Src kinase activity', *Mol Cell Biol*, 24(15), pp. 6788-98.
Manner, J., Perez-Pomares, J.M., Macias, D. and Munoz-Chapuli, R. (2001) 'The origin, formation and developmental significance of the epicardium: a review', *Cells Tissues Organs*, 169(2), pp. 89-103.
Markwald, R.R. (1973) 'Distribution and relationship of precursor Z material to organizing myofibrillar bundles in embryonic rat and hamster ventricular myocytes', *J Mol Cell Cardiol*, 5(4), pp. 341-50.
Martin-Puig, S., Wang, Z. and Chien, K.R. (2008) 'Lives of a heart cell: tracing the origins of cardiac progenitors', *Cell Stem Cell*, 2(4), pp. 320-31.
Mass, E., Wachten, D., Aschenbrenner, A.C., Voelzmann, A. and Hoch, M. (2014) 'Murine Creld1 controls cardiac development through activation of calcineurin/NFATc1 signaling', *Dev Cell*, 28(6), pp. 711-26.
Matos, P., Skaug, J., Marques, B., Beck, S., Verissimo, F., Gespach, C., Boavida, M.G., Scherer, S.W. and Jordan, P. (2000) 'Small GTPase Rac1: structure, localization, and expression of the human gene', *Biochem Biophys Res Commun*, 277(3), pp. 741-51.
Matsuda, C., Kameyama, K., Suzuki, A., Mishima, W., Yamaji, S., Okamoto, H., Nishino, I. and Hayashi, Y.K. (2008) 'Affixin activates Rac1 via betaPIX in C2C12 myoblast', *FEBS Lett*, 582(8), pp. 1189-96.
McCright, B., Gao, X., Shen, L., Lozier, J., Lan, Y., Maguire, M., Herzlinger, D., Weinmaster, G., Jiang, R. and Gridley, T. (2001) 'Defects in development of the kidney,

heart and eye vasculature in mice homozygous for a hypomorphic Notch2 mutation', *Development*, 128(4), pp. 491-502.
McCright, B., Lozier, J. and Gridley, T. (2002) 'A mouse model of Alagille syndrome: Notch2 as a genetic modifier of Jag1 haploinsufficiency', *Development*, 129(4), pp. 1075-82.
McDaniell, R., Warthen, D.M., Sanchez-Lara, P.A., Pai, A., Krantz, I.D., Piccoli, D.A. and Spinner, N.B. (2006) 'NOTCH2 mutations cause Alagille syndrome, a heterogeneous disorder of the notch signaling pathway', *Am J Hum Genet*, 79(1), pp. 169-73.
McKeown, C.R., Nowak, R.B., Gokhin, D.S. and Fowler, V.M. (2014) 'Tropomyosin is required for cardiac morphogenesis, myofibril assembly, and formation of adherens junctions in the developing mouse embryo', *Dev Dyn*, 243(6), pp. 800-17.
Meilhac, S.M., Kelly, R.G., Rocancourt, D., Eloy-Trinquet, S., Nicolas, J.F. and Buckingham, M.E. (2003) 'A retrospective clonal analysis of the myocardium reveals two phases of clonal growth in the developing mouse heart', *Development*, 130(16), pp. 3877-89.
Meissner, M., Michailidou, D., Stein, M., Hrgovic, I., Kaufmann, R. and Gille, J. (2009) 'Inhibition of Rac1 GTPase downregulates vascular endothelial growth factor receptor-2 expression by suppressing Sp1-dependent DNA binding in human endothelial cells', *Exp Dermatol*, 18(10), pp. 863-9.
Merki, E., Zamora, M., Raya, A., Kawakami, Y., Wang, J., Zhang, X., Burch, J., Kubalak, S.W., Kaliman, P., Izpisua Belmonte, J.C., Chien, K.R. and Ruiz-Lozano, P. (2005) 'Epicardial retinoid X receptor alpha is required for myocardial growth and coronary artery formation', *Proc Natl Acad Sci U S A*, 102(51), pp. 18455-60.
Meyer, D. and Birchmeier, C. (1995) 'Multiple essential functions of neuregulin in development', *Nature*, 378(6555), pp. 386-90.
Migeotte, I., Grego-Bessa, J. and Anderson, K.V. (2011) 'Rac1 mediates morphogenetic responses to intercellular signals in the gastrulating mouse embryo', *Development*, 138(14), pp. 3011-20.
Migeotte, I., Omelchenko, T., Hall, A. and Anderson, K.V. (2010) 'Rac1-dependent collective cell migration is required for specification of the anterior-posterior body axis of the mouse', *PLoS Biol*, 8(8), p. e1000442.
Mikawa, T. and Gourdie, R.G. (1996) 'Pericardial mesoderm generates a population of coronary smooth muscle cells migrating into the heart along with ingrowth of the epicardial organ', *Dev Biol*, 174(2), pp. 221-32.
Milgrom-Hoffman, M., Harrelson, Z., Ferrara, N., Zelzer, E., Evans, S.M. and Tzahor, E. (2011) 'The heart endocardium is derived from vascular endothelial progenitors', *Development*, 138(21), pp. 4777-87.
Mima, T., Ueno, H., Fischman, D.A., Williams, L.T. and Mikawa, T. (1995) 'Fibroblast growth factor receptor is required for in vivo cardiac myocyte proliferation at early embryonic stages of heart development', *Proc Natl Acad Sci U S A*, 92(2), pp. 467-71.
Minden, A., Lin, A., Claret, F.X., Abo, A. and Karin, M. (1995) 'Selective activation of the JNK signaling cascade and c-Jun transcriptional activity by the small GTPases Rac and Cdc42Hs', *Cell*, 81(7), pp. 1147-57.
Miquerol, L., Langille, B.L. and Nagy, A. (2000) 'Embryonic development is disrupted by modest increases in vascular endothelial growth factor gene expression', *Development*, 127(18), pp. 3941-6.

Mjaatvedt, C.H., Nakaoka, T., Moreno-Rodriguez, R., Norris, R.A., Kern, M.J., Eisenberg, C.A., Turner, D. and Markwald, R.R. (2001) 'The outflow tract of the heart is recruited from a novel heart-forming field', *Dev Biol*, 238(1), pp. 97-109.
Mo, F.E. and Lau, L.F. (2006) 'The matricellular protein CCN1 is essential for cardiac development', *Circ Res*, 99(9), pp. 961-9.
Momboisse, F., Lonchamp, E., Calco, V., Ceridono, M., Vitale, N., Bader, M.F. and Gasman, S. (2009) 'betaPIX-activated Rac1 stimulates the activation of phospholipase D, which is associated with exocytosis in neuroendocrine cells', *J Cell Sci*, 122(Pt 6), pp. 798-806.
Moore, K.A., Sethi, R., Doanes, A.M., Johnson, T.M., Pracyk, J.B., Kirby, M., Irani, K., Goldschmidt-Clermont, P.J. and Finkel, T. (1997) 'Rac1 is required for cell proliferation and G2/M progression', *Biochem J*, 326 (Pt 1), pp. 17-20.
Moorman, A.F. and Christoffels, V.M. (2003) 'Cardiac chamber formation: development, genes, and evolution', *Physiol Rev*, 83(4), pp. 1223-67.
Moretti, A., Caron, L., Nakano, A., Lam, J.T., Bernshausen, A., Chen, Y., Qyang, Y., Bu, L., Sasaki, M., Martin-Puig, S., Sun, Y., Evans, S.M., Laugwitz, K.L. and Chien, K.R. (2006) 'Multipotent embryonic isl1+ progenitor cells lead to cardiac, smooth muscle, and endothelial cell diversification', *Cell*, 127(6), pp. 1151-65.
Mornet, D., Pantel, P., Audemard, E. and Kassab, R. (1979) 'Involvement of an arginyl residue in the catalytic activity of myosin heads', *Eur J Biochem*, 100(2), pp. 421-31.
Mortensen, K.H., Andersen, N.H. and Gravholt, C.H. (2012) 'Cardiovascular phenotype in Turner syndrome--integrating cardiology, genetics, and endocrinology', *Endocr Rev*, 33(5), pp. 677-714.
Moses, K.A., DeMayo, F., Braun, R.M., Reecy, J.L. and Schwartz, R.J. (2001) 'Embryonic expression of an Nkx2-5/Cre gene using ROSA26 reporter mice', *Genesis*, 31(4), pp. 176-80.
Mudry, R.E., Perry, C.N., Richards, M., Fowler, V.M. and Gregorio, C.C. (2003) 'The interaction of tropomodulin with tropomyosin stabilizes thin filaments in cardiac myocytes', *J Cell Biol*, 162(6), pp. 1057-68.
Muller, S.L., Portwich, M., Schmidt, A., Utepbergenov, D.I., Huber, O., Blasig, I.E. and Krause, G. (2005) 'The tight junction protein occludin and the adherens junction protein alpha-catenin share a common interaction mechanism with ZO-1', *J Biol Chem*, 280(5), pp. 3747-56.
Munoz-Soriano, V., Belacortu, Y. and Paricio, N. (2012) 'Planar cell polarity signaling in collective cell movements during morphogenesis and disease', *Curr Genomics*, 13(8), pp. 609-22.
Murdoch, J.N., Henderson, D.J., Doudney, K., Gaston-Massuet, C., Phillips, H.M., Paternotte, C., Arkell, R., Stanier, P. and Copp, A.J. (2003) 'Disruption of scribble (Scrb1) causes severe neural tube defects in the circletail mouse', *Hum Mol Genet*, 12(2), pp. 87-98.
Nagy, II, Railo, A., Rapila, R., Hast, T., Sormunen, R., Tavi, P., Rasanen, J. and Vainio, S.J. (2010) 'Wnt-11 signalling controls ventricular myocardium development by patterning N-cadherin and beta-catenin expression', *Cardiovasc Res*, 85(1), pp. 100-9.
Nakagawa, O., Nakagawa, M., Richardson, J.A., Olson, E.N. and Srivastava, D. (1999) 'HRT1, HRT2, and HRT3: a new subclass of bHLH transcription factors marking specific cardiac, somitic, and pharyngeal arch segments', *Dev Biol*, 216(1), pp. 72-84.

Nakano, Y., Chayama, K., Ochi, H., Toshishige, M., Hayashida, Y., Miki, D., Hayes, C.N., Suzuki, H., Tokuyama, T., Oda, N., Suenari, K., Uchimura-Makita, Y., Kajihara, K., Sairaku, A., Motoda, C., Fujiwara, M., Watanabe, Y., Yoshida, Y., Ohkubo, K., Watanabe, I., Nogami, A., Hasegawa, K., Watanabe, H., Endo, N., Aiba, T., Shimizu, W., Ohno, S., Horie, M., Arihiro, K., Tashiro, S., Makita, N. and Kihara, Y. (2013) 'A nonsynonymous polymorphism in semaphorin 3A as a risk factor for human unexplained cardiac arrest with documented ventricular fibrillation', *PLoS Genet*, 9(4), p. e1003364.
Naqvi, N., Li, M., Calvert, J.W., Tejada, T., Lambert, J.P., Wu, J., Kesteven, S.H., Holman, S.R., Matsuda, T., Lovelock, J.D., Howard, W.W., Iismaa, S.E., Chan, A.Y., Crawford, B.H., Wagner, M.B., Martin, D.I., Lefer, D.J., Graham, R.M. and Husain, A. (2014) 'A proliferative burst during preadolescence establishes the final cardiomyocyte number', *Cell*, 157(4), pp. 795-807.
Neeb, Z., Lajiness, J.D., Bolanis, E. and Conway, S.J. (2013) 'Cardiac outflow tract anomalies', *Wiley Interdiscip Rev Dev Biol*, 2(4), pp. 499-530.
Neuhaus, H., Rosen, V. and Thies, R.S. (1999) 'Heart specific expression of mouse BMP-10 a novel member of the TGF-beta superfamily', *Mech Dev*, 80(2), pp. 181-4.
Nobes, C.D. and Hall, A. (1995) 'Rho, rac, and cdc42 GTPases regulate the assembly of multimolecular focal complexes associated with actin stress fibers, lamellipodia, and filopodia', *Cell*, 81(1), pp. 53-62.
Nohata, N., Uchida, Y., Stratman, A.N., Adams, R.H., Zheng, Y., Weinstein, B.M., Mukouyama, Y.S. and Gutkind, J.S. (2016) 'Temporal-specific roles of Rac1 during vascular development and retinal angiogenesis', *Dev Biol*, 411(2), pp. 183-94.
Noren, N.K., Liu, B.P., Burridge, K. and Kreft, B. (2000) 'p120 catenin regulates the actin cytoskeleton via Rho family GTPases', *J Cell Biol*, 150(3), pp. 567-80.
Nusse, R. (2008) 'Wnt signaling and stem cell control', *Cell Res*, 18(5), pp. 523-7.
Oda, T., Elkahloun, A.G., Pike, B.L., Okajima, K., Krantz, I.D., Genin, A., Piccoli, D.A., Meltzer, P.S., Spinner, N.B., Collins, F.S. and Chandrasekharappa, S.C. (1997) 'Mutations in the human Jagged1 gene are responsible for Alagille syndrome', *Nat Genet*, 16(3), pp. 235-42.
Oechslin, E. and Jenni, R. (2011) 'Left ventricular non-compaction revisited: a distinct phenotype with genetic heterogeneity?', *Eur Heart J*, 32(12), pp. 1446-56.
Ohno, S. (2001) 'Intercellular junctions and cellular polarity: the PAR-aPKC complex, a conserved core cassette playing fundamental roles in cell polarity', *Curr Opin Cell Biol*, 13(5), pp. 641-8.
Osmani, N., Vitale, N., Borg, J.P. and Etienne-Manneville, S. (2006) 'Scrib controls Cdc42 localization and activity to promote cell polarization during astrocyte migration', *Curr Biol*, 16(24), pp. 2395-405.
Palmer, B.M., Valent, S., Holder, E.L., Weinberger, H.D. and Bies, R.D. (1998) 'Microtubules modulate cardiomyocyte beta-adrenergic response in cardiac hypertrophy', *Am J Physiol*, 275(5 Pt 2), pp. H1707-16.
Pang, J., Xu, X., Getman, M.R., Shi, X., Belmonte, S.L., Michaloski, H., Mohan, A., Blaxall, B.C. and Berk, B.C. (2011) 'G protein coupled receptor kinase 2 interacting protein 1 (GIT1) is a novel regulator of mitochondrial biogenesis in heart', *J Mol Cell Cardiol*, 51(5), pp. 769-76.

Park, E.J., Watanabe Y Fau - Smyth, G., Smyth G Fau - Miyagawa-Tomita, S., Miyagawa-Tomita S Fau - Meyers, E., Meyers E Fau - Klingensmith, J., Klingensmith J Fau - Camenisch, T., Camenisch T Fau - Buckingham, M., Buckingham M Fau - Moon, A.M. and Moon, A.M. (2008) 'An FGF autocrine loop initiated in second heart field mesoderm regulates morphogenesis at the arterial pole of the heart', (0950-1991 (Print)).

Parrini, M.C., Lei, M., Harrison, S.C. and Mayer, B.J. (2002) 'Pak1 kinase homodimers are autoinhibited in trans and dissociated upon activation by Cdc42 and Rac1', *Mol Cell*, 9(1), pp. 73-83.

Pashmforoush, M., Lu, J.T., Chen, H., Amand, T.S., Kondo, R., Pradervand, S., Evans, S.M., Clark, B., Feramisco, J.R., Giles, W., Ho, S.Y., Benson, D.W., Silberbach, M., Shou, W. and Chien, K.R. (2004) 'Nkx2-5 pathways and congenital heart disease; loss of ventricular myocyte lineage specification leads to progressive cardiomyopathy and complete heart block', *Cell*, 117(3), pp. 373-86.

Pasumarthi, K.B. and Field, L.J. (2002) 'Cardiomyocyte cell cycle regulation', *Circ Res*, 90(10), pp. 1044-54.

Patel, D.M. and Green, K.J. (2014) 'Desmosomes in the heart: a review of clinical and mechanistic analyses', *Cell Commun Adhes*, 21(3), pp. 109-28.

Perala, N.M., Immonen, T. and Sariola, H. (2005) 'The expression of plexins during mouse embryogenesis', *Gene Expr Patterns*, 5(3), pp. 355-62.

Perez-Pomares, J.M., Carmona, R., Gonzalez-Iriarte, M., Atencia, G., Wessels, A. and Munoz-Chapuli, R. (2002) 'Origin of coronary endothelial cells from epicardial mesothelium in avian embryos', *Int J Dev Biol*, 46(8), pp. 1005-13.

Perona, R., Montaner, S., Saniger, L., Sanchez-Perez, I., Bravo, R. and Lacal, J.C. (1997) 'Activation of the nuclear factor-kappaB by Rho, CDC42, and Rac-1 proteins', *Genes Dev*, 11(4), pp. 463-75.

Peshkovsky, C., Totong, R. and Yelon, D. (2011) 'Dependence of cardiac trabeculation on neuregulin signaling and blood flow in zebrafish', *Dev Dyn*, 240(2), pp. 446-56.

Phillips, H.M., Hildreth, V., Peat, J.D., Murdoch, J.N., Kobayashi, K., Chaudhry, B. and Henderson, D.J. (2008) 'Non-cell-autonomous roles for the planar cell polarity gene Vangl2 in development of the coronary circulation', *Circ Res*, 102(5), pp. 615-23.

Phillips, H.M., Murdoch, J.N., Chaudhry, B., Copp, A.J. and Henderson, D.J. (2005) 'Vangl2 acts via RhoA signaling to regulate polarized cell movements during development of the proximal outflow tract', *Circ Res*, 96(3), pp. 292-9.

Phillips, H.M., Rhee, H.J., Murdoch, J.N., Hildreth, V., Peat, J.D., Anderson, R.H., Copp, A.J., Chaudhry, B. and Henderson, D.J. (2007) 'Disruption of planar cell polarity signaling results in congenital heart defects and cardiomyopathy attributable to early cardiomyocyte disorganization', *Circ Res*, 101(2), pp. 137-45.

Porrello, E.R., Mahmoud, A.I., Simpson, E., Hill, J.A., Richardson, J.A., Olson, E.N. and Sadek, H.A. (2011) 'Transient regenerative potential of the neonatal mouse heart', *Science*, 331(6020), pp. 1078-80.

Prall, O.W., Menon Mk Fau - Solloway, M.J., Solloway Mj Fau - Watanabe, Y., Watanabe Y Fau - Zaffran, S., Zaffran S Fau - Bajolle, F., Bajolle F Fau - Biben, C., Biben C Fau - McBride, J.J., McBride Jj Fau - Robertson, B.R., Robertson Br Fau - Chaulet, H., Chaulet H Fau - Stennard, F.A., Stennard Fa Fau - Wise, N., Wise N Fau - Schaft, D., Schaft D Fau - Wolstein, O., Wolstein O Fau - Furtado, M.B., Furtado Mb Fau - Shiratori,

H., Shiratori H Fau - Chien, K.R., Chien Kr Fau - Hamada, H., Hamada H Fau - Black, B.L., Black Bl Fau - Saga, Y., Saga Y Fau - Robertson, E.J., Robertson Ej Fau - Buckingham, M.E., Buckingham Me Fau - Harvey, R.P. and Harvey, R.P. (2007) 'An Nkx2-5/Bmp2/Smad1 negative feedback loop controls heart progenitor specification and proliferation', (0092-8674 (Print)).
Putkey, J.A., Sweeney, H.L. and Campbell, S.T. (1989) 'Site-directed mutation of the trigger calcium-binding sites in cardiac troponin C', *J Biol Chem*, 264(21), pp. 12370-8.
Qi, C.H., Zhao, X.Q., Ma, D., Ma, X.J., Zhou, G.M. and Huang, G.Y. (2011) 'Downregulation of Rho associated coiled-coil forming protein kinase 1 in the process of delayed myocardialization of cardiac proximal outflow tract septum in connexin 43 knockout mice embryo', *Chin Med J (Engl)*, 124(13), pp. 2021-7.
Ram, R., Wescott, A.P., Varandas, K., Dirksen, R.T. and Blaxall, B.C. (2014) 'Mena associates with Rac1 and modulates connexin 43 remodeling in cardiomyocytes', *Am J Physiol Heart Circ Physiol*, 306(1), pp. H154-9.
Ramsbottom, S.A., Sharma, V., Rhee, H.J., Eley, L., Phillips, H.M., Rigby, H.F., Dean, C., Chaudhry, B. and Henderson, D.J. (2014) 'Vangl2-regulated polarisation of second heart field-derived cells is required for outflow tract lengthening during cardiac development', (1553-7404 (Electronic)).
Rana, M.S., Horsten, N.C., Tesink-Taekema, S., Lamers, W.H., Moorman, A.F. and van den Hoff, M.J. (2007) 'Trabeculated right ventricular free wall in the chicken heart forms by ventricularization of the myocardium initially forming the outflow tract', *Circ Res*, 100(7), pp. 1000-7.
Ray, R.M., Vaidya, R.J. and Johnson, L.R. (2007) 'MEK/ERK regulates adherens junctions and migration through Rac1', *Cell Motil Cytoskeleton*, 64(3), pp. 143-56.
Red-Horse, K., Ueno, H., Weissman, I.L. and Krasnow, M.A. (2010) 'Coronary arteries form by developmental reprogramming of venous cells', *Nature*, 464(7288), pp. 549-53.
Rhee, D.Y., Zhao, X.Q., Francis, R.J., Huang, G.Y., Mably, J.D. and Lo, C.W. (2009) 'Connexin 43 regulates epicardial cell polarity and migration in coronary vascular development', *Development*, 136(18), pp. 3185-93.
Ridley, A.J. (2001) 'Rho GTPases and cell migration', *J Cell Sci*, 114(Pt 15), pp. 2713-22.
Ridley, A.J. and Hall, A. (1992) 'The small GTP-binding protein rho regulates the assembly of focal adhesions and actin stress fibers in response to growth factors', *Cell*, 70(3), pp. 389-99.
Ridley, A.J., Paterson, H.F., Johnston, C.L., Diekmann, D. and Hall, A. (1992) 'The small GTP-binding protein rac regulates growth factor-induced membrane ruffling', *Cell*, 70(3), pp. 401-10.
Roberts, A.E., Allanson, J.E., Tartaglia, M. and Gelb, B.D. (2013) 'Noonan syndrome', *Lancet*, 381(9863), pp. 333-42.
Roszko, I., Sawada, A. and Solnica-Krezel, L. (2009) 'Regulation of convergence and extension movements during vertebrate gastrulation by the Wnt/PCP pathway', *Semin Cell Dev Biol*, 20(8), pp. 986-97.
Rupert, C.E. and Coulombe, K.L. (2015) 'The roles of neuregulin-1 in cardiac development, homeostasis, and disease', *Biomark Insights*, 10(Suppl 1), pp. 1-9.

Rusu, M.C., Poalelungi, C.V., Vrapciu, A.D., Nicolescu, M.I., Hostiuc, S., Mogoanta, L. and Taranu, T. (2015) 'Endocardial tip cells in the human embryo - facts and hypotheses', *PLoS One*, 10(1), p. e0115853.
Samsa, L.A., Yang, B. and Liu, J. (2013) 'Embryonic cardiac chamber maturation: Trabeculation, conduction, and cardiomyocyte proliferation', *Am J Med Genet C Semin Med Genet*, 163c(3), pp. 157-68.
Satoh, M., Ogita, H., Takeshita, K., Mukai, Y., Kwiatkowski, D.J. and Liao, J.K. (2006) 'Requirement of Rac1 in the development of cardiac hypertrophy', *Proc Natl Acad Sci U S A*, 103(19), pp. 7432-7.
Sauzeau, V., Jerkic, M., Lopez-Novoa, J.M. and Bustelo, X.R. (2007) 'Loss of Vav2 proto-oncogene causes tachycardia and cardiovascular disease in mice', *Mol Biol Cell*, 18(3), pp. 943-52.
Sawada, N., Li, Y. and Liao, J.K. (2010) 'Novel aspects of the roles of Rac1 GTPase in the cardiovascular system', *Curr Opin Pharmacol*, 10(2), pp. 116-21.
Sawada, N., Salomone, S., Kim, H.H., Kwiatkowski, D.J. and Liao, J.K. (2008) 'Regulation of endothelial nitric oxide synthase and postnatal angiogenesis by Rac1', *Circ Res*, 103(4), pp. 360-8.
Schleiffarth, J.R., Person, A.D., Martinsen, B.J., Sukovich, D.J., Neumann, A., Baker, C.V., Lohr, J.L., Cornfield, D.N., Ekker, S.C. and Petryk, A. (2007) 'Wnt5a is required for cardiac outflow tract septation in mice', *Pediatr Res*, 61(4), pp. 386-91.
Schmittgen, T.D. and Livak, K.J. (2008) 'Analyzing real-time PCR data by the comparative C(T) method', *Nat Protoc*, 3(6), pp. 1101-8.
Sedmera, D., Pexieder, T., Vuillemin, M., Thompson, R.P. and Anderson, R.H. (2000) 'Developmental patterning of the myocardium', *Anat Rec*, 258(4), pp. 319-37.
Serini, G., Valdembri, D., Zanivan, S., Morterra, G., Burkhardt, C., Caccavari, F., Zammataro, L., Primo, L., Tamagnone, L., Logan, M., Tessier-Lavigne, M., Taniguchi, M., Puschel, A.W. and Bussolino, F. (2003) 'Class 3 semaphorins control vascular morphogenesis by inhibiting integrin function', *Nature*, 424(6947), pp. 391-7.
Severs, N.J., Rothery, S., Dupont, E., Coppen, S.R., Yeh, H.I., Ko, Y.S., Matsushita, T., Kaba, R. and Halliday, D. (2001) 'Immunocytochemical analysis of connexin expression in the healthy and diseased cardiovascular system', *Microsc Res Tech*, 52(3), pp. 301-22.
Shalaby, F., Rossant, J., Yamaguchi, T.P., Gertsenstein, M., Wu, X.F., Breitman, M.L. and Schuh, A.C. (1995) 'Failure of blood-island formation and vasculogenesis in Flk-1-deficient mice', *Nature*, 376(6535), pp. 62-6.
Sharp, W.W., Simpson, D.G., Borg, T.K., Samarel, A.M. and Terracio, L. (1997) 'Mechanical forces regulate focal adhesion and costamere assembly in cardiac myocytes', *Am J Physiol*, 273(2 Pt 2), pp. H546-56.
Sheehan, K.A., Ke, Y. and Solaro, R.J. (2007) 'p21-Activated kinase-1 and its role in integrated regulation of cardiac contractility', *Am J Physiol Regul Integr Comp Physiol*, 293(3), pp. R963-73.
Shi, Q.Y., Zhang, J.B., Mi, Y.Q., Song, Y., Ma, J. and Zhang, Y.L. (2014) 'Congenital heart defects and maternal fever: systematic review and meta-analysis', *J Perinatol*, 34(9), pp. 677-82.

Shin, C.H., Liu, Z.P., Passier, R., Zhang, C.L., Wang, D.Z., Harris, T.M., Yamagishi, H., Richardson, J.A., Childs, G. and Olson, E.N. (2002) 'Modulation of cardiac growth and development by HOP, an unusual homeodomain protein', *Cell*, 110(6), pp. 725-35.
Shiraishi, I., Simpson, D.G., Carver, W., Price, R., Hirozane, T., Terracio, L. and Borg, T.K. (1997) 'Vinculin is an essential component for normal myofibrillar arrangement in fetal mouse cardiac myocytes', *J Mol Cell Cardiol*, 29(8), pp. 2041-52.
Shou, W., Aghdasi, B., Armstrong, D.L., Guo, Q., Bao, S., Charng, M.J., Mathews, L.M., Schneider, M.D., Hamilton, S.L. and Matzuk, M.M. (1998) 'Cardiac defects and altered ryanodine receptor function in mice lacking FKBP12', *Nature*, 391(6666), pp. 489-92.
Simeone, R.M., Devine, O.J., Marcinkevage, J.A., Gilboa, S.M., Razzaghi, H., Bardenheier, B.H., Sharma, A.J. and Honein, M.A. (2015) 'Diabetes and congenital heart defects: a systematic review, meta-analysis, and modeling project', *Am J Prev Med*, 48(2), pp. 195-204.
Sinha, T., Lin, L., Li, D., Davis, J., Evans, S., Wynshaw-Boris, A. and Wang, J. (2015) 'Mapping the dynamic expression of Wnt11 and the lineage contribution of Wnt11-expressing cells during early mouse development', *Dev Biol*, 398(2), pp. 177-92.
Sinha, T., Wang, B., Evans, S., Wynshaw-Boris, A. and Wang, J. (2012) 'Disheveled mediated planar cell polarity signaling is required in the second heart field lineage for outflow tract morphogenesis', *Dev Biol*, 370(1), pp. 135-44.
Sjoblom, B., Salmazo, A. and Djinovic-Carugo, K. (2008) 'Alpha-actinin structure and regulation', *Cell Mol Life Sci*, 65(17), pp. 2688-701.
Snarr, B.S., Kern, C.B. and Wessels, A. (2008) 'Origin and fate of cardiac mesenchyme', *Dev Dyn*, 237(10), pp. 2804-19.
Snider, P., Simmons, O., Wang, J., Hoang, C.Q. and Conway, S.J. (2014) 'Ectopic Noggin in a Population of Nfatc1 Lineage Endocardial Progenitors Induces Embryonic Lethality', *J Cardiovasc Dev Dis*, 1(3), pp. 214-236.
Snowball, J., Ambalavanan, M., Cornett, B., Lang, R., Whitsett, J. and Sinner, D. (2015) 'Mesenchymal Wnt signaling promotes formation of sternum and thoracic body wall', *Dev Biol*, 401(2), pp. 264-75.
Soonpaa, M.H., Kim, K.K., Pajak, L., Franklin, M. and Field, L.J. (1996) 'Cardiomyocyte DNA synthesis and binucleation during murine development', *Am J Physiol*, 271(5 Pt 2), pp. H2183-9.
Sridurongrit, S., Larsson, J., Schwartz, R., Ruiz-Lozano, P. and Kaartinen, V. (2008) 'Signaling via the Tgf-beta type I receptor Alk5 in heart development', *Dev Biol*, 322(1), pp. 208-18.
Srinivas, S., Watanabe, T., Lin, C.S., William, C.M., Tanabe, Y., Jessell, T.M. and Costantini, F. (2001) 'Cre reporter strains produced by targeted insertion of EYFP and ECFP into the ROSA26 locus', *BMC Dev Biol*, 1, p. 4.
Srivastava, D. and Olson, E.N. (2000) 'A genetic blueprint for cardiac development', *Nature*, 407(6801), pp. 221-6.
Stanley, E.G., Biben, C., Elefanty, A., Barnett, L., Koentgen, F., Robb, L. and Harvey, R.P. (2002) 'Efficient Cre-mediated deletion in cardiac progenitor cells conferred by a 3'UTR-ires-Cre allele of the homeobox gene Nkx2-5', *Int J Dev Biol*, 46(4), pp. 431-9.
Staudt, D.W., Liu, J., Thorn, K.S., Stuurman, N., Liebling, M. and Stainier, D.Y. (2014) 'High-resolution imaging of cardiomyocyte behavior reveals two distinct steps in ventricular trabeculation', *Development*, 141(3), pp. 585-93.

Stoll, C., Dott, B., Alembik, Y. and Roth, M.P. (2015) 'Associated congenital anomalies among cases with Down syndrome', *Eur J Med Genet*, 58(12), pp. 674-80.
Sugihara, K., Nakatsuji, N., Nakamura, K., Nakao, K., Hashimoto, R., Otani, H., Sakagami, H., Kondo, H., Nozawa, S., Aiba, A. and Katsuki, M. (1998) 'Rac1 is required for the formation of three germ layers during gastrulation', *Oncogene*, 17(26), pp. 3427-33.
Sugishita, Y., Watanabe, M. and Fisher, S.A. (2004) 'The development of the embryonic outflow tract provides novel insights into cardiac differentiation and remodeling', *Trends Cardiovasc Med*, 14(6), pp. 235-41.
Sumandea, M.P., Pyle, W.G., Kobayashi, T., de Tombe, P.P. and Solaro, R.J. (2003) 'Identification of a functionally critical protein kinase C phosphorylation residue of cardiac troponin T', *J Biol Chem*, 278(37), pp. 35135-44.
Sun, Y., Liang, X., Najafi, N., Cass, M., Lin, L., Cai, C.L., Chen, J. and Evans, S.M. (2007) 'Islet 1 is expressed in distinct cardiovascular lineages, including pacemaker and coronary vascular cells', *Dev Biol*, 304(1), pp. 286-96.
Suri, C., Jones, P.F., Patan, S., Bartunkova, S., Maisonpierre, P.C., Davis, S., Sato, T.N. and Yancopoulos, G.D. (1996) 'Requisite role of angiopoietin-1, a ligand for the TIE2 receptor, during embryonic angiogenesis', *Cell*, 87(7), pp. 1171-80.
Sussman, M.A., Welch, S., Walker, A., Klevitsky, R., Hewett, T.E., Price, R.L., Schaefer, E. and Yager, K. (2000) 'Altered focal adhesion regulation correlates with cardiomyopathy in mice expressing constitutively active rac1', *J Clin Invest*, 105(7), pp. 875-86.
Sutoh, K. (1982) 'An actin-binding site on the 20K fragment of myosin subfragment 1', *Biochemistry*, 21(19), pp. 4800-4.
Suzuki, A., Yamanaka, T., Hirose, T., Manabe, N., Mizuno, K., Shimizu, M., Akimoto, K., Izumi, Y., Ohnishi, T. and Ohno, S. (2001) 'Atypical protein kinase C is involved in the evolutionarily conserved par protein complex and plays a critical role in establishing epithelia-specific junctional structures', *J Cell Biol*, 152(6), pp. 1183-96.
Szilagyi, L., Balint, M., Sreter, F.A. and Gergely, J. (1979) 'Photoaffinity labelling with an ATP analog of the N-terminal peptide of myosin', *Biochem Biophys Res Commun*, 87(3), pp. 936-45.
Ta-Shma, A., Pierri, C.L., Stepensky, P., Shaag, A., Zenvirt, S., Elpeleg, O. and Rein, A.J. (2013) 'Isolated truncus arteriosus associated with a mutation in the plexin-D1 gene', *Am J Med Genet A*, 161a(12), pp. 3115-20.
Takamatsu, H., Takegahara, N., Nakagawa, Y., Tomura, M., Taniguchi, M., Friedel, R.H., Rayburn, H., Tessier-Lavigne, M., Yoshida, Y., Okuno, T., Mizui, M., Kang, S., Nojima, S., Tsujimura, T., Nakatsuji, Y., Katayama, I., Toyofuku, T., Kikutani, H. and Kumanogoh, A. (2010) 'Semaphorins guide the entry of dendritic cells into the lymphatics by activating myosin II', *Nat Immunol*, 11(7), pp. 594-600.
Takashima, S., Kitakaze, M., Asakura, M., Asanuma, H., Sanada, S., Tashiro, F., Niwa, H., Miyazaki Ji, J., Hirota, S., Kitamura, Y., Kitsukawa, T., Fujisawa, H., Klagsbrun, M. and Hori, M. (2002) 'Targeting of both mouse neuropilin-1 and neuropilin-2 genes severely impairs developmental yolk sac and embryonic angiogenesis', *Proc Natl Acad Sci U S A*, 99(6), pp. 3657-62.
Takegahara, N., Takamatsu, H., Toyofuku, T., Tsujimura, T., Okuno, T., Yukawa, K., Mizui, M., Yamamoto, M., Prasad, D.V., Suzuki, K., Ishii, M., Terai, K., Moriya, M., Nakatsuji, Y., Sakoda, S., Sato, S., Akira, S., Takeda, K., Inui, M., Takai, T., Ikawa, M.,

Okabe, M., Kumanogoh, A. and Kikutani, H. (2006) 'Plexin-A1 and its interaction with DAP12 in immune responses and bone homeostasis', *Nat Cell Biol*, 8(6), pp. 615-22.
Talukder, M.A., Elnakish, M.T., Yang, F., Nishijima, Y., Alhaj, M.A., Velayutham, M., Hassanain, H.H. and Zweier, J.L. (2013) 'Cardiomyocyte-specific overexpression of an active form of Rac predisposes the heart to increased myocardial stunning and ischemia-reperfusion injury', *Am J Physiol Heart Circ Physiol*, 304(2), pp. H294-302.
Tam, P.P., Parameswaran, M., Kinder, S.J. and Weinberger, R.P. (1997) 'The allocation of epiblast cells to the embryonic heart and other mesodermal lineages: the role of ingression and tissue movement during gastrulation', *Development*, 124(9), pp. 1631-42.
Tamagnone, L., Artigiani, S., Chen, H., He, Z., Ming, G.I., Song, H., Chedotal, A., Winberg, M.L., Goodman, C.S., Poo, M., Tessier-Lavigne, M. and Comoglio, P.M. (1999) 'Plexins are a large family of receptors for transmembrane, secreted, and GPI-anchored semaphorins in vertebrates', *Cell*, 99(1), pp. 71-80.
Tan, W., Palmby, T.R., Gavard, J., Amornphimoltham, P., Zheng, Y. and Gutkind, J.S. (2008) 'An essential role for Rac1 in endothelial cell function and vascular development', *FASEB J*, 22(6), pp. 1829-38.
Tao, H., Suzuki, M., Kiyonari, H., Abe, T., Sasaoka, T. and Ueno, N. (2009) 'Mouse prickle1, the homolog of a PCP gene, is essential for epiblast apical-basal polarity', *Proc Natl Acad Sci U S A*, 106(34), pp. 14426-31.
Tapon, N. and Hall, A. (1997) 'Rho, Rac and Cdc42 GTPases regulate the organization of the actin cytoskeleton', *Curr Opin Cell Biol*, 9(1), pp. 86-92.
Tcherkezian, J. and Lamarche-Vane, N. (2007) 'Current knowledge of the large RhoGAP family of proteins', *Biol Cell*, 99(2), pp. 67-86.
Temsah, R. and Nemer, M. (2005) 'GATA factors and transcriptional regulation of cardiac natriuretic peptide genes', *Regul Pept*, 128(3), pp. 177-85.
ten Klooster, J.P., Jaffer, Z.M., Chernoff, J. and Hordijk, P.L. (2006) 'Targeting and activation of Rac1 are mediated by the exchange factor beta-Pix', *J Cell Biol*, 172(5), pp. 759-69.
Tepass, U., Truong, K., Godt, D., Ikura, M. and Peifer, M. (2000) 'Cadherins in embryonic and neural morphogenesis', *Nat Rev Mol Cell Biol*, 1(2), pp. 91-100.
Terracio, L., Simpson, D.G., Hilenski, L., Carver, W., Decker, R.S., Vinson, N. and Borg, T.K. (1990) 'Distribution of vinculin in the Z-disk of striated muscle: analysis by laser scanning confocal microscopy', *J Cell Physiol*, 145(1), pp. 78-87.
Thomas, P.S., Kim, J., Nunez, S., Glogauer, M. and Kaartinen, V. (2010) 'Neural crest cell-specific deletion of Rac1 results in defective cell-matrix interactions and severe craniofacial and cardiovascular malformations', *Dev Biol*, 340(2), pp. 613-25.
Thornell, L., Carlsson, L., Li, Z., Mericskay, M. and Paulin, D. (1997) 'Null mutation in the desmin gene gives rise to a cardiomyopathy', *J Mol Cell Cardiol*, 29(8), pp. 2107-24.
Tian, X., Hu, T., Zhang, H., He, L., Huang, X., Liu, Q., Yu, W., He, L., Yang, Z., Yan, Y., Yang, X., Zhong, T.P., Pu, W.T. and Zhou, B. (2014) 'Vessel formation. De novo formation of a distinct coronary vascular population in neonatal heart', *Science*, 345(6192), pp. 90-4.
Tian, X., Hu, T., Zhang, H., He, L., Huang, X., Liu, Q., Yu, W., He, L., Yang, Z., Zhang, Z., Zhong, T.P., Yang, X., Yang, Z., Yan, Y., Baldini, A., Sun, Y., Lu, J., Schwartz, R.J., Evans, S.M., Gittenberger-de Groot, A.C., Red-Horse, K. and Zhou, B. (2013) 'Subepicardial

endothelial cells invade the embryonic ventricle wall to form coronary arteries', *Cell Res*, 23(9), pp. 1075-90.
Timmerman, L.A., Grego-Bessa, J., Raya, A., Bertran, E., Perez-Pomares, J.M., Diez, J., Aranda, S., Palomo, S., McCormick, F., Izpisua-Belmonte, J.C. and de la Pompa, J.L. (2004) 'Notch promotes epithelial-mesenchymal transition during cardiac development and oncogenic transformation', *Genes Dev*, 18(1), pp. 99-115.
Timpl, R., Rohde, H., Robey, P.G., Rennard, S.I., Foidart, J.M. and Martin, G.R. (1979) 'Laminin--a glycoprotein from basement membranes', *J Biol Chem*, 254(19), pp. 9933-7.
Togi, K., Yoshida, Y., Matsumae, H., Nakashima, Y., Kita, T. and Tanaka, M. (2006) 'Essential role of Hand2 in interventricular septum formation and trabeculation during cardiac development', *Biochem Biophys Res Commun*, 343(1), pp. 144-51.
Tokuyasu, K.T. (1989) 'Immunocytochemical studies of cardiac myofibrillogenesis in early chick embryos. III. Generation of fasciae adherentes and costameres', *J Cell Biol*, 108(1), pp. 43-53.
Tong, Y. and Buck, M. (2005) '1H, 15N and 13C Resonance assignments and secondary structure determination reveal that the minimal Rac1 GTPase binding domain of plexin-B1 has a ubiquitin fold', *J Biomol NMR*, 31(4), pp. 369-70.
Tong, Y., Chugha, P., Hota, P.K., Alviani, R.S., Li, M., Tempel, W., Shen, L., Park, H.W. and Buck, M. (2007) 'Binding of Rac1, Rnd1, and RhoD to a novel Rho GTPase interaction motif destabilizes dimerization of the plexin-B1 effector domain', *J Biol Chem*, 282(51), pp. 37215-24.
Toole, B.P. (2001) 'Hyaluronan in morphogenesis', *Semin Cell Dev Biol*, 12(2), pp. 79-87.
Tovell, V.E., Chau, C.Y., Khaw, P.T. and Bailly, M. (2012) 'Rac1 inhibition prevents tissue contraction and MMP mediated matrix remodeling in the conjunctiva', *Invest Ophthalmol Vis Sci*, 53(8), pp. 4682-91.
Toyofuku, T., Yoshida, J., Sugimoto, T., Zhang, H., Kumanogoh, A., Hori, M. and Kikutani, H. (2005) 'FARP2 triggers signals for Sema3A-mediated axonal repulsion', *Nat Neurosci*, 8(12), pp. 1712-9.
Toyofuku, T., Zhang, H., Kumanogoh, A., Takegahara, N., Suto, F., Kamei, J., Aoki, K., Yabuki, M., Hori, M., Fujisawa, H. and Kikutani, H. (2004a) 'Dual roles of Sema6D in cardiac morphogenesis through region-specific association of its receptor, Plexin-A1, with off-track and vascular endothelial growth factor receptor type 2', *Genes Dev*, 18(4), pp. 435-47.
Toyofuku, T., Zhang, H., Kumanogoh, A., Takegahara, N., Yabuki, M., Harada, K., Hori, M. and Kikutani, H. (2004b) 'Guidance of myocardial patterning in cardiac development by Sema6D reverse signalling', *Nat Cell Biol*, 6(12), pp. 1204-11.
Turner, L.J., Nicholls, S. and Hall, A. (2004) 'The activity of the plexin-A1 receptor is regulated by Rac', *J Biol Chem*, 279(32), pp. 33199-205.
Urness, L.D., Bleyl, S.B., Wright, T.J., Moon, A.M. and Mansour, S.L. (2011) 'Redundant and dosage sensitive requirements for Fgf3 and Fgf10 in cardiovascular development', *Dev Biol*, 356(2), pp. 383-97.
van den Hoff, M.J., Kruithof, B.P., Moorman, A.F., Markwald, R.R. and Wessels, A. (2001) 'Formation of myocardium after the initial development of the linear heart tube', *Dev Biol*, 240(1), pp. 61-76.

van den Hoff, M.J., Moorman, A.F., Ruijter, J.M., Lamers, W.H., Bennington, R.W., Markwald, R.R. and Wessels, A. (1999) 'Myocardialization of the cardiac outflow tract', *Dev Biol*, 212(2), pp. 477-90.
van den Hoff, M.J., van den Eijnde, S.M., Viragh, S. and Moorman, A.F. (2000) 'Programmed cell death in the developing heart', *Cardiovasc Res*, 45(3), pp. 603-20.
Verzi, M.P., McCulley, D.J., De Val, S., Dodou, E. and Black, B.L. (2005) 'The right ventricle, outflow tract, and ventricular septum comprise a restricted expression domain within the secondary/anterior heart field', *Dev Biol*, 287(1), pp. 134-45.
Vikis, H.G., Li, W. and Guan, K.L. (2002) 'The plexin-B1/Rac interaction inhibits PAK activation and enhances Sema4D ligand binding', *Genes Dev*, 16(7), pp. 836-45.
Vikis, H.G., Li, W., He, Z. and Guan, K.L. (2000) 'The semaphorin receptor plexin-B1 specifically interacts with active Rac in a ligand-dependent manner', *Proc Natl Acad Sci U S A*, 97(23), pp. 12457-62.
Viragh, S. and Challice, C.E. (1981) 'The origin of the epicardium and the embryonic myocardial circulation in the mouse', *Anat Rec*, 201(1), pp. 157-68.
Vliegen, H.W., van der Laarse, A., Cornelisse, C.J. and Eulderink, F. (1991) 'Myocardial changes in pressure overload-induced left ventricular hypertrophy. A study on tissue composition, polyploidization and multinucleation', *Eur Heart J*, 12(4), pp. 488-94.
Wagner, M. and Siddiqui, M.A. (2007) 'Signal transduction in early heart development (I): cardiogenic induction and heart tube formation', *Exp Biol Med (Maywood)*, 232(7), pp. 852-65.
Waldo, K., Miyagawa-Tomita, S., Kumiski, D. and Kirby, M.L. (1998) 'Cardiac neural crest cells provide new insight into septation of the cardiac outflow tract: aortic sac to ventricular septal closure', *Dev Biol*, 196(2), pp. 129-44.
Waldo, K.L., Hutson, M.R., Stadt, H.A., Zdanowicz, M., Zdanowicz, J. and Kirby, M.L. (2005a) 'Cardiac neural crest is necessary for normal addition of the myocardium to the arterial pole from the secondary heart field', *Dev Biol*, 281(1), pp. 66-77.
Waldo, K.L., Hutson, M.R., Ward, C.C., Zdanowicz, M., Stadt, H.A., Kumiski, D., Abu-Issa, R. and Kirby, M.L. (2005b) 'Secondary heart field contributes myocardium and smooth muscle to the arterial pole of the developing heart', *Dev Biol*, 281(1), pp. 78-90.
Waldo, K.L., Kumiski, D. and Kirby, M.L. (1996) 'Cardiac neural crest is essential for the persistence rather than the formation of an arch artery', *Dev Dyn*, 205(3), pp. 281-92.
Waldo, K.L., Kumiski, D.H., Wallis, K.T., Stadt, H.A., Hutson, M.R., Platt, D.H. and Kirby, M.L. (2001) 'Conotruncal myocardium arises from a secondary heart field', *Development*, 128(16), pp. 3179-88.
Walmsley, M.J., Ooi, S.K., Reynolds, L.F., Smith, S.H., Ruf, S., Mathiot, A., Vanes, L., Williams, D.A., Cancro, M.P. and Tybulewicz, V.L. (2003) 'Critical roles for Rac1 and Rac2 GTPases in B cell development and signaling', *Science*, 302(5644), pp. 459-62.
Wang, H.U., Chen, Z.F. and Anderson, D.J. (1998) 'Molecular distinction and angiogenic interaction between embryonic arteries and veins revealed by ephrin-B2 and its receptor Eph-B4', *Cell*, 93(5), pp. 741-53.
Wang, L. and Zheng, Y. (2007) 'Cell type-specific functions of Rho GTPases revealed by gene targeting in mice', *Trends Cell Biol*, 17(2), pp. 58-64.
Wang, T., Li, B.Y., Danielson, P.D., Shah, P.C., Rockwell, S., Lechleider, R.J., Martin, J., Manganaro, T. and Donahoe, P.K. (1996) 'The immunophilin FKBP12 functions as a common inhibitor of the TGF beta family type I receptors', *Cell*, 86(3), pp. 435-44.

Wang, X., Gorospe, M., Huang, Y. and Holbrook, N.J. (1997) 'p27Kip1 overexpression causes apoptotic death of mammalian cells', *Oncogene*, 15(24), pp. 2991-7.
Wang, Y., Wu, B., Chamberlain, A.A., Lui, W., Koirala, P., Susztak, K., Klein, D., Taylor, V. and Zhou, B. (2013) 'Endocardial to myocardial notch-wnt-bmp axis regulates early heart valve development', *PLoS One*, 8(4), p. e60244.
Wang, Z. and Huang, J. (2014) 'Neuregulin-1 increases connexin-40 and connexin-45 expression in embryonic stem cell-derived cardiomyocytes', *Appl Biochem Biotechnol*, 174(2), pp. 483-93.
Watanabe, M., Choudhry, A., Berlan, M., Singal, A., Siwik, E., Mohr, S. and Fisher, S.A. (1998) 'Developmental remodeling and shortening of the cardiac outflow tract involves myocyte programmed cell death', *Development*, 125(19), pp. 3809-20.
Watanabe, M., Jafri, A. and Fisher, S.A. (2001) 'Apoptosis is required for the proper formation of the ventriculo-arterial connections', *Dev Biol*, 240(1), pp. 274-88.
Watanabe, Y., Kokubo, H., Miyagawa-Tomita, S., Endo, M., Igarashi, K., Aisaki, K., Kanno, J. and Saga, Y. (2006) 'Activation of Notch1 signaling in cardiogenic mesoderm induces abnormal heart morphogenesis in mouse', *Development*, 133(9), pp. 1625-34.
Watanabe, Y., Miyagawa-Tomita, S., Vincent, S.D., Kelly, R.G., Moon, A.M. and Buckingham, M.E. (2010) 'Role of mesodermal FGF8 and FGF10 overlaps in the development of the arterial pole of the heart and pharyngeal arch arteries', *Circ Res*, 106(3), pp. 495-503.
Webb, S., Brown, N.A. and Anderson, R.H. (1998) 'Formation of the atrioventricular septal structures in the normal mouse', *Circ Res*, 82(6), pp. 645-56.
Wei, L., Imanaka-Yoshida, K., Wang, L., Zhan, S., Schneider, M.D., DeMayo, F.J. and Schwartz, R.J. (2002) 'Inhibition of Rho family GTPases by Rho GDP dissociation inhibitor disrupts cardiac morphogenesis and inhibits cardiomyocyte proliferation', *Development*, 129(7), pp. 1705-14.
Weisleder, N., Soumaka, E., Abbasi, S., Taegtmeyer, H. and Capetanaki, Y. (2004) 'Cardiomyocyte-specific desmin rescue of desmin null cardiomyopathy excludes vascular involvement', *J Mol Cell Cardiol*, 36(1), pp. 121-8.
Wells, C.M., Walmsley, M., Ooi, S., Tybulewicz, V. and Ridley, A.J. (2004) 'Rac1-deficient macrophages exhibit defects in cell spreading and membrane ruffling but not migration', *J Cell Sci*, 117(Pt 7), pp. 1259-68.
Weninger, W.J., Geyer, S.H., Mohun, T.J., Rasskin-Gutman, D., Matsui, T., Ribeiro, I., Costa Lda, F., Izpisua-Belmonte, J.C. and Muller, G.B. (2006) 'High-resolution episcopic microscopy: a rapid technique for high detailed 3D analysis of gene activity in the context of tissue architecture and morphology', *Anat Embryol (Berl)*, 211(3), pp. 213-21.
Wikenheiser, J., Doughman, Y.Q., Fisher, S.A. and Watanabe, M. (2006) 'Differential levels of tissue hypoxia in the developing chicken heart', *Dev Dyn*, 235(1), pp. 115-23.
Williams, R., Lendahl, U. and Lardelli, M. (1995) 'Complementary and combinatorial patterns of Notch gene family expression during early mouse development', *Mech Dev*, 53(3), pp. 357-68.
Wilson, E., Leszczynska, K., Poulter, N.S., Edelmann, F., Salisbury, V.A., Noy, P.J., Bacon, A., Rappoport, J.Z., Heath, J.K., Bicknell, R. and Heath, V.L. (2014) 'RhoJ interacts with the GIT-PIX complex and regulates focal adhesion disassembly', *J Cell Sci*, 127(Pt 14), pp. 3039-51.

Worzfeld, T., Swiercz, J.M., Senturk, A., Genz, B., Korostylev, A., Deng, S., Xia, J., Hoshino, M., Epstein, J.A., Chan, A.M., Vollmar, B., Acker-Palmer, A., Kuner, R. and Offermanns, S. (2014) 'Genetic dissection of plexin signaling in vivo', *Proc Natl Acad Sci U S A*, 111(6), pp. 2194-9.
Wu, B., Zhang, Z., Lui, W., Chen, X., Wang, Y., Chamberlain, A.A., Moreno-Rodriguez, R.A., Markwald, R.R., O'Rourke, B.P., Sharp, D.J., Zheng, D., Lenz, J., Baldwin, H.S., Chang, C.P. and Zhou, B. (2012) 'Endocardial cells form the coronary arteries by angiogenesis through myocardial-endocardial VEGF signaling', *Cell*, 151(5), pp. 1083-96.
Wu, H., Wang, X., Liu, S., Wu, Y., Zhao, T., Chen, X., Zhu, L., Wu, Y., Ding, X., Peng, X., Yuan, J., Wang, X., Fan, W. and Fan, M. (2007) 'Sema4C participates in myogenic differentiation in vivo and in vitro through the p38 MAPK pathway', *Eur J Cell Biol*, 86(6), pp. 331-44.
Xie, L., Hoffmann, A.D., Burnicka-Turek, O., Friedland-Little, J.M., Zhang, K. and Moskowitz, I.P. (2012) 'Tbx5-hedgehog molecular networks are essential in the second heart field for atrial septation', *Dev Cell*, 23(2), pp. 280-91.
Xin, M., Small, E.M., van Rooij, E., Qi, X., Richardson, J.A., Srivastava, D., Nakagawa, O. and Olson, E.N. (2007) 'Essential roles of the bHLH transcription factor Hrt2 in repression of atrial gene expression and maintenance of postnatal cardiac function', *Proc Natl Acad Sci U S A*, 104(19), pp. 7975-80.
Xing, Y., Li, C., Li, A., Sridurongrit, S., Tiozzo, C., Bellusci, S., Borok, Z., Kaartinen, V. and Minoo, P. (2010) 'Signaling via Alk5 controls the ontogeny of lung Clara cells', *Development*, 137(5), pp. 825-33.
Xue, Y., Gao, X., Lindsell, C.E., Norton, C.R., Chang, B., Hicks, C., Gendron-Maguire, M., Rand, E.B., Weinmaster, G. and Gridley, T. (1999) 'Embryonic lethality and vascular defects in mice lacking the Notch ligand Jagged1', *Hum Mol Genet*, 8(5), pp. 723-30.
Yamamoto, S., Tsutsui, H., Takahashi, M., Ishibashi, Y., Tagawa, H., Imanaka-Yoshida, K., Saeki, Y. and Takeshita, A. (1998) 'Role of microtubules in the viscoelastic properties of isolated cardiac muscle', *J Mol Cell Cardiol*, 30(9), pp. 1841-53.
Yamamura, H., Zhang, M., Markwald, R.R. and Mjaatvedt, C.H. (1997) 'A heart segmental defect in the anterior-posterior axis of a transgenic mutant mouse', *Dev Biol*, 186(1), pp. 58-72.
Yanazume, T., Hasegawa, K., Wada, H., Morimoto, T., Abe, M., Kawamura, T. and Sasayama, S. (2002) 'Rho/ROCK pathway contributes to the activation of extracellular signal-regulated kinase/GATA-4 during myocardial cell hypertrophy', *J Biol Chem*, 277(10), pp. 8618-25.
Yang, J., Bucker, S., Jungblut, B., Bottger, T., Cinnamon, Y., Tchorz, J., Muller, M., Bettler, B., Harvey, R., Sun, Q.Y., Schneider, A. and Braun, T. (2012) 'Inhibition of Notch2 by Numb/Numblike controls myocardial compaction in the heart', *Cardiovasc Res*, 96(2), pp. 276-85.
Yang, J. and Xu, X. (2012) 'alpha-Actinin2 is required for the lateral alignment of Z discs and ventricular chamber enlargement during zebrafish cardiogenesis', *Faseb j*, 26(10), pp. 4230-42.
Yang, L., Cai, C.L., Lin, L., Qyang, Y., Chung, C., Monteiro, R.M., Mummery, C.L., Fishman, G.I., Cogen, A. and Evans, S. (2006) 'Isl1Cre reveals a common Bmp pathway in heart and limb development', *Development*, 133(8), pp. 1575-85.

Yashiro, K., Shiratori, H. and Hamada, H. (2007) 'Haemodynamics determined by a genetic programme govern asymmetric development of the aortic arch', *Nature*, 450(7167), pp. 285-8.
Yelbuz, T.M., Waldo, K.L., Kumiski, D.H., Stadt, H.A., Wolfe, R.R., Leatherbury, L. and Kirby, M.L. (2002) 'Shortened outflow tract leads to altered cardiac looping after neural crest ablation', *Circulation*, 106(4), pp. 504-10.
Young, K.G. and Copeland, J.W. (2010) 'Formins in cell signaling', *Biochim Biophys Acta*, 1803(2), pp. 183-90.
Yu, H., Ye, X., Guo, N. and Nathans, J. (2012) 'Frizzled 2 and frizzled 7 function redundantly in convergent extension and closure of the ventricular septum and palate: evidence for a network of interacting genes', *Development*, 139(23), pp. 4383-94.
Zaffran, S., Robrini, N. and Bertrand, N. (2014) 'Retinoids and Cardiac Development', *Journal of Developmental Biology*, 2(1), p. 50.
Zhang, H., Pu, W., Li, G., Huang, X., He, L., Tian, X., Liu, Q., Zhang, L., Wu, S.M., Sucov, H.M. and Zhou, B. (2016) 'Endocardium Minimally Contributes to Coronary Endothelium in the Embryonic Ventricular Free Walls', *Circ Res*, 118(12), pp. 1880-93.
Zhang, W., Chen, H., Qu, X., Chang, C.P. and Shou, W. (2013) 'Molecular mechanism of ventricular trabeculation/compaction and the pathogenesis of the left ventricular noncompaction cardiomyopathy (LVNC)', *Am J Med Genet C Semin Med Genet*, 163c(3), pp. 144-56.
Zhang, W., Chen, H., Wang, Y., Yong, W., Zhu, W., Liu, Y., Wagner, G.R., Payne, R.M., Field, L.J., Xin, H., Cai, C.L. and Shou, W. (2011) 'Tbx20 transcription factor is a downstream mediator for bone morphogenetic protein-10 in regulating cardiac ventricular wall development and function', *J Biol Chem*, 286(42), pp. 36820-9.
Zhang, Y., Singh, M.K., Degenhardt, K.R., Lu, M.M., Bennett, J., Yoshida, Y. and Epstein, J.A. (2009) 'Tie2Cre-mediated inactivation of plexinD1 results in congenital heart, vascular and skeletal defects', *Dev Biol*, 325(1), pp. 82-93.
Zhang, Z. and Zhou, B. (2013) 'Accelerated coronary angiogenesis by vegfr1-knockout endocardial cells', *PLoS One*, 8(7), p. e70570.
Zhao, X.Q., Huang, G.Y., Xie, L.J., Peng, T. and Zhou, G.M. (2005) '[Abnormal development of conotruncal region in Cx43 knockout mice]', *Zhonghua Yi Xue Za Zhi*, 85(38), pp. 2715-8.
Zhao, Y.Y., Sawyer, D.R., Baliga, R.R., Opel, D.J., Han, X., Marchionni, M.A. and Kelly, R.A. (1998) 'Neuregulins promote survival and growth of cardiac myocytes. Persistence of ErbB2 and ErbB4 expression in neonatal and adult ventricular myocytes', *J Biol Chem*, 273(17), pp. 10261-9.
Zhou, B., Ma, Q., Rajagopal, S., Wu, S.M., Domian, I., Rivera-Feliciano, J., Jiang, D., von Gise, A., Ikeda, S., Chien, K.R. and Pu, W.T. (2008) 'Epicardial progenitors contribute to the cardiomyocyte lineage in the developing heart', *Nature*, 454(7200), pp. 109-13.
Zhou, J., Pashmforoush, M. and Sucov, H.M. (2012) 'Endothelial neuropilin disruption in mice causes DiGeorge syndrome-like malformations via mechanisms distinct to those caused by loss of Tbx1', *PLoS One*, 7(3), p. e32429.
Zuppinger, C., Eppenberger-Eberhardt, M. and Eppenberger, H.M. (2000) 'N-Cadherin: structure, function and importance in the formation of new intercalated disc-like cell contacts in cardiomyocytes', *Heart Fail Rev*, 5(3), pp. 251-7.